Synthesis, Characterisation, and Development of Photo-activated Carbon monoxide-releasing Molecules

Jonathan Stuart Ward

Doctor of Philosophy

University of York

Chemistry

September 2014

i Abstract

Several series of photo-activated carbon monoxide-releasing molecules have been synthesised and characterised for use as potential pharmaceutical molecules.

Initial CO-RMs synthesised were based on a tetracarbonyl phenylpyridine(I) complex, with substitutions in the *para*-phenyl position. All were shown to release CO when irradiated with light of wavelength 365 nm.

An LED system was developed to irradiate samples in CO-release quantification assays.

A carboxylic acid-containing CO-RM was then developed to improve solubility. The new CO-RM is water compatible and releases three molecules of CO per molecule of CO-RM. It has been shown to be viable with sensitive RAW 264.7 macrophage cells, and to exhibit a toxic effect on *E. coli* in combination with light of wavelength 400 nm.

An L tryptophan-containing CO-RM was synthesised and is water compatible; and releases CO when irradiated at 465 nm light. It is viable with RAW 264.7 cells and is capable of suppressing an inflammatory response initiated by LPS and IFN-γ and been shown to have a detrimental effect on *E. coli, S. aureus,* and *N. gonorrhoeae*.

An alkyne-containing CO-RM was designed so that it could be used in Huisgen [3+2] cycloaddition chemistry. This CO-RM was functionalised using 4-azidobenzoic and biotin to give two new triazole-containing CO-RMs. The biotin-containing CO-RM has been shown to release CO and bind strongly with an avidin target.

Bacterial studies with a tryptophan-containing CO-RM show that increased optical density of cultures decreases the effectiveness of the CO-RM, due to reduced light penetration. This lead to the development of dye-containing CO-RM, which is based on a benzothiazole azodye. This dye-CO-RM contains a UV-band associated with CO-release that tails out to a higher wavelength than any of the previous CO-RMs prepared in this project.

ii List of Contents

iii List of figures, tables and schemes

iv Acknowledgements

I would first of all like to thank my collection of supervisors, Prof. Ian Fairlamb, Dr Jason Lynam, and Dr James Moir for letting be part of team CO-RM. It has been a really interesting project that spans more areas expertise than you can shake a stick at. I want to also thank them for supporting me through all the ups and downs of the project, both scientific and personal; I really couldn't have done it without them.

I would also like to thank all the members in each of these respective groups. Particularly Tom, Sarah, and Amanda for helping me getting off to a great start to my PhD, and for giving me those little practical tips that you just do not often find in experimental procedures (Although perhaps you should!).

I would also like to thank the more recent members of the for keeping the *badinage* within the group at the highest level and making everyday entertaining and interesting: Prof. Sir Rev. Tom 3.0, Jozzers Bray, Big Al, Phili't'pa, Geordie Kate, Hellooo there Lyndsay, Technical Charlotte, Keeping it real George, 'it's a meeee Jessica', Get off my keyboard Margot!, Selena and Nasiru, you know what I'm talking about!

I could not have done this project without the fantastic technical staff we have at York, and I thank all of them for their expertise and advice.

I would also like to thank all the members of the L1 floor in biology. I am chemist by training and I was taken in as one of their own. Everyone was really helpful in getting me up to speed with the dark arts.

I would like to express my gratitude to David Sanin and Adrian Mountford for allowing me to carry out studies in their laboratory. You guys did not have to help me but you really helped me with the project.

I also want to thank my parents Judith and Colin for always supporting me through all the years, and helping me progress this far with my education. I really could not have done it without you.

v Author’s declaration

I declare that this thesis is a presentation of original work and I am the sole author. This work has not previously been presented for an award at this, or any other, University. All sources are acknowledged as references.

1 Introduction

1.1 Carbon monoxide (CO) as a ligand

Carbon monoxide (CO) is a di-atomic species consisting of one carbon and oxygen atom with a double bond and a dative bond. The bonding in carbon monoxide can be considering in the following way (**Figure 1**).

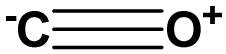

Figure 1. The structure of carbon monoxide

There are two covalent bonds between the carbon and oxygen with an additional dative bond from the oxygen. This makes the bond very strong compared to a typical CO or CC double bond.[1] Carbon monoxide is relatively inert compared to triplet dioxygen (O_2) which has two unpaired electrons. However this is situational and carbon monoxide can still undergo many reactions. In particular, it can bond strongly to metal centres.[2-3] CO bonds strongly to metal centres because it can donate and receive electron density into different orbitals. The two types of bonding are shown in **Figure 2**.

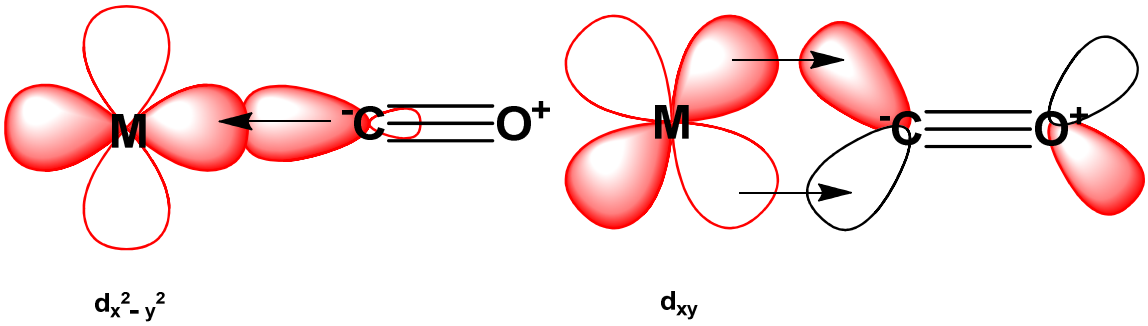

Figure 2. The bonding of carbon monoxide with a metal centre. Left: σ-donation into an empty metal d-orbital, Right: π-back donation from a full metal d-orbital into the CO π* anti bonding orbital.

The use of d-orbitals with a 45° rotation respective to each other allows for this synergistic bonding, giving a strong interaction. This bonding could involve d_{xy} and d_{x2-y2} orbitals to give the correct orientation. To demonstrate how a metal centre binds with CO, a molecular orbital diagram of CO needs to be considered (**Figure 3**).

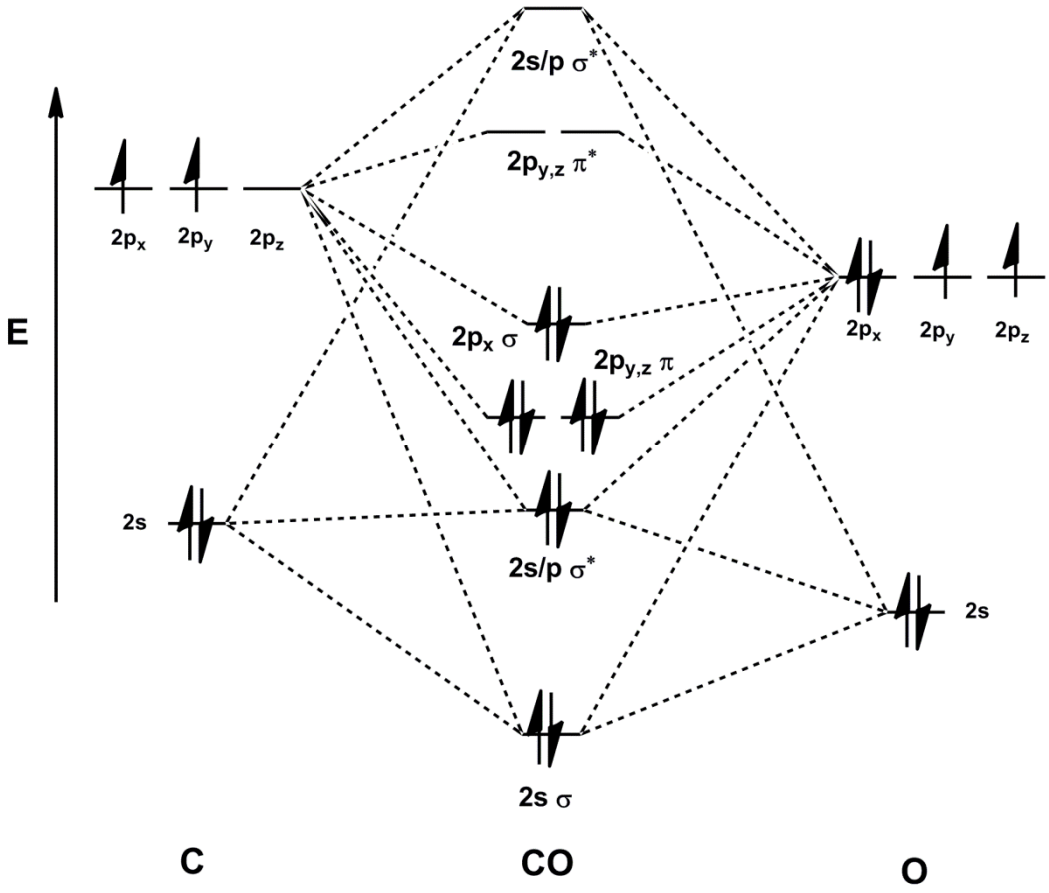

Figure 3. The molecular orbital diagram for carbon monoxide.

The diagram in **Figure 3** shows that in carbon monoxide, the π* anti-bonding orbital is empty, which explains why a metal centre d_{xy} orbital can donate electron density into this orbital. The d_{xy}–π* interaction is bonding with respect to a metal carbonyl bond but anti-bonding with respect to the C–O bond. This is why metal carbonyl stretching frequencies typically come at lower wavenumber than free CO due to a weaker C–O bond because of the π-back-bonding. The full σ orbital on CO can donate electron density into the empty $d_{x^2-y^2}$ on a metal centre. **Figure 4** shows how a metal centre can bind with carbonyl ligands in an octahedral configuration. This demonstrates how the resulting molecular orbitals are filled with electrons.[4]

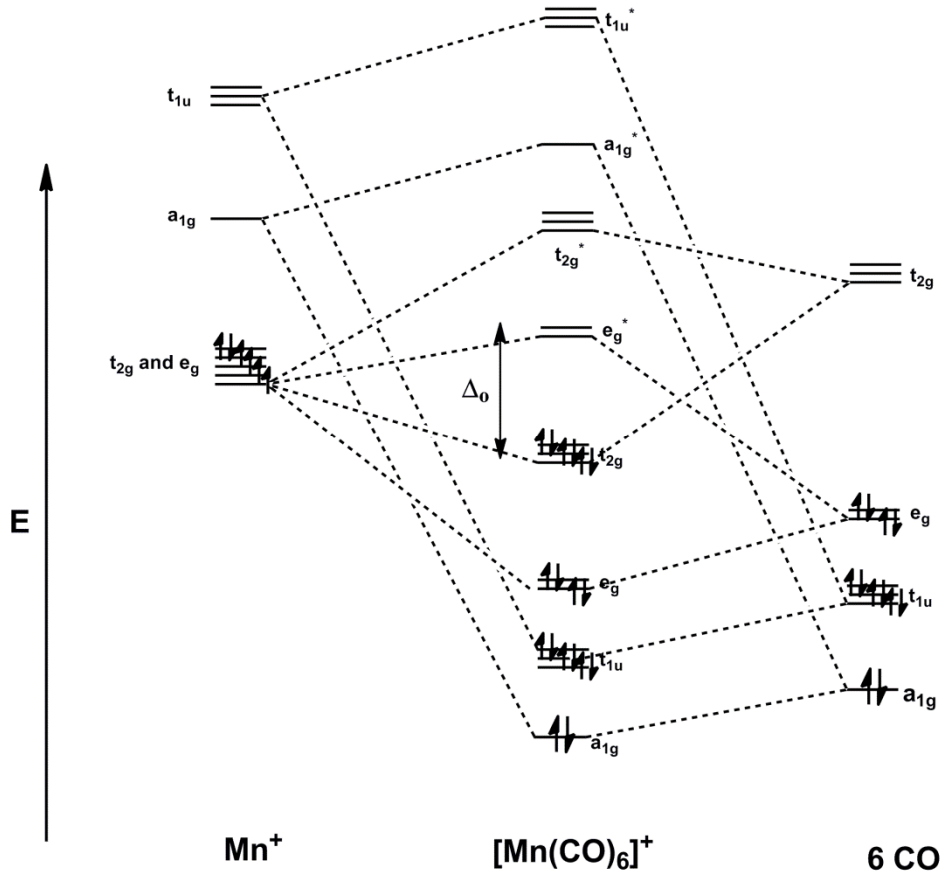

Figure 4. The bonding of a manganese(I) centre with carbon monoxide with octahedral geometry

Considering a manganese(I) metal centre it has a d_6 electron shell configuration. The six CO ligands will donate two electrons each to the metal centre giving 12 electrons from these in total. The atomic orbitals on the metal and carbonyl ligands of matching symmetry overlap to form the molecular orbitals. The 18 electrons are situated in the lowest energy orbitals available. Due to the large splitting of the t_{2g} and e_g orbitals by the strong field CO ligands; the six highest energy electrons are situated in orbitals of t_{2g} symmetry (d_{xy}, d_{xz}, and d_{yz}). The Δ_o is too large to allow for electron promotion to the e_g orbitals (dz^2 and $d_x{}^2$-$_y{}^2$). The highest occupied molecular orbitals are the t_{2g} orbitals which are involved in the donation of electron density to the π^* orbital on the CO ligand. The lowest unoccupied molecular e_g orbitals can accept electron density from σ orbitals on the CO ligand. Irradiation of a metal complex with light of energy Δ_o can result in promotion of an electron in to the e_g anti-bonding orbital. This can result in the loss of CO photolytically.

Nitric oxide (NO) is another diatomic ligand which is similar to carbon monoxide and can also bind to metal centres. The structure of NO is shown in **Figure 5**.

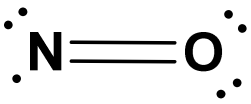

Figure 5. The structure of nitric oxide.

NO contains a double bond between its two atoms is a radical. This makes the ligand much more reactive and opens up more modes of binding. When NO bonds to a metal it can bind in a linear or bent fashion as shown in **Figure 6**.[5]

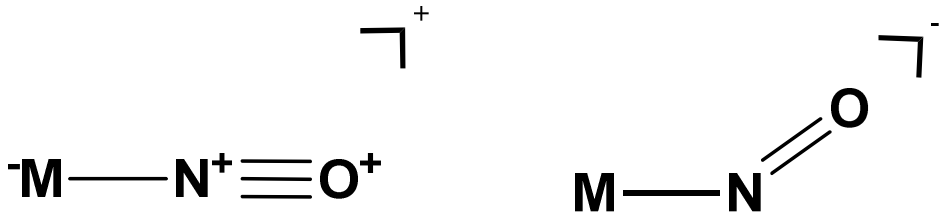

Figure 6. Binding modes of NO to a metal centre. Left: linear binding, Right: bent NO binding.

With linear NO binding, the unpaired electron is donated to the metal giving M-NO^+. With NO^+ now being isoelectronic to CO, it donates a further two electrons *via* σ-donation just like CO does making it a three-electron donor.

With bent NO binding to a metal centre, the metal donates an electron in to the same orbital as the radical creating a lone pair, giving NO^-, which is isoelectronic with di-oxygen (O_2). This then donates two electrons to the metal centre and therefore is overall a one-electron donor. O_2 also typically binds to metal centres in a bent fashion and it is clear why NO does this too when it becomes NO^-.[6]

1.2 Carbon monoxide and nitric oxide in biology

Carbon monoxide and nitric oxide both play an important role in biological systems.[7-8] Both of these are signalling molecules and it is not surprising considering their similar structures, that the signalling pathway of these molecules overlaps significantly.[8] This could be considered to be counter-intuitive as in relatively high concentrations CO is toxic to many organisms.[9] At lower concentrations, both of these molecules are involved in: the regulation of the immune system, muscle relaxation, vasodilation, blood pressure regulation, and healing processes such as thrombosis.[7, 10]

1.2.1 Carbon monoxide binding targets and protein regulation

1.2.1.1 Carbon monoxide toxicity

It is well known that CO can induce negative symptoms in humans. These effects start to occur at levels above 70 ppm.[9] At these levels, the concentration of CO-Hb in the blood can reach 10-15%. When the CO-Hb concentration is much higher than this, more severe symptoms are observed.

There are two main reasons for CO toxicity with the first being that CO has a high affinity for myoglobin and haemoglobin. CO will bind strongly to the haem group in both of these proteins. This reduces the amount of oxygen available to the organism, inducing symptoms such as fatigue and headaches but is not the main reason for its toxicity.

CO can also inhibit the action of cytochrome c oxidase.[11] This protein is found in mitochondria and is an essential part of the respiratory chain. If this chain is severely damaged, the cells cannot produce ATP and therefore cannot survive. One can consider this to be like having no fuel in the tank of a vehicle.

Cytochrome c oxidase is a large integral membrane protein consisting of 13 subunits.[12] The enzyme contains two haem centres.[13] The haem centres can bind oxygen which is essential to the transfer of electrons into the mitochondria. Carbon monoxide can compete with oxygen with respect to haem centre binding. This competition interrupts the smooth operation of this enzyme resulting in significant inhibition.

Miró carried out experiments using human muscle tissue to demonstrate the discussed mechanism of action.[11] Mitochondria were isolated and each complex of the mitochondrial respiratory chain was assayed for enzyme activity at different CO concentrations. **Table 1** shows the results obtained for cytochrome c oxidase.

Table 1. The variation in cytochrome c oxidase activity in human mitochondria at varying CO concentrations.

CO concentration / ppm	Cytochrome c oxidase activity/ nmol min^{-1} mg^{-1}
Air	836 ± 439
50	670 ± 401
100	483 ± 182
500	379 ±131

The results obtained shows statistical significance despite the large error in the measurements obtained. All the other protein complexes in the respiratory chain tested did not show any statistical significance and did not vary with CO concentration. This is an important study and it shows the site of action of carbon monoxide at higher concentrations.

Interestingly, despite the high binding affinity of CO for haem proteins such as haemoglobin and cytochrome c oxidase, Killick and Marchant showed that dogs could be rescued under certain conditions.[14] Dogs which had been poisoned with CO, giving rise to CO-Hb levels of up to 70%, could be rescued by immediate breathing of CO_2/O_2 mixtures. This work shows that with significant flushing of the system with fresh gas that the CO bound to various proteins is actually reversible. **Figure 7** shows the reduction of CO-Hb within the experiment dogs while breathing various gas mixtures.

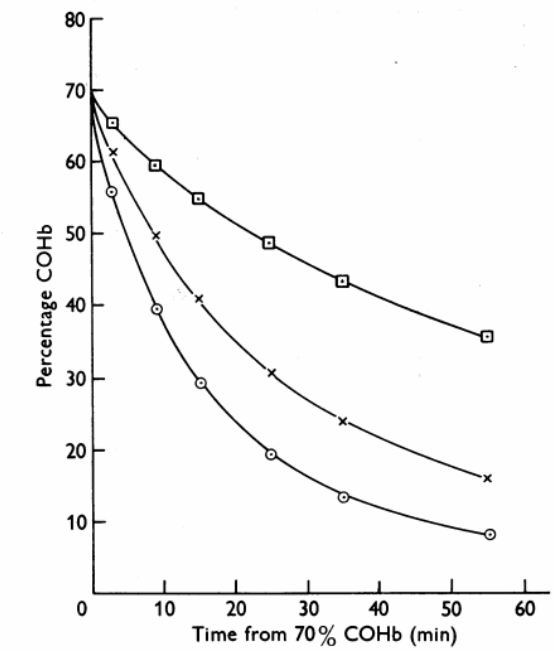

Figure 7. The percentage of CO-Hb in dogs acutely poisoned with CO. Reduction over time when breathing various gas mixtures. Square - dogs breathing air, Cross - dogs breathing 100% O_2, Circle - dogs breathing 5:95% CO_2:O_2 mixture. (Figure taken from ref. **14**: Resuscitation of dogs from severe acute carbon monoxide poisoning, Killick, E. M.; Marchant, J. V. *J. Physiol.* **1959**, 147, 274-98, Copyright Wiley 1959)

It is clear that the recovery of the dogs is improved when breathing pure oxygen or a CO_2/O_2 mixture. This is expected as nitrogen in the air does not have any affinity for these proteins so cannot compete with the bound CO at all. It is interesting to see that results like this were obtained in the late 1950s, yet these kind of gas mixtures are not readily available where CO poisoning is a possible risk. Immediate access to gas mixtures like this could save someone's life.

1.2.1.2 Haem degradation pathway - Natural CO production

As a signalling molecule, CO can bind strongly with various proteins, which triggers regulation of further proteins. CO could be considered to be a signalling molecule early on in many pathways as it is produced during the degradation of haem. **Scheme 1** shows how carbon monoxide is produced naturally within mammals and fish.[15-17]

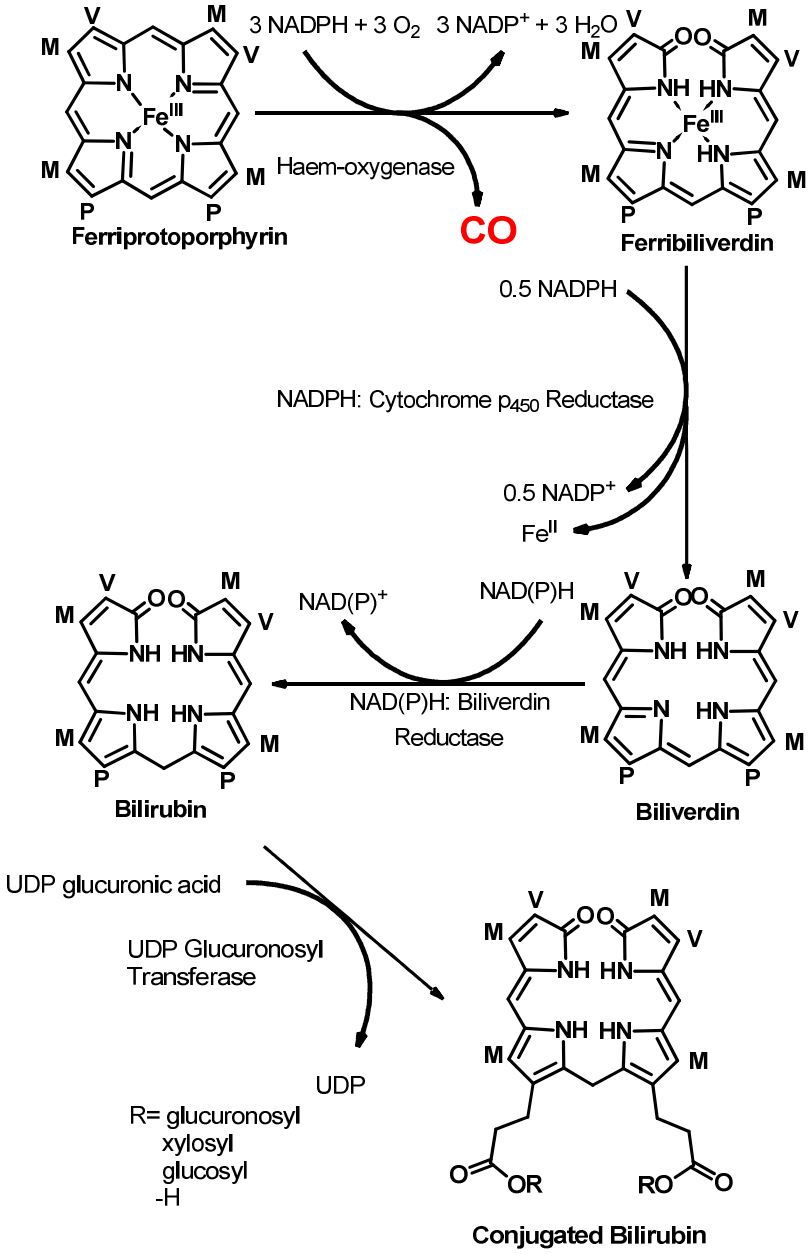

Scheme 1. The conversion of haem to Bilirubin. Side chains: M= Methyl,V= Vinyl, P= Proprionate.

Haems like in **Scheme 1** are present within many proteins such as haemoglobin, myoglobin, and many other enzymes. The haem is essential for protein function and as proteins break down the

haem material needs to be recycled/excreted. The haem also contributes to significant absorption in the 500-600 nm region of the spectrum and is often responsible for observed Q-bands.

Carbon monoxide is released in the first step of the haem degradation pathway. Haem oxygenase cleaves a carbon-carbon bond and introduces two carbonyl groups to form amides, giving ferribiliverdin. This molecule of CO can then go on to up-regulate many enzymes including the ones in this cycle.

Cytochrome p450 then removes the iron centre from the biliverdin structure by reducing it to iron(II). Biliverdin reductase then reduces a double bond in the structure introducing another pyrrole ring to giving the unconjugated bilirubin. If unconjugated bilirubin accumulates it can cause jaundice, particular in babies, which can cause serious health problems and can be potentially fatal.[18] This highlights how important this pathway is and that smooth catalysis is constantly required. This could occur for many reasons but could potentially be due to the lack of glucuronidation leading to a lack of excretion because of poor solubility.

1.2.1.3 Haem oxygenases and their importance

As mentioned in section **1.2.1.2**, haem oxygenases are essential to the haem degradation pathway. They catalyse the natural production of CO, and this then up regulates many further enzymes.[10] Haem oxygenase is present in three forms: HO-1, HO-2 and HO-3.[19] HO-1 is an inducible form of the enzyme, which is activated in the presence of increased CO levels and various forms of stress including H_2O_2 and cytokines.[20] HO-2 is a constitutive form of the enzyme that is present in lower levels and is not regulated by CO.[21] HO-1 carries out the majority of the catalysis in this pathway; however both HO-1 and 2 are expressed at higher levels than each other in certain organs. For example, HO-2 is strongly expressed in the testes and HO-1 tends to be expressed strongly in areas of erythrocyte and haem degradation. HO-3 has a very similar structure to HO-2 but little is known about what regulates HO-3 expression.[19]

HO-1 is very important during times of injury and stress. Chen and co-workers showed that aortic transplant in mice without the HO-1 enzyme resulted in death within four days in all cases due to arterial thrombosis. Mice able to produce HO-1 survived the operation for at least 56 days.[22] The low concentrations of CO due to the absence of HO-1 then results in many further enzymes not being up-regulated. This then results in: blood clotting, slow healing, and poor resistance to infection.

The presence of HO-2 which is constitutive allows initial haem decomposition. This enzyme is important as cells are dying continually within a biological system and a mechanism is needed

for constant decomposition. During periods of physical and oxidative stress, an increased haem decomposition rate is essential and the up regulation of HO-1 from increase CO levels then provides this.

Initial studies have shown the importance of the two haem oxygenase enzymes. A study by Gronert and co-workers compares injury repair rates in mice.[23] HO-2 wild type and knockout mice were wounded and the cornea was stained with fluorescein; the rates and quality of healing was then compared. **Figure 8** shows the results from this study.

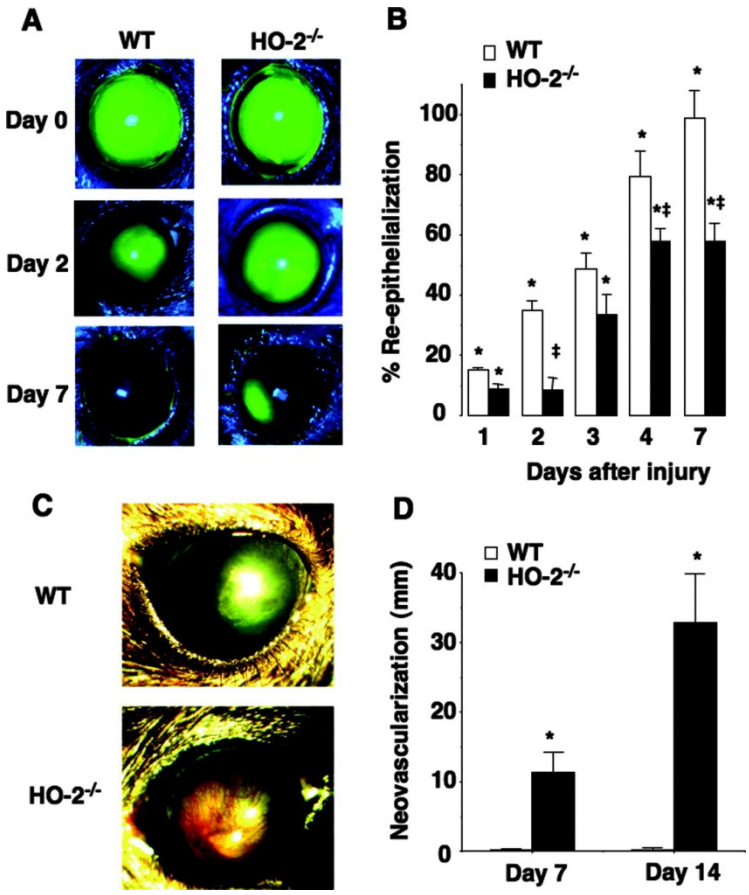

Figure 8. Results from a healing rate study in wild type and HO-2 null mice. A - Fluorescein stained cornea in wild type and HO-2 null mice. B - Study of re-epithelialisation, C - Photograph of specimens D - Neovascularisation study expressed as total length of penetrating vessels. (Figure taken from ref. **23**: Heme Oxygenase-2 Is a Critical Determinant for Execution of an Acute Inflammatory and Reparative Response, Gronert, K.; Seta, F.; Bellner, L.; Rezzani, R.; Regan, R. F.; Dunn, M. W.; Abraham, N. G.; Laniado-Schwartzman, M. *Am. J. Pathol.* **2006**, 169, 1612-1623. Copyright Elsevier 2006).

The study shows that the constitutive HO-2 enzyme is essential in initialising haem breakdown. Without this initial breakdown, the up-regulation of HO-1 due to CO release is not possible. Many other enzymes cannot be appropriately regulated, and this is evident from the slower

healing observed in the HO-2-null mice. The study also shows that healing in HO-2 null mice can be improved by administration of biliverdin. This shows that even though the CO released from the initial cleavage is important in homeostasis but there are many interlinked pathways which evolution has created to bypass certain situations.

1.2.1.4 Guanylyl cyclase - regulation and implications

Guanylyl cyclase is an important enzyme that is regulated by both CO and NO.[20, 24] This links back to the similarity between NO and CO, and explains why they work in tandem in regulation and communication. Guanylyl cyclase catalyses the conversion of guanosine triphosphate (GTP) to cyclic guanosine monophosphate (cGMP). The structures of these two compounds are shown in **Scheme 2**.[25]

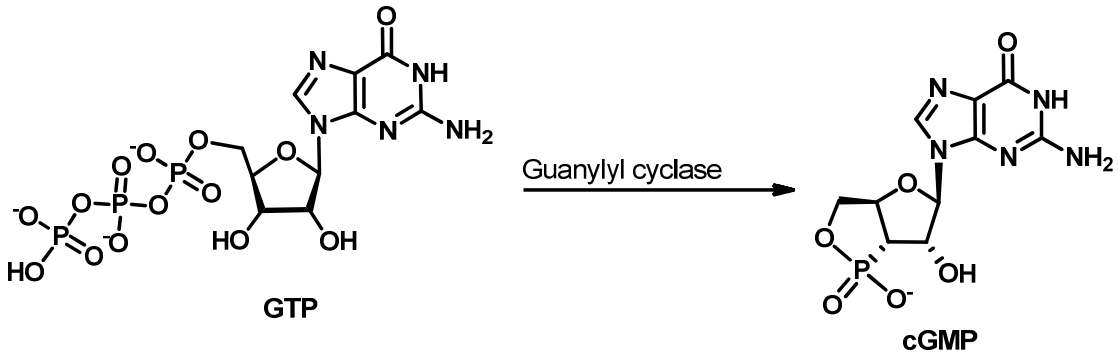

Scheme 2. The conversion of GTP to cGMP by guanylyl cyclase

This is an important process associated with key biological pathways in homeostasis. The cGMP molecule produced by guanylyl cyclase is involved in the regulation of vasodilation, immune responses and neurotransmission. Zhang and co-workers have shown that guanylyl cyclase is involved in platelet synthesis and activation.[25] The group have prepared mice that were guanylyl cyclase deficient only in the megakaryocytes and platelets. The platelets in these mice did not efficiently aggregate when required. These mice also showed extended bleeding times due to poor thrombosis when exposed to low doses of agonist.

cGMP produced by guanylyl cyclase has been found to activate cGMP-dependent protein kinase I.[10, 26] This protein is involved in a long chain of regulation pathways, including myosin phosphatase and vasodilator-stimulated phosphoprotein(VASP).[27-28] The end of this chain results in platelet inhibition and aggregation does not occur. Gawaz and co-workers have shown that platelets deficient in VASP show increased aggregation, highlighting how guanylyl cyclase and VASP work together to control aggregation. This will depend on many factors and stimuli.

This pathway explains why lack of CO results in thrombosis; due to low guanylyl cyclase concentrations, which then interrupts the rest of this regulatory pathway. The end of this pathway is also significantly involved in smooth muscle relaxation and vasodilation and can be a strong contributor to blood pressure regulation.

1.2.1.5 Inducible nitric oxide synthase (iNOS): Suppression by CO

iNOS is a cytochrome p450 type protein, and is responsible for the synthesis of nitric oxide (NO), which is known to cause an inflammatory response.[29-30] Carbon monoxide has been shown to suppress the activity of this enzyme. It is clear that the CO binds to the haem in this protein and inhibits the two step reaction that occurs at the protein haem centre.[31] CO can be considered as an anti inflammatory molecule as it can suppress the production of a molecule associated with pro-inflammatory action. This is useful and important when potentially using CO as a therapeutic molecule.

1.2.1.6 Calcium-activated potassium channels

Calcium-activated potassium channels are important membrane proteins associated with a wide range of biological functions including: smooth muscle tone,[32-33] neurotransmitter release,[34] proliferation of white blood cells,[35] red blood cell size, and many more.[36-37] This channels functions by pumping out K^+ ions when they detect Ca^{2+} ions, resulting in hyperpolarisation due to subsequent calcium channel deactivation.

Carbon monoxide and other small signalling molecules such as H_2S are known to target these channels and are associated with activating them.[38] This information emphasises the wide range of processes that CO is associated with regulating. The single molecule of carbon monoxide released from haem degradation could be extremely important in regulating all of the biological processes discussed.

1.3 Carbon Monoxide as a therapeutic molecule

1.3.1 Direct administration

With all the knowledge in the literature about how carbon monoxide interacts in biological systems, it is clear that this molecule could be exploited for use in medicine. Carbon monoxide regulates many biological functions and the introduction of CO from an external source could potentially remediate many diseases and conditions.

Within the past two decades, a significant amount of research has been carried out on the use of carbon monoxide as a therapeutic molecule. The direct administration of carbon monoxide has been used in a variety of cases.

1.3.2 Covox DS™ system for CO delivery

The Covox DS™ system is a complex machine consisting of pumps and safety valves; which can repeatedly control the amount of carboxy-haemoglobin (CO-Hb) within healthy human patients. The problem with administering CO as a gas is that the CO can freely diffuse throughout the blood stream to all areas of the patient and can pass through all cell membranes.[7] It seems somewhat inefficient to have compound evenly distributed throughout an entire system, when it may only be required in localised environments. The Covox DS™ system was used on healthy patients, and it is not known if CO delivered in this way could be beneficial.

1.3.3 Small intestine preservation and transplantation improvements

A trial carried out by Nakao and co-workers using Lewis rats has shown that CO in a University of Wisconsin solution (UW) can significantly improve the preservation of a small intestine prior to transplantation.[39] This includes reducing the amount of erosion to mucus, and helping to maintain sufficient membrane permeability.

Carbon monoxide can also improve the percentage survival of the rats after a transplantation operation was performed. Suitable controls show that the UW solution without CO does not give the same beneficial effects. Carbon monoxide also prevents reperfusion injury after an innate blood supply returns to the organ. The work also shows that the CO infused into the intestine

before transplantation then circulates around the animal when blood supply is restored. This CO could also have beneficial effects elsewhere in the animal.

There is also significantly reduced weight loss when CO is used in this experiment, which also links to the improved preservation of the intestine. The weight loss without CO treatment following transplantation could be due to poor nutrient absorption. This research also indicates that when CO is used, there is a significant reduction in concentration of several inflammatory cytokines. This is a strong indication that CO exhibits anti-inflammatory activity. This is a very promising study and is significant progress towards the use of CO in human medicine; it is impressive to see CO acting on several factors all at once.

1.3.4 CO and its potential to treat liver disease

The number of liver disease cases in the UK has been on the increase for many years. There is an increasing requirement to find treatments to prevent and treat liver failure; as thousands of people are dying every year due to this condition.[40] Otterbein and co-workers have shown that apoptosis in liver cells can be prevented by the administration of 250 ppm CO.[41] This is because the production of apoptosis inducing cytokines such as TNF-α, are reduced.

Tsui and co-workers have carried out similar research, and found that TNF-α induced apoptosis of liver cells also occurs when mice are sensitised with D-galactosamine.[42] The survival of these mice to this treatment can be significantly improved by the administration of CO. The work also shows that HO-1 deficiency increases sensitivity to liver damage. This work is in agreement with the research of Nakao and co-workers, and shows a key link between haem oxygenase and CO in cytoprotective action.

1.3.5 Carbon monoxide as an antimicrobial agent

There is an urgent need for new potent antimicrobial agents. There has been a significant increase in antibiotic resistance and some species are becoming untreatable with current medicines.[43] There has been significant interest in using carbon monoxide as an anti bacterial agent, as bacteria contain CO-binding proteins.[44-47] Binding these proteins with CO may interrupt many functions including electron transport and could increase bacterial susceptibility to attack from host immune systems. CO under the right circumstances is beneficial to the mammalian host, and this presents a multitude of potential uses for carbon monoxide.

The direct use of CO against *Escherichia coli* and *Staphylococcus aureus* was investigated by Saraiva and co-workers. It was found that a flux of gas could kill both strains of bacteria after a 15 minute CO gas flux.[48] **Figure 9** shows how the percentage survival of bacteria decreases after exposure to a flux of CO gas.

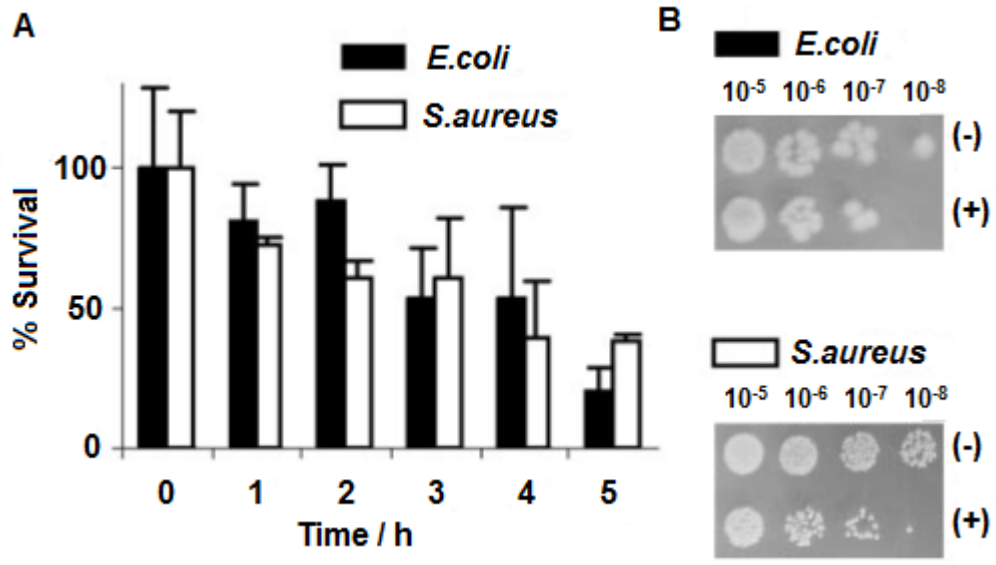

Figure 9. A: Percentage survival of E. coli and S. aureus over a five hour period after exposure to CO gas for 15 minutes. B: Sensitivity tests by spreading out diluted aliquots after four hours exposure to CO gas (+) and N_2 gas (-). (Figure taken from ref. **48**, Antimicrobial Action of Carbon Monoxide-Releasing Compounds, Nobre, L. S.; Seixas, J. D.; Romao, C. C.; Saraiva, L. M., *Antimicrob. Agents Ch.* **2007**, 51, 4303-4307) Copyright American Society for Microbiology 2007

The data in **Figure 9** shows that CO has a toxic effect on both strains of bacteria and there is a significant decrease in the percentage survival. The question is, with a 'flux' of CO gas, how much CO was actually delivered? This highlights the problem with directly delivering CO as gas or a solution that it can be difficult to administer accurate concentrations. This links in with the problems associated with the Covox DS™ system used to deliver CO into humans. It is clear there is a toxic effect but CO is also toxic to mammalian cells at a high enough concentration. This initial study highlights the need for a better method of delivering CO, so that accurate concentrations of CO can be delivered where they are required. This is why carbon monoxide-releasing molecules (CO-RMs) were developed.

1.4 Carbon monoxide-releasing molecules as therapeutics

The problems with the administration of CO gas are currently being addressed by the development of CO releasing pro-drugs. These take advantage of the reactivity of inorganic metal carbonyl complexes. There are some organic reactions that will liberate CO but most of these conditions are biologically incompatible and reagents can react very violently at room temperature.[49] An example of this is the reaction of oxalyl chloride with DMSO. The reaction is explosive at room temperature and has to be carried out at −60 °C. This temperature is too low and makes this kind of molecule unsuitable for CO release applications.

CO-RMs can be thought of as a pro-drug, a means of delivering CO to a target. This typically requires a transition metal carbonyl complex stabilised by a multidentate ligand.[50] The ligand could then be functionalised to enable the molecule to accumulate at a desired location.

1.4.1 Methods of CO-RM activation

CO-RMs require a method of activation and there are three key ways this can be achieved. These three methods include: thermal, enzyme-triggering, and photo-activation.

1.4.1.1 Thermal CO-RM activation

This method of CO-release involves a molecule that releases CO when in solution without any complicated stimulation.[51]

Lynam and co-workers reported a series of tricarbonyl iron(0) complexes. Some of these release CO rapidly on dissociation of the norbornadiene ligand in solution, without the need of a target such as myoglobin. This presents advantages such as definitely getting CO-release from the molecule on administration. The issue is that the CO-release rate is fixed at a given concentration. The CO-release begins immediately and could all be released before it reaches a desired target. With careful tuning of the norbornadiene ligand, optimal CO-release rates could still be obtained in a system like this.

Motterlini and co-workers have also developed a thermally-activiated CO-RM known as CO-RM **A1**.[52] The structure of this compound is shown in **Figure 10**.

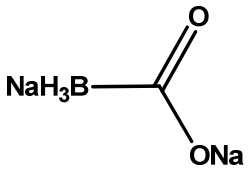

Figure 10. The structure of boron based CO-RM **A1**

In contrast to the majority of CO-RMs in the literature CO-RM **A1** does not contain any transition metals, but contains two sodium atoms. A previously reported myoglobin assay was used to assess if this compound could release CO at different pH.[53] **Figure 11** shows the details of the experiments performed.

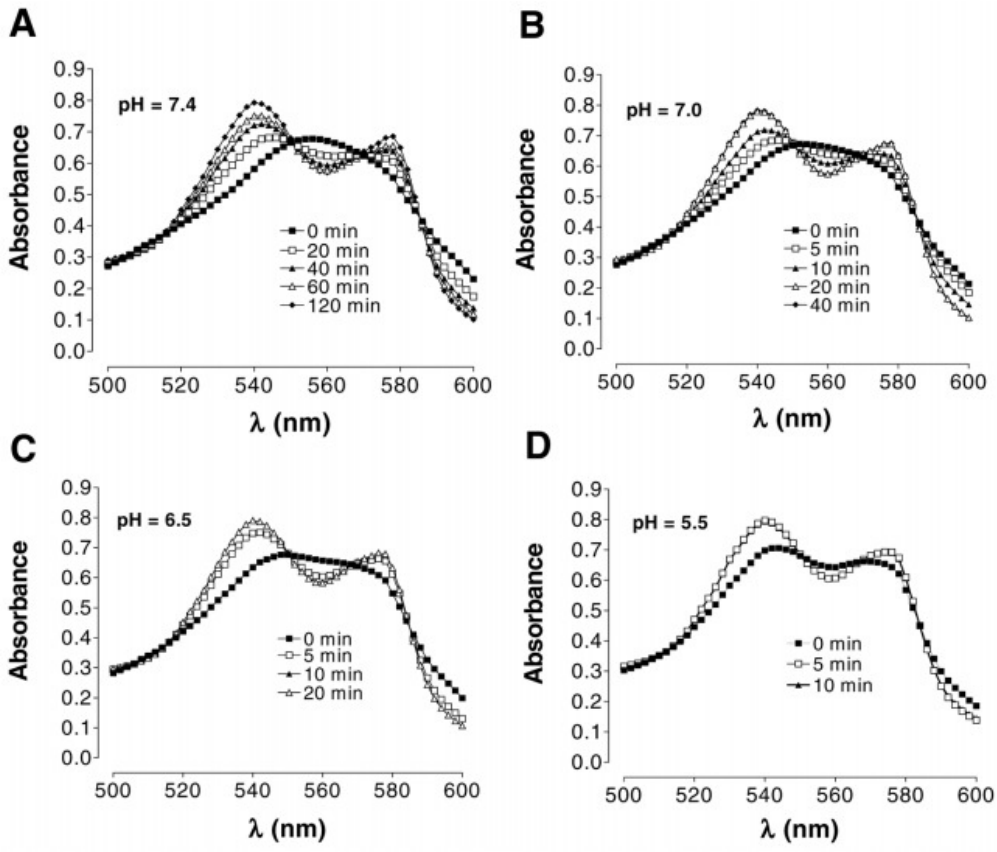

Figure 11. The conversion of deoxy-Mb to carboxy-Mb at varying pH. pH 7.4 (**A**), 7.0 (**B**), 6.5 (**C**), and 5.5 (**D**) after addition of 60 µM CO-RM **A1**.(Figure taken from ref. **52**, CORM-**A1**: a new pharmacologically active carbon monoxide-releasing molecule, Motterlini, R.; Sawle, P.; Hammad, J.; Bains, S.; Alberto, R.; Foresti, R.; Green, C. J., *FASEB J*., **2005**, 19, 284-6) Copyright FASEB 2014.

CO-RM **A1** releases CO faster at pHs 5.5 and 6.5, but is much slower at physiological pH. This could present problems under certain circumstances where higher concentrations of CO are required. This also means that there could be problems with administering this CO-RM orally.

The pH in the stomach may promote extremely fast CO release before the CO-RM gets to the desired location.

CO-RM **A1** was also used in an assay which employed amperometric electrodes to measure the amount of CO-released in solution at various pHs and temperatures. The performed assay is in agreement with the results of the myoglobin assays that were carried out. CO is released faster at lower pH and with increasing temperature. The amperometric assay works in the absence of myoglobin showing that CO-RM **A1** is a true thermally activated CO-RM.

It is also important to highlight that both of the CO release assays also employed i-CO-RM **A1** as a control. i-CO-RM **A1** is a collection of the by-products generated by the CO release from the original CO-RM. i-CO-RM **A1** did not show any signs of CO release in any of these experiments. The group also used $NaBH_4$ as a control in this experiment to assess if a boron reagent could cause any of the effects observed. However, this is not really an appropriate control as the concentration of by-products is not likely to be reflected by the concentration used in the experiments. In a biological system, the concentration of many metabolites will be varying over time, and the addition of a single by product is not the best control. The i-CO-RM experiments employed here are close to giving by-products like what is observed from fresh CO-RM. However, in a biological system, enzymes may accelerate degradation and produce different metabolites to simple thermal decomposition.

CO-RM **A1** has been employed in biological studies which show significant vasorelaxation on aortic rings isolated from rats. This effect can also be exaggerated if 1 μM YC-1 is administered alongside CO-RM **A1**. YC-1 is a stimulator of guanylyl cyclase and this is in agreement with the regulatory pathways discussed previously.

Other research groups have also carried out research on CO-RM **A1**. Stec and co-workers have shown that CO-RM **A1** increases the blood flow to the kidneys after administration to mice.[54] The work also shows that inhibition of sGC with ODQ significantly reduces the CO-RM **A1** mediated renal blood flow. This suggests that the effects observed are linked to carbon monoxide released from CO-RM **A1**. Nicoletti and co-workers have also carried out experiments with CO-RM **A1** on mice investigating its medicinal capabilities at treating experimental allergic encephalomyelitis (EAE).[55] EAE is a good model for multiple sclerosis which affects the lives thousands of people worldwide. This study shows that prolonged administration of CO-RM **A1** to mice with EAE show improvement in many areas including: reduced incidence of the disease, less inflammation of the brain and nervous system, and improved clinical and histopathological signs of the disease. This research is extremely promising and all the research discussed above shows CO-RM **A1** is a potential treatment for multiple sclerosis and many other ailments.

There are also many other thermo-CO-RMs reported in the literature such as molybdenum based CO-RMs **ALF062** and **ALF186**, developed by Alfama.[7, 56-57] The structure of these CO-RMs are shown in **Figure 12**.

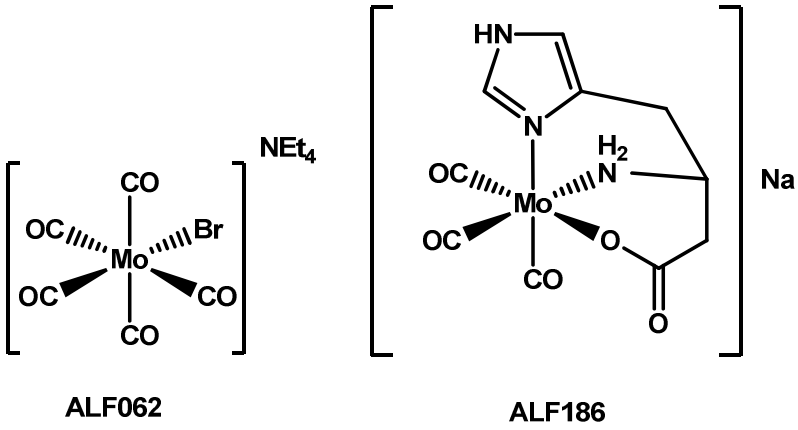

ALF062 ALF186

Figure 12. The structure of CO-RMs **ALF062**(left) and **ALF186**(right).

These CO-RMs are unstable in the presence of air. ALF186 is stable in an anaerobic aqueous solution but not in the presence of O_2 and under these conditions spontaneously releases CO.

CO-RM **ALF186** has been employed in experiments with rats to prevent gastric ulcery which arises from treatment with non-steroidal anti-inflammatory drugs (NSAIDs). **ALF186** was shown to significantly reduce the formation and severity of ulcers that were induced by ethanol administration. **ALF186** was also found to have the same effect in the presence of indomethacin, without significantly reducing the effectiveness of the anti-inflammatory drug. The potential of CO-RM conjugation to known NSAIDs is certainly a possibility.

CO-RM **ALF186** has a similar half-life to CO-RM **A1** in aqueous solution at aqueous pH. However, *in vivo* **ALF186** releases its CO very quickly. This could present problems as high concentrations of CO could be released quickly in the stomach and intestine preventing peristalsis. It is suggested that a more gradual CO-RM such as CO-RM **A1** may be more appropriate for this kind of treatment. On the other hand, the quick CO release from this CO-RM may still have its uses to treat conditions such as blood pressure reduction.

A large number of CO-RMs in the literature typically adopt an octahedral type structure, often with a metal$(CO)_n$ motif commonly reappearing.[58-62] Fairlamb and co-workers developed a new series of CO-RMs based on a μ_2-alkyne dicobalt(0)hexacarbonyl motif (**Figure 13**), with some distinctly different structural features compared to many other CO-RMs in the literature.[63]

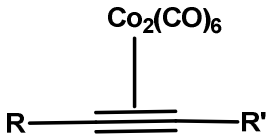

1, R = CO_2Me, R' H
2, R = CO_2Me, R' = CO_2Me
3, R = CH_2OH, R' = H
4, R = ^tBu, R' = H
5, R = Ph, R' = H
6, R = Ph, R' = Ph

Figure 13. The structure of a new alkyne cobalt(0) complexes **1**-**6**.

This series presents some of the first examples where a CO-RM uses a bimetallic centre to bind the CO ligands. It is beneficial to the pharmaceutical industry as a whole if interesting/unusual functionality is explored. Exploring a wide range of 'structural space' is likely to bring about interesting effects. If research is carried out within a narrow range of structural space then wide ranging bacterial resistance/allergies, and all sorts of other issues could become common.

The bi-metallic hexacarbonyl dicobalt(0) motif has been functionalised with a variety of substituted alkyne ligands. This structural set up provides the potential to functionalise this CO-RM with a wide variety of functionality in the future as any alkyne could be potentially introduced into the structure of a CO-RM using this chemistry.

This series of CO-RMs demonstrates how the electronics of the ligand (the alkyne) can be tuned to alter the rate of the CO-release drastically. All the CO-RMs in **Figure 13** were used in myoglobin CO-release quantification assays, and were all found to release-CO without the need for irradiation. The CO-RMs were also found to thermally release CO in DMSO. These CO-RMs do not need myoglobin to induce CO-release. Complex **2** has a $t_{½}$ of 1-2 minutes depending on concentration whereas **3** had a $t_{¼}$ of 67 minutes which is considerably longer considering there is not that much different in the structure: Increasing the the electron density of the alkyne increases the ability of the metal to back-bond into the π^* orbital on CO. Less back-bonding into this orbital results in a stronger C–O bond. This explains why Complex **2** releases so quickly due to strong electron withdrawing ester groups. This demonstrates a really good way to tune a CO-RM to get difference types of CO-release. As discussed previously, different rates of CO-release are required to treat different conditions.

Fairlamb and co-workers have carried out some detailed mechanistic investigations into the mechanism of CO-release from **2** in DMSO. ReactIR™ instrumentation which takes regular real time IR spectroscopic measurements shows that **2** is clearly unstable in DMSO. The IR spectra obtained over time show depletion of many of the M–CO vibration bands. A new strong band at 1890 cm^{-1} appears on degradation which remains present and it is likely that was due to the formation of $[Co(CO)_4]^-$. **Scheme 3** shows the proposed CO-release pathways devised from the degradation studies obtained.

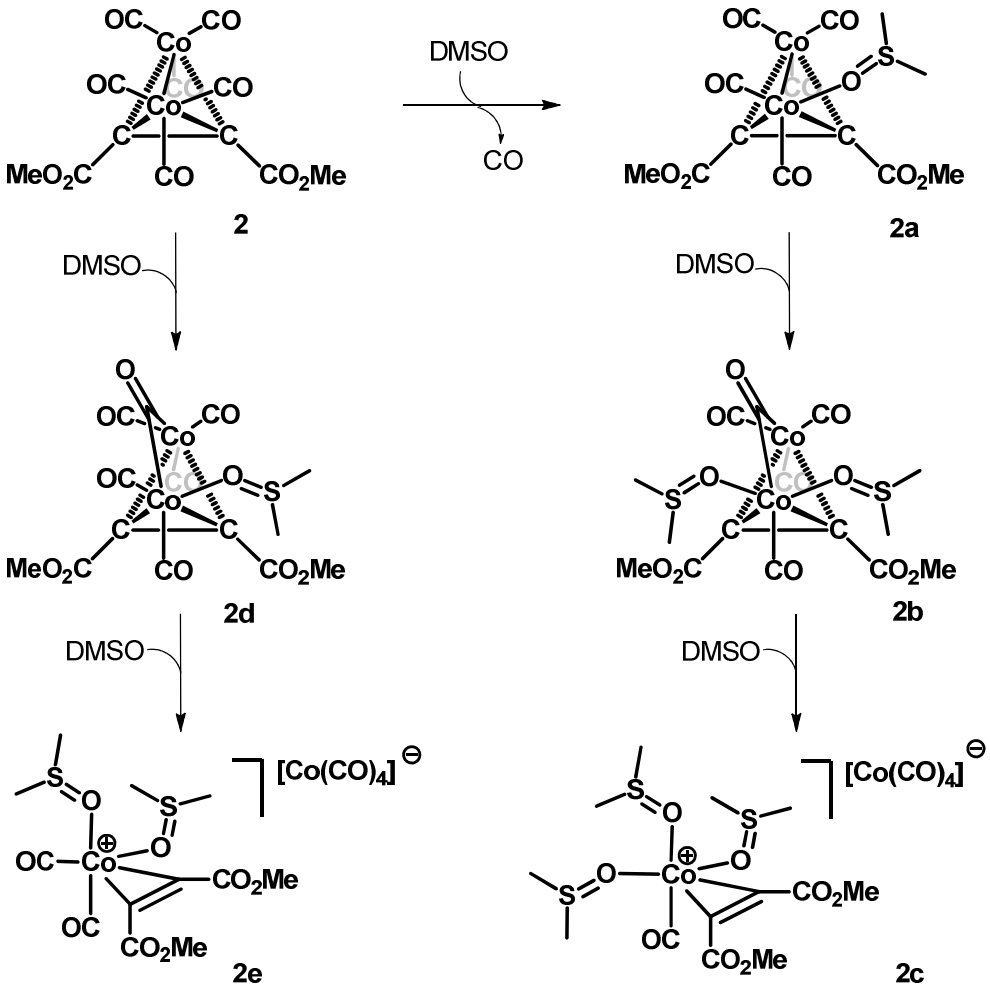

Scheme 3. Proposed degradation/CO-release pathway for CO-RM **2** in DMSO.

It is proposed that a molecule of DMSO solvent can either displace a CO ligand *via* coordination to the cobalt centre in **2** to produce **2a**. It could also coordinate to the cobalt centre without CO displacement to produce **2d**. Both of these species can then bind more DMSO, eventually resulting in cleavage of the Co–Co bond. This gives an oxidised cobalt carbonyl species with DMSO ligands, and a reduced $[Co(CO)_4]^-$ species. This then acts as a counter ion to fragments **2c** and **2e**. One may want to think carefully about how much of this mechanism occurs in aqueous solution rather than in DMSO. Breakdown in aqeuous solution is much more relevant considering that these compounds are potential pharmaceutical agents. However, one could imagine that water could act as a two electron donor in the same fashion as DMSO, and similar pathways using H_2O are likely. Carrying out mechanistic studies in water can be problematic as water can reduce the sensitivity in IR and NMR measurements making it difficult to follow what species a present. The development of better techniques to carry out detailed CO-RM degradation analysis in aqueous would be of great intrest to CO-RM researchers.

This series of CO-RMs is interesting from a structural and future synthetic perspective. This initial CO-RM series does not contain much polar functionality and structural diversity. However with the alkyne system with an R group that can be varied, many new interesting CO-RMs could be developed based on this alkyne dicobalt(0) hexacarbonyl motif.

1.4.1.2 Enzyme-triggered/chemically triggered CO-RMs

The second method of CO-RM activation is by a chemical trigger such as an enzyme.[64] These CO-RMs in contrast to thermo-CO-RMs have long-term stability in aqueous solution. The CO-release is induced by a chemical trigger, and it typically can be a haem-containing protein/enzyme which can tightly bind the CO.

CO-RM-**2** is a di-nuclear ruthenium complex with bridging chloride ligands and is sparingly water soluble. The structure of CO-RM-**2** is shown in **Figure 14**.

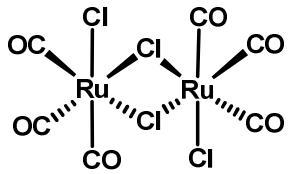

Figure 14. The structure of ruthenium-containing CO-RM-**2**

CO-RM-**2** is classed as an enzyme-triggered CO-RM (ET-CO-RM) as no CO can be detected by GC from the headspace of an aqueous solution. However in the presence of myoglobin *in vitro*, CO is transferred to the myoglobin with a half-life of one minute. This is exceptionally rapid CO-release in comparison with CO-RMs such as CO-RM **A1** and **ALF186**.

For biological studies CO-RM-**2** typically requires pre-dissolution in DMSO or another polar solvent due to solubility issues.[65] However, this compound can exhibit various beneficial effects within a biological system. Chen and co-workers have shown that mice unable to produce HO-1 undergoing aortic transplants can be rescued by administering CO-RM-**2**.[22] The CO-RM provides the CO that the mice cannot naturally produce without HO-1, restoring CO regulatory pathways and preventing severe thrombosis. **Figure 15** shows cross-sections of the aorta after the aortic transplantations were performed under various conditions.

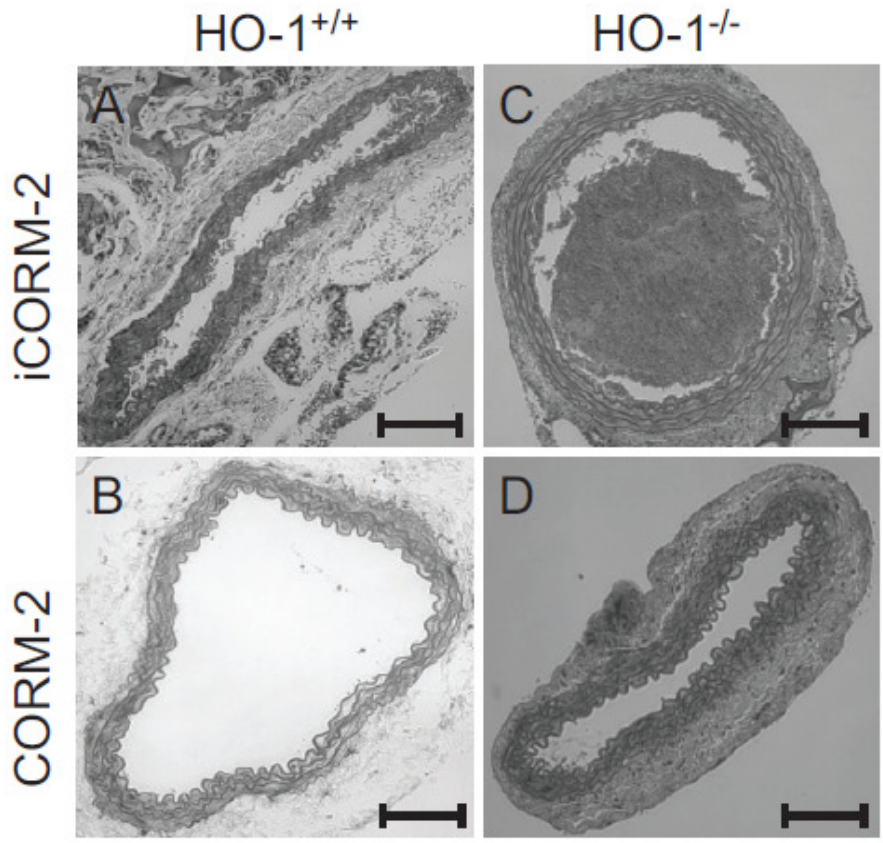

Figure 15. Aortic across sections from HO-$1^{+/+}$ and $^{-/-}$ mice having undergone an aortic graft. Administration of CO-RM-2 and inactive CO-RM-2 in both cases.(Image taken with permissions from ref. **22**) Carbon Monoxide Rescues Heme Oxygenase-1-Deficient Mice from Arterial Thrombosis in Allogenic Aortic Transplantation, George, J. F.; Chen, B.; Guo, L. L.; Fan, C. L.; Bolisetty, S.; Joseph, R.; Wright, M. M.; Agarwal, A., Am. J. Pathol. **2009**, 175, 422-429 Copyright Elsevier 2009. Note : HO-$1^{+/+}$ indicates a mouse group that can naturally produce HO-1, and HO-$1^{-/-}$ indicates a group that cannot produce the enzyme.

When a HO-$1^{+/+}$ mouse is administered CO-RM-**2**, the artery shows clear signs of vaso-dilation, typical of CO action. However with the i-CO-RM-**2** as a control, this vasodilation effect is not observed, showing that some of the ruthenium degradation species are not responsible for the effect.

When a HO-$1^{-/-}$ mouse is given the i-CO-RM-**2** control, the same arterial thrombosis occurs as when no CO-RM is administered at all. When these mice are given fresh CO-RM-**2**, the platelet rich thrombosis does not occur and normal conditions are restored. This is an excellent demonstration of how a CO-RM can be used to restore normal function.

Ruthenium-based CO-RM-**2** has also been employed in anti bacterial studies with *E. coli* and *S. aureus*.[48] Viability studies were performed in the same fashion as was done with CO gas. **Figure 16** shows the results of bacterial viability studies with CO-RM-**2**.

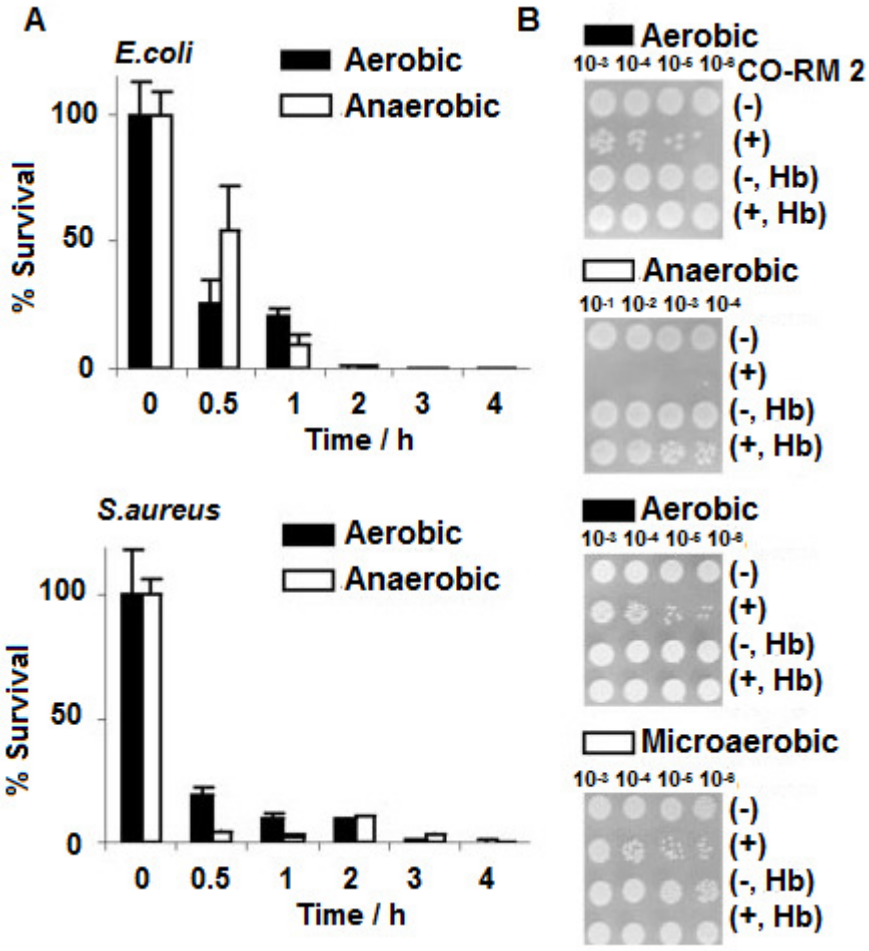

Figure 16. **A**: Use of CO-RM-**2** to assess percentage survival of *E. coli* and *S. aureus* under aerobic and anaerobic conditions. **B**: Plating studies with haemoglobin controls to assess bacterial viability. (Figure taken from ref. **48**, Antimicrobial Action of Carbon Monoxide-Releasing Compounds, Nobre, L. S.; Seixas, J. D.; Romao, C. C.; Saraiva, L. M., *Antimicrob. Agents Ch.* **2007**, 51, 4303-4307. Copyright 2007 American Society for Microbiology.

The studies illustrated in **Figure 9** and **Figure 16** show that the use of ruthenium CO-RM-**2** shows improved anti-bacterial activity compared to using CO gas alone. The addition of haemoglobin as a control prevents the anti-bacterial effect observed by the CO-RM, suggesting that CO produced from the CO-RM is causing the effect.

There are also other studies that have been carried out that show the potential problems with CO-RM-**2**.[66] Dong and co-workers have shown that ruthenium-based CO-RM-**2** activates K^+ channels in an inselective manner in human endothelial cells. Experiments carried out with ruthenium

monomer CO-RM-**3** also induced currents by activating the K^+ channels in the cells. The current generated by CO-RM-**3** matches that of the currents generated by CO gas. The currents generated by CO-RM 2 show a different profile. The CO-RM-**2** induced current generated was not diminished even after administration of 2-aminoethoxydiphenyl borate, which is a selective K^+ channel blocker. More experiments would need to be carried out to discover why CO-RM-**2** is activating the channels in this fashion. It is undesirable for a CO-RM to bind to a target in this way as it is unselective. On the other hand it is difficult to tell what the true consequences of this channel activation are, because there are many *in vivo* studies with mice that show very positive and promising properties from CO-RM-**2**.

CO-RM-**3** is a water soluble CORM that has attracted considerable research interest within the past few years. CO-RM-**3** is a ruthenium complex containing a glycinato ligand, one chloride ligand and three CO ligands. It is synthesised from ruthenium dimer CO-RM-**2** and the details are shown in **Scheme 4**.[53]

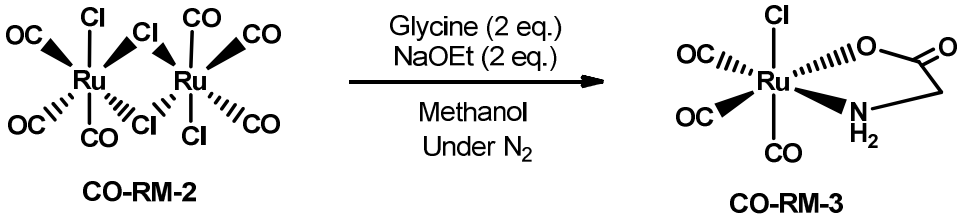

Scheme 4. Synthesis of tricarbonylchloro(glycinato)ruthenium(II) (CORM-**3**)

CO-RM-**3** is an protein-triggered CO-RM, and is stable in aqueous solution with minimal degradation. In the presence of myoglobin the CO-RM has a half-life for CO-release of only one minute . This is a rapid rate of CO-release and is similar to the half-life of CO-RM-**2**.

Studies by Desmard and co-workers have shown that CO-RM-**3** is a potential treatment for *Pseudomonas aeruginosa* infection.[67] Infected mice treated with CO-RM-**3** show increased survival rates. Clark and co-workers have shown that administration of CO-RM-**3** to mice that have had a heart transplant enables them to survive longer than ones that receive no CO-RM-**3**. In addition to this, i-CO-RM-**3** is a solution of CO-RM-**3** that has been allowed to release one CO thermally and this solution shows no improvement compared to the control, suggesting the effect is due to the action of CO. There are however some problems with i-CO-RM-**3**. Only one CO from CO-RM-**3** is released thermally and the exact composition of the material after release is unknown. There may not be any significant thermal release from i-CORM-**3** but there could be further interactions of the remaining complexes with the host proteins and other targets.

Even though a lot of research into the effect of CORM-**3** has been carried out, and the results are very promising, the synthesis and characterisation does not exhibit defined stereoselectivity. It is

possible to have the chloride ligand *trans*- to a carbonyl ligand, oxygen ligand or an amine ligand. Differences in the isomers within the compounds produced could easily affect the CO release rates and even the way that the compound binds to proteins.

It has also been shown by X-ray diffraction that CORM-3 forms ruthenium adducts with various proteins, including hen egg white lysozyme (HEWL). The structure of these adducts are shown in **Figure 17**.[64]

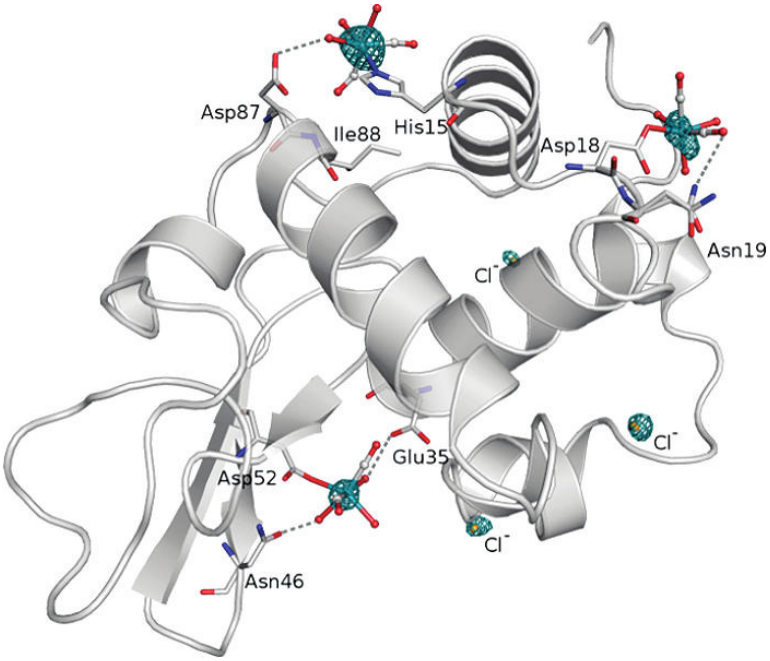

Figure 17. The structure of a ruthenium CO-RM 3/ HEWL protein adduct. (Image taken from ref. **64**, CORM-3 Reactivity toward Proteins: The Crystal Structure of a Ru(II) Dicarbonyl−Lysozyme Complex, Bernardes, G. J. L.; Santos-Silva, T.; Mukhopadhyay, A.; Seixas, J. D.; Romão, C. C.; Romão, M. J. *J. Am. Chem. Soc*. **2011**, 133, 1192-1195) Copyright 2011, American Chemical Society.

The ruthenium moiety bound to the protein is a triaqua, dicarbonyl species. Even though 80% of the ruthenium is bound to a histidine residue, it also can bind to many other sites on protein such as Glu35. This binding is unselective and it is likely that this ruthenium species could bind to many other proteins in a similar fashion and this could give rise to undesirable side effects. More investigations into how CO-RM-**3** interacts with proteins to distinguish the difference between CO release effects and the newly discovered ruthenium binding. This binding could be responsible for some of the biological effects observed in recent studies and it may be difficult to differentiate between the two.

An efficient CO-RM would interact selectively with proteins for targeting purposes only, providing that the CO is responsible for the observed therapeutic effects. Once CO-release is

complete, any degradation products need to be non toxic and it would be ideal if they did not bind to unwanted targets. The purpose of the metal centre and ligands are for selectivity and CO transportation. Multidentate ligands can prevent leeching of any toxic metal species by keeping them tightly bound as a soluble complex.

CO-RM-**3** has been employed in many *in vivo* experiments and it has been shown to exhibit many positive effects. Drago and co-workers have carried out experiments with rabbits, showing that administration of CO-RM-**3** lowers intraocular pressure induced by α-chymotrypsin.[68] The inactive form of CO-RM-**3** does not lower intraocular pressure, suggesting the action of carbon monoxide in this treatment. These studies demonstrate a potential use of CO-RM-**3** for the treatment of ocular hypertension.

Chlopicki and co-workers have carried out experiments on human platelets with CO-RM-**3** and demonstrated that it inhibits platelet aggregation in a concentration-dependent manner.[69] The administration of a guanylate cyclase inhibitor increases the effect observed by the CO-RM. Considering the X-ray structure in **Figure 17**, it could be possible that CO-RM-**3** is having its effect by binding to a protein and altering its function. i-CO-RM-3 would not be a suitable control here as fresh complex might be required to get transfer of the ruthenium centre on to a protein. It is also important to note that addition of an sGC activator did not affect the outcome of CO-RM-**3** administration. This suggests a guanylate cyclase independent mechanism is involved in inhibition of platelet aggregation. However this study was carried out with washed platelets *in vitro,* and the lack of other cells types and proteins that are present *in vivo* could significantly alter how the platelets aggregate. It is worth questioning how comparable an *in vitro* study is to what occurs in a live organism.

$[Mn(CO)_4\{S_2CNMe(CH_2CO_2H)\}]$(**7**), a CO-RM developed by Mann and co-workers, is stable in phosphate buffered saline for several hours (**Figure 18**).[58]

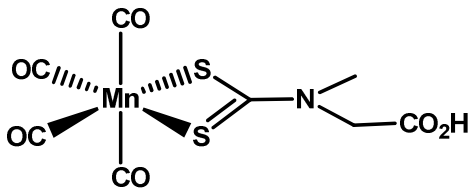

Figure 18. The structure of CO-RM **7**

In the presence of myoglobin, CO is rapidly released from CO-RM **7** to the haem. One of the real advantages of this molecule in comparison with previous CO-RMs, is that it can release several molecules of CO per molecule of CO-RM. This was determined by the myoglobin assay data shown in **Figure 19**.

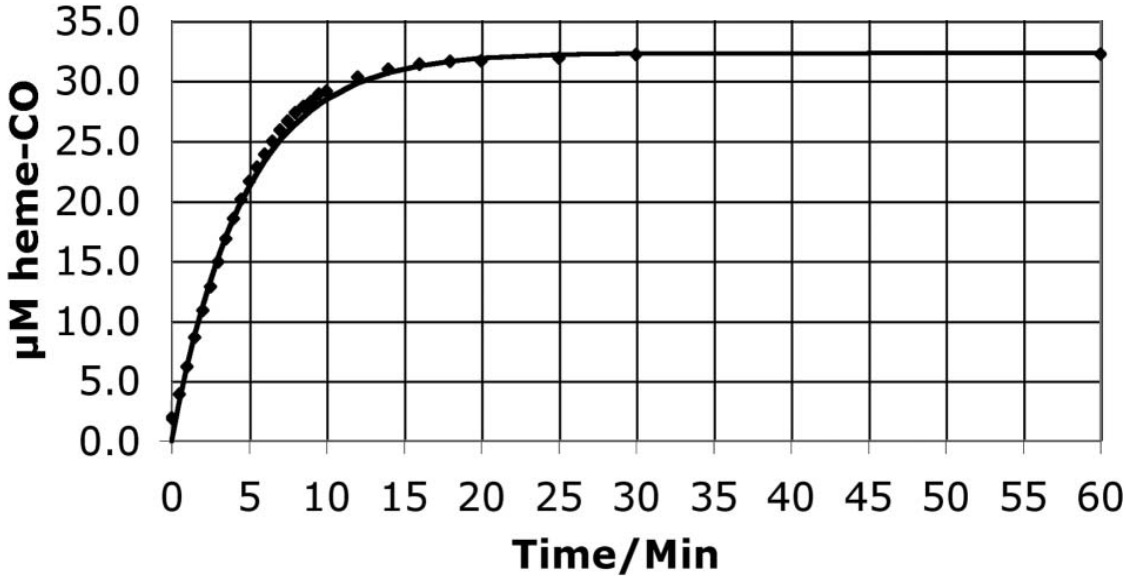

Figure 19.[$Mn(CO)_4\{S_2CNMe(CH_2CO_2H)\}$] (**7**) at a concentration of 10 µM in a myoglobin assay.(Image taken from ref. **58**, [$Mn(CO)_4(\{S_2CNMe(CH_2CO_2H\})$], a new water-soluble CO-releasing molecule, Crook, S. H.; Mann, B. E.; Meijer, A. J.; Adams, H.; Sawle, P.; Scapens, D.; Motterlini, R., *Dalton Trans*. **2011**, 40, 4230-5. Copyright The Royal Society of Chemistry 2011.

Only 10 µM of CO-RM **7** can produce around 30 µM of CO-Mb, meaning that this molecule releases three molecules of CO per molecule of CO-RM. This is advantageous as less of the original molecule is required to get the same amount of CO that can be released from ruthenium-based CO-RM-**3**. [$Mn(CO)_4\{S_2CNMe(CH_2CO_2H)\}$] (**7**) has been used in viability tests with RAW 264.7 cells, a macrophage cell line. An Alamar blue assay which detects the metabolism of live cells indicates that there is a 25% reduction in cell viability at 50 and 100 µM concentrations of this complex. An LDH assay that detects the release of LDH from dead cells shows only 10% cytotoxicity. CO-RM **7** is only killing 10% of cells, but is clearly interfering with the metabolism of the cells. This is potentially concerning from a pharmacological point of view.

It is known that CO can suppress the production of nitric oxide (NO) in cells.[70] It is also known that NO can exhibit an anti-inflammatory response,[29] and if NO is suppressed then an anti-inflammatory response can be observed. NO_2^- (nitrite) is a stable degradation product of NO and so it can be used as a way of quantifying the amount of NO produced by cells. This means that by using carefully designed controls, it is possible to determine if the CO released by CO-RMs is causing a suppression of NO production in RAW 264.7 cells and thus anti-inflammatory action.

A nitrite assay was performed to assess if $[Mn(CO)_4\{S_2CNMe(CH_2CO_2H\})]$ (**7**) could be used to induce an anti-inflammatory response in RAW 264.7 macrophages, and results are shown in **Figure 20**.

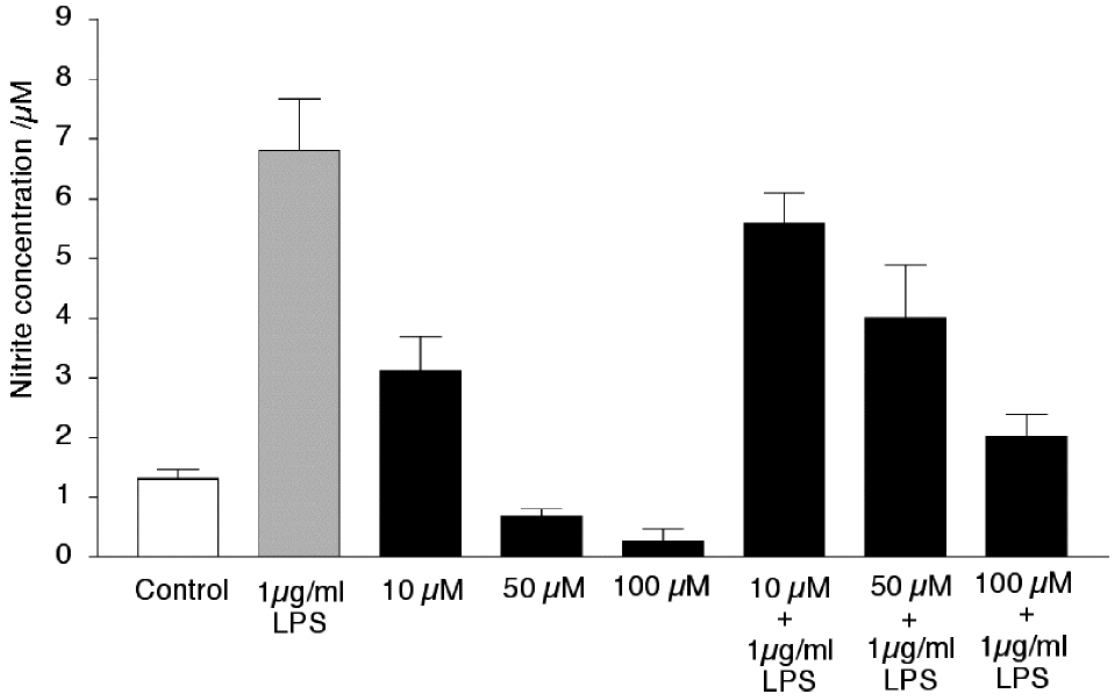

Figure 20. Nitrite quantification assay to assay NO suppression on administration of CO-RM **7** to RAW 264.7 cells. LPS (1 μl) was used to stimulate an initial inflammatory response.(Image from ref. **58**, $[Mn(CO)_4\{S_2CNMe(CH_2CO_2H)\}]$, a new water-soluble CO-releasing molecule, Crook, S. H.; Mann, B. E.; Meijer, A. J.; Adams, H.; Sawle, P.; Scapens, D.; Motterlini, R. *Dalton Trans*. **2011**, 40, 4230-5) Copyright The Royal Society of Chemistry 2011

Results in **Figure 20** show a larger percentage reduction in nitrite compared to the drop in viability, and toxicity. This suggests that CO-RM **7** can induce an anti-inflammatory response, although the percentage cell viability in these studies is of some concern. Testing cells in a plate is not always likely to be representative of what may happen *in vivo* and further studies are required with this molecule.

Fairlamb and co-workers have also developed a series of CO-RMs based on an η^4-2-pyrone motif coordinated to a tricarbonyl iron(0) centre.[71-74] One could think of these CO-RMs being similar to the norbornadiene iron complexes prepared by Lynam and co-workers due to the η^4-diene mode of coordination.[51] The pyrone ligand is a planar molecule where as the norbornadiene ligand has a bent structure with the two parallel alkenes being forced closer together in space. Pyrone based CO-RMs are of particular importance as this type of free ligand is known to possess anti-bacterial activity.[75] One could imagine administering the CO-RM which will release CO and the

antibacterial pyrone at the same time, which has great potential. The structure of the 2-pyrone CO-RMs from this research are shown in **Figure 21**.

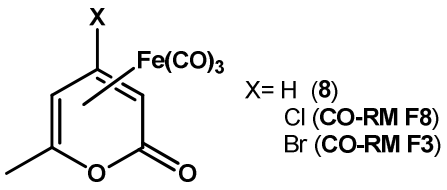

Figure 21. The structure of 2-pyrone containing CO-RMs prepared by Fairlamb and co-workers.

Parent CO-RM **8** was the first pyrone compound to be tested in a myoglobin assay and it was unfortunately discovered that it did not release-CO in a myoglobin assay. This shows that this particular CO-RM is stable in aqueous solution and in the presence of myoglobin. It was not tested for CO-release using irradiation but it is certainly possible that it could.

CO-RM **F8** was tested at 60 μM in a myoglobin assay and was found to release only 3 μM of CO in the presence of myoglobin without irradiation. This is slow release compared to other CO-RMs such as CO-RM-**3**. This CO-RM could still be used if a steady release of CO is required. It was not established whether the gradual CO-release from CO-RM **F8** was due to myoglobin extraction or thermal degradation. However, it is clear that the introduction of a halogen in the 4-position on the ring alters the properties of the molecule. It either alters the electronics of the Fe–CO bonds allowing for some thermal release, or it could alter the binding constant of the pyrone ring to the $Fe(CO)_3$ moeity. Dissociation of the pyrone ring from the metal centre could then result in spontaneous CO-release from the resulting fragment just like what occurs when substituents are changed in norbornadiene complexes.[51]

CO-RM **F8** was tested for viability/toxicity with RAW 264.7 cells as has been done with previous CO-RMs. It was found to be viable up to a concentration of 100 μM which is encouraging. Considering that previous $Fe(CO)_3$-based CO-RMs have been shown to release two molecules of CO per molecule of CO-RM, it is likely that this CO-RM could do the same. The production of 200 μM CO from 100 μM CO-RM is likely to be more than enough CO to exhibit many of the effects previously discussed, although the CO-release rate is rather slow for CO-RM **F8**.

The pyrone ring was also substituted with a bromine atom in the 4-position to give CO-RM **F3**. This CO-RM was tested in a myoglobin assay and was found to release 11 μM of CO over one hour. This is a relatively slow release but is almost four times faster than CO-RM **F8**. There is something significant about substituent 4 position on the ring. Exchanging a chlorine atom for a bromine atom in this structure has significantly increased the rate of CO-release. CO-RM **F3** was

also shown to be just as viable as CO-RM **F8** with RAW 264.7 cells despite the increased rate of CO-release. It is important to be aware of the fact that a higher rate of CO-release also means a higher rate of production of by-products which could be potentially toxic. **Figure 22** shows the details of the CO-release studies and some biological work carried out on CO-RM **F3**.

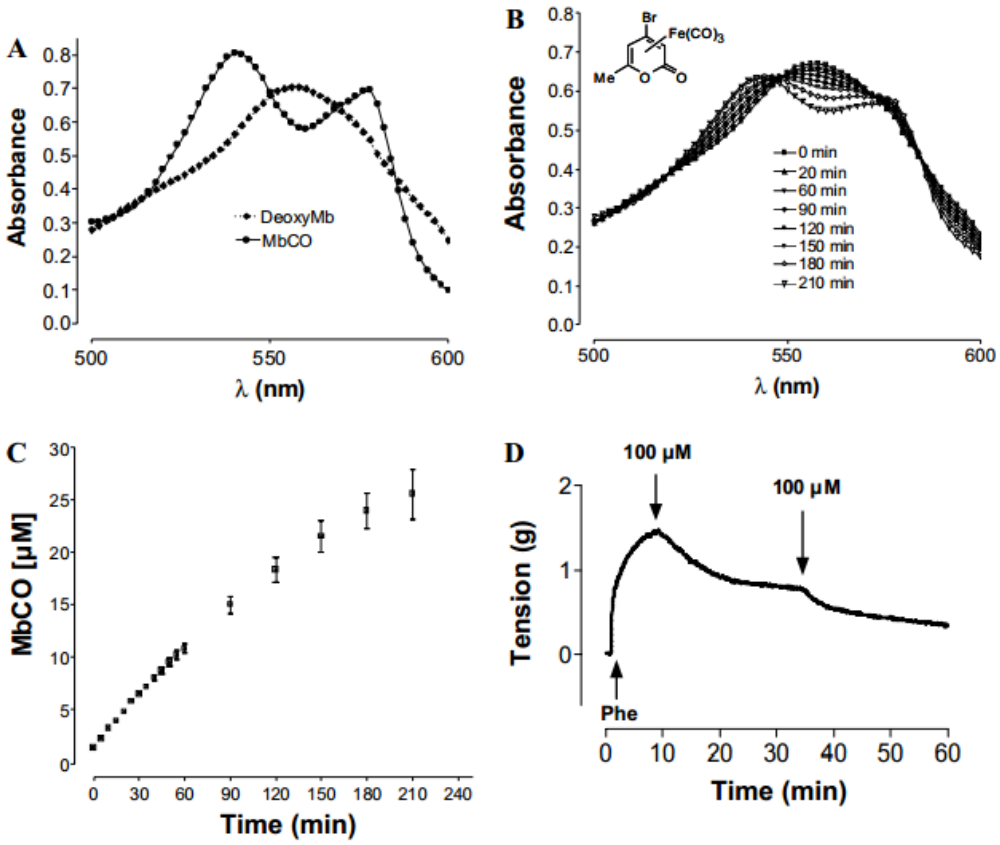

Figure 22. A: Reference UV-Vis spectra of deoxy-Mb and carboxy-Mb. B: UV showing clear conversion of deoxy-Mb to carboxy-Mb using CO released from CO-RM **F3**. C: Calculated concentrations of carboxy-Mb on CO-release from CO-RM **F3**. D: Demonstration of vasorelaxation on isolated aortic rings from rats using CO-RM **F3**, rings were pre-contracted with administration of phenyl ephedrine (Phe). (Figure taken from ref. **72**, η_4-Pyrone iron(0)carbonyl complexes as effective CO-releasing molecules (CO-RMs), Fairlamb, I. J. S.; Duhme-Klair, A. K.; Lynam, J. M.; Moulton, B. E.; O'Brien, C. T.; Sawle, P.; Hammad, J.; Motterlini, R. *Bioorg. Med. Chem. Lett.* **2006**, 16, 995-8).Copyright Elsevier 2006

CO-RM **F3** is a promising CO-releasing molecule, and a smooth conversion to carboxy-Mb is observed over a three hour period. This CO-RM was also shown to induce vasodilation to aortic rings when 100 µM portions of the CO-RM were administered. There is a change in gradient in the tension in the aortic ring on addition of CO-RM **F3**, which had been deliberately contracted prior to starting the experiment. The vasodilatory properties of CO-RM **F3** are likely to be due to

the CO that is released from this CO-RM. Considering that there is an immediate drop in tension on CO-RM addition, is it also suggesting that low concentrations CO are required to induce this effect. This CO-RM releases CO as a slow rate so a small amount of CO will have been released on the time scale of this vasodilation experiment.

CO-RM **F3** has also been used in Greiss assay experiments as was performed with $[Mn(CO)_4(\{S_2CNMe(CH_2CO_2H\})]$ (**7**). CO-RM **F3** shows a concentration-dependent reduction in nitrite production from RAW 264.7 cells. This occurs at concentrations which are significantly below signs of any toxicity, strongly suggesting CO-RM **F3** can induce an anti-inflammatory response. CO-RM **F3** is a promising CO-releasing molecule and further studies into its action, is justified by the discussed research. It would be important to determine whether this CO-RM is a thermo- or enzyme-triggered-CO-RM as this has not yet been established.

Schatzschneider and co-workers have also developed CO-RMs which are activated by enzymes.[76] CO-RMs **9**-**12** are based on an tricarbonyl iron(0) motif bound by an acyloxybutadiene ligand. The structures of these CO-RMs are shown in **Figure 23**.[77]

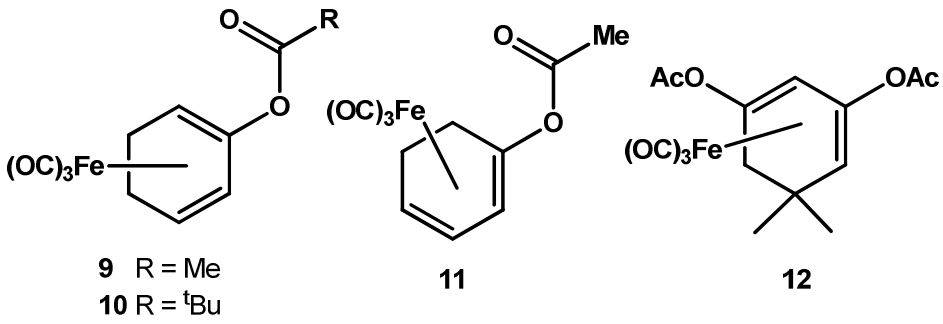

Figure 23. The structure of tricarbonyl iron(0) acyloxybutadiene complexes **9**-**12**.

The four complexes above including **12**, which was previously prepared by Boháč and co-workers for non medicinal purposes, have been utilised in this enzyme-triggered CO-RM study. It was determined that these CO-RMs **9**-**12** are relatively stable compared to many thermo-CO-RMs, which made them suitable ET-CO-RMs candidates. It was found that these complexes could be activated by the use of esterase enzymes. Interestingly each CO-RM could be hydrolysed by some esterase enzymes but not others. This creates a fantastic platform for selectively activated ET-CO-RMs. **Table 2** shows which of the CO-RMs above degrade when treated with two different esterase enzymes.

Table 2. Esterase ability to activate CO-RM **9**-**12**.PLE = Pig-liver esterate.LCR = Lipase from Candida rugosa. + indicates activity, − indicates no activity.

Enzyme	9	10	11	12
PLE	−	−	+	+
LCR	+	+	+	-

It was found through kinetic resolution experiments that PLE could not degrade **9** and **10** but could degrade **11** and **12**. Conversely, LCR could degrade **9-11** but not **12**. This variation in selectivity is useful when thinking about administering a CO-RM *in vivo.* Understanding which enzymes are degrading/activating a drug is essential for compounds to progress as medicinal candidates.

Interestingly a myoglobin assay was used with these CO-RMs as standard to assess their CO releasing ability and it was found that without esterase, there was no significant CO release from these CO-RMs with myoglobin present. This is a key result as many CO-RMs are readily degraded by myoglobin as CO is transferred to them very quickly. In the presence of the appropriate enzyme, CO-release to myoglobin can then be observed. Cleavage of the ester bond in CO-RMs **9-12** leaving an alcohol significantly alters the ability of the diene ligand to donate and receive electron density from the iron centre. **Figure 24** shows details of esterase-mediated CO release to myoglobin from CO-RM **11**.

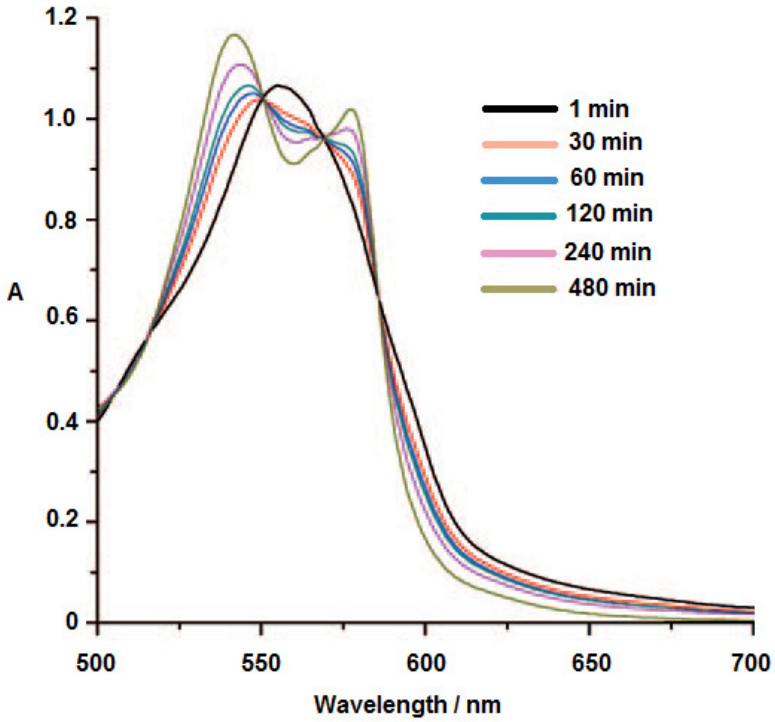

Figure 24. CO-release from 99 µM CO-RM **11** indicated by a clean deoxy-Mb to carboxy-Mb transition. 0.01 eq. PLE used as a CO-RM activation agent.(Image taken from Ref. **77**, Acyloxybutadiene Iron Tricarbonyl Complexes as Enzyme-Triggered CO-Releasing Molecules (ET-CORMs), Romanski, S.; Kraus, B.; Schatzschneider, U.; Neudorfl, J. M.; Amslinger, S.; Schmalz, H. G., *Angew. Chem. Int. Ed.* **2011**, 50, 2392-6) Copyright Wiley 2011.

In the presence of PLE, CO from CO-RM **11** results in clean conversion of reduced myoglobin to carboxy myoglobin over a period of eight hours. This slow release is similar to the CO-RM **A1** release rate. The kinetic rates of CO release here could be easily controlled by varying the concentrations of esterase in the solution. This gives a very strong degree of control.

CO-RMs **9**-**12** were all tested for cell viability with RAW 264.7 macrophages. The CO-RMs show varying degrees of toxicity in the presence of LPS. **10** showed the most promising results with no signs of toxicity within the 100 µM range. However, **11** shows an IC_{50} of only 39 µM which is relatively toxic with respect to **10**. Unfortunately the authors did not carry out any sub-stoichiometric myoglobin assays to determine how many CO molecules were released per molecule of CO-RM. With an iron tricarbonyl CO-releasing moeity, it would be reasonable to expect more than one CO molecule released per molecule of CO-RM.

The authors did however test the four CO-RMs for their ability to suppress NO production in RAW 264.7 cells, thus eliciting an anti-inflammatory response as described previously. All the CO-RMs were found to suppress the production of NO by a greater percentage than their toxicity at the same CO-RM concentration. **11** and **12** were found to be the best NO suppressors with

reduction values of 33% at only 5 μM CO-RM concentrations. This is one of the most potent anti-inflammatory responses from a CO-RM in the literature and is promising.

Future research with these acyloxybutadiene complexes could focus around its enzyme related activation. Screening needs to be carried out with a larger variety of enzymes to find out which *in vivo* esterases could activate the CO-RMs. There are also many other enzymes which could activate this CO-RM and this is clearly going to be important when calculating *in vivo* CO release kinetics. One could also think about the co-administration of a CO-RM with an esterase enzyme to aid its degradation under certain circumstances. The CO-RM could be administered first, and allowed to accumulate at its required location. The appropriate enzymes could then be administered to trigger controlled CO-release. Careful selection would have to be made to find an enzyme that would not interfere with other biological processes.

1.4.1.3 Photo-activated CO-RMs

The final method of CO-RM activation is by photo-irradiation. There are now many new photo CO-RMs being published in the literature.[59-62, 78] This class of CO-RM does not degrade over a short period of time; either thermally or in the presence of a CO binder such as myoglobin. Using light to activate a CO-RM provides an extra degree of control to the CO-release kinetics. Both the light intensity and CO-RM concentration can be varied. There are issues with the wavelength of light in terms of getting effective tissue penetration, and research towards photo-CO-RMs that edge away from low wavelength UV light is desirable.

One of the first photo-CO-RMs prepared was CO-RM-**1** ($Mn_2(CO)_{10}$). CO-RM-**1** is a di-manganese compound containing a metal-metal bond with each manganese bearing five carbonyl ligands. This compound is an efficient photo-CO-RM with a short half-life, but is apolar. This gives rise to poor water solubility and therefore low bioavailability.[79-80] This molecule is shown to release CO efficiently in organic solvent when irradiated as detected by myoglobin through a CO permeable membrane. Considering the wavelength of light being used to photolyse CO-RMs in the current literature; UV light is too high in energy for medical use and CO-RMs which release when irradiated at a higher wavelength are more desirable.

Arregui and co-workers have carried out some initial studies with CO-RM-**1** in similar fashion to what has been carried out with previous CO-RMs.[81] In rats, CO-RM-**1** was shown to increase the level of CO-Hb in the blood and increase the levels of cGMP in urine. It was also shown to increase renal blood flow by a significant amount. This CO-RM was an important starting point in the development of CO quantification procedures and photo-activated CO release, however

this molecule does not contain interesting structural features for further modification to alter properties like in the case of the acyloxybutadiene complexes.[76] New, more soluble and more structurally appropriate CO-RMs have now been prepared.

Lynam and co-workers prepared a series of cyclopentadienyl molybdenum tricarbonyl complexes with varying alkynyl ligands. The synthesis and structure of the more promising CO-RMs from this work is shown in **Scheme 5** .[82]

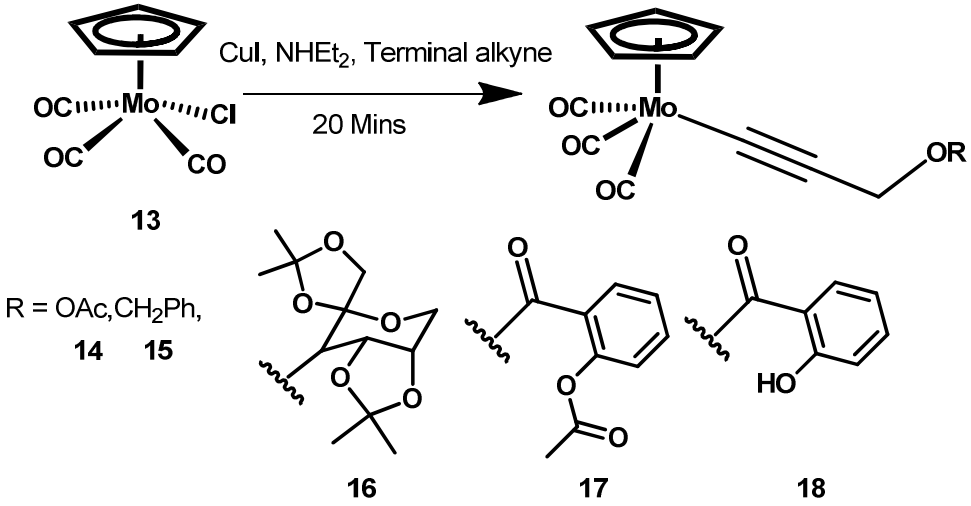

Scheme 5. Cyclopentadienyl molybdenum tricarbonyl complexes with varying alkynyl ligands

CO-RMs **14-18** are prepared by reaction of a terminal alkyne with a tricarbonyl chloro molybdenum complex (**13**) in the presence of CuI to activate the alkyne, with $NHEt_2$ as a base. This reaction is very versatile and produces a structurally diverse selection of potentially therapeutic CO-RMs. The most promising of these CO-RMs is **16**. This CO-RM is water soluble presumably because of the β-D-fructopyranose group. This group significantly increases the polarity and therefore water solubility of the complex.

CO-RM **16** was used in a myoglobin assay and was found not to release CO to the myoglobin without any irradiation. However with irradiation from a 6 W TLC lamp, clean generation of CO-Mb was observed. More studies into the cytotoxicity of this CO-RM and how it may breakdown *in vivo* would be essential if this CO-RM was to be taken forward. The use of a sugar to improve its solubility makes it structurally interesting. The method of attaching the ligand to the metal carbonyl moeity allows almost endless variation of the R group and further synthetic investigation could produce more interesting candidates.

Westerhausen and co-workers developed another photo-CO-RM based on a cystamine iron structure.[83] The synthesis and structure of CO-RM **S1** is shown in **Scheme 6**.

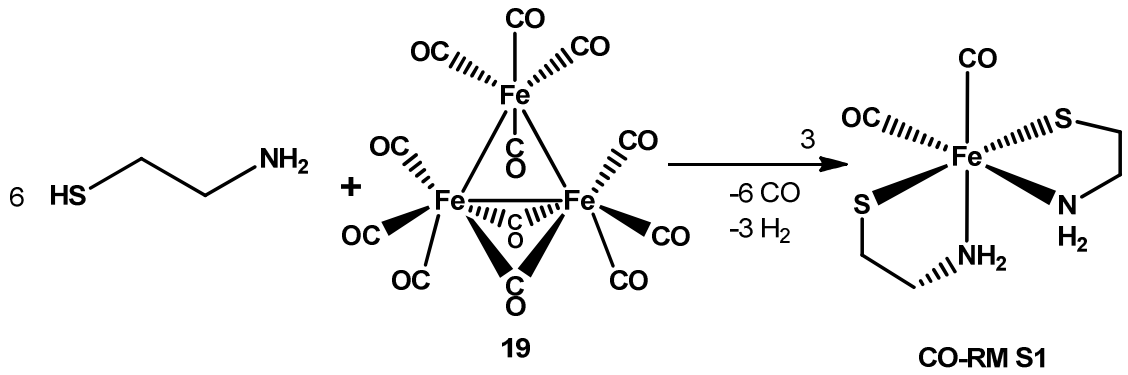

Scheme 6. The synthesis of CO-RM **S1**

CO-RM **S1** is prepared by reaction of 6 eq. of cystamine with dodecyl carbonyl species **19**, which forms three equivalents of CO-RM **S1**. This reaction is fairly efficient with the only waste products being small gasses. A myoglobin assay was used to assess and classify the CO-release behaviour of CO-RM **S1**. It was found that CO-RM **S1** that was stored in solution in the dark for 15 mins before addition to myoglobin only released marginal amounts of CO. When a repeat solution was irradiated for 15 mins with light of wavelength 470 nm. Complete conversion of deoxy-Mb to carboxy-Mb was observed. CO-RM **S1** was also irradiated directly in the presence of myoglobin after an initial 'dark' period. No release was observed in the dark period followed by quick CO release with irradiation (**Figure 25**).

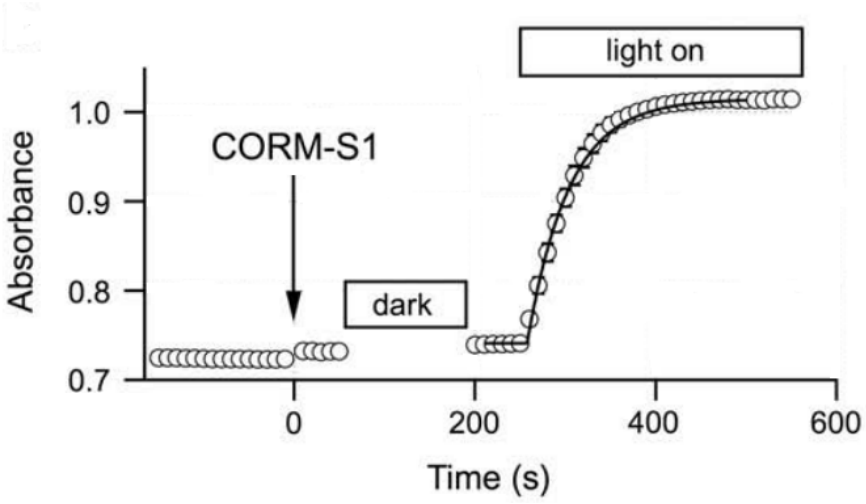

Figure 25. Myoglobin assay absorbance profile with CO-RM **S1**. Initially in the dark followed by 470 nm irradiation. (Graph taken from Ref. **83** with permissions, Dicarbonyl-bis(cysteamine)iron(II): A light induced carbon monoxide releasing molecule based on iron (CORM-S1), Kretschmer, R.; Gessner, G.; Gorls, H.; Heinemann, S. H.; Westerhausen, M., *J. Inorg. Biochem.,* **2011**, 105, 6-9) Copyright Elsevier 2011.

CO-RM **S1** shows good stability in the dark in the presence of myoglobin and releases in a controlled an efficient manner on irradiation at 470 nm. This is one of the most promising photo-activated CO-RMs in terms of wavelength in the literature. 470 nm is one of the highest wavelengths used the promote CO-release from a CO-RM and this wavelength will penetrate further in to tissue than some of the lower wavelengths used to activate previous CO-RMs.

CO-RM **S1** was also employed in a key study which shows that it can activate the Ca^{2+}-dependent K^+ channels in the presence of irradiation. **Figure 26** shows the results of this study.

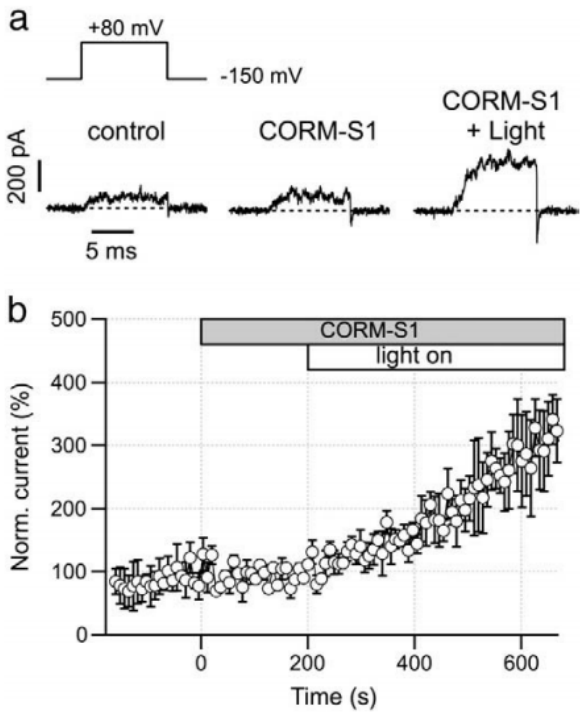

Figure 26. Current measured across a membrane containing BK Slo1 Ca^{2+}-activated K^+ channels. Current measurements carried out in the presence (1mM) and absence of CO-RM **S1**(control). Light was also turned on after an initial dark period as indicated. (Image taken from Ref. **83**, Dicarbonyl-bis(cysteamine)iron(II): A light-induced carbon monoxide releasing molecule based on iron (CORM-S1), Kretschmer, R.; Gessner, G.; Gorls, H.; Heinemann, S. H.; Westerhausen, M., *J. Inorg. Biochem.* **2011**, 105, 6-9). Copyright Elsevier 2011

There is negligible current detected with CO-RM **S1** in the absence of light which matches with the control. When the light is turned on there is a statistically significant increase in the current measured across the membrane. This strongly suggests that the CO-RM is not releasing a significant amount of CO in the dark and then CO is being released on irradiation and causing a strong activation of the K^+ channels. This is an encouraging result although using the CO-RM at 1mM seems like a clinically irrelevant concentration. Cytotoxicity studies need to be carried out with macrophages such as RAW 264.7 cells. The CO-RM may activate the channel at 1mM but cell viability assays or *in vivo* studies have not being carried out to show that this complex is not toxic at 1 mM. Most CO-RMs are typically administered at a much lower concentration and it would be better to see if 1 mM is really necessary. The binding site on the K^+ may be saturated at a much lower concentration of CO-RM.

Mohr and co-workers have also developed a class of photo-CO-RM developed on unprotected L-histidine.[78] The synthesis and structure of CO-RM **21** is shown in **Scheme 7**.

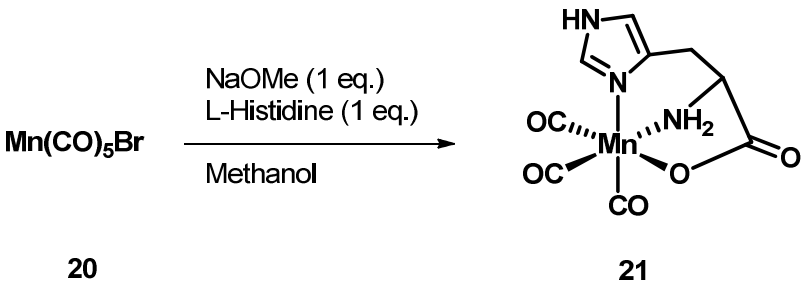

20 **21**

Scheme 7. The synthesis and structure of CO-RM **21**

CO-RM **21** has a structurally desirable unprotected L-histidine ligand. L-histidine is a natural amino acid and is of course non-toxic. This is likely to reduce the chance of toxicity when developing a new CO-RM, because if free L-histidine is released then it is less likely to be a problem from a pharmacological point of view compared to an unknown newly designed ligand. Having said that, CO-RM **21** has not been tested for toxicity/viability yet which would need to be done if it were to be used in further studies.

The molecule has been show to be stable in aqueous solution and in the presence of myoglobin. On irradiation at 365 nm with a 6 W TLC lamp there is CO-release observed with a half-life of 93 mins. This is slow release for a photo-CO-RM and irradiation for such long periods of time in a clinic is impractical. Irradiation with light of wavelength 365 nm is now outdated, and there are better photo-CO-RMs in the literature such as CO-RM **S1**. I*n vivo* experiments could be carried out to assess if there is any enzymatic activity that could degrade CO-RM **21**. It could potentially have a role as an ET-CO-RM under the correct conditions.

Zobi and co-workers have recently developed CO-RM **22** based on vitamin-B_{12} (**Figure 27**).[60] This is a clever strategy to take as the use of essential biological molecules is likely to decrease toxicity, as everyone needs vitamin-B_{12} to live and stay healthy. Vitamin-B_{12} is also water soluble and due to its porphyrin ring absorbs strongly in the visible region, making an excellent potential CO-RM tag. A similar strategy was also taken with the Mohr histidine CO-RM **21** by using unprotected L-histidine, which is a biologically essential compound.

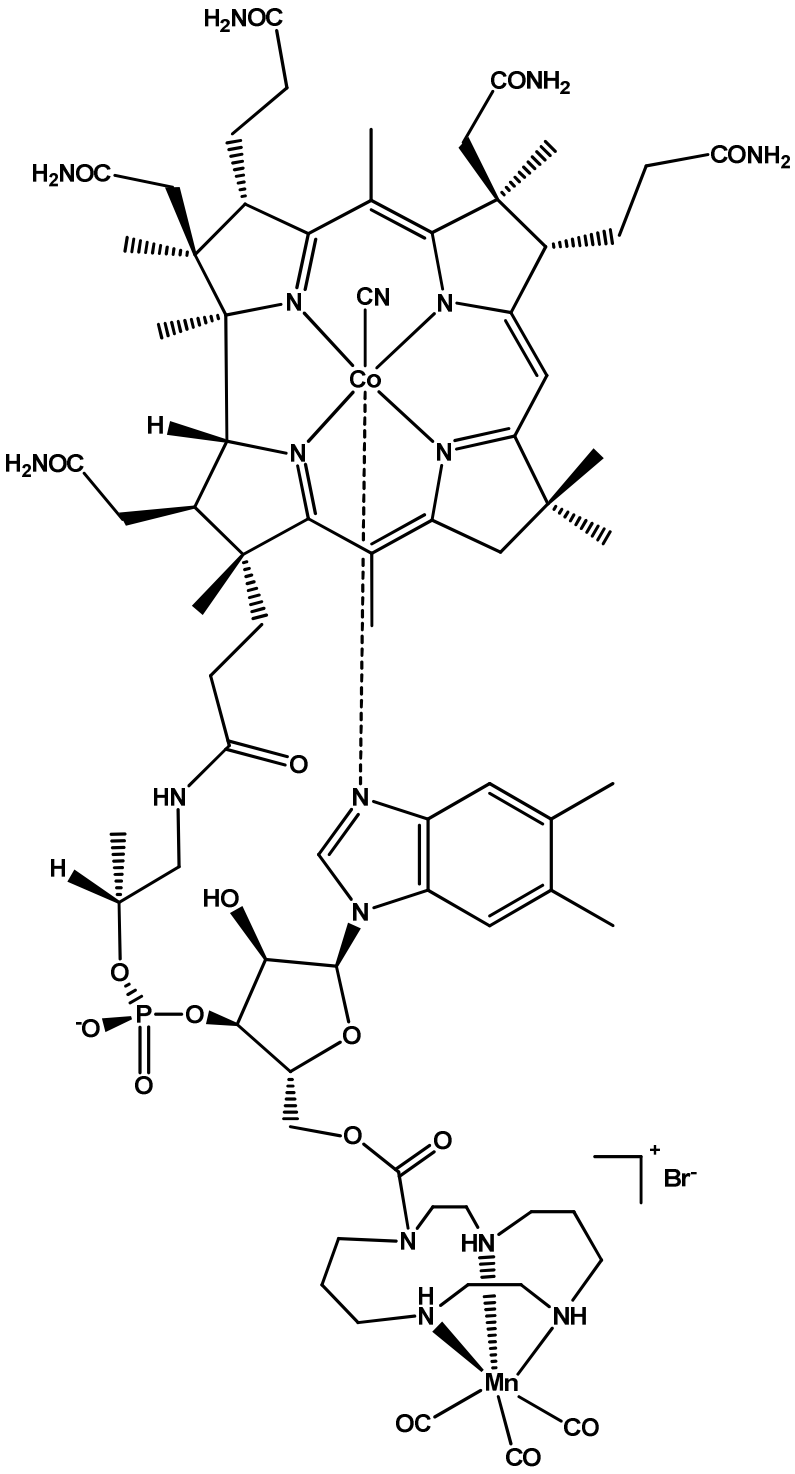

Figure 27. The structure of Vitamin-B_{12} conjugate CO-RM **22**

The structure of CO-RM **22** is quite remarkable, and is one of the most structurally complex and diverse CO-RMs ever prepared. This is made possible by using an already complex naturally occurring compound. Trying to synthesise this compound from scratch would prove extremely difficult involving many steps. By using a natural compound and some clever linking chemistry it is possible to make this compound in only a few synthetic steps.

CO-RM **22** contains a tetraazacyclotetradecane (tacd) manganese(I) tricarbonyl species, which has been conjugated using carbamate functionality. Manganese carbonyl CO-release motifs are very commonly used and for good reasons. Many manganese(I) CO-RMs as discussed previously are not toxic, reducing the risk when developing new CO-RMs that contain this moeity.

CO-RM **22** is soluble in water, which of course is due to the vitamin-B_{12} functionality with its primary amide functionality. CO-RM **22** is stable in aqueous solution for long periods of time setting up to be a promising photo-CO-RM. In a solution of methanol, the CO-RM is stable for a prolonged period, and on irradiation the M–CO bands in the IR spectrum slowly deplete showing that CO-RM **22** is acting as a photo-CO-RM. Myoglobin assays also show CO-release from this CO-RM on irradiation with a 470 nm LED and a green Ar Laser.

A UV-Vis spectrum of the tetraazacyclotetradecane (tacd) manganese(I) tricarbonyl species prior to conjugation shows overlap of the LED and laser emission with the compound's absorption band. This (tacd)$Mn(CO)_3$ moeity has some interesting spectral properties with the absorption band tailing well into the visible region. Carrying out some detailed DFT calculations on this structure could be very beneficial in terms of finding out what features of this moeity shifts the absorption to such high wavelength. CO-RM **22** is one of the highest wavelength photo activated CO-RMs presented in the literature and this kind of conjugation is something that should be taken on board by other researchers with other interesting biological molecules.

Schatzschneider and co-workers have taken complex **24** previously synthesised by Trofimenko and co-workers, and investigated its potential as a photo-CO-RM.[62, 84] The synthesis of **24** is shown in **Scheme 8**.

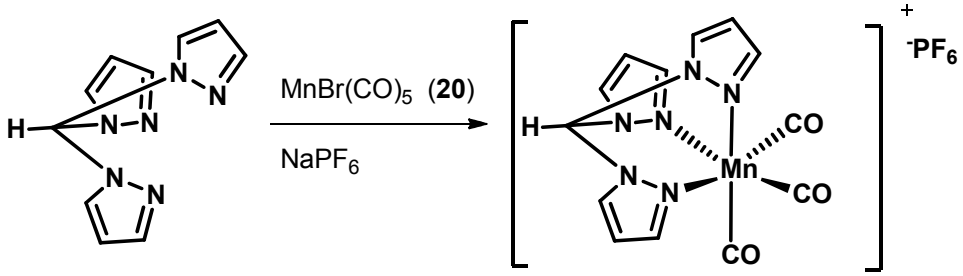

23 **24**

Scheme 8. The synthesis and structure of CO-RM **24**

Complex **20** has become a very useful metal carbonyl precursor for the preparation of CO-RMs. CO-RM **24** is prepared by reaction of **20** with tpm ligand **23** in the presence of $NaPF_6$.

CO-RM **24** has been shown to be stable in aqueous buffer and in the presence of myoglobin in the dark. No spectroscopic changes were observed when **24** was mixed with myoglobin. However upon irradiation with a 365 nm TLC lamp conversion to carboxy-Mb was observed. It is important to note that the CO-release from this tricarbonyl manganese(I) species is much faster compared with the similar Histidine complex **21.** With myoglobin in excess of CO-RM **24**, it was found that 1.9 moles of CO per mole of **24** which is advantageous for pharmacological reasons.

CO-RM **24** was also used in studies with HT29 colon cancer cells for cytotoxicity studies. The results from this study are shown in **Figure 28**.

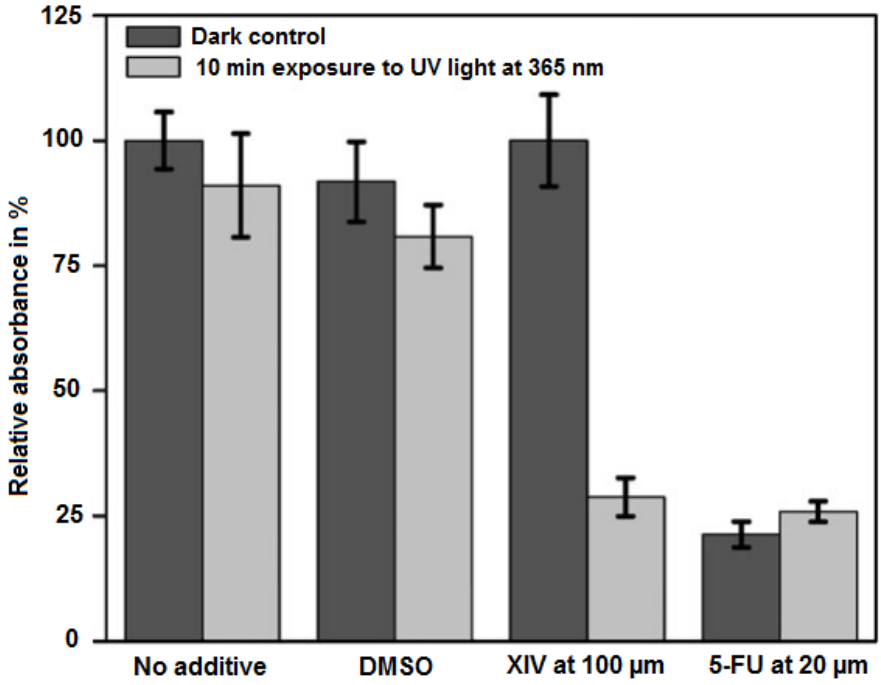

Figure 28. Cytotoxicity test of CO-RM **24** at 100 µM against HT29 colon cancer cell.(graph taken from ref.**62**: Photoinduced CO release, cellular uptake and cytotoxicity of a tris(pyrazolyl)methane (tpm) manganese tricarbonyl complex Niesel, J.; Pinto, A.; Peindy N'Dongo, H. W.; Merz, K.; Ott, I.; Gust, R.; Schatzschneider, U., Chem Comm. **2008**, 1798-800) Copyright The Royal Society of Chemistry 2008.

The controls in this experiment show that the DMSO is not causing any significant toxicity. The irradiation only causes a small reduction, but this is expected considering the wavelength of irradiation used. CO-RM **24** does not cause any cytotoxicity to the cancer cells in the dark but a large increase in cytotoxicity is observed when the cells are irradiated for 10 mins in the presence of **24**. This reduction is comparable to 5-fluorouracil (FU) which is an established anti-cancer agent. These results are initially very promising but more investigations in to the mechanism of

toxicity need to be carried out. Pre-irradiation of **24** to generate a 'photo-i-CO-RM' would be a suitable starting point in assessing if photo products were responsible for toxicity.

CO-RM **24** was also developed further by Schatzschneider and co-workers using some procedures developed by Regal and co-workers. The methane proton in tpm ligand **23** was removed using base to provide an anchor for further synthesis. **Scheme 9** shows how CO-RM **25** was synthesised, which can then be easily functionalised by various reactions.

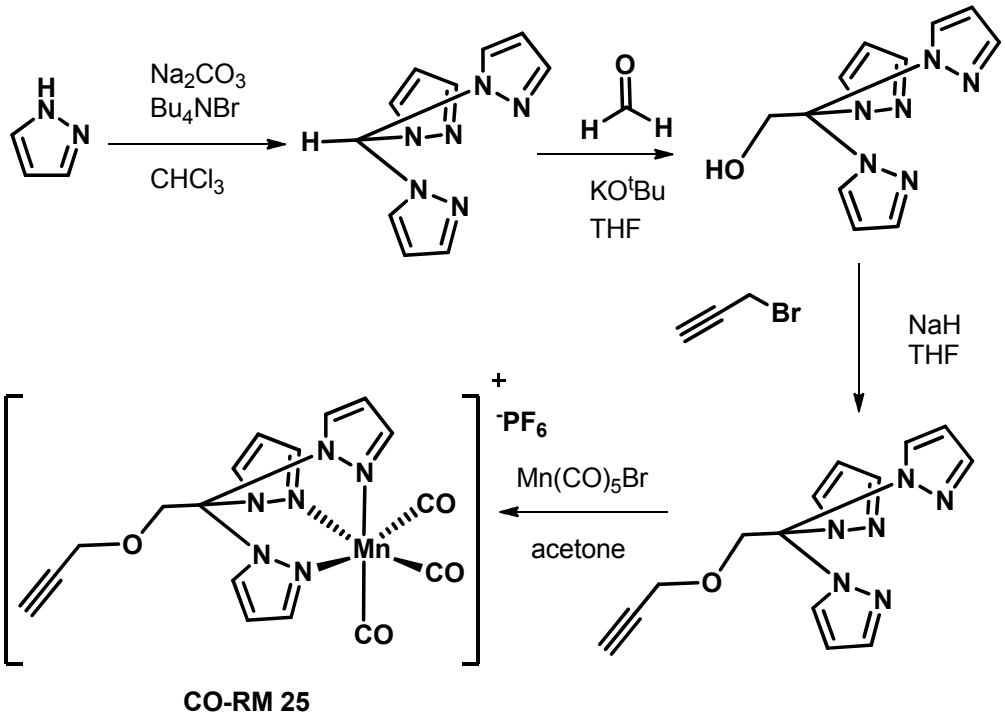

Scheme 9. The synthesis of CO-RM **25**, a substituted variant of CO-RM **24**.

The final step in the system of CO-RM **25** is prepared by the same complexation as with CO-RM **24**. However the ligand is pre-functionalised before the complexation step in this case. Alkyne functionality was introduced with a spacer which was used to keep the alkyne distanced from the metal complex. This would have been done so that any groups that are subsequently attached on to the alkyne are less likely to interfere with the CO-releasing properties of the manganese unit.

Schatzschneider and co-workers then developed some synthetic peptides which could be conjugated with CO-RM **25** using either a Sonogashira reaction, or a Huisgen [3 + 2] cycloaddition reaction. **Figure 29** shows the structures of the different peptides prepared.

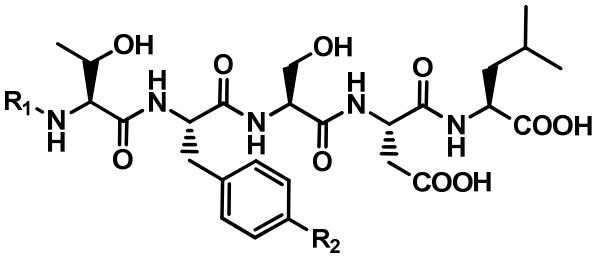

$R_1 = p\text{-I-}C_6H_4CO$ $R_2 = H$ = **26**
$R_1 = H$ $R_2 = I$ = **27**
$R_1 = N_3CH_2CO$ $R_2 = H$ = **28**

Figure 29. The structure of synthetic peptides used for coupling with CO-RM **25**

Peptides **26** and **28** contain functionality at the N-terminus while **27** is functionalised on the phenylalanine side chain. This provides an excellent opportunity to functionalise on different areas in the molecule depending on what is required. The azides are used in the [3 + 2] cycloaddition reactions and the iodine is used for Sonogashira cross-coupling reactions.

Scheme 10 shows reaction of **28** with CO-RM **25** to produce a peptide-CO-RM conjugate **29**.

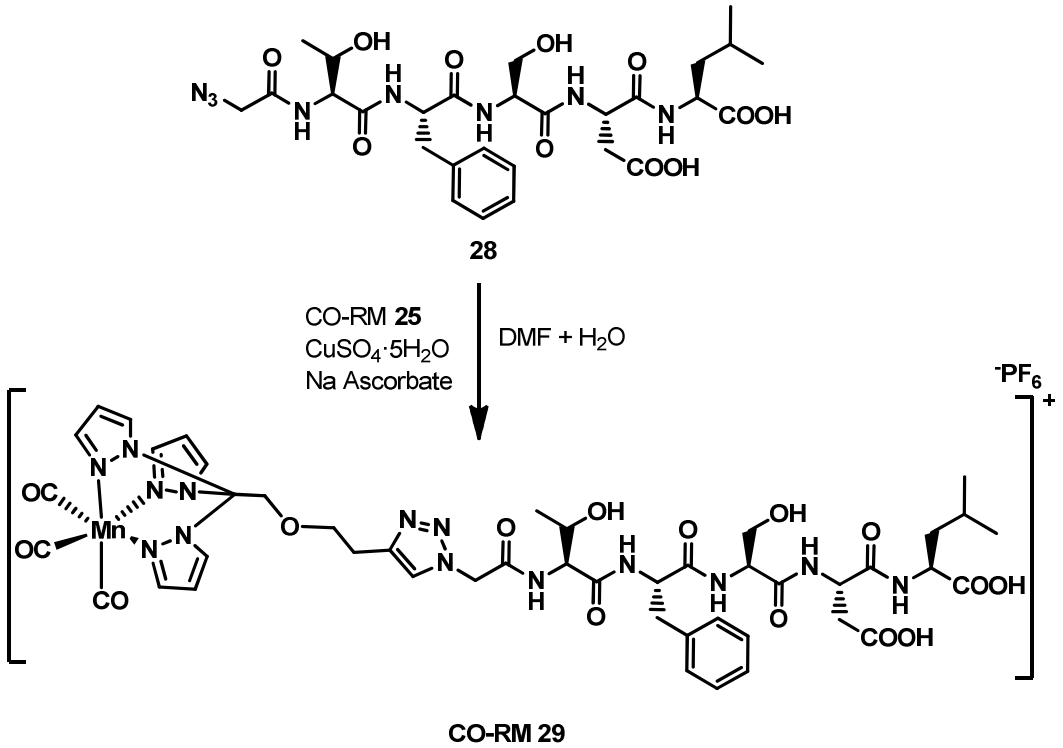

Scheme 10. The synthesis of peptide-CO-RM conjugate **29** using [3 + 2] cycloaddition chemistry.

The peptide sequence Thr-Phe-Ser-Asp-Leu is found in the transactivation domain of tumour suppression protein p53[85] which binds with regulatory MDM2. If MDM2 gets over expressed due

to too much p53-MDM2 binding, then p53 activity gets reduced and cells with damaged DNA can divide and grow unchecked. This then leads to cancerous growth.[85] The authors chose this peptide as a means of trying to interrupt this interaction and prevent MDM2 over expression.

CO-RM **29** was successfully synthesised by conjugation of **25** and **28** using [3 + 2] cycloaddition chemistry. ESI-MS, IR spectroscopy and HPLC were used to indicate high purity. To date, CO-RM **29** has only be employed in a myoglobin assay but acts as a photo-CO-RM and releases 1.7 moles of CO per mole of CO-RM. This is encouraging considering the complex amount of functionalisation carried out with this molecule and that the uncoupled CO-RM **25** releases 1.9 moles of CO. Despite the complex peptide attached, the CO-releasing moeity in **29** still remains stable and releases CO in a very similar fashion to the unfunctionalised CO-RM **25**.

It is clear that [3+2] cycloaddition chemistry and Sonogashira cross-coupling reactions are a powerful tool for the development of more complex CO-RMs and indeed other pharmaceuticals agents. Once a suitable CO-RM has been developed there are thousands of possible interesting structures that can then be attached on to the CO-releasing moeity. The cyclopentadienyl molybdenum tricarbonyl complexes shown in Scheme **3** could also be easily modified to give a complex with a terminal alkyne functionality which would allow the same sort of chemistry to be carried out on those too.

1.5 Potential for CO-RM use as a labelling/imaging agent

Schatzschneider and co-workers have also developed CO-RMs for more than just use as a pharmaceutical agent. It is possible take advantage of the diagnostic infrared M–CO stretching frequencies and use a 'CO-RM' like moeity to act as a labelling or imaging agent.[86]

The first way that a CO-RM like molecule was used as an imaging agent was to use CO-RM **24** but with a chloride counter ion to provide increased solubility (**24a**). The work establishes that there is a diagnostic M–CO Raman stretch at 1963 cm^{-1} from the CO-RM which is not present when analysing cells without **24a** present. This allows for images to be taken of the cells clearly showing where the CO-RM is located. **Figure 30** shows the difference between an optical image and a Raman microspectroscopy image of a HT29 colon cancer cell taken in the presence CO-RM **24a**.

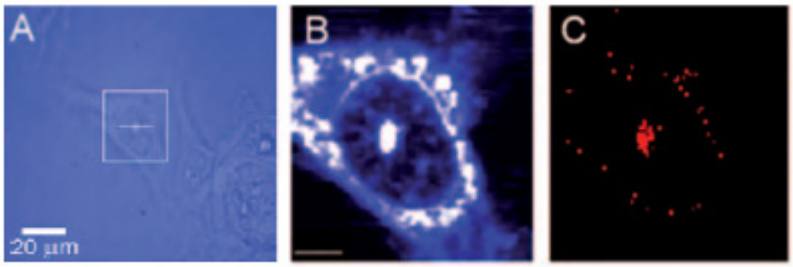

Figure 30. A) Optical image of a HT29 human colon cancer cell incubated with an aqueous solution (2 mM) of **24a** for 3 h. B, C) Raman images reconstructed from integrating the intensities of the CO and CH stretching peaks. The integration range was 2800–3050 cm^{-1} for (B) and 1945–1965 cm^{-1} for (C). The scale bar for the Raman images is 6 µm.(adapted image taken from Ref.**86** with permissions, Label-Free Imaging of Metal–Carbonyl Complexes in Live Cells by Raman Microspectroscopy, Meister, K.; Niesel, J.; Schatzschneider, U.; Metzler-Nolte, N.; Schmidt, D. A.; Havenith, M., Angew. Chem. Int. Ed. **2010**.) Copyright Wiley 2010.

Image A shows little information about the cell and only an outline of the cell can be observed. However using Raman microspectroscopy in the presence of $[Mn(tpm)(CO)_3]Cl$ (**24a**) observing at 1945 cm^{-1} clearly shows an intense signal of the CO-RM around the cell and inside, especially within the nucleus. Using C–H frequencies (Image C) is much less selective and informative as many biological molecules will contain Raman active C-H vibration modes. The use of the C–O stretch can be attributed specifically to the CO-RM and shows important localisation information. One would imagine that many other CO-RMs could also be used in the same way.

Schatzschneider and co-workers also developed a cyclopentadienyl tricarbonyl manganese(I) system which can be used to label biologically important peptides.[87] The $CpMn(CO)_3$ 'tag'

provides metal carbonyls which can be used for infrared imaging. This makes it possible to view where these biological important molecules are located inside a cell. **Figure 31** shows the structure of cymantrene-peptide conjugate **30**.

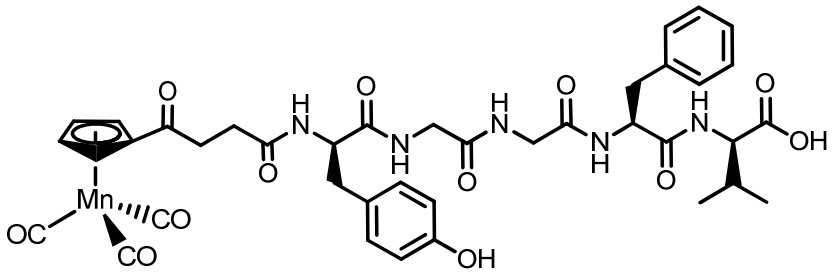

30

Figure 31. The structure of **30**, a cymantrene tagged biological probe.

The 'CO-RM' like moeity was attached to the peptide with a succinic acid linker to space out the metal fragment from the rest of the peptide sequence. This could help prevent any interference with the peptide binding to its natural targets.

Complex **30** has three diagnostic IR stretches at 1916, 1943 and 2016 cm^{-1}, which are similar to the stretches observed in the tpm CO-RM system. These peaks give a strong signal that would not be naturally produced by cells. This molecule has been shown to be non toxic to MCF-7 human breast cancer cells making it suitable for use as a probe. Any toxicity would be undesirable as it could strongly interfere with the location of the unconjugated peptide. This is a promising molecule but imaging studies with this peptide have yet to be carried out.

1.6 Overview and remarks

In summary, CO has been shown to play an essential role in eukaryotic biology and is a key molecule with respect to homeostasis. Many researchers have shown that CO as a gas or locked within a CO-RM can be used as an extremely beneficial molecule to treat many conditions and diseases and to preserve organs. The multiple benefits that carbon monoxide-releasing molecules (CO-RMs) could potentially give present a large advantage over many traditional organic drugs, which may only treat one condition. A single CO-RM has the potential to treat a variety of ailments rather than needing a complex mixture of different drugs. CO-RMs also have the potential to alleviate harmful side effects from current drugs already on the market.

The other great benefit of using CO-RMs as pharmaceuticals is that there are numerous different structures capable of releasing CO as previously described. This spans a wide variety of coordinating ligands, geometries, CO-release modes and transition metal centres. This means that if one particular CO-RM was toxic to a patient in the future, another one could be potentially used.

It is important to remember that the CO is the drug and the ligand is a means of getting the CO where it is required. With the right ligand, the properties of CO-release and localisation can be fine tuned and modified, which can simply not be achieved using CO gas alone. This highlights the benefits of a CO-RM over the use of CO gas. Ramão and co-workers have shown that a $[Mo(CO)_3(CNR)_3]$ CO-RM motif is an encouraging candidate for treating acute liver injury.[88] This CO-RM accumulates in the liver but it was not designed to do this. While this work is encouraging, developing more functionalised CO-RMs for less random localisation could be more beneficial. Rather than making a CO-RM in the hope that it accumulates where it is required; it would be more logical to bind to specific proteins that are at high concentrations within an organ/tissue.

One of the other benefits is that CO is already produced in the body naturally. So providing that the CO dose is controlled carefully there are unlikely to be too many side effects due to the CO itself. Although great care needs to be taken in assessing the behaviour of the fragments that are left behind after CO release. Currently, there is not much detail in the literature about the characterisation of the fragments left behind after CO-release; even if they have shown that it is non-toxic and not responsible for the beneficial effects observed.

CO-RMs clearly have the potential to become some of the most important pharmaceuticals invented to date.

2 Aims and Objectives

The aims of this project are to:

- Synthesise a new generation of photo-active CO-RMs that are water compatible, and release CO in a controlled manner
- Increase the wavelength of light required to release CO while retaining stability.
- Introduce a site for functionalisation to allow targeting
- To prepare CO-RMs that can be used to exhibit detrimental effects on various bacterial strains, while being viable with eukaryotic cells
- Carry out investigations to elucidate the mechanism of action of the CO-RMs on bacteria

The objectives of this project are to:

- To design new ligands based on initial research and then synthesise complexes of these new designs using synthetic chemistry
- Carry out a wide variety of myoglobin assay experiments to establish CO release profiles for the CO-RMs synthesised. Water compatibility can be assessed with data from these assays
- Carry out growth curves and plating studies with *E. coli* and *S. aureus.* Careful controls are required to confirm effects and to assess what is causing these
- Carry out Alamar blue and LDH assays with RAW 264.7 macrophages using CO-RMs to assess their viability

3 Manganese(I) complexes as potential CO-RMs

3.1 Synthesis and characterisation of new manganese(I) complexes

The main aim of this project was to prepare a new class of photo-active CO-RMs. To do this, it was necessary to find a promising CO-releasing moeity that could be used as a basis for further studies. Tetracarbonyl phenylpyridine manganese(I) complexes have been prepared by Bruce and co-workers in the 1970's, however they had not yet been reported for use in a medicinal context.[89-90] The structure of parent complex **37** is shown in **Figure 32**.

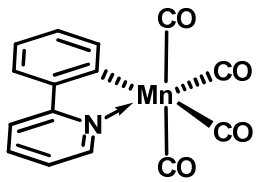

37

Figure 32. The structure of a potential CO-RM manganese(I) complex **37**

This octahedral structure consists of a 2-phenylpyridine bidentate ring system with a covalent bond to the manganese from the phenyl ring. There is also dative bond to the manganese from the nitrogen in the pyridine ring. The central manganese(I) atom has four carbon monoxide ligands. This structure was taken as a starting point for further research into using this moeity as a CO-RM.

It was known from work by Fairlamb and co-workers that this molecule was known to release CO in the presence of light on a nano-second time scale;[91] but a more in-depth study of this potential CO-RM was required. Initial work was required to establish if the '$Mn(CO)_4$' motif attached to the 2-phenylpyridine ligand could be used in CO-RMs for further studies.

The aim was to assess if simple structural variation on the phenyl ring would influence how the molecule behaves in terms of general stability and CO-release rates. If small structural variations caused dramatic changes in the rate/mode of the CO-release then this would make the CO-RM unsuitable when considering the aims of this project. The aim is to discover a CO-releasing moeity that can be functionalised with lots of different substituents to allow altering a variety of chemical properties. These include solubility, localisation, and wavelength of CO-release, and also for the potential to introduce fluorescence in to the structure.

Initial modification of CO-RM **37** involved synthesising a series of complexes substituted at the *para*-position on the phenyl ring. This position was chosen to avoid steric interaction of this group with the $Mn(CO)_4$ moeity, and also to maintain symmetry in the molecule to avoid the potential for isomerism. The structure of the initial target molecules are shown in **Figure 33**.

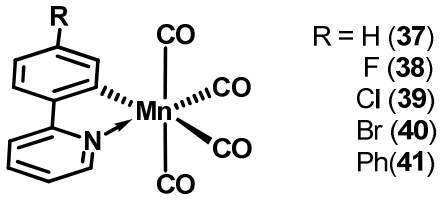

Figure 33. The target structures for initial CO-RM studies

The series of structures includes halogen substituents and the introduction of a third aromatic ring. All of these substitutions could affect how each CO-RM releases CO. Different substituents could alter the amount of electron density within the aromatic rings, subsequently changing the electron density on the metal. This could then weaken the M–CO bond depending on the substituent, and alter CO-releasing properties.

To synthesise these ligands, a two step linear strategy was developed based on the previous synthesis of the parent compound **37**. Firstly the ligands were prepared by a series of palladium-mediated Suzuki–Miyaura cross-coupling reactions in one step from commercially available materials. The general synthetic route to the substituted 2-phenylpyridine ligands required is shown in **Scheme 11**.

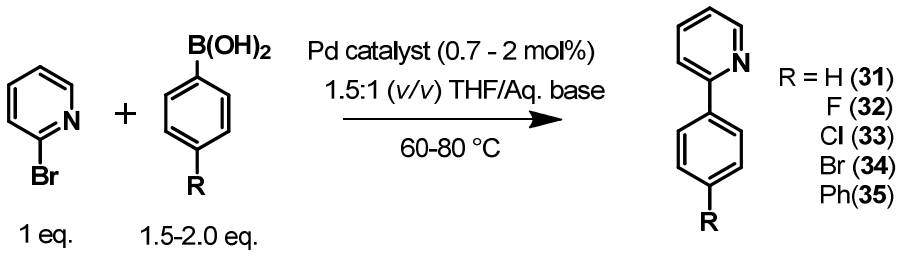

Scheme 11. General reaction scheme for preparation of substituted phenyl pyridine ligands. (R = H (**31**) was purchased from Sigma Aldrich).

The Suzuki–Miyaura cross-coupling reaction has long been established for synthesising linked aromatic systems,[92] and this made it suitable for preparing ligands **32**-**35**. The reactions use a palladium catalyst in low loading (0.7-2 mol%) to turn over the reaction using a THF/water system with the aqueous layer containing a base. The reactions were performed at 60-80 °C depending on the substrate, and the yields for the reactions are shown in **Table 3**.

Table 3. Percentage yields obtained from Suzuki–Miyaura cross-coupling reactions.

Compound	R	Catalyst	Base	% Yield
32	F	AB cat (0.7 mol %)	1.9M $Na_2CO_{3(aq)}$	79
33	Cl	$Pd(PPh_3)_4$ (2 mol %)	2M $K_2CO_{3(aq)}$	83
34	Br	$Pd(PPh_3)_4$ (2 mol %)	1.9M $Na_2CO_{3(aq)}$	59
35	Ph	$Pd(PPh_3)_4$ (2 mol %)	1.9M $Na_2CO_{3(aq)}$	59

Ligand **32** was synthesised using an alternative catalyst **ABcat**, which is a palladium dimer species bridged by 2-bromopyridine ligands (**Figure 34**).[93]

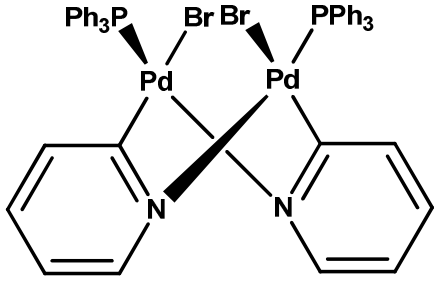

36

Figure 34. The structure of palladium dimer pre-catalyst **ABcat** (**36**)

Palladium dimer pre-catalyst **36** has been previously used in Suzuki–Miyaura reactions, and is particularly effective because it slowly degrades in solution to give mono-ligated Pd–PPh_3, which is catalytically active in cross-coupling reactions.[93] The slow release of active palladium into solution can prevent aggregate formation and subsequent turnover reduction. This catalyst had not been previously used with an electron withdrawing substituent such as fluorine on a benzene ring before. **ABcat** (**36**) was used in this case to test if the reaction could tolerate different functionality. Pleasingly **ABcat** in this reaction gave compound **32** in 79% yield, which gave satisfactory material for further characterisation.

Bromo-containing compound **34** had to be synthesised using a lower temperature of 60 °C. This was performed at 60 °C to prevent the *para*-bromophenylboronic acid from coupling with itself and the target product to give undesired tri-aromatic chains. *ortho*-Bromopyridines generally react faster than bromobenzene derivatives and 60 °C is low enough to efficiently promote the reaction of 2-bromopyridine, but low enough to avoid activation of the C–Br bond in the bromobenzene derivatives. The reaction in **Scheme 11** gave product **34** in 59% yield. The chloro substituent in the starting material used to prepare **33** is much more suited to this reaction as these typically react at higher temperature. 80 °C gives a fast reaction of the 2-bromopyridine species with negligible cross-coupling observed from the chloro containing species in the reaction. This is reflected in the respectable 83% yield obtained for ligand **33**.

Ligand **35** was only synthesised in 59% yield, which seems rather low considering that biphenyl boronic acid will not be coupling with itself like in the case of *para*-bromophenylboronic acid. The extended conjugation and larger system could slow down the reaction rate. However sufficient material was obtained to move forward with the synthesis of CO-RM **41**.

With all the synthesised ligands purified and fully characterised by: $^{1}H/^{13}C$ NMR, ESI mass spectrometry, elemental analysis and IR spectroscopy, the target CO-RMs **37**-**41** could then be prepared using the reaction presented in **Scheme 12**.[89-90]

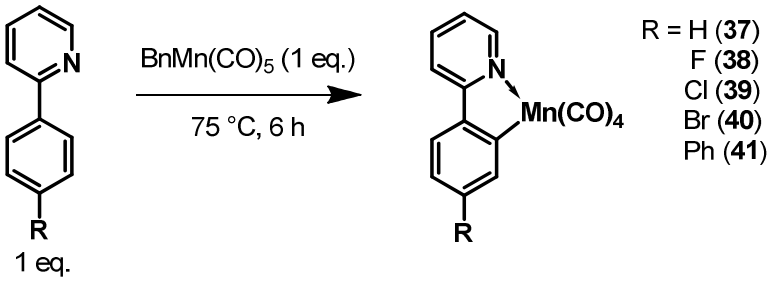

Scheme 12. The synthesis of CO-RMs **37**-**41** using $BnMn(CO)_5$

The phenylpyridine species react with $BnMn(CO)_5$(**42**) to give a tetracarbonyl phenylpyridine manganese(I) species. Toluene is produced as a reaction by-product, which can easily be removed under reduced pressure. **Figure 35** shows the ^{1}H NMR of ligand **34** and its corresponding purified manganese complex **40**.

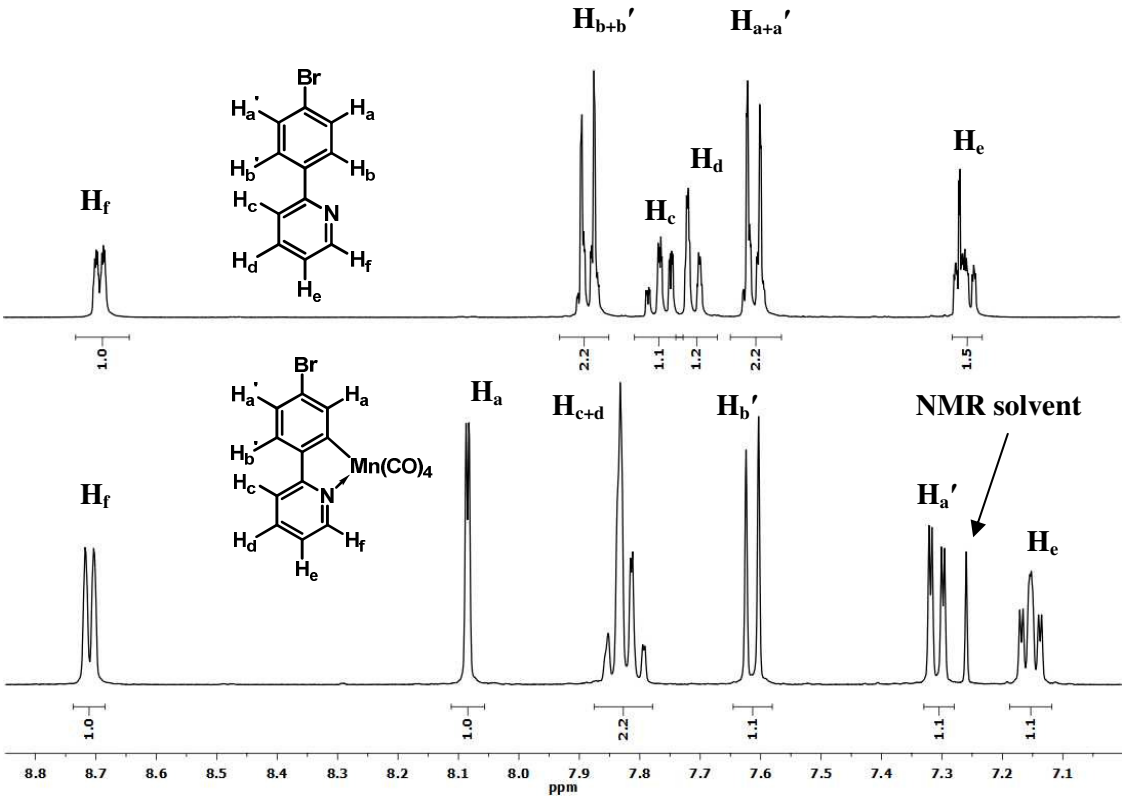

Figure 35. The 400 MHz ^{1}H NMR spectrum of ligand **34** (top) and CO-RM **40** (bottom) recorded in $CDCl_3$

In the ^{1}H NMR spectra shown in **Figure 35**, it is clear that the pair of doublets (H_a-H_a', H_b-H_b' 7.6–7.9 ppm, ^{3}J = 8.3 Hz) due to the *para*-substituted aromatic starting material (**34**) are lost on reaction with $BnMn(CO)_5$. This was a good indication that the cyclo-metallation had taken place. There is a resonance at 8.05 ppm (^{4}J = 1.9 Hz), which is typical of long-range W-coupling between H_a and H_a' as indicated in **Figure 35**. The removal of a proton H_b by the cyclo-metallation reaction isolates H_a, which can then only couple to H_a' at the other side of the ring. This also changes proton H_b' in the product which can only couple to H_a' (^{3}J = 8.5 Hz). The nitrogen in the pyridine ring in CO-RM **40** coordinates to the manganese(I) centre and this results in shifting of the pyridine proton signals $H_{c\text{-}f}$. Protons H_{c+d} have shifted so that they are partially overlapping. These data together suggests the desired compound has been synthesised.

3.1.1 IR spectroscopic and group theory analysis of CO-RM 40

Figure 36 shows the IR spectra of the starting material and product from the cyclo-metallation reaction of ligand **34** to produce **40**.

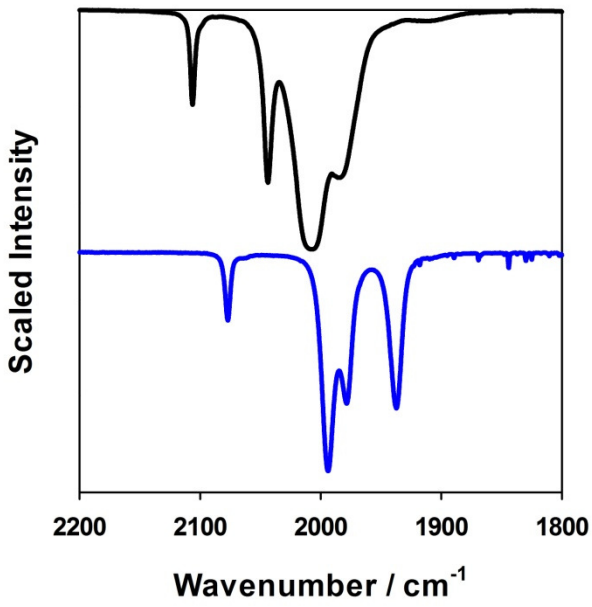

Figure 36. The solution IR spectra in THF of $BnMn(CO)_5$ (black) and CO-RM **40** (blue)

The IR spectrum of CO-RM **40** confirms that all the benzyl pentacarbonyl manganese(I) has been consumed in the reaction as there is no peak at 2107 cm^{-1}. There are also new peaks at 2074 and 1933 cm^{-1} corresponding to the new complex. It is possible to use group theory to analyse the symmetry of the complex, and determine the correct number of CO stretches that should be observed in the IR spectrum. A diagram of CO-RM **40** with appropriate axes is shown in **Figure 37**.

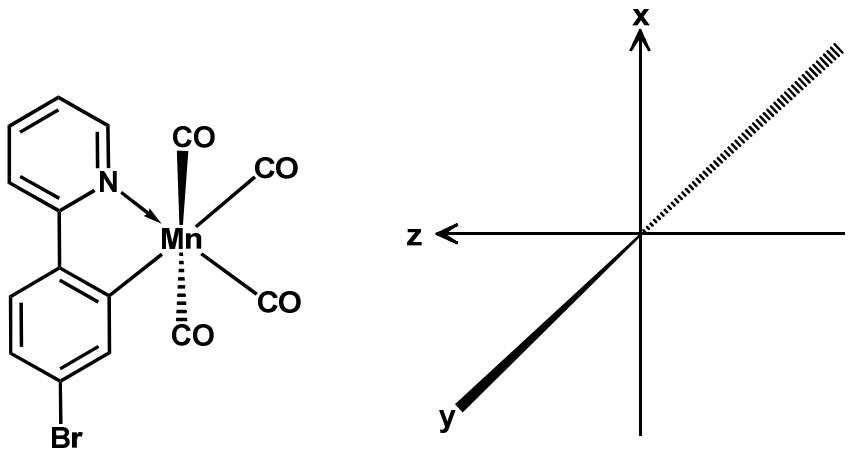

Figure 37. The structure of a tetracarbonyl manganese(I) complex **40**, with the axis relevant to the C_{2v} point group. Note: y axis is perpendicular to the xz plain, as are the CO ligands with wedge and dashed bonds respectively.

If complex **40** was treated purely by symmetry, it would belong to the C_s point group. If a C_2 operation is performed around the z axis considering the metal octahedron, only a carbon and nitrogen atom switch places. This means that this molecule may show pseudo C_{2v} symmetry. In some cases pendant groups away from the central metal octahedral structure do not affect the number of IR stretches.

The molecule contains four metal carbonyls and the symmetric stretches of each carbonyl can be represented as vectors pointing away from the molecule in the direction of the M-C≡O bond. The vectors can have each operation in the C_{2v} point group performed on it. The number of vectors that move on performing an operation in the relevant point group are removed from the total number of vectors, and the reducible representation can be calculated. The irreducible representation can be calculated by finding which components of the C_{2v} point group contribute to the reducible representation. **Table 4** shows the reducible representation obtained for complex **40** using the C_{2v} point group.

Table 4. The reducible representation for the CO symmetric stretches in complex **40** using the C_{2v} point group.

C_{2v}	E	C_2	σ(xz)	σ(yz)
Γ	4	0	2	2

E is the identity operation and involves no movement and so no vectors move, hence giving a contribution of four. C_2 is a 180° rotation about the z axis, and the two carbonyl vectors in the xz plain switch places. The two carbonyls *trans* to each other in the yz plane also switch places and

so the C_2 operation contributes zero. The σ operation is a reflection in the plane indicated, and in both cases each plain dissects two of the vectors and these remain the same in each case. Both σ operations give a contribution of two each. **Table 5** shows the point group C_{2v}.

Table 5. The C_{2v} point group

C_{2v}	E	C_2	σ(xz)	σ(yz)	
A_1	1	1	1	1	z,
A_2	1	1	-1	-1	R_z
B_1	1	-1	1	-1	x,R_y
B_2	1	-1	-1	1	y,R_x

The irreducible representation components in the C_{2v} point group that combine to give the reducible representation are 2 A_1 + B_1 + B_2. All components are IR active and four stretches are expected. This is in agreement with the data obtained for the CO-RM **40**.

It may be possible that the complex could behave like it belongs to the C_s point group due to the bromine atom and the difference in mass between the C and N atoms. The reducible representation can be obtained by treating the compound in the same way as before but using the C_s point group operations. The new reducible representation is shown in **Table 6** and the group table for the C_s point group is shown in **Table 7**.

Table 6. The reducible representation for the CO symmetric stretches in complex **40** using the C_s point group.

C_s	E	σ_h
Γ	4	2

Table 7. The C_s point group table

C_s	E	σ_h	
A′	1	1	x, y, R_z
A″	1	-1	z, R_x, R_y

The irreducible representation components in the C_s point group that combine to give the reducible representation are 2 A′ + 2 A″. This would also give rise to four peaks. It could be possible that the molecule is behaving like either point group but it is difficult to assign it to one looking at the analysis given. The IR spectra of all the CO-RMs **37-41** all show very similar IR

spectra with four peaks all in almost identical positions. It is clear that this molecule is not affected significantly by the presence of a substituent in the para position on the phenyl ring. This can provide confidence that the pattern of IR signals observed in the metal carbonyl region is diagnostic and typical of a manganese tetracarbonyl species.

3.1.2 X-ray crystal structure of CO-RM 40

To confirm the structure of CO-RM **40**, crystals have been obtained by diffusion of hexane in to a solution of **40** in CH_2Cl_2. The structure was confirmed by X-ray crystallography. The X-ray structure for complex **40** is shown in **Figure 38**.

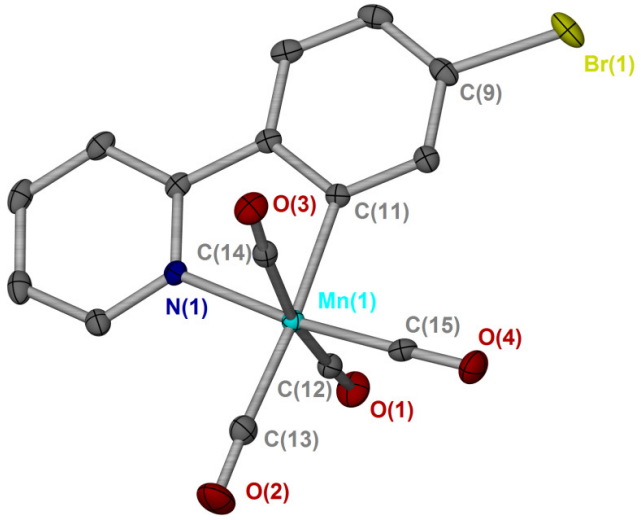

Figure 38. X-ray crystal structure of complex **40**. Atoms displayed as ellipsoids at 50% probability. Hydrogen atoms omitted for clarity. Selected bond lengths (Å) and angles (°):Mn(1)-C(11) = 2.0477(17) , Mn(1)-N(1) = 2.0638(14), Mn(1)-C(15) = 1.8007(18), Mn(1)-C(12) = 1.8642(19), Mn(1)-C(13) = 1.8401(19), Mn(1)-C(14) = 1.8544(19); C(14)-Mn(1)-C(12) = 168.51(8), C(13)-Mn(1)-C(12) = 95.58(8),C(11)-Mn(1)-C(15) = 93.25(7), C(13)-Mn(1)-N(1) =96.04(7), C(15)-Mn(1)-N(1) = 172.80(7), C(14)-Mn(1)-N(1) =90.03(7) , C(12)-Mn(1)-N(1) =88.03(7), N(1)-Mn(1)-C(11) = 79.55(6)

It is interesting to note the C(14)-Mn(1)-C(12) bond angle of 168.51(8) ° is quite distorted from an ideal octahedron. This is due to the size of the phenylpyridine system, which forces the system due to the N-Mn-C(11) bond angle of only 79.55(6) °. This geometry could play an important role in the determining the properties of the CO-RM. The slight distortion could alter how electron density passes from the ligand to the metal, potentially altering the mode of CO-release.

3.1.3 Yields for CO-RMs 37-41

Table 8 shows the yields obtained from the reaction of all the phenylpyridine ligands in the initial series with $BnMn(CO)_5$ (**42**).

Table 8. The isolated yields for CO-RMs **37**-**41** obtained from reactions using $BnMn(CO)_5$.

Compound	R	% Yield
37	H	88
38	F	43
39	Cl	83
40	Br	72
41	Ph	72

The complexes were all isolated in moderate to excellent yield following a simple filtration. Although further purification by column chromatography could be performed if required. Due to a slower rate of reaction in the synthesis of fluorinated CO-RM **38** (determined by ^{1}H NMR analysis), a further 0.2 eq. of $BnMn(CO)_5$ was added to react with any remaining ligand to give pure product. It is unknown why this reaction proceeded much slower than all the others; however enough material was obtained in all cases to carry out further testing.

3.1.4 In situ infrared spectroscopic analysis (ReactIR™) of CO-RM 41

With five manganese(I) complexes that are potential releasers of CO, the first step was to assess if there was any short term degradation of the complexes in air. This was followed using ReactIR™ instrumentation (Mettler-Toledo). A 1 mM solution of CO-RM **41** was prepared in DMSO and was stirred ca. three hours with IR spectra being recorded every minute. **Figure 39** shows the results of this ReactIR™ experiment. This CO-RM was the only complex analysed by ReactIR™ in this series due to limited availability of the instrument.

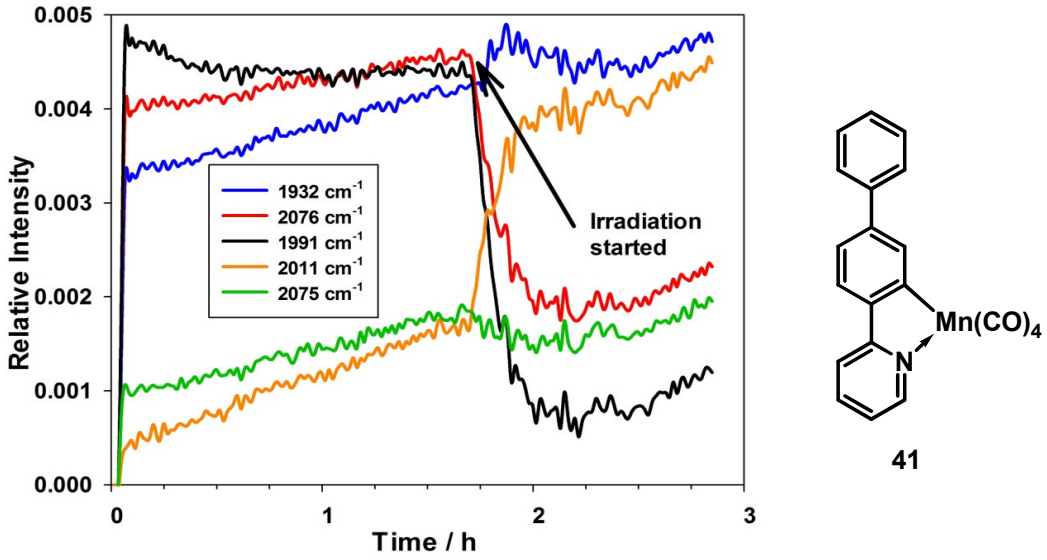

Figure 39. ReactIR™ profile showing the stability of complex **41** in the dark, followed by continuous irradiation at 365 nm with a 4 W TLC hand lamp.

Over a one hour 40 min period, The IR peaks associated with complex **41** do not significantly change in intensity. This suggests that this CO-RM is not a fast thermal CO-releaser at room temperature. When CO-RM **41** is irradiated after an initial period in the dark with light of wavelength 365 nm, many spectral changes occur. The most significant of these changes is the bleaching of the two peaks at 2076 and 1991 cm^{-1}. This suggests that photolysis is initiating loss of carbon monoxide from the complex. However in this situation all the CO is not lost as a new species is formed which is suggested by a new peak forming at 2011 cm^{-1}. The peak at 1932 cm^{-1} does not decrease in intensity which suggests that there is a peak in the new formed species in the same position as a CO-RM peak. This IR spectroscopic data shows that **41** is a photo-CO-RM in DMSO but does not provide details concerning the degraded products of the CO-RM. This has however been done with other CO-RMs in this project.

3.2 Correction details for the myoglobin assay

It has been established by ReactIR™ experiments that CO-RM **41** is not a significant thermally promoted CO-RM in a solution of DMSO and can be activated with light of wavelength 365 nm. More experiments were required to show that the complex was definitely releasing CO, and to assess whether there was any promotion of CO release by myoglobin. The quantification of CO release and assessment of reactivity towards a protein can be done in the same experiment using a myoglobin assay. This assay will also assess thermal stability in an aqueous solution, better representing physiological type conditions compared to the initial DMSO studies.

Myoglobin is a CO binding protein that shows clear spectroscopic changes when CO binds to the porphyrin metal centre.[94] The spectra in **Figure 40** shows myoglobin that has been deoxygenated with sodium dithionite, and then subsequently flushed with CO gas to generate Mb-CO.

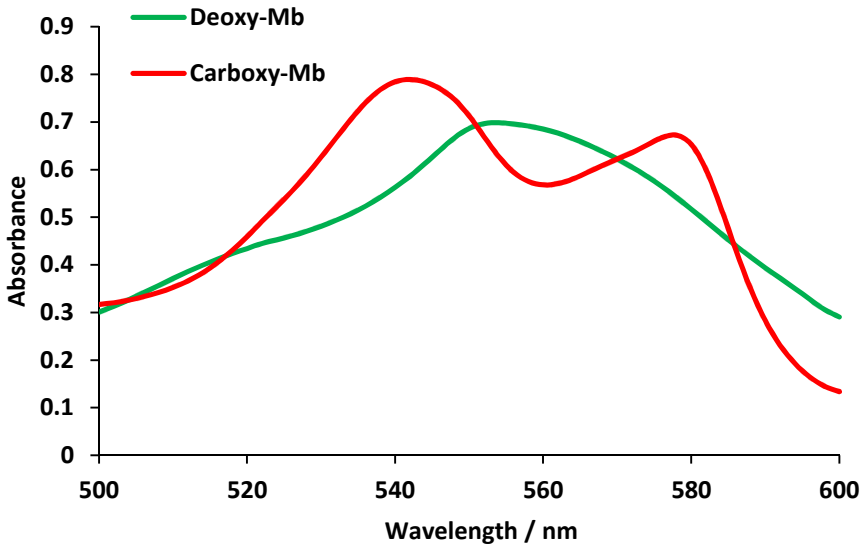

Figure 40. The UV spectra of 50 µM deoxy-Mb (green) and carboxy-Mb (red) in PBS buffer pH 7.4.

The data in **Figure 40** shows that there are clear spectral changes on the binding of CO to deoxy-Mb. The four isosbestic points suggest that there is a conversion from one species to another. Myoglobin has been used in an established assay to quantify the CO release from many reported CO-RMs.[51, 53, 80, 94]

3.2.1 Correction of the myoglobin assay due to insolubility

CO-RMs **37-41** are unfortunately only partially water soluble at 40 µM, and precipitation occurs when added to PBS buffer in a small amount of DMSO (0.5%). This is undesirable from a pharmacological point of view; however the main aim of this series of CO-RMs is to assess how varying the substituent affects the CO-release rates. Despite these CO-RMs being apolar, there are many water insoluble drugs on the market and solublising agents could be used to make them more compatible.[95]

The assessment of CO-release can be still performed with myoglobin due to the complex still being partially soluble. As the CO-RM is irradiated more complex will be pulled in to solution and CO-release can be quantified. For the CO-release to be quantitative, a correction procedure has been developed by Fairlamb and co-workers, and has been further refined here.[94] The full details of how the myoglobin assay is corrected is described in this section. It is not possible to discuss the CO-release data in detail until this correction has been performed.

Figure 41 shows the changes to the UV spectrum of a deoxy-myoglobin solution when a solution of CO-RM **37** in DMSO is added.

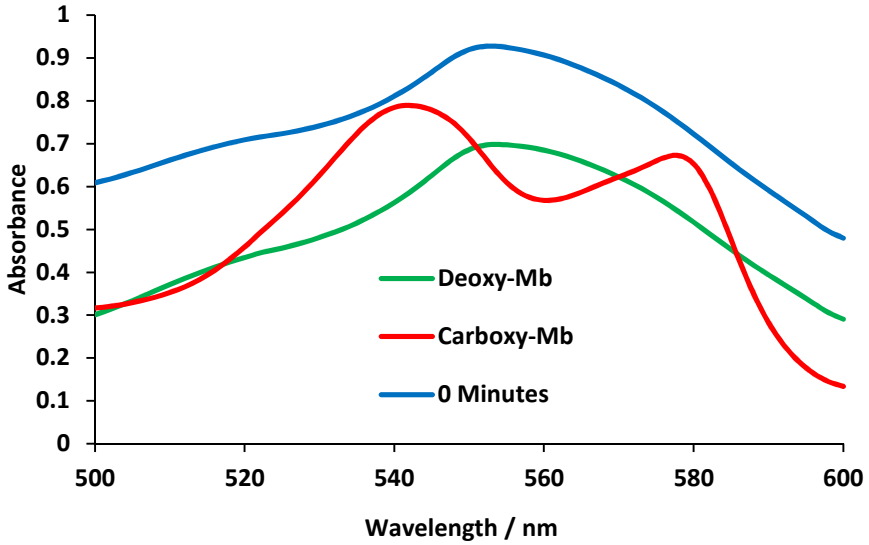

Figure 41. The UV spectra of 50 µM deoxy-Mb (green) and carboxy-Mb (red) and deoxy-Mb with 40 µM CO-RM **37** in PBS buffer pH 7.4.

On addition of CO-RM **37** to a solution of deoxy-Mb, there is a large increase in absorbance due to CO-RM precipitation. The important feature of this up-shifted spectrum is that it is still the same shape as the deoxy-Mb curve, suggesting that the complex has not released any CO on initial addition of CO-RM **37** to the myoglobin solution. The majority of additional absorbance from the CO-RM precipitation can be removed by fixing all the spectra at a reference point of 510 nm. This reference point is at the position of one of the isosbestic points and was chosen in line with a published literature procedure.[96] It is scientifically acceptable to fix all the spectra in the assay at this point, as regardless of how much CO is released, the absorbance will not change at 510 nm when considering the conversion of deoxy-Mb to carboxy-Mb. **Figure 42** shows the spectra from **Figure 41**, after they have been corrected at 510 nm.

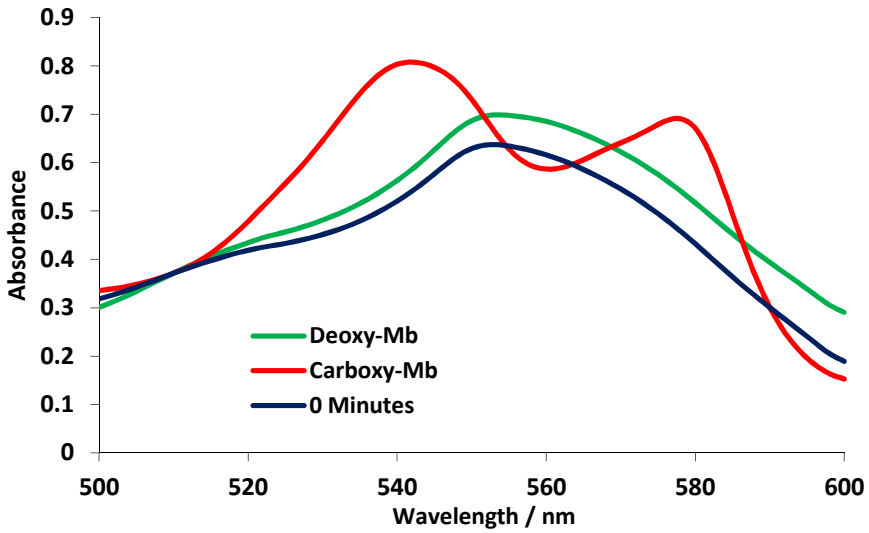

Figure 42. Spectra from **Figure 41** after correction at 510 nm (spectra adjusted to match the absorbance of deoxy-Mb at 510 nm).

After correction of the curves at 510 nm, the spectra just after addition of the CO-RM appears more like the deoxy-Mb curve that was taken without CO-RM. However there is a slight difference between them due to the precipitate from CO-RM **37**. The 510 nm correction shifts the whole spectrum down by the same amount. This does not correct for any precipitate that scatters/absorbs light to varying degrees across the 500–600 nm region. This difference also needs to be subtracted and this can be done by mapping-out the difference at the isosbestic points. The difference at the four isosbestic points creates four positions to which a curve can be fitted. The equation of the curve can be used to calculate difference across the whole spectrum. These values can then be subtracted from the spectrum. **Figure 43** shows the spectrum of the four isosbestic points representative of the difference between the two curves in **Figure 42**.

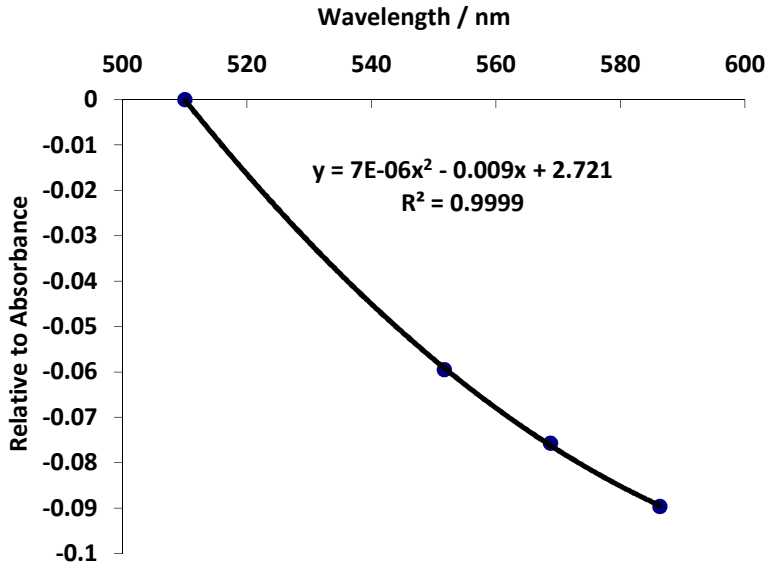

Figure 43. The difference between a deoxy-Mb spectra and a deoxy-Mb solution containing 40 μM CO-RM **37** mapped out at the isosbestic points.

Fitting a curve to the four points representing the difference between the two spectra, due to CO-RM interference, can provide a good fit, from which an equation can be determined. The curve was fitted using Sigmaplot[94] and new data points along the line between the first and last isosbestic point were generated at a 2 nm interval to match with the data obtained from the UV-Vis spectrometer. The data is only valid within the isosbestic points because the curve for correction is only fitted to values within the 510-585 nm range.

The relative absorbance here has ended up less than the original deoxy-Mb spectrum because it was originally higher up but has been pulled down during the correction at 510 nm. There happened to be less absorbance at the higher wavelength in the raw spectrum.

Once this data has been subtracted from the spectrum representing deoxy-Mb and 40 μM CO-RM **37**, the data in **Figure 44** was obtained.

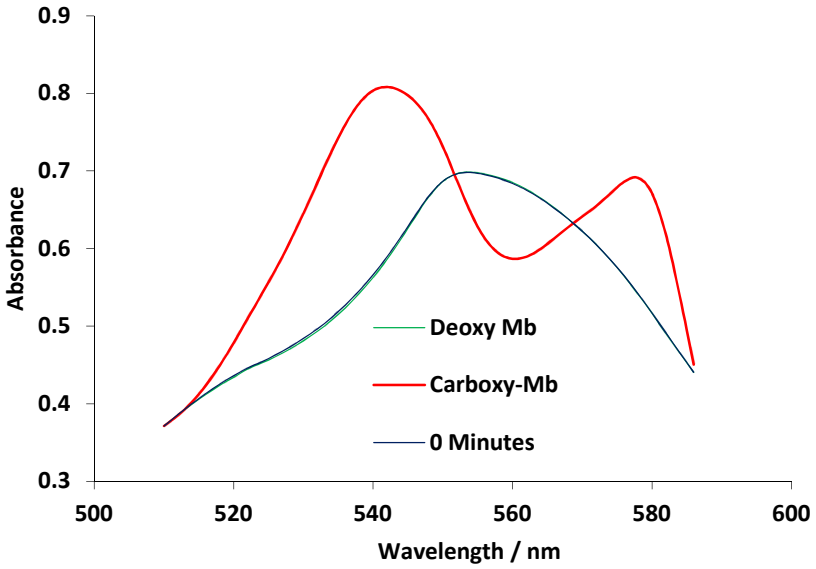

Figure 44. Fully corrected data for 40 µM CO-RM **37** in a myoglobin assay at zero minutes.

The myoglobin assay data that has been fully corrected fits the deoxy-myoglobin curve well as shown by **Figure 44**. The errors associated with this correction are calculated by taking the Mb-CO concentration and calculating a theoretical Mb-CO concentration. This is done by combining the carboxy-Mb and deoxy-Mb reference spectra by the appropriate percentage and comparing this to the corrected spectrum containing the CO-RM. If the total concentration of myoglobin is 50 µM, and at a particular time in the assay the measured value for Mb-CO is 25 µM, then 50% of the reference spectra for both deoxy-Mb and carboxy-Mb would be combined to provide a 'correct' spectrum. The difference between the 'correct' and measured spectra gives the error. **Figure 45** shows the error for the spectra acquired at zero minutes in the myoglobin assay for CO-RM **37**.

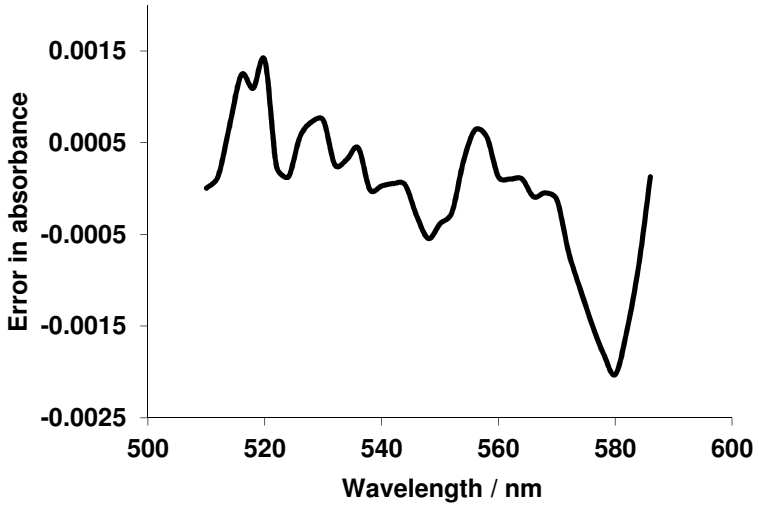

Figure 45. The error in absorbance for a fully corrected UV-Vis spectrum at zero minutes in a myoglobin assay with 40 μM CO-RM **37**. Error calculated as described above.

The error in the measurement at zero minutes does not go above 0.0021. This error represents less than 1% of the absorbance values measured at these wavelengths, demonstrating that the corrected spectrum closely matches the calculated spectrum. For the full myoglobin assay with CO-RM **37**, the aim was to assess if the CO-RM was stable in the presence of myoglobin. For this assay the solution was kept in the dark for a 45 minute period and then was irradiated with a 6 W TLC hand lamp emitting irradiation of wavelength 365 nm from above the solution. This would then confirm if the CO-RM was releasing CO on irradiation at the given wavelength.

The process described above for correcting the zero minute spectrum was then applied to all the spectra which were recorded every five minutes from this point. **Figure 46** shows all the UV-Vis spectra from the myoglobin assay with CO-RM **37** corrected only at 510 nm.

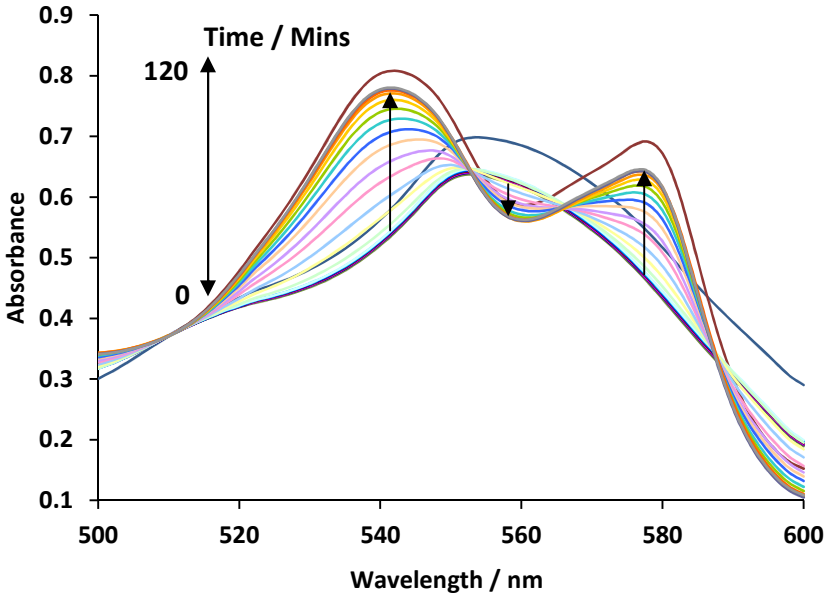

Figure 46. Myoglobin assay UV spectra with 40 µM CO-RM **37** corrected at 510 nm.

The data shows that all the isosbestic points for the experimental data do not yet match with the deoxy-Mb and Mb-CO reference curves. This is due to the difference in light scattering as previously discussed.

Figure 47 shows the four points curves (like in **Figure 43**) for each spectrum in the myoglobin assay of CO-RM **37**.

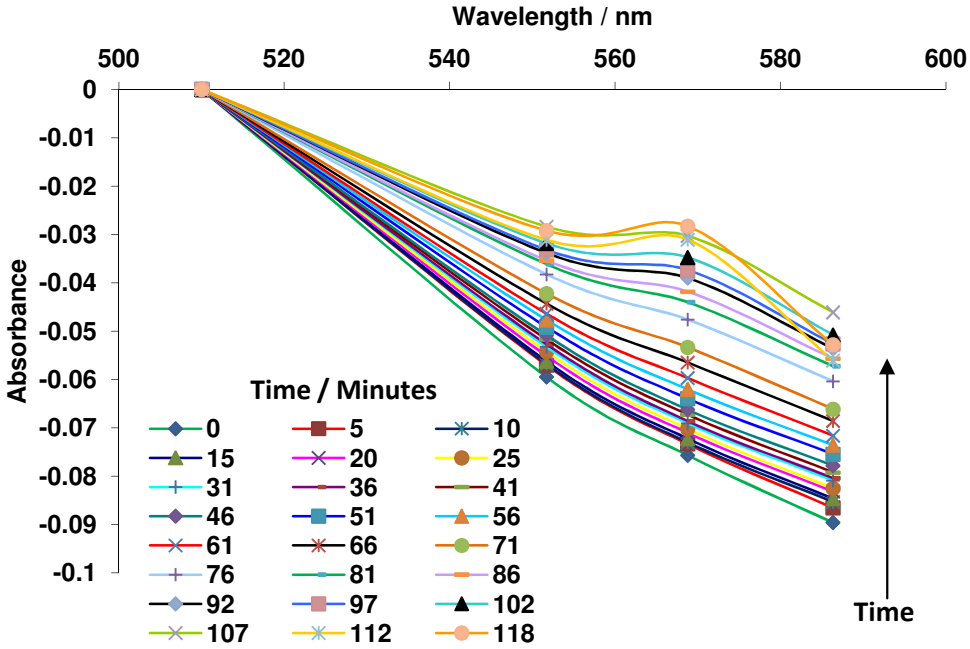

Figure 47. The four point correction curves for every spectra in the myoglobin assay of CO-RM **37**

All of the four point curves shown in **Figure 47** were put through the same non linear regression process as the four points shown in **Figure 43**. There were some problems with the curves towards the end of the assay (as Mb-CO evolves) due to a change in curve shape. The nature of turbidity changes as the assay progresses due to irradiation affecting the composition of the solution. The curves become more complex, and this makes it harder to fit a curve to the four points. Many different equations were used in the fitting process and the whole Sigmaplot™ equation library was used to find a curve with the most suitable fit. The most suitable fit was determined by how close the modelled curve was to the four isosbestic points. The key wavelength in these measurements is at 540 nm, as the absorbance at this wavelength is used to calculate the myoglobin concentrations. So the modelling between the first two isosbestic points (510 and 550 nm) was given priority. The non-linear regression curve for every spectrum is subtracted to generate a fully corrected curve and this is shown in **Figure 48**.

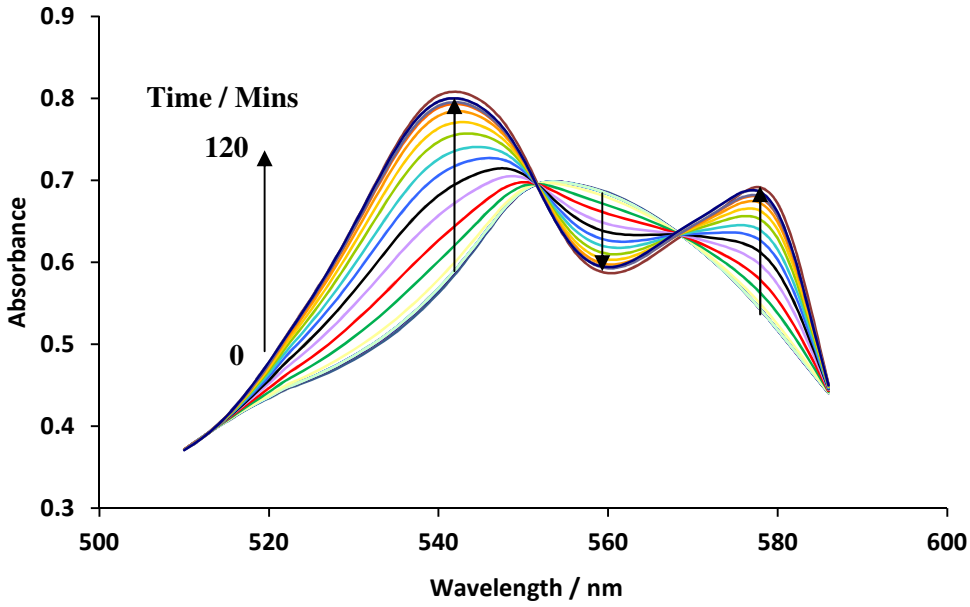

Figure 48. Fully corrected myoglobin assay data using 40 μM CO-RM **37**.

The corrected data matches well with the deoxy-Mb and carboxy-Mb curves, and all the isosbestic points match closely throughout the assay. It is clear from this experiment that there is a smooth conversion from deoxy-Mb to carboxy-Mb. This is because the conversion matches tightly around the isosbestic points with only variation between these values. **Figure 49** shows the errors for all the time points in the myoglobin assay of complex **37**.

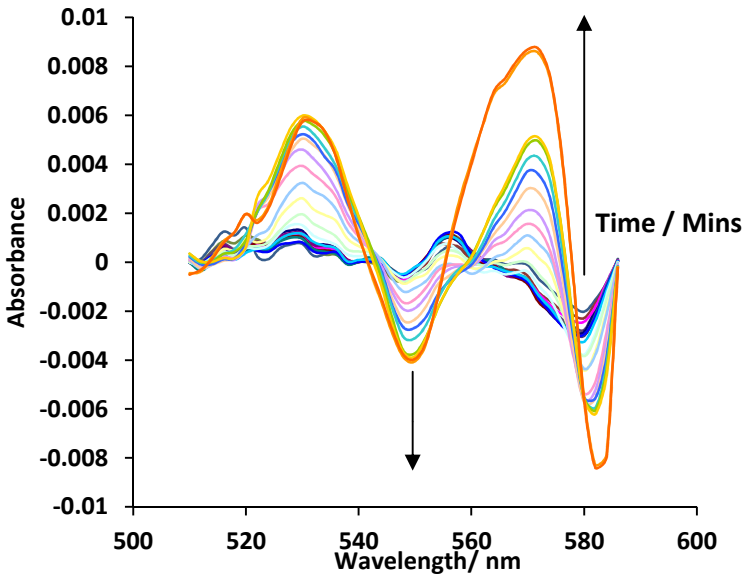

Figure 49. The error in absorbance for a fully corrected myoglobin assay using 40 μM CO-RM **37**.

The data in **Figure 49** shows that the error increases with time. The error is highest when fitting the four point curve for time points 112 and 118 mins. This is expected as the myoglobin will have degraded slightly over time by this point, and some shifts in the spectrum are expected. Considering the largest error in **Figure 49** of 0.0087 at 572 nm, and a corresponding absorbance at this wavelength of 0.661, the error equates to 1.3% of the absorbance measurement. This small percentage error shows that the myoglobin assay correction described, maps out the CO-RM absorbance effectively. The myoglobin assay was deemed a suitable technique for measuring the CO-releasing from these complexes and the information obtained can now be fully analysed. **Figure 50** below shows a plot of the measured Mb-CO concentration before any correction and after the full four point correction.

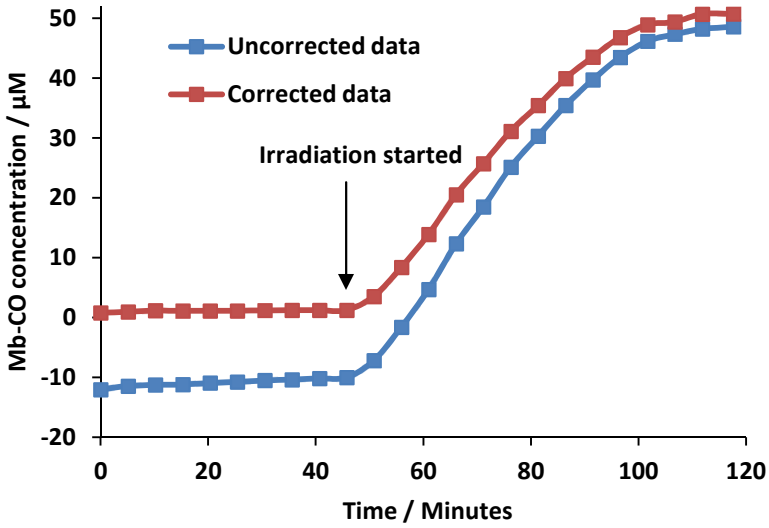

Figure 50. A plot of Mb-CO concentration vs. time for the myoglobin assay for 40 µM CO-RM **37**, showing raw and fully corrected data. Mb-CO concentration calculated from the absorbance at 540 nm.

Figure 50 shows that without the correction, the data are unsuitable for analysis as the calculations give a large negative concentration of Mb-CO. With the correction, the initial absorbance of Mb-CO is just above zero which is consistent with the fact that the initial spectrum appears like the deoxy-Mb spectrum. It is important to note that CO-RM **37** does not release any CO in the initial 45 mins dark period. When the solution was irradiated from above with a 6 W TLC lamp emitting irradiation of wavelength 365 nm, CO was released from the CO-RM and the concentration of Mb-CO increased. The total Mb-CO concentration observed at the end of the assay was 51 µM, representing myoglobin saturation with CO. This suggests that 40 µM CO-RM **37** is releasing more than 40 µM CO. If the CO-RM is releasing more than one CO per molecule of CO-RM, then this can make a potentially efficient CO-releasing molecule. This is because lower concentrations are required to administer a given concentration of CO. This assay shows that this CO-RM is a photo-CO-RM and not an ET-CO-RM with respect to myoglobin. The CO-RM does not degrade in the presence of sodium dithionite which has been previously shown to induce CO-release from CO-RMs.[97] This assay confirms that this complex is robust under aqueous and reducing conditions.

CO-RM **37** is structurally similar to the $[Mn(CO)_4\{S_2CNMe(CH_2CO_2H)\}]$ (**7**) prepared by Mann and co-workers.[58] CO-RM **7** is thermally stable in buffer solution for long periods of time but when it is exposed to myoglobin, CO-release is then observed. The 2-phenylpyridine-based CO-RM **37** does not release CO in solution with myoglobin or sodium dithionite until irradiated with light. This suggests that there is something significantly different about the bonding in the phenylpyridine complex that stops the myoglobin binding up CO. The covalent carbon–

manganese bond may be stronger than that of a thioacetate type ligand. This may help keep the complex stable in the presence of myoglobin. This is an encouraging result as it gives control over when the CO is released.

There are however some limitations when it comes to correcting the myoglobin assay and this includes the fact that only four points of correction are used to remove any interference. This means that it can be difficult to correct for the any slight changes that occur in between these points. The error analysis in this project shows that correction closely maps the calculated spectra. This may not always be the case and great care needs to be taken. If there are large un-predictable changes in absorbances that need to be corrected for then this analysis could be unsuitable.

Significant human input is required for the correction procedure. This includes analysing the UV spectra qualitatively to assess if the imperfections in the spectra are due to precipitation or from the formation of new species/reaction with myoglobin. It also requires observation of solutions being analysed to assess for visible signs of precipitation. If there is too much interference in the spectra then the myoglobin assay is unsuitable for analysis. In the analysis discussed in this section. The shift up due to CO-RM precipitation still results in a curve shaped very much like the deoxy-Mb curve demonstrating little if any initial interaction of the myoglobin with the added CO-RM.

Also as shown in **Figure 50**, if the uncorrected curve was considered, then the change in Mb-CO concentration would exceed the concentration of Mb-CO in the solution and this needs correcting for considering that a negative concentration of Mb-CO does not make sense. It is also important to consider that because this change exceeds the concentration of Mb-CO present; it means that the rate of CO release would be altered. Calculating the half-life of CO-release requires data points up to half the concentration of CO-RM used and the rate would differ. The interference from CO-RM precipitation in the UV-spectra needs to be removed to allow accurate and comparable half-lives to be calculated.

The myoglobin assay correction is necessary so that comparison within a series can be performed. One may want to consider that the precipitate may dissolve at different rates across a series, but a standard method of analysis needed to be established. This method was further developed from an established widely cited literature procedure.[96]

3.2.2 Two part non-linear myoglobin assay correction

As mentioned in section **3.2.1**, towards the end of the assay the smooth curve that represents the CO-RM absorbance/interference gets more complex. Rather than a smooth decrease with increasing wavelength, due to changes that occur on CO-release there is more of an S-shaped curve. This is difficult to fit with just one equation and results in increase error following four point correction. In this situation the four points can be fitted using two separate equations. The first equation fits a line to the first three points. The two segment linear equation in Sigmaplot software fits two linear lines to the points in one go with a fairly smooth transition between the intermediate point. This is performed for the first three isosbestic points. The correction between the 3rd and 4th isosbestic point can then be mapped out using a simple linear y = mx + c equation. **Figure 51** shows the isosbestic points that need to be mapped out for correction for a typical set of CO-release curves (from CO-RM **77** discussed in section **7**).

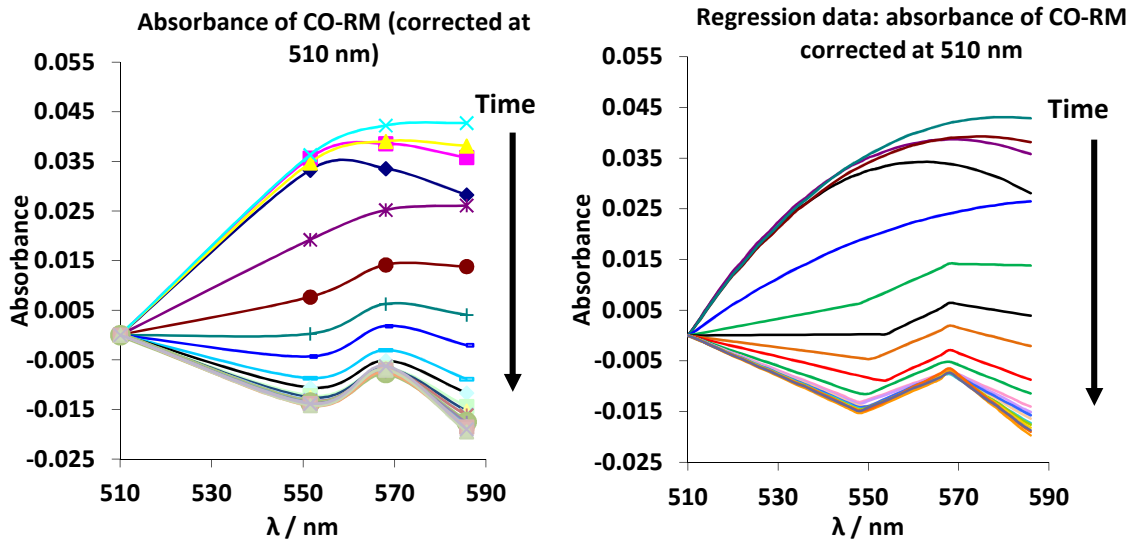

Figure 51. Comparison of absorbance/precipitation of CO-RM **77** in a myoglobin assay with the mapped absorbance using non-linear regression so that 2 nm spaced data points can be generated for spectral correction.

As time progresses it is clear that an S-shaped curve develops as this particular CO-RM is irradiated in solution. A quadratic type equation will typically map out the first few curves in this series but will not accurately model the later ones. Using the two segment linear equations to correct from 510 to 568 nm and the linear equation from 568 nm to 586 nm gives a closely modelled absorbance for each CO-RM/by-product interference.

Figure **52** shows the errors from the corrected data in **Figure 51**.

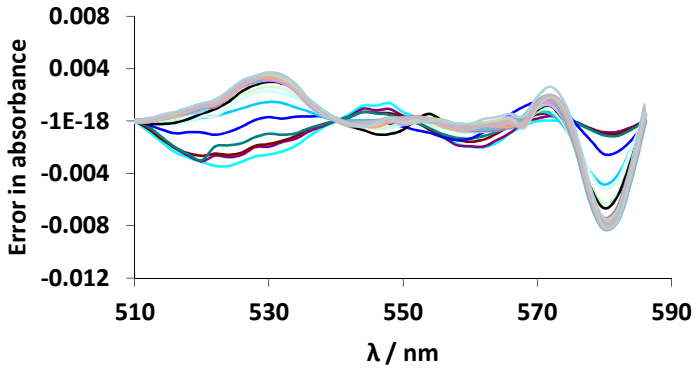

Figure 52. The error in absorbance after a correction of a myoglobin assay using CO-RM **77**

The S shaped curves are modelled well as determined by the error above. The error here is lower compared to the errors shown in **Figure 49**; showing that using the two-part correction is efficient when the four points cannot be accurately modelled with a single equation. The correction at 510 nm removes the majority of the CO-RM interference/absorbance, and the two part correction removes the remaining differences. This correction procedure allows for interference in the UV-Vis spectra to be removed from this assay and produces accurate data with relatively small errors.

3.3 Discussion of CO-release from CO-RMs 37-41

With all the correction procedures established in the myoglobin assay that is used in this work, all of the CO-RMs in this initial phenylpyridine series can be corrected and the data can be analysed. **Figure 53** shows data from myoglobin assays using 40 µM CO-RMs **37-41** in each separate experiment. In these myoglobin assays a 6 W TLC lamp emitting light of wavelength 365 nm was used. Irradiation was initiated after 45 mins and was used for two minutes every five minute period to allow for a spectrum to be recorded.

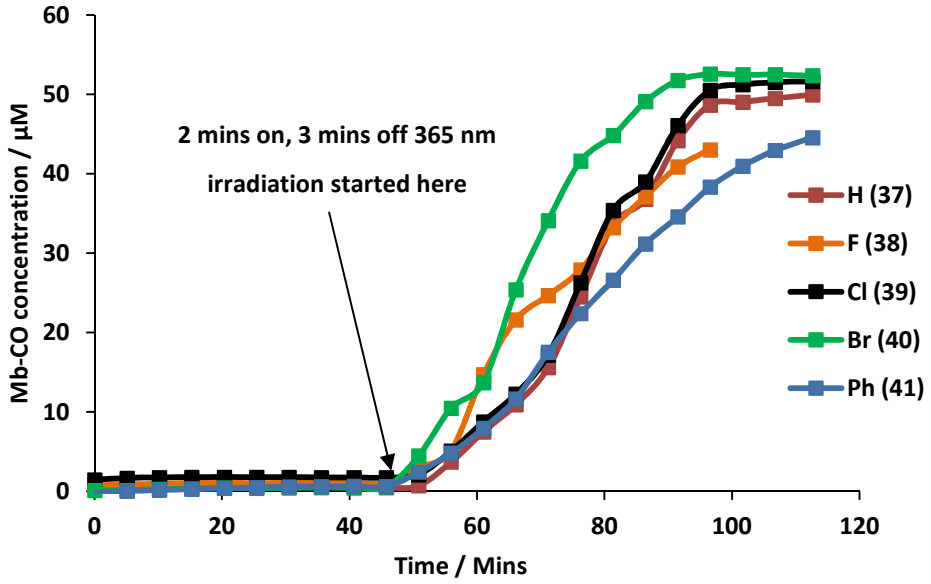

Figure 53. Myoglobin assays using 50 µM myoglobin with 40 µM of each CO-RM at 37 °C. Solutions irradiated from above after 45 mins with a 6 W TLC lamp emitting light of wavelength 365 nm above the sample. Irradiation on for two mins every five minute period.

The data in **Figure 53** shows that the series of substituted phenylpyridine CO-RMs are photo-activated CO-releasing molecules. During the dark period (45 mins) for CO-RMs **37**-**41**, there is no CO-release observed. The CO-RMs are all stable in the presence of myoglobin and phosphate buffered saline. When the solutions were irradiated, conversion to carboxy-Mb is observed in all cases. The correction procedures used yielded spectra with well defined isosbestic points in all cases. The half-life ($t_{½}$) has been calculated from these data and are shown in **Figure 54**. The half-life for CO-release from a CO-RM is calculated by assessing how many minutes from initiating irradiation it takes to release half the concentration of CO compared to the CO-RM concentration used. This is the standard method of reporting the half-life because a CO-RM may release multiple CO ligands. The kinetics shown in **Figure 53** are a combination of several release rates and so the discussed half-life determination method is used. A t = 0 value was taken

as the start of irradiation as no significant CO-release was detected until this point by a thermal or enzyme-triggered mechanism.[94]

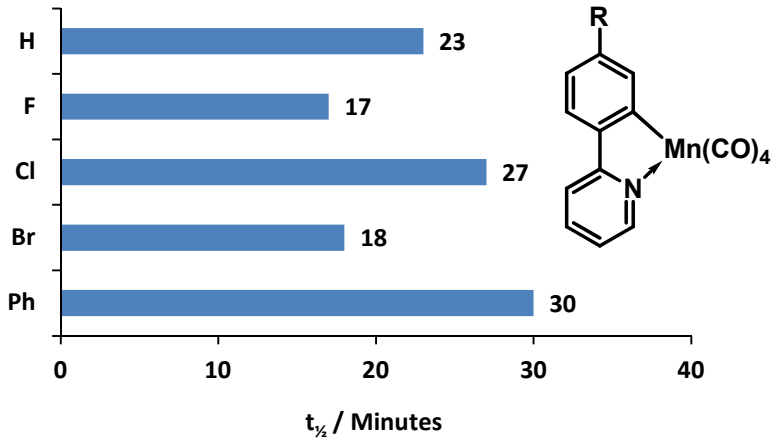

Figure 54. Half-life values for CO-release from CO-RMs **37**-**41**, t = 0 taken as the start of irradiation with a 6 W TLC lamp emitting light of wavelength 365 nm. Irradiation carried out for two mins per five mins.

Under the same irradiation conditions, it is clear that varying the substituent at the *para*-position on the phenyl ring alters the half-life for CO-release. CO-RM **38** (F) and **40** (Br) release faster than the other CO-RMs with half-lives of 17 and 18 mins respectively. The introduction of an extra phenyl ring in to CO-RM **41** appears to have lowered the half life. It is likely that this extra apolar substituent has decreased aqueous solubility and reduced the amount of CO-RM available in solution for efficient irradiation. A similar amount of Mb-CO is generated with CO-RMs **37**-**41** however it takes different amounts of time to achieve this depending on the substituent and this is important The increased amount of precipitation will also scatter more light reducing the amount of light that penetrates further into the solution.

Molar extinction coefficient determination was also carried out on these complexes at 330 nm to see if altering the substituent changed the coefficient to some extent. A high molar absorption coefficient of the band associated with CO-release could lead to more efficient CO-release. **Table 9** shows the molar extinction coefficients for CO-RMs **37**-**41**.

Table 9. Molar extinction coefficients (ε) for CO-RMs **37**-**41** in acetonitrile at 330 nm.

Compound	ε / mol^{-1} dm^3 cm^{-1} (330 nm)	R^2
37 (H)	4054 ± 96	0.9997
38 (F)	4522 ± 83	0.9998
39 (Cl)	4534 ± 163	0.9993
40 (Br)	4872 ± 25	1
41 (Ph)	13166 ± 374	0.9996

Substituting the *para*-position of the phenyl ring on the parent phenyl pyridine complex with a halogen increases the molar extinction coefficient by a maximum of 20% (**40**). This is not surprising considering that this substituent does not increase conjugation or significantly alter the electronic character of the system. Introduction of another phenyl ring (CO-RM **41**) which is in conjugation with the original motif, increases the molar extinction coefficient over three fold compared to the parent complex (**37**). This is a significant change and if the solubility of this complex was not reduced by decreasing polarity, it is expected that there would be a significantly increased CO-release rate.

The half-lives in this series of CO-RMs vary to some degree, however the CO-RMs are stable in aqueous solution *ca.* 45 mins. The CO-RMs do not release CO until irradiation is initiated. It is also important to note that the half lives reported are for the specific conditions used. If the sample was irradiated for longer in one period then the half-life for these complexes would be shorter. It is important to correlate irradiation time and power with the CO-release rates.

3.3.1 Re-evaluation of CO-RMs 39 and 40 using an LED irradiation system.

In contrast to the careful experimental conditions typically used in thermal reactions, there is less focus on how light is used as a reaction parameter. As shown in **Figure 53**, light is the most important parameter in this kinetic study when determining the CO-release rates. The wavelength, intensity, and distance of the source from the solution all significantly contribute to the kinetic data. This applies not only to a myoglobin assay, but to any reaction that requires significant contribution of light to make the reaction proceed.

With this knowledge in mind, a cost effective LED system was developed to address the general issues associated with using a TLC lamp. When using a TLC hand-lamp the wavelength and intensity are fixed and the irradiation is emitted over a wide cone angle due to the lamp being 10

cm above the cuvette. A small LED with dimensions of only 4 mm × 4 mm allows development of a system that can clip directly on to a UV cuvette (**Figure 55**).

Figure 55. The LED irradiation cap mounted on a UV-Vis cuvette

The LED in **Figure 55** is close to the sample meaning that a large proportion of the light passes through the sample, increasing efficiency. The LEDs can operate at a power consumption of up to 5 W, which is similar to that of a hand lamp. This is a high power consumption considering the size of the LED relative to a TLC lamp.

A control unit was also developed, which can automatically control when the LED comes on and off. This helps to reduce error arising from manual control (**Figure 56**).

Figure 56. The LED control unit developed at the University of York.

The device in **Figure 56** monitors and controls the LED power consumption. This means that the device can repeatedly deliver the same amount of light. This system was used in further CO-release studies.

With the new LED system developed, CO-RMs **39** and **40** were re-tested in the myoglobin assay to compare the efficiency of the LED to the TLC lamp. **Figure 57** shows myoglobin assays with 40 μM CO-RM.

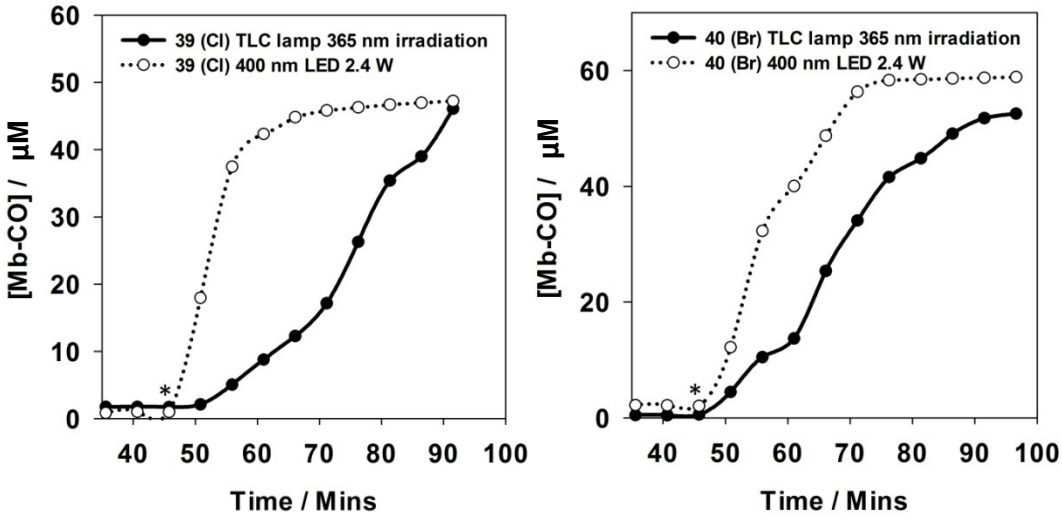

Figure 57. CO-release from 40 μM CO-RM **39**(left) and **40** (right) using 50–60 μM myoglobin. Irradiation with 365 nm TLC lamp and LED (400 nm, 2.4 W). On for 2m per 5m period. * indicates start of irradiation cycles. 0-35 mins omitted for clarity as it stays close to zero throughout this period.

The myoglobin assays in **Figure 57** demonstrate that the use of a 400 nm LED is more efficient than a TLC lamp. The LED was set to a power consumption of 2.4 W which is less than 50% of the output of a TLC lamp. With less power consumption than a TLC lamp, the CO-release rate from both CO-RM **39** and **40** is much faster when irradiation from an LED is used. With CO-RM **39** the myoglobin is saturated 20 mins earlier when the LED is used. The half-life for CO-RM **39** was reduced from 27 to 6 mins, and for CO-RM **40** is cut from 18 to 8 mins. This is a significant change and highlights the importance of the light source.

These half-life values were determined using an LED emitting irradiation of wavleength 400 nm, with a power consumption of 2.4 W light. The light intensity could easily be increased further to shorten the half-life if required (this is shown with CO-RM **47** in section **4**). This data clearly shows that the half-life of these CO-RMs is variable depending on what type of irradiation system is used. This provides an extra degree of control that some thermo- and enzyme-triggered-CO-RMs cannot provide.

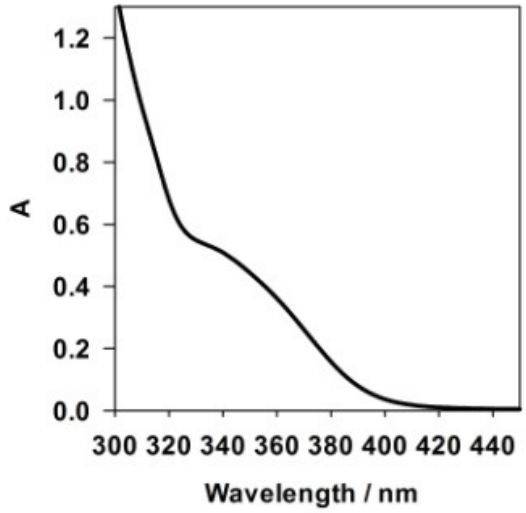

Figure 58. UV spectrum in MeCN at 1.125×10^{-4} mol dm^{-3} for CO-RM **40**(Br)

The UV-Vis spectrum in **Figure 58** shows that CO-RM **40** has a weak absorbance at 400 nm. The 400 nm LED has a spectral width of ± 20 nm, with maximum intensity at 400 nm. This means that a large portion of the light from the LED is not being absorbed. Yet fast conversion from deoxy-Mb to carboxy-Mb is observed. CO-release is still faster than using the TLC lamp. The LED light is being absorbed at a wavelength with a lower absorption coefficient compared with 365 nm, emphasising how efficient the $Mn(CO)_4$ motif is at releasing CO on photolysis. Even though some of the 400 nm light is not being absorbed, the use of 400 nm light is much more desirable since it is less likely to damage important biological molecules compared to 365 nm light.

It was then necessary to quantify how many molecules of CO are released from CO-RMs **39** and **40**. This was done by using a substoichiometric concentration of CO-RM relative to the concentration of myoglobin in an assay. The amount of CO-RM used was lower than the maximum possible amount of CO that could be released (four with an $Mn(CO)_4$ system), so that myoglobin saturation was not possible. **Figure 59** shows CO-release profiles from CO-RMs **39** and **40** at only 10 μM in a myoglobin assay.

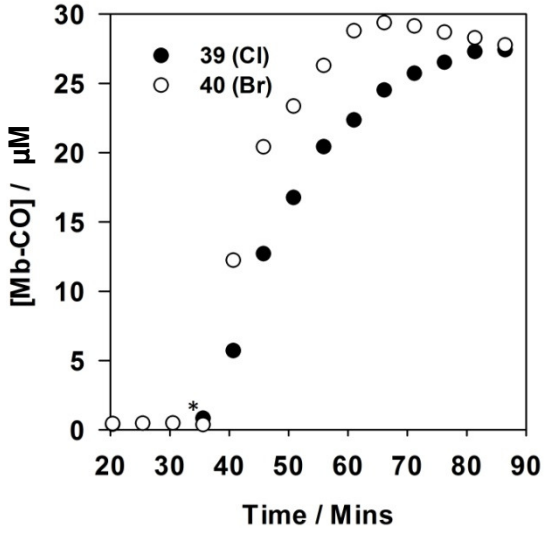

Figure 59. CO release from 10 µM CO-RMs **39** and **40** using 50-60 µM myoglobin in a myoglobin assay. Irradiation with LED (400 nm, 2.4 W). On for two mins per five min period. * indicates start of irradiation cycles. CO-release profiles carried out by Conrad Wagner

The CO-release profiles in **Figure 59** show that both CO-RMs release almost three molecules of CO per molecule of CO-RM. This is advantageous compared to ruthenium-based CO-RM-**3** in the literature that only releases one CO,[80] as a lower concentration of CO-RM is required to get the same amount of CO. The kinetic curves are much smoother with the automatically timed LED system. The TLC lamp studies were still essential in gaining initial information but moving forward, the LED system is much more suited to these kinetic studies.

3.4 Palladium-mediated cross-coupling on a CO-RM

CO-RMs **39** and **40** contain a halide substitent, providing the opportunity to functionalise these CO-RMs and improve their properties. This has been previously carried out on a tricarbonyl iron pyrone complex using palladium chemistry.[73] A palladium-mediated cross-coupling has been carried out directly on CO-RM **40** using phenyl boronic acid to give CO-RM **41** *via* a different route to what was previously used in this project, based on a modified literature procedure.[98] This demonstrates that this CO-RM is directly functionisable. **Scheme 13** shows the conditions developed by Buchwald and co-workers with some modifiations to carry out this reaction on potentially sensitive CO-RM **40**.

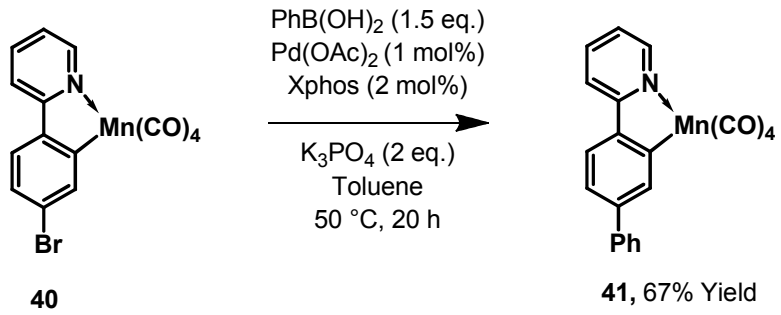

40 **41,** 67% Yield

Scheme 13. Modified Suzuki–Buchwald conditions carried out on **40** to prepare CO-RM **41** *via* an alternative route. Conditions developed in collaboration with Joshua Bray.

Despite the presence of base, phosphine ligand and palladium catalyst; it is possible to carry out a cross-coupling reaction directly on CO-RM **40**. It is impressive that these conditions work at 50 °C lower than for similar organic substrates reported in the literature (100 °C).[98] Performing this reaction at higher temperature (70 °C) in an attempt to improve the yield, resulted in degradation of both the starting material and cross coupled product to their corresponding free ligands. The lower temperature is necessary to maintain stability of the cyclometalled species. The reactivity of the C–Br bond appears activated under the conditions in **Scheme 13**. With the manganese centre back-bonding into the π^* orbtial on the metal carbonyl, it is expected that the manganese atom is then electron deficicent. This results in withdrawal of electron density out of the ring and subsequently the C–Br bond. This type of cross-coupling reaction has not been previously performed on a manganese complex, such as CO-RM **40** before.

The product from **Scheme 13** was already previously prepared by reaction of ligand **35** with $BnMn(CO)_5$ (**42**) and comparison of ^1H and ^{13}C NMR, IR and LIFDI-MS data with the original

reported synthesis confirms the presence of cross-coupled product. This reaction was carried out as an example to show that the cross-coupling conditions are effective.

3.5 Conclusions on initial phenylpyridine CO-RM series

This initial CO-RM series establishes that the phenylpyridine-$Mn(CO)_4$ motif has the potential to progress into further CO-RM studies. Synthesis of CO-RMs **37-41** was carried out in two linear steps; which is a short route to some encouraging structural motifs. The CO-RMs were characterised using a variety of techniques demonstrating high purity, and there can be confidence in the assigned structures. Group theory analysis was also carried out to demonstrate that CO-RMs **37-41** had the correct number of CO stretches in their IR spectra: this is an useful technique when working with metal carbonyl complexes. It is essential that CO-RMs taken forward for further study can be made in high purity to avoid false positive or negative results.

CO-release quantification using a myoglobin assay has shown that the CO-RMs **37**-**41** are robust photo-CO-RMs. They have controllable half-lives making the motif suitable for further development. The myoglobin assay procedure has been optimised for CO-release quantification with CO-RMs that precipitate at the required concentration and assays were shown to have a low percentage of error compared to the absorbances measured. This gives a degree of confidence and reliability to the Mb-CO concentrations obtained from these assays. Some expertise and careful judgment is required when fitting the curves to the four isobestic points during correction procedures. This procedure is not trivial, but yields high-quality final results.

Unfortunately there is a degree of precipitation in aqueous medium with 40 μM CO-RMs **37-41**. This is a serious issue that had to be addressed, and was carried out by further functionalisation shown in section **4**. Even though CO-RMs **37**-**41** are not as drug-like as other molecules synthesised in this project, they were essential for the development of all the other CO-RMs.

4 Developement of water compatible CO-RMs

4.1 Synthesis and characterisation of ester CO-RM 45

With the knowledge that the initial phenylpyridine CO-RM series **37**-**41** releases CO efficiently under photochemical conditions, the next step in this project was to develop more polar CO-RMs. These need to be either water soluble or compatible (i.e. remains in solution on addition to aqueous solution in a small amount of DMSO). DMSO is commonly used in biological testing at low concentrations and there are many solubilising agents available in the pharmaceutical industry that can be used as a DMSO replacement.[95]

The first step in the synthesis of a new series of CO-RMs was to prepare more polar substituted phenylpyridine ligands. A 2-(4-hydroxy-phenyl)pyridine **43** scaffold was prepared using a Suzuki–Miyaura reaction and the details are shown in **Scheme 14**.

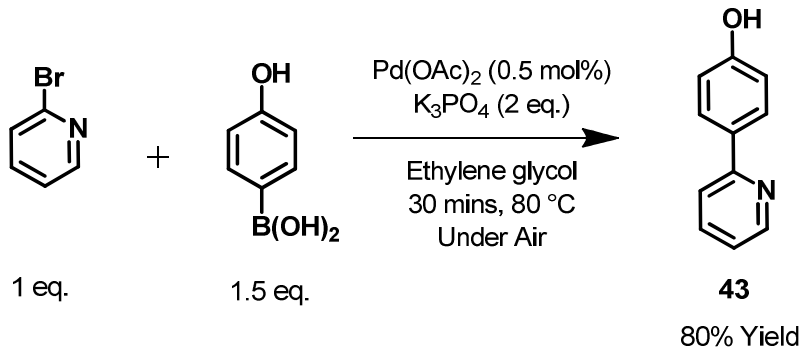

Scheme 14. The synthesis of 2-(4-hydroxy-phenyl)pyridine (**43**)

The procedure developed by Liu and co-workers is efficient at coupling bromopyridine substrates with various boronic acids:[92] Polar *para*-hydroxyphenylboronic acid is tolerated well in this reaction giving an 80% yield after only 30 minutes reaction. Ligand **43** was then used in a Williamson ether synthesis to extend the molecule further, and **Scheme 15** shows the details for the synthesis.[99]

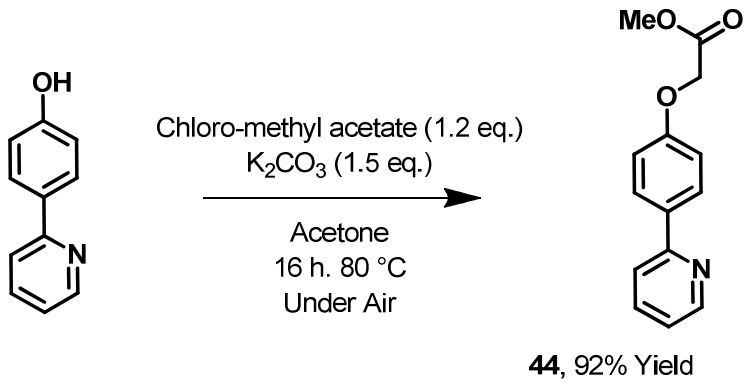

Scheme 15. The synthesis of methyl [4-(pyridin-2-yl)phenoxy]acetate **44**.

Zhang and co-workers showed that reaction of similar substrates in acetone gave poor yields using one equivalent of chloro-methylacetate and K_2CO_3.[99] Slight adjustments to the procedure gave **44** in 92% Yield. The use of 1.2 eq. of chloromethyl acetate and 1.5 eq. of K_2CO_3 in acetone in a sealed thick-walled round-bottomed flask provided optimal conditions for this synthesis. Sealing the flask allowed the acetone to reach higher temperatures and the reaction then went to completion, as determined by TLC analysis. The low boiling point of both acetone and chloromethyl acetate makes the removal of unwanted starting material under reduced pressure straight forward. Only an extraction workup was required to obtain the pure product **44**.

Compound **44** was then treated with $BnMn(CO)_5$ (**42**) in toluene in a similar fashion to the preparation of CO-RMs **37-41**. Toluene was used as an alternative solvent in this reaction due to poor solubility of **44** in hexane. The reaction did not go to full completion and column chromatography was required to remove small amounts of remaining $BnMn(CO)_5$ (**42**), and unreacted ligand **44**. The new ester CO-RM **45** was isolated with a yield of 81%.

The ^{1}H NMR of CO-RM **45** shows similar changes on complexation (**Figure 60**).

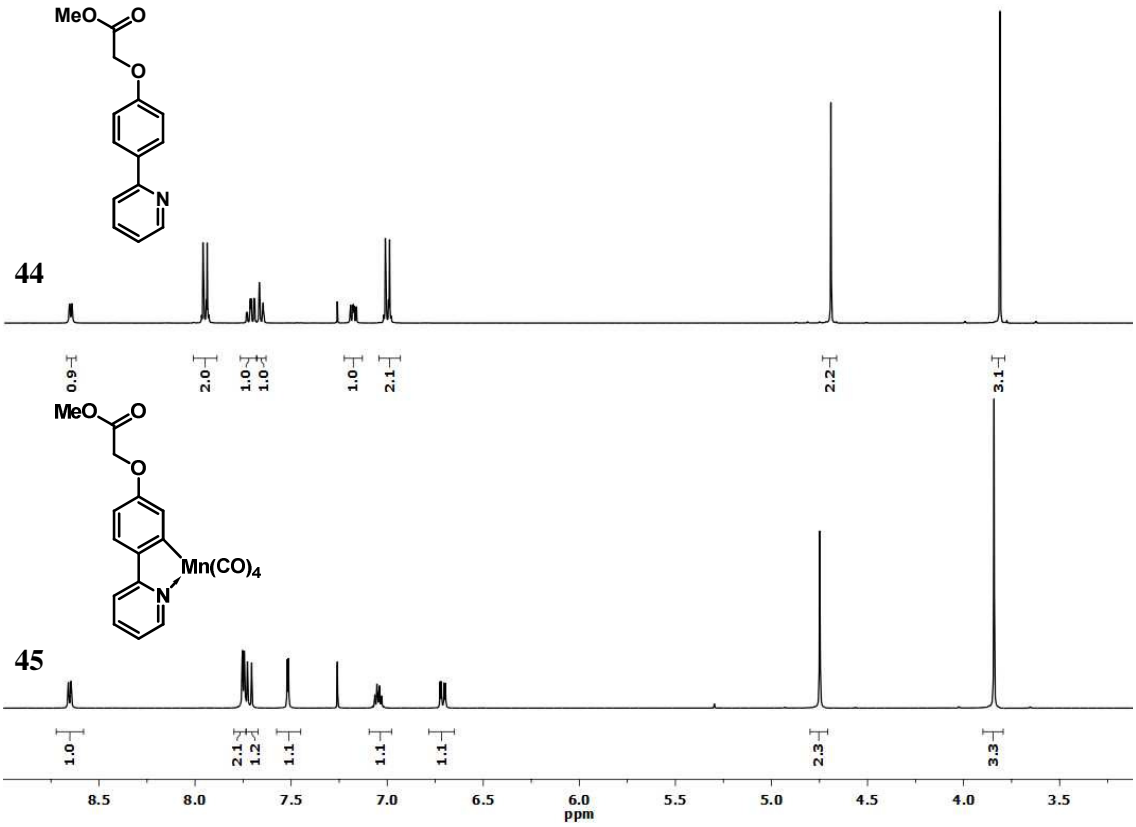

Figure 60. The 400 MHz ^{1}H NMR spectra in $CDCl_3$ of ligand **44** (top) and CO-RM **45** (bottom) at 300 K.

The NMR data in **Figure 60** shows that on complexation, the loss of the *para*-substituted aromatic splitting is observed. The two doublets at 6.99 and 7.94 ppm (^{3}J = 9.0 Hz) are not present in the spectra of CO-RM **45**. The IR spectrum of CO-RM **45** shows four bands in a similar position as for CO-RMs **37**-**41**. Crystals of **45** were obtained by diffusion of hexane into a solution of **45** in CH_2Cl_2 which were analysed by X-ray crystallography, and the solved X-ray structure is shown in **Figure 61**.

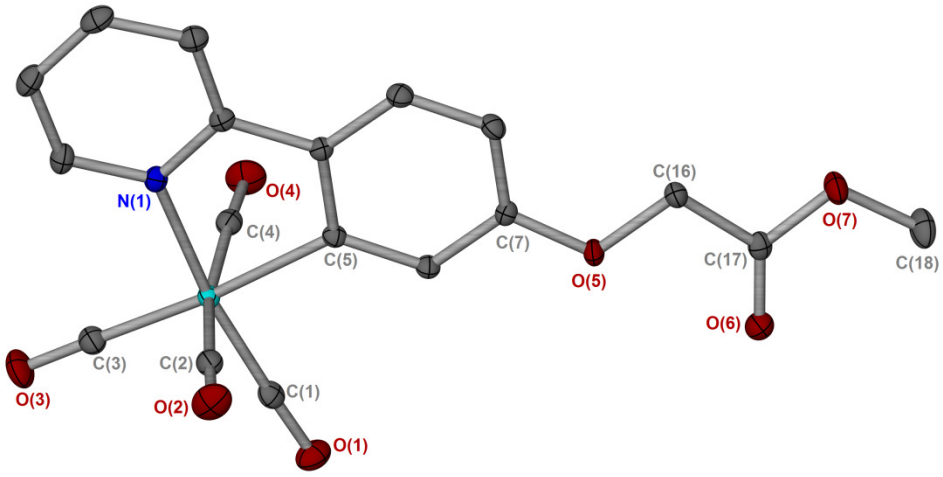

Figure 61. X-ray crystal structure of CO-RM **45**. Atoms displayed as ellipsoids at 50% probability. Hydrogen atoms omitted for clarity. Selected bond lengths (Å) and angles(°): Mn(1)-N(1) = 2.0672(11), Mn(1)-C(1) = 1.8148(14), Mn(1)-C(2) = 1.8660(14), Mn(1)-C(3) = 1.8263(14), Mn(1)-C(4) = 1.8527(14), Mn(1)-C(5) = 2.0528(13); N(1)-Mn(1)-C(1) = 172.00(5), N(1)-Mn(1)-C(2) = 88.23(5), N(1)-Mn(1)-C(3) = 95.30(5), N(1)-Mn(1)-C(4) =90.38(5), N(1)-Mn(1)-C(5) = 80.08(5), C(2)-Mn(1)-C(4) =169.52(6), C(1)-Mn(1)-C(3) = 92.67(6).

The X-Ray structure in **Figure 61** shows that the desired compound has been successfully synthesised. It also shows that the distorted geometry in CO-RM **45** is different to that of bromo-substituted CO-RM **40**. The N-Mn-C(5) bond angle of 80.08(5)° indicates a similar 'pincer' effect from the phenylpyridine ligand in this complex as observed in X-ray structure of CO-RM **40** .

4.1.1 CO-release from ester CO-RM 45

Having successfully prepared CO-RM **45**, the next step was to evaluate the CO-release rate to see if there was improved solubility and increased CO-release rates. **Figure 62** shows details of a myoglobin assay using 40 µM CO-RM **45**. A 6 W TLC hand lamp emitting light of wavelength 365 nm was used in these initial studies to allow a comparison with the data from the initial series of complexes.

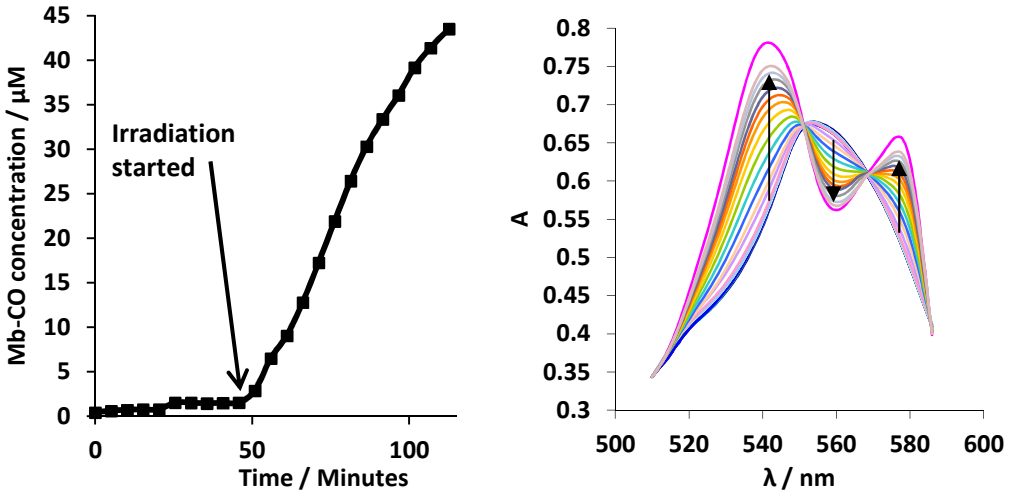

Figure 62. Left: CO-release profile for CO-RM **45** at 40 µM in PBS buffer pH 7.4. Irradiation with a 6 W 365 nm TLC hand lamp for 2 mins per 5 min period. Right: Full UV/vis spectra from 510-586 nm after four point correction.

The data in **Figure 62** shows that CO-RM **45** releases CO in a similar fashion to the previous series of complexes. Unfortunately the ester group is not polar enough to solubilise CO-RM **45** in solution and some precipitation was observed as seen previously with CO-RMs **37-41**. A half-life for CO-release of 29 mins was observed for this complex. This is similar to bi-phenylpyridine CO-RM **41**. On the other hand, it is promising that this molecule still behaves like a photo-CO-RM. Introduction of even more complex functionality does not affect the CO-RMs reactivity to aqueous buffer solution and myoglobin.

4.2 Development and synthesis of acid-containing CO-RM 47

The myoglobin assay for CO-RM **45** showed that a more polar moiety was required to make a water compatible CO-RM. The approach taken was to consider hydrolysing the methyl ester in CO-RM **45** to give carboxylic acid functionality. This functional group should be deprotonated in PBS buffer at pH 7.4 and the complex should be more water soluble. This was a promising strategy because only one reaction from CO-RM **45** could yield a structure with considerably different physical properties.

Initial synthetic studies involved attempting hydrolysis of ligand **44** to develop a set of conditions that could then be used on ester-containing CO-RM **45.** In order to circumvent possible problems during ester hydrolysis, a mild procedure developed by Karlsson and co-workers that can

hydrolyse esters at ambient temperature was utilised.[100] **Scheme 16** shows the conditions used to hydrolyse the methyl ester in ligand **44**.

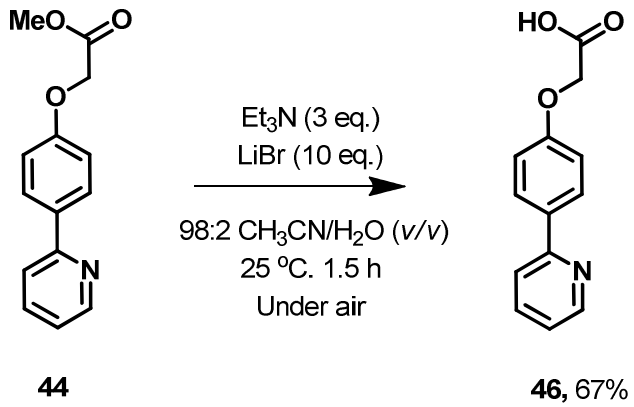

Scheme 16. The ester hydrolysis of ligand **44** to form carboxylic acid ligand **46**.

The hydrolysis of ester ligand **44** in wet acetonitrile under the given conditions was efficient giving **46** in 67% yield. The same conditions were used to hydrolyse the ester in CO-RM **45**, however the reaction was carried out under a nitrogen atmosphere initially followed by argon. This precaution was taken in case the product (**47**) was air sensitive. **Scheme 17** shows the conditions used on CO-RM **45** to hydrolyse the ester.

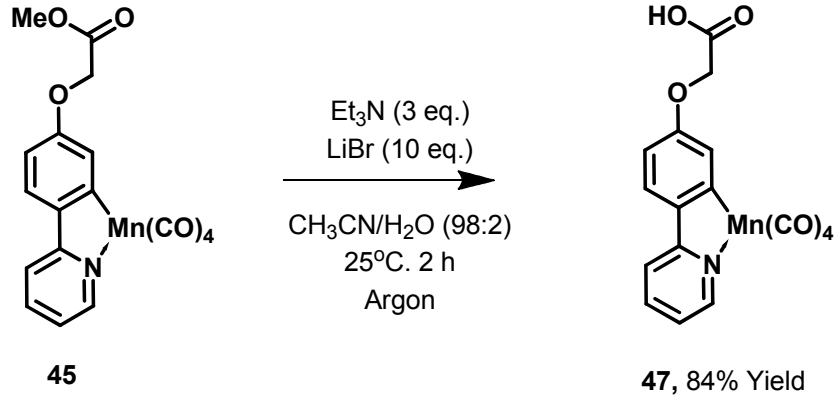

Scheme 17. The hydrolysis of CO-RM **45** under mild conditions to give CO-RM **47**

The hydrolysis was successful giving CO-RM **47** in 84 % yield, up from 67% in the ligand test reaction. This synthetic route provided sufficient amounts of CO-RM for further studies. This approach to preparing complex **47** was taken as the complexation with benzyl pentacarbonyl manganese is typically efficient in hydrophobic solvents. Ligand **46** is significantly more polar than any other ligand previously prepared, and is poorly soluble in hexane or toluene. It was therefore deemed appropriate to hydrolyse the ester of CO-RM **45** instead of attempting to find alternative cyclo-metallation conditions.

The ^{1}H NMR spectra in **Figure 63** show the changes to CO-RM **45** on ester hydrolysis.

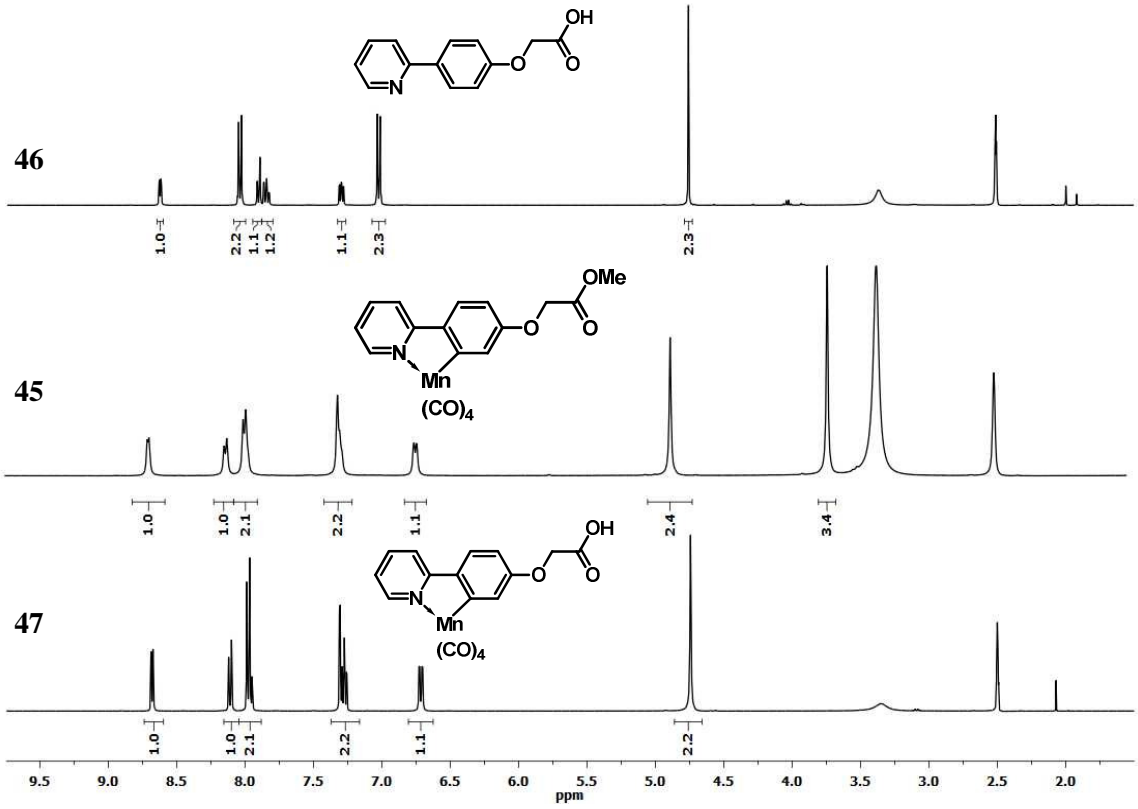

Figure 63. 400 MHz ^{1}H NMR spectra in d_6-DMSO of ligand **46** (top) CO-RM **45**(middle) and CO-RM **47** (bottom) at 300 K.

The NMR data in **Figure 63** shows that the singlet signal for the CH_3 on the methyl ester at 3.8 ppm is not present in either ligand **46** or CO-RM **47**. This suggests that the ester has been successfully hydrolysed. There is also a broad singlet at 13.15 ppm in the ^{1}H NMR spectrum of CO-RM **47**, and this chemical shift is diagnostic of carboxylic acid functionality. The IR spectrum of CO-RM **47** still contains the four peaks diagnostic of the tetracarbonyl manganese unit. It is pleasing that the '$Mn(CO)_4$' moiety is stable under the reaction conditions used. The data obtained suggests synthesis of pure carboxylic acid CO-RM **47**.

4.3 CO-release investigations with acid-containing CO-RM 47.

With the new acid-containing CO-RM **47** synthesised and characterised, it was then necessary to test its CO-release properties using a myoglobin assay. Initial studies were carried out before the development of the LED system and assays were carried out using 20, 40 and 60 µM CO-RM **47**. The results from this assay are shown in **Figure 64**.

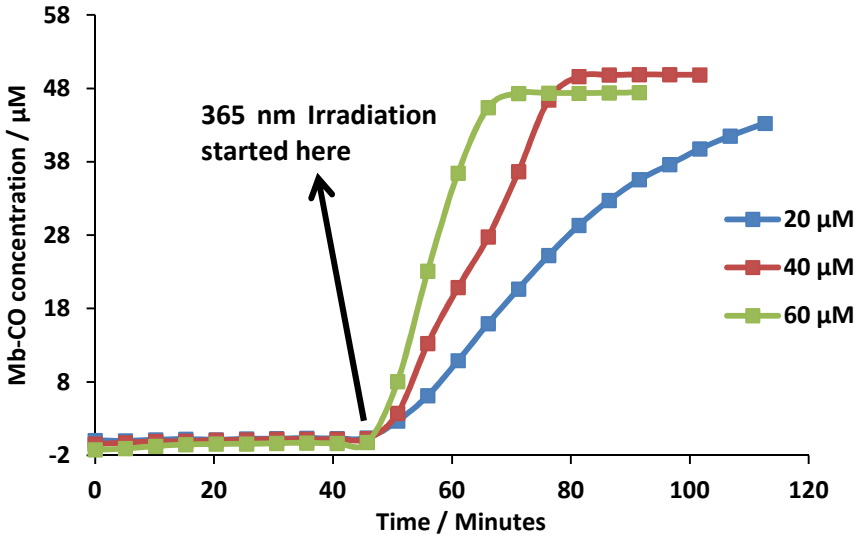

Figure 64. The CO-release profile of CO-RM **47** at 20, 40 and 60 µM concentrations in the presence of 50 µM myoglobin. Irradiation (365 nm, 6 W) initiated after 45 mins with two mins on, three mins off cycles.

The myoglobin assays in **Figure 64** show that CO-RM **47** is an efficient CO-releasing molecule. CO is not released until irradiation is initiated, which results in saturation of myoglobin at all the above concentrations. The half-life for CO-RM **47** under these conditions was found to be faster than any CO-RM previously prepared in this project, and the values are shown in **Figure 65**.

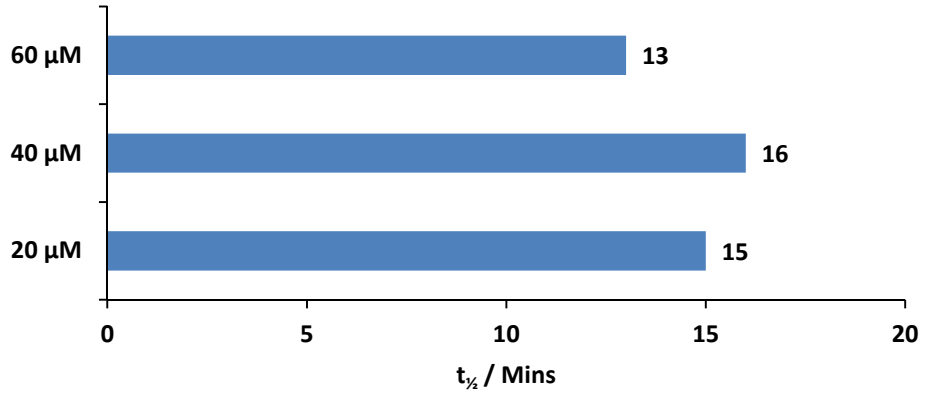

Figure 65. The $t_{½}$ values for CO-RM **47** at 20, 40 and 60 µM under 365 nm 6 W TLC lamp irradiation with two mins irradiation every five min period.

CO-RM **47** releases more CO in the same amount of time on irradiation at higher concentrations but the observed half-life values do not significantly vary with different concentrations.

CO-RM **47** does not precipitate in aqueous solution when added in 5 µl DMSO to 1 ml PBS buffer. This is a significant step forward in the development of this class of CO-RMs as it can be administered in solution without any precipitation or interference. This lack of precipitation is a potential reason for a shorter half-life with more CO-RM being in solution. **Figure 66** shows all the UV spectra for the 40 µM assay shown in **Figure 64**. This data has only been corrected at 510 nm.

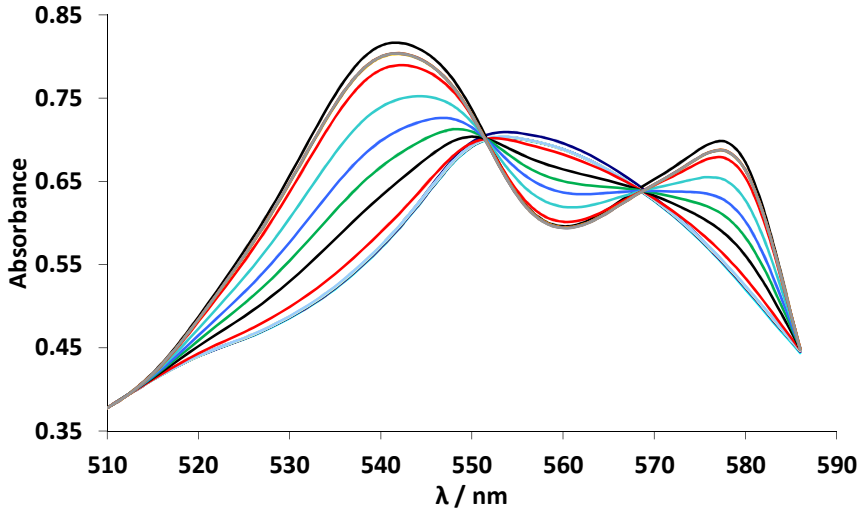

Figure 66. All UV-Vis absorption spectra for myoglobin assay using 40 µM CO-RM **47**. Only 510 nm correction applied.

CO-RM **47** is soluble on administration to the myoglobin solution and there is no skewing of the UV spectra, and the solution remains clear. Four point corrections for this assay is not required.

A comparison of CO-release from CO-RM **47** using TLC lamp and LED irradiation was then performed. Substiochiometric assays were also carried out to determine the number of CO molecules released from CO-RM **47**. **Figure 67** shows the CO-release data from these experiments.

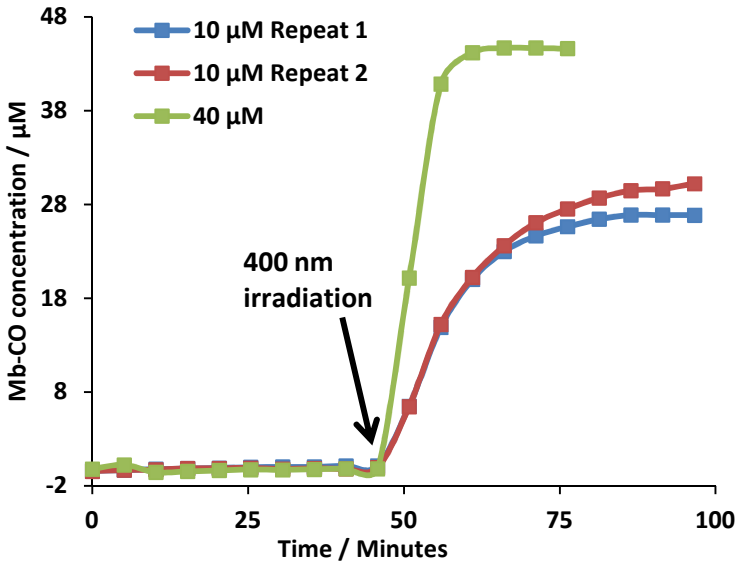

Figure 67. CO release profile of CO-RM **47** at 10 and 40 µM concentrations. Irradiation (400 nm 2.4 W) on for two mins per five min period. Irradiation started after 45 mins as indicated.

The myoglobin assays in **Figure 67** show that use of the LED significantly increases the rate of CO-release from CO-RM **47**. The half-life is reduced from 16 to 5 mins when using the 400 nm LED system. This further highlights the increased efficiency of using an LED close to the sample. Use of 10 µM CO-RM **47** shows that three molecules of CO are released from each molecule of CO-RM. This is comparable with the data obtained using halogenated CO-RMs **39** and **40**. The substituent in the *para*-phenyl position is still not altering the number of CO molecules released. The initial rate of CO-release for the two 10 µM repeats is the same. There is a small amount of error in the total CO-release but this would be expected due to some degree of myoglobin degradation over the course of the experiment.

The LED system in combination with CO-RM **47** releases CO rapidly, with a half-life of only five minutes (this equates to only two mins of irradiation). As discussed previously, different CO-release rates can be required depending on the type of treatment required.[7] Fast CO release rates in the stomach could result in over-vasodilatory action giving rise to lack of peristalsis.[101] Therefore further CO-release assays were carried out with CO-RM **47**. These were designed to assess the control that could be achieved when initiating CO-release. The next myoglobin assay used only 0.5 W of power instead of 2.4 W using an LED emitting light of wavelength 400 nm.

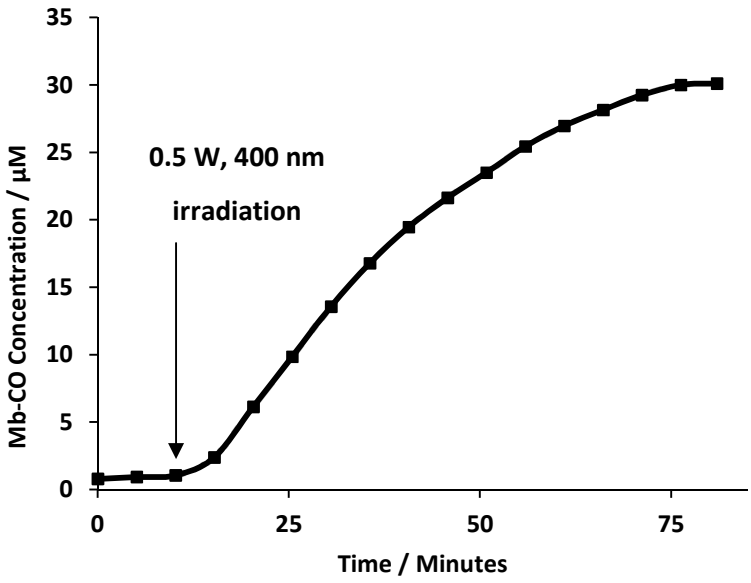

Figure 68. Myoglobin assay with 10 µM CO-RM **47**. Irradiation (400 nm, 0.5 W) for two mins per five min period after 10 mins in the dark.

The CO-release $t_{½}$ value for the experiment in **Figure 68** using 0.5 W irradiation was determined to be 8 mins. This increased by four mins compared to experiments performed at the same concentration of CO-RM when using a power consumption of 2.4 W. The change in half-life is not linear and this is expected due to the fact that not all of the irradiation passing through the sample will be absorbed. This is an important experiment as it shows that the half-life of CO-RM **47** can be controlled by varying the intensity of the irradiation. This variation in CO-release rate has not yet been demonstrated by any other photo-CO-RM in the literature.

Having established that the CO-RM **47** does not release CO until irradiation is initiated, the next step was to establish if CO-release could be halted if irradiation was stopped mid-experiment. This would give an extra degree of control over the CO-release process if the compound was to be irradiated *in vivo*. If the amount of CO *in vivo* was monitored as irradiation was used, then the irradiation could be stopped in the event of excessive CO-release. **Figure 69** shows the results from a myoglobin assay in which a stepwise irradiation procedure was used.

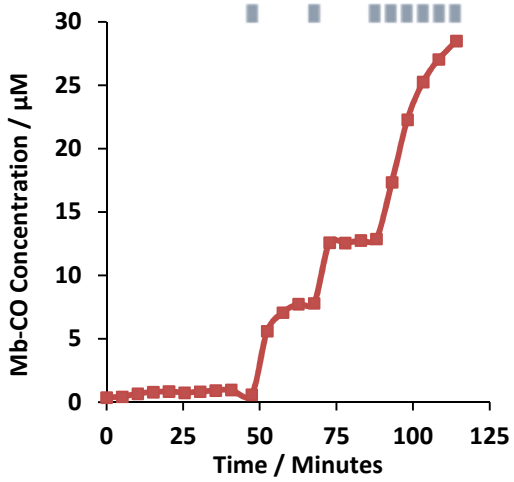

Figure 69. CO-release data using 10 µM CO-RM **47** with stepwise irradiation. Blue rectangles indicate two mins (400 nm, 2.4 W) irradiation.

The myoglobin assay data in **Figure 69** shows that CO-release from CO-RM **47** can be halted by turning off the LED. This means that the resulting species produced after initial irradiation are stable in aqueous solution and in the presence of myoglobin. A photo-CO-RM demonstrating the ability to switch off and back on again after initial irradiation has not yet been shown in the literature until publication of this research.[59] It is encouraging that if the irradiation is resumed that the same amount of CO is released compared to previous experiments.

The CO-release behaviour of CO-RM **47** has been well characterised, and it has been established it is an efficient photo-CO-RM with thermal stability. The next step was to establish what species were formed in solution on the irradiation of the CO-RM. This was performed using ESI mass spectrometry. A 0.5 mg ml^{-1} solution of CO-RM **47** in 50:50 (*v/v)* CH_3CN/H_2O was measured using ESI-MS (+ve mode). The experiment was performed using CH_3CN to aid solubility; as DMSO could not be used here due to incompatibility with ESI-MS instrumentation. The solution was then irradiated with light of wavelength 400 nm for one minute in between each subsequent ESI-MS measurement. **Figure 70** shows the profile of peaks that were observed how they changed over the time of the irradiation experiment.

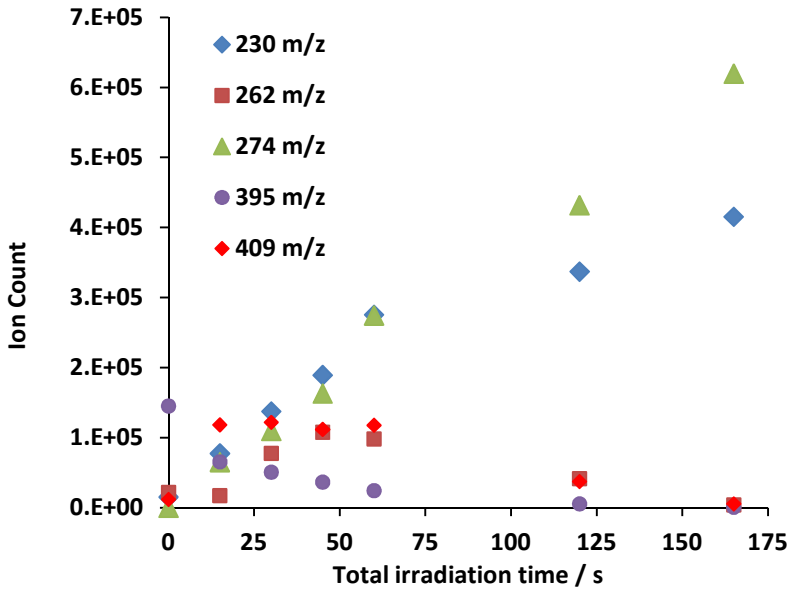

Figure 70. ESI-MS (+ve mode) profile for peaks detected on the 400 nm irradiation of CO-RM **47** in 50:50 (*v/v*) CH_3CN/H_2O.

On irradiation the molecular ion for CO-RM **47** at 395 *m/z* is depleted. Some species attributable to the peaks at 230 and 274 *m/z* accumulate. **Scheme 18** shows a proposed degradation pathway based on the ESI-MS data in **Figure 70**.

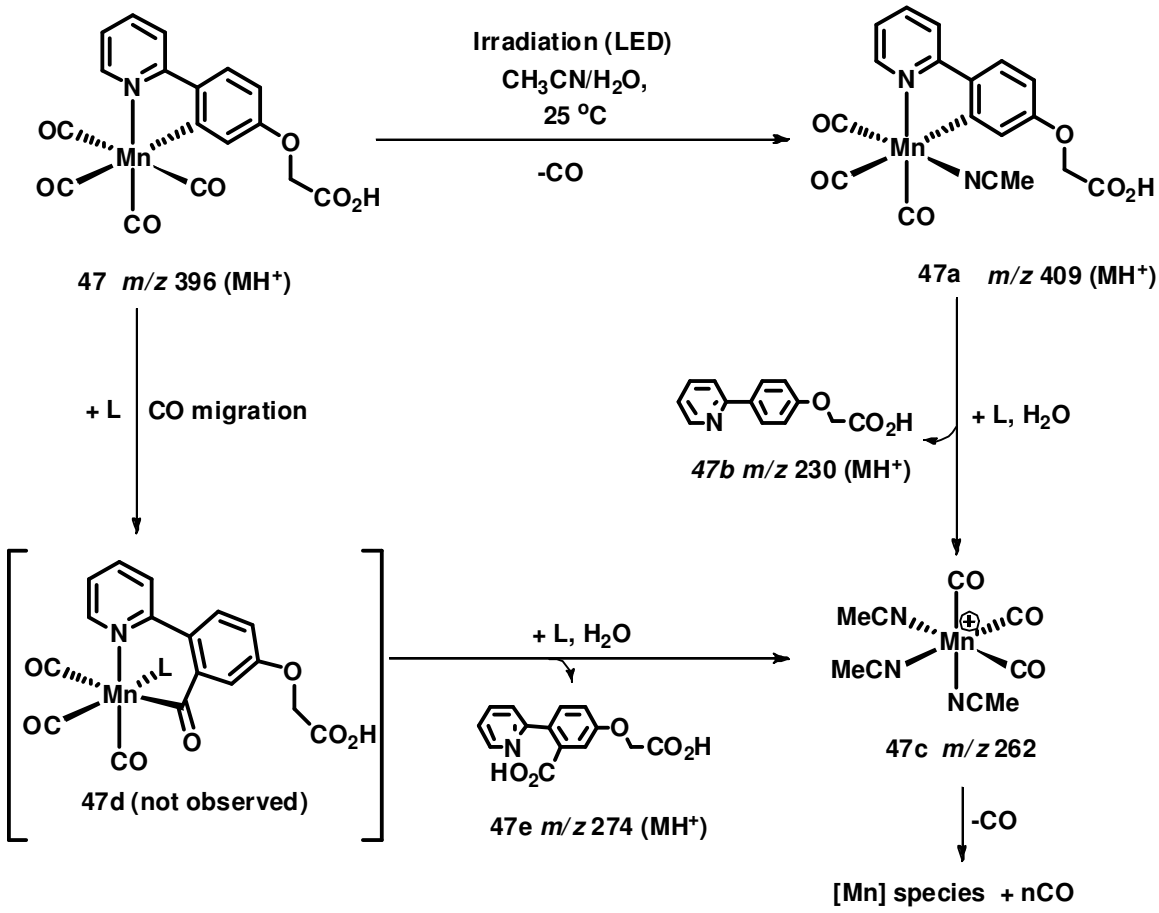

Scheme 18. Proposed degradation pathway for CO-RM **47** in 50:50 (*v/v*) CH_3CN:H_2O on irradiation with light of wavelength 400 nm (2.4 W).

On irradiation of CO-RM **47**, an intermediate species with 409 *m/z* was detected (**47a**). This matches with the loss of CO from the molecule ion followed by coordination of an acetonitrile ligand from solution. This is expected as the vacant coordination site following CO loss would give a 16 electron complex, which would rapidly result in coordination of another ligand. Species **47a** is an intermediate and its intensity rises and then decreases close to zero. As the peak at 409 *m/z* accumulates, peaks at 230 and 262 *m/z* were detected (**47b** and **c**). The peak at 262 *m/z* is also an intermediate, which is likely to be a tricarbonyl manganse(I) species (**47c**). This has resulted from cleavage of the manganacycle giving uncoordinated free ligand **47b** at 230 *m/z*. Species **47c** also depletes on further irradiation, and is likely to be responsible for further CO-release. Myoglobin assay studies indicate release of three molecules of CO released per molecule of CO-RM **47**. This means that the species at 262 *m/z* may be responsible for further CO-release.

It is proposed that CO-RM **47** can also degrade by a secondary pathway. A peak at 274 *m/z* was detected with significant intensity (**47e**). This peak did not deplete following further irradiation just like free ligand **47b**. It is proposed that **47e** has an additional carboxylic acid group at the

ortho-phenyl position. It is likely that **47e** results from a CO migration from the manganese centre over to the phenyl ring (**47d**).This can then be attacked by water to give a carboxylic acid-containing species **47e** at *m/z* 274. The mechanistic process that forms **47e** consumes one CO ligand from the manganese centre, and this could be a significant contributor to why only three out of a possible four CO ligands are released in aqueous solution. Another potential reason is that increased back-bonding from the manganese to remaining CO ligands following initial CO-release may increase the energy needed to release further CO ligands. With only one CO ligand remaining, is it likely that the M–CO bond is too strong to be broken using 400 nm light.

In summary, CO-RM **47** has been shown to be an efficient photo-CO-RM with suitable water compatibility. Even though **47** has to be administered in DMSO, it does not precipitate on addition to aqueous solution. DMSO is not the ideal solvent to use for these studies but it is used at a low concentration and is typically used in biology for the administration of drug compounds in initial studies.[59] CO-RM **47** has been shown to have a variable half-life of CO-release dependent on the intensity of irradiation. CO-release can be halted by simply turning the light off during an experiment. This CO-RM has a strong degree of control in terms of its CO-release, that many CO-RMs in the literature have not been shown to possess.

4.4 Biological investigations with CO-RM 47

With the CO-releasing properties of CO-RM **47** established, it was then necessary to take this CO-RM forward into biological studies. CO-RM **47** has been shown to release CO efficiently in 0.01 M PBS buffer at pH 7.4, however further investigations into its CO-release in biological media were required.

LB media (Lysogeny broth) is a biological medium commonly used for the growth of *E. coli* and *S. aureus*. It is a nutient rich medium containing all the nutrients these species need to grow. DMEM (Dulbecco's modified eagle medium) in combination with foetal calf serum (FCS) is an even richer medium used for the growth of eukaryotic cell lines. This medium contains a complex mixture of defined amino acids, hormones, sugars and other nutrients. DMEM/FCS is also typically used for the growth of RAW 264.7 macrophage cells.

With the knowledge that these media would be used in biological investigations with CO-RM **47**, it seemed appropriate to test the CO-release behaviour of this CO-RM in these solutions. Myoglobin assays using 20 μM CO-RM **47** in PBS, LB medium and 90% (*v/v*) DMEM:FCS medium with 400 nm 2.4 W irradiation were carried out as performed previously. **Figure 71** shows the results from these CO-release investigations.

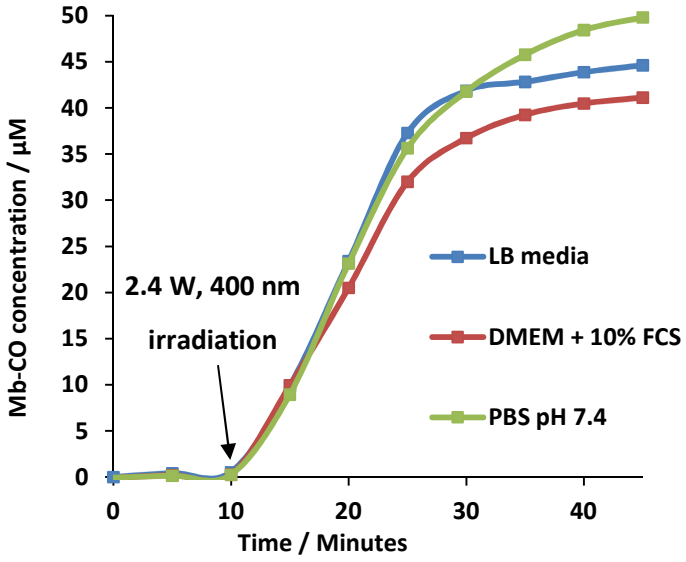

Figure 71. The use of 20 µM CO-RM **47** in a 50 µM myoglobin assay using different aqueous media (monitored by UV-Vis spectroscopic analysis). Arrow indicates start of irradiation (400 nm, 2.4 W). LED on for two mins every five minute period.

DMEM:FCS medium contains: various proteins, amino acids, hormones, sugars, and other nutrients. Despite this, CO-RM **47** is stable in this medium. The CO-RM can then be activated with light when required. Furthermore, the initial CO-release rates are almost identical in the different aqueous mixtures. CO-RM **47**'s CO-release rate under the conditions tested is independent of all the additional species in solution. This demonstrates how robust this CO-RM **47** is under thermal conditions.

4.4.1 Eukaryotic cell studies with CO-RM 47

If CO-RM **47** is to progress as a potential pharmaceutical agent, the viability of RAW 264.7 macrophages cells along with CO-RM toxicity had to be assessed. RAW 264.7 cells are white blood cells and are associated with the detection of foreign bodies within an organism. This potentially makes them very sensitive to new drug compounds/foreign species, since these cells will contain many receptors capable of detecting foreign functionality. The sensitivity of these cells makes them a suitable starting point for initial viability tests.

With the knowledge that CO-RM **47** is a thermally stable compound, the toxicity of the by-products formed by irradiation in solution was assessed. This was performed by irradiating the CO-RM in DMSO before it was added to the cells. This allowed the toxicity of the combined by-products, following irradiation to be assessed.

RAW 264.7 cells were grown in culture plates in 10% (*v/v*) DMEM:FCS medium until they were confluent. Fresh medium containing 10, 50 and 100 µM CO-RM was then added to the cells, which were then incubated overnight at 37 °C under a 5% CO_2 atmosphere.

The viability and cytotoxicity of the compound tested were assessed using two complementary assays. Alamar Blue and LDH assays required live cells and dead cells respectively to detect a response. Using two complementary assays means that information obtained *via* different mechanisms can be obtained, increasing the reliability of the results obtained.

The Alamar blue assay uses a sterile 10% reazurin solution in culture medium.[102] The reazurin can only be reduced to resorufin if the cells are alive. On reduction of reazurin (**48**) to resorufin (**49**) (**Scheme 19**), a distinct blue to red colour change is observed. This can be quantified using UV-Vis spectroscopic analysis. Wells with no compound added are counted as the live control, and cells with 1% Triton X-114 added are counted as a dead control. The percentage viability can then be scaled between the absorbance values for the dead and live control.

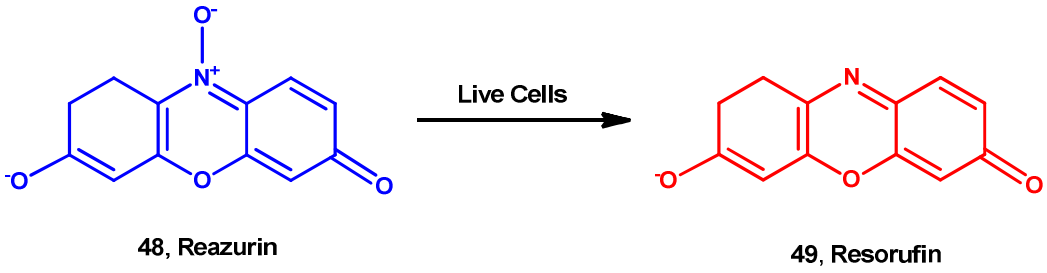

Scheme 19. The conversion of reazurin (**48**) to resorufin (**49**) which can only be carried out in live cells. Spectrometric change detected by UV-Vis spectroscopic analysis.

The LDH assay measures the amount of lactate dehydrogenase released from cells up on death.[103] On cell death the membrane ruptures and cellular contents are released. LDH is a stable enzyme which converts lactate to pyruvate, and this conversion can be quantified by using the enzyme that is released from cells in to the medium upon death. The more cells that die means that more catalysis to produce pyruvate will take place due to increased LDH levels. The assay is scaled between a live and dead control in the same way as the Alamar blue assay.

Ester CO-RM **45** and acid-containing CO-RM **47** were tested using an Alamar blue and LDH assay together to assess the viability of these CO-RMs. The photo-degradents were also tested by pre-irradiation as previously described. CO-RM **F8** was also tested along side the other CO-RMs to ensure that the tests were comparable with previously published results.[74] **Figure 72** shows results from the Alamar blue assays performed.

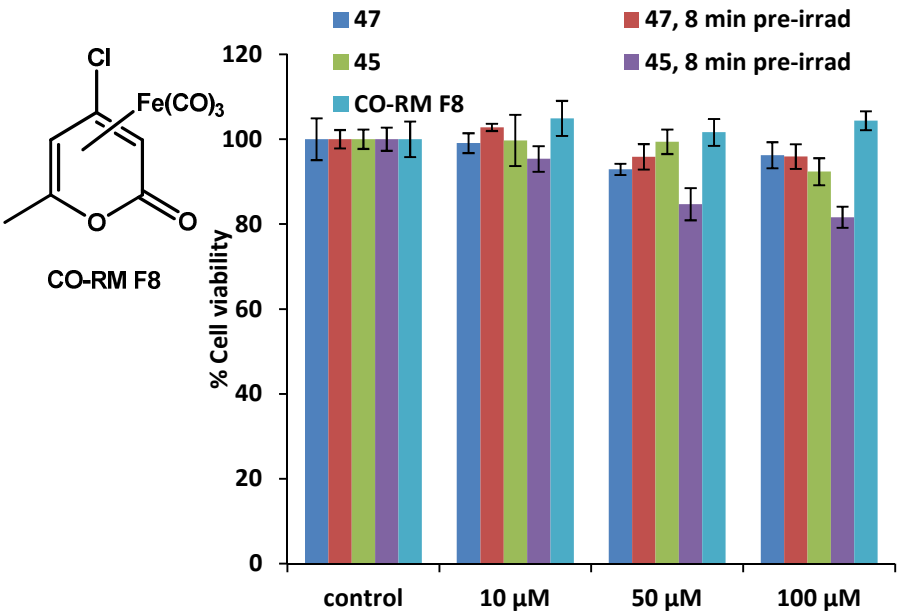

Figure 72. Alamar blue assay data from CO-RMs **45**, **47**, and **F8** using RAW 264.7 cells in 24/96 well plates. Compounds tested at the above concentrations with and without irradiation (400 nm, 2.4 W) before addition to the cell culture.

CO-RM **47** is > 90% viable with RAW 264.7 cells at all the tested concentrations. This includes when the CO-RM is directly added to the medium with the cells, and also when it has been irradiated for eight mins before it is added to the culture. This means that both the CO-RM and its biological and photo-degradents, are viable at the tested concentrations. These initial tests are encouraging and further bioligcal studies can be carried out using CO-RM **47**. Ester CO-RM **45** shows a slight reduction in viability and this highlights the importance of hydrolysing the ester from CO-RM **45** to make a more water compatible CO-RM **47**. The viability of CO-RM **F8** closely matches the previously published results validating the method.[71-72, 74]

Figure 73 shows the complimentary LDH assay results for the same tests carried out in **Figure 72**.

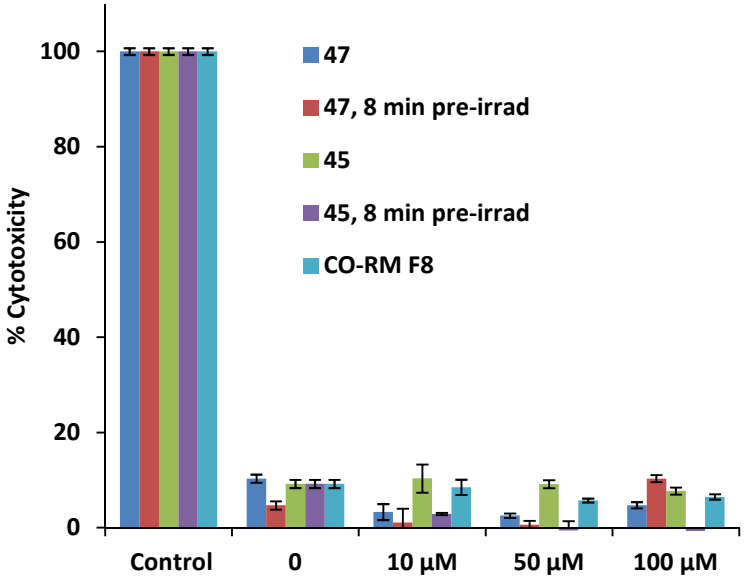

Figure 73. LDH for CO-RMs **45**, **47** and CO-RM **F8** with RAW 264.7 cells. Compounds tested at the above concentrations with and without irradiation (400 nm, 2.4 W) before addition to the cell culture.

The LDH assay data in **Figure 73** is in agreement with the Alamar blue assay data results in **Figure 72**. The percentage LDH release with CO-RM **47** does not go above the cell only control. It is expected that there will be a small amount of LDH release without compound, as some cells will die over the experiment period. This is because a plastic plate is not a natural environment for the cells. It is important to note that these assays may not perfectly mirror each other, since they assess the cells *via* a different method. Additionally, cell viability and cytotoxicity are not the same thing, and there can be some difference between the tests. While there is viability with ester CO-RM **45** as determined by the Alamar blue assay, there is no significant LDH production on the administration of this compound. This suggests some biological pathways are interupted with out killing the cells. Literature CO-RM **F8** also does not show any LDH production in these studies matching with literature studies carried out.

These studies show that CO-RM **47** is a viable molecule with respect to chemically sensitive RAW 264.7 cell. This biological work represents a significant step towards the development of a new photo-CO-RM.

4.4.2 NO suppression using CO-RM 47 with RAW 264.7 macrophages.

It is known that CO can suppress the production of nitric oxide (NO) in cells.[70] It is also known that NO can exhibit an inflammatory response,[29] and if NO is suppressed then an anti-inflammatory response can be observed. NO_2^- (nitrite) is a stable degradation product of NO and so it can be used to quantify the amount of NO produced by cells. This means that by using certain controls, it is possible to observe if the CO released by CO-RMs is causing a suppression of NO production in RAW 264.7 cells.

The concentration of nitrite can be quantified using a Greiss assay.[104] To assess if the CO-RMs synthesised can stop the production of nitrite, RAW 264.7 cells need to be stimulated to produce NO. This can be done using LPS, which is found on the surface of bacteria. Macrophages such as RAW 264.7 can detect LPS, and this can trigger the production of NO. IFN-γ is a cytokine that, together with LPS, can trigger a potent anti-inflammatory response.[105] Part of this response involves the production of high concentrations of NO.

LPS and IFN-γ were used together to stimulate the production of a high concentrations of NO from RAW 264.7 cells. A CO-RM can be added to see if there is a reduction in NO production. This would then suggest that the CO-RMs are producing CO and that this CO is suppressing the NO production.

Greiss assay experiments were carried out using CO-RM **47** at a concentration of 50 μM. This concentration was chosen because it was well within viable limits as determined by Alamar blue and LDH assays. Two separate 96 well plates were prepared with RAW 264.7 cells. One plate was irradiated for eight minutes with an LED (3.6 W, 400 nm) and the other was not. This was to assess if the light was causing any unusual effects. The results of the initial study are shown in **Figure 74**.

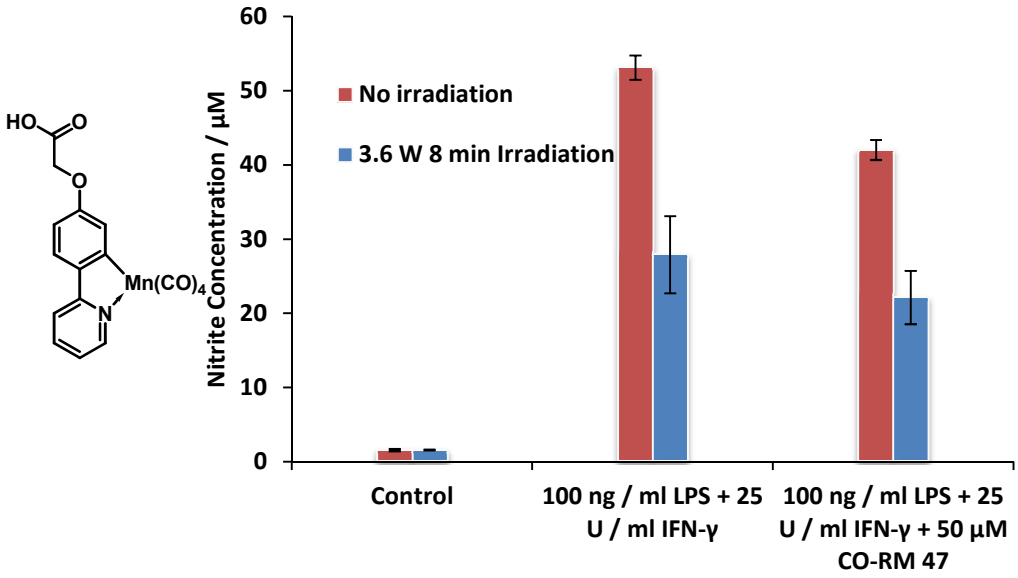

Figure 74. Greiss assay data: observation of nitrite levels in supernatant from RAW 264.7 murine macrophages after incubation with 50 µM CO-RM **47**. Identical plates set up except one is irradiated for eight mins (3.6 W, 400 nm).

The Greiss assay data in **Figure 74** shows that there is an issue with irradiating the cells with light of wavelength 400 nm. There is a reduction in nitrite production on irradiation in the absence of CO-RM. This could be due to damage to the cells due to the light. Macrophages will not experience such intense light compared to skin cells and perhaps this could explain their sensitivity.

However, in the presence of 50 µM CO-RM **47** without light, there is a statistically significant reduction in amount of nitrite produced by the cells in compared to the control. There is a 21% reduction in nitrite production in the presence of the CO-RM. This is also at a concentration of CO-RM that shows no signs of significant toxicity. This suggests anti-inflammatory action of CO-RM **47**. Even though this reduction percentage is less than observed with some other CO-RMs in the literature, both LPS and IFN-γ are used together in these experiments. This induces a significantly stronger inflammatory response than just LPS in isolation. CO-RM **47** can suppress a strong inflammatory response which is particularly encouraging. Initial results were carried out with LPS in isolation; but it was found that the concentrations of NO produced from this stimulation were too low for accurate Greiss assay quantification. This is why a stronger stimulation method was used.

4.4.3 Investigations with CO-RM 47 on *E. coli* W3110

RAW 264.7 macrophage cell studies have established that CO-RM **47** is a viable molecule with respect to a sensitive eukaryotic cell line. It has also been established that the CO-RM also possesses some anti-inflammatory properties. As discussed in section **1.3.5**, CO can be toxic towards bacteria under the correct conditions and the next step in this research was to assess the effect of CO-RM **47** on bacteria.

Initial investigations were carried out using *E. coli* W3110 with CO-RM **47** in LB medium at 100 µM. Special LED system attachments were developed so that bacteria could be irradiated in sterile conditions under repeatable conditions. **Figure 75** shows the attachments developed.

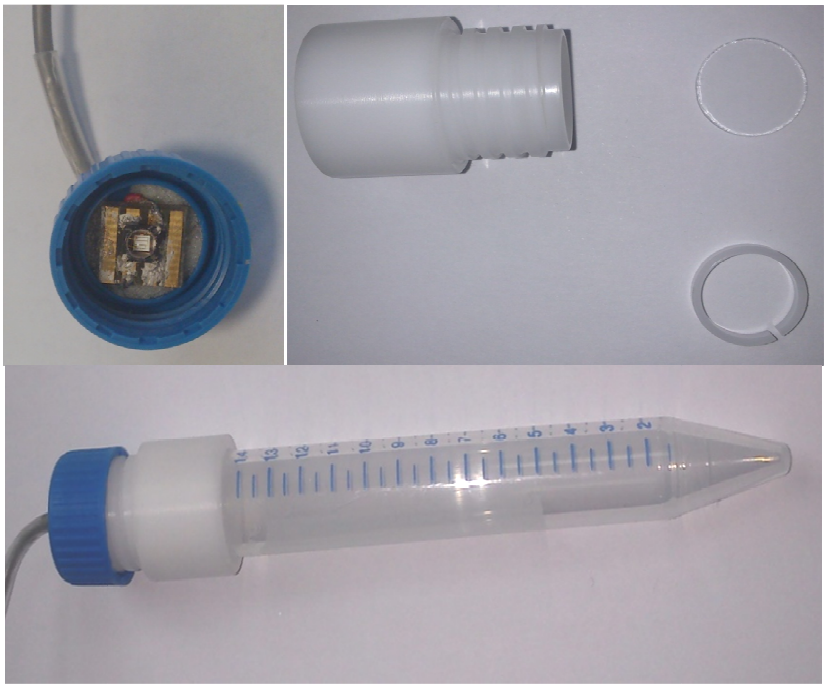

Figure 75. LED system developed for irradiation of bacteria under sterile conditions. Top left: LED mounted in Falcon™ tube cap. Top right: Sterile attachment to separate LED from bacteria with a glass window, Bottom: Full set up

Initial experiments involved growing *E. coli* W3110 under rotation at 200 rpm in LB media with CO-RM **47** at varying concentrations to carry out an initial toxicity test under rapid growth conditions. *E. coli* W3110 was chosen because it is a wild type strain so should not have any major genetic defects which could enhance the effects of a CO-RM. **Figure 76** shows the details of the initial growth curve experiments.

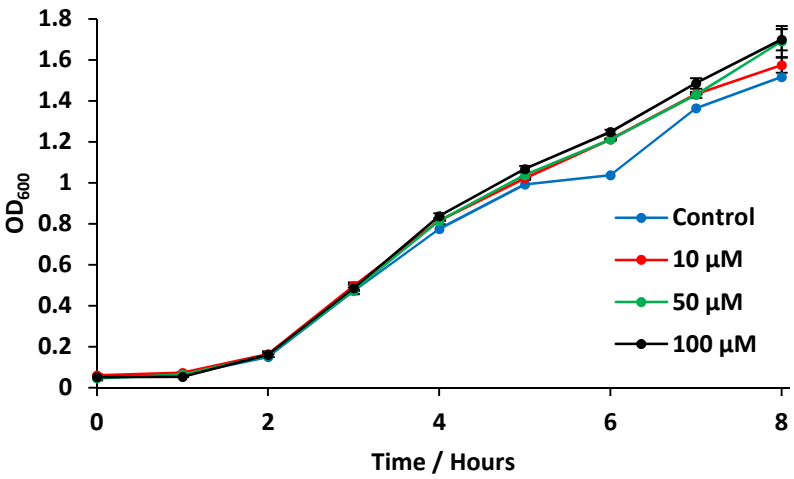

Figure 76. *E. coli* W3110 growth with varying concentration of CO-RM **47** at 37 °C with 200 rpm rotation in 15 ml Falcon™ tubes.

E. coli are not affected by the presence of CO-RM **47** under all the tested concentrations. The bacteria grow at the same rate with the compound present. This means that the compound is not toxic to *E. coli* (however there is no irradiation present). It is known from myoglobin assay studies that the CO-RM does not degrade in LB media until irradiation is initiated, so unless *E. coli* can breakdown this CO-RM, it is not expected that there will be much thermal CO-release occurring in these particular experiments.

In order to evaluate the effects of rotation speed, it was decided that future experiments should be carried out with 100 rpm rotation on the orbital shaker. This is because at 200 rpm rotation, the solutions would be well oxygenated. This would not reflect an *in vivo* situation because the majority of oxygen would be tightly bound in haem-containing proteins such as myoglobin and haemoglobin. The bacteria in this situation would have to compete for the oxygen to allow efficient growth, and so shaking at 100 rpm to reduce the oxygen to more realistic levels seems appropriate.

With the knowledge that CO-RM **47** is stable in LB media, it seemed logical to deliberately degrade it before adding it to the bacteria in the way that was done in the RAW 264.7 cell studies. CO-RM **47** was therefore irradiated for eight minutes (400 nm, 2.4 W) in LB media prior to addition of the bacteria. **Figure 77** shows the results of this initial irradiation study.

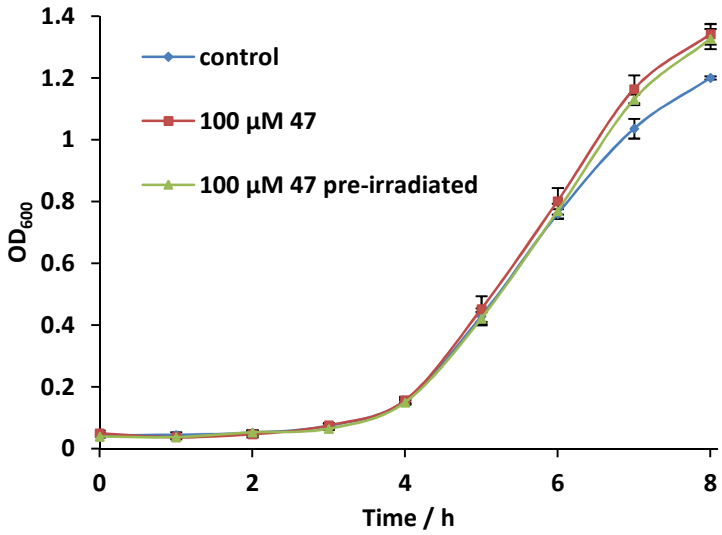

Figure 77. Pre-irradiation study with 100 µM CO-RM **47**. Eight mins irradiation (400 nm, 2.4 W) of CO-RM **47** in LB media before addition to the *E. coli* culture. Growth was then carried out for eight hours at 37 °C.

The by-products formed after eight minutes irradiation are also not toxic towards *E. coli* under the given conditions. Direct irradiation of *E. coli* in the presence of CO-RM **47** was then carried out. **Figure 78** shows the growth curve from this initial direct irradiation study. Note: This study was carried out separately from the curve in **Figure 77**

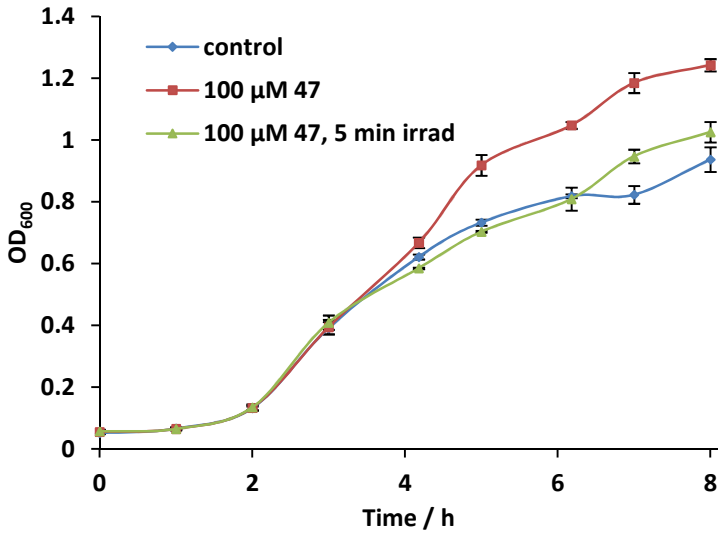

Figure 78. Five mins direct irradiation (400 nm, 2.4 W) of *E. coli* W3110 in the presence of 100 µM CO-RM **47**. Irradiation carried out at three hours into the experiment for 5 mins total.

Figure 78 shows that at 100 µM CO-RM **47** in LB media (with 0.5% DMSO) appears to increase the growth of *E. coli* compared to control. However, with five mins irradiation the growth is reduced to the OD of the bacteria-only control. This suggests that there is a reduction in growth

of *E. coli* on irradiation. This increase in growth was expected to be due to DMSO and not the CO-RM, and so a growth curve with DMSO under these conditions was performed (**Figure 79**).

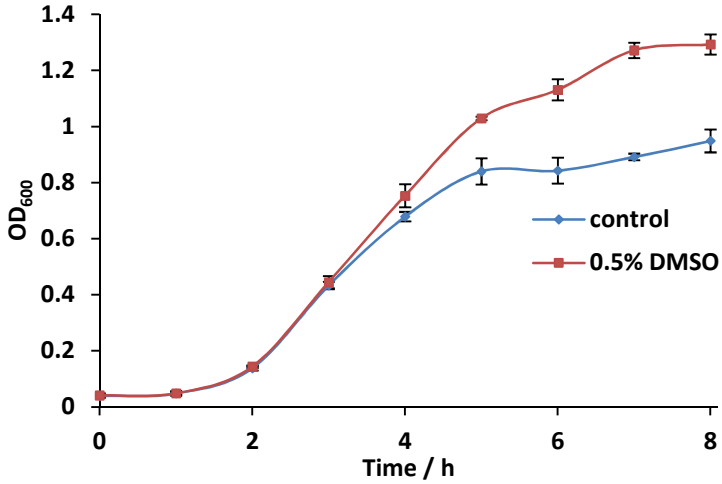

Figure 79. Growth of *E. coli* W3110 with and without DMSO at 37 °C in LB media, with rotation in Falcon™ tubes at 100 rpm on an orbital shaker.

The curve in **Figure 79** confirms that DMSO is responsible for increased growth at 100 rpm. It is known that *E. coli* can use DMSO as an electron source *via* the use of membrane protein DMSO reductase.[106] This extra electron source in the presence of DMSO may increase growth rates.

With the knowledge that CO-RM **47** causes a slight decrease in growth rates on irradiation in the presence of DMSO, controls were required to assess if the irradiation was responsible for this decrease. **Figure 80** shows the details of this irradiation-only control.

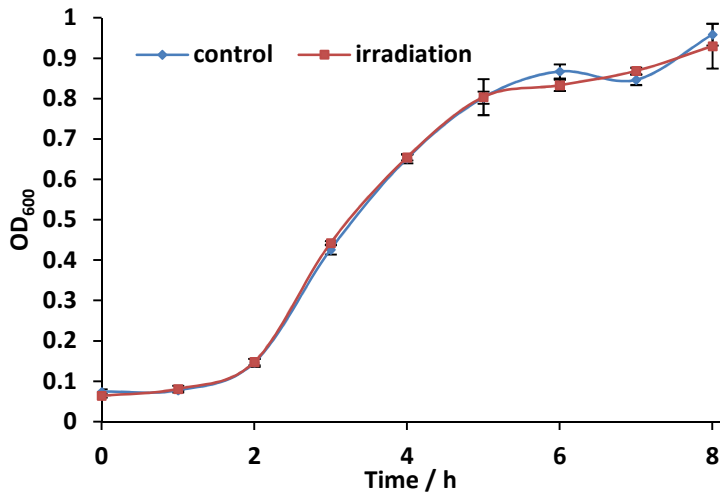

Figure 80. Growth curve with 32 mins direct irradiation (400 nm, 2.4 W) of *E. coli* W3110 at 37 °C in LB media with 100 rpm rotation.

With 32 mins direct irradiation of *E. coli* there is no change in the growth of the bacteria. This strongly suggests that the decrease observed in **Figure 78** was due to the action of CO-RM **47**. This control was carried out for 32 mins to allow further irradiation in future experiments.

The decrease observed with five minutes of irradiation is not very encouraging, as the OD does not decrease below the value observed without DMSO. This is why the duration of irradiation was increased in further experiments. **Figure 81** shows a repeat of the experiment in **Figure 78** but with 32 mins total irradiation instead of five.

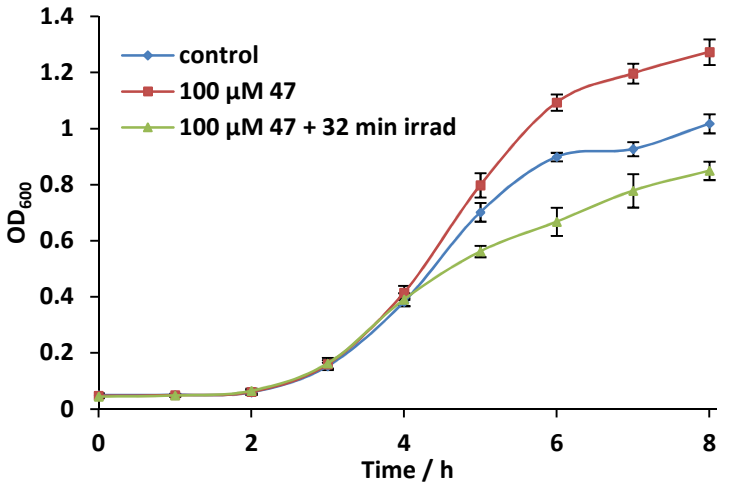

Figure 81. Growth curve with 32 mins direct irradiation (400 nm 2.4 W) of *E. coli* W3110 with 100 µM CO-RM **47**. Irradiation carried out between three and four hours into the experiment.

With an increased irradiation time, there is an improved reduction in the OD reduction of *E. coli* on irradiation in the presence of CO-RM **47**. Following eight hours growth, the OD is reduced by

35% to below the OD of the control without any DMSO. This represents a significant improvement in the action of CO-RM **47** on *E. coli*.

With a significant decrease in the growth of *E. coli* observed, the next step was to modify the conditions to assess if they could be optimised. Two modifications were made and the first was to switch from Falcon™ tubes to eight ml Bijou tubes. The length of a bijou tube is shorter and so the light path length to all the bacteria will be shorter. **Figure 82** shows the set-up that was used for new bacterial irradiation conditions.

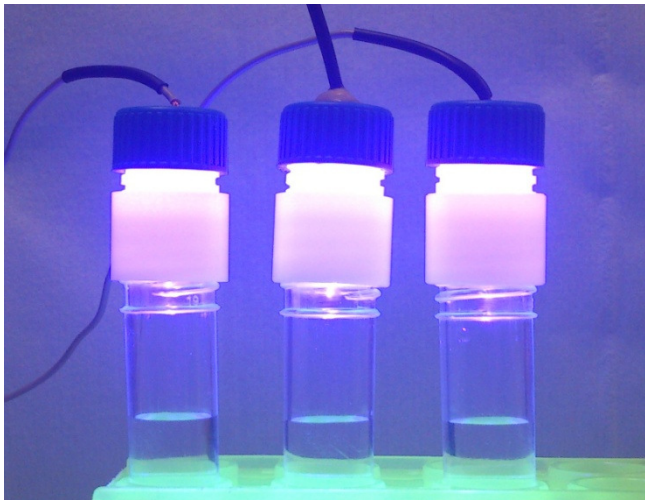

Figure 82. Irradiation set-up with new eight ml Bijou tubes.

The second modification involved increasing the irradiation duration to 68 mins delivered over two hours (irradiation on for four mins and off for one minute to prevent over heating of the LED and to maintain 37 °C growth temperature in the medium). **Figure 83** shows the results with the two disscussed modifications.

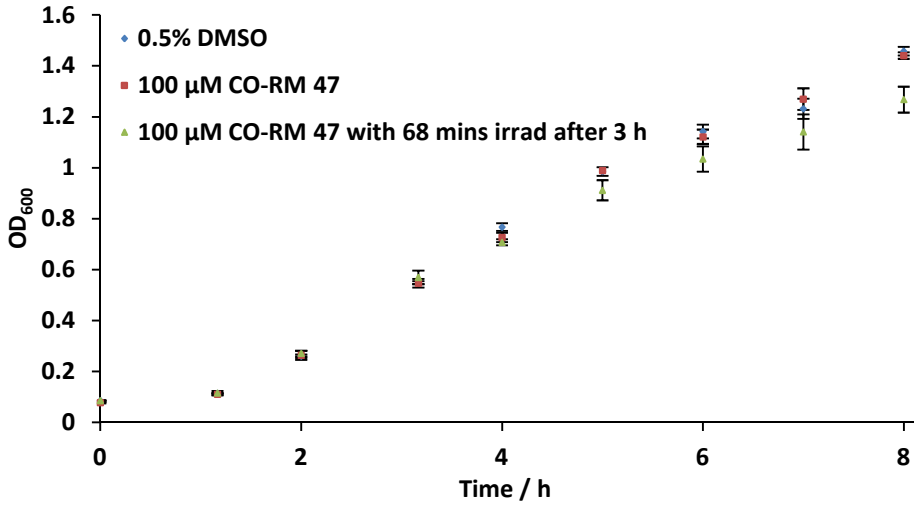

Figure 83. Growth curve with 68 mins direct irradiation (400 nm, 2.4 W) of *E. coli* W3110 with 100 µM CO-RM **47** in LB media. Irradiation was carried out between three and five hours.

Despite the increase in irradiation time, there was no improvement in the toxicity of CO-RM **47** towards *E. coli*. This could be because the increased irradiation is degrading some of the by-products that may participate in antibacterial action. It also could be variation between experiments and that the increase in irradiation is not actually releasing further CO.

It was postulated that with irradiation commencing at three hours, the OD of the bacteria has increased enough to significantly interfere with penetration of light through the culture medium. This could reduce the rate of CO-release. A further experiment was designed so that irradiation was started two hours earlier allowing less growth from the initial starting OD value of 0.05. **Figure 84** shows the results from this irradiation study.

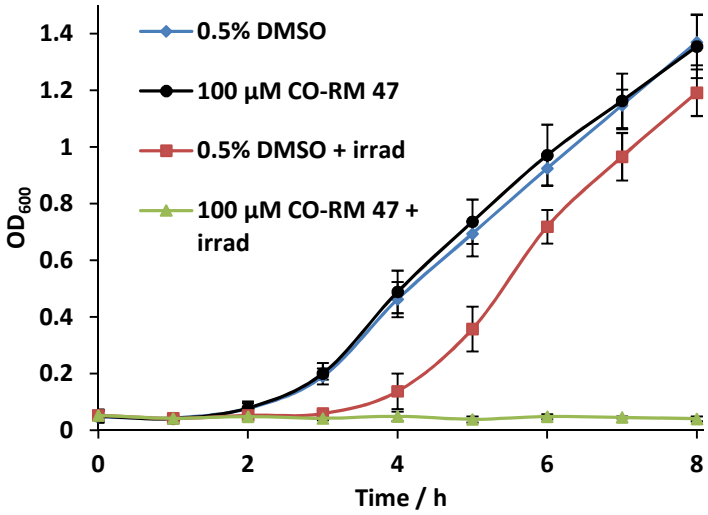

Figure 84. Growth curve with 68 mins direct irradiation (400 nm, 2.4 W) of *E. coli* W3110 with 100 µM CO-RM **47** in LB media. Irradiation carried out between one and three hours.

Starting irradiation two hours earlier has a dramatic effect on the action of CO-RM **47**. Irradiation on its own without the CO-RM causes a lag in the growth of *E. coli*. The lower OD appears to improve the action of the CO-RM. On irradiation of the CO-RM at one hour there is no growth of *E. coli* above the starting OD over an eight hour period. This suggests either strong inhibition of growth or antibacterial activity. To distinguish between the two, three further repeats of this experiment were carried out but with an additional plating study. This involved taking aliquots from cultures at zero and four hours. This represents before and after irradiation. The aliquots were diluted so that individual colonies could be counted after incubation on agar plates. **Table 10** shows the numbers obtained from this plating study.

Table 10. Colony counts from *E. coli* W3110 cultures, before and after 68 mins irradiation (0 and 4 h) (400 nm, 2.4 W). Incubation in LB media with 100 μM CO-RM **47**.

Repeat	Time/ h	Dilution	Colony count
1	0	500	229
1	4	No dilution	33
1	4	500	0
2	0	500	283
2	4	No dilution	46
2	4	50	0
2	4	500	0
3	0	500	235
3	4	No dilution	180
3	4	500	0

The plating study was carried out with three further repeats which all show the similar curves as shown in **Figure 84**. The dilution study shows that the reduction in growth is a strong antibacterial effect and not a bacteriostatic. This antibacterial effect is in the order of 99-99.9%, and this is particularly encouraging. It is interesting that simply moving the irradiation to after one hour initial growth turns this CO-RM into a potent antibacterial agent. This result was obtained with bacteria that were 13-14 days old from when they were initially grown from stocks. It was therefore necessary to examine how effective CO-RM **47** would be on younger *E. coli.* **Figure 85** shows the results from the use with *E. coli* that were six days old.

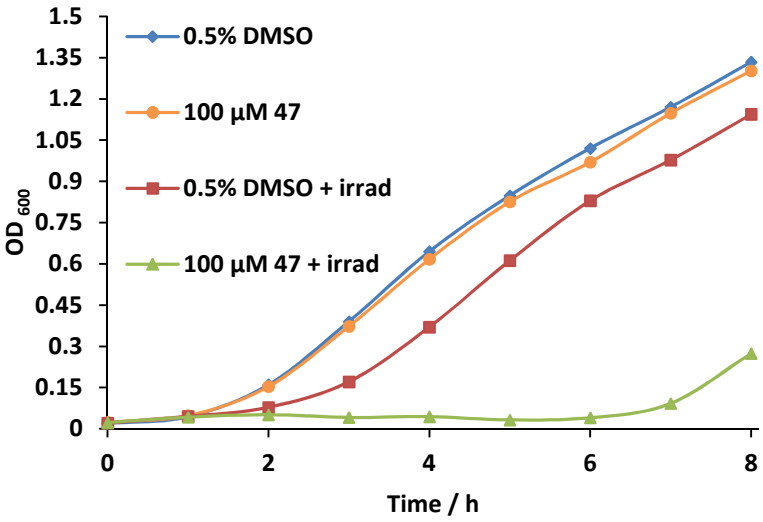

Figure 85. Growth of *E. coli* W3110 in LB media with 100 µM CO-RM **47**. Irradiation (400 nm, 2.4 W) started at one hour for 68 mins total. *E. coli* was from a six day old plate used for experiment.

CO-RM **47** is still effective at stopping the growth of *E. coli* that is six days old for several hours, but re-growth occurs in the 7th hour of the experiment. This should still represent a large percentage of killing, as *E. coli* is capable of doubling in population every 30 mins as shown by earlier experiments.

It has been established that under the correct conditions, CO-RM **47** shows potent antibacterial activity against *E. coli* in combination with irradiation of wavelength 400 nm. It was then necessary to carry out a control experiment to test if the photo-products of irradiation were toxic to *E. coli*. A pre-irradiation experiment was performed to match the irradiation times used in previous experiments. The results from this control experiment are shown in **Figure 86**.

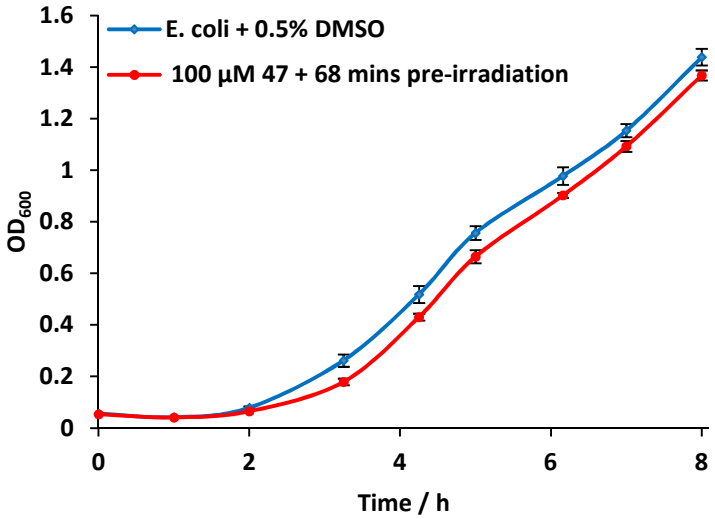

Figure 86. Growth curve of *E. coli* W3110 in LB media with 100 µM CO-RM **47**. Media with 100 µM CO-RM **47** was irradiated for 68 mins (400 nm, 2.4 W) before addition of *E. coli*. The culture was then allowed to grow with no further irradiation.

Presence of the by-products from 68 mins irradiation does not affect the growth of *E. coli* very much. The media was not flushed with air before the bacteria was added, and this is suggests that all the photo-products are not toxic. This includes some remaining extra cellular CO that was not expelled from the medium after irradiation. The data suggests that fresh CO-RM is required to get the antibacterial effect.

In summary, CO-RM **47** has been shown under certain conditions to be an effective antibacterial agent against *E. coli*. The controls also suggest that CO is likely to be responsible for the effect observed as pre-irradiation experiments fail to show the same antibacterial effect. One of the draw backs with this experimental procedure is that a significant amount of irradiation is required to get a potent antibacterial effect.

In comparison with histidine photo-CO-RM **21**, the CO-release rate of CO-RM **47** is significantly faster.[78] This means that CO-RM **21** may struggle to show any antibacterial activity due to such a slow CO-release rate. A short half-life is likely to be required for this treatment, which may explain why ruthenium CO-RM-**3** ($t_{½}$ = 1 minute) has also been shown to be effective against *E. coli*.[107]

4.4.4 Investigations with CO-RM 47 on *S. aureus* 8325-4

Staphylococcus aureus is another strain of bacteria which is responsible for a number of severe infections, particularly in hospitals. Older patients and those with a reduced immune system are particularly vulnerable to infection. There are also many strains which are becoming resistant to a wide range of antibiotics and alternative treatments for these strains are urgently required.[108] As shown with ruthenium dimer CO-RM-**2**, it is possible to use a CO-RM to induce a detrimental effect on *S. aureus*. Having shown that under the correct conditions, CO-RM **47** can be antibacterial towards *E. coli*, it seemed logical to expand its scope to further strains of bacteria. The next strain to be tested was *S. aureus*.

Initial investigations with CO-RM **47** and *S. aureus* established the viability under thermal conditions. Initial growth curves were also used to establish if DMSO was affecting the growth rate. **Figure 87** shows the first growth carried out with CO-RM **47** on *S. aureus*.

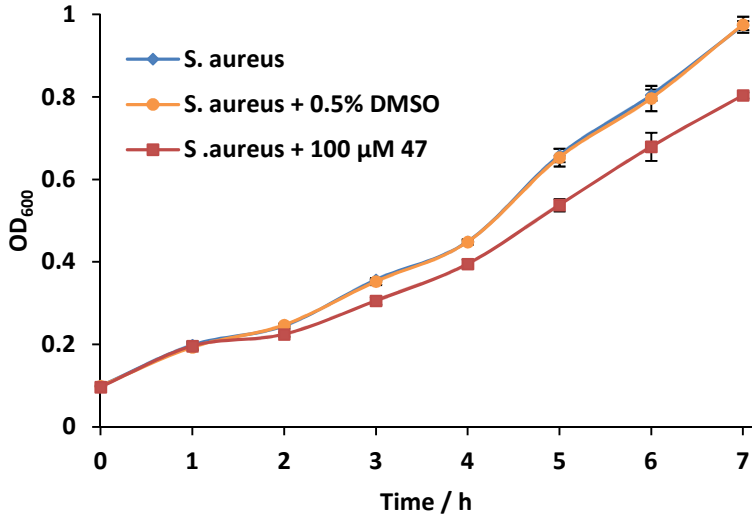

Figure 87. Growth of *S. aureus* 8325-4 in LB media with 100 rpm rotation with 100 µM CO-RM **47** at 37 °C. 0.5% DMSO used as a control.

Initial investigations show that *S. aureus* cannot use DMSO beneficially like *E. coli* can. The results also show that there is a decrease in the growth of *S. aureus* without the need for irradiation. This suggests that there might be a small amount of CO released from CO-RM **47** thermally over the long-term. The reduction is not very significant and there is not a potent antibacterial effect here.

Following on from the experiment in **Figure 87**, it was appropriate to proceed with irradiation of CO-RM **47** with *S. aureus.* These studies were carried out prior to knowledge about irradiating at

one hour after inoculation. This next study was carried out with 68 mins of irradiation after three hours of initial growth (**Figure 88**).

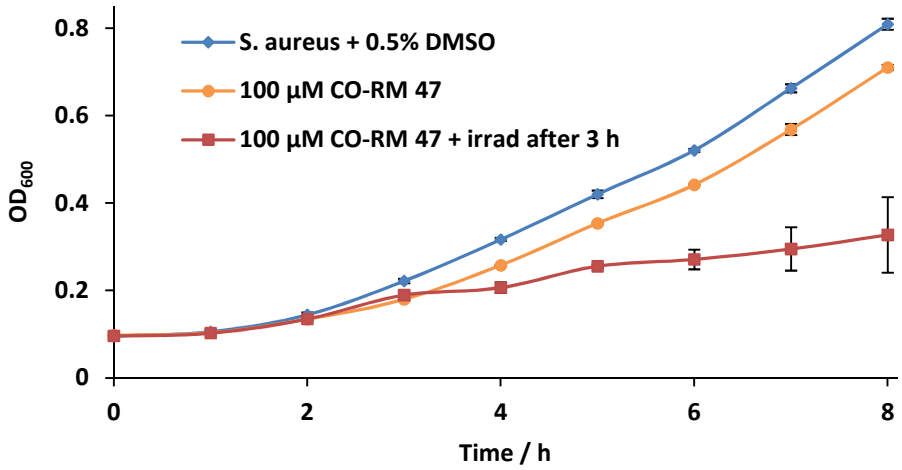

Figure 88. Growth of *S. aureus* in LB media with 100 rpm rotation with 100 µM CO-RM **47** at 37 °C. 0.5% DMSO used as a control. Irradiation (400 nm, 2.4 W) started at three hours for a total of 68 mins (4 mins on, 1 min off cycles).

The data in **Figure 88** shows that with irradiation, there is a significant reduction in the growth of *S. aureus*. It has been reported in the literature that *S. aureus* can be particularly sensitive to 400 nm irradiation.[109-110] Therefore a further control with light only was required to assess the difference between irradiation, both with and without CO-RM.

Figure 89 shows this additional experiment.

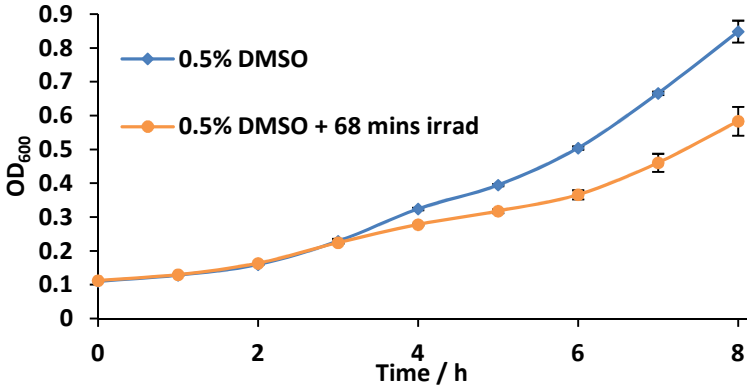

Figure 89. Growth curve with *S. aureus* 8325-4 in LB medium at 37 °C with 100 rpm rotation. 68 mins irradiation (400 nm, 2.4 W) started after three hours (LED on for four mins per five min period).

The control experiment in **Figure 89** shows that irradiation and CO-RM **47** together give a more potent effect that irradiation on its own.

After it was realised in studies with *E. coli* that irradiation after one hour initial growth improves the effectiveness of the treatment; the same strategy was then employed in studies with *S. aureus*. **Figure 90** is a repeat of the study in **Figure 88** with irradiation starting after one hour initial growth instead of three.

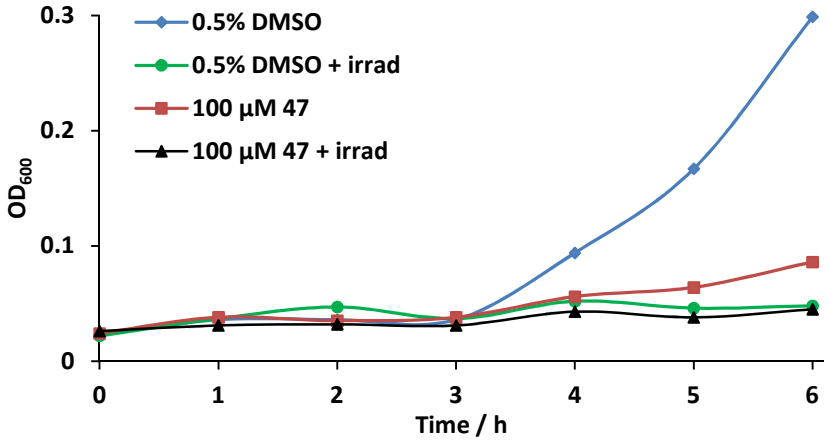

Figure 90. Growth of *S. aureus* in LB media with 100 rpm rotation with 100 µM CO-RM **47** at 37 °C. 0.5% DMSO used as a control. Irradiation (400 nm) started at three hours for a total of 68 mins (four mins on, one min off). Starting OD lower than carried out in previous experiments.

It is important to note that the curves in **Figure 90** were carried out with a lower starting OD than previously carried out. This results in CO-RM **47** having a potent effect on *S. aureus* without irradiation. This is unusual considering the stability of CO-RM **47** in this medium. At the lower OD (fewer bacteria), there could be a higher CO-RM/target ratio, which could explain why this effect with no irradiation is observed. Without irradiation there is still slow growth throughout the experiment suggesting it is not killing a large percentage of bacteria.

When irradiation is used the OD is static throughout the whole experiment both with and without CO-RM **47**. However a plating viability study was carried out with *S. aureus* to verify if a difference between the two could be observed. **Table 11** shows the colony numbers from aliquots taken at one and three hours, representing before and after irradiation respectively.

Table 11. Plating study with *S. aureus*, aliquots taken at one hour and three hours from the cultures used in **Figure 90**. Study with 100 μM CO-RM **47** in LB media. Dilutions are noted in bold

1 h CO-RM	3 h CO-RM (irrad)	1 h DMSO	3 h DMSO (irrad)
500x	**500x**	**500x**	**500x**
530	0	565	13
5000x	**5000x**	**5000x**	**5000x**
78	0	71	0

As previously shown in the literature, irradiation of wavelength 400 nm has a potent effect on *S. aureus,* and this is also shown in the case with DMSO only.[109-110] With 400 nm irradiation only, there is a 97% killing rate under the given irradiation conditions. This shows how sensitive *S. aureus* is to the irradiation used. With 100 μM CO-RM **47** this killing rate is increased to over 99%. The difference is very slight, but the 13 remaining bacteria detected in that aliquot could turn in to 1000's after treatment. Using a lower starting OD and irradiating earlier in these experiment results in a more potent effect.

4.5 Conclusions on CO-RM 47 and its properties

CO-RM **47** has been prepared in 50% overall yield in four linear steps, and complicated purification was not required. CO-RM **47** has also been fully characterised using a wide variety of techniques demonstrating high purity. This is essential when carrying out biological tests on potentially sensitive cells. False results at this stage could have large implications in further studies.

CO-RM **47** has been shown to release three molecules of CO per molecule of CO-RM. This is beneficial as less CO-RM will be required to get a desired concentration of CO released. The tetracarbonyl phenylpyridine manganese(I) motif does not exhibit different modes of CO-release in myoglobin assays when it is structurally modified in the *para*-phenyl position. This is encouraging when considering the aims of this project. CO-RM **47** has been shown to be viable with RAW 264.7 cells and to have varying detrimental effects on both *E. coli* and *S. aureus* at concentrations that do not kill RAW 264.7 cells. Ester CO-RM **45** was mildly toxic to RAW 264.7 macrophage cells, highlighting the importance of hydrolysing the ester to give CO-RM **47**.

CO-RM **47** has been shown to suppress the effect of inflammatory stimulation and it is likely that CO released from CO-RM **47** is responsible for this. This CO-RM has great potential and further studies in the future to get this CO-RM closer to clinical trials would be desirable. Irradiation of wavelength 400 nm is out of the harmful UV region of the spectrum. People experience 400 nm irradiation on their skin when simply outside in the sun. At low bacterial densities, there is a possibility that the irradiation might not even be required (**Figure 90**). The results in this section justify further biological studies using CO-RM **47**

5 Development of Functionisable CO-RMs

5.1 Synthesis and characterisation of alkyne tagged CO-RMs

CO-RM **47** has been developed from an initial tetracarbonyl phenylpyridine manganese(I) structure to improve its solubility and subsequently CO-release rates. However, this CO-RM has no intentional means of protein targeting. There is a possibility to use the acid functionality on CO-RM **47** in esterification and amide formation reactions to introduce functionality capable of protein binding. It was however decided that using a Huisgen [3+2] cycloaddition approach that has been previously used on $(tpm)Mn(CO)_3$ developed by Schatzschneider and co-workers would be a more suitable initial approach.[61] Functionalisation on 4-hydroxyphenylpyridine (**43**) was used to develop a new target CO-RM. A second derivative with an extra CH_2 group between the phenyl group and the oxygen was also prepared amid concerns of potential phenolic ether hydrolysis. **Figure 91** shows the structure of the designed target CO-RMs.

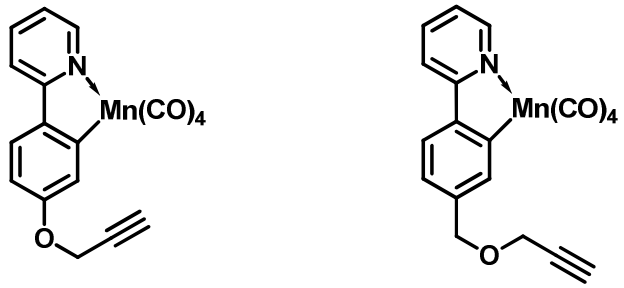

62 **63**

Figure 91. The structure of target alkyne CO-RMs **62** and **63**.

The target structures contain terminal alkyne functionality, which has the potential to be used in cycloaddition chemistry. This could introduce variation in functionality to generate an analogue library. As mentioned, CO-RM **63** has an additional methylene group that could help reduce steric and electronic interference from the attached groups with the tetracarbonyl manganese. This chemistry can be used in the following way to generate new structures (**Scheme 20**).[111]

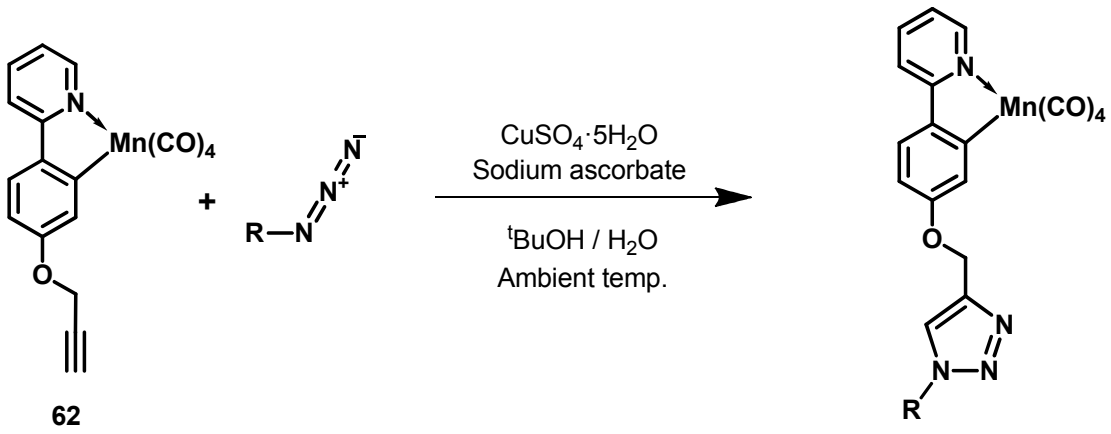

Scheme 20. Potential Huisgen [3+2] cycloaddition conditions to introduce desired R group on CO-RM **62**. The same conditions could also be used on CO-RM **63**.

By activating the alkyne functionality on CO-RM **62** with copper(II) sulfate pentahydrate, the azide and alkyne can then undergo a cycloaddition reaction to give a 1,4-triazole ring with the desired R group attached. It is possible that 1,5-triazole regio-isomers of the desired product could be formed in this reaction where the azide adds in the cycloaddition rotated by 180 degrees, but a literature procedure was found that exclusively gave only the 1,4-isomer, and this was important when trying to design an efficient synthesis.[111]

The synthesis of CO-RM **62** started from phenol compound **43**, but for the synthesis of CO-RM **63** an additional alcohol-containing ligand was required. **Scheme 21** shows the synthesis of extended alcohol **50**.

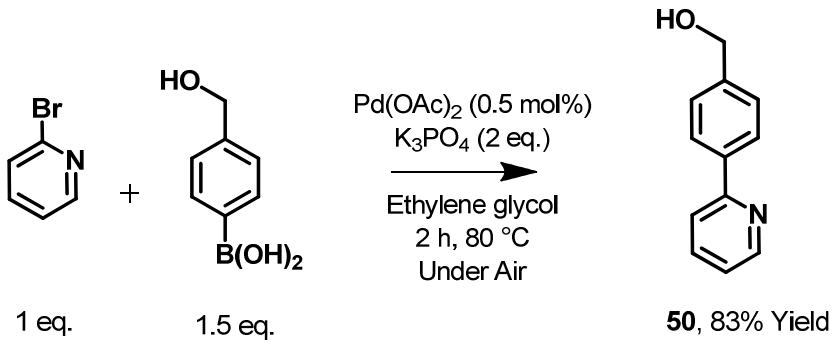

Scheme 21. Suzuki–Miyaura coupling conditions used to prepare ligand **50**

Similar conditions were used to prepare phenolic ligand **43**, however a longer reaction was required to get full conversion. This is likely to be due to the alcohol functionality not being in conjugation with the ring system in this case, Pleasingly, two hours reaction time gave ligand **50** in a respectable 83% yield.

With the two alcohol-containing ligands **43** and **50** synthesised, the next step was to introduce alkyne functionality into the system. Similar conditions used by Schatzschneider and co-workers on their tpm ligand system were adopted here, as this had been shown to work successfully.[61]

The Williamson ether synthesis conditions used to make the propargyl ligand **52** is shown in **Scheme 22** . The same conditions were also used to make shorter ligand **51**.

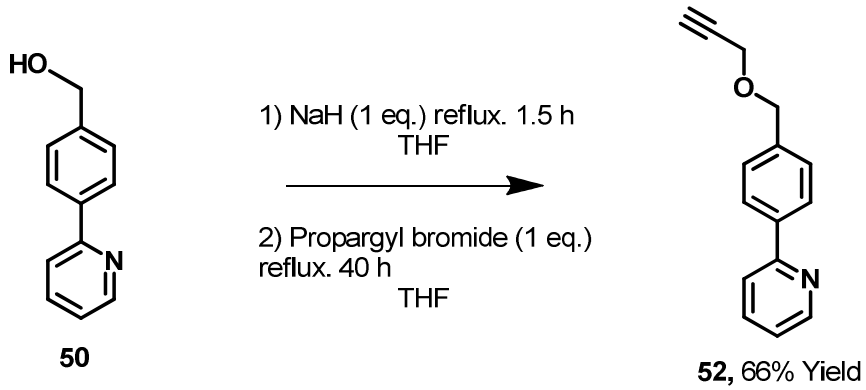

Scheme 22. The synthesis of compound **52** using a William ether synthesis.

By converting alcohol **50** to its corresponding sodium salt, the oxygen atom is then activated, allowing nucleophilic attack on propargyl bromide to give the target alkyne **52**. Alkyne **52** was isolated with a yield of 66%, which is comparable with the yields obtained on the tpm ligands by Schatzschneider and co-workers.[112] The shorter ligand **51** was also synthesised using these conditions and was isolated with a yield of 75%. This is a slight improvement on the extended ligand. Both of these reactions yielded sufficient quantities of alkyne ligand to continue with the next synthesis.

The next step in the synthesis of CO-RMs **62** and **63** was intended to be the final step in the synthesis and involved reacting the synthesised alkyne ligands with $BnMn(CO)_5$ to introduce the tetracarbonyl manganese(I) system. **Scheme 23** shows the conditions used in an attempt to synthesise CO-RM **63**.

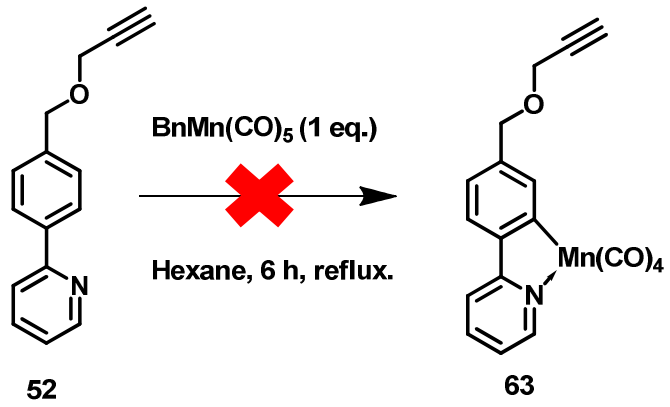

Scheme 23. Attempted conditions used to cyclometallate ligand **52**.

After initial heating at 75 °C, rather than turning the yellow/light brown colour typically observed with previous cyclo-metallation reactions; this reaction turned dark brown/black and significant amounts of precipitation occurred. The desired product was not isolated from attempted cyclo-metallation of either ligand **51** or **52**. It was postulated that the alkyne functionality was reacting with the tetracarbonyl manganese unit, resulting in precipitation of manganese(IV) species which are typically are dark brown in colour. Analysis of literature research carried out by Nicholson and co-workers provided a potential explanation for what was occurring in this reaction (**Scheme 24**).[113]

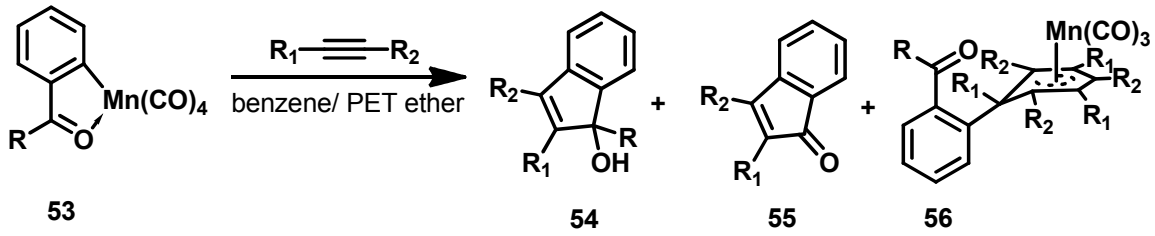

Scheme 24. Reaction of an *ortho*-$Mn(CO)_4$ aryl ketone with alkynes to produce indenols, indenones, and hexadienyl manganese tricarbonyl species.

When *ortho*-$Mn(CO)_4$ aryl ketones (**53**) are heated with a wide variety of alkynes, these react to produce indenols (**54**), indenones (**55**), and a structurally interesting hexadienyl manganese(0) tricarbonyl species (**56**). Generation of **56** arises from triple insertion of the alkyne species. It was suspected that some kind of insertion process was occurring with the phenylpyridine system, which involved alkyne ligand **52** reacting with a molecule of CO-RM **63** once it has been formed.

The research by Nicholson and co-workers explored a wide variety of alkynes in their reactions, and this was very useful in solving the synthetic problem of synthesising CO-RM **63**. Many functional groups on either side of the alkyne used in these reactions were tolerated, with the

exception of two $SiMe_3$ substituents. Reflux of **53** in benzene with the TMS alkyne for 64 hours yielded only 9% of indenol **54**. The TMS group is likely associated with blocking the reaction of the alkyne with **53**. This information was then employed in stopping the terminal alkyne in ligand **52** reacting. It was decided that since only one side of the alkyne in ligand **52** could be functionalised, that a bulky TIPS group could be used to try and reduce the alkyne reactivity. **Scheme 25** shows the synthesis of TIPS protected alkyne **58** using a modified literature procedure.[114]

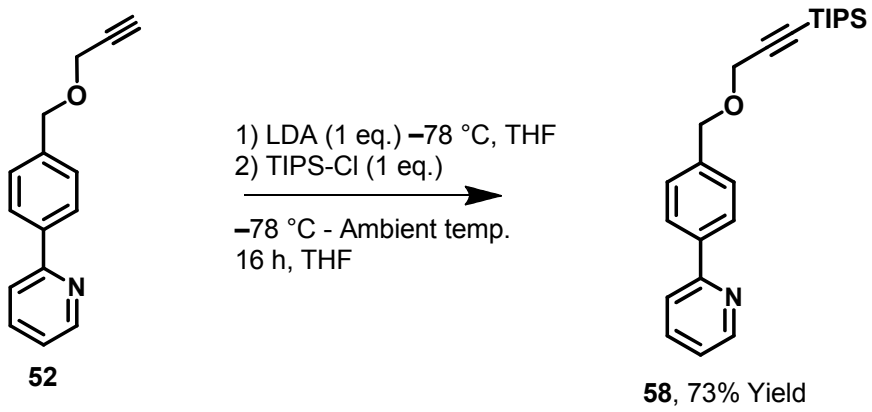

Scheme 25. Synthesis of TIPS protected alkyne ligand **58**

Lithiation of the terminal alkyne in **52**, followed by trapping with TIPS chloride gave **58** in a respectable 73% yield. The corresponding shorter TIPS alkyne **57** was also synthesised using the same method and was isolated with a yield of 76%.

With protected TIPS alkyne ligands **57** and **58** prepared, the next step was to attempt a cyclometallation reaction to see if the introduction of TIPS group would allow cyclometallation to occur. **Scheme 26** shows the conditions used to form TIPS protected complex **60**.

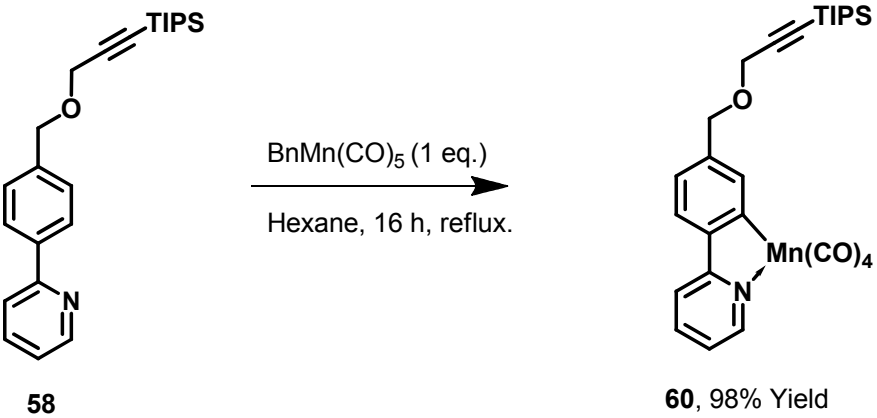

Scheme 26. Reaction of TIPS protected ligand **58** with $BnMn(CO)_5$ to give complex **60.**

Pleasingly, introduction of TIPS functionality on the alkyne eliminates any significant side reactions, and pure product was isolated with a 98% yield following a simple filtration. The success of this reaction highlights the importance of reporting unsuccessful reactions in the literature. While Nicholson and co-workers were deliberately trying to react alkynes with manganese complexes, the reporting of their 'less successful' reaction was useful in this research. Without this knowledge the synthesis of complex **60** may have not been achievable in the same time-frame. The corresponding shorter TIPS complex **59** was also prepared in 97% yield.

An additional communication was published by Wang and co-workers.[115] This paper helps to further explain what was occurring in the unprotected cyclometallisation reactions. The research shows how heating tetracarbonyl phenylpyridine manganese(I) complexes in the presence of terminal alkynes yields alkenyl products (**Scheme 27**).

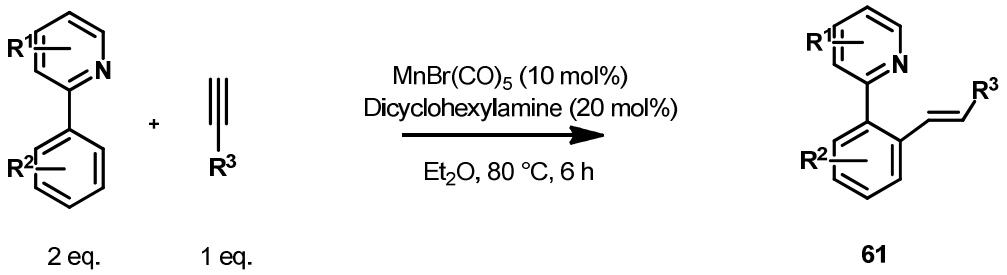

Scheme 27. Literature synthesis of alkenyl phenylpyridines using a manganese catalyst system.

In this reaction $MnBr(CO)_5$ (**20**) with the amine base, produces tetracarbonyl phenylpyridine manganese(I) complex **37** *via* a different route. This complex then reacts with alkynes to form the alkenyl phenylpyridine **61**. This is another potential pathway that could have occurred when attempting to cyclometallate the unprotected alkynes with $BnMn(CO)_5$ (**42**).

With the TIPS protected complex synthesised, the final step in the synthesis of CO-RMs **62** and **63** was a TIPS deprotection. This was done using TBAF·$3H_2O$ at ambient temperature. **Scheme 28** shows the conditions used to isolate target complex **63**.

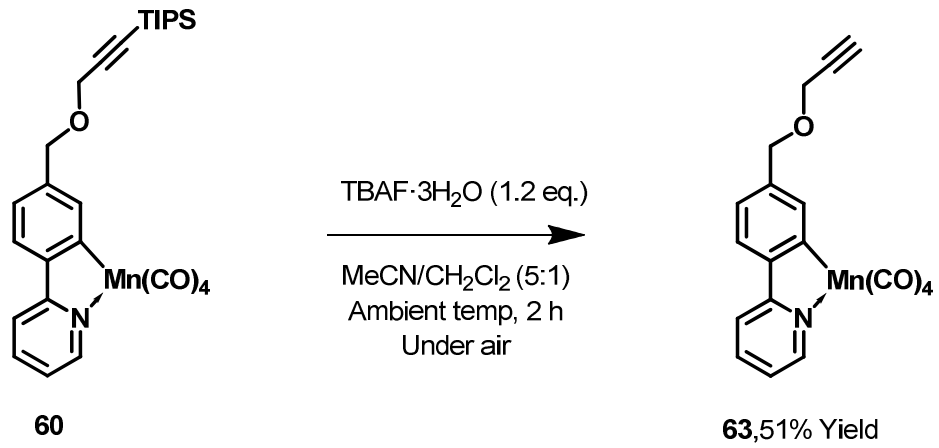

60 **63**,51% Yield

Scheme 28. The synthesis of CO-RM **59** from its corresponding TIPS protected complex **56**.

A CH_3CN/CH_2Cl_2 mixture was used to enable full dissolution of the apolar TIPS protected complex. The complex was unfortunately only synthesised in 51% yield, and it was discovered that the TBAF reagent converted a significant amount of TIPS complex **60** to its corresponding free ligand **52**. However a sufficient quantity of CO-RM **63** was isolated, which could then be used for further studies. The corresponding alkyne complex **62** was also prepared using the same method with 1 eq. of TBAF·$3H_2O$ in 52% yield.

Complexes **62** and **63** have been successfully prepared and isolated for use in further studies including synthesis, CO-release, and biology (see section **5.2**).

5.2 CO-release studies with alkyne CO-RMs 62 and 63

The CO-release rates of CO-RMs **62** and **63** was quantified using myoglobin assays. These were performed with each CO-RM at 10 and 40 μM concentrations. Irradiation of wavelength 400 nm was used as before, so that half-life values for CO-release could be compared with previously synthesised CO-RMs. **Figure 92** shows the CO-release profiles for CO-RMs **62** and **63** at 10 and 40 μM.

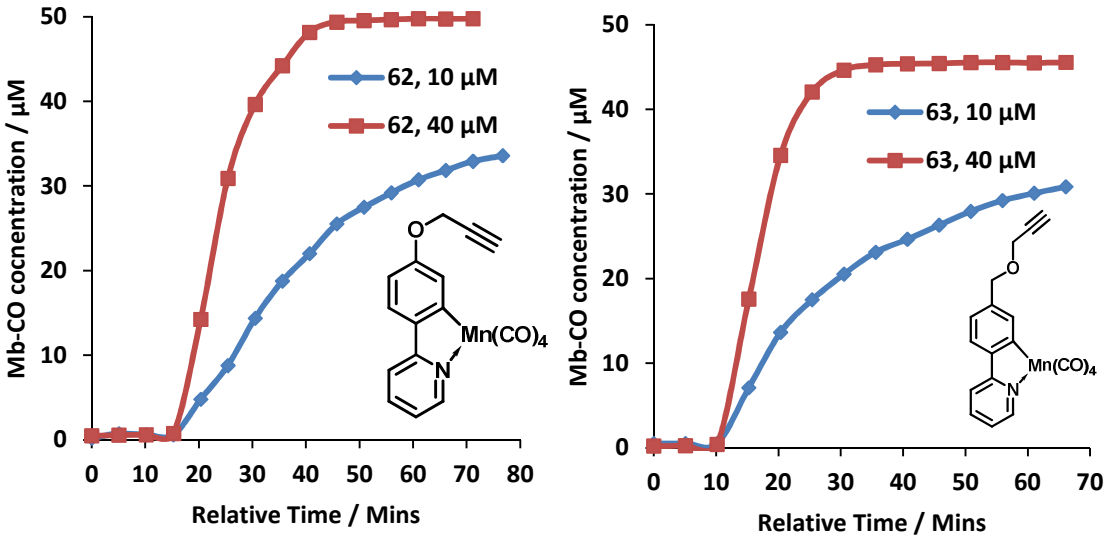

Figure 92. The CO-release profiles of CO-RM **62** (left) and **63** (right) at 10 and 40 µM with 45-50 µM myoglobin in PBS buffer pH 7.4. Irradiation (400 nm, 2.4 W) on for two minutes per five minute period. CO-RM **62** 40 µM curve and CO-RM **63** 10 µM curve shifted left to match starting irradiation times for comparison at different concentrations. CO-release not observed in any case until irradiation was initiated.

The CO-release profiles for CO-RM **62** and **63** show that despite changing the functionality on the phenyl ring quite significantly, it does not affect the mode of CO-release. Both **62** and **63** do not release CO until the irradiation is initiated. At 40 µM, both CO-RMs saturate the myoglobin, and at 10 µM both CO-RMs are releasing three molecules of CO per molecule of CO-RM. This matches the number of CO molecules released from CO-RM **47**. It appears that despite the change in functionality in the *para*-phenyl position, that the $Mn(CO)_4$ moeity is acting as an isolated CO-releasing unit. **Figure 93** shows the half-life values calculated from the data in **Figure 92**.

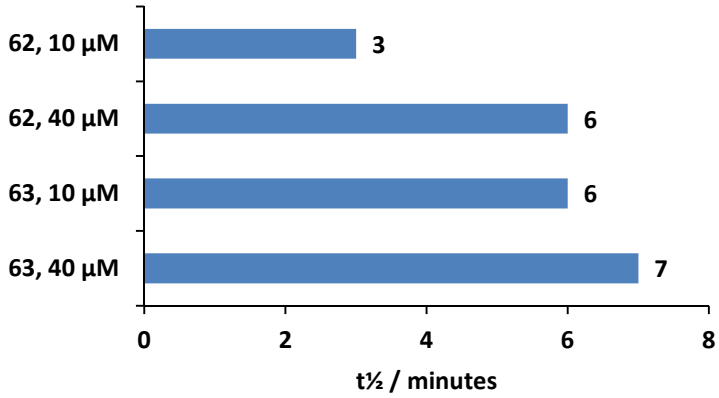

Figure 93. Half-life values for CO-release from CO-RM **62** and **63** at 10 and 40 µM.

The half-lives of CO-RMs **62** and **63** are comparable to CO-RM **47** (5 mins). This further emphasises how changing functionality is not altering the CO-release properties of the '$Mn(CO)_4$' unit. CO-RM **63** at a concentration of 10 µM appears to have a fast half-life of three minutes. This could be due to complete solubility at this concentration. It is unfortunate that there is a small amount of precipitation with CO-RMs **62** and **63** at a concentration of 40 µM, but this was corrected as previously using four point correction.

5.2.1 Biological studies with CO-RM 62 and 63 on RAW 264.7 cells

Even though CO-RMs **62** and **63** show a small amount of precipitation, it was still important to test their viability against RAW 264.7 cells. In the pharmaceutical industry there are many drugs that are not directly soluble in water including many steroids and solubilising agents which can be used in formulation with such compounds.[95] This could be done with the CO-RMs in this project. It is also important to note that there was significantly less precipitation with these functionalised compounds compared to the initial CO-RM series (**37-41**) discussed previously in section **3**.

CO-RMs **62** and **63** were therefore tested with RAW 264.7 cells in both Alamar blue and LDH assays using the same conditions that were used with CO-RM **47** (**Figure 94**).

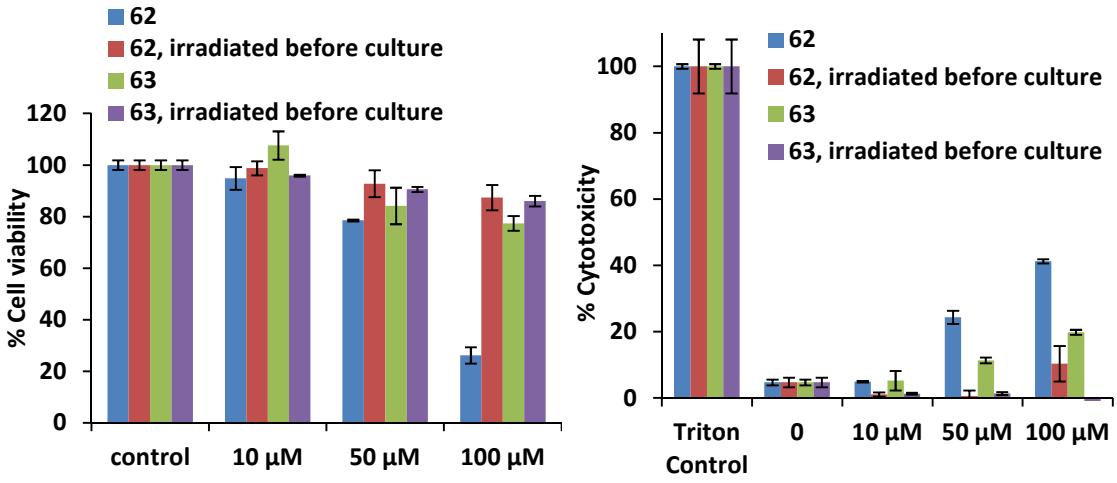

Figure 94. Alamar blue assay (left) and LDH assay (right) for CO-RMs **62** & **63** using RAW 264.7 cells in a 24/96 well plate with DMEM + 10% FCS medium. Compounds tested at the above concentrations with and without irradiation (400 nm, 2.4 W, 8 mins) before addition to the cell culture.

Unfortunately CO-RM **62** shows cytotoxicity at 50 and 100 µM concentrations. Both the Alamar blue and LDH assay shows complementary data with CO-RM **62** inducing significant amounts of LDH being released. Perculiarly, when CO-RM **62** is irradiated for eight minutes prior to addition to the cells, the toxicity is almost completly alleviated. The photo by-products generated do not affect cell viability or induce LDH release. This CO-RM is likely to produce free ligand (**51**) and $(CH_3CN)_3Mn(CO)_3$ (**47c**) just like CO-RM **47** does and it has already been shown that **47c** is viable in pre-irradiation experiments. It is possible that there is something about the geometry of CO-RM **62** that targets an important enzyme resulting in the observed cytotoxicity and viability reductions.

CO-RM **63** with an additional methylene linker, unlike CO-RM **62** is viable with and without irradiation. CO-RM **62** and **63** are similar in structure and this methylene group is important with respect to macrophage cell viability and cytotoxicity. It was proposed that the phenolic propargyl group in CO-RM **62** could be hydrolysed to produce a phenol containing species (**64**), causing a significant degree of toxicity. The presence of the $Mn(CO)_4$ group withdrawing electron density out of the aromatic rings, could increase the rate of hydrolysis compared to the free ligand.

With the above propositions in mind, a new phenolic CO-RM **64** was prepared from ligand **43** to test the above hypotheses. **Scheme 29** shows the synthesis of phenol-containing CO-RM **64**.

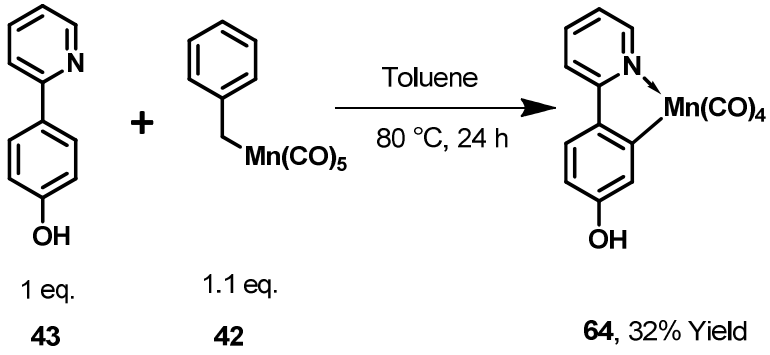

Scheme 29. The synthesis of CO-RM **64**

This CO-RM was particularly difficult to synthesise due to insolubility of ligand **43** in suitable cyclometallation solvents. The CO-RM was prepared in 32% yield, giving sufficient material to carry out biological investigations.

CO-RM **64** was tested in both Alamar blue and LDH assays (**Figure 95**).

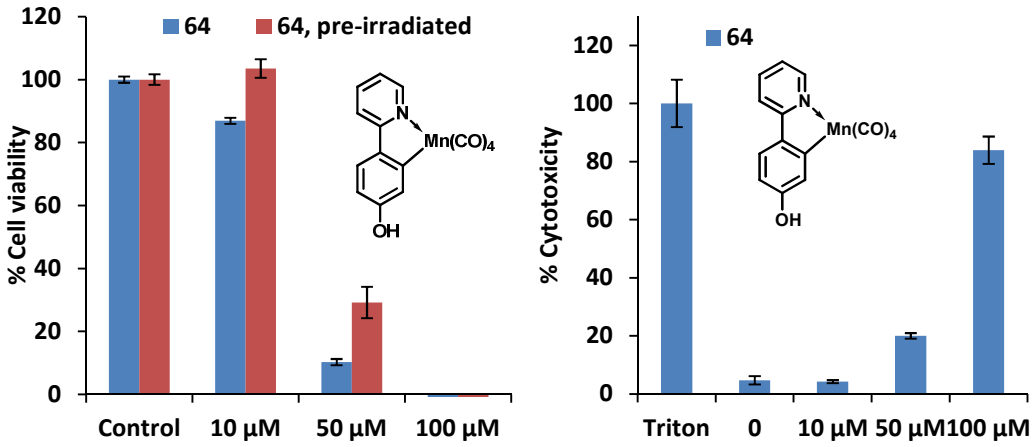

Figure 95. Cell viability tests using CO-RM **64** on RAW 264.7 murine macrophages after overnight incubation. Left: Alamar blue assay with straight addition (blue) and pre-irradiation (red), right: LDH assay. Both assays are referenced to a 1% triton X-114 control. CO-RM **64** wass pre-irradiated for eight mins (2.4 W, 400 nm) before addition to RAW 264.7 cell culture.

Phenol-containing CO-RM **64** shows potent reductions in cell viability and significant cytotoxicity at even 50 µM, with 0% viability at 100 µM. There is also a slight improvement in cell viability when the CO-RM is irradiated before addition to culture. This matches with the unusual behaviour of propargyl-containing CO-RM **62**, and suggests that phenolic CO-RM **64** is produced on administration of CO-RM **62**. The presence of a CH_2 linker between the main functionality in CO-RM **63** could prevent ether bond hydrolysis as no significant cell death observed with CO-RM **63**.

5.3 Cycloaddition chemistry for the functionalisation of CO-RM 63

CO-RM **63** has been shown to be an efficient CO-releaser and is viable with RAW 264.7 cells. CO-RM **62** shows signs of toxicity potentially due to propargyl hydrolysis. This may not be an issue once cycloaddition chemistry has introduced a triazole ring, but with the data available it was deemed less risky to take CO-RM **63**, rather than CO-RM **62** forward for further synthetic studies.

5.3.1 The synthesis and characterisation of extended CO-RM 65

The next stage was to demonstrate that CO-RM **63** could be used as a substrate in [3+2] cycloaddition chemistry. The first reaction carried out was used to improve the solubility of CO-RM **63** to produce a CO-RM similar to acid-containing CO-RM **47**. The conditions used to functionalise CO-RM **63** to produce triazole containing CO-RM **65** are shown in **Scheme 30**.[111]

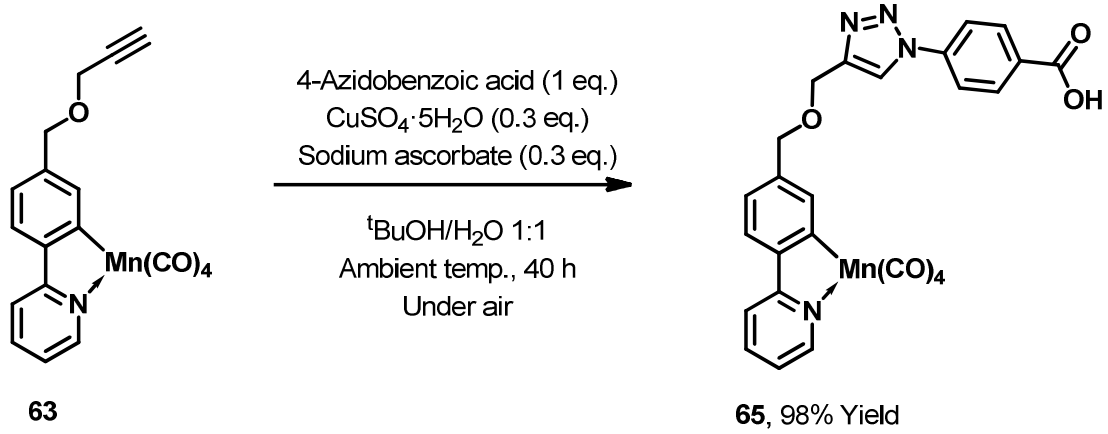

63 **65**, 98% Yield

Scheme 30. Huisgen [3+2] cycloaddition conditions to synthesise CO-RM **65**.

Initial attempts at this reaction using lower concentrations of $CuSO_4 \cdot 5H_2O$ (0.1 eq.) and sodium ascorbate (0.2 eq.) resulted in an incomplete reaction. It was then difficult to purify the compound by column chromatography due to the free acid functionality which caused streaking on TLC plates. With an increased catalyst loading and sodium ascorbate concentration (0.3 eq. of each), complete reaction and purification was achieved with an acid work up to get the polar CO-RM in to the organic layer. The compound was prepared in an excellent 98% yield. **Figure 96** shows the ^{1}H NMR spectrum of CO-RM **65** in DMSO, which shows evidence for key structural features. It is also important to note that reactions carried out on a 45 mg scale (based on CO-RM **63**), only worked in 8 ml medium size sample vials. The original reaction that was scaled up to

45 mg in a small 2 ml sample vial did not go to completion. This is possibly due to deactivation of catalyst by oxygen and stirring issues.

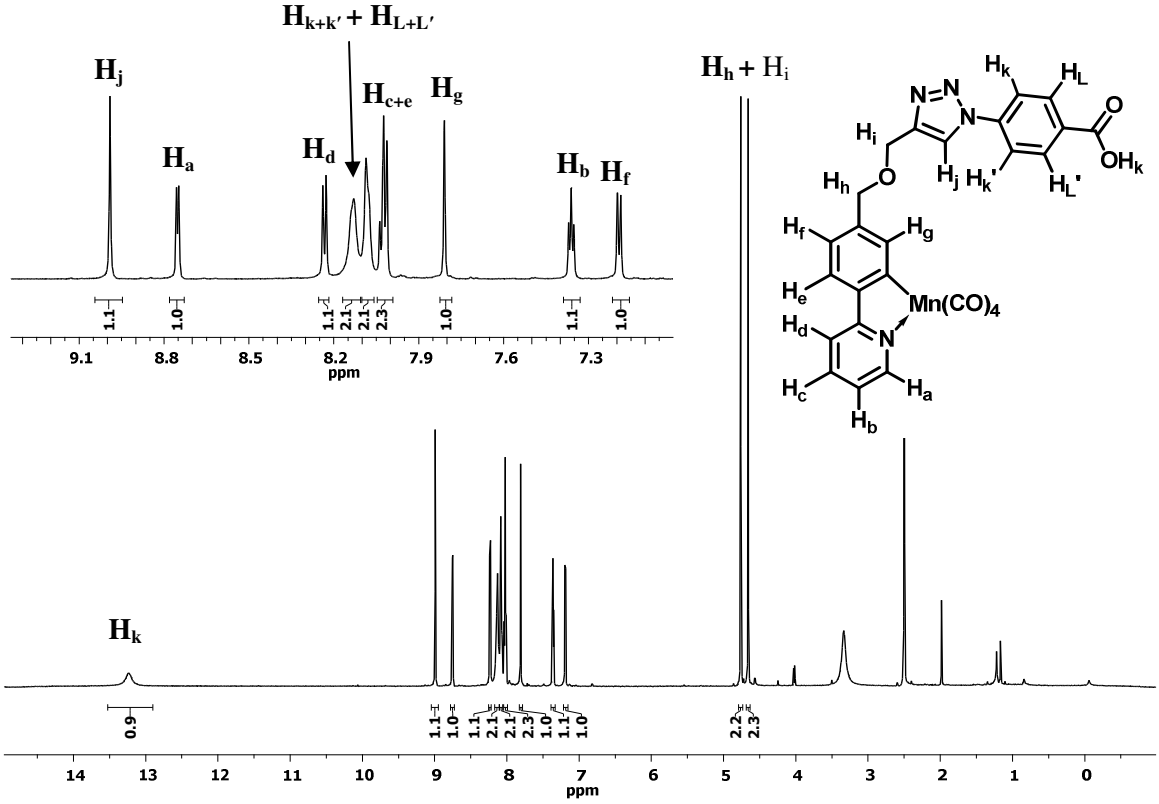

Figure 96. 700 MHz ^{1}H NMR spectrum of CO-RM **65** in DMSO-d_6 at 300 K.

The ^{1}H NMR spectrum of CO-RM **65** shows clear evidence for the presence of pure target compound. There is a singlet at 8.99 ppm corresponding to the triazole proton in the cycloaddition product. Importantly the integration of this proton matches correctly with the integration of all the protons within phenylpyridine structure strongly suggesting that each molecule of alkyne-containing CO-RM **63** has reacted to produce one molecule of triazole-containing species. The two broad peaks at 8.1 ppm correspond to the new phenyl protons k+k′ and L+L′ and these show strong correlation in a ^{1}H COSY NMR experiment. These peaks are unusually broad compared to the phenyl-pyridine proton signals suggesting there are some unusual secondary effects. It is possible that there is some restricted rotation about the phenyl-triazole bond on the NMR time scale. The data obtained suggests the presence of pure CO-RM **65**.

5.3.2 CO-release and biological studies with CO-RM 65

CO-RM **65** was tested in three myoglobin assays to verify if further structural modification affects the CO-release from the $Mn(CO)_4$ motif. CO-RM **65** was initially synthesised to develop cycloaddition chemistry conditions, but it still has some drug like features such as the triazole ring and the carboxylic acid, and could have some interesting properties. One myoglobin assay at 40 µM and two assays with 10 µM CO-RM were carried out. The second 10 µM assay employed stepwise irradiation to see if structural modification still allows 'on and off' switching as demonstrated with CO-RM **47**. These myoglobin assays are shown in **Figure 97**.

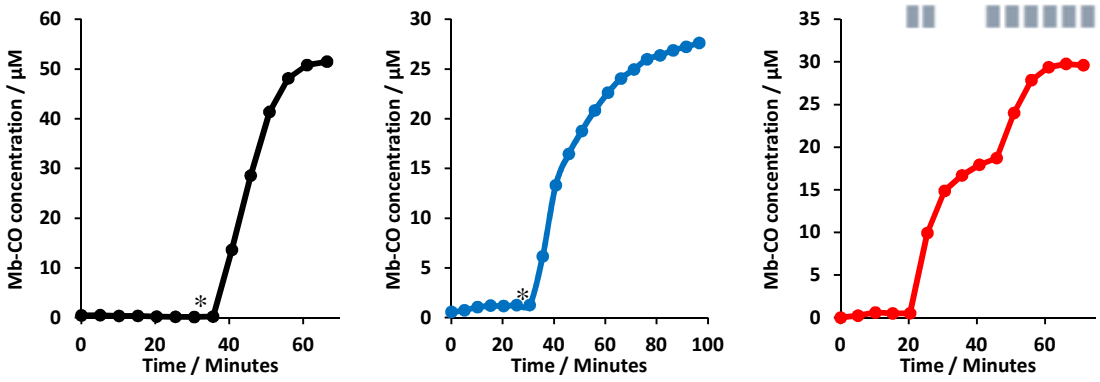

Figure 97. Myoglobin assays in PBS buffer pH 7.4 for CO-RM **65**. Left: 40 µM assay, middle: 10 µM assay. Right: 10 µM assay with step wise irradiation.* marks start of two mins irradiation every five mins or blue rectangles mark two mins irradiation (400 nm, 2.4 W) at the given point in time.

CO-RM **65** can be classified a photo-activated CO-RM under the given myoglobin assay conditions. It is stable in the dark and releases CO efficiently when irradiated with light of wavelength 400 nm. It is capable of saturating 50 µM of myoglobin when using 40 µM CO-RM **65**. CO-RM **65** also releases three molecules of CO just like all previous CO-RMs in this phenylpyridine-containing series. This CO-RM does not precipitate in aqueous solution at the concentrations used in **Figure 97**. This [3+2] cycloaddition chemistry example shows how these methods can be used to improve the properties of a CO-RM, and in this case the solubility is improved.

CO-RM **65** was also tested in viability studies with RAW 264.7 cells to see how the further structural modification would affect cell viability (**Figure 98**).

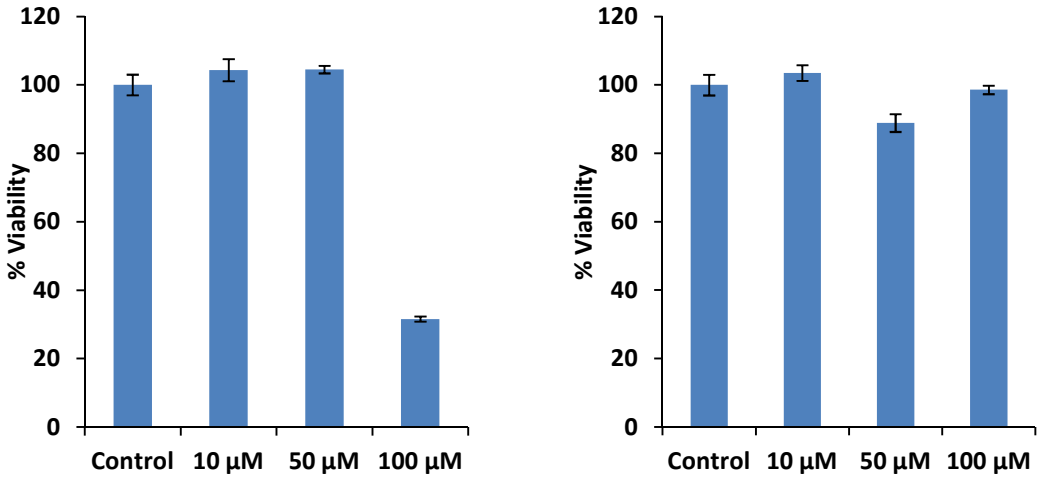

Figure 98. Alamar blue assay for CO-RM **65** with RAW 264.7 murine macrophages. Left: direct addition at the given concentration. Right: Irradiation (2.4 W, 400 nm, 8 mins) performed in DMSO before addition to the cells.

There is a reduction in cell viability at higher concentrations of CO-RM **65** which is then eradicated if the CO-RM is irradiated in DMSO before addition to the cell culture. Unfortunately a degree of colour was formed on the irradiation of this CO-RM in DMSO. This does not interfere with the Alamar blue assay as all the medium is replaced following incubation with the cells. However, with the LDH assay the CO-RM remains in the medium and this colour makes this CO-RM unsuitable for testing in the LDH assay.

In summary, further mechanistic studies would need to be carried out in future to find out the true cause of this reduction in cell viability. CO-RM **65** contains a CH_2 linker between the phenyl pyridine and the rest of the structure so phenolic CO-RM **64** would not be produced on hydrolysis of the linker. This suggests that the original molecule or one of its biological by-products is responsible for the toxicity observed. It is important to note that at 50 µM CO-RM **65** is viable, and can release three molecules of CO per molecule of CO-RM. This means that up to 150 µM CO can be produced on the irradiation of 50 µM CO-RM **65**. Much lower concentrations of CO released from CO-RMs in the literature have been shown to give beneficial biological effects. There is still future promise for CO-RM **65** and it should be taken forward for further biological studies.

5.4 Functionalisation of CO-RM 63 with a biotin marker

As shown in section **5.3.1**, CO-RM **63** can successfully be used as a substrate in cycloaddition chemistry. It seemed logical to try this chemistry with more biologically relevant structures. The more complex biological target chosen for studies was a d-biotin conjugate. Biotin is found in both eukaryotic and prokaryotic biological systems and is associated with a wide range of biological functions.[116] It can bind strongly with avidin/streptavidin ($K_D \approx 10^{-15}$ M), and will not dissociate from the binding site without avidin denaturation.[117] The binding is so strong that radioactive biotin (containing ^{14}C) is required to detect the minute amount of free biotin in solution.

The strong binding of biotin to avidin makes it an excellent model for making a targeted CO-RM. A conjugate with biotin can be synthesised, and this can then be assessed for binding to avidin as a target. It has been shown by Walker and co-workers that under certain conditions *E. coli* will take up large peptide-biotin conjugates through their biotin transporter which they would not usually take up without the biotin linker.[116] This is a potentially method for forcing bacteria to take up pharmaceutical agents, including CO-RMs; although there might be difficulties with getting sufficient uptake. This is because *E. coli* can synthesise its own biotin and in some cases requires nanomolar concentrations to survive.[118]

The following target biotin-CO-RM conjugate **71** was proposed (**Figure 99**).

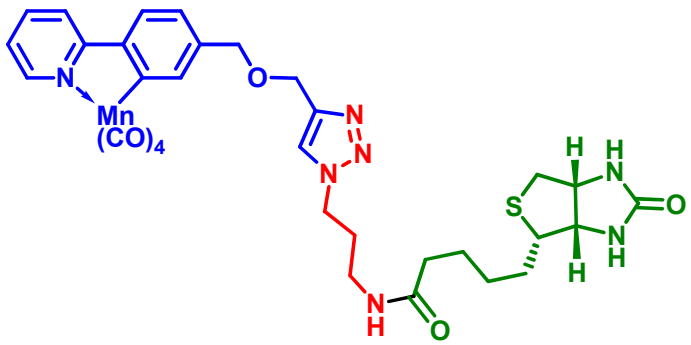

71

Figure 99. Target structure for a biotin-CO-RM conjugate **71**

Target structure **71** contains CO-RM **63** (blue) which is then to be conjugated with a biotin (green) azide structure containing a three carbon linker. The linker (red) acts as a spacer to prevent the CO-RM structure from interfering with biotin-avidin binding. The biotin azide (**70**) and CO-RM **62** can be linked using cycloaddition chemistry in the same way that was used to prepare CO-RM **65**. The synthesis of CO-RM **71** is discussed below.

With the synthesis of CO-RM **62** already completed, all that remained was to synthesise the biotin azide linker (**70**) and this was done by methods shown in **Scheme 31**.

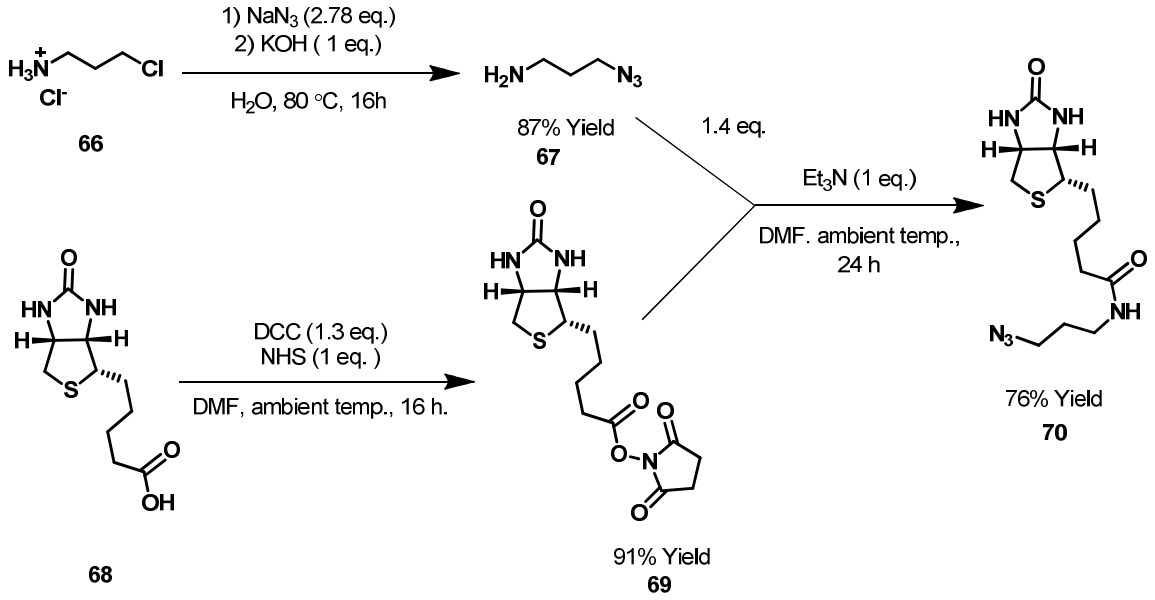

Scheme 31.Synthesis of biotin-containing azide **70**

Conversion of 3-chloropropylamine hydrochloride (**66**) to 3-azidopropylamine (**67**) by nucleophilic attack with NaN_3 was performed in aqueous solution using a literature procedure.[119] The azide product was obtained in 87% yield in comparison with 99% yield reported in the literature. This synthesis of **67** was repeated several times and it is suspected that 87% is a more realistic yield as this compound was particularly volatile. The reaction gave sufficient quantities of **67** for further synthesis. It is important to be aware of the safety precautions associated with handling small azide compounds such as **66**. This compound has a very high nitrogen content and is therefore potentially explosive. Due to this, plastic spatulas, clear-seal glassware, and a blast shield were all used in the synthesis of **66** to prevent any explosion occurring.

To form an amide bond between **67** and **68**, the carboxylic acid functionality on biotin required activation to allow further reactions to be carried out under mild conditions. Biotin (**68**) was activated by the formation of an *N*-hydroxysuccinimide ester. This was achieved using DCC as a coupling agent to give NHS-biotin (**69**) in a respectable 91% yield.

With an *N*-hydroxysuccinimide ester (**69**) prepared, the coupling of biotin and 3-azidoamine propane could be carried out under mild conditions with only triethylamine in DMF at ambient temperature. There was no requirement for an additional coupling agent in this reaction, and this made purification by silica gel chromatography trivial. The required biotin azide (**70**) was successfully synthesised with a yield of 76%.

The final step in the synthesis of biotin conjugate CO-RM **71** was to perform the [3+2] cycloaddition reaction with CO-RM **63** and biotin azide **70** using the following conditions (**Scheme 32**).

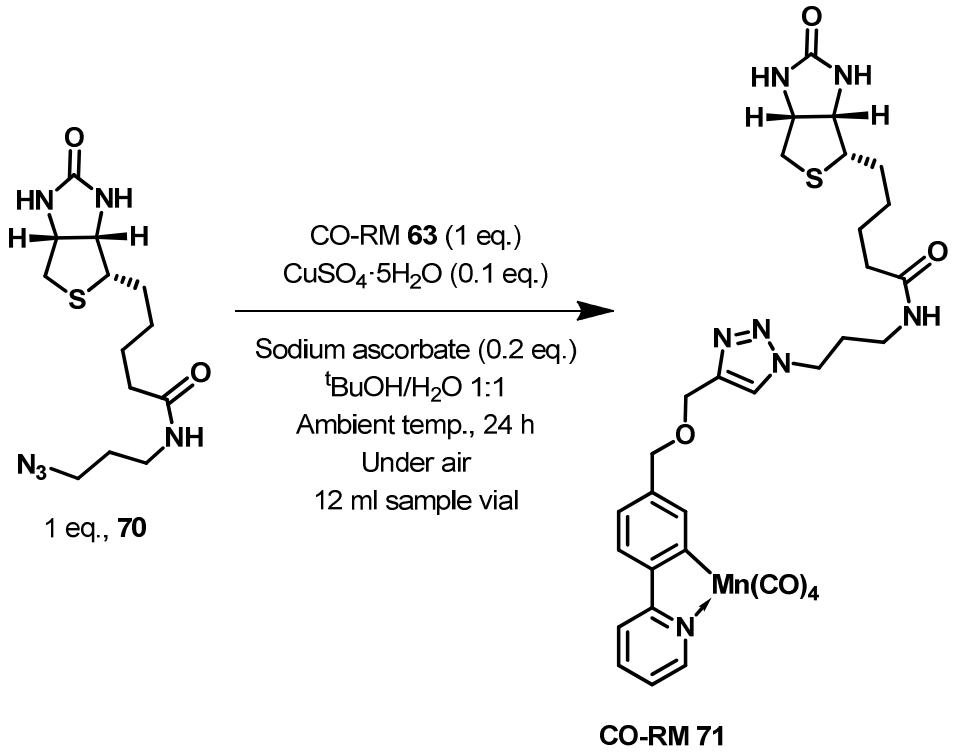

Scheme 32. Initial attempted [3+2] cycloaddition additions for the synthesis of CO-RM **71**

Initial reactions started using lower concentrations of $CuSO_4 \cdot 5H_2O$ and sodium ascorbate (0.1 and 0.2 eq.), which resulted in an incomplete reaction as was the case with CO-RM **65**. Silica gel column chromatography could easily remove any unreacted alkyne CO-RM **63**. One spot was shown by TLC analysis of the column fractions, but ^{1}H NMR spectroscopic analysis indicated that the biotin and 'CO-RM' sections of the molecule did not match in integration. The biotin azide starting material was co-eluting with the product. This means that azide (**70**) needed to be consumed in this reaction or purification would prove extremely difficult. Further reactions with increased catalyst concentration (0.3 eq. and 1 eq.) did not result in complete reaction as determined by ^{1}H NMR spectroscopic analysis. A reaction time of 48 hours also did not result in a compete reaction with 1 eq. $CuSO_4 \cdot 5H_2O$.

These initial reaction attempts were carried out in large sample vials (12 ml) under air (**Figure 100**) and it was postulated that the air may be slowly deactivating the catalyst. Leaving the reaction for longer (48 h) also did not result in complete reaction.

Even with the possibility that air was deactivating the catalyst, it was decided that the conditions would be modified further. This was done so that the reaction could still work without the need to deoxygenate the solvent, making the reaction easier to perform.

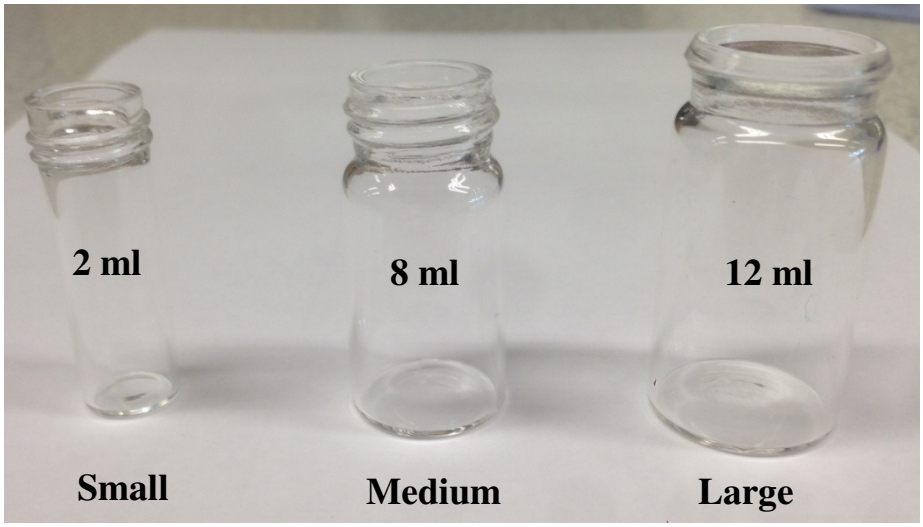

Figure 100. Sample vials used for small scale [3 + 2] cycloaddition reactions to synthesise CO-RMs **65** and **71**.

The reaction proceeded significantly in the large sample vials but never to completion. On switching to the medium size vial with 1 eq. of $CuSO_4 \cdot 5H_2O$ and 2 eq. sodium ascorbate, the reaction goes to completion within 24 hours. Pure product (95 % as determined by ^{1}H NMR spectroscopic analysis) was obtained with only a work up extraction. Under the same conditions in a medium vial there is a clear difference in the conversion to product and the reaction was repeated to give the same results. It is proposed that in the medium sized vial the smaller head space means that over the course of the experiment, there is not enough oxygen within the vial to completely deactivate the catalyst. This means that the reaction proceeds to completion under these conditions. There may also be some differences in the stirring, affecting how starting materials and products come in and out of solution, and it is evident from the image in **Figure 100** how the vortexes formed on solution stirring could vary in vials of different size. **Figure 101** shows the ^{1}H NMR spectrum of the product obtained from both reaction repeats using 1 eq. of CO-RM **63** and 1 eq. of biotin azide **70**.

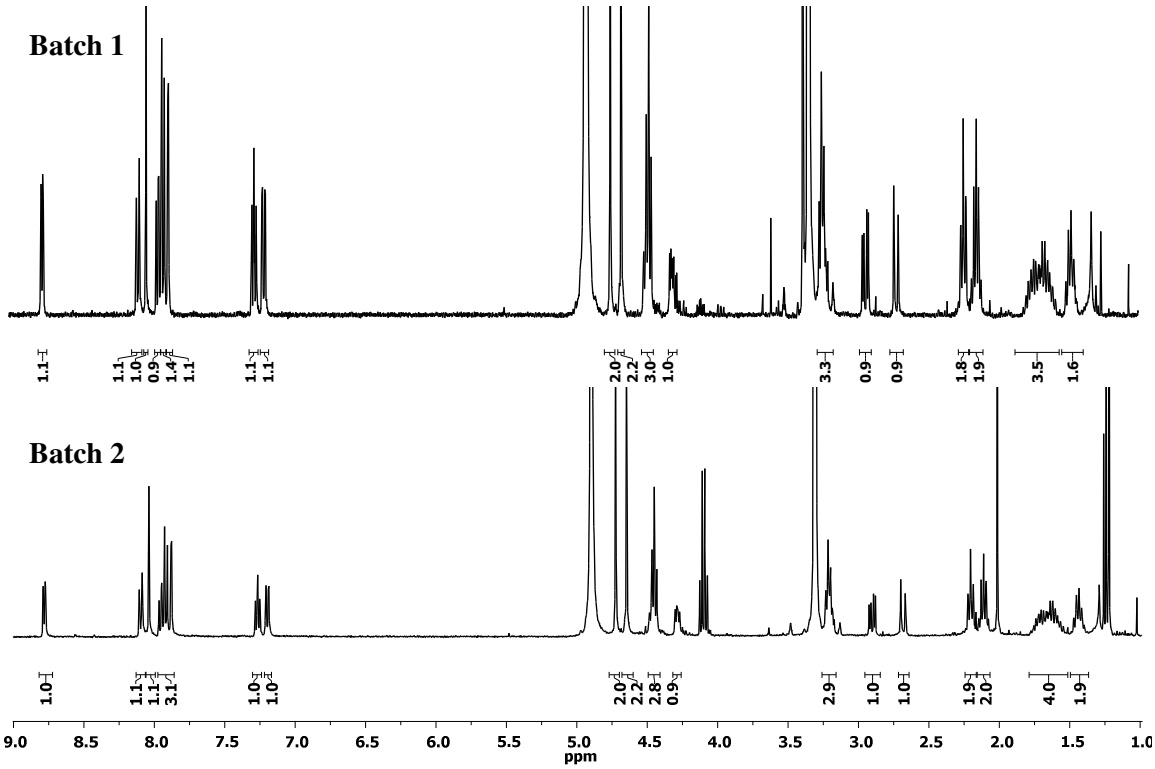

Figure 101. 400 MHz ^{1}H NMR spectrum of two batches of biotin conjugate CO-RM **71** in MeOD-d_4 at 300 K. Note: Batch 2 contains some residual ethyl acetate from workup .

The ^{1}H NMR spectra in **Figure 101** above show that both batches are >90% pure without significant amounts of starting material left in the reaction. All the proton resonances with the exception of the amine signals are observed in the NMR spectrum above. Presumably the amine signals will not be observed in methanol due to exchange. There are however some small amounts of unknown impurities and EtOAc present, especially in the second batch of material. This was not desirable despite the promising reaction conversion without any further purification following workup. CO-RM **71** was obtained in 72% yield using this method.

It was proposed that reaction with 1 eq. of alkyne and azide, any small weighing errors could result in small amounts of remaining starting material that do not react. Therefore two further reactions were attempted using 0.5 eq. of biotin azide **70** and 1 eq. of alkyne CO-RM **63**. With these conditions all of the biotin azide should be completely consumed in the reaction and the remaining 0.5 eq. of alkyne CO-RM **63** can be easily removed by column chromatography due a significant difference in polarity. These new conditions including 48 hours reaction time to ensure complete azide consumption. **Scheme 33** shows the conditions used to prepare biotin-containing CO-RM **71**.

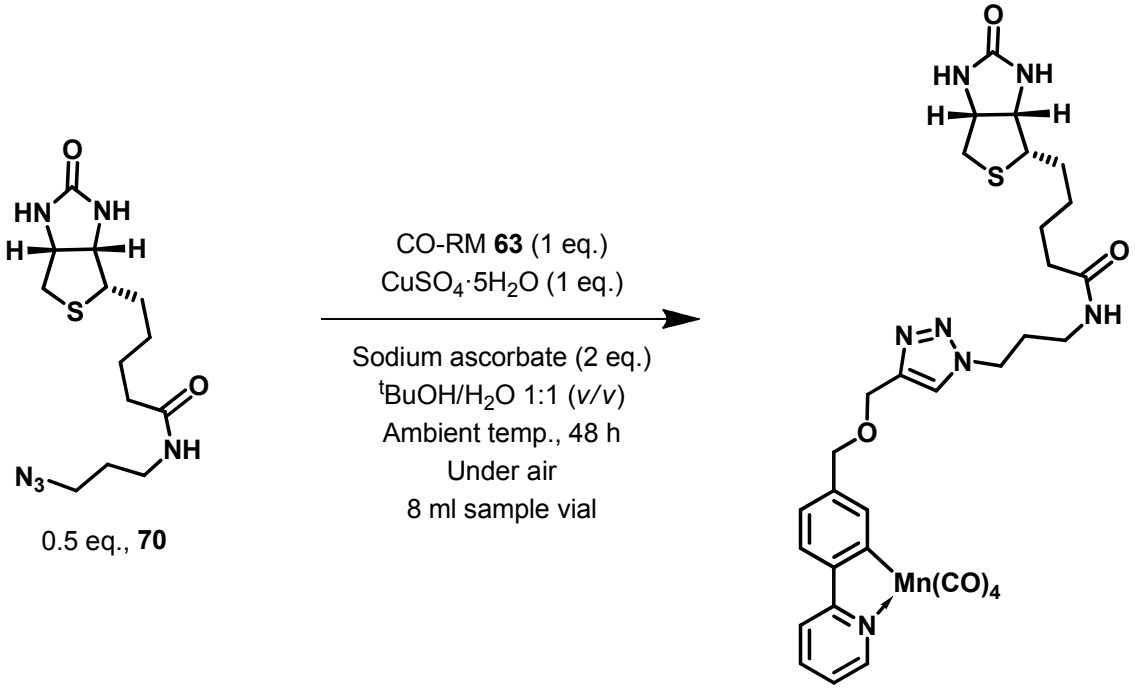

Scheme 33. The synthesis of CO-RM **71** using modified optimised conditions

Using the modified conditions in **Scheme 33** followed by silica gel column chromatography, pure batches of CO-RM **71** were obtained with a 50% yield. The yield is somewhat reduced compared to previous conditions and some product is likely lost during further purification. This new method results in very pure material which is much more suited to detailed characterisation studies. Batches 1 and 2 are still >90% pure as shown by ^{1}H NMR spectroscopy. **Figure 102** shows the ^{1}H NMR spectrum of the material obtained from these new conditions (**batch 3**).

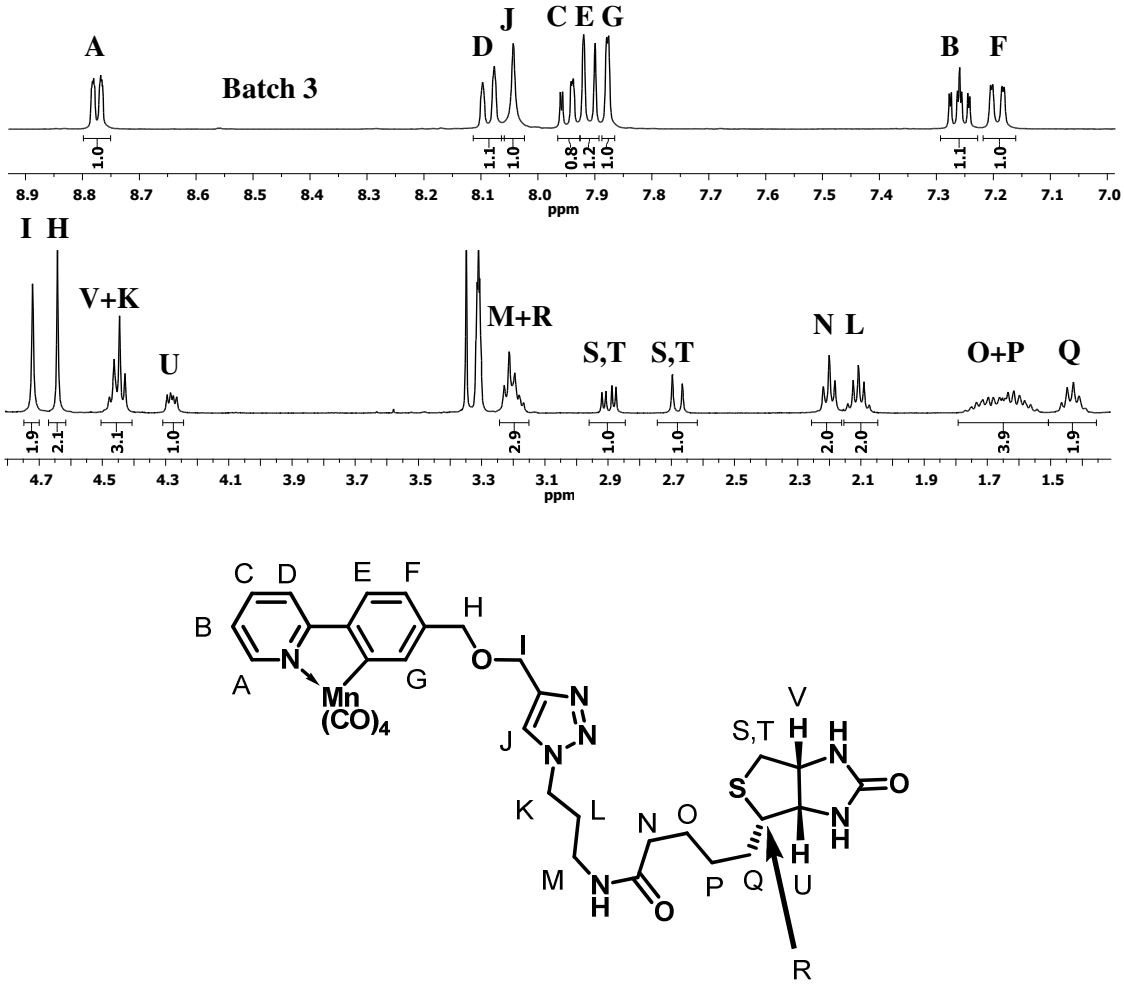

Figure 102. 400 MHz ^{1}H NMR spectrum of CO-RM **71** in MeOD-d_4 at 300 K. Spectrum has been expanded for clarity, with the structure below.

The ^{1}H NMR spectrum in **Figure 102** shows that batch 3 is >98% pure compared to >95% achieved with the previous batches. The use of a substoichiometric concentration of azide **70** meant that all of it reacted prior to column chromatography, so co-elution was no longer an issue. The relative integration between the 'CO-RM' and biotin sections in this batch match closely. In the ^{1}H NMR spectrum of **71**, the triazole proton signal is also detected at 8.05 ppm and its integration matches with the rest of the resonances from the molecule. Further NMR studies including: ^{1}H{^{1}H}, ^{1}H COSY, ^{13}C DEPT-135, HSQC and HMBC, were used to fully characterise CO-RM **71**. It was possible to map out the entire structure of the molecule using these techniques. ESI mass spectrometry and IR spectroscopy data also supports the proposed structure of CO-RM **71**. Four batches of this CO-RM **71** were made and the elemental analysis for each batch was out particularly on the nitrogen. The large molecular weight and series of fused rings of this compound could result in incomplete combustion during the elemental analysis procedure altering the CHN ratio. However, the ^{1}H NMR spectrum of CO-RM **71** batch 3 does not show

any significant impurities. Further binding studies (discussed in section **5.4.2**) suggest that batch 3 is sufficiently pure.

5.5 CO-release and biological studies with biotin conjugate CO-RM 71

It has been established in section **5.3** that biotin CO-RM **71** has been successfully synthesised. The next step was to assess if this molecule could release CO. CO-RM **71** was utilised in myoglobin assays at 10 and 40 μM concentrations. **Figure 103** shows the CO-release profiles for CO-RM **71** in PBS pH 7.4 using conditions typically used previously.

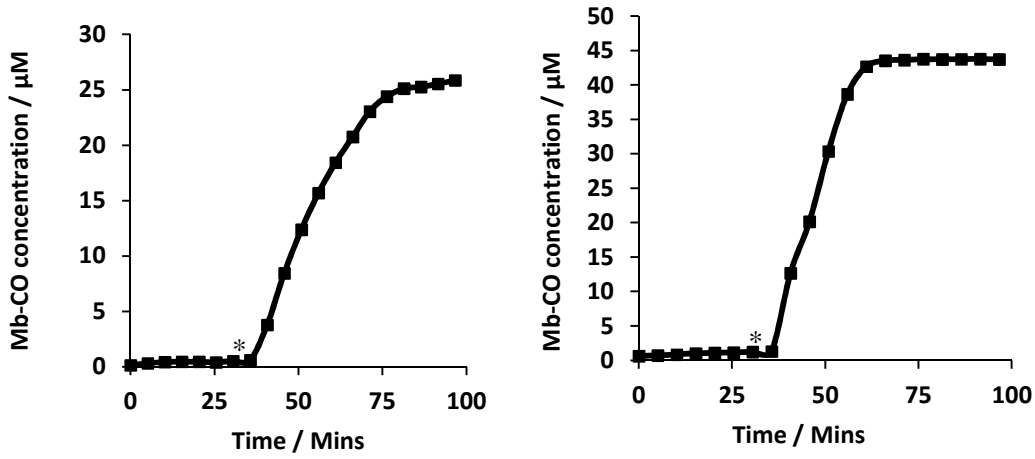

Figure 103. 10 (left) and 40 μM (right) CO-RM **71** used in myoglobin assays. * marks the start of two mins irradiation (2.4 W, 400 nm) every five mins.

Despite the complexity of CO-RM **71**, it still acts as a photo-CO-RM. There is no CO-release from this structure to myoglobin in the dark, and fast CO-release is observed on irradiation at 400 nm. CO-RM **71** releases 2.5 molecules of CO per molecule of CO-RM, which is slightly lower than the previous CO-RMs prepared. This type of reduction was expected as a similar decrease was observed with the (tpm)$Mn(CO)_3$ peptide conjugates prepared by Ulrich and co-workers.[61] CO-RM **71** unfortunately precipitates slightly at concentration of 40 μM in PBS buffer, and some four point correction was required to correct for this. This lack of solubility is likely to be related to the large molecular weight in combination with the apolar section of the CO-RM. However, it was found that reducing the concentration to 30 μM resulted in no precipitation and the CO-RM remains in solution at this concentration. CO-RM **71** can release up to 75 μM of CO at this concentration, which is enough to consider using it in further studies.

5.5.1 RAW 264.7 cell studies with biotin-containing CO-RM 71

CO-RM **71** was then tested in viability studies with RAW 264.7 studies using an Alamar blue assay. It was found that CO-RM **71** photo-products absorb a small amount of light in the visible region and was therefore deemed unsuitable for testing in LDH assays. However the Alamar blue assay can still provide a significant amount of information as the cells must be alive to detect a response. **Figure 104** shows the results obtained from this Alamar blue assay.

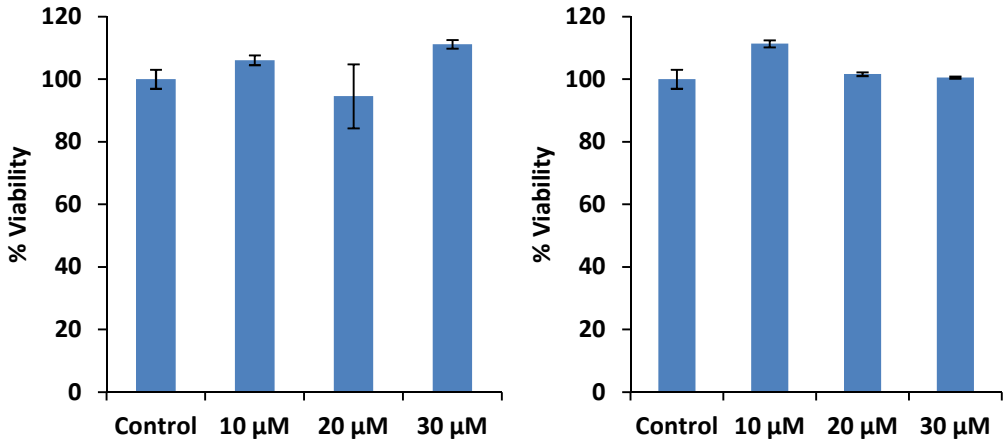

Figure 104 .Alamar blue assay using varying concentrations of CO-RM **71** with RAW 264.7 murine macrophages. Left: direction addition in DMSO. Right: Eight mins (400 nm, 2.4 W) irradiation in DMSO before addition to cells.

CO-RM **71** has been shown to be completely viable with RAW 264.7 cells at various concentrations. It was decided that this CO-RM should not be tested above its known solubility limit as the large molecular weight would likely result in considerable precipitation at a concentration of 100 µM.

As with many of the previous CO-RMs prepared in this project, CO-RM **71** is still viable following eight minutes irradiation in DMSO prior to addition to the cells. The photo by-products of this compound are also viable. Excluding the CO-RMs prepared in this project, there are no photo-CO-RMs in the literature to date that make an *in situ* i-CO-RM by pre-irradiation. It is essential to assess whether the products of irradiation are viable. If these products are toxic to cells, then irradiation would result in the death of many cells in further studies and this is undesirable.

5.5.2 Binding studies using CO-RM 71 and avidin: an example of targeting.

It has been shown that with varying degrees of functionalisation, that the parent phenylpyridine complex maintains its stability, and is a photo-CO-RM in the presence of myoglobin in aqueous solution. The next step with CO-RM **71** was to investigate if it can bind to a target. The selected target is avidin to which biotin binds strongly, with a high dissociation constant.[117, 120] It is important to assess if the linker and CO-RM fragment conjugated to biotin affects the binding to avidin. The three carbon linker should provide sufficient distance between the CO-RM and the biotin unit to prevent any significant interference.

5.5.2.1 HABA/avidin assay with CO-RM 71

The ability of biotin to bind to avidin was assessed using two methods, and the first of these was a HABA/avidin assay. **Figure 105** shows how the HABA avidin assay can be used to quantify the concentration of biotin within a sample.[121]

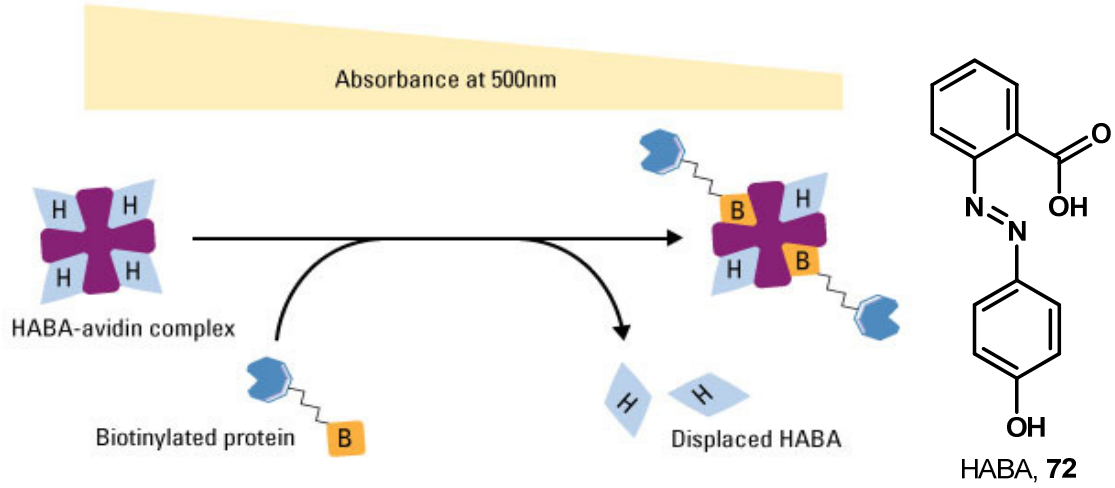

Figure 105. The HABA avidin assay method for biotin quantification (Image by Thermo scientific, Copyright 2014)

Hydroxyazobenzoic acid (**72**) is an orange dye that absorbs strongly at 500 nm. It can bind strongly to avidin but binds weaker than biotin. The biotin can displace HABA out of a HABA-avidin complex, resulting in a lower molar extinction coefficient of the dye. This is due to a change in local environment, resulting in a change in absorbance. This change in absorbance is linearly dependent on the amount of HABA dye displacement, and consequently the amount of biotin in solution. The HABA/avidin assay can be used to quantify the amount of biotin within a sample and this can help assess if CO-RM **71** binds to avidin in solution.

Four solutions were prepared containing 30 µM of a defined compound. The solutions of each compound were based on their molecular weight and were prepared in 0.5% (*v/v*) DMSO/0.01 M PBS pH 7.4. If there is a pure compound in the solution at 30 µM which contains a biotin moeity, then it will quickly displace 30 µM of HABA from avidin, giving an assay read out of 30 µM. If there are any impurities that do not bind, or significant amounts of free biotin are present, then the assay read out concentration will deviate from the calculated concentration. This is because the initial weight of compound used was based on the molecular weight of the compound. All of the solutions in 0.5% DMSO had their UV spectrum with no HABA/avidin measured as a control and these values were subtracted in concentration determination calculations.

Assay read-out values for CO-RM **71** and various controls used in the HABA/avidin assay are shown in **Table 12**.

Table 12. HABA avidin assay data for various compounds in 0.5% DMSO:0.01M PBS buffer pH 7.4. Assay shows intended solution concentration and the read out determined from the assay.

Compound added	**Added conc.**	**Assay conc.**
CO-RM **71**	30 µM	30.6 µM
Free biotin (**68**)	30 µM	24.9 µM
CO-RM **65** (**control**)	30 µM	0 µM
DMSO (**0.5%**)	0.5% *(v/v)*	0 µM

When a 30 µM solution of CO-RM **71** is added to a HABA/avidin solution, the shift in absorbance at 500 nm gives a concentration read out of 30.6 µM, which is close to the intended concentration. This suggests high purity and also suggests that the compound is displacing equimolar concentrations of HABA. Free biotin (**68**) was also tested at 30 µM and the assay gave a read out of 24.9 µM. This is close to the intended concentration; it may be slightly lower due to commercial d-biotin not always being 100% active/pure. It is possible that the purification of all the biotin reagents throughout synthesis of CO-RM **71** has actually enriched the biotin activity. This control shows that CO-RM **71** is binding in this assay in a similar fashion to free biotin.

Acid-containing CO-RM **65** was also tested in the HABA/assay as an extra control. This CO-RM has many structural features found within biotin CO-RM **71**. It contains the phenylpyridine $Mn(CO)_4$ unit and the triazole functionality from the cycloaddition reaction. It was important to test CO-RM **65** in this assay to assess if a similar structure without biotin could not displace HABA from the avidin protein, giving a false read out. CO-RM **65** did not reduce the absorbance at 500 nm showing that it does not displace HABA from avidin. It is the biotin section of CO-RM **71** that is responsible for binding to avidin.

All these data together show that CO-RM **71** is binding with avidin efficiently with a binding constant higher than HABA. This data in conjugation with all the NMR characterisation shows that a pure compound with strong avidin binding has been prepared.

5.4.2.2 Isothermal Titration Calorimetry (ITC) studies with CO-RM 71

The disadvantage of the HABA/avidin assay is that it does not give detailed information relating to the binding strength of CO-RM **71**. This is why isothermal titration calorimetry (ITC) was used as an additional technique.

ITC experiments involve titrating a biotin ligand (or a biotin containing species) into a solution of avidin. Both solutions are regulated to 25 $^{\circ}$C and the ITC apparatus then detects temperature changes due to any interactions taking place. The instrument calculates energy changes by maintaining a temperature of 25 °C, and the amount of energy that the instrument has to add or or take out due to thermodynamic processes is recorded.

The avidin containing cell has a volume of 1.4 ml and the ligand syringe has a volume of 0.28 ml. This means that if the concentration of ligand is 10-fold higher than the protein, then there will be a 2:1 ratio of ligand to protein at the end of the titration experiment. The 0.28 ml of ligand can be added over 20 injections so a saturation point can be observed when a 1:1 molar ratio has been achieved. Once the avidin binding site is saturated, no more binding occur and so the energy released from binding will cease.

Biotin (or CO-RM **71**) at a concentration of 20 μM was titrated in to 2 μM avidin monomer (4 identical binding sites in the tetramer protein) to give a 2:1 ligand:binding site ratio as discussed. Both CO-RM **71** and free biotin were tested in this assay. The ITC titration curves for free biotin are shown in **Figure 106**.

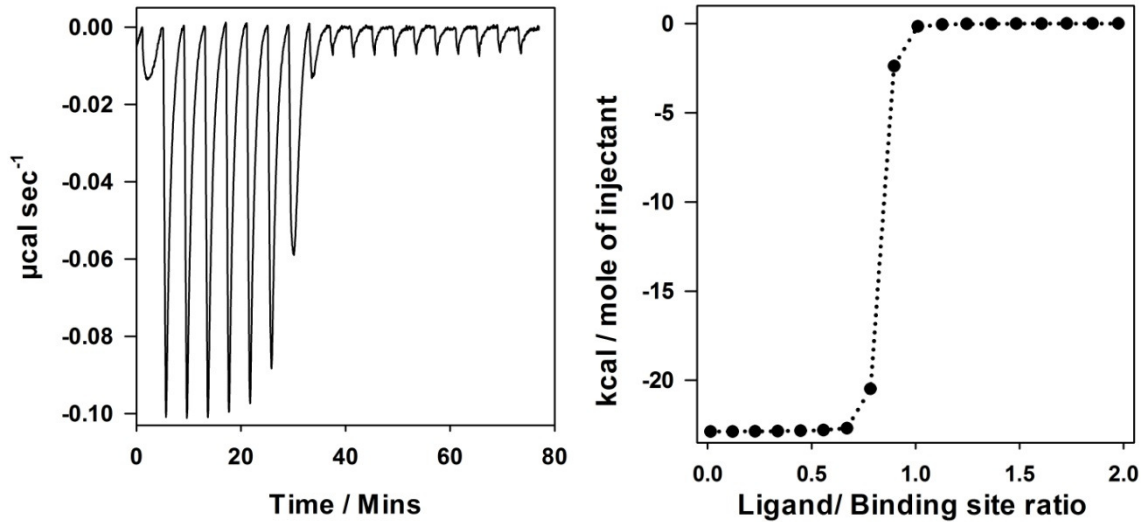

Figure 106. ITC titration curves for the addition of free biotin (**68**) into avidin in PBS buffer pH 7.49. End of the titration results in a 2:1 ligand/protein binding site ratio.

This initial ITC titration shows free biotin binding with avidin showing clear 1:1 binding with the avidin monomer binding site. The energy released from the binding drops off dramatically once a 1:1 ligand to binding site ratio has been achieved, suggesting a high binding constant which is already expected for free biotin. The energy released on biotin/avidin binding has been calculated to be 22 kcal mol^{-1}, which matches closely to the literature value obtained by Stjurkuusk and Wadsö.[120] This control experiment shows that the ITC experiment is correctly calibrated and that CO-RM **71** can be reliably tested. **Figure 107** shows the same experiment, but carried out with CO-RM **71** instead of free biotin.

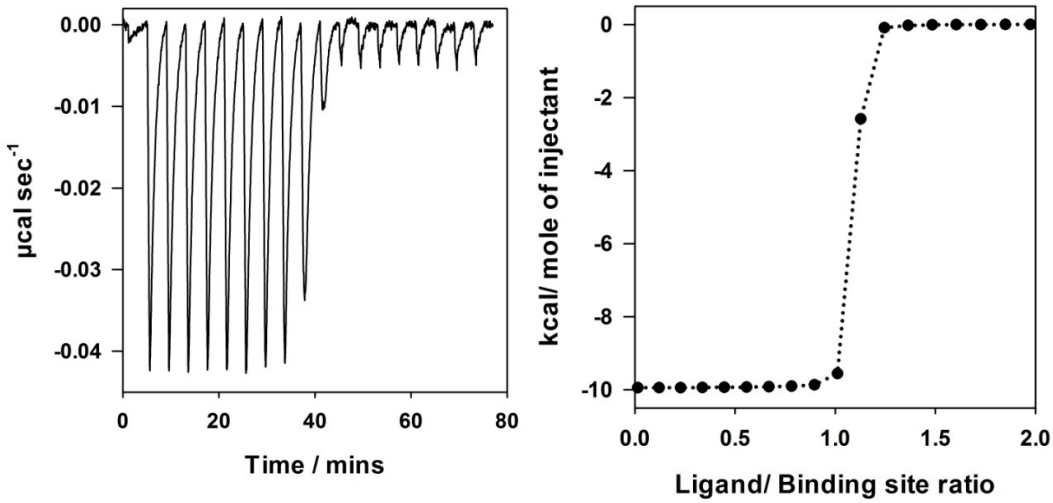

Figure 107. ITC titration curves for the addition of CO-RM **71** into avidin in PBS buffer pH 7.49. End of the titration results in a 2:1 ligand/protein binding site ratio.

The ITC data for CO-RM **71** is similar to free biotin but with a few differences. The enthalpy change from CO-RM **71**-avidin binding has been found to be 10 kcal mol^{-1}, which is 12 kcal mol^{-1} less than free biotin. This means that the CO-RM **71** does not bind as strongly as free biotin but there is still a significant enthalpy change. The binding energy does not always reflect the dissociation constant which is related to both the on and off rates.

Even though the binding energy is lower compared to free biotin, there is still a steep drop in energy release when one equivalent of CO-RM **71** has been titrated in to avidin. The gradient of the curve is large for both free biotin and CO-RM **71**, suggesting they have similar dissociation constants. The curves from this ITC data are so steep that the binding constants for both complexes are out of range of the technique, demonstrating that the CO-RM **71** binds strongly to avidin, just like free biotin. A ^{14}C-containing biotin conjugate would be required to accurately compare dissociation constants.[117]

With the knowledge that CO-RM **71** was binding strongly to avidin, it was then employed in a myoglobin assay in the presence of avidin to show that the CO-RM can release CO while bound to avidin. The avidin binding site was in excess of CO-RM **71** (2:1 ratio) so that all of the CO-RM would be bound to avidin (**Figure 108**).

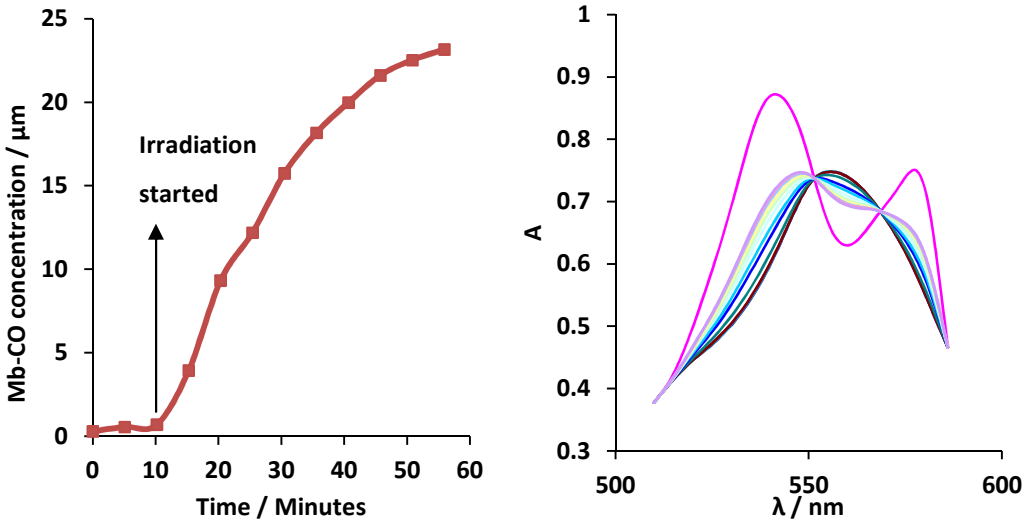

Figure 108. Left: Myoglobin assay with 10 µM CO-RM with 20 µM avidin binding site. Irradiation (400 nm, 2.4 W) started after 10 mins. Irradiation on for two mins per five minute period. Right: UV-Vis spectra corresponding to the myoglobin assay in the left graph.

The myoglobin assay data in **Figure 108** shows that biotin-containing CO-RM **71** can effectively release CO when irradiated while bound to avidin. Only small amounts of four point correction were required to reduce the error to acceptable values as discussed in section **3**. These data show how a CO-RM was tagged to a protein, and despite all this functionalisation and conjugation, the '$Mn(CO)_4$' CO-release motif still acts in isolation as a photo-CO-RM in the presence of myoglobin.

5.6 Conclusions on alkyne-containing functionalised CO-RMs

CO-RMs **62** and **63** were successfully synthesised despite some initial problems with alkyne reactivity. This reactivity was controlled using a triisopropylsilyl (TIPS) protecting group and inspiration for this came from 'unsuccessful' reactions from other researchers work, highlighting the importance of reporting unsuccessful results.

CO-RM **62** was found to be toxic towards RAW 264.7 cells, but fortunately CO-RM **63** was prepared alongside this as a reserve, and this CO-RM is viable with RAW 264.7 cells. This shows that considering what functionality is typically associated with toxicity, can be beneficial when synthesising a series of potential drug compounds.

CO-RM **63** was used in [3+2] cycloaddition chemistry to develop a CO-RM (**71**) that was conjugated to biotin. ITC binding studies are encouraging and suggest strong binding between CO-RM **71** and avidin. This is one of the first examples where a CO-RM has been designed to bind to a specific target, and has then been show to do just that. There are solubility issues with CO-RM **71**, but it is still soluble at 30 μM and is capable of releasing 75 μM CO at this concentration. It is also possible that once this CO-RM is bound to its avidin target, that the protein could improve solubility. Sequential administration could be used to allow accumulation of the CO-RM, although future testing would be required. Initial success with the conjugation of biotin into CO-RM **71** opens up many possibilities to synthesis a library of CO-RMs containing a variety of selective tags.

6 A CO-RM based on natural L-tryptophan.

In chapters **3**-**5**, several new series of CO-RMs have been developed which are capable of releasing efficiently on irradiation with light of wavelength 400 nm. This is starting to push out of the harmful irradiation region and this wavelength could certainly be considered for treatment with CO-RMs on skin and a short distance into skin tissue. However if photo-CO-RMs are to be considered for treatment of ailments deeper within tissue then a higher wavelength of light would be required to prevent mass absorption of all the light by macromolecules etc. Blue light is absorbed a lot more by tissue compared to red light and one can imagine the potential advantages of having a CO-RM which can be activated by light externally without the need to use fibre optic probes.[122] The absorption of light by tissue and other molecules highlights one of the main disadvantages of photo-CO-RMs. One of the main aims of this project it to begin solving this issue.

6.1 Synthesis and characterisation of CO-RM L-75

Initially, the idea to use tryptophan as a ligand in a CO-RM was based around the inherent fluorescent properties of the indole ring on the amino acid side chain. This indole ring could allow for excitation by light for potential use in cellular imaging studies. It was also desirable to introduce a natural ligand in to a CO-RM because of its non-toxic properties. It has already been shown that CO-RM **47** releases free ligand on irradiation, and knowing that the free ligand released is not cytotoxic could reduce the chances of producing a viable CO-RM.

With the above in mind, the initial intention was to react L-tryptophan (**73**) with $BnMn(CO)_5$ (**42**) to produce similar cyclometallated manganese(I) species. **Scheme 34** shows the initial intended synthesis of a tryptophan containing CO-RM.

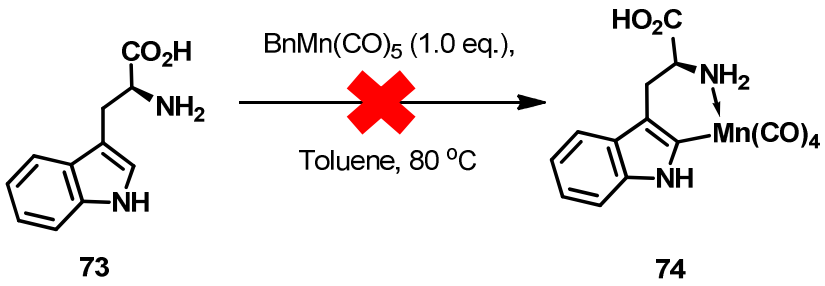

73 74

Scheme 34. Initial attempted synthesis of target CO-RM structure **74**.

The intention was to produce a tetracarbonyl manganese(I) species (**74**) but with a six-membered manganacycle, contrasting with the five-membered rings previously prepared. Unfortunately reaction of $BnMn(CO)_5$ with L-tryptophan did not result in conversion to a new species other than what appeared to be thermal degradation of some $BnMn(CO)_5$. L-Tryptophan (**73**) is a polar molecule (water soluble) and it was proposed that reaction in this solvent would not occur simply due to solubility issues. This reaction was then attempted in methanol in which L-tryptophan is more soluble. **Scheme 35** shows the conditions used to synthesise new CO-RM **75**.

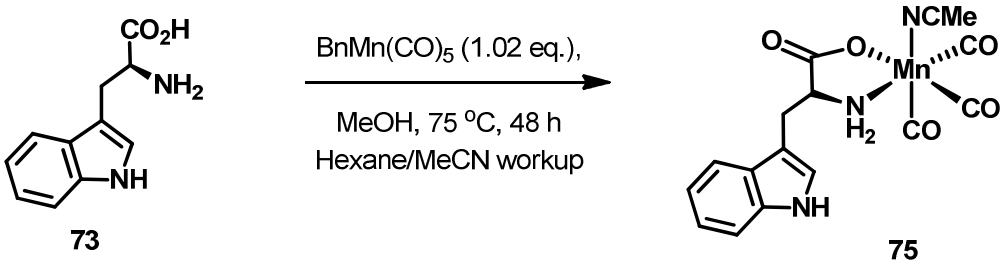

73 75

Scheme 35. The synthesis of a new L-tryptophan-containing manganese(I) CO-RM **75**

The conditions were modified based on previous knowledge that removing some unreacted polar species from a compound can be difficult. With this in a mind a slight excess of $BnMn(CO)_5$ (**42**) was used so that the L-tryptophan (**73**) could completely react. The small remaining quantity of $BnMn(CO)_5$ starting material could be removed using a specialised hexane/MeCN work up. These two organic solvents are not miscible, and it is unlikely that any tryptophan-containing complex would be soluble in the hexane layer, and so would remain in the MeCN phase allowing facile isolation. A bright yellow powder was obtained at the end of the reaction.

Interestingly, the intended six-membered manganacycle **74** was not the product of the reaction. Significant consumption of $BnMn(CO)_5$ was observed by TLC analysis suggesting some reaction was occurring. The ^{1}H NMR spectrum of the isolated material indicated that all of the indole protons were still present. There was little if any shifting of the indole proton signals, suggesting that C–H activation of the indole 2-position had not occurred (**Figure 110**).

The ^{1}H NMR spectra of L-tryptophan and CO-RM L-**75** are shown in **Figure 109**.

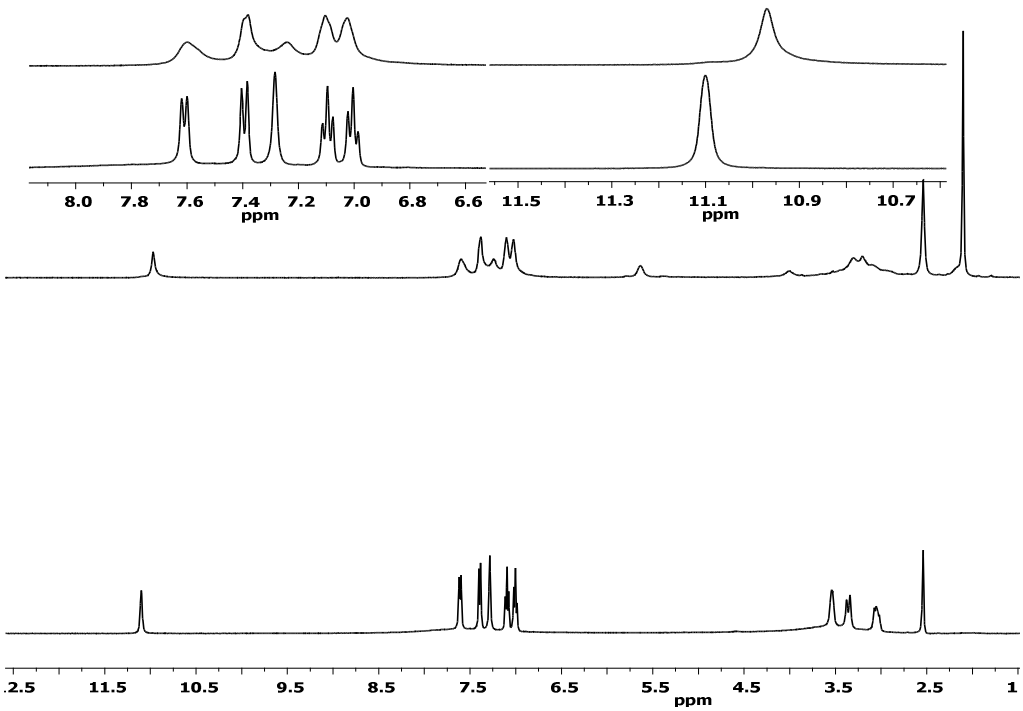

Figure 109. 400 MHz ^{1}H NMR spectrum of L-tryptophan (bottom) and CO-RM L-**75** (top) in DMSO-d$_6$ at 300 K. Note: Assignments for CO-RM L-**75** are shown in the spectra in Figure **A24** in Appendix 1

In the ^{1}H NMR spectrum of L-tryptophan, there is a very broad signal underneath the indole proton signals between 6.5-8,5 ppm, which is likely to be due to the amine protons. It is clear that some exchange on the NMR time scale is occurring in solution.

Even though there is some broadening in the peaks in the spectrum of CO-RM L-**75**, it is still possible to make out the indole proton peaks from the tryptophan part of the structure. With referencing to the DMSO solvent peak there is clearly no shift of these indole protons, including the indole N–H proton compared the peaks from L-tryptophan (**Figure 109**).

There is also a new singlet at 5.63 ppm which is likely to be due to the amine resonance. There is some exchange in this spectrum and some exchange will be expected. This amine is likely to have arisen from shifting of the broad signal under the indole proton signals in the L-tryptophan ^{1}H NMR spectrum, which is now no longer present. On coordination of the amine to the manganese centre, the signal has sharpened and has shifted to lower field (5.63 ppm), which is expected due to the electron withdrawing nature of the manganese(I) carbonyl centre. Addition of D_2O to the NMR sample confirms that the NH_2 signal at 5.63 ppm is exchanging as its intensity with respect to the indole protons was decreased by 50%.

The water peak at 3.25 ppm is broad, but is not a completely smooth Gaussian peak, and it is proposed that the alkyl C–H proton signals are overlapping with the water peak. Alkyl protons H, I, and J are not in direct bonding with the manganese centre and are not expected to shift. **Figure 109** shows that these alkyl protons H, I and J are under the water signal in the ^{1}H NMR spectrum of L-tryptophan.

There is a key signal at 2.10 ppm in the ^{1}H NMR spectrum of CO-RM L-**75** that integrates for close to three protons. It is proposed that this singlet arises from the methyl group of a coordinated acetonitrile ligand. The integration is likely to be slightly less than three due to some exchange in solution. There is also a signal at a chemical shift of 1.6/1.2 ppm in both the solution and solid state ^{13}C NMR respectively for CO-RM L-**75**. This is diagnostic of a coordinated acetonitrile ligand. The ^{13}C solid state NMR spectra also shows key resonances at 220 ppm with corresponding spinning side bands typical of a metal carbonyl environment.

The IR spectrum of the new species also provided key information on what had occurred during in the reaction (**Figure 110**).

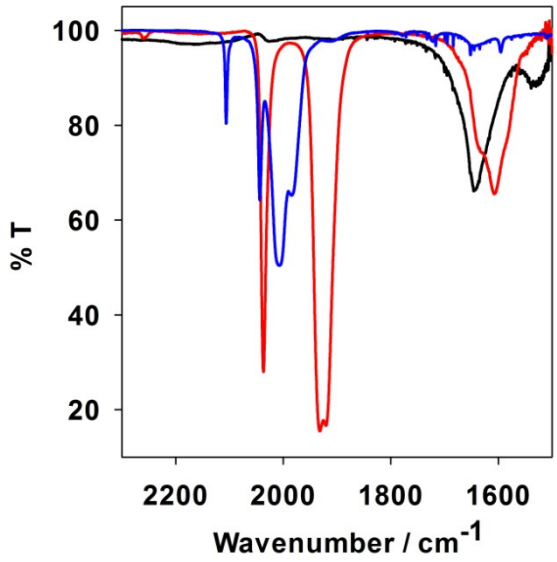

Figure 110. The solution IR spectrum of L-tryptophan-containing CO-RM L-**75** (red) and L-tryptophan (black) and $BnMn(CO)_5$ (blue)

The IR spectrum of tryptophan-containing CO-RM L-**75** contains no peak at 2107 cm^{-1} indicating no remaining $BnMn(CO)_5$ starting material. CO-RM L-**75** still has three sharp metal carbonyl signals in its IR spectrum. The spectrum indicates a species was present with pseudo C_{3v} symmetry. A new metal carbonyl species has been formed in this reaction, but typically reaction with $BnMn(CO)_5$ produces an $Mn(CO)_4$ species, so it appears that further CO loss has occurred in the synthesis of CO-RM L-**75**. There is also a shift in the frequency of the carboxylic acid

C=O stretch in L-**75** when compared to frequency of the same functional group in L-tryptophan. This peak shifts to lower energy from 1644 to 1604 cm^{-1}. This suggests interaction of the carboxylic acid functionality with the metal centre rather than the indole ring. An alternative five-membered manganacycle could be formed between the acid and amine within the L-tryptophan structure.

With all the data obtained for this complex, it was proposed that the likely structure is the one shown in **Figure 111**.

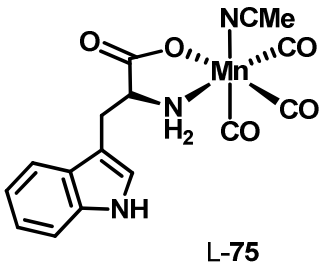

L-**75**

Figure 111. Proposed structure of new L-tryptophan containing CO-RM L-**75**.

The IR spectrum suggests the presence of a tripodal $Mn(CO)_3$ structure with interaction of the amine and acid from the L-tryptophan shown in **Figure 111**. This complex is isostructural with the Mohr histidine complex **21** when analysing the coordination around the manganese(I) centre. The Mohr histidine complex **21** was prepared according to literature procedure and its IR spectrum was analysed alongside the tryptophan complex prepared in this work. **Figure 112** shows the IR spectra of **21**,**73** and L-**75**.

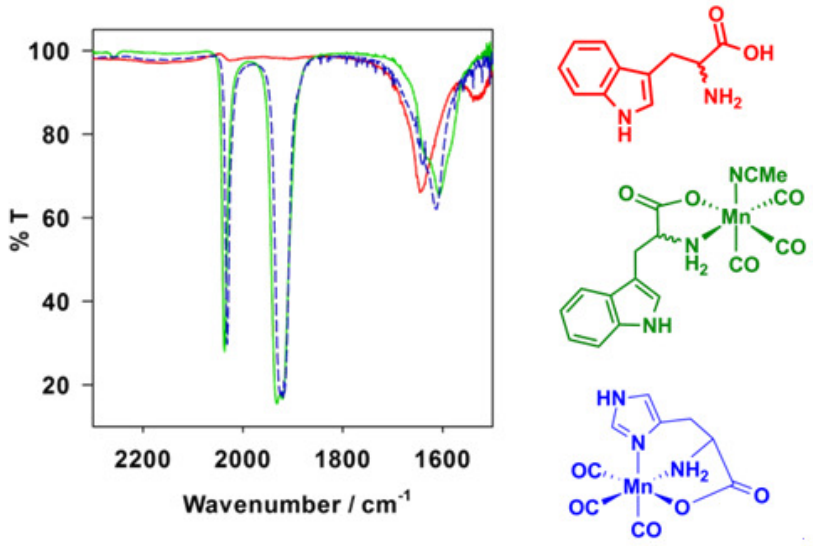

Figure 112. Solution IR spectra of tryptophan (red), CO-RM **75** (green) and Mohr histidine complex **21** (blue).[78]

The IR spectrum of the Mohr histidine complex (**21**) is similar to the spectrum of CO-RM **L-75**. This suggests the presence of a similar $Mn(CO)_3$ unit with a primary amine coordinated to the metal centre. With the C=O stretch of the acid functionality in both complexes having a similar frequency, it is likely that they have the same coordination mode, with the acid deprotonated and covalently bonded to the manganese centre. These data support the proposed structure in **Figure 111**.

6.1.1 Further structural investigations on CO-RM 75 and its isomers

With the presence of a stereocenter within CO-RM **75**, it is imperative that this structural feature is investigated and characterised. None of the techniques used in the previous section discussed distinguish between the L and D enantiomers of this complex. This needs to be analysed as some racemisation may occur during synthesis. CO-RM **75** was also prepared in the same way with both D- and DL-tryptophan to prepare an enantiomer and racemate complex of **75**. L-**75**, DL-**75** and D-**75** were then analysed by circular dichroism and optical rotation ($[\alpha]_D^{20}$).

The optical rotation recorded for D-**75** was $[\alpha]_D^{20}$ +248.2 (*c*=1, DMSO), and for L-**75** was $[\alpha]_D^{20}$ –286.5 (*c*=1, DMSO). The magnitude these two values are consistent with the starting enantiopurities of purchased D- and L-tryptophan respectively. The DL-racemate gave an $[\alpha]_D^{20}$ of −7.30 which is close to zero in comparison to the intensity obtained for the D- and L-**75** batches.

Circular dichroism spectra of CO-RM L-**75**, D-**75** and DL-**75** were recorded to get information about how each isomer interacts with light between wavelengths 280-550 nm (**Figure 113**).

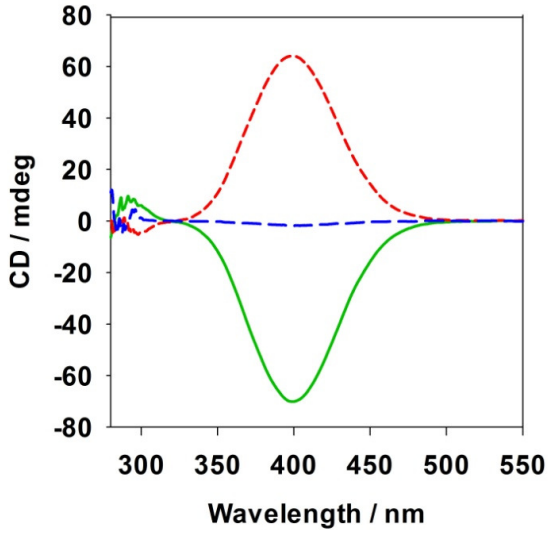

Figure 113. CD spectra of D-**75** (red), L-**75**(green) and DL-**75**(blue) in DMSO (c = 6×10^{-4} mol dm^{-3}). Each spectrum is an average of four runs.

The CD spectra complement the data obtained from the $[\alpha]_D^{20}$ experiments. The L-**75** CD mirrors the D-**75** isomer CD spectrum taking into account the enantiopurities of tryptophan starting materials. Pleasingly the DL-**75** CD spectrum is flat showing no indication of enantioenrichment.

Both the optical rotation experiments suggest that the L-tryptophan remains as the L-isomer in its corresponding manganese complex. There is no conversion from one isomer to the other during

synthesis. This is promising from a pharmacological point of view as fewer species to deal with in a pharmaceutical mixture is certainly an advantage.

To add an extra degree confidence to the data already obtained, some DFT calculations were performed by Dr. Jason Lynam on various potential isomers of CO-RM **75** to calculate the relative energies of possible structures. **Figure 114** shows the proposed potential structures for CO-RM **75** along with their calculated energies relative to isomer A1. Solvation in MeOH was also included in further calculations. The reaction was performed in methanol and so performing calculations in this solvent is relevant.

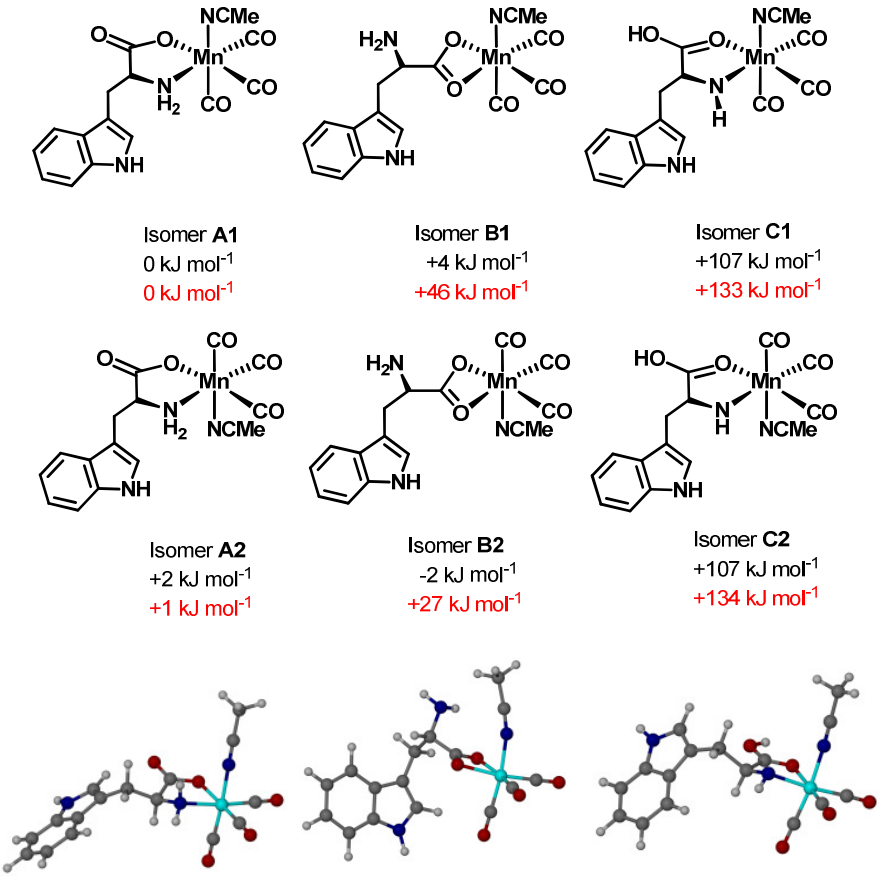

Figure 114. Isomeric structures (A, B and C) and DFT calculated structures considered as products resulting from the reaction of L-tryptophan with $BnMn(CO)_5$. Energies are Gibbs Free Energies in the gas phase (black) and with solvent correction for MeOH (red). Energies are relative to Isomer **A1** determined at the (RI-)PBE0/def2-TZVPP level. Calculated by Dr. Jason Lynam.

The DFT calculations show thermodynamically how potential structures differ from each other and if all were to exist, this data gives information about the relative quantities of each isomer in solution. The **C** isomers are over 100 kJ mol^{-1} higher in energy relative to the **A** isomer when

solvated with methanol. This is a large energy difference making the formation of isomer **C** at 75 °C particularly unlikely. The **B** isomers are closer in energy compared to the **C** isomers but ^{1}H NMR and IR spectra rule out the presence of κ^2-binding from the carboxylic acid and interaction from the amine functionality. The initial proposed structure (**Scheme 34/**Structure **74**) was not run in these calculations as experimental evidence strongly suggests that this structure was not formed; The ^{1}H NMR spectrum of the material shows that the indole ring has clearly not been cyclometallated as all the protons on the indole ring are still intact.

All the data suggests either of **A** isomers but unfortunately it is not possible to distinguish between the two. CO-RM **75** is proposed to be either isomer **A1** or **A2** but could be a mixture of the two which are inter-converting. Considering the broadening of the ^{1}H NMR spectra compared to L-tryptophan it is certainly possible that some inter-conversion between isomer **A1** and **A2** is taking place. There can be a degree in confidence in the characterisation of CO-RM L-**75** and the material prepared can be taken forward for further studies.

6.2 CO-release and mechanistic studies with CO-RM L-75

With CO-RM L-**75** sufficiently characterised it was then necessary to assess how it releases CO in aqueous medium. A myoglobin assay was used again to assess this CO-release at both 10 and 40 μM concentrations. **Figure 115** shows these assays with irradiation at 400 nm.

More myoglobin assays have been carried out to assess the CO release from CO-RM L-**75**. The first assay carried out uses a 400 nm LED at 2.4 W to release the CO.

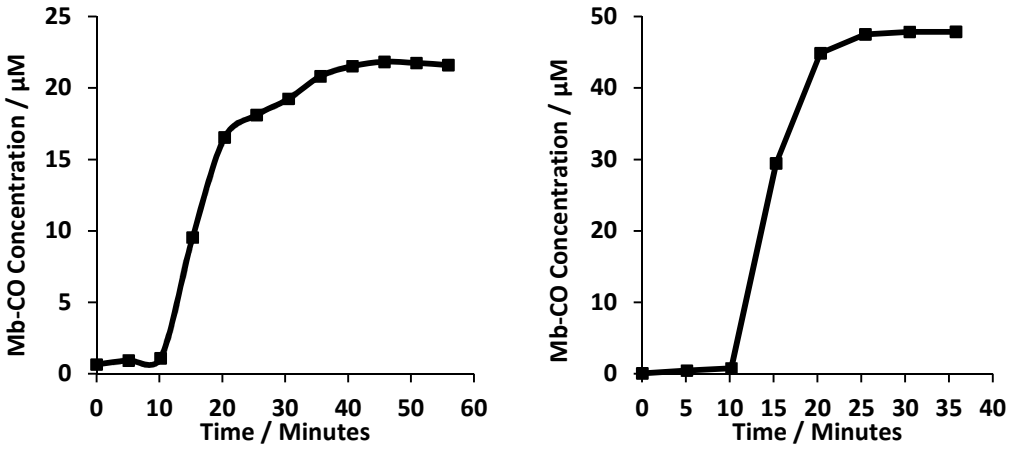

Figure 115. Myoglobin assay CO release profiles in PBS pH 7.4 at 37 °C for CO-RM L-**75**. Left: 10 μM assay producing 20 μM Mb-CO. Right : 40 μM assay saturating myoglobin. CO-release initiated at ten mins with two mins of irradiation (2.4 W, 400 nm) every five mins.

One of the initial promising properties of CO-RM L-**75** is that it remains completely soluble after addition in DMSO to aqueous medium.

The CO releasing properties of CO-RM L-**75** are similar to that of many of the phenylpyridine derivatives. The photo-activated CO-release from L-**75** is faster than anything previously prepared in this project. With 400 nm light, the half-life of CO-release for L-**75** is reached within 2.5 mins at 10 μM and within 3.5 minutes at 40 μM. Within both these time periods, only two mins of irradiation has been delivered. This is quick CO-release compared to many of the CO-RMs previously prepared.

This CO-RM can be photo-activated to induce CO-release and is stable in the presence of myoglobin. A further myoglobin assay was carried out with 40 μM CO-RM L-**75**, showing that it is fairly stable for at least 45 minutes with myoglobin in the dark with minimal CO-release (**Figure 116**).

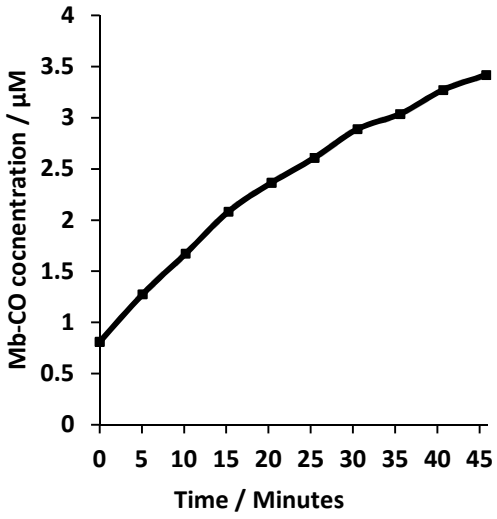

Figure 116. A 50µM myoglobin assay with no irradiation using 40 µM CO-RM L-**75** in PBS buffer pH 7.4.

There is slow CO-release in the dark but this is less than 4 µM of CO over this period. This is only a small fraction percentage of the total CO that could be released on irradiation (up to 80 µM at this concentration). Complex L-**75** is still acting very much like a photo-CO-RM. This small amount of release may come from increased reactivity due to the potentially exchangeable acetonitrile ligand. This small amount of either thermal or ET-triggered CO-release may prove useful in further studies.

CO-RM L-**75** only releases two molecules of CO per molecule where as previous CO-RMs release three. The phenylpyridine-based CO-RMs prepared so far are releasing one fewer CO per molecule than the number of CO ligands in the molecule. This is expected as the manganese centre will back-bond more strongly as each CO is released, and when there is only one CO ligand bound to the manganese, it will be so strongly bound that it will not be photolytically released.[123] A UV-Vis spectrum of CO-RM L-**75** was recorded and this suggests that it could release CO using irradiation of lower energy than 400 nm light (**Figure 117**).

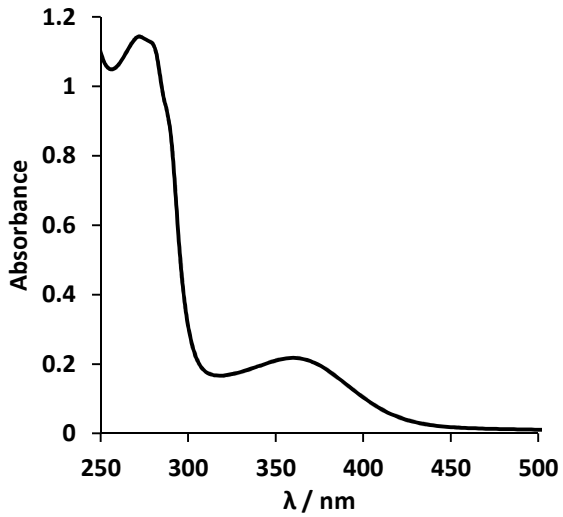

Figure 117. UV-Vis spectrum of CO-RM L-**75** in MeCN at 1.5×10^{-4} mol dm^{-3}.

There is a small band in the UV spectrum of CO-RM L-**75** with a λ_{max} at 360 nm. This is a possible reason why the CO-RM releases CO quickly when irradiated with 400 nm light. This small band tails off past 450 nm. In more myoglobin assays, new LEDs were used that emit irradiation of wavelength 465 nm ± 20 nm. This blue light is at the high end of the visible spectrum. This LED was used in a myoglobin assay to see if this lower energy light could still release CO from CO-RM L-**75**. These data are shown in **Figure 118**.

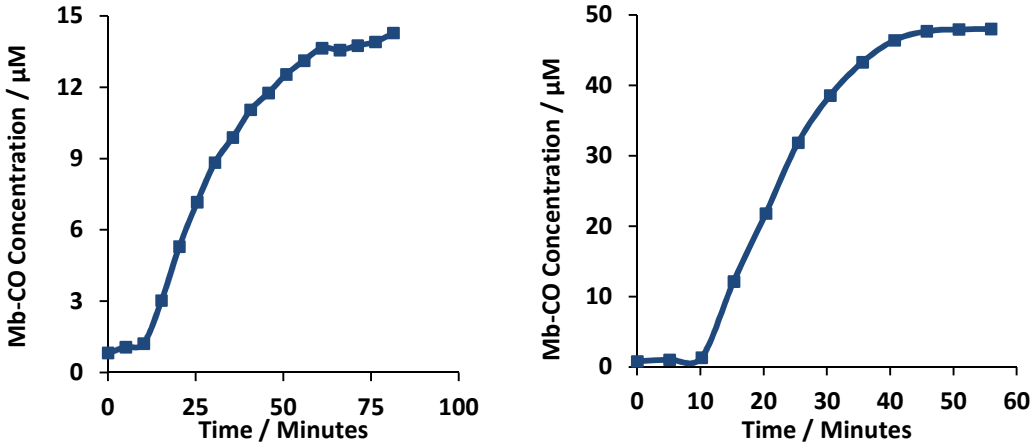

Figure 118. Myoglobin assay CO release profiles in PBS pH 7.4 at 37 °C for CO-RM L-**75**. Left: 10 µM assay producing 14 µM Mb-CO. Right: 40 µM assay saturating 50 µM myoglobin. CO release was initiated at 10 mins with two mins of irradiation (2.4 W, 465 nm) every five mins.

CO-RM L-**75** can release CO when irradiation of wavelength 465 nm is used. The CO-release rate is slower compared to using irradiation of wavelength 400 nm. This is expected as the molar extinction coefficient is lower at 465 nm decreasing the chance of photon absorption. CO-RM L-**75** at a concentration of 40 µM can convert all the myoglobin to Mb-CO. This is particularly

efficient considering that the CO-RM has a weak absorbance at the irradiation wavelength. Unfortunately there are 0.5 eq. fewer CO molecules released with light of wavelength 465 nm.

A UV-Vis spectroscopy study was also carried out to assess if the smaller absorption band is associated with photo-initiated CO release (**Figure 119**). A solution of CO-RM L-**75** was prepared in DMSO and an initial UV spectrum was recorded.

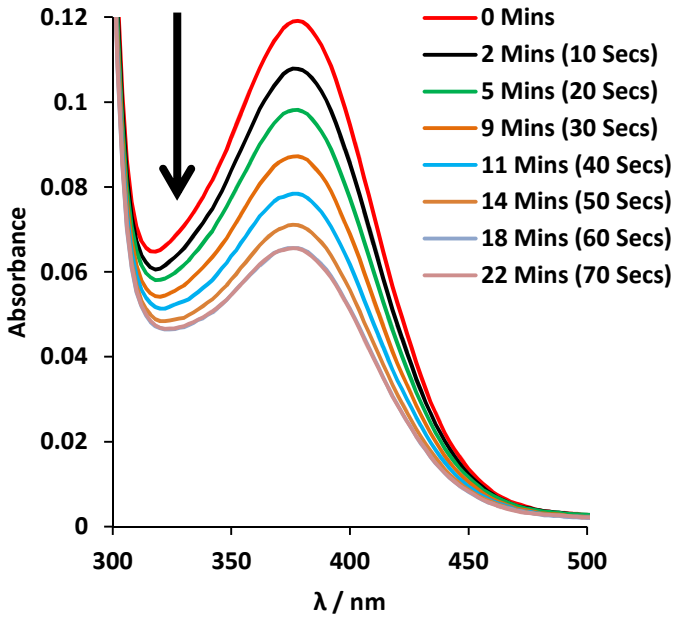

Figure 119. Decay of the M–CO UV absorption band from L-**75** over time when photo-irradiated (400 nm, 2.4W) in DMSO (the time in brackets refer to the irradiation time between UV-vis measurements).

On irradiation of this smaller UV band in DMSO, there is a significant decrease in intensity as the total irradiation time increases. This suggests that the absorption band is associated with photo-activated CO-release from CO-RM L-**75**.

6.2.1 ReactIR™ studies with CO-RM 75

ReactIR™ studies were also carried out with CO-RM **75** to follow the loss of the metal carbonyl C=O stretches by real time IR spectroscopy. This was done in both methanol and a DMSO/PBS mixture. A solution of CO-RM DL-**75** was added into a solution of methanol and was followed over time (**Figure 120**).

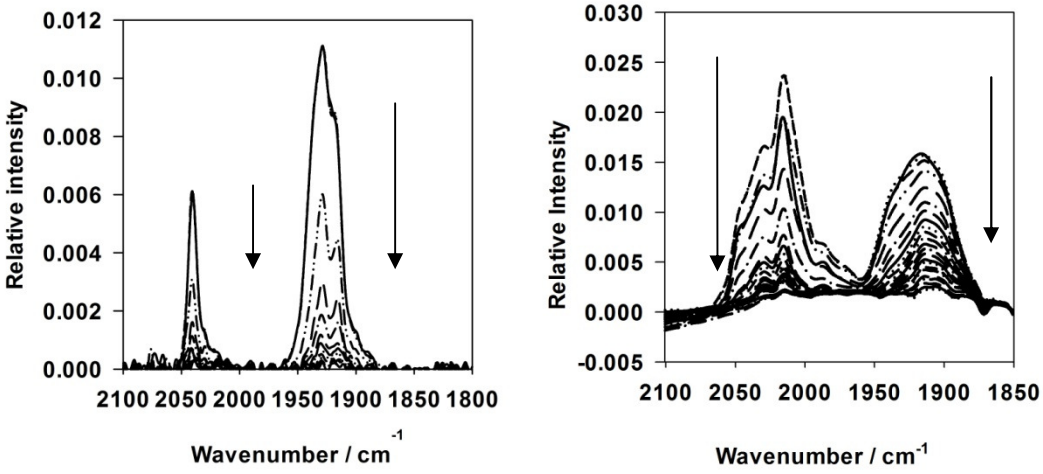

Figure 120. Decay of metal carbonyl C=O stretches from 1 mM DL-**75** measured by *in situ* ReactIR™. Continuous irradiation performed (2.4 W, 400 nm). Left: methanol, right: 10% DMSO/ 0.01M PBS pH 7.4.

Unusually all of the metal carbonyl signals are depleted in these ReactIR™ experiments. This may appear contradictory to the myoglobin assays which suggests that all the CO is not released from the CO-RM. It is not possible to measure the IR spectrum in real time in 0.5% (*v/v*) DMSO/H_2O due to needing such high concentrations of CO-RM (3 mM) to get a good signal/noise ratio. This means that in the myoglobin assay mixture, all the CO is likely not released. It is possible that on irradiation, a large number of different species are produced, broadening the IR bands and therefore lowering their intensity below the lower limit of detection. These studies still confirm that the metal carbonyl stretches significantly decrease on, and not until irradiation occurs (**Figure 121**).

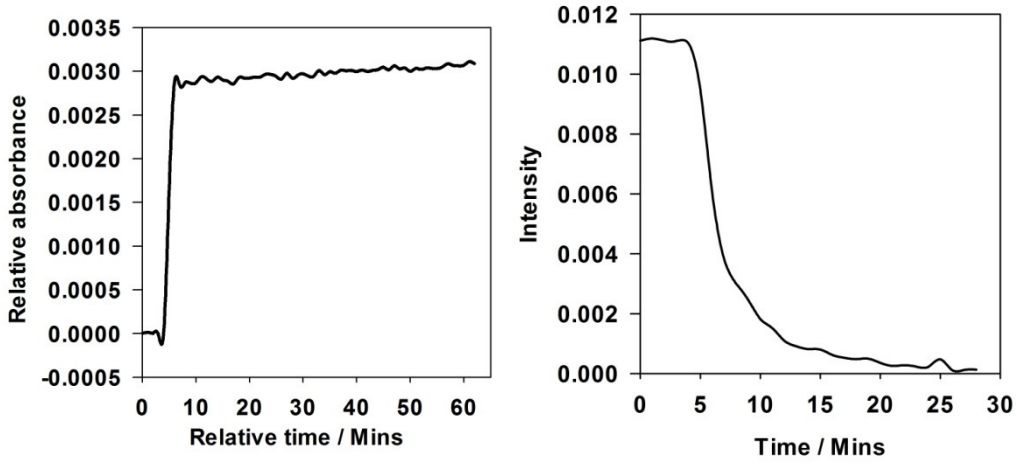

Figure 121. Decay/stability studies by observation of metal carbonyl C=O stretch at 1935 cm^{-1} from DL-**75** measured by *in situ* ReactIR™. Left: methanol with no irradiation, right: methanol with continuous irradiation (400 nm, 2.4 W) after five mins initial darkness.

ReactIR™ data in **Figure 121** shows that CO-RM DL-**75** is not degraded significantly in the dark. These data shows that the intensity of the metal carbonyl C=O stretch at 1935 cm^{-1} does not decrease over a one hour period. With 400 nm irradiation a smooth kinetic curve is obtained with a half-life of only two minutes, and this matches closely with the $t_{½}$ observed from the myoglobin assay in **Figure 115**.

6.2.2 ESI-MS degradation studies with CO-RM DL-75

With the kinetics of CO-release from CO-RM L-**75** characterised, it was then necessary to carry out the same +ve mode ESI-MS degradation study that was done with CO-RM **47**. It would be important to have an idea of what species would be formed on irradiation of this compound. Two ESI-MS degradation studies with different capillary exit voltages were carried out. The two experiments were carried out using a skimmer voltage of 42 V and a capillary exit voltage of 43 and 80V respectively. By changing the capillary exit voltage it was possible to optimise the sensitivity and detection of particular CO-RM **75** fragments. A 0.5 mg ml^{-1} solution of CO-RM DL-**75** in 50:50 CH_3CN/H_2O was irradiated for one minute (465 nm, 2.4 W) in between ESI-MS measurements. **Figure 122** and **Figure 123** shows the relevant ESI-MS ions detected in this study at the two different capillary exit voltages.

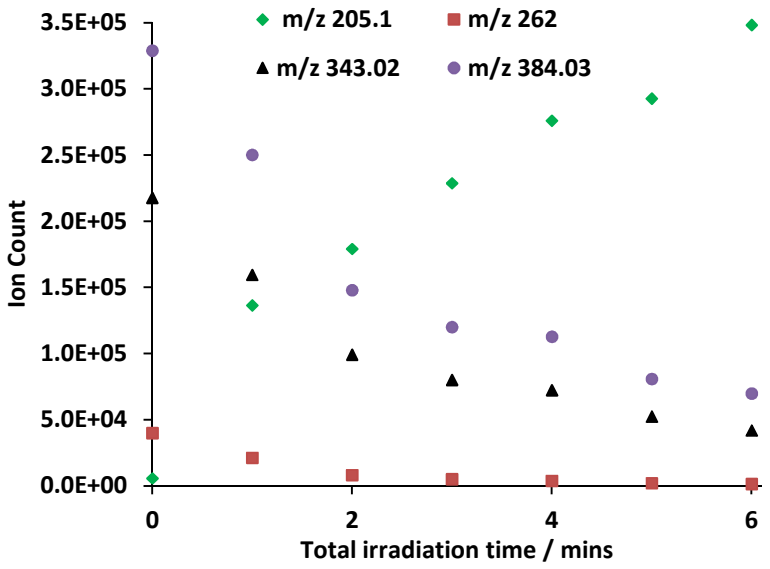

Figure 122. ESI-MS degradation study for CO-RM DL-**75** in 50:50 (*v/v*) CH_3CN/H_2O. Capillary exit voltage = 43 V. Skimmer voltage = 42 V. (465 nm, 2.4 W irradiation used)

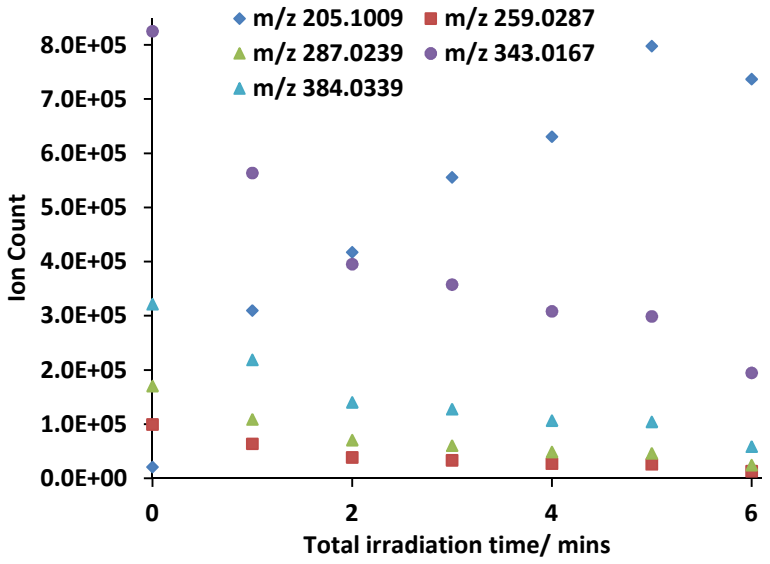

Figure 123. ESI-MS degradation study for CO-RM DL-**75** in 50:50 (*v/v*) CH_3CN/H_2O. Capillary exit voltage = 80 V. Skimmer voltage = 42 V. (465 nm, 2.4 W irradiation used).

Both ESI-MS studies show the reduction of the molecular ion at *m/z* 384 and increase of a signal at *m/z* 205, which corresponds to free L-tryptophan. This matches with the data obtained for acid CO-RM **47**. However, there are clearly some differences in the mechanism of degradation with tryptophan CO-RM **75**. The peak at *m/z* 262 which corresponds to $[(CH_3CN)_3Mn(CO)_3]^+$ (**47c**) is detected in these experiments, but only using the reduced capillary exit voltage. In the profiles shown in **Figure 122** and **Figure 123**; this peak at *m/z* 262 does not increase and diminish in

intensity like an intermediate as was observed with CO-RM **47**. In the degradation of CO-RM **75** a small amount of **47c** was detected initially which then depletes over time with irradiation. This suggests that $[(CH_3CN)_3Mn(CO)_3]^+$ (**47c**) does not play such an important role in the degradation pathway for CO-RM **75**. It is possible that in this situation that the peak at *m/z* 262 is from small amounts of thermal degradation and decreases in intensity due to further irradiation. This is not the case with acid CO-RM **47** as the ion at 262 *m/z* (**47c**) in that case is not present before irradiation. The peak for **47c** in this case grows in and depletes over the course of the experiment.

Scheme 36 shows the other peaks detected in the ESI-MS degradation study of CO-RM DL-**75** and shows what they may correspond to.

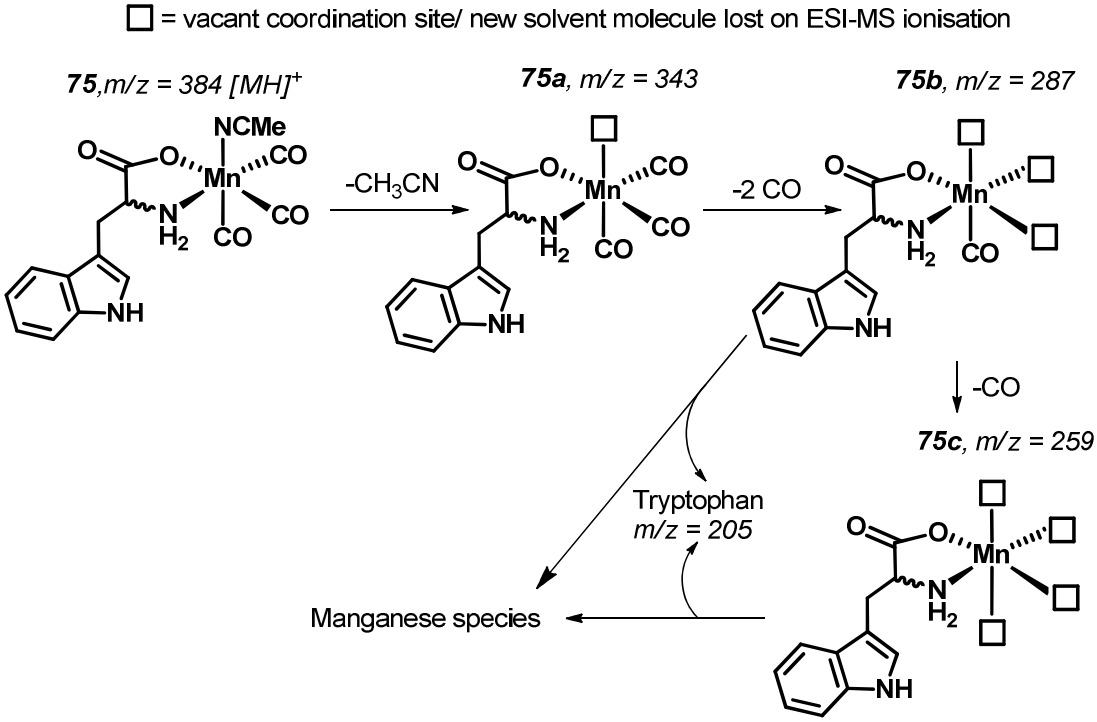

Scheme 36. Proposed degradation of CO-RM DL-**75** during 465 nm irradiation in 50:50 (*v/v*) CH_3CN/H_2O.

It is proposed that after initial solvation of CO-RM **75**, there will be some ligand exchange of the CH_3CN for H_2O. This was not detected by ESI-MS, but the loss of the CH_3CN is observed by with *m/z* 343 (**75a**). Irradiation of this species will also result in further CO loss followed by additional ligand coordination. Both double and triple CO-loss products are detected at *m/z* 287 and 259 respectively (**75b** and **75c**). Significant amounts of free tryptophan were formed but it is not clear at which point in the degradation pathway this is formed. It could be formed at several different stages by competing pathways. It is difficult to assess whether some of the species in **Scheme 36** are formed in the ESI-MS instrument or whether they are formed in solution.

However, Brian Mann and co-workers have proposed similar CO-dissociation/solvent coordination degradation pathways for their [$Mn(CO)_4\{S_2CNMe(CH_2CO_2H)\}$] (**7**) and it is certainly possible that some of the species in **Scheme 36** are present in solution.[58] There can be a degree of confidence in the formation of free tryptophan ligand from CO-RM **75**.

6.3 Eukaryotic biological studies with CO-RM L-75 on RAW 264.7 cells

With detailed mechanistic studies on the CO-release and degradation of CO-RM L-**75** in hand, it was then necessary to carry out cell viability and cytotoxicity studies on RAW 264.7 murine macrophages. This compound was tested using Alamar blue and LDH assays as done previously and these results are shown in **Figure 124**.

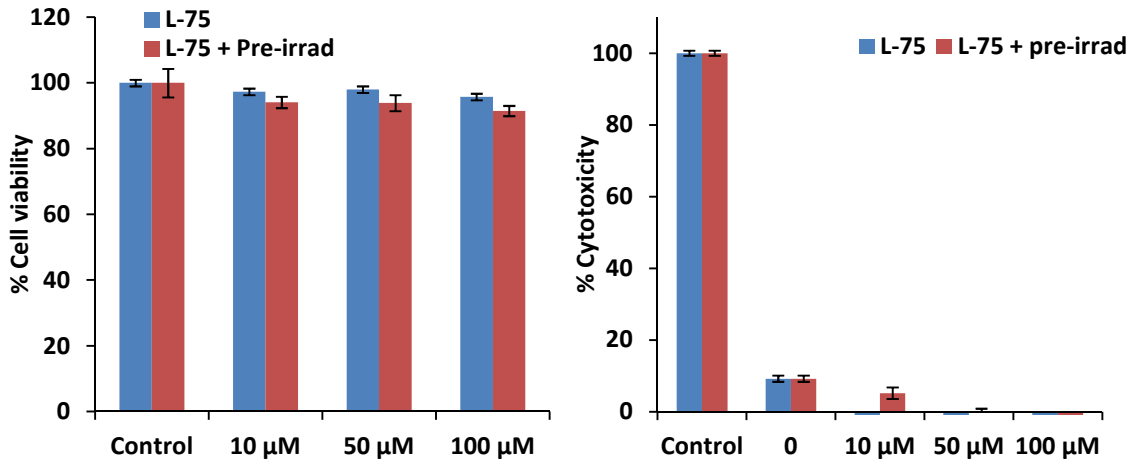

Figure 124. Alamar blue assay (left) and LDH assay (right) with RAW 264.7 cells in 10% (*v/v*) HI-FCS/DMEM medium. Addition of 10-100 µM CO-RM L-**75** by direct addition and pre-irradiation (8 mins, 2.4 W, 465 nm) in DMSO.

The data in **Figure 124** shows that CO-RM L-**75** is viable with RAW 264.7 cells both before and after eight minutes irradiation of wavelength 465 nm, which has been shown to efficiently induce CO-release from CO-RM L-**75**. This CO-RM shows similar viability to acid-containing CO-RM **47**, as well as literature CO-RMs **F3**, **F8**, and [$Mn(CO)_4\{S_2CNMe(CH_2CO_2H)\}$] (**7**).[58, 71-72, 74] The CO-RM appears to exhibit some cytoprotective action as the RAW 264.7 cells release less LDH in the presence of CO-RM L-**75** compared to without.

6.3.1 NO suppression using CO-RM L-75 with RAW 264.7 macrophages

CO-RM **47** has previously been tested and shown to induce an anti-inflammatory response with RAW 264.7 macrophages that were strongly stimulated with LPS and IFN-γ. This study was also carried out with CO-RM L-**75**. With the knowledge that 400 nm light appeared to affect the cells without CO-RM, 465 nm light was used in these experiments with the anticipation that this would not affect the cells as much with it being well in to the visible region of the spectrum. **Figure 125** shows the Greiss assay data for tests with CO-RM L-**75** using four mins irradiation.

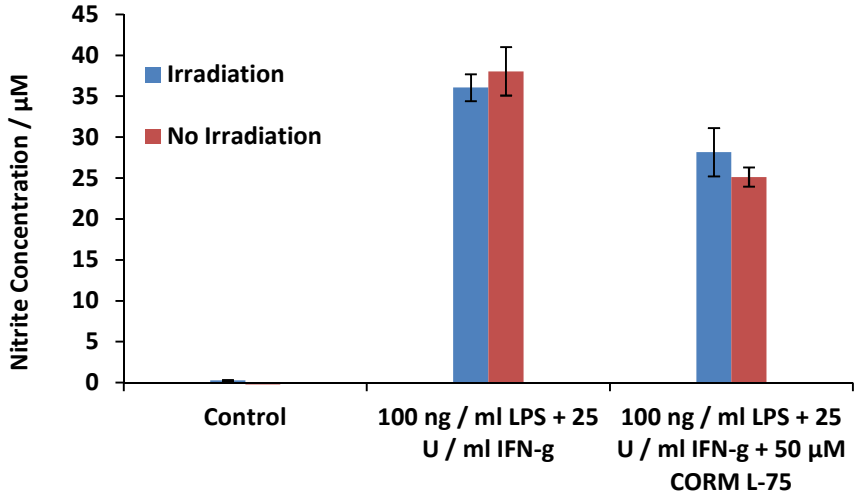

Figure 125. Greiss assay data - determination of nitrite levels in supernatant from RAW 264.7 murine macrophages after incubation with 50 µM CO-RM L-**75**. Identical plates set up except one is irradiated for 4 mins (3.6 W, 465 nm).

Interestingly, in the absence of CO-RM L-**75** with only four mins 465 nm light, there is no change in the amount of NO_2^- production from the macrophages. With CO-RM L-**75** present, there is a clear reduction in NO_2^- production. This reduction is present without the need for irradiation. There is a 35% reduction in nitrite levels in the presence of 50 µM CO-RM L-**75** which is a significant drop considering the intensity of the inflammatory response. This decrease is 14% higher than the reduction observed with acid-containing CO-RM **47**. This experiment was carried out at a completely viable concentration of CO-RM L-**75** and an LDH assay was also carried out alongside the Greiss assay in **Figure 125** as an extra control. The assay detected less LDH in the wells with CO-RM L-**75**, LPS and IFN-γ than they did in the wells with only cells. This suggests that the reduction in nitrite production arises from the anti-inflammatory action of CO-RM L-**75** and not direct toxicity issues. It was postulated that the anti-inflammatory action of CO-RM L-**75** in the absence of light comes from the small amount of thermal or enzyme-triggered CO-release detected in the myoglobin assay before any irradiation. This suggests that

only a small amount of CO is required to suppress the potent inflammatory response induced by LPS and IFN-γ. This could also explain why four minutes irradiation, which should release significant amounts of CO, does not further reduce the NO_2^- production.

It is unfortunate that irradiation of CO-RM L-**75** does not enhance the effects observed with RAW 264.7 cells considering it was designed to be a photo-CO-RM. However there are still great advantages to designing CO-RMs to be photo-activated, even if they might not be irradiated in treatment. The main reason is that if the CO-RM does not release significantly to myoglobin then it is likely to be fairly stable towards many CO binding proteins. In reality, one would not want all the CO from this CO-RM to be sequestered by myoglobin *in vivo* as this would not induce any significant beneficial biological effect. Releasing CO to other important targets is more desirable and designing the CO-RM not to donate CO to myoglobin has its advantages. The irradiation of CO-RM L-**75** does not enhance the CO-RMs properties in these studies but it may still have its uses in bacterial studies where more CO might be required to get a beneficial effect.

6.4 Studies on *E. coli* W3110 with CO-RM L-75

CO-RM **L-75** has been shown to efficiently release CO and is viable with RAW 264.7 cells. The next stage in this research is to take this promising tryptophan-based CO-RM forward into bacterial studies. CO-RM L-**75** has been shown to be viable up to a concentration of 100 μM with RAW 264.7 cells, and so bacterial viability/toxicity assays were not carried out above this concentration. If CO-RM L-**75** was found to inhibit bacterial growth at 100 μM, then there is a chance it could do so without killing sensitive macrophages.

Initial studies with *E. coli* involved taking a similar approach to that which was carried out with CO-RM **47**. *E. coli* W3110 were grown in LB media and then irradiated after one hour at 400 nm for a total of 68 minutes. This study was done with bacteria that had been grown on a LB agar plate and were stored at 4 °C for six days before use. **Figure 126** shows the results from an initial growth/irradiation study.

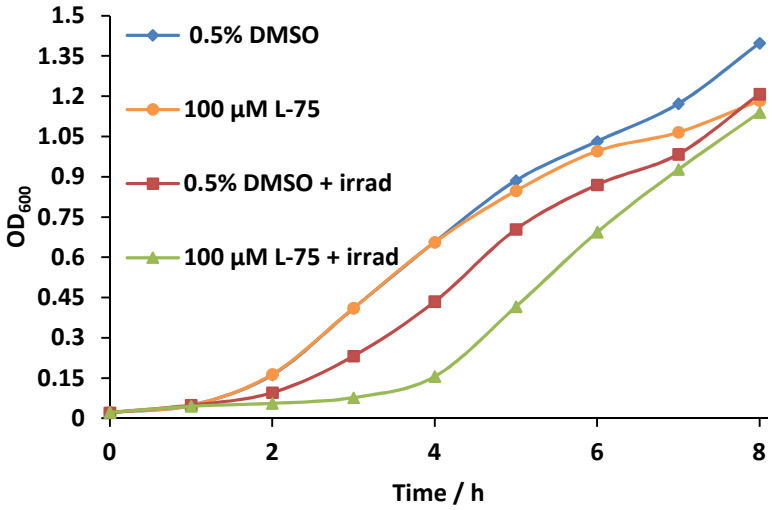

Figure 126. The growth curve for six day old *E. coli* W3110 in LB media at 37 °C with 100 µM L-**75**. Irradiation (400 nm, 2.4 W, 68 mins) performed between one and three hours.

CO-RM L-**75** is not as effective on six day old *E. coli* as acid CO-RM **47**. CO-RM **47** was capable of keeping the OD_{600} from increasing for seven hours before re-growth under these conditions. With CO-RM L-**75** the *E. coli* grew back only one hour after irradiation ceases. There is still promise from this study as CO-RM and irradiation together caused a more detrimental effect than each of these variables in isolation. This experiment was repeated with *E. coli* from the same plate but when they were 7-8 days old (**Figure 127**).

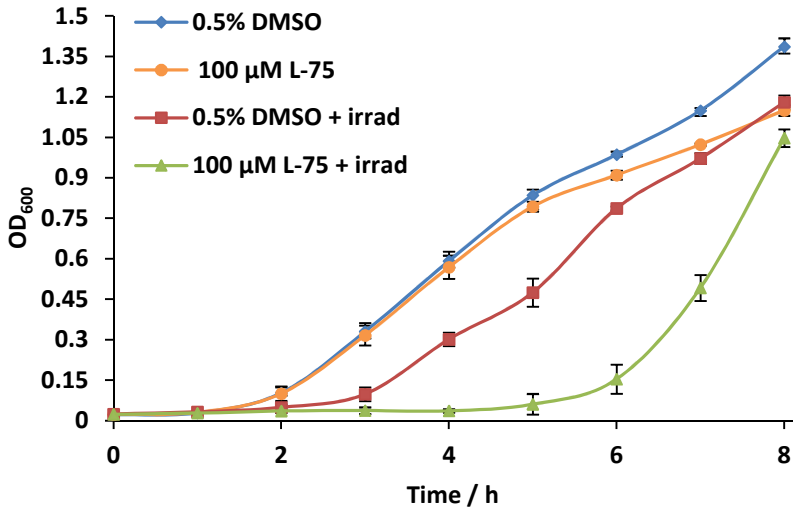

Figure 127. The growth curve for 7-8 day old *E. coli* W3110 in LB media at 37 °C with 100 µM L-**75**. Irradiation (400 nm, 2.4 W, 68 mins) performed between one and three hours. Data is an average of experiments from 7-8 day old bacteria used in repeat experiments.

With the bacteria being stored at 4 °C for a further 1-2 days, the effectiveness of CO-RM L-**75** on *E. coli* has increased by a significant amount. The bacteria take an extra hour to grow back compared to the study carried out with six day old *E. coli* (**Figure 126**). This is not as effective as CO-RM **47** at this irradiation wavelength. A final set of irradiation repeats were carried out using *E. coli* that were 13-14 days old (**Figure 128**).

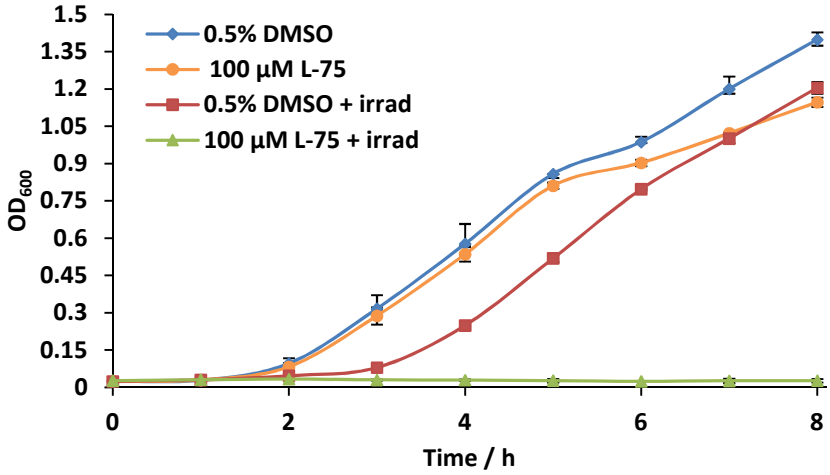

Figure 128. The growth curve for 13-14 day old *E. coli* W3110 in LB media at 37 °C with 100 µM L-**75**. Irradiation (400 nm, 2.4 W, 68 mins) performed between one and three hours. Data is an average of experiments from 13 and 14 day old bacteria used in identical repeat experiments.

With the *E. coli* at 13-14 days old there is a dramatic change in the effectiveness of CO-RM L-**75** with 68 mins irradiation. These data are comparable to the data obtained with CO-RM **47** on *E.*

coli of the same age. Irradiation or CO-RM only is not causing a significant detrimental effect. There is a clear difference in the bacteria as their age increases and this will be discussed further.

A plating viability study was carried out on *E. coli* three times to assess how many bacteria were capable of forming colonies after irradiation treatment on *E. coli* that are 13-14 days old. The growth curves for these plating studies match what was observed in **Figure 128** and the data from the plating studies is shown in **Table 13**.

Table 13. Colony counts from *E. coli* W3110 cultures corresponding to **Figure 128**, representing before and after irradiation (0 h and 4 h) (400 nm, 2.4 W, 68 minutes). Incubation in LB media with 100 µM CO-RM L-**75**. Stock plate with *E. coli* was 13-14 days old.

Repeat	Time taken / h	Dilution	Colony count
1	0	500x	282
1	4	500x	0
2	0	500x	330
2	4	0x	80
2	4	500x	0
3	0	500x	258
3	4	0x	330
3	4	500x	4

The plating study shows that on average over 99% of the *E. coli* are killed under conditions tested. There is a small amount of variation with slightly less killing in repeat three, but this is really promising work showing that CO-RM L-**75** can exhibit anti bacterial activity on *E. coli.* This is one of first examples of a photo-CO-RM showing a potent anti-bacterial effect in *E. coli*. **Figure 129** shows an example of plates before and after irradiation which gave the data in **Table 13**.

Figure 129. Left: colony counts of *E. coli* W3110 in the presence of 100 μM CO-RM L-**75** at t = 0 h (50x dilution) in LB media. Right: effect of L-**75** at t = 4 h incubation after 68 mins irradiation (400 nm, 2.4 W).

Recently, Schatzschneider and co-workers have also carried out studies on *E. coli* with $[(tpa)Mn(CO)_3]^+Br^-$, and a mild effect is seen with this CO-RM and irradiation of wavelength 365 nm.[124] This irradiation wavelength is too low for effective tissue penetration and is likely to be damaging to eukaryotic cells. The effect observed with CO-RM L-**75** in these studies is much more potent compared to the literature CO-RM $[(tpa)Mn(CO)_3]^+Br^-$, and uses irradiation closer to the visible region of the electromagnetic spectrum.[124]

6.4.1 *E. coli* W3110 aging study

There is a significant change in the effectiveness of CO-RM L-**75** on *E. coli* relating to age, and further investigations into the potential source of this was required. In all experiments carried out at different ages so far, the *E. coli* all eventually grow to the same OD_{600} after eight hours, suggesting that they are not just significantly weakened by being older. There is however greater susceptibility to CO-RM L-**75** in the presence of light.

The age of the *E. coli* was drastically affecting the ability of CO-RM L-**75** to kill them. A study was carried out to assess if this was to do with there being less bacteria alive on the plate, or if it was to do with the increased OD at 1 h in the fresh cultures due to fast initial growth. A plating study was performed to assess how the viable colony numbers on a plate changed over one month. The bacteria were put in to a solution of LB media with 100 μM CO-RM L-**75** and were plated out as previously. This was done with fresh, 9, 18, and 27 day old *E. coli* (**Table 14**).

Table 14. Plate counting for *E. coli* W3110 at varying age. Samples prepared in LB media to an OD_{600} of 0.2 with 100 µM CO-RM L-**75** and was immediately diluted and plated.

Days old	Dilution	Colony count
27	500x	40
18	500x	282
9	5000x	234
1	5000x	397

The study shows that over a period of one month, a significant proportion of the *E. coli* had died. After 18 days approx. 90% had died, and this explains the extended the lag phase observed with older cultures. Even though the culture was prepared each time so that it had the same starting OD there is a clear difference in the number of living bacteria. This could contribute to age dependent ability of the CO-RMs to kill *E. coli*. When the *E. coli* is fresh there is no lag phase and the OD increases quickly, giving a higher OD at the time of irradiation compared to older cultures. This increased turbidity could contribute to the decreased effectiveness of the CO-RMs, as the light gets scattered rather than passing all the way through the solution and inducing CO-release.

A study with CO-RM L-**75** was carried out with fresh *E. coli* that had just grown up on the plate. The OD was started ten times lower than carried out to see if turbidity was infact a significant issue in these experiments. The *E. coli* grew after one hour to the same OD as observed in the older experiments due to the bacteria being fresh out of 37 °C overnight growth. Results from the experiment are shown in **Figure 130**.

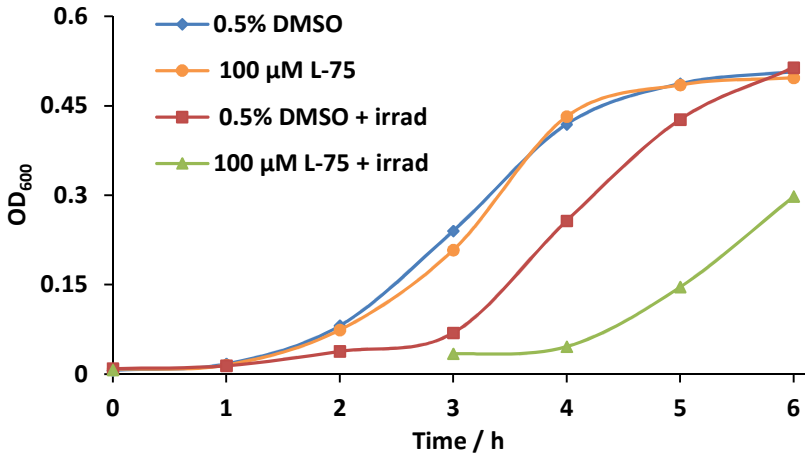

Figure 130. Growth of fresh *E. coli* W3110 with 100 µM CO-RM L-**75** in LB media. Starting cultures made from stock with an OD = 0.2 and diluted by 100 for the experiment. Irradiation (400 nm, 2.4 W, 68 mins) was carried out between one and three hours.

The OD_{600} at the point of irradiation is the same in **Figure 130** as in experiments with older cultures, suggesting similar numbers of bacteria at this point in the experiment. The *E. coli* grows less with CO-RM L-**75** and irradiation but do not die at a 99% rate as was the case with the older *E. coli*. This is suggesting that over time something significant is happening to the *E. coli*'s biology that causes it to be much more susceptible to CO release. Even though it is known that the majority of *E. coli* die after a few weeks, the ones that are still alive are capable of growing efficiently as shown by the control curves in all these experiments.

The aging effect observed could possibly be related to the oxidises that *E. coli* uses such as bd and bo oxidases.[47] The ratio of these essential CO-binding proteins could change over the aging process. If CO can inactivate one of these essential enzymes more easily, and it is in major excess at the time, it is postulated that this could explain the aging effect observed.

Despite this aging effect, there is a potent effect observed with CO-RM L-**75** on irradiation of 14 day old *E. coli.* Further studies were required to discover the source of this antibacterial effect.

6.4.2 Further controls to suggest CO is the cause of antibacterial activity

Current experiments demonstrate both CO-RM L-**75** and irradiation have to be present *together* to see the desired effect. CO-RM L-**75** is not toxic to *E. coli* without irradiation, suggesting that this molecule and its by-products are not toxic either. The photo-products of CO-RM L-**75** were also tested for toxicity, as this might not be produced in the dark.

In the literature, using the by-products of a CO-RM to suggest the action of CO is widely carried out. This is known as an i-CO-RM (inactive CO-RM).[22] Many tests involve using 'proposed' fragments as an i-CO-RM. This presents many disadvantages as adding an intermediate at a certain concentration may not reflect the concentration profile in the real experiment. The proposed intermediates might not even be present, and so it is difficult to draw a strong conclusion in relation to CO action from this kind of i-CO-RM control experiment.

An alternative method to assess the toxicity of CO-RMs by-products is to make an *in situ* i-CO-RM. This involves either leaving a CO-RM in solution for a known time period if it degrades thermally, or irradiating it in solution for the same period of time that would be used in main experiments. The advantage of doing this is that the products produced in this situation should closely mirror those of the main experiment with bacteria. After degradation has been carried out, the bacteria can be added to this solution after, and growth curves can be carried out. This experiment gives a realistic profile of the products that will be in solution. Even though it is not known exactly what all the degradation products are, these experiments are likely to match the concentrations of products from the bacteria experiments. **Figure 131** shows results from this pre-irradiation experiment with CO-RM L-**75**.

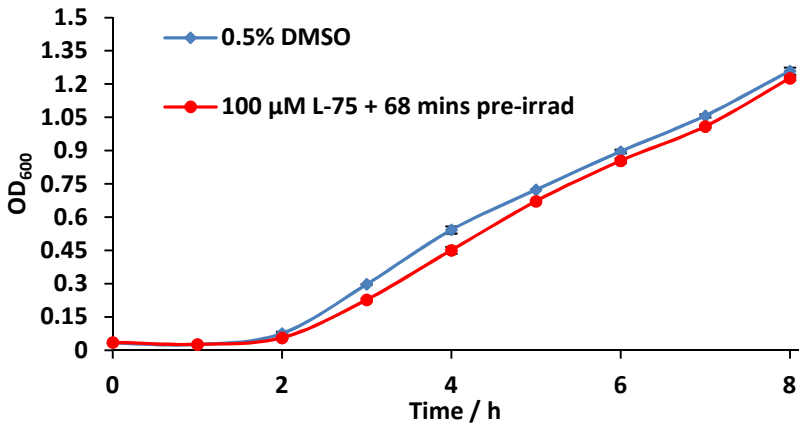

Figure 131. Growth curve of *E. coli* W3110 in LB media with 100 µM CO-RM L-**75**. Media with 100 µM CO-RM was irradiated for 68 mins (400 nm, 2.4 W) before addition of *E. coli* to culture. The culture was then allowed to grow with no further irradiation.

With 100 µM irradiated CO-RM L-**75**, the presence of the photo-products from the 68 mins irradiation does not affect the growth of *E. coli* significantly. The media was not flushed with air before the bacteria were added. This suggests that the photo-products were not toxic at the concentrations generated by 68 mins irradiation at 400 nm. It also suggests that what causes the toxic effect when the *E. coli* are directly irradiated with the CO-RM has to be inside or on the surface of the cell.

The next control experiment carried out was similar to that shown in **Figure 131** but involves irradiating the bacteria directly after the 'pre-irradiation' of the CO-RM. This will assess the toxicity of the photo-products in the presence of light. It could be possible that light sensitises the bacteria then making some of the by-products toxic. Considering the myoglobin assay data for this CO-RM, it is expected that all the CO will have been released within the 68 minutes irradiation. The results from the 'CO-RM pre-irradiation + direct bacterial irradiation' study are shown in **Figure 132**.

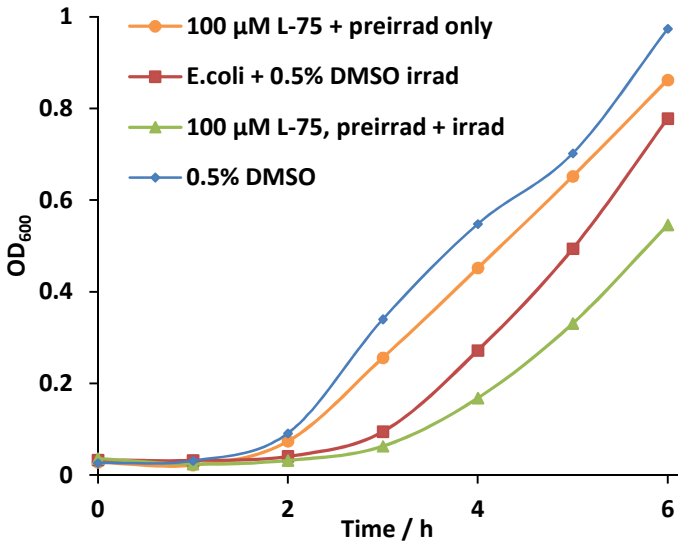

Figure 132. Growth curve with *E. coli* W3110 in LB media with 100 µM CO-RM L-**75** was irradiated **without** *E. coli* for 68 mins. *E. coli* was then added to culture and was **directly** for 68 mins (400 nm, 2.4 W) after one hour initial growth.

The photo-products of CO-RM L-**75** with irradiation causes some reduction in growth compared to the DMSO control, but this is not as effective as irradiating directly with freshly dissolved CO-RM L-**75**. This suggests the initial starting molecule and irradiation are required to get the strong antibacterial effect. This experiment has been repeated twice and also shows the same effect. These controls were done using *E. coli* with a similar age used in the direct irradiation experiments (**Figure 128**).

All the controls carried out strongly suggest that the CO is causing the toxic effect, but only when the CO is released directly from CO-RM L-**75**. Such detailed controls/mechanistic investigations have not been previously carried out on a photo-CO-RM. It is hoped that these detailed control experiments will be adopted by other researchers when investigating the antibacterial action their photo-CO-RMs.

The final control that has been carried out involves establishing if one of the photo-degradents was toxic under irradiation conditions. It is known from mass spectrometry studies in section **6.6.2** that irradiation of CO-RM L-**75** liberates free L-tryptophan. It was necessary to investigate if the presence of L-tryptophan and irradiation at the same concentrations caused any effect. An irradiation experiment was carried out using 100 µM L-tryptophan administered in 0.5% DMSO just like the CO-RM. The results of this precautionary control are shown in **Figure 133**.

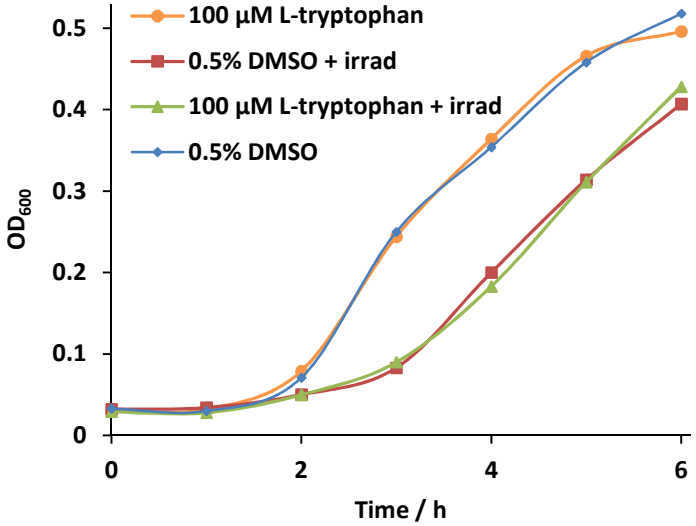

Figure 133. Growth of *E. coli* W3110 with 100 µM L-tryptophan in the presence and absence of light. Irradiation after 1 h initial growth for a total of 68 mins (400 nm, 2.4 W).

L-tryptophan (**73**) with irradiation does not alter the growth rate of *E. coli*. Both irradiated cultures with and without tryptophan grow in the same fashion, showing that it is the irradiation causing the slight inhibition and not L-tryptophan. This result was expected as L-tryptophan does not absorb where the 400 nm LED emits, so no photo-degradation was expected.

To summarise, CO-RM L-**75** has been well characterised in terms of CO-release and has been shown to exhibit a strong effect against *E. coli*, which are more sensitive to treatment with increasing age. Both CO-RM **47** and L-**75** appear to be more effective on dormant *E. coli,* which could present its own advantages. Many current antibiotics target actively growing bacteria by the inhibition of cell wall synthesis.[125] Dormant bacteria may not be targeted due to the lack of cell wall synthesis using previous antibiotics. CO-RMs tested in this project are more potent against older bacteria and this could prove very useful if this CO-RM was used in tandem with a current antibiotic to ensure complete bacterial death. Further studies would be necessary to confirm this.

6.4.3 Further *E. coli* studies with CO-RM L-75 and 465 nm irradiation.

Detailed studies have been carried out with CO-RM L-**75** showing its antibacterial ability against *E. coli* in conjugation with irradiation of wavelength 400 nm. It has been shown by myoglobin assay studies in section **6.2** that this CO-RM releases CO with irradiation of wavelength 465 nm; and so investigations into the effect of CO-RM L-**75** with 465 nm irradiation were carried out. These are the first studies of a CO-RM activated by visible light being tested on *E. coli*.

The first test that was carried out using irradiation of wavelength 465 nm, and was essentially a repeat of studies with irradiation of wavelength 400 nm. *E. coli* of a similar age (14 days) were used so that data could be directly compared (**Figure 134**).

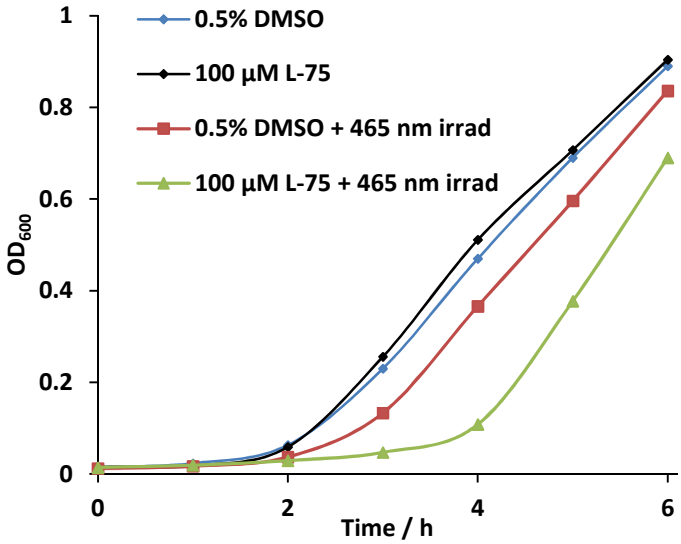

Figure 134. Growth curve with14 day old *E. coli* W3110 and 100 µM CO-RM L-**75** from a starting OD of 0.159 diluted by 10. Irradiation (465 nm 2.4 W, 68 mins) started after one hour initial growth. Irradiation stopped after 3 hours. LED on for 4 mins per 5 min cycle

CO-RM L-**75** with irradiation of wavelength 465 nm is not as effective against *E. coli* under the same conditions used with 400 nm irradiation. Re-growth is observed after irradiation stops and is comparable to the effect seen in younger *E. coli* with 400 nm treatment (**Figure 126**). This is expected as irradiation of wavelength 465 nm was shown to release CO more slowly in myoglobin assays. Also 0.5 eq. less total CO is released with 465 nm irradiation compared to at 400 nm. This may explain why it is not as effective.

A repeat of the experiment shown in **Figure 134** was carried out in the same way but with a 10-fold lower starting OD. This experiment was designed to assess if turbidity has much of an effect under these conditions (**Figure 135**).

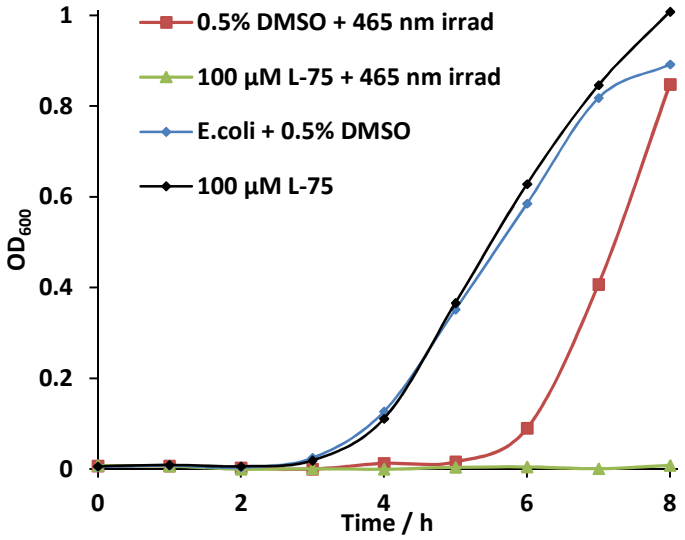

Figure 135. Growth curve with 14 day old *E. coli* W3110, and 100 µM CO-RM L-**75** from a starting OD of 0.15 diluted by 100. Irradiation (465 nm, 2.4 W, 68 mins) started after one hour initial growth.

CO-RM L-**75** with irradiation of wavelength 465 nm has a more potent effect when the initial starting OD of *E. coli* is lower. The lower OD will allow for improved light penetration through the liquid medium; meaning that more CO-RM will absorb irradiation over the same time period. Irradiation at wavelength 465 nm also has a fairly detrimental effect on *E. coli* without CO-RM. However, with 100 µM CO-RM L-**75** there is a much more potent effect with no growth observed over an eight hour period. A plating study was also carried out along side this study to assess the viability of *E. coli* with and without CO-RM L-**75** on exposure to irradiation of wavelength 465 nm (**Table 15**).

Table 15. *E. coli* W3110 plating viability study data obtained alongside results from **Figure 135**. Aliquots taken before and after 465 nm irradiation (one and three hours respectively). Plating dilutions are shown in bold.

1 h (Before irradiation)	**3 h Irradiated**	**1 h (before irrad DMSO only)**	**3 h irrad (DMSO only)**
50x	**50x**	**50x**	**50x**
300	14	259	206
500x	**500x**	**500x**	**500x**
35	3	42	33

The data in **Table 15** shows that under the given conditions, there is a 95% antibacterial effect on *E. coli* with 465 nm irradiation and 100 μM CO-RM L-**75**. The DMSO control only shows a 20% killing rate presumably due to irradiation. This suggests that both CO-RM and irradiation together are required to get a potent antibacterial effect. This is the first example of a visible-light-induced CO-RM showing a detrimental effect on *E. coli.*

Tryptophan-based CO-RM L-**75** has potential for the treatment of *E. coli* as determined by all the growth curves/viability studies performed. There are some issues with turbidity reducing the effectiveness of the CO-RM and more studies with increased irradiation power could be carried out in the future to solve this issue. This highlights the requirement for CO-RMs which release CO with irradiation of lower energy; however CO-RM L-**75** is certainly a step in the right direction and still has potential to be used in further studies. Despite the turbidity issues this CO-RM could potentially be used for surface treatment due to the lack of turbidity issues in this situation although more studies would need to be carried out for this.

Finally, in our publication of CO-RM L-**75**, it is referred to as TryptoCO-RM.[126]

6.5 Investigations with CO-RM L-75 on S. aureus 8325-4

CO-RM L-**75** has been employed in further studies to assess its action on *S. aureus*.

CO-RM L-**75** has shown potent antibacterial activity on *E. coli* W3110 with both 400 and 465 nm irradiation. The next step in this research was to extend the scope of CO-RM L-**75** and test it on more strains of bacteria. The first of these is *S. aureus* 8325-4 which is a wild type strain.

Initial studies with *S. aureus* were based on similar studies carried out on *E. coli*. *S. aureus* was grown in LB medium in the presence and absence of CO-RM L-**75**. Irradiation of wavelength 400 nm was also used so that a comparison to *E. coli* studies could be made. **Figure 136** shows the initial growth curve carried out with *S. aureus* in the presence of CO-RM L-**75**.

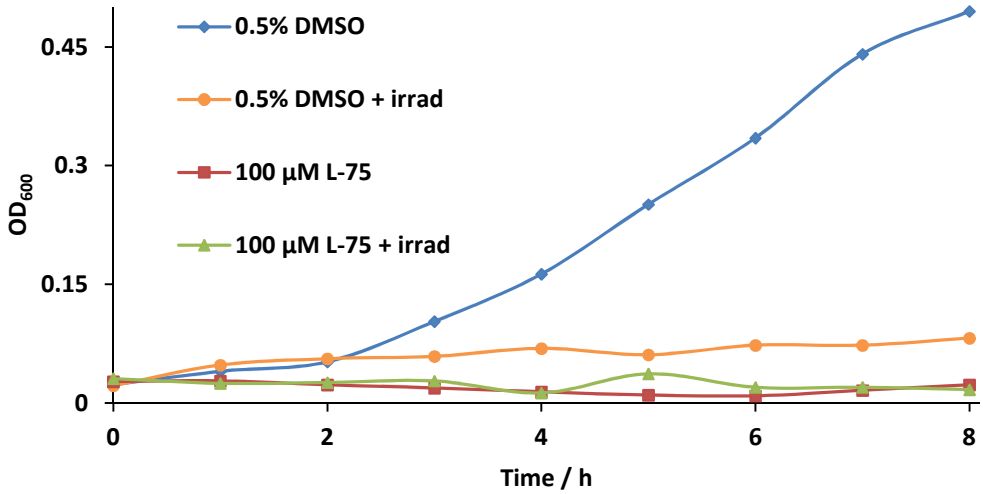

Figure 136. Growth of one day old *S. aureus* with 100 µM CO-RM L-**75** in LB medium at 37 °C with 100 rpm shaking in 8 ml bijou tubes. Irradiation (400 nm, 2.4 W, 68 mins) started after one hour initial growth.

Initial studies with one day old *S. aureus* with CO-RM L-**75** show that it prevents the growth of *S. aureus* without the need for irradiation. This is unusual considering that these bacteria were fresh. Older bacteria were required to get this kind of effect when using acid CO-RM **47**. It is possible that *S. aureus* is much more sensitive to CO from CO-RMs than *E. coli*. It was shown that CO-RM L-**75** can release very small amounts of CO thermally (**Figure 116**), and this could be the source of this inhibitory effect. A plating study was carried along side this initial study to assess the affect of CO-RM L-**75** and 400 nm irradiation together (**Table 16**).

Table 16. Plating study for *S. aureus* 8325-4 before and after irradiation (400 nm, 2.4 W, 68 minutes) in the presence of 100 μM CO-RM L-**75**

Days old	Time taken / h	Dilution	Colony count
1	1	50x	634
1	3	50x	32

CO-RM L-**75** with 400 nm irradiation kills 95% of *S. aureus* under the tested conditions. This is a encouraging result considering that the bacteria tested were only one day old. With 400 nm irradiation there is much less of an aging effect here, in contrast to the *E. coli* studies.

It was important to establish whether the effect observed without irradiation was bacteriostatic or bactericidal. A repeat of the growth curve in **Figure 136** was performed and a plating study was carried out by taking aliquots from the non-irradiated culture with CO-RM L-**75** (**Table 17**).

Table 17. *S. aureus* plating study taken from non-irradiated samples with 100 μM CO-RM L-**75**.

Days old	Time taken / h	Dilution	Colony count
4	0	50x	870
4	4	50x	783
4	7	50x	820

The 'thermal' effect on *S. aureus* with relatively fresh bacteria is infact bacteriostatic. The CO-RM is preventing *S. aureus* from growing over a seven hour period without killing them.

Investigations into the source of this bacteriostatic effect were performed. Initial studies centred on establishing if the effect was coming from a small amount of photo-activated CO-release by ambient light; or from very slow thermal release as determined by a myoglobin assay. Growth curves with *S. aureus* were therefore set up with CO-RM L-**75** in ambient light and in the complete dark (bijou tubes were wrapped in foil). This study was repeated and results with errors are shown in **Figure 137**.

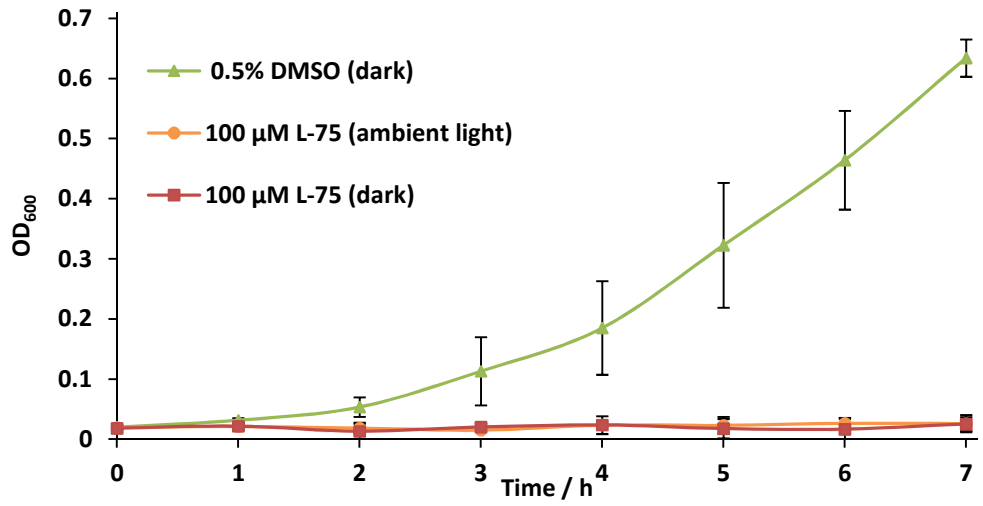

Figure 137. Growth of *S. aureus* 8325-4 in LB media at 37 °C with 100 µM CO-RM L-**75** in ambient light, and the dark. 0.5% DMSO in ambient light used as a control. No irradiation was used.

The 'thermal' effectiveness of CO-RM L-**75** on *S. aureus* is not changed by being grown in the dark. Great care was taken to keep the sample in the dark as much as possible. This was not possible when taking aliquots for analysis but this is only for a small amount of time compared to the duration of the experiment. Given the precautions taken, it is difficult to rationalise the amount of CO-release on the basis of stray light. There is some slow thermal CO-release, or the bacteria are initiating degradation either inside or on the surface of the cell.

The next step in this investigation was to pre-irradiate CO-RM L-**75** in LB medium to generate its corresponding i-CO-RM. CO-RM L-**75** was pre-irradiated for 68 mins and the *S. aureus* were then cultured as performed previously (**Figure 138**).

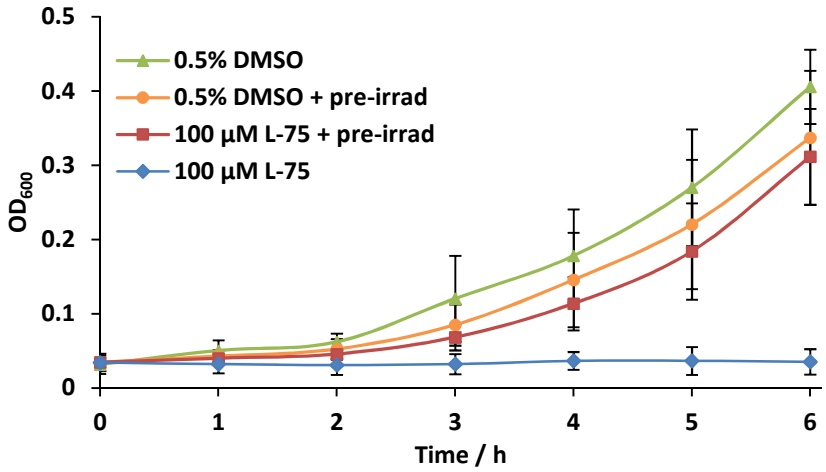

Figure 138. Growth curve with *S. aureus* 8325-4 in LB media with 100 µM CO-RM L-**75**. CO-RM L-**75** was pre-irradiated in LB media (2.4 W, 400 nm, 68 mins) in the **absence** of the bacteria. *S. aureus* was subsequently added to the i-CO-RM/LB media solution and cultured for six hours at 37°C.

The experiment in **Figure 138** was carried out with three independent repeats on separate days, which explains why there is some variation between repeat measurements. It is difficult to obtain exactly the same starting OD when starting a new experiment. Each batch of bacteria are slightly different so it can be difficult to directly compare these experiments. However taking the variation between experiments into account, it is clear that fresh CO-RM is required to get the bacteriostatic effect. When the CO-RM has been irradiated without bacteria, the bacteria grow only marginally slower than the controls without CO-RM. This mechanistic study suggests that CO-release from the CO-RM is responsible for the inhibition of growth observed.

6.5.1 Further Irradiation (400 nm) studies with *S. aureus* and CO-RM L-75

It has been shown that CO-RM L-**75** can exhibit a 95% bactericidal effect with irradiation on *S. aureus*, and a bacteriostatic effect without irradiation. These data was obtained using bacteria that were fresh. Previous studies show improved results on older *E. coli* with CO-RM L-**75** and this strategy was also taken with *S. aureus*.

S. aureus was grown with and without CO-RM L-**75** at a concentration of 100 µM using bacteria stored at 4 °C for 8 days. This batch of bacteria was older than previously used batches and was designed to see if there was an improved effect. Irradiation was also used in this study (**Figure 139** and **Table 18**).

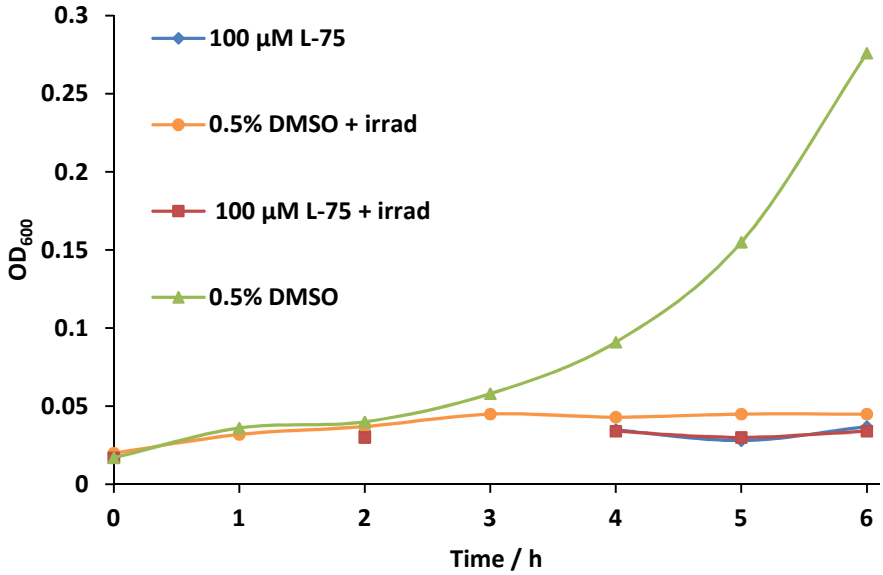

Figure 139. Growth of eight day old *S. aureus* 8325-4 with 100 µM CO-RM L-**75** in LB medium at 37 °C with 100 rpm shaking in 8 ml bijou tubes. Irradiation (400 nm, 2.4 W, 68 mins) started after one hour initial growth.

Table 18. Plating study with eight day old *S. aureus* corresponding to aliquots taken at one and three hours from the cultures used in **Figure 139**. Aliquots taken from both irradiated and non-irradiated cultures with 100 µM CO-RM L-**75**. Dilution factors shown in bold

1 h (Before irradiation)	**3 h Irradiated**	**1 h 'Thermal'**	**3 h 'Thermal'**
50x	**50x**	**50x**	**50x**
>2000	5	>2000	>2000
500x	**500x**	**500x**	**500x**
458	0	490	533

The experiments with eight day old *S. aureus* show that they are much more susceptible to CO-RM L-**75** in the presence of irradiation; but the bacteriostatic effect without irradiation does not improve. With irradiation in this case there is a greater than 99% toxicity with the use of irradiation compared to the previous 95% observed.

With the knowledge that CO-RM L-**75** was acting efficiently on *S. aureus*, a repeat of the above experiment was performed using 50 µM CO-RM L-**75** (**Figure 140** and **Table 19**).

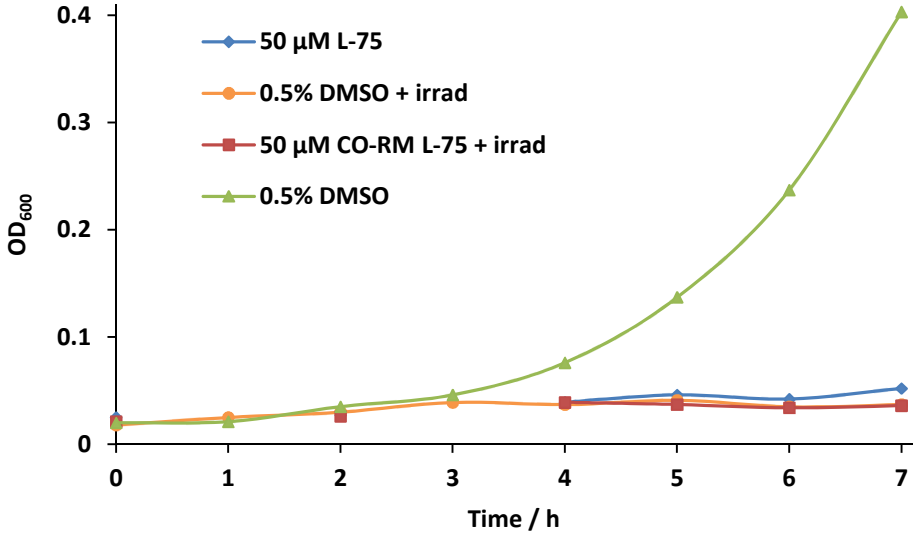

Figure 140. Growth of nine day old *S. aureus* 8325-4 with 50 µM CO-RM L-**75** in LB medium at 37 °C with 100 rpm shaking in 8 ml bijou tubes. Irradiation (400 nm, 2.4 W, 68 mins) started after one hour initial growth.

Table 19. Plating study with nine day old *S. aureus* corresponding to aliquots taken at 1 and 3h from the cultures used in experiments from **Figure 140**. Aliquots taken from both irradiated and non irradiated cultures with 50 µM CO-RM L-**75**. Dilution factors shown in bold

1 h (CO-RM, before)	3 h CO-RM Irrad	1 h Thermal	3 h Thermal
50x	**50x**	**50x**	**50x**
>2000	63	>2000	>2000
500x	**500x**	**500x**	**500x**
403	3	337	531

On the older cultures of *S. aureus*, CO-RM L-**75** is still effective with 400 nm irradiation with a >95% killing observed under the given conditions. This is not as effective as it is with CO-RM L-**75** at a concentration of 100 µM. The bacteriostatic effect is starting to drop away at lower concentrations with a fair degree of growth over the two hours of the experiment without irradiation. The growth is still slower compared to the 0.5% DMSO control. It is promising that this CO-RM can have a detrimental effect on *S. aureus* at a concentration that is viable with RAW 264.7 cells.

6.5.2 Visible-light irradiation studies with CO-RM L-75 on *S. aureus* 8325-4

Tryptophan-based CO-RM L-**75** has an antibacterial effect when irradiated at 400 nm with *S. aureus,* but as demonstrated on *E. coli* CO-RM L-**75** can be effective when irradiated with light of wavelength 465 nm. This justified further irradiation studies on *S. aureus* using irradiation of wavelength 465 nm.

Initial studies using irradiation of wavelength 465 nm were based on the previous conditions that used 400 nm irradiation but using different LEDs (**Figure 141** and **Table 20**).

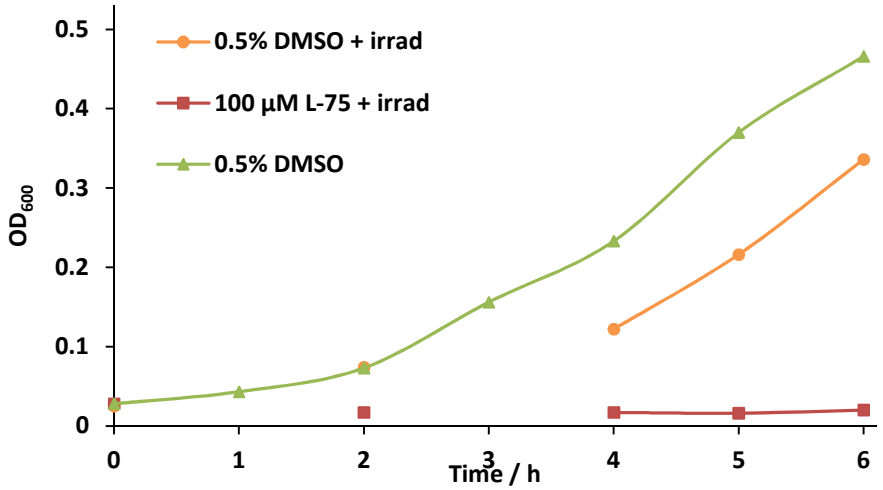

Figure 141. Growth of one day old *S. aureus* 8325-4 with 100 µM CO-RM L-**75** in LB medium at 37 °C with 100 rpm shaking in 8 ml bijou tubes. Irradiation (465 nm, 2.4 W, 68 mins) started after one hour initial growth. Missing points due to aliquots taken for plating studies.

Table 20. Plating study with one day old *S. aureus* corresponding to aliquots taken at one and three hours from the cultures used in experiments from **Figure 141**. Aliquots taken from both irradiated cultures with 100 µM CO-RM L-**75** and irradiated DMSO only controls. Dilution factors shown in bold

1 h CO-RM (Before)	**3 h CO-RM Irrad**	**1 h (before, DMSO)**	**3 h Irrad (DMSO)**
500x	**500x**	**500x**	**500x**
255	17	479	787

The initial study using CO-RM L-**75** with 465 nm irradiation exhibits a 90-95% killing rate on *S. aureus* when analysing the colony numbers before and after irradiation. The DMSO control

shows significant growth over the same period, demonstrating that both CO-RM and light are required together.

The unusual feature about these results is that unlike the previous results, the colony numbers before irradiation do not match between the DMSO and CO-RM control. There are more colonies in the DMSO control after one hour incubation compared to the CO-RM culture. This suggests that some colonies have died in the first hour in the presence of CO-RM without irradiation. This suggests that there is some degree of antibacterial action of CO-RM L-**75** on *S. aureus* without the need for irradiation. Is it evident that there is some degree of variability between experiments and every set of cells used in each repeat will vary in some way. However, all repeats at 100 µM are showing at least a bacteriostatic effect when assessed by plating study.

The above experiment (**Figure 141** and **Table 20**) with irradiation at wavelength 465 nm was then repeated again using a 10-fold lower starting OD. This experiment was designed to assess how turbidity affects irradiation studies; and to assess if the number of bacteria per unit volume at the same concentration of CO-RM altered the effectiveness of the treatment (**Figure 142** and **Table 21**)

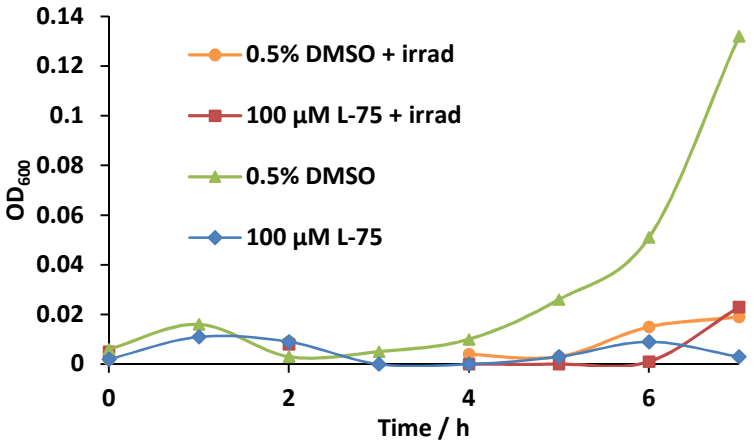

Figure 142. Growth of one day old *S. aureus* 8325-4 with 100 µM CO-RM L-**75** in LB medium at 37 °C with 100 rpm shaking in 8 ml bijou tubes. Irradiation (465 nm, 2.4W, 68 mins) started after one hour initial growth. Missing points due to aliquots taken for plating studies. Starting OD 10-fold lower than the experiment in **Figure 141**.

Table 21. Plating study with one day old *S. aureus* corresponding to aliquots taken at 1 and 3h from the cultures used in experiments from **Figure 142**. Aliquots taken from both irradiated cultures with 100 μM CO-RM L-**75** and irradiated (465 nm) DMSO only controls. Dilution factors given in bold.

1 h CO-RM (Before)	**3 h CO-RM Irrad**	**1 h (before, DMSO)**	**3 h Irrad (DMSO)**
50x	**50x**	**50x**	**50x**
71	3	384	507

With a starting OD 10-fold lower, there is an even bigger mismatch between the one hour colony counts with 100 μM CO-RM L-**75** and DMSO only. This strongly suggests that having fewer bacteria in the same volume of medium increases the bactericidal effect of CO-RM L-**75** without irradiation. If there are 384 colonies before irradiation in DMSO, then this could actually be taken as the starting number rather than the 71 colonies with CO-RM. This would mean that lowering the OD also increases the effectiveness of CO-RM L-**75** with 465 nm irradiation. This would be expected due to less light scattering and increased light absorption by the CO-RM.

6.6 Leghaemoglobin mechanistic studies: a CO scavenger rescue agent

The pre-irradiation studies carried out in section **6.5** suggest that CO released from CO-RM L-75 is responsible for the effects observed on *S. aureus*. To support this claim it was necessary to carry out some more detailed studies.

Leghaemoglobin (LegHb) is an oxygen and CO binding protein found within many leguminous plants within their root nodules.[127] LegHb has a fast CO binding rate of 13.5 μM^{-1} s^{-1} compared with only 0.51 μM^{-1} s^{-1} for myoglobin. LegHb and Mb have similar CO dissociation rates (0.012 s^{-1} and 0.019 s^{-1}), and this makes LegHb a potentially useful mechanistic tool for CO-RM studies.[128] LegHb can be added to bacterial cultures and used as a 'CO sponge' to quickly sequester CO that is released from the CO-RM. It will bind the CO faster than myoglobin can making it potentially more efficient for this application. If the use of this protein can reverse the action of a CO-RM on bacteria, then this would strongly support the action of CO rather than any metallic fragments.

With the above information in mind, David Richardson at the University of East Anglia kindly provided an *E. coli* BL21 sample containing a plasmid with multiple copies of the LegHb

genome sequence. This sample was prepared as reported previously.[129] The modified strain was cultured in auto induction medium at 37 °C to a high OD to obtain sufficient quantities of protein. The crude protein extract containing LegHb was obtained by sonication of cultured cells to break the cell wall and membrane. LegHb was purified by using an anionic exchange column eluting with a NaCl gradient. An SDS page gel was run to confirm protein purity and this is shown in **Figure 143**.

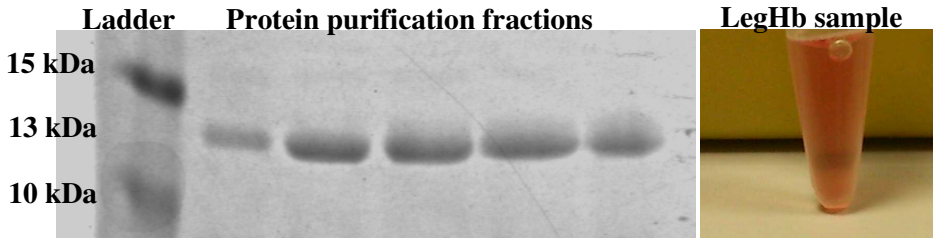

Figure 143. Left: SDS Page gel of LegHb. Right: Pure LegHb sample in Tris Buffer.

With pure LegHb protein obtained, it could be used in further bacterial studies as a CO scavenger. *S. aureus* appears to be much more sensitive to CO from CO-RM L-**75** compared to *E. coli.* To investigate this, a substoichiometric concentration of LegHb was added to cultures relative to the CO-RM concentration (100 μM). LegHb at concentration of 22 μM was added to LB media in a solution of 10 mM tris buffer pH 7.8 (protein storage buffer). Control experiments without LegHb had the same volume of tris buffer added to ensure everything was at the same concentration. The OD was measured at 650 nm in these experiments to reduce interference from the LegHb absorbance. **Figure 145** and **Table 22** show the first growth curve and plating study carried out with LegHb.

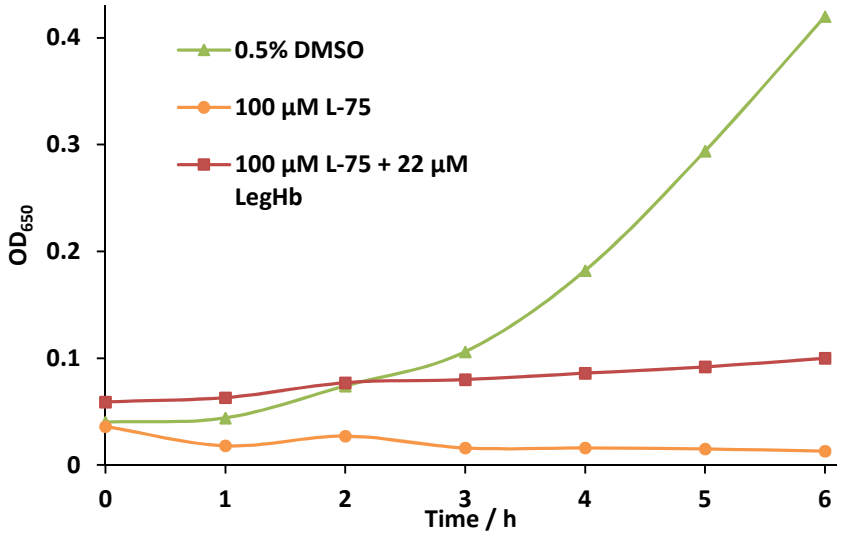

Figure 144. Growth curve with 10 day old *S. aureus* growth curve in LB medium at 37 °C with 100 µM CO-RM L-**75** and 22 µM LegHb CO scavenger.

Table 22. Plating study results matching with **Figure 144** comparing treatment of nine day old *S. aureus* with 100 µM CO-RM L-**75** after six hours of growth. Dilution factors shown in bold

6 h CO-RM	6 h CO-RM + LegHb
500x	**500x**
6	855
5000x	**500x**
0	136

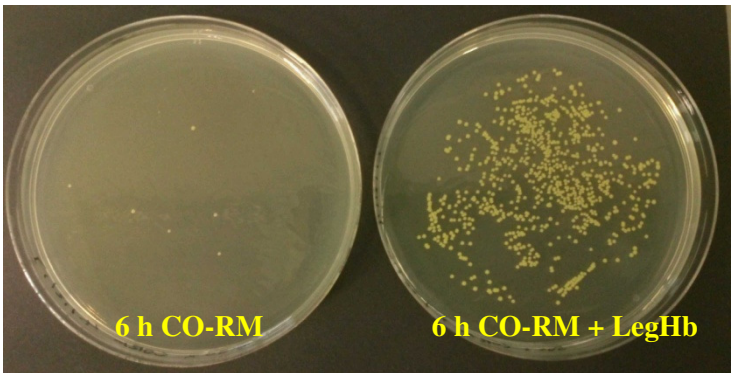

Figure 145. Images of 500× dilution plates which gave the data in **Figure 144**.

This experiment shows that LegHb protects *S. aureus* from the action of CO-RM L-**75**. Treatment with LegHb results in many more colonies surviving six hours CO-RM treatment. **Figure 145** shows that despite the slight increase in absorbance due to LegHb, the absorbance continues to increase by nearly two-fold over the six hour period. Without LegHb the OD of the culture immediately drops below its starting value and continues to decrease. LegHb does not completely mitigate the effects of CO-RM L-**75**, but reduces its potency, suggesting it is binding free CO that is released from CO-RM L-**75**.

A substoichiometric amount of LegHb is able to rescue *S. aureus* and this suggests that only a small amount of CO is associated with the antibacterial effect observed. This would match with the slow amount of CO-release from CO-RM L-**75** detected in the myoglobin assay without irradiation.

It is postulated that that CO-RM L-**75** may be degraded inside the bacteria releasing CO to its target. This would be difficult to prove with bacteria having natural manganese uptake mechanisms[130-131]. CO released inside the cell may diffuse outside of the cell and be bound up tightly by the LegHb. This could then prevent this molecule of CO from diffusing back inside another cell and binding to a target. Regardless of the mechanism of CO-release from CO-RM L-**75**, there can be confidence that *S. aureus* is more sensitive to CO than *E. coli.*

When nine day old *S. aureus* is used in these experiments, they appear more sensitive to CO-RM L-**75** at this age without light, with a large proportion of *S. aureus* dying when LegHb is not present. There appears to be a similar age based effect with *S. aureus* just like with *E. coli*.

A repeat of the experiment in **Figure 144** was performed to help confirm the observed results and the data is shown in **Figure 146** and **Table 23**.

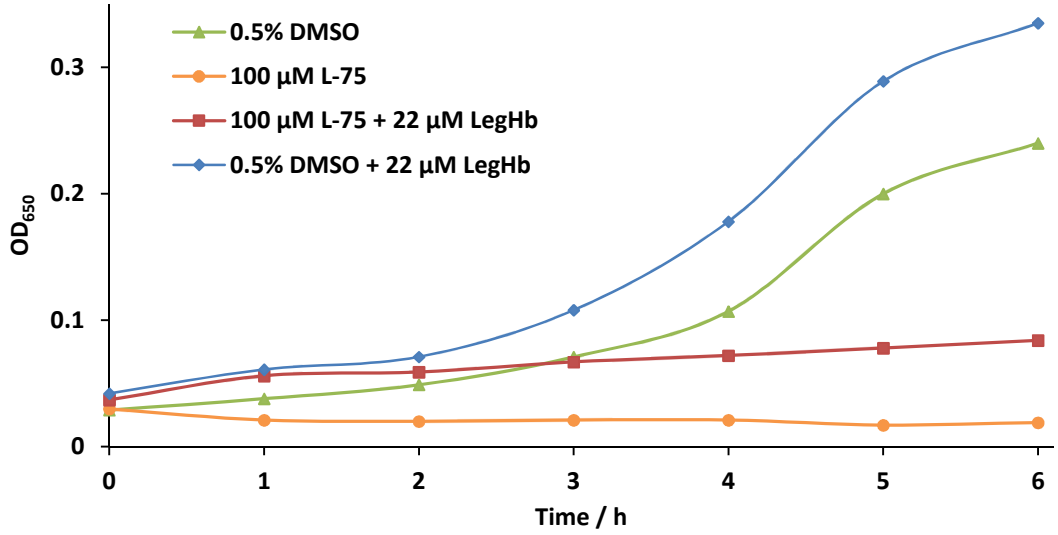

Figure 146. A growth curve with 10 day old *S. aureus* in LB medium at 37 °C with 100 µM CO-RM L-**75** and 22 µM LegHb CO scavenger. Additional LegHb only control added.

Table 23. Plating study results matching with **Figure 146** comparing treatment of 10 day old *S. aureus* with 100 µM CO-RM L-**75** after six hours growth. Repeat experiment of **Figure 144**.

6 h CO-RM	**6 h CO-RM + LegHb**
500x	**500x**
0	673
5000x	**500x**
0	71

The repeat experiment demonstrates that LegHb is rescuing *S. aureus* from the effects of CO-RM. The bacteria which were one day older show similar rates of rescue with LegHb with similar levels of antibacterial action without LegHb are observed. The extra control with LegHb was also carried out to rule out any interference LegHb itself.

This repeat experiment further contributes to the suggested mechanism of action. It would be difficult to use LegHb in photo-activated studies because LegHb significantly absorbs where the 400 and 465 nm LEDs emit and the decreased light penetration could give false positive results.

This experiment was repeated a final time with fresher *S. aureus* (five days old). This experiment was performed to confirm the age dependent action of CO-RM L-**75** (**Figure 147** + **Table 24**)

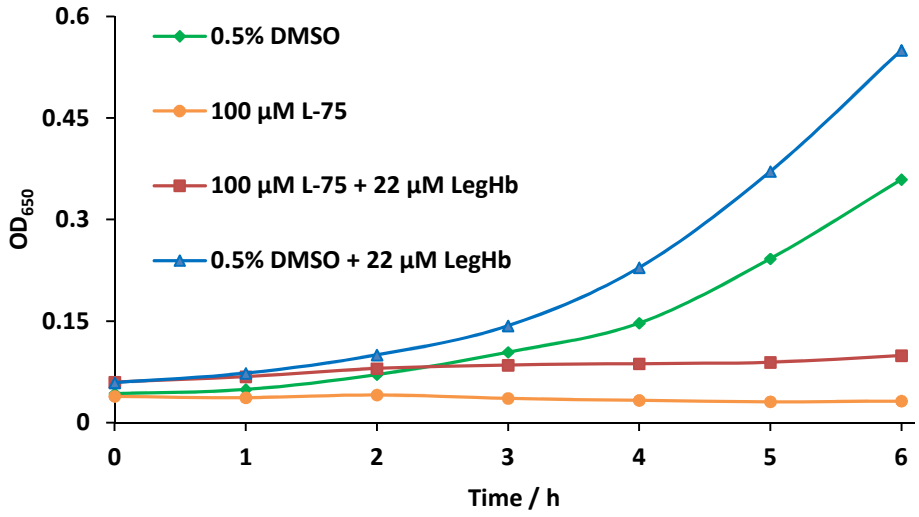

Figure 147. Five day old *S. aureus* growth curve in LB medium at 37 °C with 100 µM CO-RM L-**75** and 22 µM LegHb CO scavenger. Additional LegHb only control added. Second repeat experiment.

Table 24. Plating study results matching with **Figure 147** comparing treatment of five day old *S. aureus* with 100 µM CO-RM L-**75** after six hours of growth. Second repeat experiment.

6 h CO-RM	**6 h CO-RM + LegHb**
500x	**500x**
477	762
5000x	**5000x**
57	155

The second repeat of these LegHb investigations shows an age dependent antibacterial action of CO-RM L-**75** on *S. aureus*. With five day old bacteria there is less of an anti bacterial effect. However this experimental repeat still demonstrates the ability of LegHb to rescue the *S. aureus* from the action of CO-RM L-**75**.

6.6.1 Dual repeat studies with CO-RM L-75 on *S. aureus* using LegHb

Despite three repeat experiments showing that LegHb can reduce the potency of CO-RM L-**75**, further experiments were carried out. Previous results were carried out on separate days with different batches of bacteria and only one plate was used for each dilution study. This was done because there were concerns regarding the time it takes to obtain bacterial aliquots and perform plating studies. The bacteria are grown in a 37 °C room and must be removed for samples to be taken. Keeping the time at lower temperature to a minimum is essential. Studies with more simultaneous repeats were required to allow for some more statistical analysis. LegHb incubations were repeated using two vials for each type of measurement with a plate for each vial. Considering that the DMSO and LegHb only controls do the same thing previously, these were omitted from these experiments so as to keep the time samples were out of the 37 °C room to a minimum. The detailed growth curve and colony counting study is shown in **Figure 148** and **Table 25**.

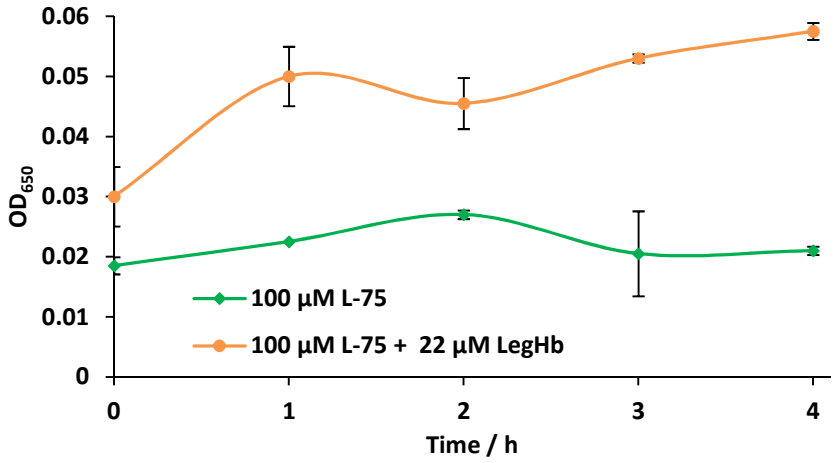

Figure 148. Seven day old *S. aureus* 8325-4 growth curve with 100 µM CO-RM L-**75** and 22 µM LegHb at 37 °C. Curves are an average of two side by side repeats.

Table 25. Plating study values for aliquots taken from seven day old *S. aureus* cultures used in **Figure 148**. Repeat one and two: aliquots taken from separate vials and spread out in the same fashion. Dilution factors indicated in bold.

Repeat 1			
0 h CO-RM	**4 h CO-RM**	**0 h CO-RM + LegHb**	**4 h CO-RM + LegHb**
500x	**500x**	**500x**	**500x**
234	1	202	307
5000x	**5000x**	**5000x**	**5000x**
26	0	31	54
Repeat 2			
500x	**500x**	**500x**	**500x**
221	4	196	284
5000x	**5000x**	**5000x**	**5000x**
13	0	22	29

With the plating study in **Figure 148** aliquots were taken at four hours, instead of six hours, to assess if the antibacterial effect of CO-RM L-**75** had occurred earlier than previously observed. The variation in numbers between the two repeats is small and there is antibacterial action from the CO-RM after four hours which can be significantly reduced with the presence of LegHb. In this experiment the *S. aureus* increases in numbers over the four hours when CO binding agent LegHb is present.

To summarise, CO-RM L-**75** has been shown to exhibit a variety of effects against *S. aureus* 8325-4, both with and without light. The CO-RM has a significant effect without irradiation suggesting *S. aureus* is sensitive to low concentrations of CO. The effects of the CO-RM are enhanced by irradiation of wavelength 400 and 465 nm, and with increasing age. Pre-irradiation studies and studies with Leg-Hb which scavenges CO from the solution suggest that CO is released from CO-RM L-**75**. It also suggests that the antibacterial effects of CO-RM L-**75** are not due to metal fragments. To date, these studies in keeping with the studies performed with *E. coli*, represent some of the most detailed mechanistic studies carried out on these bacteria in the literature.

6.7 Investigations with CO-RM L-75 on *Neisseria gonnorhoeae* MS11

Tryptophan-based CO-RM L-**75** has shown some very promising antibacterial activity on both *E. coli* and *S. aureus*. *N. gonorrhoeae* is a sexually transmitted disease which if left untreated can cause serious health problems.[132-134] In the first-world this has typically not been a top health concern due to being easily treatable with a course of antibiotics. However recently, new strains of *N. gonnorhoeae* have been discovered which are resisting many commonly used antibiotics.[132-134] There have been human *N. gonorrhoeae* infections in Japan where all current treatments have proved ineffective and many peoples' health is at serious risk.[132-134] The persistence of these *N. gonorrhoeae* strains increases the chance of these strains spreading rapidly and causing serious problems. There is an urgent requirement for new effective treatments of *N. gonorrhoeae*, and CO-RM L-**75** could potentially be a new treatment. This warrants detailed testing of CO-RM L-**75** on *N. gonorrhoeae.*

Initial investigations with *N. gonorrhoeae* MS11 drew upon the previous knowledge obtained from tests on *E. coli and S. aureus.* A growth curve was carried out using BHI medium with a yeast autolysate supplement (YAL) in the presence and absence of CO-RM L-**75** at a concentration of 100 μM. BHI + YAL was found to be a suitable medium for *N. gonorrhoeae,* with significant growth over the period of the experiment. It is undesirable to use a medium in which the bacteria were particularly weakened, and this is why a YAL supplement was used. *N. gonorrhoeae* throughout these investigations were cultured from stocks on Columbia agar plates with 5% horse blood for 48 hours. Bacteria were used within two days after this initial growth and were stored at 37 °C under 5% CO_2 prior to use. Aging studies were not performed here due to their sensitivity. Cells cannot be stored for as long as other strains of bacteria without significantly weakening them. **Figure 149** shows the initial growth experiment carried out with CO-RM L-**75** on *N. gonorrhoeae.*

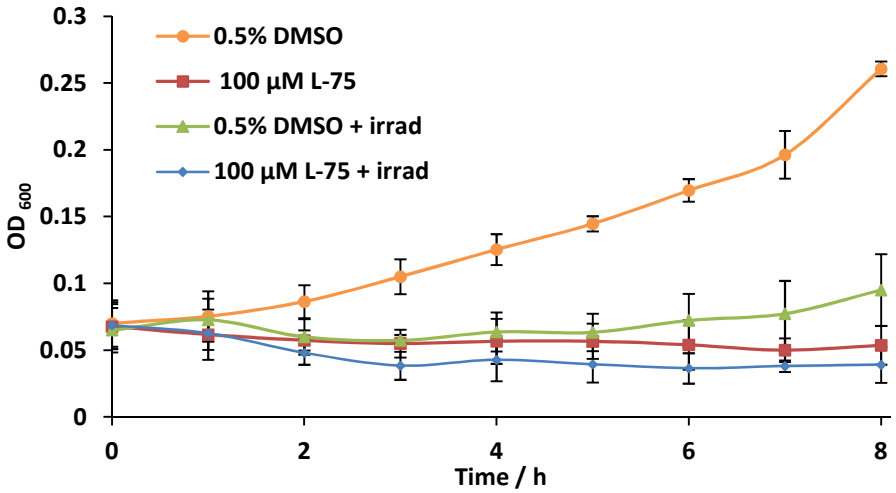

Figure 149. Growth curve with *N. gonorrhoeae* MS11 in BHI + YAL growth medium with 100 µM CO-RM L-**75**. Irradiation was used as indicated after one hour initial growth (400 nm, 2.4 W, 68 mins)

As shown in **Figure 149**, *N. gonorrhoeae* is capable of growing successfully in this medium with a four-fold increase in OD_{600} over the eight hour growth period. Irradiating *N. gonorrhoeae* at 400 nm for 68 mins without CO-RM L-**75** results in a large reduction in growth, but there is evidence for re-growth towards the 8th hour of the experiment. With CO-RM L-**75** at a concentration of 100 µM, the same significant drop in OD_{600} occurs but there is no re-growth later in the experiment. The same applies to both irradiated and non-irradiated cultures with CO-RM L-**75**. This suggests that CO-RM L-**75** is having a similar action on *N.gonnorhoeae* as it is on *S. aureus* and *E. coli.* The OD_{600} of cultures with CO-RM L-**75** at a concentration of 100 µM do not increase above the starting OD throughout the course of experiment without irradiation. This suggests another thermal or enzyme-triggered mechanism of CO-RM activation.

As carried out with previous strains of bacteria, plating studies were carried out to assess the percentage cytotoxicity of CO-RM L-**75** on *N. gonorrhoeae* (**Figure 150**). This study was done with and without irradiation.

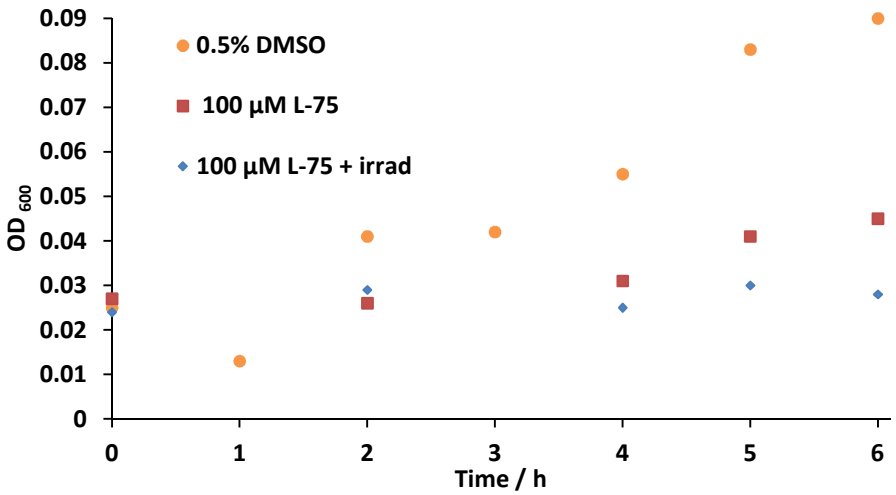

Figure 150. *N. gonorrhoeae* MS11 growth curve in BHI + YAL medium with 100 µM CO-RM L-**75**. Carried out in the presence and absence of irradiation (400 nm, 2.4 W, 68 mins) which was started at one hour. Aliquots taken at one and three hours representing before and after irradiation for a plating study. Trend lines not included due to the low OD used and single repeats in this experiment

Table 26. Plating study corresponding to **Figure 150**. Both samples contain 100 µM CO-RM L-**75**. Left pair: irradiation between 1-3h), right pair: no irradiation. Dilutions indicated in bold

1 h (CO-RM)	**3 h (CO-RM irrad)**	**1 h CO-RM**	**3 h CO-RM**
500x	**500x**	**500x**	**500x**
260	71	230	127
5000x	**5000x**	**5000x**	**5000x**
35	7	29	17

CO-RM L-**75** at a concentration of 100 µM in BHI + YAL shows a detrimental effect to *N. gonorrhoeae* both with and without irradiation. There is a 45% reduction in numbers without irradiation confirming that *N. gonorrhoeae* is also sensitive to CO released from a CO-RM as seen against *S. aureus*. With irradiation there is an increase in cytotoxicity giving a 73% reduction in numbers. However considering the large amount of CO that should be released from CO-RM L-**75** on irradiation, this is not having a significant effect on the bacteria. The BHI + YAL medium is a rich medium and contains many species that absorb at the point of irradiation. In this medium it is proposed that a significant proportion of irradiation is being absorbed and is not being used to activate the CO-RM. It is promising that CO-RM L-**75** shows a mild antibacterial effect without irradiation but an alternative growth medium was required for remaining experiments in this work.

RPMI medium has been previously been used within the Moir research group to grow *Neisseria meningitidis*. *N. meningitidis* is closely related to *N. gonorrhoeae* and RPMI medium was used as an alternative medium for further experiments. Initial studies showed that RPMI medium on its own was not sufficient to allow for efficient growth of *N. gonorrhoeae*. Using YAL together with RPMI created a new medium which *N. gonorrhoeae* could grow efficiently in.

Initial experiments were carried out using CO-RM L-**75** without irradiation to assess the antibacterial effect observed without irradiation in this new medium. A short growth curve and complimentary plating study was carried out (**Figure 151** and **Table 27**)

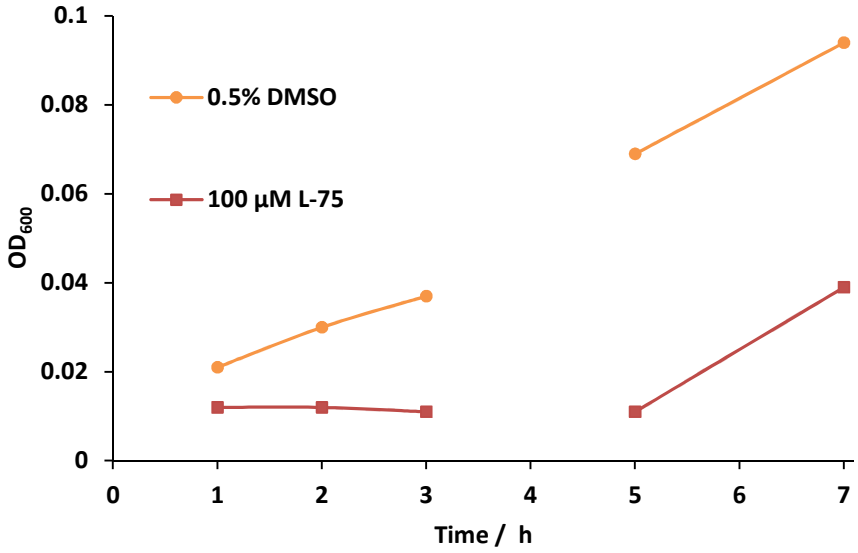

Figure 151. Growth curve with *N. gonorrhoeae* at 37 °C in RPMI + YAL medium. Use of 0.5% DMSO with or without 100 µM CO-RM L-**75**. Aliquots removed at zero and four hours during the experiment Lines not included due to fewer data points. Data points missing due to aliquots taken for plating study.

Table 27. *N. gonorrhoeae* plating study corresponding to the aliquots taken from **Figure 151** at zero and four hours. Dilutions indicated in bold

0 h CO-RM	4 h CO-RM	0 h DMSO	4 h DMSO
500x	**500x**	**500x**	**500x**
438	0	534	717
5000x	**5000x**	**5000x**	**5000x**
55	0	75	80

In RPMI + YAL medium there is a potent antibacterial effect without the need for irradiation. 438 colonies were present at the start of the experiment at 500× dilution, with none present at the same dilution after 4 hours incubation. Without CO-RM L-**75** the bacteria survive and increase in

numbers over the same period of time. This suggests that moving to this new medium is not weakening the bacteria. However, CO-RM L-**75** does appear to be much more potent in this new medium. It is postulated that the protein rich BHI medium, which contains a large number of undefined contents, could cause degradation of the CO-RM reducing its effectiveness. A repeat of this experiment was carried out at a higher starting OD to assess how toxic this CO-RM actually is (**Figure 152** and **Table 28**).

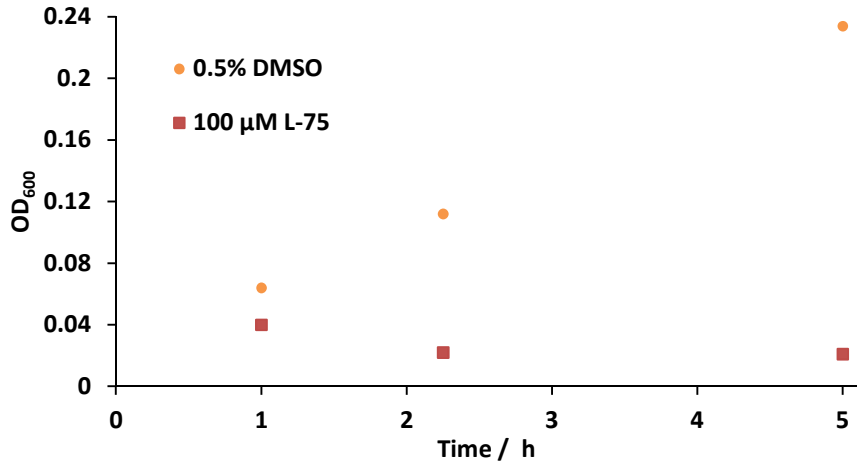

Figure 152. Repeat growth curve with *N. gonorrhoeae* MS11 at 37 °C in RPMI + YAL medium. Use of 0.5% DMSO with or without 100 µM CO-RM L-**75**. Aliquots removed at zero and four hours during the experiment. Higher starting OD was used for this experiment. Lines not included due to fewer data points. Data points missing due to aliquots taken for plating study.

Table 28. *N. gonorrhoeae* MS11 plating study corresponding to the aliquots taken from **Figure 152** at zero and four hours. Dilutions indicated in bold.

0 h CO-RM	4 h CO-RM	0 h DMSO	4 h DMSO
500x	**500x**	**500x**	**500x**
>2000	0	>2000	>2000
5000x	**5000x**	**5000x**	**5000x**
365	0	459	1264

The data in **Figure 152** shows that there is a significant increase in bacterial growth when a higher starting OD is used. The OD of the culture with CO-RM L-**75** present drops well below the starting OD, but with 0.5% DMSO the bacteria grow significantly in numbers over the experiment. The plating study shows that the cytotoxicity of CO-RM L-**75** in this medium is even more potent than initially thought. There is >99.9% bactericidal effect in the presence of the CO-RM L-**75**. This is the first time a CO-RM has been used to show detrimental effects on *N. gonorrhoeae* MS11.

6.7.1 *N. gonorrhoeae* MS11 studies using LegHb as a rescue agent.

With CO-RM L-**75** showing a potent antibacterial effect against *N. gonorrhoeae*. It was then necessary to carry out further mechanistic investigations to see if CO release from CO-RM L-**75** was killing *N. gonorrhoeae*. This involved using LegHb as a rescue agent as was performed previously with *S. aureus*. The first experiment using LegHb in experiments with *N. gonorrhoeae* is shown in **Figure 153** and **Table 29**.

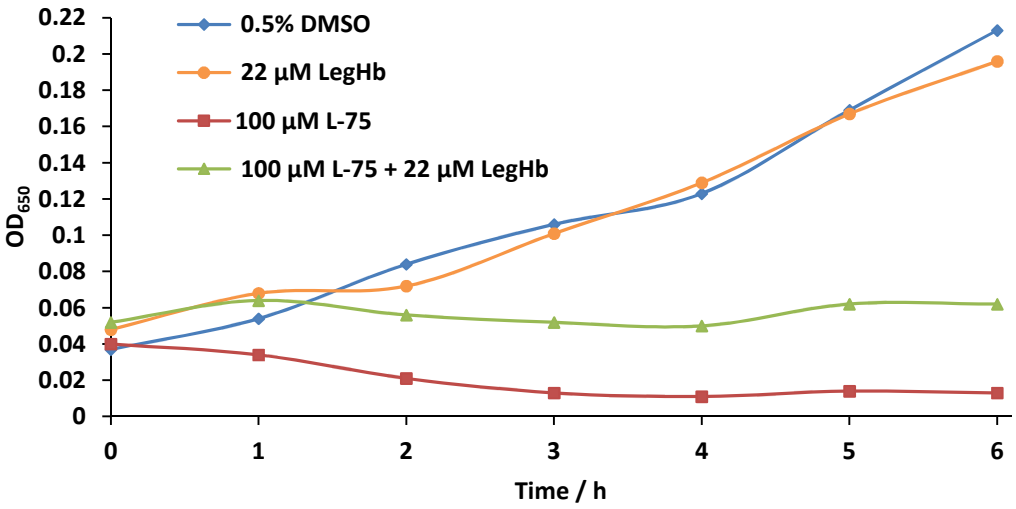

Figure 153. *N. gonorrhoeae* MS11 growth curve in RPMI + YAL medium with 100 µM CO-RM L-**75** and 22 µM LegHb.

Table 29. Plating study corresponding to aliquots taken at zero and four hours from the cultures represented in **Figure 153**. Dilutions indicated in bold.

0 h CO-RM	4 h CO-RM	0 h CO-RM + LegHb	4 h CO-RM + LegHb
5000x	**5000x**	**5000x**	**5000x**
163	4	181	32
50000x	**50000x**	**50000x**	**50000x**
13	1	17	1

The bactericidal effect observed in RPMI medium is lower than previously observed but is still > 97% toxic to *N. gonorrhoeae*. The growth curve shows that *N. gonorrhoeae* is rescued by the presence of LegHb. This suggests a similar mechanism of action (*i.e* CO) of CO-RM L-**75** on *S. aureus*. The LegHb control grows by the same amount as the DMSO-only control.

The experiment in **Figure 153** was repeated but excluding the LegHb only control, so that double repeats could be carried out (**Figure 154** and **Table 30**). *N. gonorrhoeae* is a temperature

sensitive bacteria and keeping it at its optimum growth temperature of 37 °C for as much time as possible is essential to try and reflect *in vivo* conditions.

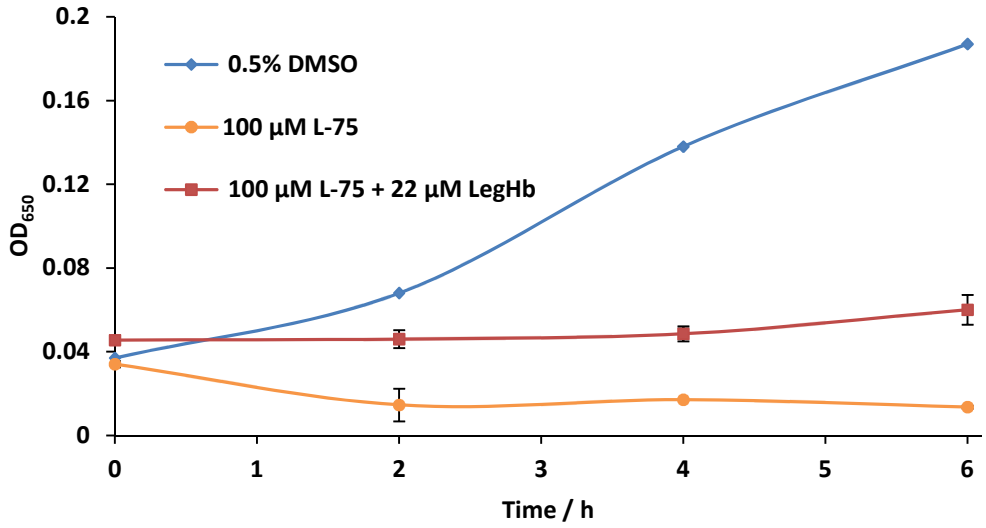

Figure 154. *N. gonorrhoeae* growth curve in RPMI + YAL medium with 100 µM CO-RM L-**75** and 22 µM LegHb. Cultures with CO-RM L-**75** and LegHb are an average of two side by side repeats.

Table 30. Plating study data corresponding to aliquots taken at zero and four hours from cultures represented in **Figure 154**. Dilutions indicated in bold

Repeat 1			
0 h CO-RM	**4 h CO-RM**	**0 h CO-RM + LegHb**	**4 h CO-RM + LegHb**
500x	**500x**	**500x**	**500x**
>1000	0	>1000	106
5000x	**5000x**	**5000x**	**5000x**
157	0	141	9
Repeat 2			
500x	**500x**	**500x**	**500x**
>1000	0	>1000	110
5000x	**5000x**	**5000x**	**5000x**
118	0	123	8

These repeat studies show that *N. gonorrhoeae* can be rescued by the use of substoichiometric amounts of LegHb relative to the amount of CO-RM L-**75**. There is an antibacterial effect above 99% in these repeats which is reduced to only 90% by the use of LegHb. The degree of rescue in these experiments is less than that observed in the experiments with *S. aureus*. However, there is a significant enough change here to be confident that there is a similar mechanism of action on *N.*

gonorrhoeae as there is with *S. aureus*. Both *S. aureus* and *N. gonorrhoeae* are both very sensitive to CO.

6.8 Spectral investigations with CO-RM L-75, LegHb and Mb

With LegHb acting as a potential 'CO sponge' in the presence CO-RM L-**75** in bacterial cultures, further UV-Vis spectroscopic studies were carried out with CO-RM L-**75** and LegHb to investigate how the CO is transferred to the LegHb.

Initial studies explored whether LegHb could bind CO gas without the need for sodium dithionite. Then CO-RM L-**75** was tested as the CO source (**Figure 155**).

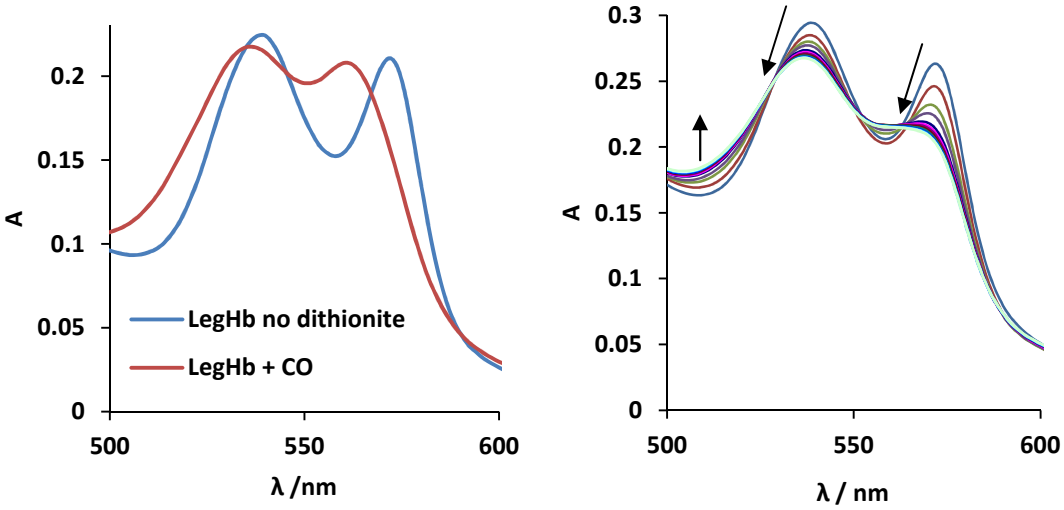

Figure 155. Left: UV spectrum of 22 µM LegHb and the changes upon binding CO gas. Right: UV-Vis spectra of 22 µM LegHb with 100 µM CO-RM L-**75** taken every five mins. Sample was kept in the dark once the experiment was started.

The UV-Vis data in **Figure 155** shows that a similar set of spectral changes occur on binding CO from gas and from CO-RM L-**75**. It also shows that CO-RM L-**75** is capable of releasing CO without the need for a sodium dithionite. There is potential for the bacteria to produce a reducing environment as they use up all the oxygen in the culture, but with the presence of CO-RM L-**75** the majority of the cells are not actively growing. This is therefore unlikely to be the case. The fact that it takes 55 minutes to saturate only 22 µM LegHb using 100 µM CO-RM L-**75**, suggests that the CO-RM is slowly releasing its CO as shown in the myoglobin assay (**Figure 116**). The LegHb is not just sequestering the CO straight from the CO-RM, it is appears to be binding the CO as it is gradually released thermally into solution.

It is proposed that this small amount of CO is responsible for the antibacterial effects observed in the *N. gonorrhoeae* experiments.

The same experiment with CO gas was also carried out to assess if myoglobin would bind CO in the same way without sodium dithionite. It was found that no spectral change was observed on bubbling with CO gas. Myoglobin does not bind CO strongly/fast enough to displace the bound oxygen without the use of sodium dithionite.

With the above taking in to consideration, a final *N. gonorrhoeae* experiment was carried out using CO-RM L-**75**. Myoglobin was employed as a second potential rescue agent although it was expected that it would not bind up the CO in solution. **Figure 156** and **Table 31** shows the growth curves and corresponding plating study carried out alongside this.

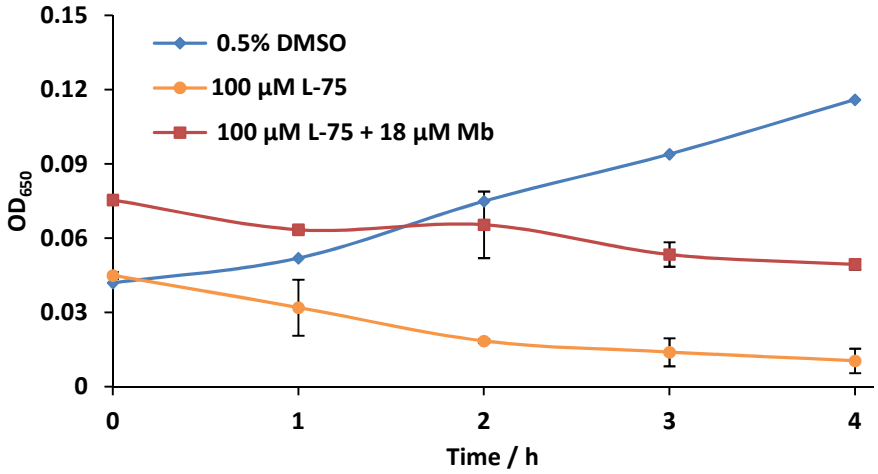

Figure 156. *N. gonorrhoeae* growth curve with CO-RM L-**75** and 18 µM myoglobin in RPMI + YAL medium at 37 °C with 100 rpm rotation.

Table 31. Plating study data corresponding to aliquots taken at zero and four hours from cultures represented in **Figure 156**. Dilutions factors are shown in bold.

Repeat 1			
0 h CO-RM	**4 h CO-RM**	**0 h CO-RM + Mb**	**4 h CO-RM + Mb**
500x	**500x**	**500x**	**500x**
>1000	39	>1000	65
5000x	**5000x**	**5000x**	**5000x**
173	8	174	5
Repeat 2			
500x	**500x**	**500x**	**500x**
>1000	36	>1000	46
5000x	**5000x**	**5000x**	**5000x**
188	6	187	4

The myoglobin experiments above suggest that myoglobin is not binding any CO released from solution both with and without bacteria. The variation between repeats is small and there is not a large degree of rescue with myoglobin.

The studies in this section show that LegHb is a new mechanistic tool for gaining insight in to how CO-RMs exhibit detrimental effects against bacteria. LegHb has not been previously used in this manner and has been useful in the bacterial studies presented in this study.

6.9 Concluding remarks on CO-RM L-75 and its properties

In summary, CO-RM L-**75** has been shown to have a potent antibacterial effect against *N. gonorrhoeae.* The most potent effect was observed in RPMI + YAL medium without the need for irradiation with a killing rate over 99%. CO-RM L-**75** is similar to the previous phenylpyridine CO-RMs prepared in this project; but differs by an exchangeable acetonitrile ligand and an N^O mode of coordination as opposed to C^N. It is proposed that this exchangeable ligand site allows for slow thermal CO release which is believed to cause the thermal or enzyme-triggered action on *S. aureus* and *N. gonorrhoeae*. It may be possible that an enzyme within each strain of bacteria can facilitate CO release inside the cell at a much faster rate. This CO could then immediately bind a target within the cell. CO-RM L-**75** has proven to be a promising new potential pharmaceutical molecule with many possible applications.

CO-RM L-**75** was designed to be a photo-CO-RM, however it possesses some antibacterial activity without the need for irradiation. Designing a CO-RM to be a photo-CO-RM with respect to aqueous solution and proteins such as myoglobin and LegHb can be advantageous. *In vivo*, one would not want to administer a CO-RM for it to be immediately be bound up by myoglobin as this is not the desired target. CO-RM L-**75** does not rapidly release its CO to myoglobin; which means it can be administered into the body and will not immediately degrade due to the presence of myoglobin. Subsequent irradiation allows for rapid CO-release, and could be metabolised inside bacterial cells which kills them due to CO then binding to important respiration enzymes.

There is variation in the degree of antibacterial effects being observed throughout different repeats and experiments. There are also unusual aging effects observed with *E. coli* and *S. aureus*. The cells at older ages still grow rapidly and it is difficult to draw conclusions to what the aging effect means in the broader context of a potential *in vivo* study. Bacteria *in vivo* are under many forms of stress from human immune responses and other factors. The key conclusion from all of the research in this section is that under certain conditions, the CO-RMs synthesised in the project exhibit a potent effect on three infectious strains of bacteria, and the only way to find out if they will work *in vivo*, is to test them as such.

7 Visible-light-induced CO-release using a dye CO-RM.

7.1 Synthesis and characterisation of a dye $Mn(CO_4)$ CO-RM.

To widen the potential applications of photo-CO-RMs, creating new analogues and discovering structural features which increase the wavelength of light required for CO-release is desirable as shown with previous CO-RMs. CO-release at higher wavelength allows for deeper tissue penetration by light[122], increasing the type of potential conditions that could be treated using photo-activated CO-RMs. Irradiation at lower wavelengths is quickly absorbed by macromolecules which could prevent efficient CO-release. This would limit the use of these CO-RMs to skin/wound treatment if photolysis was required to get an effect.

To discover a new motif with structural features that would increase the wavelength of CO-release, A literature search was performed to find a lead molecule. Initial literature searches were carried out in *dyes pigments* journal. There was particular interesting in using dyes to create a new CO-RM, as these molecules are designed to absorb well into the visible region of the spectrum. They are often designed to have a very high molar absorption coefficient with extended conjugation systems with 'push-pull' electronic systems.

Research by Wang and co-workers reported a series of structurally interesting azodyes.[135] **Scheme 37** reports the synthesis of a dye selected for use in further synthetic studies.

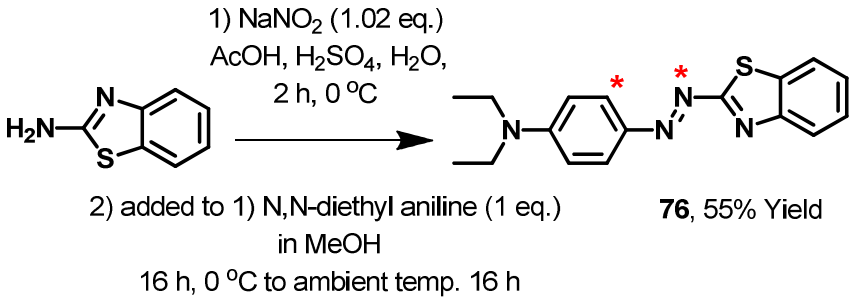

Scheme 37. The synthesis of benzothiazole containing azo-dye **76**, stars indicate future target atoms for functionalisation

Azo dye **76** was selected for further studies because of the interesting spectral properties it has. **76** has a λ_{max} at 512 nm with a reported molar extinction coefficient of 52000 mol^{-1} dm^3 cm^{-1}. This is a high wavelength and molar extinction coefficient considering the size of the molecule and the amount of conjugation. The 'push-pull' conjugated system within this molecule is likely to be responsible for its interesting optical properties. The strong mesomeric effect from the *N,N*-

diethyl group in tandem with the electron deficient benzothiazole allows for efficient electron transfer across the molecule. Ligand **76** is clearly efficient at absorbing at this wavelength which makes it an excellent candidate ligand for photo-CO-RM synthesis.

Dye **76** was used in many reactions in an attempt to install an $Mn(CO)_4$ group like that which had previously been introduced onto phenylpyridine ligands. The initial intention with this molecule was to install the $Mn(CO)_4$ which could be potentially linked to the π-conjugation system of the dye. The idea was that this π-system could alter the d-d energy gap, subsequently resulting in lower wavelength photo-activated CO-release.

Initial attempts to cyclometallate **76** using $BnMn(CO)_5$ gave a large number of coloured products as seen by TLC and column chromatography (**Figure 157**).

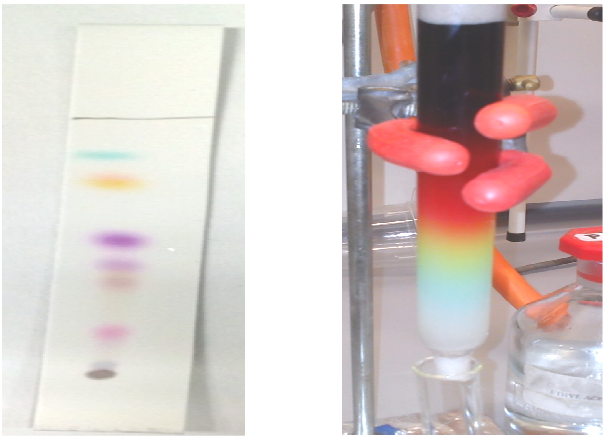

Figure 157. Left: TLC of crude reaction mixture when synthesizing CO-RM **77**. Right: Column from the purification of the crude reaction mixture.

It is proposed that the azo dye starting material was decomposing, and swapping its substituents to create different azo dyes giving rise to the array of colours observed on the TLC plate/column. Optimisation proved unsuccessful in preventing degradation. Reactions were attempted using lower temperatures (40 and 75 °C) with longer reaction times (48 and 16 h respectively). At 40 °C little conversion to any new products was observed, and at 75 °C no product was isolated following column chromatography. A reaction temperature of 95 °C was required to get the $BnMn(CO)_5$ to react with the dye substrate in the desired fashion, but this simultaneously causes degradation. Optimised conditions to get the desired cyclo-metalated complex are shown in **Scheme 38**.

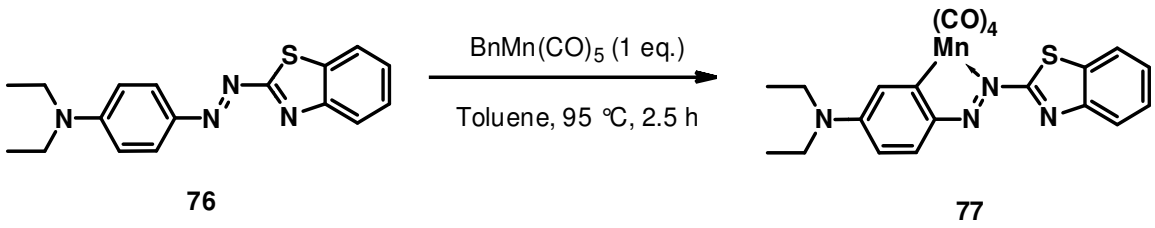

Scheme 38. Optimised conditions for the synthesis of CO-RM **77**.

Reaction of azodye **76** with $BnMn(CO)_5$ at 95 °C for two hours provided enough time and energy to allow reaction of **76** to give CO-RM **77** following column chromatography. **Figure 158** shows the TLC of column fractions that resulted in obtaining sufficiently pure product.

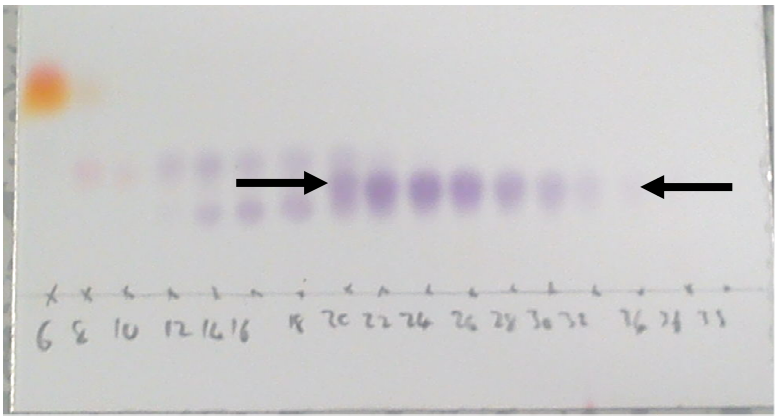

Figure 158. TLC of column fractions from the purification of CO-RM **77**, arrow indicates fractions taken.

Comparing the above TLC to the crude TLC (**Figure 157**), it shows that the majority of the coloured species have degraded on passing through the column. Several purple species were observed and fractions 24–32 were found to contain the target complex **77** with sufficient purity for further analysis.

Figure 159 shows the ^{1}H NMR spectrum of CO-RM **77**

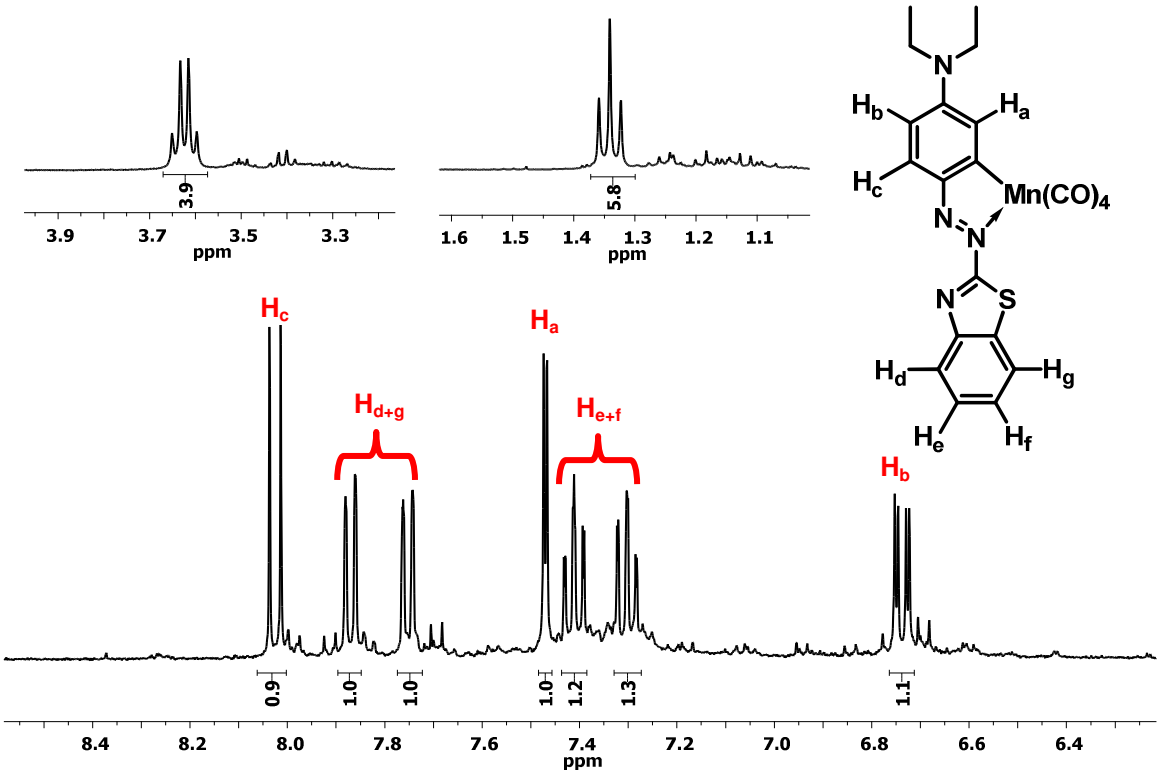

.

Figure 159. 400 MHz ^{1}H NMR spectrum of CO-RM **77** in CD_2Cl_2 at 300 K

On cyclometallation of dye **76**, a typical resonance pattern is seen around the phenyl ring. The signal for H_a only contains a long range ^{4}J W-coupling to H_b as expected. H_b is a doublet of doublets due to W coupling with H_a and a shorter range ^{3}J coupling with H_c. H_c only has a matching coupling constant back to H_b. A ^{1}H-^{1}H COSY experiment confirms these discussed couplings and assignments. The COSY experiments also show coupling between protons H_{d+e} and H_{f+g}. These data suggests the proposed structure for CO-RM **77**.

A solution IR spectrum of CO-RM **77** was obtained in CH_2Cl_2 to confirm the presence of the metal carbonyl ligands within the structure (**Figure 160**).

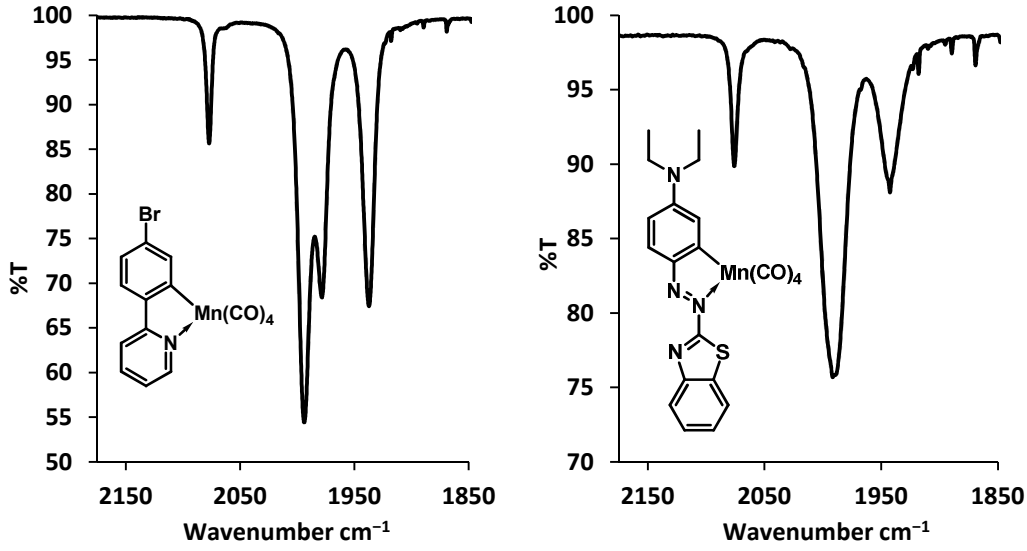

Figure 160. Left: IR spectrum of CO-RM **40** for comparison. Right: IR spectrum of azodye CO-RM **77**

The main difference between the two IR spectra is that the spectrum for CO-RM **77** appears to have three peaks instead of four. The IR spectrum of bromo-phenylpyridine CO-RM **40** was shown for comparison to demonstrate that the frequency, shape and spacing of the peaks similar. It is proposed that the change in structure has resulted in the middle two M–CO peaks from CO-RM **77** significantly overlapping. This is why there are three apparent peaks are observed instead of four. This could certainly be expected with the nitrogen that coordinates to the manganese being in a different chemical environment. The peak at 1990 cm^{-1} in the spectra of CO-RM **77** is not symmetrical which suggests two overlapping peaks. LIFDI and ESI mass spectrometry measurements both show a molecular ion peak corresponding to the target $Mn(CO)_4$ complex as opposed to a tricarbonyl species. With the data in hand there can be a strong degree of confidence that the target CO-RM **77** has been successfully synthesised.

CO-RM **77** was unfortunately only isolated with a yield of 5%, which can be linked to the significant amount of thermal degradation shown by TLC and column chromatography. Despite the poor yield, this CO-RM could possess some unique properties, and this warrants further investigations

7.2 Spectral, CO-release and mechanistic studies with dye CO-RM 77

With sufficiently pure CO-RM **77** to hand, the next step was to characterise its relevant properties. CO-RM **77** was designed to increase the wavelength of irradiation required to initiate CO-release, and so spectral properties were the first to be investigated. Initial experiments involved UV-Vis spectral analysis (**Figure 161**).

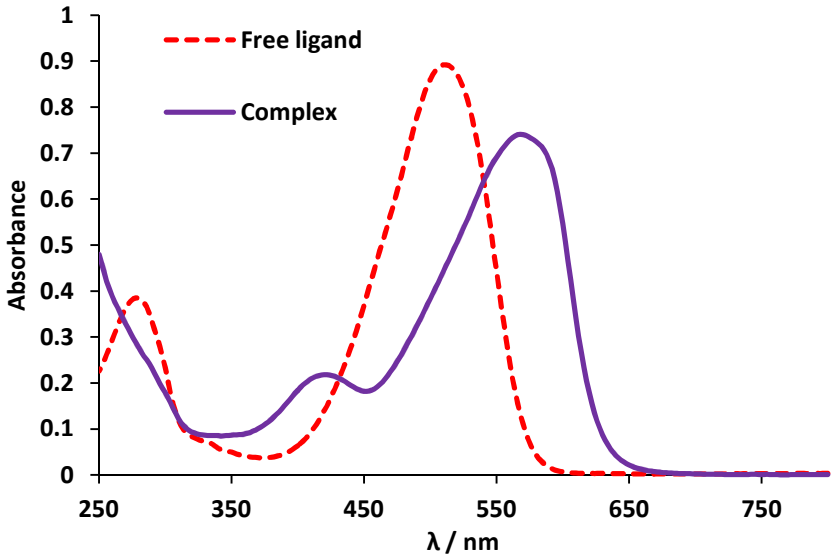

Figure 161. UV-Vis spectra of azo dye **76** and its corresponding $Mn(CO)_4$ complex **77** in CH_2Cl_2.

As mentioned previously, the dye ligand **76** has a λ_{max} at 512 nm and is a vibrant red colour. Complexation of dye **76** to produce a tetracarbonyl manganese(I) dye species (**77**) significantly shifts the λ_{max} of CO-RM **77** up by 60 nm giving a dark purple colour. The λ_{max} of the free ligand is already relatively high considering the size of the molecule and the amount of conjugation. So the shift observed on complexation is an improvement to the optical properties of this system.

Using UV-Vis spectroscopy, the molar extinction coefficient of both the dye and CO-RM **77** were determined for comparison and for purity information (**Figure 162**). Trend lines were forced through zero and concentrations were based on the molecular weight of the compound. Any significant error in the measurements would result in a line which does not pass through zero without a reduction in R^2.

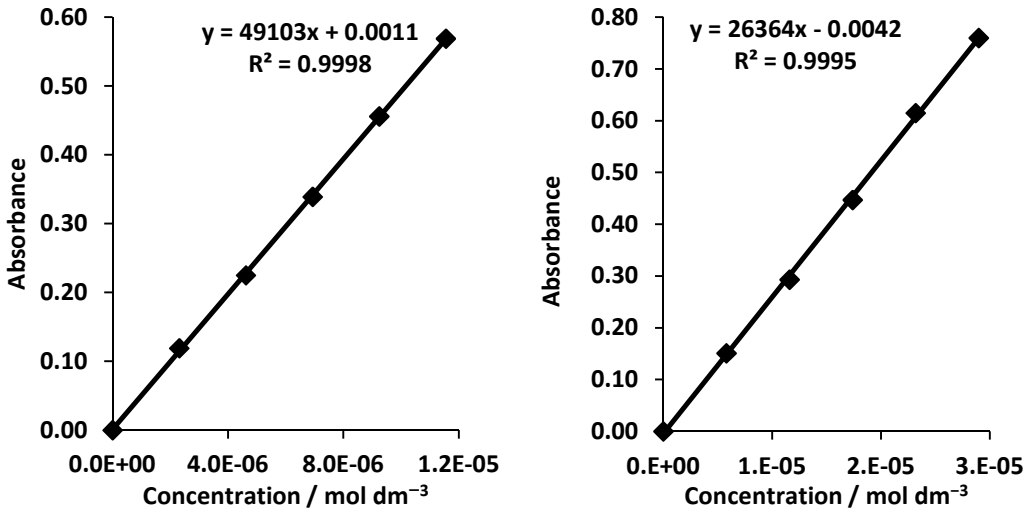

Figure 162. Molar extinction coefficient determination in CH_2Cl_2 for dye **76** (left) and CO-RM **77** (right).

With a literature ε_{512} for dye **76** of 52000 mol^{-1} dm^3 cm^{-1}, this matches fairly closely with the value obtained from this experiment of 49100 ± 881 mol^{-1} dm^3 cm^{-1}, adding a degree of reliability to the result. There will be some error within measurements carried out in both cases but the R^2 value obtained here is very close to one when forced through zero matching the concentration measurements. CO-RM **77** has a ε_{576} of 26300 ± 830 mol^{-1} dm^3 cm^{-1}. This is lower than the value obtained for the free dye **76**, but considering the shift to higher wavelength this is still a high molar extinction coefficient.

There is also a new band present in the UV-Vis spectrum of CO-RM **77** with a λ_{max} at 422 nm. This band has a ε_{422} of 8204 ± 264 mol^{-1} dm^3 cm^{-1} which higher than for any other CO-RM prepared in this project at this wavelength.

With the UV-Vis profile of CO-RM **77** characterised, it was then necessary to see if the UV spectrum would change on irradiation at various wavelengths. To obtain information about which bands might be associated with any spectral changes seen, blue (465 nm), green (525 nm) and amber (590 nm) LEDs were used to irradiate CO-RM **77** in CH_2Cl_2 (**Figure 163**).

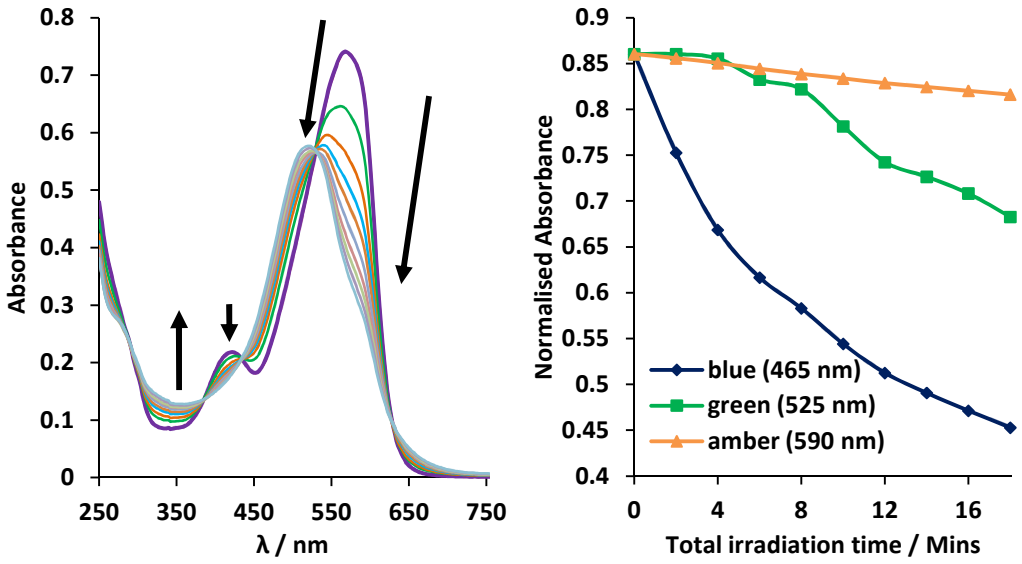

Figure 163. Left: Spectral changes of CO-RM **77** on irradiation (465 nm, 2.4 W) in CH_2Cl_2, each interval represents two minutes of irradiation. Experiment also carried out in the same fashion using 525 and 590 nm irradiation. Right: Normalised absorbance for CO-RM **77** at 565 nm as it is being irradiated at the given wavelengths.

On the irradiation of CO-RM **77** with irradiation of wavelength 465 nm, there are clear and defined spectral changes. The peak from the π-system at 576 nm decreases in intensity and shifts back over to 520 nm, close to the λ_{max} of free ligand. This suggests that free ligand might be released just like many of the other CO-RMs in this project. No spectral change was observed in the dark for 25 minutes, and irradiation and the given wavelengths is responsible for the spectral changes observed.

The most important feature about the results in **Figure 163** is that CO-RM **77** shows the same spectral changes when irradiated with light of wavelength 525 and 590 nm. The changes are significantly slower than with irradiation of wavelength 465 nm, but this is significant increase in the wavelength that has been used to release CO from a CO-RM previously. This is the highest wavelength of irradiation that has ever been used to show a change in the spectral profile of a CO-RM. However it is clear from these results that the absorption band at 576 nm is not associated with CO-release/spectral change. If it was then it is likely that the CO-release would be fast due to the large molar extinction coefficient and this wavelength. The M–CO absorption band at 420 nm is likely to be responsible for CO-release in all these cases. This band is estimated to tail off to close to 600 nm. Despite the π-system in this CO-RM not being associated with CO-release; using a dye to make a CO-RM has created a system with an M–CO absorption band higher in wavelength than anything previously prepared this project.

The spectral studies in **Figure 163** suggest that free ligand is produced on irradiation of the CO-RM. To confirm this, an ESI-MS degradation study was performed as previously (**Figure 164**).

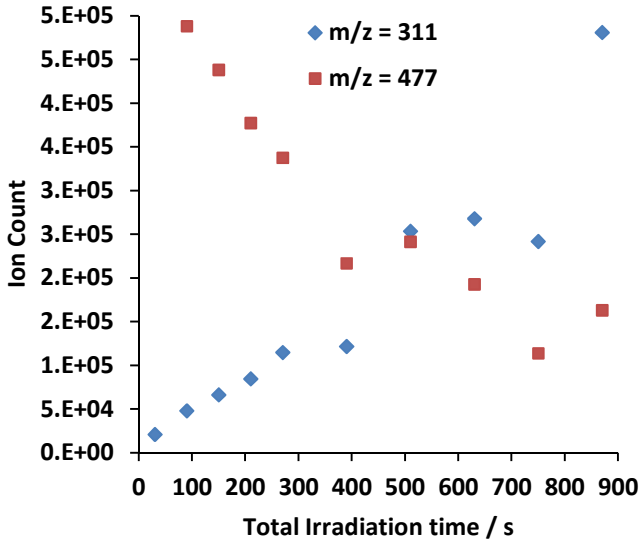

Figure 164. ESI-MS degradation study of CO-RM **77** in CH_2Cl_2 using irradiation (465 nm, 2.4 W).Irradiation was stopped while running each ESI-MS measurement.

When a solution of CO-RM **77** is irradiated at 465 nm, the intensity of the molecular ion at 477 *m/z* decreases, and increasing peaks matching the mass of free ligand **76** is observed at 311 *m/z*. This suggests a similar type of degradation process as observed with previous CO-RMs. This data also confirms why the λ_{max} of the irradiated species shifts down back towards the λ_{max} of the free ligand. Compiling the ESI-MS degradation data obtained in this project, it is likely that most bidentate tetracarbonyl manganese(I) complexes release free ligand during their photo-degradation process.

7.2.1 CO-release from dye CO-RM 77 initiated by visible-light

It has been shown that CO-RM **77** undergoes a significant spectral change on irradiation with 465 nm light producing free ligand. The next step was to assess how CO-RM **77** behaves in aqueous solution with myoglobin as carried out with other CO-RMs previously. There were however significant initial concerns with using this CO-RM in the myoglobin assay. This was due to the large absorbance from the CO-RM during same region of the spectrum as myoglobin. To tackle this problem the myoglobin assays were carried out with low concentrations of CO-RM to reduce the absorbance from the CO-RM in comparison to the myoglobin. Two myoglobin assays were carried out using 5 and 10 µM CO-RM **77** (**Figure 165**).

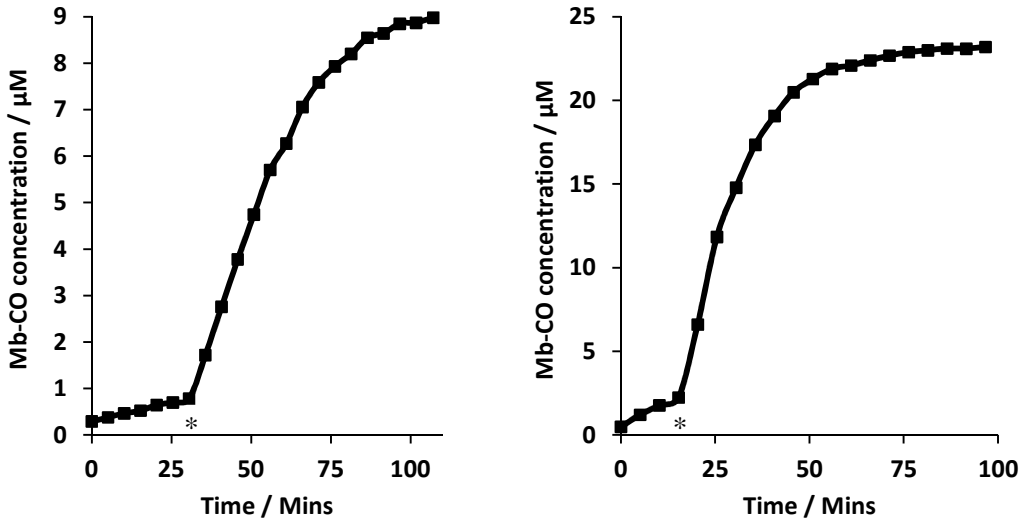

Figure 165. Myoglobin assays in PBS buffer pH 7.4 for CO-RM **77**. Left: 5 µM CO-RM assay, Right: 10 µM CO-RM assay.* marks start of irradiation (465 nm, 2.4 W, two mins every five mins)

With reduction in the used concentration of CO-RM **77** in the myoglobin assays, it was possible to correct for the CO-RM absorption profile throughout the experiment. The myoglobin assay correct procedures in section **3** shows the corrected CO-RM absorption profiles and the mapped absorbances for subtraction. The errors after correction are just as low as described in that section.

CO-RM **77** shows a small amount of CO-release before irradiation just like CO-RM L-**75**. This might be useful when treating sensitive bacteria such as *S. aureus* and *N. gonorrhoeae*. This thermal or enzyme-triggered release is very slow in comparison with the CO-release observed on irradiation at 465 nm. Irradiating CO-RM **77** with light of wavelength 465 nm releases CO effectively at both 5 and 10 µM, with half-life values of 13 and five mins respectively. This is relatively quick considering that 465 nm irradiation is being used here, and this must relate to the shifted M–CO absorption band at 420 nm.

CO-RM **77** is releasing two molecules of CO per molecule of CO-RM which is less than other tetracarbonyl CO-RMs previously prepared. However this is still more than some CO-RMs in the literature such as ruthenium-based CO-RM **3**.

7.3 Concluding remarks on azodye-containing CO-RM 77

In summary, a promising dye CO-RM structure (**77**) has been prepared and characterised in terms of its spectral and CO-release properties. The preparation of this CO-RM significantly increased our knowledge about how to increase the wavelength of CO-release. Further investigations into how this structure increases the wavelength of CO release could be useful. The CO-RM releases CO efficiently when irradiated with light of wavelength 465 nm, and it is likely that it will release CO using higher wavelengths (considering the spectral changes observed on irradiation with light of wavelength 525 and 590 nm). Further myoglobin assay studies would be required to assess this

CO-RM **77** has some really interesting properties, but the yield for the synthesis is poor and requires further optimisation. The current synthesis presents problems when biological and chemical tests are required, as the yield cannot meet the required amount of compound required. The expected reason for the low yield is due to the azo dye structure decomposing due to the heat required for the cyclometallisation reaction as observed by TLC and column chromatography. A potential alternative structure and synthesis is discussed in section **8**.

8 Overall conclusions

8.1 Initial phenylpyridine complex series

This project has taken an initial tetracarbonyl (2-phenylpyridine-κ^2N,C^8)manganese(I) structure and developed it in several different ways to improve various properties. A relatively simple complex has been functionalised with a variety of functional groups including: halogens, carboxylic acids, alkynes, and biotin.

Initial investigations were focused on establishing if the tetracarbonyl (2-phenylpyridine-κ^2N,C^2)manganese(I) structure would be a suitable starting point in terms of creating a photo-CO-RM that could be functionalised without significantly changing its properties. By creating a series of substituted phenylpyridine complexes, it was established *via* a myoglobin assay that the phenylpyridine$Mn(CO)_4$ moeity was indeed a suitable candidate for further CO-RM synthesis.

Despite changing substituents at the *para*-position on the phenyl ring, the stability of all the CO-RMs in an initial series (R = H, F, Cl, Br, Ph) was not affected. All five CO-RMs in this initial series (**37-41**) were stable in aqueous medium in the presence of myoglobin, but released CO efficiently on irradiation at 365 nm with a UV hand lamp. It would be undesirable if adding functionality on to the parent structure significantly changed how the CO-RM released CO.

All the CO-RMs in this series precipitated at concentrations that would be required to release significant amounts of CO in a biological setting. This is undesirable and it was concluded that further functionalisation was required to make a compound that could potentially progress into clinical trials. These initial target are simply not water compatible enough compared to ruthenium-based CO-RM-**3** and $[Mn(CO)_4\{S_2CNMe(CH_2CO_2H)\}]$ (**7**) detailed in the literature.[58, 136] This meant that further structural modifications were required to improve the properties of the CO-RMs.

8.2 Improving the solubility of phenylpyridine based CO-RMs

The solubility problem with the initial series of CO-RMs was solved by the introduction of carboxylic acid functionality on a small chain in the *para*-position of the phenyl ring. This group is ionised at physiological pH meaning it is deprotonated in most biological environments. This extra charge improved the solubility of CO-RM **47**. This CO-RM can be prepared in high yield and on scale that provides enough material for a significant number of biological studies (**Figure 166**).

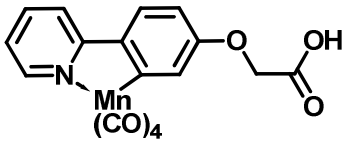

Figure 166. The structure of water compatible CO-RM **47**

Introduction of the carboxylic acid functionality meant that when the CO-RM was added to aqueous solution it did not precipitate. This was a significant step from having analogues which were more proof of principle, to something which may actually progress forward as a potential pharmaceutical agent. CO-RM **45** releases three molecules of CO per molecule of CO-RM which is comparable to $[Mn(CO)_4\{S_2CNMe(CH_2CO_2H)\}]$ (**7**) prepared by Mann and co-workers.[58] It is also important to note that with the lack of precipitation, this CO-RM has a half-life shorter than the initial CO-RM series. With more CO-RM in solution and no turbidity to scatter irradiation, the rate of CO-release from this complex is much more efficient.

Many of the CO-RMs reported in the literature do not release CO in the dark, and then release CO on irradiation.[61-62, 78, 137] However, many papers do not report enough details on how irradiation experiments are carried out. It was demonstrated with CO-RM **47** that its half-life significantly decreases on switching from a 365 nm TLC hand lamp to a 400 nm LED system. In all the irradiation studies using LEDs in this project, the LEDs have been at a set distance, and defined power consumption. The LED irradiation system developed at the University of York has demonstrated that photo-CO-RMs can have their half-life varied by changing the intensity of the irradiation. This provides advantage over thermo- and enzyme-triggered CO-RMs; as the CO-release from these complexes is somewhat fixed by the thermodynamics of the interactions between their targets. With photo-CO-RMs both the irradiation and concentration can be used to control how CO is released within a system; because the irradiation intensity can be varied. CO-RM **47** could be used as fast releaser like ruthenium CO-RM-**3** using high intensity irradiation,[136] or could be used a slow steady CO-releaser such as CO-RM **A1** by using low intensity irradiation power.[138]

8.2.1 Antibacterial action of CO-RM 47

CO-RM **47** has been shown to possess potent antibacterial properties against *E. coli* W3110 with irradiation of wavelength 400 nm. CO-RM **47** is also viable at the same concentration with RAW 264.7 cells meaning that it has the potential to be used in further *in vivo* studies. CO-RM **47** kills 99% of *E. coli* which were stored at 4 °C for 14 days. This could be advantageous as these bacteria are likely to be more dormant compared to bacteria taken straight out of a 37 °C culture room. Dormant bacteria which avoid antibiotic treatment can be a serious problem following a course of antibiotics. This CO-RM has the potential to treat against these kinds of problematic bacteria.

It is important to discuss that a potent antibacterial effect has been found under the conditions tested, but this will of course not reflect the conditions *in vivo*. There are many factors to take into consideration. For example if this CO-RM was to be used to treat a skin infection with 400 nm irradiation. The CO-RM may not be effective due to poor light penetration, but it could be enhanced by working together with the immune system. CO-RMs can boost the immune system and reduce inflammation, among numerous other beneficial biological changes. It may be possible that a CO-RM will not have a direct antibacterial effect, but could enhance the ability of the immune system to deal with the infection. The only real way to know if this CO-RM can actually be an effective treatment is to start *in vivo* studies. It is important to emphasise that CO-RM **47** could be viable with 20 different cell strains in a 96 well plate, but toxic *in vivo*, wasting considerable money and time on initial studies. There is also an urgent requirement for more antibacterial agents, and taking this in to account there is enough data on CO-RM **47** to take it to further studies.[139]

8.3 Development of biologically compatible CO-RMs

CO-RM **47** releases a molecule of its corresponding free ligand on irradiation, and this could be of concern when developing new analogues. This creates a metabolite which could be toxic following irradiation. Luckily this is not the case with the CO-RM **47** but when designing new analogues this is certainly something to bear in mind. Taking this into consideration, a new CO-RM containing unprotected L-tryptophan was developed (**Figure 167**).

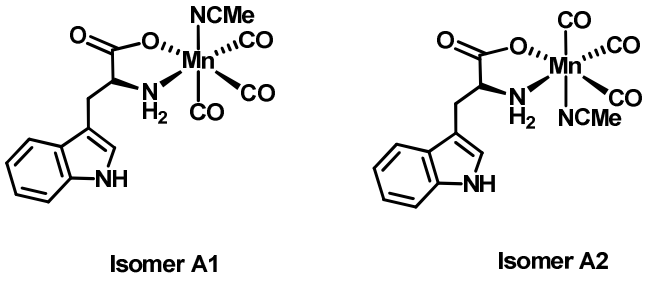

Figure 167. The isomers of CO-RM L-**75**.

By using L-tryptophan as ligand, it was anticipated that free L-tryptophan would be released on irradiation. This turned out to be the case and was confirmed by ESI-MS studies. L-tryptophan (**73**) is a natural biological molecule required by most organisms, and the release of a benign metabolite is certainly desirable in terms of reducing toxicity and potential side effects. While the free ligands from other CO-RMs have been shown to be non toxic, it is unknown what side effects they may have. With the release of L-tryptophan from CO-RM L-**76**, there can be a strong degree of confidence that the release of L-tryptophan is unlikely to cause any significant side effects.

In the structure of CO-RM L-**75**, L-tryptophan is bound to a manganese(I) centre *via* a bidentate N^O coordination mode. This differs from the C^N binding mode of the phenylpyridine complex. There are also only three CO ligands in this system with a potentially exchangeable acetonitrile ligand. These differences result in a shift of the UV absorption bands associated with CO-release to higher wavelength in comparison with the phenylpyridine derivatives. This results in efficient CO-release from CO-RM L-**75** when irradiated at 465 nm, which cannot be achieved with CO-RM **47**. Irradiation of wavelength 465 nm will penetrate deeper in tissue (0.5 mm) and this means that CO-RM L-**75** could still be used to treat conditions within the skin.[122] It is also important to consider that this CO-RM does not need irradiation to have a detrimental effect on *S. aureus* and *N. Gonorrhoeae* and has the potential to be used deep within tissue.

8.3.1 CO-RM L-75 exhibits antibacterial activity against three species

CO-RM L-**75** has also been to shown to possess a potent anti-bacterial effect on *E. coli* under the same conditions as CO-RM **75**. This CO-RM can also exhibit a detrimental effect on *E. coli* at 465 nm which is the first example where a CO-RM has been used in conjunction with visible light to kill bacteria.

Acid-containing CO-RM **47** failed to show any significant effect on *S. aureus* compared to the effect of the irradiation, where as CO-RM L-**75** has been shown to have a potent effect, both with and without irradiation. It is postulated that the acetonitrile coordination site allows for small amounts of thermal CO-release while still maintaining stability in the presence of proteins such as myoglobin. It is clear from these studies that *S. aureus* is much more susceptible to CO than *E. coli.* This means that using CO-RMs as a means of treating *S. aureus* is a promising research direction.

CO-RM L-**75** also shows the same type of anti bacterial activity against *N. gonorrhoeae* MS11 in RPMI + YAL medium. There is antibacterial activity in order of 99% without the need for irradiation. *N. gonorrhoeae* is also very sensitive to CO just like *S. aureus,* and this is good news from a research prospective. It is likely to be sensitive due to only containing one cytochrome c oxidase enzyme making it very vulnerable to inactivation by CO.[45-46] Control experiments show that *N. gonorrhoeae* grows efficiently in this medium with DMSO, showing that it is not weakened in this medium.

8.3.2 LegHb as a CO scavenger for mechanistic studies

A strong CO binding protein LegHb can significantly reduce the antibacterial effects of CO-RM L-**75** when used in substoichiometric concentrations relative the amount of CO-RM. CO-RM L-**75** at a concentration of 100 μM is capable of releasing 200 μM CO; and only 22 μM LegHb is capable of reducing the antibacterial effect significantly. This suggests that only a small amount of CO is released in these experiments contributing to the suggestion that *N. gonorrhoeae* is sensitive to CO.

CO-RM L-**75** is also viable with RAW 264.7 macrophages and shows evidence of an anti-inflammatory action in the presence of LPS and IFN-γ. This means that the CO-RM could be used for more than just antibacterial purposes.

There are significant results showing that CO-RM L-**75** is a promising potential therapeutic molecule, and this CO-RM should be taken in to further studies. This should include further mechanistic studies in to the source of antibacterial action without irradiation, and possible *in vivo* studies.

8.4 Modifying CO-RMs using [3+2] Huisgen cycloaddition chemistry

Previously prepared CO-RMs have been shown to possess excellent CO-releasing properties and *in vitro* biological activity. However, these CO-RMs have no means of targeting a specific location within a biological system making them potentially inefficient. It would be desirable if functionality could be a attached to a CO-RM, allowing it to accumulate in a particular organ. This means very low concentrations could be administered which would potentially reduce toxicity. The CO-RM could then accumulate in the desired organ where an infection was present.

In this project, the phenyl pyridine manganese(I) lead complex has been functionalised with a terminal alkyne group allowing to be used as a substrate in azide-alkyne [3+2] cycloaddition chemistry (**Scheme 39**).

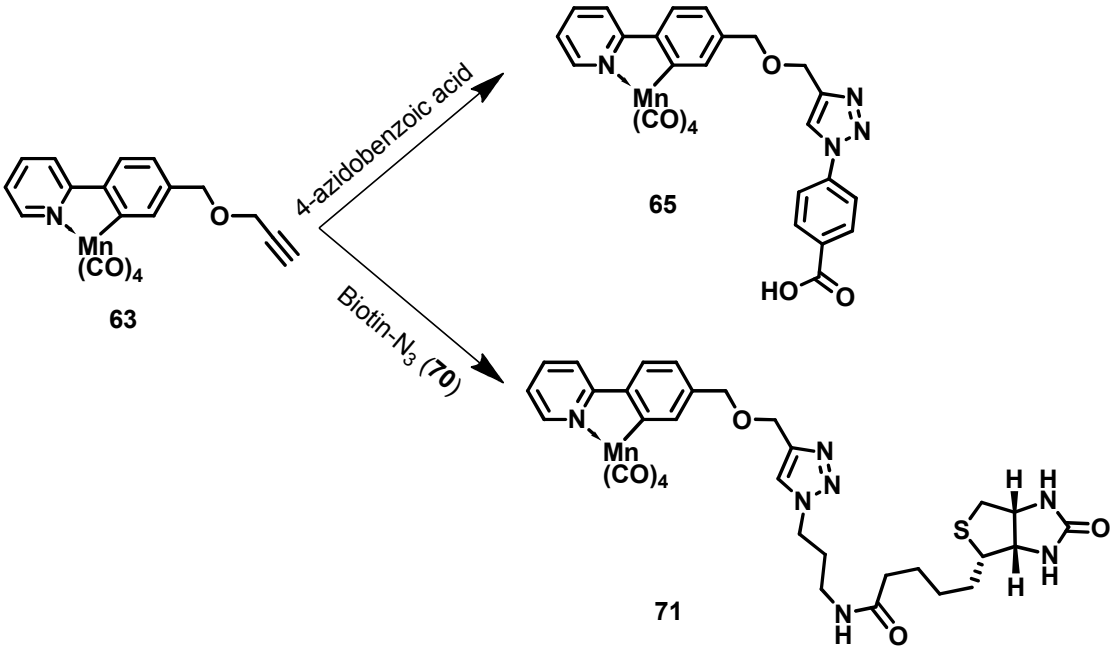

Scheme 39. Functionisable CO-RM **63** employed in [3+2] cycloaddition chemistry to introduce further functionality.

Para-azidobenzoic acid was used as a substrate to functionalise CO-RM **63** to generate acid CO-RM **65**. This CO-RM is an extended analogue very similar to acid CO-RM **47** with its carboxylic acid functionality. While CO-RM **65** was initially synthesised to develop methodology, it releases CO efficiently and does not precipitate in aqueous solution. It is also viable with RAW 264.7 cells up to a concentration of 50 μM. This analogue has the potential to be taken forward for further study and the extended structure may possess some interesting biological activity.

Following success with *para*-azidobenzoic acid, CO-RM **63** was functionalised with an azide linked biotin compound (**70**) to generate a CO-RM with significant functionality and complexity (**71**). CO-RM **71** releases CO-efficiently, is viable with RAW 264.7 cells at its soluble concentrations (up to 30 μM), and binds strongly with avidin. This makes it one of the first CO-RMs designed to bind to a desired target. It has also been shown to release-CO while bound to its avidin target. This shows how this CO-RM system could be used to develop analogues which could localise in a particular biological location.

The inspiration to use click chemistry to functionalise CO-RMs came from a paper by Schatzschneider and co-workers.[61] In this work a manganese(I) CO-RM wass tagged with various peptides to create complex conjugates. While it has been shown that these peptide-CO-RM conjugates release-CO, it has not been shown that these conjugates can then be used for localisation. In this work biotin CO-RM **71** has been shown to release CO efficiently on irradiation and has been shown to bind strongly to its desired target.

8.5 Increasing the wavelength of light required to initiate CO-release

Longer wavelengths of light penetrate further in tissue and the aim of this work was to prepare a new analogue which would absorb higher in the visible spectrum than previously obtained. This was achieved by preparing a CO-RM based on an azodye (**Figure 168**).

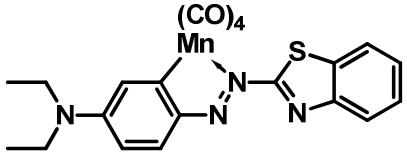

77

Figure 168. Structure of an azodye-$Mn(CO)_4$ complex synthesised in this project.

While the π-π^* transition that gives the compound an intense purple colour is not associated with CO-release, the CO-release from this complex can be initiated at a wavelength much higher than anything previously prepared. CO-RM **S1** shows efficient CO release at 470 nm, which is one of the highest wavelengths of irriadiation used photo-CO-RM currently the literature.[137] CO-RM **77** shows efficient CO-release at 465 nm in a myoglobin assay. CO-RM **77** also shows the same spectral change in aqueous solution when irradiated 465, 525 and 590 nm light. The rates are different but the same type of change is observed, suggesting that this CO-RM also releases CO at these wavelengths. This is one of the most promising CO-RMs prepared to date, although yield of CO-RM **77** is poor and requires optimisation.

The structural features in CO-RM **77** provide information about what kind of motif is required to increase the wavelength of light required to initiate CO-release. Development of further analogues based on this structure could yield CO-RMs which could release CO with red light. Red light penetrates deep into tissue significantly increasing the range of treatments that photo-CO-RMs could be used for.

To close discussions, this project has developed several new interesting pharmaceutical molecules, which have the potential to make it in to pre-clinical trials. The majority of the aims in this project have been achieved and further study with these CO-RMs has been justified.

9 Future work

9.1 Initial phenylpyridine series

It has been shown that bromo-CO-RM **40** can be functionalised with Suzuki-Buchwald chemistry. The substrate used may not be as biologically relevant as some of the work carried out later on this project, but the conditions work giving pure product in good yield (67%). There is potential for more biologically interesting molecules to be tagged on to initial CO-RM **40**. The initial functionalisation reaction was carried out in toluene, and some modifications might be required to introduce more polar substrates.

9.2 Future derivation of CO-RM 47

CO-RM **47** has improved solubility and CO-releasing properties compared to the initial CO-RM series. As discussed previously the structure is promising and should go into initial *in vivo* studies. However it has no current means of localisation. Future work could focus on the development of a coupling system directly on to CO-RM using amide synthesis (**Scheme 40**).

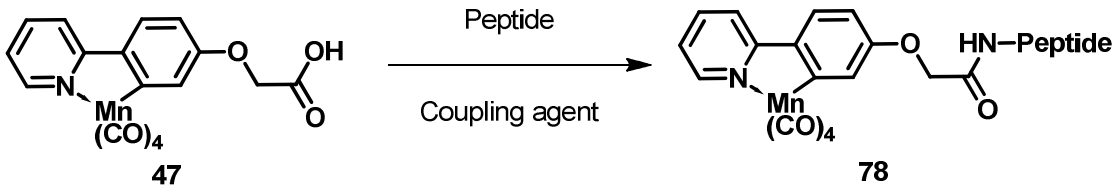

Scheme 40. Potential to use CO-RM **47** in further analogue (**78**) synthesis.

Amide synthesis is well documented and there are a huge variety of coupling agents that could be used to carry out this reaction efficiently.[140] This chemistry could allow endless functionality to be attached on to this molecule just like with the alkyne derivatives. This would allow for peptide targeting. Peptides which are known to bind strongly with target proteins could be used in the synthesised proposed in **Scheme 40**. This means that localisation of a peptide in a particular organ or type of tissue could be achieved. However great care must be taken in choosing peptides which do not illicit a potent immune response as this could cause serious inflammation. One could imagine using short sequences such as Thr-Phe-Ser-Asp-Leu which has already been conjugated to CO-RM **29** as shown in the literature.[61]

9.3 Future work with alkyne CO-RM 63

Alkyne CO-RM **63** has been used in two reactions to create molecules tagged with desired substrates. This chemistry could be extended to tag in a wide variety of substrates including peptides as proposed for CO-RM **79**. This could be achieved in a similar way to the way it was done to synthesis biotin CO-RM **71**. A proposed synthesis could be as shown in **Scheme 41**

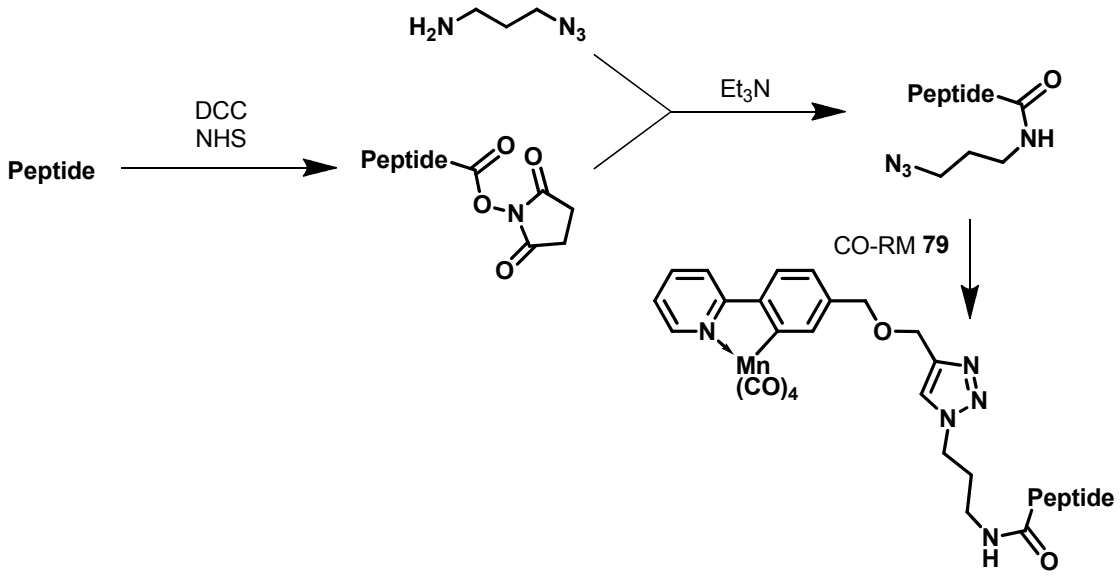

Scheme 41. Proposed synthesis for conjugating peptides with CO-RM **63**

Using this synthesis method, a library of peptide conjugates could be created. One may ask why would it be advantageous to have two different methods of making CO-RM conjugates? Well it may be possible that certain peptides are not compatible with one synthetic procedure but are with others. It may also be possible that the different structural motifs described with the same peptide may bind differently to their target. Having a several different synthetic routes to similar complexes would certainly be desirable.

9.4 Future studies with Tryptophan based CO-RM L-75

CO-RM L-**75** is one of the most promising CO-RMs prepared in this project with exciting properties against three strains of bacteria, and viability with RAW 264.7 macrophages. For mechanistic purposes CO-RM L-**75** is not fluorescent enough at the correct wavelength to be used in cell microscopy studies. This kind of studies could give large amounts of information including whether the CO-RM gets in to prokaryotic and eukaryotic cells, and where it is localised. This would required the development of second generation tryptophan CO-RMs.

Synthetic work by Fairlamb and co-workers uses palladium chemistry to prepare functionalised tryptophan derivatives (**Scheme 42**)[141].

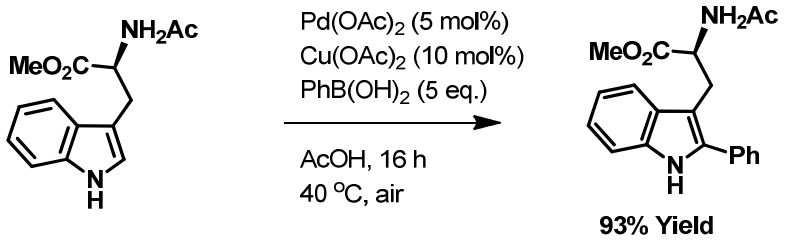

Scheme 42. C–H activation chemistry used to functionalise protected L-tryptophan

Using a palladium acetate catalyst system, it is possible to synthesise analogues of tryptophan substituted on the *ortho*-position of the indole. Several different boronic acids were used in this study to prepare a library of substituted tryptophan compounds. These analogues have a shifted λ_{em} of fluorescence to lower energy compared to unfunctionalised tryptophan. These derivates could be used to prepare a whole series of new CO-RMs based on CO-RM L-**75**, which could be fluorescent enough at the appropriate wavelength of excitation for confocal microscopy studies. **Scheme 43** shows the proposed synthesis of these potential new analogues.

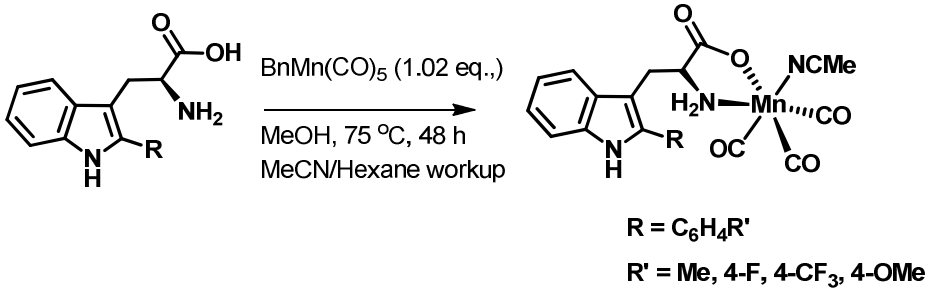

Scheme 43. Proposed synthesis for new a new generation of Tryptophan based CO-RMs.

The new CO-RMs in **Scheme 43** could enable a wide variety of visual mechanistic studies to be undertaken to allow more to be understood about how these CO-RMs cause the potent antibacterial effects that they exhibit. Some detailed localisation studies could also be carried out in RAW 264.7 cells. This could be done by fluorescence studies using the proposed CO-RMs detailed in **Scheme 43**. It could also be performed using Raman imaging techniques carried out by Schatzschneider and co-workers.[142] This may give more insight into why CO-RM L-**75** has anti-inflammatory properties.

As well as the mechanistic studies, CO-RM L-**75** on its own is still a promising potential pharmaceutical molecule and further studies need to be carried out to get this molecule closer to clinical trials. CO-RM L-**75** has not yet been tested for its vasodilatory properties where as CO-RM **S1**, CO-RM **F3**, and ruthenium CO-RM-**3** has been. Tests to see if CO-RM L-**75** can relax

aortic rings like these other CO-RMs is important in terms of establishing what kind of applications CO-RM L-**75** may have. As well as these initial studies *in vivo* viability tests need to be carried out, and if these are successful then discovering what conditions CO-RM L-**75** could treat could truly commence.

9.5 Future studies with dye related CO-RMs

With dye CO-RM **77** exhibiting some very interesting and useful properties, further research into this azodyeMn(CO)$_4$ motif is a high priority. The push-pull electronic π-system within CO-RM **77** is likely responsible for the interesting shift up of the M–CO absorption band. Performing DFT calculations on free ligand **76** and CO-RM **77** to find out how the electrons are distributed in this system could provide some useful information in terms of designing new analogues which release CO at an even higher wavelength could be obtained. One may also want to consider making a similar analogue of CO-RM **77** with fewer CO ligands in an attempt to reduce energy required to promote an electron from the t_{2g} to the e_g orbitals on the metal. This could lead to longer wavelength CO release at the sacrifice of releasing fewer CO molecules per CO-RM.

The current synthesis of CO-RM **77** is poor due to thermal degradation during the synthesis. Future work could involve developing a new CO-RM with the azo dye functionality in π-conjugation with the main structure. This removes the need to heat the azo-dye in the synthesis, potentially preventing any degradation. A potential synthesis route is proposed in **Scheme 44**.

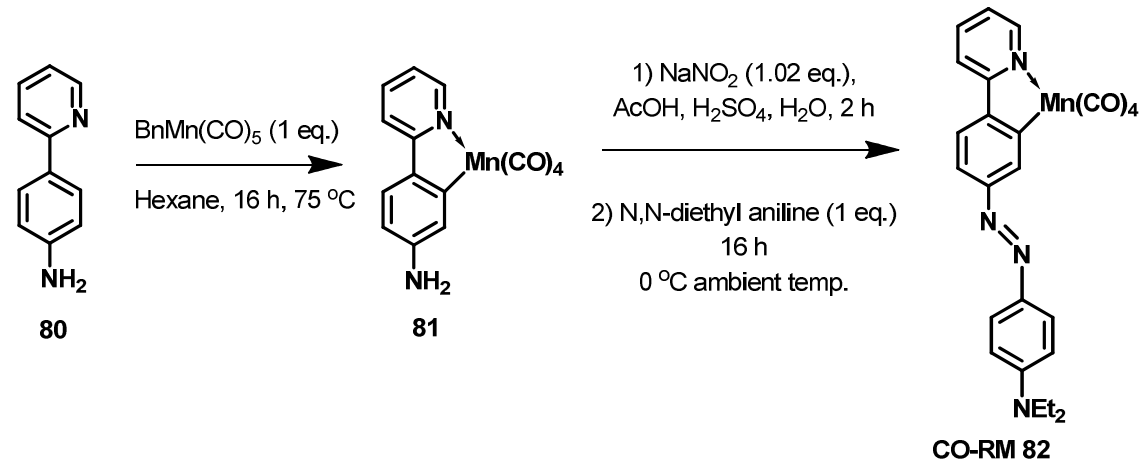

Scheme 44. The proposed synthesis of a second generation dye CO-RM **82** inspired by azodye **76**

Target molecule CO-RM **82** has a similar end structure to the dye used to make CO-RM **77**. The benzothiazole unit has been replaced with CO-RM **81** which could be easily made using its corresponding commercially available ligand (**80**). This synthesis could create a new CO-RM

with high wavelength release and more interesting spectral properties. If the manganese unit in CO-RM **81** can survive the diazotisation conditions, the yields for this synthesis could be much higher compared to CO-RM **77**. CO-RMs **47** and **65** are exposed to acidic work up conditions during their synthesis and both are isolated in high yield, suggesting that the manganese unit should be sufficiently stable to withstand the acidic conditions needed to carry out diazotisation.

10 Experimental Section

10.1 Chemistry general experimental details

All reactions were carried out under a nitrogen atmosphere unless otherwise stated. Chemical reagents were purchased from Sigma Aldrich, Alfa Aesar or Frontier Scientific and used as received. All dry solvents were obtained from a Pure Solv MD-7 solvent machine and were stored in ampoules under nitrogen until required. Ethers from this machine were deoxygenated by sonication with nitrogen bubbling for at least 30 mins.

All TLC analysis was carried out using Merck 5554 silica plates and spots were visualised using UV light at 254 and 365 nm. Column chromatography was carried out using silica gel 60 purchased from Sigma Aldrich.

Solution ^{1}H and ^{13}C NMR analysis was carried out on Jeol ESC400/ESX400 and Bruker AV500/AV700 spectrometers. All chemical shifts in ^{1}H NMR spectra are reported in ppm (δ) and are referenced to the residual NMR solvent ($CDCl_3$: 7.26 ppm, DMSO-d_6: 2.50 ppm, MeOD-d_4: 3.31 ppm, CD_2Cl_2: 5.32 ppm). The spectra were processed in MNova software. All chemical shifts in ^{13}C NMR spectra are reported in ppm (δ) and are referenced to the NMR solvent. ($CDCl_3$: 77.36 ppm, DMSO-d_6: 39.52 ppm, MeOD-d_4: 49.00 ppm, CD_2Cl_2: 53.49 ppm). For the ^{13}C NMR of some of the tetracarbonyl manganese(I) complexes, the metal carbonyl peaks were not observed due to long relaxation time in the solvent used. IR spectroscopy confirms the presence of these metal carbonyls.

Mass spectrometry was carried out using a Bruker microTOF instrument. All data were acquired in positive ion mode using ESI or LIFDI ionisation. High resolution ESI spectrometry data is reported with less than 5 ppm error unless otherwise stated. All LIFDI data reported is within 120 ppm error.

ESI-MS degradation studies of CO-RMs **47**, **75** and **77** were performed in 50:50 (*v/v*) CH_3CN/H_2O or CH_2Cl_2 at a concentration of 0.5 mg ml^{-1}. The solution was passed through cotton wool each time a sample was required, a 100 µl aliquot was taken and diluted by 10-fold. In the experiments 4 µl injections of the diluted solution were used for all measurements. After obtaining an initial spectrum the sample was irradiated for one minute and a spectrum was taken between each irradiation. Varying capillary exit and skimmer voltages are used to optimise the experiment depending on the CO-RM used. This variation can reduce the amount of molecular

ion fragmentation making it easier to detect products of irradiation. Irradiation was carried out using either a 400 or 465 nm LED (2.4 W power).

Melting points of all complexes and ligands were obtained on a Perkin Elmer DSC 7 machine. Experiments were run using a ramp rate of 10 °C min^{-1} to above the required melting temperature. The melting point was taken as the onset of the observed endothermic peak. The machine was calibrated using an indium standard.

IR spectroscopy was carried out on a Thermo-Nicolet Avatar-370 FT-IR spectrometer. Spectra were taken in either solid state (KBr disc), or in solution.

UV-Visible spectroscopy for the myoglobin assay and molar absorption coefficient determination was carried out on a JASCO V-560 spectrometer using PMMA cuvettes of pathlength 10 mm A baseline in the required solvent was carried out prior to starting an assay. Photo-initiated carbon monoxide release was carried out using a 5 W 400 nm LED directly above the solution.

[α] measurements were carried out on a JASCO DIP-370 digital polarimeter using a concentration of 10 g L^{-1} using a cell of path length 100 mm. DMSO was used as solvent and was used for a background measurement.

CD measurements were carried out using a JASCO J-810 polarimeter using a concentration of 6×10^{-4} mol dm^{-3} using a quartz cell of path length 1 mm. DMSO was used as solvent for all measurements including backgrounds. 4 scans were taken between 280 and 550 nm for each sample.

Fluorescence emission measurements for CO-RM L-**75** were carried out on a Shimadzu RF-5301PC Spectrofluorophotometer in 95:5 *(v/v)* H_2O/DMSO using two-fold dilutions starting from $c = 1.3\times10^{-6}$ mol dm^{-3} using a quartz cell of path length 10 mm.

The decomposition of CO-RMs in solution were followed using a Mettler Toledo React IR™ iC10 IR spectrometer with a silicon probe. IR spectra are taken in real-time every 60 seconds and complex irradiation was performed using either a 365 nm 4 W TLC lamp, a 400 nm 5W LED or 465 nm 5 W LED set to power consumption level of 2.4W.

Elemental analysis was carried using an Exeter Analytical CE-440 Elemental Analyser. Elemental analysis was not performed on all compounds. In some cases this was due to limited amounts of final compound (such as dye **77**). In other cases some intermediate compounds in a synthetic route were not analysed, however the important final compound in a series was analysed and purity was demonstrated. Compounds not analysed using this technique show good purity by ^{1}H NMR and were successfully used to prepare further compounds.

10.1.1 Further general details on measurements

10.1.1.1 ^{1}H NMR details

^{1}H NMR chemical shift data are reported to two decimal places. ^{1}H NMR coupling constant data are reported to one decimal place with rounding to the nearest 0.5 Hz in cases where there is small error in the coupling constant. Coupling between peaks in these cases have been confirmed to show coupling by ^{1}H COSY correlation NMR experiments.

10.1.1.2 Myoglobin assay error analysis

Following four point correction in the myoglobin assay detailed in sections **3.2** and **10.3**, the error in the myoglobin assay is calculated at 2 nm intervals from 510 nm to 586 nm. The errors are calculated from the difference of the myoglobin assay spectra are compared to their calculated spectra. The calculated UV-Vis spectra are based on percentage combinations of reference deoxy and carboxy-Mb taken prior to starting an assay. The percentage combinations of the reference spectra depends on the conversion of deoxy-Mb to carboxy-Mb during an experiment. Increased conversion to carboxy-Mb requires a larger contribution in the calculations from the carboxy-Mb reference spectrum. These reference spectra are always recorded again when a new assay is performed to account for variations in the UV-Vis spectra over time. The error can be expressed at a particular wavelength by calculating the ratio between the calculated error and the absorbance of the measurement at this wavelength. All myoglobin assays in this work does not have an error at a particular wavelength above 4% representing a close match between the reference and experimental data.

10.1.1.3 Details on RAW 264.7 cell assays

Errors in both the Alamar Blue and LDH assays detailed in section **10.5.1** are calculated from the triplicate measurements carried out for each variable. The standard deviation for each variable is calculated and expressed as a percentage ± from the mean average value. It is expressed as a percentage because the viability and LDH released are also expressed in this way, so values with appropriate error bars can be represented graphically.

10.1.1.4 Details on bacterial cell assays

Where possible, errors are calculated from the triplicate measurements carried out for each variable. Errors are represented as ± standard deviation from the mean average value. It was

impractical to carry out three triplicate measurements on the same day due to the sensitivity of the bacteria. Due to variation in bacteria between batches this was not always possible in these cases. Therefore three repeat experiments were carried out on separate days and these could then be used in triplicate analysis in most cases. Due to how bacteria can vary between batches, this was not always possible in these cases each repeat experiment was analysed separately and conclusions were drawn from the three repeats as a whole.

10.2 New irradiation system

A new method of carrying out photochemical reactions and assays has been developed at the chemistry department at the University of York. An LED has been mounted on a special plastic cap that fits over the top of a PMMA cuvette (**Figure 169**).

Figure 169. An LED mounted on a special plastic cap fitted in to a PMMA cuvette.

This LED is connected to the control unit shown in **Figure 170** and the functions are shown in **Table 32**.

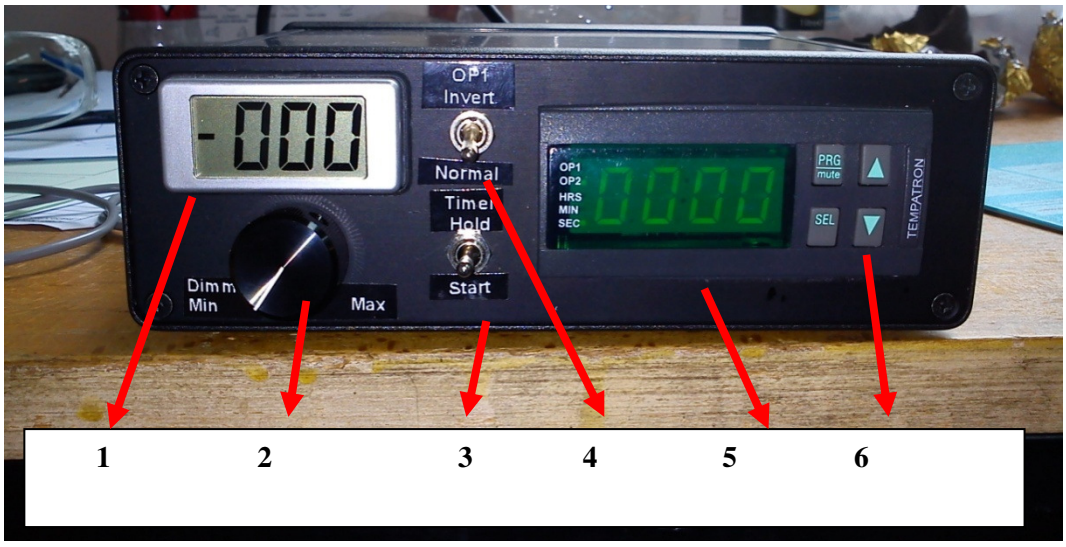

Figure 170. Control unit for the irradiation system

Table 32. Functions of different switches on the irradiation system shown in **Figure 170**.

Number	Name/Brief function
1	Current Monitor - Measures power that the LED is drawing in milliamps
2	Dimmer Switch - Turn to increase or decrease power
3	Start/Hold button, Up = hold (time will not count), Down = Start/Reset counter
4	Mode inverter- Can be used to change off/on modes
5	Timer display : Left two digits = Mins, Right two digits = Seconds
6	Timer controls – can be used to change how long the LEDs come on and off for

This irradiation system allows light intensity to be varied. It also allows for automated on and off cycles to be programmed into the system making it possible to automate experiments. This system ensures that consistent irradiation of a well defined wavelength is produced for the desired experiments.

10.3 Experimental procedure for the myoglobin assay

Lyophilised equine heart myoglobin (11 mg, purchased from Sigma Aldrich), was dissolved in 10 ml of 0.01 M PBS buffer solution (pH 7.4) to give an absorbance of approx.0.7 at 550 nm. This mass of myoglobin will give a solution with an approximate myoglobin concentration of 50 μm depending on the myoglobin batch. Sonication for five minutes will usually give full myoglobin dissolution. The solution was filtered through cotton wool to ensure optical clarity. 1 ml of myoglobin solution was added to a PMMA 1 ml UV cuvette and approx. 1 mg of sodium dithionite was added. The solution was mixed with a micropipette twice. The UV spectrum of the deoxy-Mb solution was then obtained. CO gas was bubbled through the 1 ml of solution for 15 seconds. The Mb-CO UV spectrum was then obtained. These were used as reference spectra for determining the Mb-CO concentrations at intermediate mixtures of deoxy/carboxy-Mb.

A new 1 ml cuvette containing 1 ml of myoglobin stock solution was then prepared and incubated at 37 °C ready for the assay. 1 mg of CO-RM was dissolved in 100 μl of DMSO. Using the CO-RM stock solution, 100 μl of a second stock solution was prepared. The second stock solution is 200 times the concentration required in actual assay (*e.g* 8 mM for a 40 μM assay). Sodium dithionite (approx. 1 mg) was added to the new 1 ml myoglobin cuvette and the solution was mixed twice.

Immediately after this, 5 µl of the secondary CO-RM stock solution was added to the new deoxy-Mb solution giving final CO-RM concentrations of 10, 20, 40 and 50 µM as required. The solution was mixed again twice and the solution was layered with light mineral oil (500 µl) to prevent CO escape. The assay was then started immediately. UV spectra were acquired every five minutes and irradiation was used when required but not when the spectrometer was scanning. The sample was irradiated from above at 400 or 465 nm for typically for two or three minutes every five minute period. The assay was not carried out for longer than 2.5 hours due to potential myoglobin degradation.

10.3.1 Standard data treatment for the myoglobin assay

Deoxy-Mb contains an absorption maximum at 560 nm. As CO is released from the administered CO-RM, the absorption maximum at 560 nm decreases and two new peaks at 540 nm and 578 nm arise in the spectra. These new peaks come from Mb-CO. The total concentration of myoglobin in the stock solution prepared is calculated from the maximum absorption peak at 540 nm in the saturated Mb-CO solution. **Equation 1** shows how this is calculated.[143]

$$\text{Mb-CO}_{\text{max}} = (\text{OD}_{540}/\,\varepsilon) \times 1000$$

Equation 1. Calculating the total myoglobin concentration for an assay stock solution. ε = extinction co-efficient of Mb-CO= 15.4 mM cm^{-1}, OD_{540} = Absorbance of saturated Mb-CO solution at 540nm.

The calculation of Mb-CO concentrations throughout the assay are also calculated from the OD_{540}. A second coefficient (ε_2) is required for these experiments as there are two species absorbing in solution, deoxy-Mb and Mb-CO. This coefficient takes in to account the change in absorbance at 540nm (ΔOD_{540}). This calculation also requires a second wavelength. This is used as a reference point to increase the accuracy of the calculations. The UV-Visible spectra of deoxy-Mb and Mb-CO share four isosbestic points (OD_{iso}) at 510, 550, 570, and 585 nm. The isosbestic point at 510 nm was used as the reference point to calculate the coefficient ε_2. This was done using **Equation 2**.

$$\varepsilon_2 = \frac{\Delta OD_{540} - \Delta OD_{iso510} \times 1000}{Mb{-}CO_{max}}$$

Equation 2. Calculating the second Mb-CO extinction coefficient(ε_2).ΔOD_{iso510} = Change in absorbance at the 510 nm isosbestic point, ΔOD_{540} = change in absorbance at 540 nm. Mb-CO_{max} = maximum concentration of myoglobin. ε_2 = new extinction coefficient.

Using the new extinction coefficient, the concentration of myoglobin in an unknown sample can be calculated. This is done using **Equation 3**.

$$\text{Mb-CO} = \frac{(\Delta OD_{540} - \Delta OD_{iso510})}{\varepsilon_2} \times 1000$$

Equation 3. Calculating the unknown Mb-CO concentration in a sample. ΔOD_{540} = change in absorbance at 540 nm, ΔOD_{iso510} = Change in absorbance at the 510 nm isosbestic point, ε_2 = new absorption coefficient.

10.3.2 Myoglobin assay correction using non-linear regression.

The data treatment for myoglobin assay data detailed in section **9.3.1** is only sufficient for CO-RMs that do not absorb in the 500-600 nm region of the UV-vis spectrum, and also for CO-RMs which precipitate to any extent causing turbidity. The majority of the absorbance due to turbidity can be accounted for by the correction at 510 nm; however it does not account for the difference in light scattering across the 500-600 nm region. A procedure developed by Fairlamb and co-workers was developed to account for this turbidity/CO-RM absorbance.[94] This procedure can also be used to account for other minor differences between the reference spectra and the spectra measured during the assay.

10.4 Chemical synthesis

10.4.1 Synthetic procedures for small phenyl pyridine ligands

General procedure 1 - synthesis of 2-(4-bromophenyl)pyridine (34)

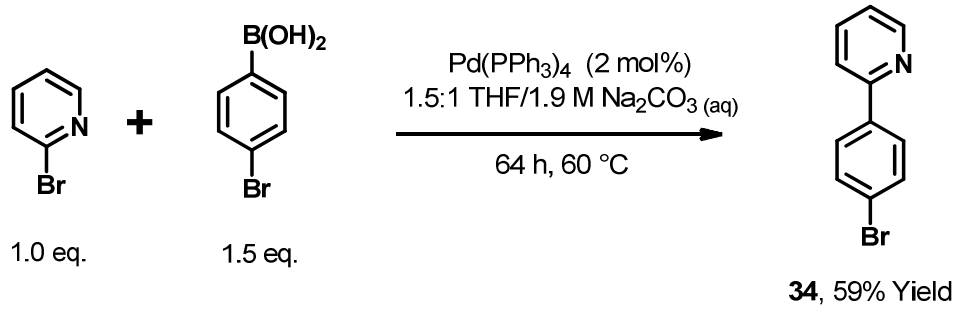

This synthesis is based on a modified literature procedure[93, 144]

In a nitrogen atmosphere glove box, to an oven dried Schlenk tube equipped with a magnetic stirrer bar was added $Pd(PPh_3)_4$ (0.02 eq., 0.033 mmol, 38.3 mg). The Schlenk tube was removed from the glove box and was attached to a Schlenk line. Under a high flow of nitrogen was added 4-bromobenzene boronic acid (1.5 eq., 1.66 mmol, 502 mg), followed by 2-bromopyridine (1 eq., 2.5 mmol, 158 µl/260 mg). 1.9 M $Na_2CO_{3\,(aq)}$ (6 ml) and THF (9 ml) was then added *via* syringe. The reaction was heated to 60 °C for 64 h. The reaction was allowed to cool and deionised water (40 ml) was added. The product was extracted with dichloromethane (3 × 40 ml), dried with $MgSO_4$ and filtered. The solvent was removed under reduced pressure to yield crude product. The crude product was purified using silica gel column chromatography using 90:10 PET ether/ethyl acetate as eluent. The solvent was removed under reduced pressure to give a crystalline, slightly off white solid (231 mg, 59% Yield).

MP (DSC): 64 °C ; ^{1}H NMR (400 MHz, $CDCl_3$) δ 8.69 (dd, *J* = 4.8, 1.0 Hz, 1H), 7.88 (d, *J* = 8.3 Hz, 2H), 7.76 (apr.td, 1H), 7.70 (dd, *J* = 8.0, 1.0 Hz, 1H), 7.60 (d, *J* = 8.3 Hz, 2H), 7.28–7.23 (m, 1H (under ref. Peak)); ^{13}C NMR (100 MHz, $CDCl_3$) δ 156.6, 150.1, 138.5, 137.2, 132.2, 128.8, 123.8, 122.8, 120.7; Elemental Analysis (CHN) C : 56.15% H: 3.49% N: 5.77% (calc.: C: 56.44% H: 3.34 %N: 5.98%); ESI-MS *m/z* = 233.9917 $[M+H]^+$ (calc. for $C_{11}NH_9Br$ = 233.9913); IR (Pressed KBr disc) : 1581, 1556, 1458, 1426, 1389, 1147, 1095, 1066, 1001, 833, 772, 625, 539, 453 cm^{-1}.

Synthesis of 2-(4-Fluorophenyl)pyridine (32)

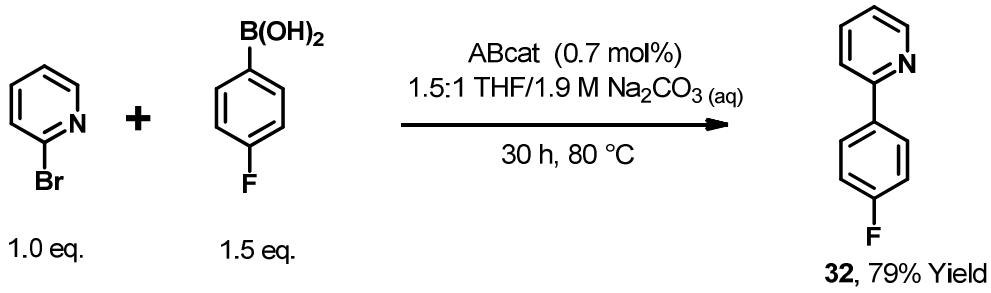

This synthesis is based on a modified literature procedure[93, 144]

32 was synthesised using general procedure **1** (see synthesis of **34**) using ABcat (0.007 eq., 11.6 µMoles, 12.2 mg), 4-fluorobenzene boronic acid (1.5 eq., 2.5 mmol, 502 mg). The product was isolated as a slightly off white solid (226 mg, 79% Yield).

MP(DSC): 42 °C ;^{1}H NMR (400MHz, $CDCl_3$) δ 8.67 (ddd, *J* = 4.8 Hz, 1.7 Hz, 1.0 Hz, 1H), 7.98 (dd, *J* = 9.0 Hz, 5.4 Hz, 2H), 7.74 (apr. td, 1H) , 7.67 (dt, *J* = 8.0 Hz, 1.0 Hz, 1H), 7.22 (ddd, *J* = 8.3, 4.8, 1.0 Hz, 1H), 7.15 (apr. t, *J* = 9.0 Hz, 2H); ^{13}C NMR (100 MHz, $CDCl_3$) δ 165.0, 162.6, 156.7, 150.0, 137.1, 135.9, 135.8, 129.0, 128.9, 122.3, 121.1, 116.0, 115.9; Elemental Analysis (CHN) C: 76.79% H: 4.71% N: 7.95%(Calculated : C: 76.29% H: 4.66% N: 8.09%) ESI-MS *m/z* = 174.0717 $[M+H]^+$ (calc. for $C_{11}NH_9F$ = 174.0713).

Synthesis of 2-(4-chlorophenyl)pyridine (33)

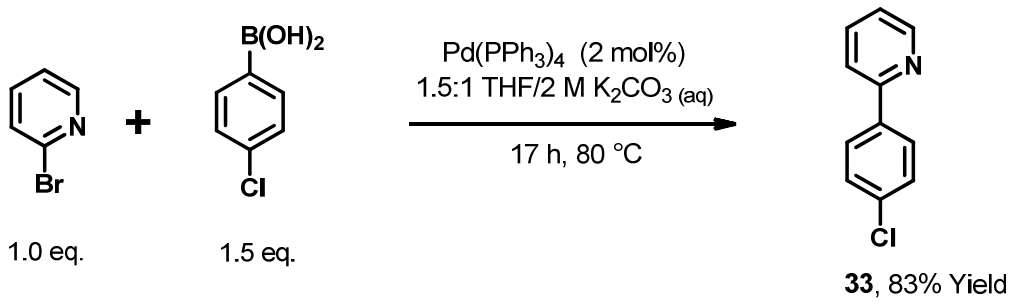

This synthesis is based on a modified literature procedure[93, 144]

33 was synthesised using general procedure **1,** but using 4-chlorobenzene boronic acid (1.5 eq., 2.5 mmol, 378 mg) and 2.0 M $K_2CO_{3(aq)}$ (6 ml). The product was isolated as a crystalline, slightly off white solid (261 mg, 83% Yield).

MP(DSC): 51°C ; ^{1}H NMR (400 MHz, $CDCl_3$) δ 8.69 (dd, *J* = 4.6, 0.7 Hz, 1H), 7.94 (d, *J* = 8.5 Hz, 2H), 7.76 (apr. td, 1H), 7.70 (d, *J* = 8.0 Hz, 1H), 7.44 (d, *J* = 8.5 Hz, 2H), 7.27–7.22 (m, 1H (under ref. peak)); ^{13}C NMR (100 MHz, $CDCl_3$) δ 156.6, 150.1, 138.1, 137.2, 135.4, 129.3,

128.5, 122.8, 120.7; Elemental Analysis (CHN) C: 69.19% H: 4.30% N: 7.18%(calc.: C: 69.67% H: 4.25% N: 7.39%) ESI-MS *m/z* = 190.0422 $[M+H]^+$ (calc. for $C_{11}NH_9Cl$ = 190.0418); IR (Pressed KBr disc): 1585, 1565, 1491, 1462, 1433, 1397, 1153, 1087, 1009, 985, 847, 829, 773, 734, 702, 676, 633, 613, 541, 491, 452 cm^{-1}.

Synthesis of 2-(4-biphenyl)pyridine (35) [93, 144]

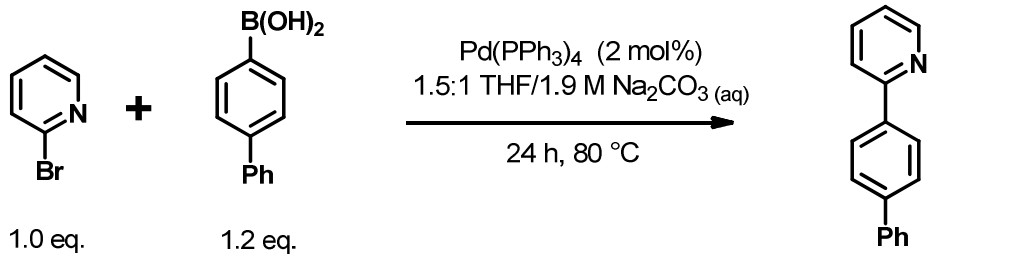

1.0 eq. 1.2 eq.

35, 59% Yield

35 was synthesised using general procedure **1** (1.66 mmol, 2-bromopyridine) but using biphenyl boronic acid (1.2 eq., 1.99 mmol, 331 mg). The product was isolated as a white solid (226 mg, 59% Yield).

MP(DSC): 144 °C; ^{1}H NMR (400 MHz, $CDCl_3$) δ 8.72 (dt, *J* = 4.7, 1.1 Hz, 1H), 8.09 (d, *J* = 8.5 Hz, 2H), 7.81–7.75 (m, 2H), 7.72 (d, *J* = 8.5 Hz, 2H), 7.67 (d, *J* = 8.0 Hz, 2H), 7.47 (t, *J* = 8.0 Hz, 2H), 7.37 (apr. t, *J* = 7.3 Hz, 1H), 7.26–7.22 (m, 1H (under ref. peak)); ^{13}C NMR (100 MHz, $CDCl_3$) δ 157.4, 150.1, 142.1, 141.0, 138.7, 137.1 129.2, 127.9, 127.8, 127.6, 127.5, 122.5, 120.9; Elemental Analysis (CHN): C: 87.84% H: 5.75% N: 5.92% (calc. C: 88.28% H: 5.67% N: 6.06%) ESI-MS *m/z* = 232.1122 $[M+H]^+$ (calc. for $C_{17}NH_{14}$= 232.1120); IR (Pressed KBr disc): 1603, 1595, 1584, 1570, 1556, 1487, 1464, 1448, 1430, 1400, 1296, 1181, 1149, 1058, 1035, 1003, 983, 906, 847, 786, 752, 711, 687, 644, 625, 608, 452 cm^{-1}.

10.4.2 Synthesis of short phenyl pyridine complexes and (Bn)$Mn(CO)_5$

Synthesis of Benzyl pentacarbonyl manganese(I)(42) [145]

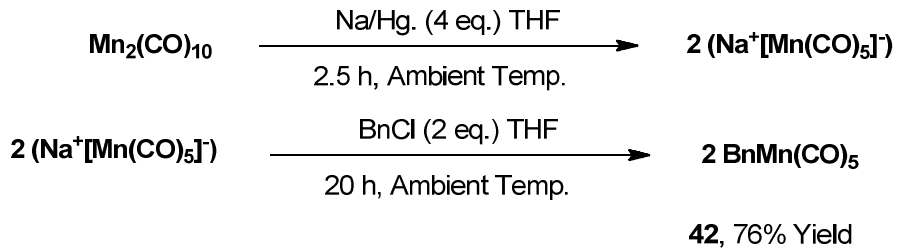

To an oven-dried Shlenk tube equipped with a magnetic stirrer under nitrogen was added mercury (3 cm^3). Sodium metal (4 eq, 1.07 mmol, 246 mg) was added in small pieces with high stirring to allow dissolution. In a separate Schlenk tube under nitrogen was added $Mn_2(CO)_{10}$ (1 eq., 2.68 mmol, 1.04 g), followed by anhydrous, deoxygenated THF (40 ml). The THF solution was then transferred by cannula on to the sodium amalgam and was stirred for 3 hours. In a separate Schlenk tube equipped with a magnetic stirrer under nitrogen was added benzyl chloride (2 eq., 5.36 mmol, 617 µl / 678 mg). The Schlenk tube containing benzyl chloride was placed in a bath of ice and water and was put under vacuum with stirring for 60 seconds. At ambient temperature, the THF solution of $NaMn(CO)_5$ was transferred by cannula into the benzyl chloride. The mixture was stirred at ambient temperature (20 °C) for 20 h. The solution was then filtered through a bed of Celite™ and was washed with diethyl ether (5 × 20 ml). The contents were then loaded on to silica gel and this was added on to a pad of silica (5 cm). The pad was washed with petroleum ether (3 × 40 ml). The solvent was removed to yield product contaminated with benzyl chloride. Benzyl chloride was removed at 35 °C under vacuum. The product must be broken up periodically with a spatula and put back under vacuum. A slightly yellow crystalline product was obtained. (1.179 g, 76% yield).

MP (DSC): 40 °C; ^1H NMR (400 MHz, $CDCl_3$); δ 7.18 (m, 4H), 6.97(m, 1H), 2.41 (s, 2H). IR (solution THF): 2107, 2047, 2009, 1987 cm^{-1}; ESI-MS *m/z:* 286.9748 $[M+H]^+$ (Calculated for $MnO_5C_{12}H_8$: 286.9747).

General procedure 2 Synthesis of Tetracarbonyl (2-(phenyl κ,C^{2}pyridine-κ,N)manganese(I) (37)[146-147]

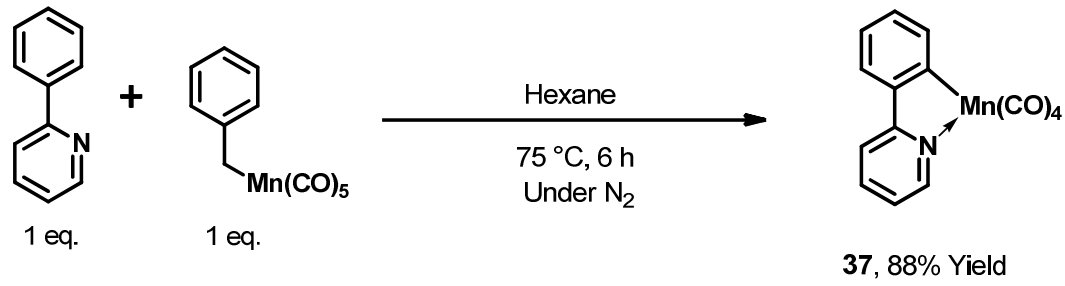

37, 88% Yield

To an oven dried Schlenk tube equipped with a magnetic flea under nitrogen was added 2-phenylpyridine (1 eq., 1 mmol, 143 µl/ 155 mg), $BnMn(CO)_5$ (1 eq., 1 mmol, 286 mg) followed by dry deoxygenated hexane (16 ml). The mixture was heated with stirring for 6 h. The reaction mixture was allowed to cool to ambient temperature. The hexane solution was filtered through a pipette packed with cotton wool and removal of solvent under reduced pressure yielded a pure yellow crystalline solid (284 mg, 88% Yield).

MP(DSC) : 114 °C; ^{1}H NMR (400 MHz, $CDCl_3$) δ 8.72 (d, *J* = 5.5 Hz, 1H), 7.97 (d, *J* = 7.5 Hz, 1H), 7.87 (d, *J* = 8.1 Hz, 1H), 7.81–7.74 (m, 2H), 7.28 (td, *J* = 7.5, 1.0 Hz, 1H), 7.17 (td *J* = 7.5, 1.5 Hz, 1H), 7.11 (ddd, *J* =7.5, 5.5, 1.5 Hz, 1H): ^{13}C NMR (100 MHz, $CDCl_3$) δ 174.9, 166.4, 153.9, 146.2, 141.7, 137.9, 130.3 124.2, 124.0, 122.4, 119.3. Elemental Analysis (CHN): C: 56.65% H: 2.98% N: 4.06% (calc.: C: 56.10% H: 2.51% N: 4.36% LIFDI-MS *m/z* = 321.0202 $[M]^+$ (calc. for $MnC_{15}H_8NO_4$ = 320.9834). IR (Solution: THF) : 2071, 1986, 1972, 1928, 1600, 1576, 1477 cm $^{-1}$.

Synthesis of Tetracarbonyl (2-(4-fluorophenyl)κ,C^2-pyridine-κ,N)Manganese(I) (38)

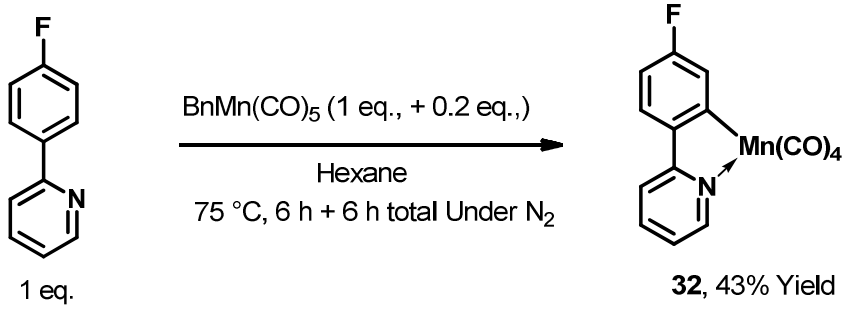

32, 43% Yield

Using the details from general procedure **2**, $BnMn(CO)_5$ (1 eq., 0.5 mmol, 143 mg), 2-(4-fluoro-phen-4-yl)pyridine (1 eq., 0.5 mmol, 86.5 mg) and hexane (8 ml) were used to prepare complex **38**. After 6 h, the reaction mixture was allowed to cool to ambient temperature. CH_2Cl_2 (10 ml) was added to dissolve the yellow precipitate. The mixture was filtered through cotton wool and solvent was removed under reduced pressure to yield product containing 20% starting material

(**32**). The impure product was reacted with more $BnMn(CO)_5$ (0.2 eq.) at 75 °C in hexane for six hours. Addition of dichloromethane and filtration as previously mentioned yielded a pure yellow solid (74 mg, 43% Yield).

MP(DSC): 163 °C; ^{1}H NMR (400 MHz, $CDCl_3$) δ 8.69 (dt, *J* = 5.6, 1.2 Hz 1H), 7.87–7.78 (m, 2H), 7.75 (dd, *J* = 8.5, 5.1 Hz, 1H), 7.68 (dd, *J* = 8.5, 2.5 Hz, 1H), 7.06-7.15 (m, 1H), 6.84 (td, *J* = 8.5, 2.5 Hz, 1H); ^{13}C NMR (100 MHz, $CDCl_3$) δ 179.6, 165.7, 165.3, 162.7, 154.2, 142.4, 138.3, 127.5, 127.3, 125.7, 125.6, 122.5, 119.5, 111.8, 111.6 ; Elemental Analysis (CHN) C: 52.94% H: 2.21% N: 3.98% (Calculated: C: 53.12% H: 2.08% N: 4.13%) ESI-MS *m/z* = 339.9827 $[M+H]^+$ (calc. for $MnC_{15}H_8FNO_4$= 339.9812). IR (Solution: THF): 2075, 1993, 1977, 1936, 1605, 1587, 1571, 1558, 1480, 1464, 1431, 1315, 1262, 1192 cm^{-1}.

Synthesis of Tetracarbonyl (2-(4-chlorophenyl)κ,C^{2}pyridine-κ,N)manganese(I) (39)

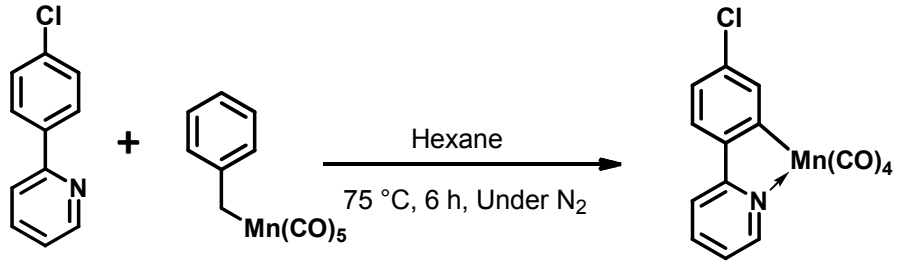

1 eq. 1 eq.

39, 83% Yield

Using the details from general procedure **2**, $BnMn(CO)_5$ (1 eq., 0.25 mmol, 72 mg), 2-(4-chlorophenyl)pyridine (1 eq., 0.25 mmol, 50 mg) and hexane (4 ml) were used to prepare complex **39**. At the end of the reaction, the reaction mixture was allowed to cool to ambient temperature. Dichloromethane (5 ml) was added to the mixture to dissolve the yellow precipitate. The solution was filtered through cotton wool packed in a pipette. Removal of solvent under reduced pressure gave pure product (82 mg, 83% Yield).

MP (DSC): 161 °C; ^{1}H NMR (400 MHz, $CDCl_3$) δ 8.71 (d, *J* = 4.3 Hz, 1H), 7.93 (s, 1H), 7.85-7.78 (m, 2H), 7.68(d, *J* = 8.0 Hz, 1H), 7.15 (d, *J* = 6.5 Hz, 2H); ^{13}C NMR (100 MHz, $CDCl_3$) δ 178.2, 165.7, 154.2, 144.7, 140.7, 138.4, 136.8, 125.1, 124.6, 122.9, 119.7. Elemental Analysis (CHN) C: 50.53% H: 2.11% N: 3.72% (calc.: C: 50.66% H: 1.98% N: 3.94%) LIFDI-MS *m/z* = 354.9831 $[M]^+$ (calc. for $MnC_{15}H_7ClNO_4$= 354.9444). IR (Solution: THF): 2077, 1993, 1978, 1936, 1605, 1567, 1543, 1478, 1424 cm^{-1}.

Synthesis of Tetracarbonyl (2-(4-bromophenyl)κ,C^{2}pyridine-κ,N)manganese^I (40)

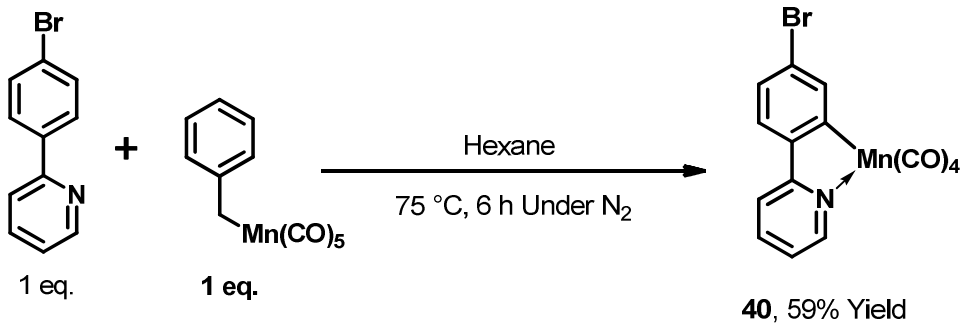

Using the details from general procedure **2**, $BnMn(CO)_5$ (1 eq, 0.75 mmol, 215 mg), 2-(4-bromophenyl)pyridine (1 eq., 0.75 mmol, 176 mg) and hexane (12 ml) were used to prepare complex **40**. At the end of the reaction, the Schlenk tube was stored at −18 °C overnight. The product had precipitated out of solution and the hexane solution was removed with a pipette. The yellow/brown solid product was then dried under reduced pressure. (217 mg, 72% Yield).

MP (DSC): 208 °C; ^{1}H NMR (400 MHz, $CDCl_3$) δ 8.71 (d, *J* = 5.6 Hz, 1H), 8.09 (d, *J* = 1.9 Hz, 1H), 7.88-7.78 (m, 2H), 7.61 (d, *J* = 8.5 Hz, 1H), 7.31 (dd, *J* = 8.5, 2.0 Hz, 1H), 7.15 (d, *J* = 6.7, 2.1 Hz, 1H); ^{13}C NMR (126 MHz $CDCl_3$) δ 219.5, 214.0, 213.2, 178.6, 165.6, 154.0, 144.8, 143.3, 138.1, 127.2, 126.1, 125.1, 122.8, 119.5. Elemental Analysis (CHN) C: 44.97% H: 1.75% N: 3.39% (calc.: C: 45.03% H: 1.76% N: 3.50%); ESI-MS *m/z* = 399.9017 $[M+H]^+$ (calc. for $MnC_{15}H_8BrNO_4$= 399.9012). IR (Solution : THF) : 2075, 1992, 1977, 1936, 1259 cm $^{-1}$.

Synthesis of Tetracarbonyl (2-(biphenyl)κ,C^{2}pyridine-κ,N)manganese^I (41)

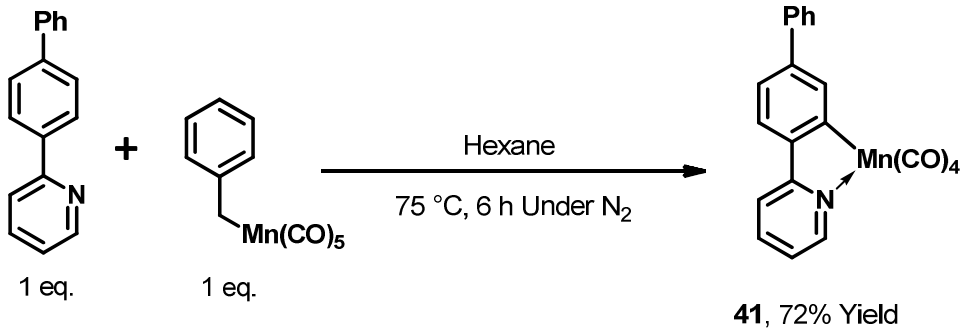

Using the details from general procedure **2**, $BnMn(CO)_5$ (1 eq., 0.5 mmol, 143 mg), 2-(biphenyl)pyridine (1 eq., 0.5 mmol, 116 mg) and hexane (8 ml) were used to prepare **41**. At the end of the reaction, the reaction mixture was allowed to cool to ambient temperature. CH_2Cl_2 (10 ml) was added to the mixture to dissolve the yellow precipitate. The solution was filtered through

cotton wool packed in a pipette. Removal of solvent under reduced pressure gave pure product as an off white solid (144 mg, 72% Yield).

MP(DSC): 138 °C; ^{1}H NMR (400 MHz, $CDCl_3$) δ 8.74 (d, *J* = 6.0, 1.7, 1.0 Hz, 1H), 8.21 (d, *J* = 1.8 Hz, 1H), 7.91 (d, *J* = 8.0 Hz, 1H), 7.85 (d, *J* = 8.0 Hz, 1H), 7.83-7.77 (m, 1H), 7.77-7.70 (m, 2H), 7.48 (t, *J* = 7.6 Hz, 2H), 7.42 (dd, *J* = 8.0, 1.8 Hz, 1H), 7.38 (t, *J* = 7.5 Hz, 1H), 7.13 (ddd, *J* = 7.5, 6.0, 1.4 Hz, 1H); ^{13}C NMR (100 MHz, $CDCl_3$) δ 175.6, 166.4, 154.2, 154.6, 142.8, 141.7, 140.2, 138.2, 129.1, 127.8, 127.7, 124.6, 123.6, 122.6, 119.7; Elemental Analysis (CHN) C: 63.61 % H: 3.44 % N: 3.39 % (calc.: C: 63.49% H: 3.04% N: 3.53%); LIFDI-MS *m/z* = 397.0349 $[M]^+$ (calc. for $MnC_{21}H_{12}NO_4$= 397.0147). IR (Solution: THF): 2073, 1989, 1974, 1932, 1602, 1582, 1562, 1477, 1475 cm^{-1}.

Alternative synthesis of complex 41 *via* a palladium-mediated cross-coupling reaction

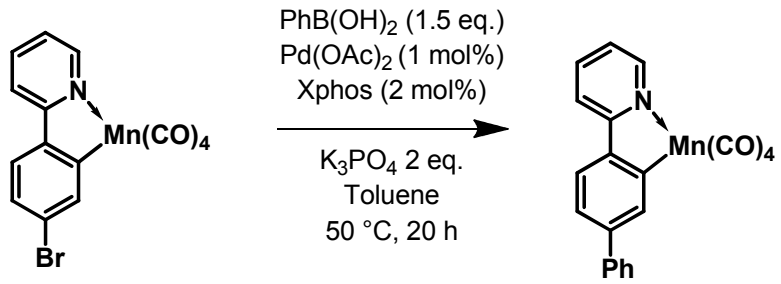

41, 67% Yield

This synthesis is based on a modified literature procedure.[98]

To a dry Schlenk tube equipped with a magnetic stirrer bar was added complex **40** (1 eq., 125 µMol, 50 mg), phenyl boronic acid (1.5 eq., 187.5 µMol, 23 mg) and K_3PO_4 (2 eq., 250 µMol, 34 mg). The Schlenk tube was evacuated and backfilled with N_2 three times. To a second Schlenk tube under N_2 was added $Pd(OAc)_2$ (5 mg) and Xphos (21.2 mg). Dry, degassed THF (1 ml) was added to the second Schlenk tube to prepare a red stock solution of catalyst/ligand, stirring is required for at least one minute to ensure dissolution. Dry degassed toluene (1 ml) was added to the Schlenk tube and the contents were stirred for 5 minutes at ambient temperature. Catalyst stock solution (60 µl) giving $Pd(OAc)_2$ (1 mol%, 0.3 mg) and Xphos (2 mol%, 1.2 mg) was added *via* syringe to the reaction Schlenk tube. The reaction mixture was then heated to 50 °C with vigorous stirring in the dark for 20 h. The reaction was quenched by cooling to ambient temperature. This was then filtered through a pipette packed with Celite™ and subsequently filtered through a silica plug in a pipette eluting with toluene collecting small fractions. Solvent was then removed under reduced pressure to give crude product. The crude mixture was purified by silica gel column chromatography. It was loaded on to silica using CH_2Cl_2, and then was charged on to a column packed with 5% EtOAc: petroleum ether. The product was eluted by

switching to 10% and finally 15% (*v/v*) EtOAc:Pet ether. Removal of column solvent under reduced pressure gave product **41** as an off white solid (32 mg, 67% yield).

10.4.3 Synthesis of polar phenylpyridine ligands

Synthesis of 2(4-hydroxyphenyl)pyridine (43) . General procedure 3

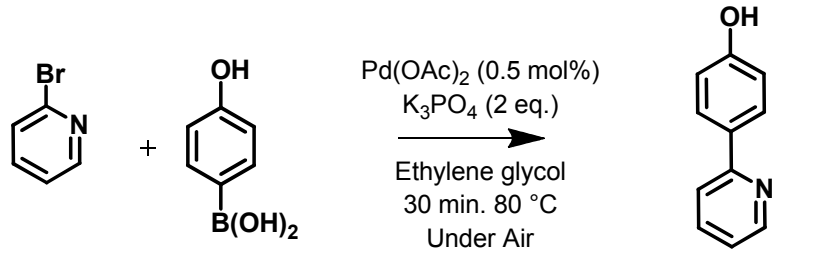

This compound was synthesised using a modified literature procedure.[92]

To a 250 ml round bottomed flask equipped with a magnetic stirrer was added $Pd(OAc)_2$ (0.005 eq., 50 µMol, 11.2 mg), 4-hydroxybenzeneboronic acid (1.5 eq., 15 mmol, 505 mg), potassium tri-phosphate (2 eq., 20 mmol, 4.24 g), 2-bromopyridine (1 eq., 10 mmol, 950 µl/1.58 g), and ethylene glycol (60 ml). The reaction was heated to 80 °C for 30 minutes and was allowed to cool to room temperature. Water (75 ml) and saturated brine (75 ml) were added and the aqueous layer was extracted with dichloromethane (4 × 100 ml). The organic layers were combined and dried with $MgSO_4$ and filtered. Solvent was removed under reduced pressure to yield the crude product. The crude product was purified by silica gel column chromatography (40:60 *v/v* PET ether/ethyl acetate followed by 50:50 (*v/v*) petroleum ether/ethyl acetate). The solvent was removed to isolate the title compound as a white solid (1.37 g, 80% yield).

M.P. (DSC): 164 °C; ^{1}H NMR (400 MHz, $CDCl_3$) δ 8.62 (ddd, *J* = 5.0, 1.8, 1.0 Hz, 1H), 7.79–7.71 (m, 3H), 7.65 (d, *J* = 8.0 Hz, 1H), 7.21 (dd, *J* = 7.4, 5.0 Hz, 1H), 6.80 (d, *J* = 8.5 Hz, 2H); ^{13}C NMR (100 MHz, $CDCl_3$) δ 158.2, 157.9, 149.2, 137.7, 130.8, 128.9, 121.9, 121.1, 116.2; Elemental Analysis (CHN) C: 76.85% H: 5.31% N: 8.04% (calc.: C: 76.17% H: 5.30% N: 8.18%); ESI-MS *m/z* = 172.0755 $[MH]^+$ (calc. for $C_{11}H_{10}NO$= 172.0762); IR (KBr disc): 3367–2120, 1603, 1560, 1523, 1470, 1425, 1381, 1273, 1245, 1183, 1153, 1097, 998, 966, 839, 778, 744, 714, 646, 623, 580, 552, 492, 473 cm^{-1}. Note: OH peak was not observed in the ^{1}H NMR spectrum, but is clearly observed in the IR spectrum.

Synthesis of methyl [4-(pyridin-2-yl)phenoxy]acetate (44).

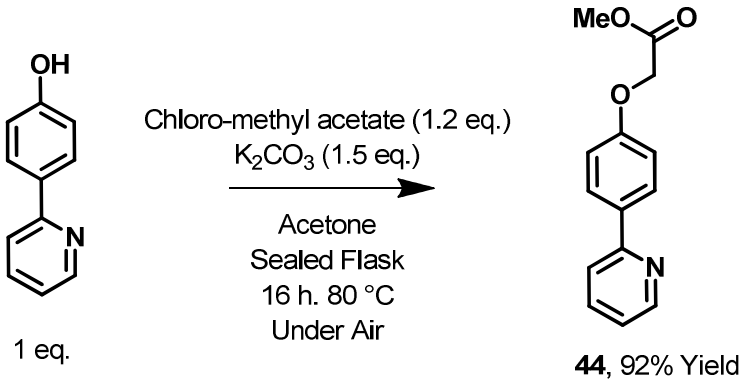

This synthesis was based on a modified literature procedure[99].

To a thick walled round bottomed flask equipped with a magnetic stirrer was added 2-(4-hydroxy-phenyl)pyridine (1 eq., 5.84 mmol, 1.00 g), potassium carbonate (1.5 eq., 8.76 mmol, 1.21 g) and chloro-methylacetate (1.2 eq., 7.01 mmol, 760 mg/615 µl). Acetone (50 ml) was added and the flask was sealed with a screw lid. The mixture was the heated to 80 °C for 20 h. The reaction mixture was allowed to cool to room temperature and deionised water was added (60 ml). The aqueous layer was extracted with dichloromethane (3 × 60 ml) and the organic layer was dried with $MgSO_4$ and filtered. Removal of solvent under reduced pressure yielded pure product as an off white solid (1.30 g, 92% yield).

M.P.(DSC): 95 °C ; ^{1}H NMR (400 MHz, $CDCl_3$) δ 8.64 (ddd, *J* = 4.8, 1.7 Hz, 1.0 Hz, 1H), 7.94 (d, *J* = 9.0 Hz, 2H), 7.71 (dd, *J* = 8.0, 1.7 Hz, 1H), 7.65 (apr. dt, 1H), 7.17 (ddd, *J* = 7.2, 4.8, 1.0 Hz, 1H), 6.99 (d, *J* = 9.0 Hz, 2H), 4.69 (s, 2H), 3.81 (s, 3H);^{13}C NMR (100 MHz, $CDCl_3$) δ 169.6, 158.9, 157.2, 149.9, 137.1, 133.5, 128.6, 122.0, 120.2, 115.1, 65.7, 52.7; ESI-MS *m/z* = 244.0971 $[M+H]^+$ (calc. for $C_{14}H_{14}NO_3$ = 244.0974); IR (Pressed KBr disc): 1757, 1601, 1587, 1561, 1512, 1467, 1435, 1396, 1314, 1307, 1275, 1212, 1177, 1157, 1114, 1080, 1029, 1005, 982, 913, 840, 825, 781, 743, 715, 702, 639, 603, 551, 490 cm^{-1}.

Synthesis of 2-(4-hydroxymethyl-phenyl)pyridine (50)

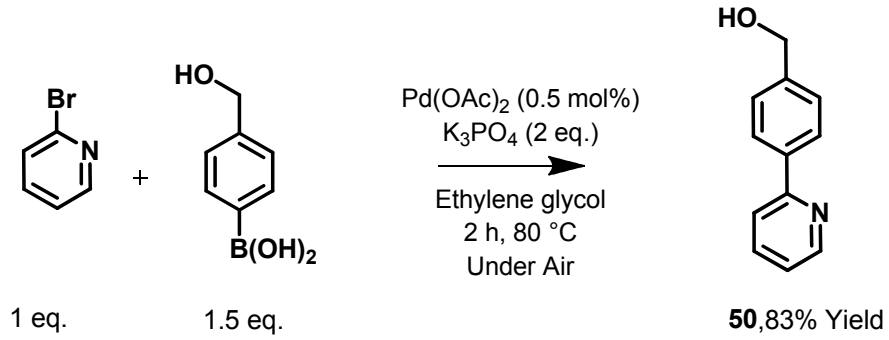

Using general procedure **3**, $Pd(OAc)_2$ (0.005 eq., 50 µMol, 11.2 mg), (4-hydroxymethyl)phenylboronic acid (1.5 eq., 15 mmol, 2.28 g), K_3PO_4 (2 eq., 20 mmol, 4.24 g), 2-bromopyridine (1 eq., 10 mmol, 950 µl/1.58 g), and ethylene glycol (60 ml) were used to synthesise the title compound. The product was isolated as a clear colourless oil (1.5 g, 83% yield).

^{1}H NMR (400 MHz, $CDCl_3$) δ 8.65–8.55 (ddd, *J* = 4.8, 1.5, 1.0 Hz, 1H), 7.83 (d, *J* = 8.0 Hz, 2H), 7.69 (apr. td, 1H), 7.63 (d, *J* = 7.9 Hz, 1H), 7.35 (d, *J* = 8.0 Hz, 2H), 7.18 (ddd, *J* = 7.3, 4.8, 1.0 Hz, 1H), 4.64 (s, 2H), 4.14 (s, 1H); ^{13}C NMR(100 MHz, $CDCl_3$) δ 157.5, 149.7, 142.5, 138.3, 137.2, 127.4 127.2, 122.4, 121.1, 64.6; ESI-MS: *m/z* = 186.0918 $[MH]^+$ (Calc. for $C_{12}H_{12}NO$ = 186.0913).

10.4.4 Synthesis of polar phenylpyridine complexes

Synthesis of tetracarbonyl (2-(4-hydroxy-phenyl)κ,C^8-pyridine-κ,N) manganese(I) (64)

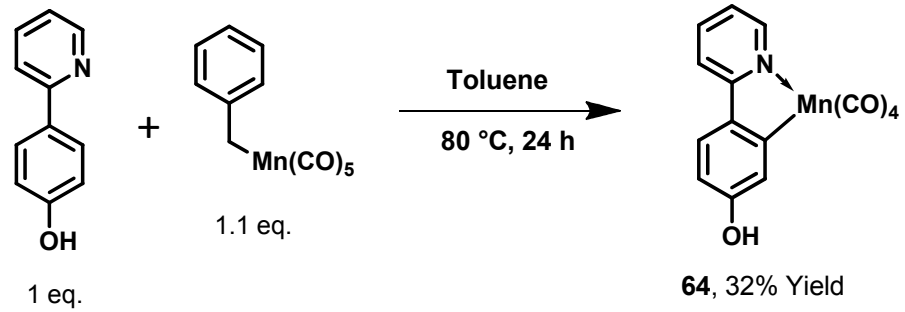

Using the details from general procedure **2**, $BnMn(CO)_5$ (1.1 eq., 2.57 mmol, 735 mg), 2-(4-hydroxy-phenyl)pyridine (1 eq., 2.34 mmol, 400 mg) and toluene (30 ml) were used to prepare the title complex **64**. At the end of the reaction, the solvent was removed under reduced pressure. The crude mixture was loaded on to silica using dichloromethane. The compound was purified by silica gel column chromatography (30:70 (*v/v*) diethyl ether/PET ether). Removal of solvent under reduced pressure yielded product as an off white solid (250 mg, 32% yield).

M.P. (DSC): 127 °C (crystalline change) 171 °C (melt); ^{1}H NMR (400 MHz, $CDCl_3$) δ 8.64 (d, *J* = 5.6 Hz, 1H), 7.74 (d, *J* = 4.2 Hz, 2H), 7.69 (d, *J* = 8.4 Hz, 1H), 7.42 (d, *J* = 2.5 Hz, 1H), 7.03 (m, 1H), 6.66 (dd, *J* = 8.4, 2.5 Hz, 1H) , 4.98 (s, 1H); ^{13}C NMR (100 MHz $CDCl_3$) δ 178.4 ,166.3, 157.2, 154.0, 139.6, 138.0, 127.5, 125.8, 121.6, 118.9, 111.9; Elemental Analysis (CHN) C: 53.38% H: 2.46% N: 3.99% (calc.: C: 53.28% H: 2.68% N: 4.14%); ESI-MS *m/z* = 337.9871 $[M+H]^+$ (calc. for $MnC_{15}H_9NO_5$= 337.9856); IR (Solution: THF): 3264, 2072, 1988, 1971, 1929, 1604, 1580, 1556, 1481, 1467, 1432, 1268, 1221, 1162 cm^{-1}.

Synthesis of tetracarbonyl (methyl [4-(pyridin-2-yl-κ,N)phen-κ,C^2-oxy]acetate) manganese(I) (45)

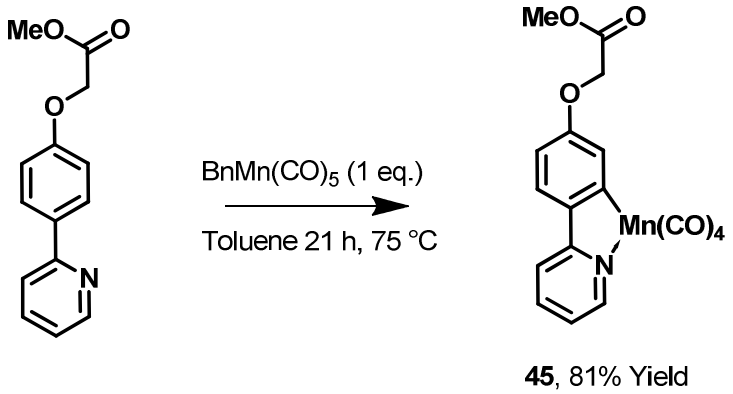

45, 81% Yield

Using the details from general procedure **2**, $(Bn)Mn(CO)_5$ (1 eq., 1.82 mmol, 521 mg), methyl [4-(pyridin-2-yl)phenoxy]acetate (1 eq., 1.82 mmol, 472 mg) and toluene (29 ml) were used to prepare the title complex **45**. After 21 h heating, the reaction mixture was allowed to cool to room temperature. The solvent was removed under reduced pressure and crude solid was loaded on to silica using dichloromethane. The crude mixture was purified using silica gel column chromatography (80:20 (*v/v*) PET ether/ethyl acetate). Removal of solvent under reduced pressure gave pure product (600 mg, 81% yield).

M.P. (DSC): 144 °C; ^{1}H NMR (400 MHz, $CDCl_3$) δ 8.65 (d, *J* = 5.6 Hz, 1H), 7.75 (d, *J* = 3.6 Hz, 2H), 7.90 (d, *J* = 8.5 Hz, 1H), 7.52 (d, *J* = 2.5 Hz, 1H), 7.04 (m, 1H), 6.71 (dd, *J* = 8.5, 2.5 Hz, 1H), 4.75 (s, 2H), 3.84 (s, 3H); ^{13}C NMR (100 MHz, $CDCl_3$) δ 175.1, 169.5, 165.9, 158.8, 153.8, 140.2, 137.8, 126.1, 125.2, 121.6, 118.9, 110.8, 65.3, 52.4; Elemental Analysis (CHN) C: 52.80% H: 2.99% N: 3.20% (calc.: C: 53.10% H: 2.48% N: 3.44%); ESI-MS *m/z* = 410.0061, $[M+H]^+$ (calc. for $MnC_{18}H_{13}NO_7$ = 410.0067); IR (THF): 2073, 1990, 1973, 1931, 1767, 1743, 1604, 1581, 1554, 1467, 1428 cm^{-1}.

Synthesis of methyl [4-(pyridin-2-yl)phenoxy]acetic acid (46)

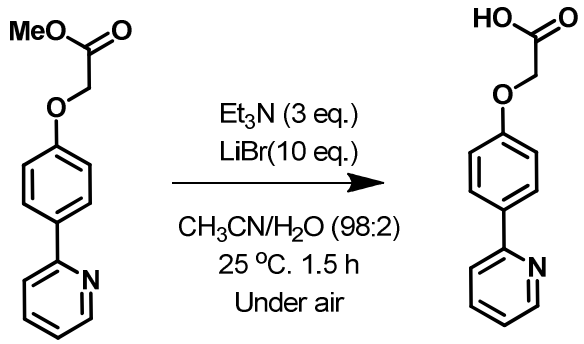

46,67% Yield

To a round bottomed flask equipped with a magnetic stirrer was added methyl [4-(pyridin-2-yl)phenoxy]acetate (1 eq., 1 mmol, 243 mg), and lithium bromide (10 eq., 10 mmol, 868 mg). Triethylamine (3 eq., 3 mmol, 303 mg/418 µl), deionised water (100 µl) and acetonitrile (5 ml) were then added. The reaction was stirred at 25 °C for 1.5 h. Deionised water (15 ml) was added to the reaction and the mixture was acidified with 2 M HCl to pH 3. The aqueous layer was extracted with ethylacetate (3 × 30 ml). The remaining aqueous extract was neutralised with NaOH to pH 5 and was extracted with ethyl acetate a further three times. The organic extract was dried with $MgSO_4$ and filtered. The solvent was removed under reduced pressure to yield pure product as a white powder (156 mg, 67% yield).

MP (DSC): 166 °C; ^{1}H NMR (400 MHz, DMSO-d_6) δ: 8.62 (ddd, *J* = 4.8, 1.8, 1.0 Hz, 1H), 8.03 (d, *J* = 8.9 Hz, 2H), 7.89 (apr. dt, 1H), 7.84 (td, *J* = 7.3, 1.8 Hz, 1H), 7.29 (ddd, *J* = 7.3, 4.8, 1.3 Hz, 1H), 7.02 (d, *J* = 8.9 Hz, 2H), 4.75 (s, 2H); ^{13}C NMR (101 MHz, DMSO-d_6) δ: 170.2, 158.7, 155.7, 149.4, 137.2, 131.7, 127.9, 121.9, 119.5, 114.7, 64.5; Elemental Analysis (CHN) C: 67.32 % H: 4.80 % N: 6.26 % (calc.: C: 68.11 % H: 4.84 % N:6.11 %); ESI-MS *m/z* = $[M+H]^+$ (calc. for $C_{13}H_{12}NO_3$ = 230.0812); IR (KBr Disc): 3432, 1728, 1601, 1563, 1516, 1471, 1432, 1277, 1234, 1181, 1073, 998, 927, 845, 778, 755, 741, 686, 645, 605, 519, 500, 436 cm^{-1}.

Synthesis of tetracarbonyl (methyl [4-(pyridin-2-yl-κ,N)phen-κ,C^2-oxy]acetic acid) manganese(I) (47)

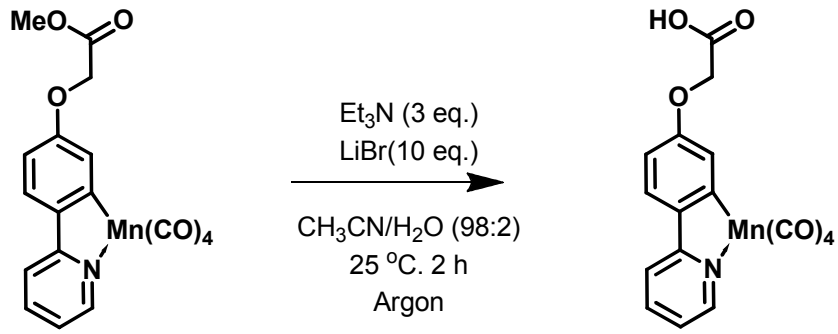

47, 84% Yield

To a round bottomed flask equipped with a magnetic stirrer was added (methyl [4-(pyridin-2-yl-κ,N)phen-κ,C_2-oxy]acetate)Manganese(I) (1 eq., 0.733 mmol, 300 mg), and lithium bromide (10 eq., 7.33 mmol, 636 mg). The flask was purged with argon using a balloon. Triethylamine (3 eq., 2.19 mmol, 223 mg/307 µl), deionised water (140 µl) and acetonitrile (7 ml) were then added. The acetonitrile was degassed by sonication with argon bubbling from a balloon for 15 minutes prior to addition. The reaction was stirred at 25 °C for 2 h. Deionised water (15 ml) was added to the reaction and the mixture was acidified with 2 M HCl to pH 2-3. The aqueous layer was extracted with dichloromethane (3 × 30 ml). The organic extract was washed with water (20 ml) and was dried with $MgSO_4$ and filtered. The solvent was removed under reduced pressure to yield pure product as a yellow solid (246 mg, 84% yield).

M.P. (DSC): 153 °C (broad); ^{1}H NMR (400 MHz, DMSO-d_6) δ 13.15 (broad s, 1H) 8.72 (d, *J* = 5.6 Hz, 1H), 8.15 (d, *J* = 8.0 Hz, 1H), 8.00 (m, 2H), 7.35 (d, *J* = 2.5 Hz, 1H), 7.31 (ddd, *J* = 7.0, 5.6, 1.2 Hz, 1H) 6.75 (dd, *J* = 8.5, 2.5 Hz, 1H), 4.78 (s, 2H); ^{13}C NMR (100 MHz, d_6-DMSO) δ 221.0, 215.4, 214.4, 175.8, 171.1, 165.7, 159.8, 155.1, 140.6, 139.8, 126.9, 126.6, 123.6, 120.3, 111.1, 65.3; Elemental Analysis (CHN) C: 51.65% H: 2.71% N: 3.49% (calc.: C: 51.67% H: 2.56% N: 3.54%); ESI-MS *m/z* = 395.9916, $[M+H]^+$ (calc. for $MnC_{17}H_{11}NO_7$ = 395.9911); IR (THF): 2071, 1989, 1972, 1931, 1766, 1731, 1604, 1581, 1554, 1469, 1428, 1314, 1284 cm^{-1}.

10.4.5 Synthesis of alkyne linked ligands

Synthesis of 2-[4-(prop-2-ynyloxy)phenyl]pyridine (51) - general procedure 4.

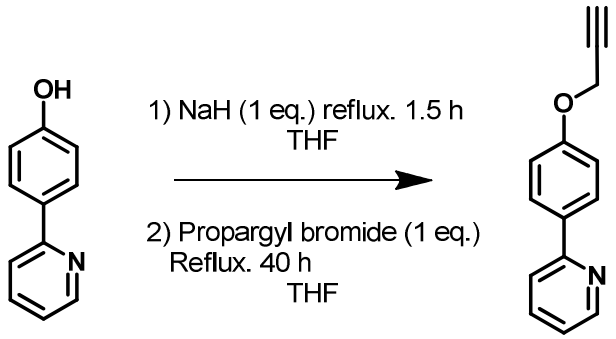

51, 75% Yield

This compound was prepared using a modified literature procedure.[61]

To a suspension of sodium hydride (1 eq., 7 mmol, 178 mg) in THF (40 ml), was added a solution of 2-(4-hydroxyphenyl)pyridine (1 eq., 7 mmol, 1.21 g) in THF (40 ml) in a Schlenk tube *via* cannula transfer over 10 mins. The resulting solution was refluxed for 1.5 h. The solution was allowed to cool and propargyl bromide (1 eq., 7 mmol, 833 mg) was then added. The solution was refluxed for a further 40 h. The reaction mixture was then allowed to cool to room temperature, and water (40 ml) was added. The aqueous phase was then extracted with CH_2Cl_2 (3 × 50 ml). The organic layers were combined, then washed with saturated sodium carbonate (2 × 50 ml), water (2 × 50 ml), were then dried with $MgSO_4$ and filtered. The solvent was evaporated to yield the crude product. The crude was dissolved in dichloromethane and was loaded on to silica. The crude mixture was purified by silica gel column chromatography using 30:70 (*v/v)* Et_2O:petroleum ether increasing to 40:60. Removal of solvent yielded pure product as an off-white solid (1.1 g, 75% yield).

M.P. (DSC): 81 °C; ^{1}H NMR (400 MHz, $CDCl_3$) δ 8.65 (d, *J* = 4.8 Hz, 1H), 7.96 (d, *J* = 8.8 Hz, 2H), 7.72 (apr. td, 1H), 7.67 (d, *J* = 8.0 Hz, 1H), 7.17 (ddd, *J* = 7.2, 4.8, 1.4 Hz, 1H), 7.07 (d, *J* = 8.8 Hz, 2H), 4.75 (d, *J* = 2.5 Hz, 2H), 2.54 (t, *J* = 2.5 Hz, 1H); ^{13}C NMR (100 MHz, $CDCl_3$) δ 158.7, 157.3 ,149.9, 137.0, 133.3, 128.5, 121.9, 120.2, 115.4, 78.7, 76.0, 56.2; ESI-MS: *m/z* = 210.0920 $[MH]^+$ (calc. for $C_{14}H_{12}NO$ = 210.0193); Elemental Analysis (CHN) C: 80.02% H: 5.26% N: 6.58% (calc.: C: 80.36% H: 5.30% N: 6.69%); IR (THF):3232, 2128, 2118, 1608, 1588, 1564, 1514, 1467, 1436, 1377, 1307, 1275, 1242, 1223, 1176, 1154, 1112 cm^{-1}.

Synthesis of 2-(4-[(prop-2-ynyloxy)methyl]phenyl)pyridine (52)

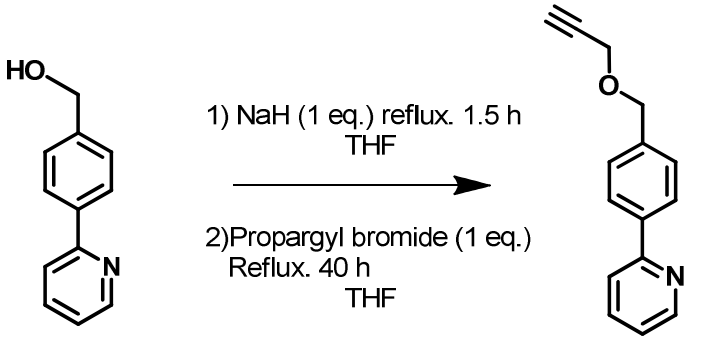

52, 66% Yield

Using general procedure **4**, 2-(4-hydroxymethyl-phenyl)pyridine (1 eq., 6 mmol, 1.11 g), sodium hydride (1 eq., 6 mmol, 143 mg) and propargyl bromide (1 eq., 6 mmol, 714 mg) were used to synthesise the title compound. Pure product was obtained as an orange oil (892 mg, 66% yield).

^{1}H NMR (400 MHz, $CDCl_3$) δ 8.68 (dt, *J* = 4.8, 1.3 Hz, 1H), 7.98 (d, *J* = 8.2 Hz, 2H), 7.75–7.67 (m, 2H), 7.46 (d, *J* = 8.3 Hz, 2H), 7.20 (ddd, *J* = 5.8, 4.9, 2.6 Hz, 1H), 4.66 (s, 2H), 4.19 (d, *J* = 2.3 Hz, 2H), 2.49 (t, *J* = 2.3 Hz, 1H); ^{13}C NMR (100 MHz, $CDCl_3$) δ 157.3, 149.8, 139.2, 138.3, 137.0, 128.7, 127.2, 122.4, 120.8, 79.9, 75.1, 71.4, 57.4; ESI-MS: *m/z* = 224.1066 $[MH]^+$ (Calc. for $C_{15}H_{14}NO$ = 224.1070); IR (CH_2Cl_2): 1607, 1589, 1564, 1515, 1467, 1435, 1375, 1220, 1177 cm^{-1}.

Synthesis of 2-[4-(3-triisopropylsilyl-prop-2-ynyloxy)phenyl]pyridine (57) - general procedure 5.

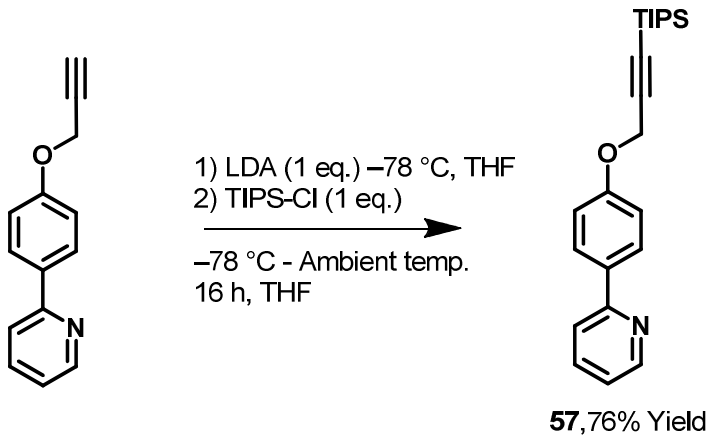

57,76% Yield

This compound was synthesised using a modified literature procedure.[114]

2-[4-(prop-2-ynyloxy)phenyl]pyridine (1 eq., 1 mmol, 209 mg) was dissolved in dry THF (10 ml). The mixture was cooled to −78 °C and LDA (1 eq., 1 mmol) was added over five mins *via* syringe. The reaction mixture was allowed to warm to 0 °C for five mins. The mixture was cooled back to −78 °C and TIPS chloride (1 eq., 1 mmol, 192 mg/214 µl) was added. The mixture was allowed to warm to ambient temperature and was stirred overnight. Saturated $NH_4Cl_{(aq)}$(10 ml) was added and the mixture was extracted with Et_2O (2 × 20 ml). The organic layer was then washed with water (10 ml) and saturated brine (10 ml) and was dried with $MgSO_4$ and filtered. Removal of solvent under reduced pressure yielded crude product. The crude product was loaded on to silica using dichloromethane. The product was purified by silica gel column chromatography. The column was started using petroleum ether to remove apolar impurities. The product was eluted with 8% Et_2O: petroleum ether (*v/v*). Removal of solvent under reduced pressure yielded the product as a clear orange oil (279 mg, 76% yield).

^{1}H NMR (400 MHz, $CDCl_3$) δ 8.65 (ddd, *J* = 4.8, 1.6, 1.0 Hz, 1H), 7.94 (d, *J* = 8.8 Hz, 2H), 7.78–7.59 (m, 2H), 7.16 (ddd, *J* = 7.0, 4.8, 1.4 Hz, 1H), 7.10 (d, *J* = 8.8 Hz, 2H), 4.78 (s, 2H), 1.04 (s, 21H); ^{13}C NMR (100 MHz, $CDCl_3$) δ 158.9, 157.3, 149.8, 137.0, 132.8, 128.3, 121.8, 120.2, 115.6, 102.1, 89.7, 57.1, 18.8, 11.4; ESI-MS: *m/z* = 366.2238 $[MH]^+$ (calc. for $C_{23}H_{32}SiNO$ = 366.2248)

Synthesis of 2-(4-[(3-triisopropylsilyl-prop-2-ynyl-oxy)methyl]phenyl)pyridine (58).

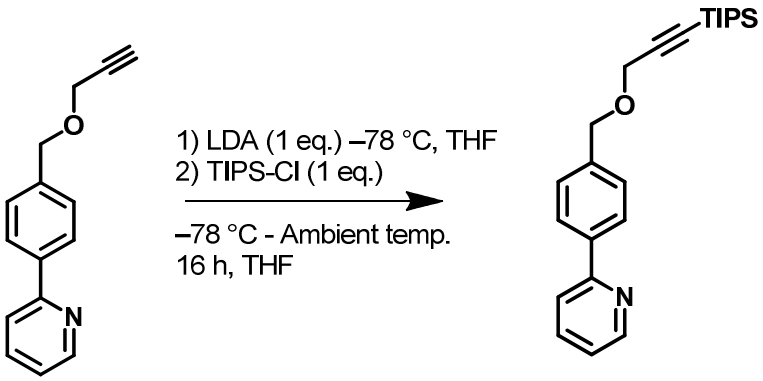

58, 73% Yield

Using general procedure **5**, 2-(4-[(prop-2-ynyloxy)methyl]phenyl)pyridine (1 eq., 1.91 mmol, 426 mg), LDA (1 eq., 1.91 mmol) and TIPS chloride (1 eq., 1.91 mmol, 368 mg/ 408 µl) in THF (15 ml) were used to synthesise the title compound **58**. The compound was purified using silica gel column chromatography starting with petroleum ether moving to 20% Et_2O: petroleum ether (*v/v*). The compound was isolated as a clear orange oil (499 mg, 73% Yield).

^{1}H NMR (400 MHz, $CDCl_3$) δ 8.69 (dt, *J* = 5.0, 1.3 Hz, 1H), 7.99 (d, *J* = 8.1 Hz, 2H), 7.78–7.68 (m, 2H), 7.47 (d, *J* = 8.1 Hz, 2H), 7.23 (ddd, *J* = 6.6, 5.0, 2.2 Hz, 1H), 4.70 (s, 2H), 4.24 (s, 2H), 1.10 (s, 21H); ^{13}C NMR (100 MHz, $CDCl_3$) δ 157.5, 150.0, 139.2, 138.7, 137.1, 128.9, 127.3, 122.4, 120.8, 103.5, 88.4, 70.9, 58.1, 18.9, 11.5; ESI-MS: *m/z* = 380.2394 $[MH]^+$ (Calc. for $C_{24}H_{34}NOSi$ = 380.2404); Elemental Analysis (CHN) C: 75.36% H: 8.72% N: 3.68% (calc.: C: 75.94% H: 8.76% N: 3.69%); IR (solution: CH_2Cl_2): 2170, 1587, 1468, 1436, 1349, 1264, 1078 cm^{-1}.

10.4.6 Synthesis of alkyne linked complexes

Synthesis of tetracarbonyl 2-[4-(3-triisopropylsilyl-prop-2-ynyloxy)phenyl]κ,C^2-pyridine-κ,N) manganese(I)(59) - general procedure 6

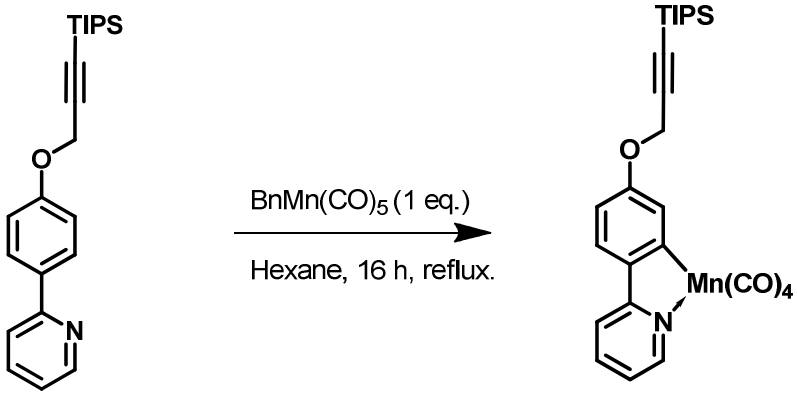

59, 97% Yield

2-[4-(3-triisopropylsilyl-prop-2-ynyloxy)phenyl]pyridine (1 eq., 2.285 mmol, 833 mg) and $BnMn(CO)_5$ (1 eq., 2.285 mmol, 654 mg) were dried under vacuum in a Schlenk tube for 15 minutes. Hexane (30 ml) was then added via cannula transfer from an ampoule. The reaction mixture was refluxed with stirring for 16 h. The solution was allowed to cool to room temperature and was filtered through a pipette packed with Celite™. The solvent was removed under reduced pressure to yield the product as an off-yellow solid (1.17 g, 97% yield). The compound did not require further purification after the reaction but if it was required this could be done using silica gel column chromatography.

M.P. (DSC): 95 °C; ^{1}H NMR (400 MHz, $CDCl_3$) δ 8.65 (dt, *J* = 5.5, 1.3 Hz, 1H), 7.77–7.72 (m, 2H), 7.71 (d, *J* = 8.6 Hz, 1H), 7.60 (d, *J* = 2.5 Hz, 1H), 7.03 (td, *J* = 5.5, 3.1 Hz, 1H), 6.79 (dd, *J* = 8.6, 2.5 Hz, 1H), 4.84 (s, 2H), 1.05 (s, 21H); ^{13}C NMR (100 MHz, $CDCl_3$) δ 177.9, 166.4, 159.3, 154.0, 139.9, 137.9, 126.3, 125.4, 121.6, 119.0, 112.0, 102.3, 89.3, 56.8, 18.9, 11.4; ESI-MS: *m/z* = 532.1345 $[MH]^+$ (calc. for $C_{27}H_{31}MnNO_5Si$ = 532.1347); Elemental Analysis (CHN) C: 60.58% H: 5.77% N: 2.56% (calc.: C: 61.01% H: 5.69% N: 2.64%); IR (Solution: THF): 2073, 1989, 1973, 1931, 1604, 1580, 1553, 1468, 1431, 1317, 1281, 1211, 1198, 1165 cm^{-1}.

Synthesis of tetracarbonyl 2-(4-[(3-triisopropylsilyl-prop-2-ynyl-oxy)methyl]phenyl) κ,C^2-pyridine-κ,N) manganese(I) (60)

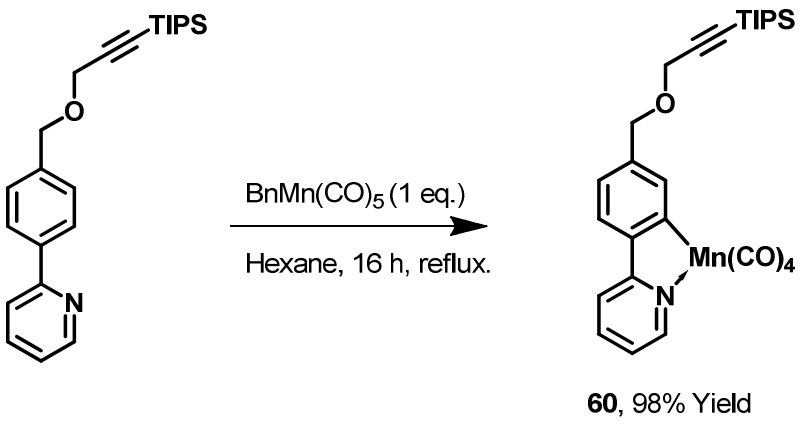

60, 98% Yield

Using general procedure **6**, 2-(4-[(3-triisopropylsilyl-prop-2-ynyl-oxy)methyl]phenyl)pyridine (1 eq., 3.24 mmol, 147 mg) and $BnMn(CO)_5$ (1 eq., 3.24 mmol, 111 mg) were used with hexane (30 ml) to synthesise the title complex as an off yellow solid (1.7 g, 98% Yield).

M.P. (DSC): 82°C; ^{1}H NMR (400 MHz, $CDCl_3$) δ 8.74–8.69 (m, 1H), 7.92 (d, *J* = 1.6 Hz, 1H), 7.88 (d, *J* = 8.2 Hz, 1H), 7.81 (d, *J* = 2.0 Hz, 1H), 7.77 (d, *J* = 7.9 Hz, 1H), 7.20(dd, *J* = 8.1, 1.7 Hz, 1H), 7.15–7.07 (m, 1H), 4.70 (s, 2H), 4.30 (s, 2H), 1.11 (s, 21H); ^{13}C NMR (100 MHz, DMSO-d_6) δ 220.0, 214.5, 213.4, 172.5, 164.7, 154.4, 145.9 , 140.9, 139.1, 139.0, 124.5, 124.0, 123.7, 120.0, 104.3, 86.8, 70.5, 57.3, 18.4, 10.6; ESI-MS: *m/z* = 546.1494 $[MH]^+$ (calc. for $C_{28}H_{33}MnNO_5Si$ = 546.1503); Elemental Analysis (CHN) C: 61.48% H: 5.91% N: 2.51% (calc.: C: 61.64% H: 5.91% N: 2.57%); IR (solution: CH_2Cl_2): 2170, 2075, 1991, 1977, 1932, 1605, 1477, 1268, 1076 cm^{-1}.

Synthesis of tetracarbonyl 2-[4-(prop-2-ynyloxy)phenyl] κ,C^2-pyridine-κ,N) manganese(I) (62) - general procedure 7

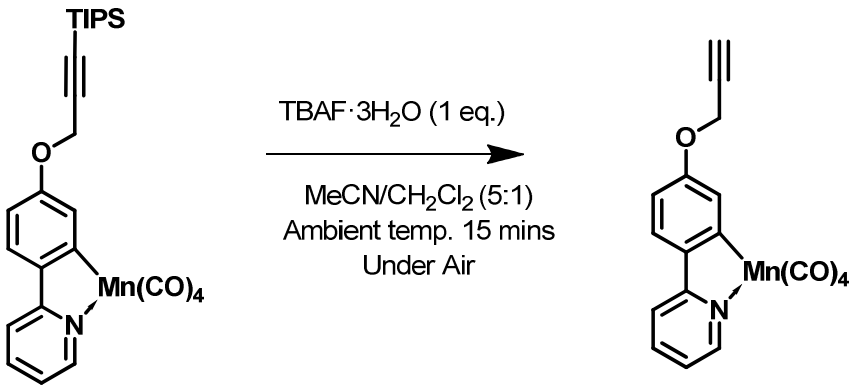

62, 52% Yield

Tetracarbonyl 2-[4-(3-triisopropylsilyl-prop-2-ynyloxy)phenyl]κ,C^2-pyridine-κ,N) manganese(I) (1 eq., 0.525 mmol, 279 mg) was dissolved in a mixture of MeCN (5 ml) and CH_2Cl_2 (1 ml). TBAF·$3H_2O$ (1 eq., 0.525 mol, 165 mg) was added to the reaction mixture with stirring. After 15 minutes, H_2O (20 ml) was added the aqueous layer was extracted with CH_2Cl_2 (3×20 ml). The organic extract was dried with $MgSO_4$ and was filtered. Removal of solvent under reduced pressure yielded crude product. The crude product was loaded on to silica using CH_2Cl_2. The crude mixture was purified by silica gel column chromatography. The column was packed using petroleum ether and the product was eluted with 10% ethyl acetate/petroleum ether. Removal of solvent under reduced pressure yielded pure product as an off white solid (103 mg, 52% Yield).

M.P. (DSC): 125 °C (decomposition); ^{1}H NMR (400 MHz, $CDCl_3$) δ 8.66 (d, *J* = 5.7 Hz, 1H), 7.79–7.68 (m, 3H), 7.59 (d, *J* = 2.5 Hz, 1H), 7.09–6.98 (m, 1H), 6.78 (dd, *J* = 8.5, 2.5 Hz, 1H), 4.80 (d, *J* = 2.3 Hz, 2H), 2.57 (d, *J* = 2.3 Hz, 1H); ^{13}C NMR (100 MHz, DMSO-d_6) δ 178.1, 166.2, 159.0, 154.0, 140.2, 138.0, 126.7, 125.4, 121.8, 119.0, 111.2, 78.9, 75.9, 56.0; LIFDI-MS: *m/z* = 374.9863 $[M]^+$ (Calc. for $C_{18}H_{10}NO_5Mn$ = 374.9939); Elemental Analysis (CHN) C: 56.80% H: 2.83% N: 3.47% (calc.: C: 57.62% H: 2.69% N: 3.73%); IR (solution: THF):3242, 2117, 2073, 1989, 1973, 1931, 1645, 1603, 1579, 1552, 1476, 1431, 1213 cm^{-1}.

Synthesis of tetracarbonyl 2-(4-[(prop-2-ynyloxy)methyl]phenyl) κ,C^2-pyridine-κ,N) manganese(I) (63)

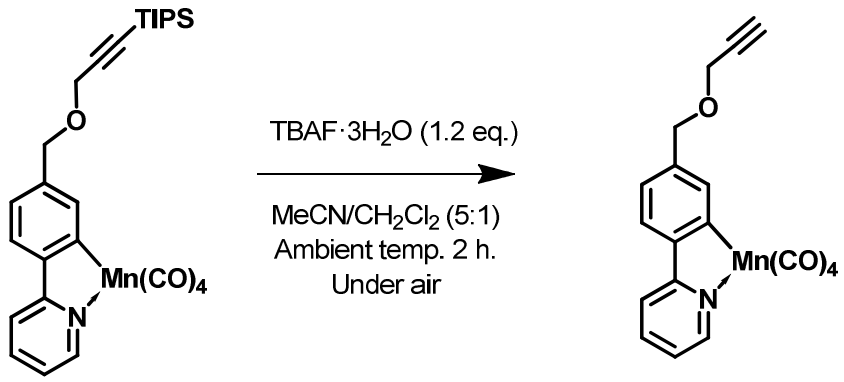

63, 51% Yield

Using general procedure **7**, tetracarbonyl 2-(4-[(3-triisopropylsilyl-prop-2-ynyl-oxy)methyl]phenyl) κ,C^2-pyridine-κ,N) manganese(I) (1 eq., 3.037 mmol, 1.657 g), MeCN (30 ml), CH_2Cl_2 (6 ml) and TBAF.$3H_2O$ (1.2 eq, 3.644 mol, 1.15 g) were used to synthesise the title complex over 2 h. The crude mixture was purified using silica gel column chromatography starting with 10% Et_2O:petroleum ether moving to 20%. Removal of solvent under reduced pressure yielded pure product as an off white solid (606 mg, 51% yield).

M.P (DSC).107 °C(decomposition);^{1}H NMR (400 MHz, DMSO-d_6) δ 8.72 (d, J = 5.5 Hz, 1H), 8.28–8.13 (m, 1H), 8.03–7.95 (m, 2H), 7.74 (d, J = 1.6 Hz, 1H), 7.33 (ddd, J = 7.2, 5.5, 1.3 Hz, 1H), 7.09 (dd, J = 8.0, 1.7 Hz, 1H), 4.53 (s, 2H), 4.21 (d, J = 2.4 Hz, 2H), 3.48 (t, J = 2.4 Hz, 1H); ^{13}C NMR (100 MHz, $CDCl_3$) δ 175.4, 166.4, 154.2, 146.1, 141.4, 139.3, 138.2, 124.34, 124.32, 122.7, 119.7, 80.1, 75.0, 72.3, 57.8; ESI-MS: m/z = 390.0184 $[MH]^+$ (calc. for $C_{19}H_{13}MnNO_5$ = 390.0169); Elemental Analysis (CHN) C: 58.58% H: 3.23% N: 3.48% (calc.: C: 58.62% H: 3.11% N: 3.60%); IR (Solution: CH_2Cl_2):3237, 2120, 2076, 1991, 1976, 1933, 1605, 1587, 1479, 1273, 1257, 1081 cm^{-1}.

10.4.7 Synthesis of a biotin azide conjugate (70)

Synthesis of 3-azido-1-propylamine (67)[112, 148]

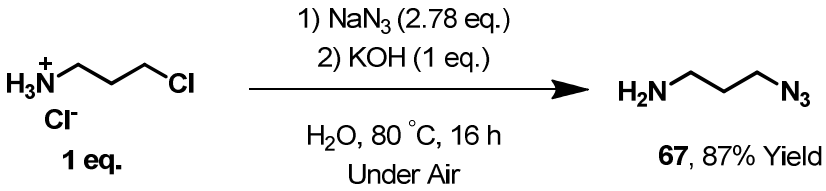

To a stirred solution of 3-chloropropylamine hydrochloride (1 eq., 4.31 mmol, 560 mg), dissolved in water (5 ml) was added NaN_3 (2.78 eq., 12.0 mmol, 840 mg), and the mixture heated to 80 °C. After 16 h, KOH pellets (1 eq.) were added to basify the solution, followed by extraction with diethyl ether (3 × 5 ml). The organic phase was dried with $MgSO_4$ and filtered. Removal of solvent under reduced pressure to gave pure product as a colourless oil (312 mg, 72% yield). Note: This molecule is volatile, and low pressure and temperature on a rotator evaporator is essential.

^{1}H NMR (400 MHz, $CDCl_3$) δ 3.33 (td, *J* = 6.8, 2.0 Hz, 1H), 2.76 (td, *J* = 6.8, 2.0 Hz, 1H), 1.68 (qnd, *J* = 6.8, 2.0 Hz, 1H), 1.39 (s, 2H); ^{13}C NMR (101 MHz, $CDCl_3$) δ 49.4, 39.5, 32.6; ESI-MS: *m/z* = 101.0822 $[MH]^+$ (Calc. for $N_4C_3H_9$ = 101.0822).

Safety in the Handling of Sodium Azide and other Azides

Sodium azide is toxic and can be absorbed through the skin. It decomposes explosively upon heating to above 275 °C. Sodium azide reacts vigorously with CS_2, bromine, nitric acid, dimethyl sulfate, and a series of heavy metals, including copper and lead. In reaction with water or Brønsted acids the highly toxic and explosive hydrogen azide is released. It has been reported that sodium azide and polymer-bound azide reagents form explosive di- and triazidomethane with CH_2Cl_2 and $CHCl_3$, respectively. Heavy-metal azides that are highly explosive under pressure or shock are formed when solutions of NaN_3 or HN_3 vapours come into contact with heavy metals or their salts. Heavy-metal azides can accumulate under certain circumstances, for example, in metal pipelines and on the metal components of diverse equipment (rotary evaporators, freeze drying equipment, cooling traps, water baths, waste pipes), and thus lead to violent explosions. Some organic and other covalent azides are classified as toxic and highly explosive, and appropriate safety measures must be taken at all times. **Plastic spatulas, clear seal glassware, and blast shields are highly important to ensure safe working conditions**.

Synthesis of Biotin-NHS (69)[119]

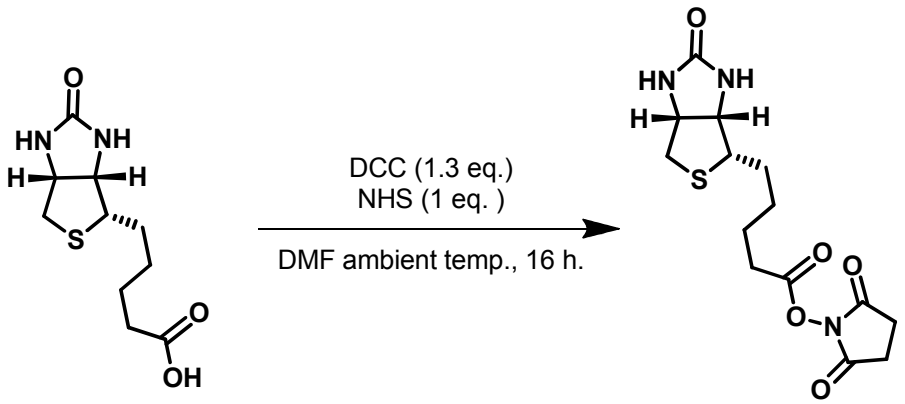

69, 91% Yield

d-Biotin (1 eq., 2.05 mmol, 0.5 g) and *N*-hydroxysuccinimide (1 eq., 2.05 mmol, 236 mg) were dissolved in hot DMF (15 ml) in a 50 ml round-bottom flask with stirring. *N,N*-dicyclohexylcarbodiimide (1.3 eq., 2.66 mmol, 0.55 g) was added, and the solution was stirred overnight at ambient temperature (20 °C), during which time a white precipitate formed. The reaction mixture was filtered, and the filtrate was evaporated and triturated with ether. The white precipitate obtained by trituration with Et_2O was filtered and washed with ether to give a white powder. (627 mg, 91% Yield).

^{1}H NMR (400 MHz, DMSO-d_6) δ 6.40 (s, 1H), 6.34 (s, 1H), 4.26 (dd, J = 7.5, 5.2 Hz, 1H), 4.10 (ddd, J = 7.5, 4.4, 1.7 Hz, 1H), 3.11–3.02 (m, 1H), 2.83–2.72 (m, 5H), 2.63 (t, J = 7.5 Hz, 2H), 2.54 (d, J = 12.4 Hz, 1H), 1.73–1.29 (m, 6H); ^{13}C NMR (101 MHz, DMSO-d_6) δ 170.8, 169.0, 163.0, 61.0, 59.2, 55.3, 33.4, 30.0, 27.8, 27.6, 25.5, 24.3. ESI-MS: m/z = 342.1122 $[MH]^+$ (Calc. for $C_{14}H_{20}N_3O_5S$ = 342.1118); Note: There are some small unknown impurities in this material. These do not affect the next step in any significant fashion. Pure material has been obtained in subsequent steps by using this material.

Synthesis of a biotin-azide-conjugate (70)

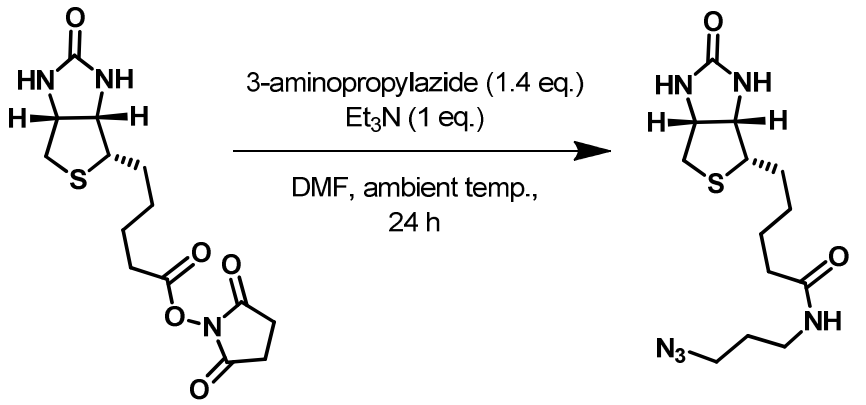

This experimental procedure is based on a modified literature procedure.[119]

Et_3N (1 eq., 0.879 mmol, 187 µL) was added to a solution of 3-aminopropylazide (1.4 eq., 1.23 mmol, 123.2 mg) in DMF (13 ml), followed by the addition of biotin-NHS (1 eq., 70 mg, 0.20 mmol) in DMF (9 ml). The resulting solution was stirred at room temperature for 24 h. The solvent was evaporated under reduced pressure. The crude residue was purified by flash chromatography (acetone/MeOH, 10:1) to give the desired biotin-azide-conjugate (220 mg, 0.674 mmol, 76 %) as an off white solid.

^{1}H NMR (400 MHz, MeOD-d_4) δ 4.49 (dd, *J* = 7.9, 4.5 Hz, 1H), 4.30 (dd, *J* = 7.9, 4.5 Hz, 1H), 3.36 (t, *J* = 6.9 Hz, 2H), 3.25 (t, *J* = 6.9 Hz, 2H), 3.23–3.18 (m, 1H), 2.93 (dd, *J* = 12.8, 5.0 Hz, 1H), 2.71 (d, *J* = 12.8 Hz, 1H), 2.21 (t, *J* = 7.5 Hz, 2H), 1.92–1.54 (m, 6H), 1.51–1.37 (m, 2H); ^{13}C NMR (101 MHz, MeOD-d_4) δ 176.2 ,166.1, 63.4, 61.6, 57.1, 50.2, 41.0, 37.7, 36.8, 29.80, 29.74, 29.5, 26.9; ESI-MS: *m/z* = 349.1411 $[MNa]^+$ (Calc. for $SO_2N_6C_{13}H_{22}Na$ = 349.1417).

10.4.8 Synthesis of CO-RMs via [3+2] cycloaddition chemistry

Synthesis of tetracarbonyl (2-[4-(([1-(4-carboxyphenyl)-1*H*-1,2,3-triazol-4-yl]methoxy)methyl)phenyl-κ,C^2]pyridine-κ,N) manganese(I) (65).

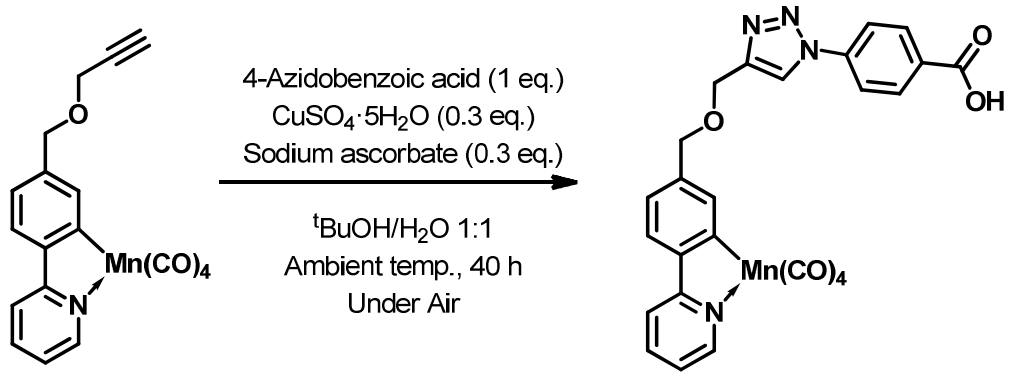

65, 98% Yield

This synthesis was carried out using a modified literature procedure.[111]

To an 8 ml screw sample vial equipped with a microwave stirrer bar was added **62** (1 eq., 0.116 mmol, 45 mg) followed by ^{t}BuOH (1.5 ml). The mixture was stirred for five minutes at ambient temperature. 4-azidobenzoic acid (1 eq., 0.115 mmol, 19 mg) was added to the reaction mixture followed by water (1.35 ml). $CuSO_4{\cdot}5H_2O$ (0.3 eq., 115 µl, 0.0348 mmol) was added to the mixture from a 0.3 M aqueous solution followed by sodium ascorbate (0.3 eq., 35 µl, 0.0348 mmol) from a 0.5 M aqueous solution. The vial was sealed with parafilm™ and the mixture was stirred in the dark for 40 h at ambient temperature. After 40 h, consumption of **63** was observed by TLC analysis. Water (10 ml) was added followed by 1 M HCl (until pH 1). The acidified aqueous layer was extracted with ethyl acetate (3 × 15 ml) and was dried with $MgSO_4$ and filtered. Removal of solvent under reduced pressure gave pure product as an off white solid (62 mg, 98% yield).

M.P. (DSC): 159 °C(decomposition);^{1}H NMR (700 MHz, DMSO-d_6) δ: 13.24 (s, 1H), 8.99 (s, 1H), 8.75 (d, *J* = 5.3 Hz, 1H), 8.23 (d, *J* = 8.1 Hz, 1H), 8.17–8.06 (m, 4H), 8.05–7.98 (m, 2H), 7.81 (s, 1H), 7.36 (t, *J* = 6.3 Hz, 1H), 7.19 (d, *J* = 7.9 Hz, 1H), 4.76 (s, 2H), 4.66 (s, 2H); ^{13}C NMR (176 MHz, DMSO-d_6) δ: 220.2, 214.6, 213.4, 172.4, 166.4, 164.7, 154.4, 145.7, 145.4, 139.8, 139.5, 139.1, 131.1, 130.6, 124.5, 123.8, 123.7, 122.5, 120.0, 119.8, 71.7, 63.0; ESI-MS: *m/z* = 553.0582 $[MH]^+$ (Calc. for $C_{26}H_{18}MnN_4O_7$ = 553.0550); Elemental Analysis (CHN) C: 56.56 % H:3.32% N:9.62 % (calc.: C: 56.53% H: 3.10% N: 10.14%); IR (Solution: CH_2Cl_2): 2075, 1991, 1976, 1932, 1733, 1699, 1695, 1607, 1586, 1093, 1042 cm^{-1}.

Synthesis of Biotin conjugate-CO-RM (71)

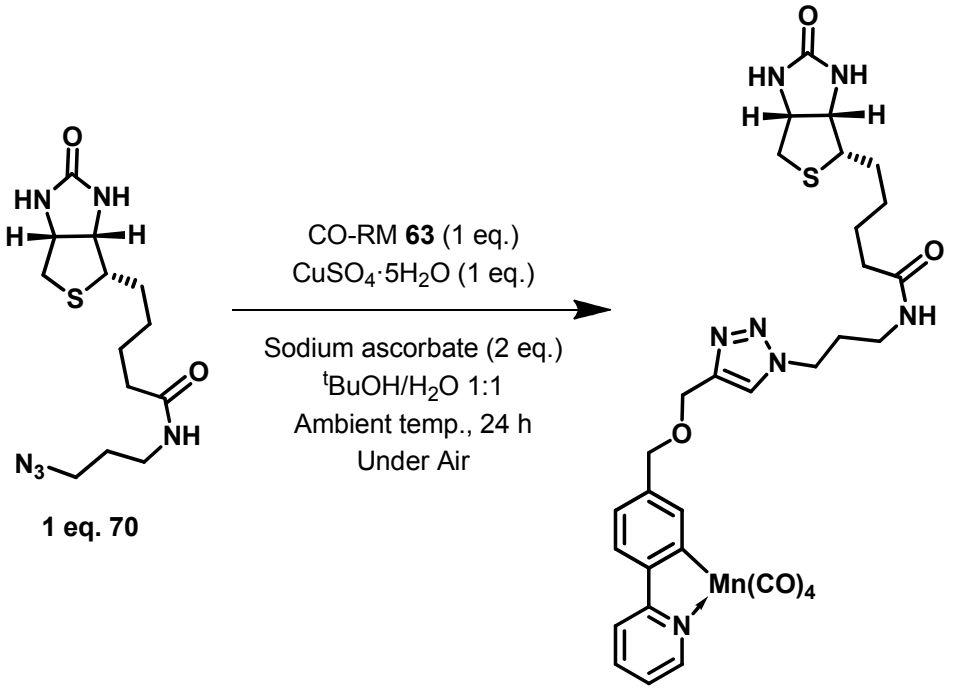

71, 72 or 50% Yield

This synthesis is based on a significantly modified literature procedure.[111]

To an 8 ml screw cap sample vial was added azide **70** (1 eq., 0.077 mmol, 25.1 mg), followed by CO-RM **63** (1 eq. 0.077 mmol, 30 mg). ^{t}BuOH (1.25 ml) was then added and the mixture was stirred with a magnetic flea to aid dissolution (complete dissolution will not occur). Water (840 µl) was then added followed by the addition of $CuSO_4 \cdot 5H_2O$ as a 0.3 M solution (1 eq., 0.077 mmol, 256 µl, 19.2 mg) and sodium ascorbate as a 1 M solution (2 eq., 0.154 mmol, 154 µl, 30.5 mg). The vial was closed and sealed with para-film™ and was stirred for 24 h at ambient temperature. TLC analysis at the end of this period showed the consumption of CO-RM **62** . The reaction mixture was diluted with EtOAc (5 ml) and was transferred to a separating funnel containing water (10 ml). The mixture was extracted with ethyl acetate (4 × 5 ml). The organic layer was dried with $MgSO_4$ and filtered. Removal of solvent under reduced pressure yielded pure product as an off white solid (40 mg, 0.056 mmol, 72% Yield).

M.P. (DSC): 75 °C (decomposition); ^{1}H NMR (400 MHz, MeOD-d_4) δ 8.77 (ddd, *J* = 5.6, 1.5, 0.7 Hz, 1H), 8.09 (apr. dt, *J* = 8.3, 1.2 Hz, 1H), 8.04 (s, 1H), 7.96-7.89 (m, 2H), 7.88 (d, *J* = 1.6 Hz, 1H), 7.26 (ddd, *J* = 7.2, 5.6, 1.3 Hz, 1H), 7.19 (dd, *J* = 8.0, 1.5 Hz, 1H), 4.72 (s, *J* = 1.9 Hz, 2H), 4.64 (s, *J* = 1.6 Hz, 2H), 4.51–4.40 (m, 3H), 4.28 (dd, *J* = 7.9, 4.5 Hz, 1H), 3.25–3.16 (m, 3H), 2.90 (dd, *J* = 12.7, 4.9 Hz, 1H), 2.68 (d, *J* = 12.7 Hz, 1H), 2.20 (t, *J* = 7.0 Hz, 2H), 2.11 (p, *J* = 7.0 Hz, 2H), 1.80-1.53 (m, 4H), 1.44 (m, 2H); ^{13}C NMR (700 MHz, MeOD-*d*$_4$) δ 221.6, 215.7,

215.0 176.3, 174.8,167.0, 155.4, 147.4, 145.8, 141.5, 140.8, 139.8, 125.5, 125.4, 125.2, 124.2, 120.8, 73.7, 64.2, 63.3, 61.6, 57.1, 49.2 (peak observed by ^{13}C DEPT-135 under solvent peak), 41.1, 37.3, 36.7, 31.1, 29.8, 29.4, 26.8; ESI-MS: *m/z* = 716.1677 $[MH]^+$ (calc. for $MnSO_7N_7C_{32}H_{35}$ = 716.1694); Elemental Analysis (CHN) C: 52.56 % H: 4.78% N: 12.42 % (calc.: C: 53.71% H: 4.79% N: 13.70%); IR (Solution: MeOH): 2075, 1992, 1977, 1936, 1681, 1653, 1605, 1588, 1567, 1333, 1313, 1269, 1231 cm^{-1}. Note: This reaction can also be performed using 0.5 eq., biotin azide **70** (0.00385 mmol, 12.6 mg) with everything else on the same scale using a reaction time of 48 h to give purer material. After work up as detailed previously, CO-RM **71** can be purified by silica gel column chromatography starting with 5% *(v/v)* $MeOH/CH_2Cl_2$ moving to 10% *(v/v)* $MeOH/CH_2Cl_2$. Removal of solvent under reduced pressure yielded pure product as yellow solid (14 mg, 0.00195 mmol 50% yield).

10.4.9 Synthesis of Amino acid containing Manganese Complexes

Synthesis of Tricarbonyl Acetonitrile (L-2-Amino-3-(1H-indol-3-yl)propanoic acid) Manganese[I] (L-**75**)

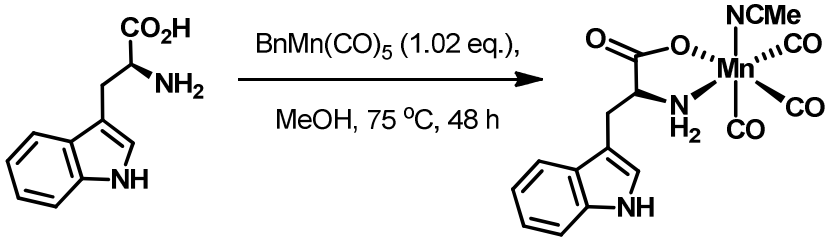

L-**75**, 82% Yield

An oven dried (130 °C) Schlenk tube equipped with a magnetic stirrer was evacuated and refilled with nitrogen three times. L-tryptophan (1 eq, 2.5 mmol, 511 mg), and $BnMn(CO)_5$ (1.02 eq, 2.55 mmol, 730 mg) were added to the Schlenk tube under a high flow of nitrogen. The two solids were then dried under vacuum for 30 mins. Under a high nitrogen flow, dry, deoxygenated methanol (50 ml) was added by cannula transfer. The mixture was heated to 75 °C with slow stirring due to the initial insolubility of tryptophan. The tube was then sealed with a hot condensing finger (to ensure the finger was dry before introduction to the flask) and was heated to 75 °C under a flow of nitrogen. Once reflux was achieved, the flask was sealed at the tap and heated at 75 °C for 48 h. Occasional periods of vigorous stirring for one minute were required to ensure all the tryptophan solid would dissolve and react. The mixture was allowed to cool to room temperature. The methanol was removed under reduced pressure in the Schlenk tube to leave a crude residue as a yellow solid. Dry CH_3CN (20 ml) was then added *via* syringe followed by dry hexane (40 ml). The solution was stirred for two minutes and the upper hexane layer was

removed by syringe. Two more portions of hexane (40 ml) were added to the Schlenk tube and were removed as described. Removal of CH_3CN under reduced pressure yielded a yellow solid. (820 mg, 82% Yield).

MP(DSC): 202 °C (decomposition) ; ^{1}H NMR (400 MHz, d_6-DMSO) δ 10.97 (broad s, 1H), 7.60 (broad s, 1H), 7.38 (broad, s, 1H), 7.24 (broad s, 1H), 7.12 (broad s, 1H), 7.02 (broad s, 1H), 5.63 (broad s ,NH_2 but exchange processes reduce integration, D_2O shake supports this), 2.10 (broad s ,3H). ^{13}C NMR (100 MHz, d_6-DMSO): 136.7, 128.1, 125.2, 121.4, 119.0 (broad s), 118.5, 111.9 (broad s), 1.6. Solid state ^{13}C NMR Direct excitation: (100 MHz) δ 220.2, 186.3, 137.1, 128.1, 120.3, 111.6, 1.3. Solid state ^{13}C NMR Cross polarisation: (100 MHz) δ 185.1, 136.7, 128.2, 109.0, 1.2. Elemental Analysis(CHN): C: 49.94% H: 3.64% N: 9.37% (Calculated containing 0.3 eq. of MeOH observed in ^{1}H NMR: C: 49.55% H: 3.79% N: 9.93%); ESI-MS *m/z* = 343.0118, $[M+H-MeCN]^+$(calc. for $MnC_{14}H_{12}N_2O_5$ = 343.0121), *m/z* = 384.0385, $[M+H]^+$ (calc. for $MnC_{16}H_{15}N_3O_5$ = 343.0387) IR (Solution: THF): 3281 (broad), 2028, 1922, 1897, 1599, 1454, 1180 cm^{-1} IR: (KBr disc): 3412, 3319, 3261, 2035, 1927, 1900, 1564, 1413 cm^{-1} IR: (Solution: MeOH): 2037, 1933, 1921, 1607 cm^{-1}. IR (Solution: CH_2Cl_2): 3680, 3465, 3343, 2253, 2032, 1929, 1906, 1606, 1418 cm^{-1}. $[\alpha]_D^{20}$: L isomer = –286.5 (*c=1,* DMSO), D isomer = $[\alpha]_D^{20}$ +248.2 (*c=1,* DMSO); UV/Vis (acetonitrile): λ_{max} (ε) = 272 (7505), 360 nm (1443 mol^{-1} dm^3 cm^{-1}).

Note: The D isomer used for CD measurements and $[\alpha]_D$ was made in same way but using D-tryptophan purchased from Sigma Aldrich. The DL racemate complex was made from a bought DL-tryptophan racemate. The $[\alpha]_D$ measurements taken above match the starting enantiopurities of the bought starting materials.

Details from EPSRC National Solid-state NMR Service at Durham for Complex L-75

The complex gives much broader lines than free tryptophan. Two spectra were recorded, a CP experiment with interrupted decoupling and a DE experiment. This should only give signals from quaternary (and methyl) carbons. There is a signal at 185 ppm from the acid group, up from 176/178 ppm in the free tryptophan ligand. The other three quaternaries are at 109, 128 and 137 ppm. The CO signal is just visible but it is clearer in the direct excitation spectrum. In the DE experiment, there is the signal at 1 ppm due to the co-ordinated acetonitrile. There is an extensive manifold of spinning sidebands, centred at 220 ppm, from the CO carbons. It is not possible to resolve individual CO lines it is not possible to tell whether these groups are all the same but IR spectroscopy confirms the presence of three carbonyls. In principle, the carbon will be coupled to the manganese which would result in a multiplet or more likely just broadening of the signal. The extensive sideband manifold, and the fact that the centreband has a lower intensity than the first high-frequency sideband, is typical of an M-C≡O environment.

Synthesis of the Mohr Histidine complex[78] (21)

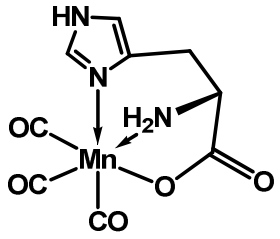

This complex was prepared exactly as reported in the literature. 50:50 MeCN-d_3/D_2O shifts the resonance of the residual solvents. The ^{1}H NMR was referenced to the peak at 7.99 ppm which appears in the literature data as the water peak shifts significantly due to a mixed solvent combination. Referencing this peak to 7.99 ppm matches all the other peaks with the literature NMR spectrum.

MP(DSC): decomp. above 250°C; ^{1}H NMR (400 MHz, d_3-MeCN/D_2O) δ 7.99 (broad s, 1H), 6.99 (broad s, 1H), 3.78 (broad, s, 1H), 3.00 (broad s, 2H), ESI-MS *m/z* = 293.9911, $[M+H]^+$ (calc. for $MnC_9H_9N_3O_5$ = 293.9917), *m/z* = 315.9733, $[M+Na]^+$ (calc. for $MnC_9H_8N_3O_5Na$ = 315.9733). IR (Solution: CH_3OH): 2031, 1925, 1917, 1613 cm^{-1}.

10.4.10 Synthesis of an azo dye based Manganese(I) complex

Synthesis of 4-[(*E*)-1,3-benzothiazol-2-yldiazenyl]-*N*,*N*-diethylaniline (76)

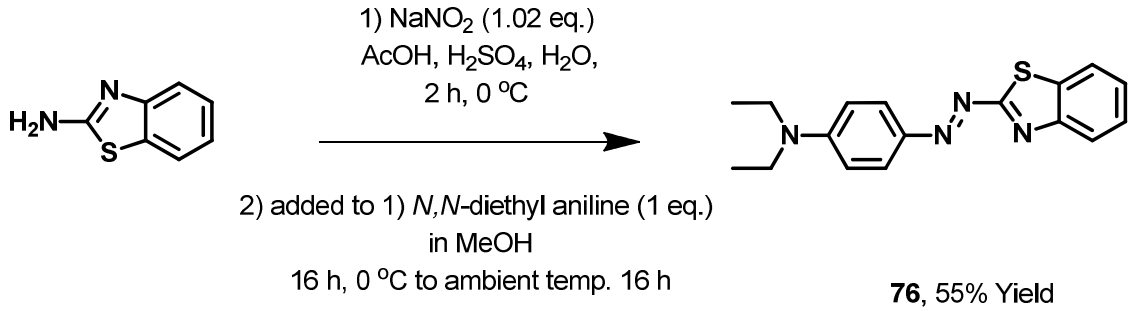

Note: 2-aminobenzathiazole was distilled using Kugelrohr apparatus prior to use (93 °C /1 Torr).

This synthesis is based on a modified literature procedure with an alternative workup.[135]

To acetic acid (6 ml) was added 2-aminobenzathiazole (1 eq., 1 mmol, 150 mg) and concentrated sulfuric acid (2 ml). $NaNO_2$ (1.02 eq., 1 mmol, 70 mg) in water (3 ml) was then added to the sulfuric acid solution and stirred for 2 hours at 0 °C during which an orange colour develops. *N,N*-diethylaniline (1 eq., 1 mmol, 149 mg/81 µl) was then added in methanol (10 ml) to the diazonium salt solution and the solution goes a dark blue. The solution was stirred and was allowed to warm up to ambient temp. (25 °C) and then was stirred for a further 16 h. Ethyl acetate (50 ml) and water (50 ml) was added to the aqueous layer in a separating funnel. 2M $NaOH_{(aq)}$ was then added until a significant amount of the bright red product goes in to the organic ethyl acetate layer. The aqueous layer was then extracted with more ethyl acetate (2 × 50 ml). The organic layer was washed with brine (50 ml) and was dried with $MgSO_4$ and subsequently filtered. The solvent was removed under reduced pressure to yield crude product as a dark powder. The product was purified by silica gel column chromatography by dry loading onto silica with CH_2Cl_2 and eluting with Ethyl acetate using a gradient from 15:85 to 40:60 (*v/v*) EtOAc: PET ether. Removal of solvent under reduced pressure yielded pure product as a dark crystalline solid (170 mg, 55% Yield).

Note: The large volumes of extraction solvent were used to enable visualisation of the layers in the separation due to strong absorption from the product.

^{1}H NMR (400 MHz, $CDCl_3$) δ 8.06 (dd, *J* = 8.0, 0.5 Hz, 1H), 7.96 (d, *J* = 9.3 Hz, 2H), 7.82 (dd, *J* = 8.0, 0.5 Hz, 1H), 7.45 (apr. t, *J* = 8.0 Hz, 1H), 7.36 (apr. t, *J* = 8.0 Hz, 1H), 6.71 (d, *J* = 9.3 Hz, 2H), 3.46 (q, *J* = 7.1 Hz, 4H), 1.23 (t, *J* = 7.1 Hz, 6H). ^{13}C NMR (101 MHz, $CDCl_3$) δ 177.9, 153.1, 152.6, 142.8, 134.3, 128.2(broad), 126.4, 126.2, 124.1, 122.3, 111.7, 45.3, 13.0. ESI-MS:

m/z = 311.1310 $[MH]^+$ (Calc. for $C_{17}H_{19}N_4S$ = 311.1325); Elemental Analysis (CHN) C: 65.60% H: 5.79% N: 17.94% (calc.: C: 65.78 % H: 5.84 % N: 18.05%);

Synthesis of dye-containing CO-RM (77)

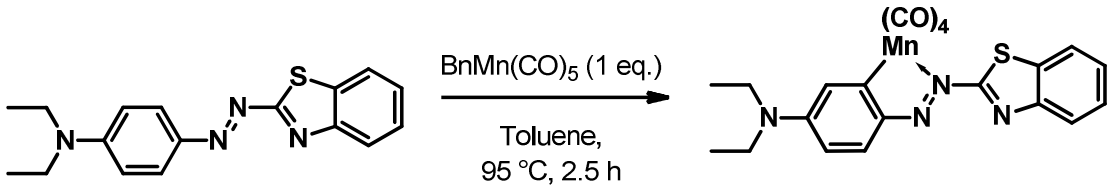

77, 5% Yield

Azodye **76** (1 eq., 0.5 mmol, 155 mg) and $BnMn(CO)_5$ (1 eq., 0.5 mmol, 143 mg) were added to a dry Schlenk tube under a flow of nitrogen. The reagents were dried under vacuum for 15 mins. Toluene (8 ml) was added *via* syringe. The mixture was heated to 95 °C, and on reaching temperature the Schlenk tube was sealed. The mixture was heated for a further 2.5 h. On cooling to room temperature the solvent was removed under reduced pressure to yield crude product. The crude mixture was purified by silica gel column chromatography by loading the crude mixture on to a minimum amount of silica with CH_2Cl_2. The product was eluted from the column using a gradient from 15:85 to 35:65 (*v/v*) Et_2O/petroleum ether (all with 0.5% Et_3N). The product was isolated as a purple solid (12 mg, 5% yield).

^1H NMR (400 MHz, CD_2Cl_2) δ 8.03 (d, *J* = 9.0 Hz, 1H), 7.87 (d, *J* = 8.0 Hz, 1H), 7.75 (d, *J* = 8.0 Hz, 1H), 7.47 (d, *J* = 2.5 Hz, 1H), 7.41 (apr.t, *J* = 7.5 Hz, 1H), 7.30 (apr.t, *J* = 7.5 Hz, 1H), 6.74 (dd, *J* = 9.0, 2.5 Hz, 1H), 3.62 (q, *J* = 7.0 Hz, 4H), 1.34 (t, *J* = 7.0 Hz, 6H); ^{13}C NMR (101 MHz, CD_2Cl_2) δ 195.2, 175.7, 156.1, 151.8, 150.5, 137.0, 134.4, 126.1, 125.0, 122.8, 122.0, 121.4, 112.5, 45.7, 12.8.; ESI-MS: *m/z* = 477.0401 $[MH]^+$ (calc. for $C_{21}H_{18}N_4O_4SMn$ = 477.0424); IR (Solution: CH_2Cl_2): 2076, 1990, 1942, 1603, 1581, 1386, 1338, 1297, 1210 cm^{-1}.

10.5 Biological general experimental details

10.5.1 Eukaryotic Cell Viability Assay details

Culturing RAW 264.7 cells from a liquid nitrogen stock.

Work with RAW 264.7 cells with was carried out in a category II laminar flow hood apart from when incubating the cells.

TOX 7 and TOX 8 kits were purchased from Sigma Aldrich and were used as directed below for Alamar blue and LDH Assays.

A 1 ml stock containing RAW 264.7 Cells using a 10% DMSO/ Media mixture was partially thawed and was added to 10 ml of fresh DMEM media containing 10% heat inactivated FCS, 2 mM L-glutamine, 100 units ml^{-1} penicillin and 0.1 mg ml^{-1} streptomycin . The cells were pelleted by centrifuging at 1200 rpm for 5 minutes. The pellet was re-suspended in 10 ml of complete medium. This was then transferred to a T-25 flask and was incubated at 37 °C under a 5% CO_2 atmosphere until confluent.

Passaging the cells

The media in the flask was disposed of and the cells were washed with 10 ml of 1x PBS pH 7.2. 10 ml of fresh media was added and the cells were re-suspended in the media using a plastic cell scraper. It is important to be gentle at this stage. 2 ml of the cell suspension was added to a new T-25 cell flask and 8 ml of fresh media was added and the cells were incubated as before. The remaining 8 ml of cell suspension could be used for cell studies. Cells were not used in studies further than 10 passages to prevent false results due to mutation/contamination.

Culturing cells in a 24 well plate

The cells from the 8 ml suspension described previously were counted using a haemocytometer and approximately 5×10^5 cells were added to each well. The total volume of media in each well was 1 ml. The cells were incubated at 37 °C overnight and were 80-90% confluent the next day.

Addition of CO-RM to cell culture in a 24 well plate.

The media from overnight culture was replaced with 1 ml of fresh medium. The compound of interest was dissolved in DMSO at a concentration 200 times the final required value. 5 µl of this solution was then added to each well to provide the correct concentration. The cells were incubated overnight.

Culturing cells in a 96 well plate

The cells from the 8 ml suspension described previously were counted using a haemocytometer and approximately 5×10^4 cells were added to each well. The total volume of media in each well was 200 µl. The cells were incubated at 37 °C overnight and were 80-90% confluent the next day.

Addition of CO-RM to cell culture in a 96 well plate.

The compound of interest was dissolved in DMSO at a concentrated 200 times the required value. 5 µl of this solution was then added to 1 ml of media in a 2 ml Eppendorf. This was shaken and 200 µ of the CO-RM /media solution was added to each well. The old media was removed from each well before addition. The cells were incubated overnight with the CO-RM solution.

Alamar blue assay in a 24 well plate.

After incubation with the CO-RM, the media from each well was removed and was replaced with 1 ml of a 10% Alamar blue (Sigma Aldrich)/90% complete media mixture. The cells were then incubated for 4 hours at 37 °C. 200 µl of the media was then transferred to a flat bottomed 96 well plate and was read on a plate reader at 570 nm with a background subtraction at 630 nm. Results were expressed as a percentage scaled between the difference in absorbance of a 1% Triton-X-114 control (dead cells) and a live control with no compound.

Alamar blue assay in a 96 well plate.

After incubation with the CO-RM, the media from each well was removed and was replaced with 220 µl of a 10% Alamar blue (Sigma Aldrich) / 90% complete media mixture. The cells were then incubated for 6 hours at 37 °C. 200 µl of the media was then transferred to a flat bottomed 96 well plate and bubbles were popped with a needle. The plate was read on a plate reader at 570 nm with a background subtraction at 630 nm. Results were expressed as a percentage scaled between the difference in absorbance of a 1% triton-X-114 control (dead cells) and a live control with no compound.

LDH assay in a 24 well plate

After incubation with the CO-RM. 50 µl of supernatant was removed from each well and was added to a flat bottomed 96 well plate. 100 µl of LDH reaction mixture (Sigma Aldrich) was then added to each well across the plate using a multi-channel pipette (this is essential to ensure comparable absorbances). The plate was protected from light and after 30 minutes 15 µl of 1M HCl was added to each well with a multi-channel pipette. Any bubbles were popped with a needle and the plate was read on a plate reader at 490 nm with a background subtraction at 630

nm. Results were expressed as a percentage scaled between the difference in absorbance of a 1% triton-X-114 control (dead cells) and a live control with no compound. Blank media was also ran in this assay and the absorbance from this was subtracted from all wells.

LDH assay in a 96 well plate

After incubation with the CO-RM. The plate with the cells was centrifuged at 500 rpm for 5 minutes. 50 µl of supernatant was removed from each well and was added to a flat bottomed 96 well plate. 100 µl of LDH reaction mixture (Sigma Aldrich) was then added to each well across the plate using a multi-channel pipette (this is desirable to ensure comparable absorbances).All bubbles were popped swith a needle and the plate was read over time at 490 nm (subtraction at 630 nm) until the absorbance of the 1% triton control reached at least 1.6. This will stop the reaction from going too far and enable the detection of low concentrations LDH. The results were expressed as a percentage scaled between the difference in absorbance of a 1% Triton-X-114 control (dead cells) and a live control with no compound. Blank media was also used in this assay and the absorbance from this was subtracted from all wells.

10.5.2 Nitric Oxide quantification: Greiss Assay Details

A Greiss reagent system was purchased from Promega™ and was used as directed.

50 µl of medium after overnight incubation with 50 µM CO-RMs **47** and L-**75** both in the presence and absence of LPS (100 ng ml^{-1}) and IFN-γ (25 U ml^{-1}) was taken and analysed in the Greiss assay as directed by the kit instructions.

10.5.3 Prokaryotic Cell Experiment Details

10.5.3.1 E.coli W3110 cells: experimental details

All culture work was carried out under sterile conditions working close to a gas burner flame.

Plating out cells

50:50 glycerol/LB media stocks of *E.coli W3110* were streaked with a loop on to LB agar plates and grown at 37 °C overnight. The plates were then stored at 4 °C and samples were used within one month.

Liquid medium culture for growth curves

Bacteria were transferred from the plates grown previously to LB media to give a stock solution of *E. coli* with an OD_{600} 10 times that of the required starting OD for the experiments. 2.7 ml of media was added to 8 ml plastic bijou tubes. DMSO (15 µl) was then added for the controls. The CO-RM was also added to the tubes in the same volume of DMSO at 200 times the required concentration (i.e 20 mM dilutes to 100 µM). 300 µl of *E. coli* stock solution was then added to the 2.7 ml CO-RM/media solutions to give a 3 ml culture volume. The cultures were then grown at 37 °C rotating at 100 rpm on an orbital shaker and OD measurements were typically taken every hour.

OD measurements were taken at 600 nm on a Jenway 6305 spectrophotometer. Measurements were taken with 300 µl aliquots in Eppendorf UVette® disposable cuvettes. The cuvettes were elevated by 3 mm in the sample holder to ensure the beam passed through the liquid correctly. Samples were shaken gently in the cuvettes immediately before measuring to ensure a homogeneous cell distribution. If the OD_{600} was expected to go over 0.8, all the samples at that time point were diluted by two to keep the OD/bacterial relationship linear.

Procedure for irradiation of culture under sterile conditions

The white sterile attachment shown in **Figure 171** was stored in ethanol and was wiped dry and immediately placed close to the Bunsen burner flame.

A 300 µl aliquot was taken from the sample and the lid was then replaced with the dry sterile attachment. The LED cap was then attached and the vials were wrapped in foil and were incubated with 100 rpm rotation.

The irradiation was then started with each LED typically drawing a current of 200 mA and therefore a power of 2.4 W. Irradiation was delivered in 4 mins on, 1 min off cycles to prevent the LED from overheating. Irradiation in these experiments was typically carried out for a total of 68 mins (17 full cycles). 34 minutes of this irradiation was done between 1 and 2 h. Another 34 mins was delivered between 2 and 3 h. This was to allow for hourly OD measurements to be taken. After irradiation was complete the sterile attachment was replaced with a new bijou tube lid and aliquots for OD measurements were then taken out as normal for the rest of the experiment.

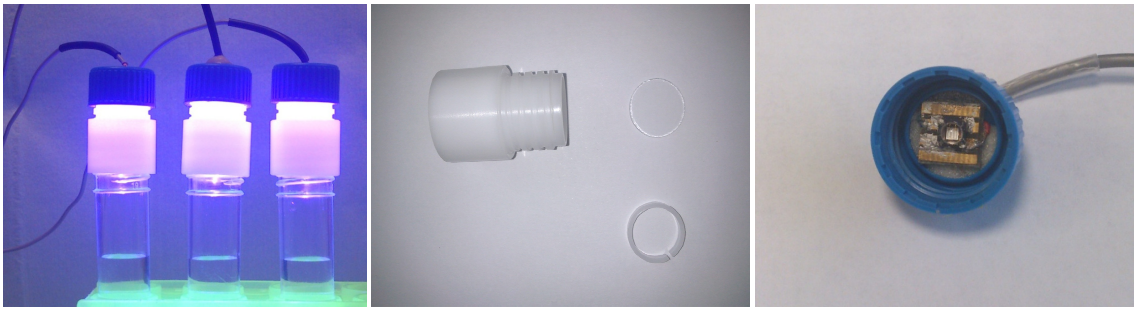

Figure 171. Left: full setup with irradiation going down. Middle: Sterile attachment with glass window. Right: 400 nm LED mounted in Falcon tube cap.

Procedure for the assessment of *E. coli* cell viability.

300 µl aliquots were taken at 0 h and 4 h during a new experiment. These time points represent before and after irradiation in the presence of 100 µM CO-RM and DMSO. These aliquots were then diluted by 50×, 500×, 5000× and 50000×. 50 µl of each dilution was then spread on to LB agar plates and were incubated at 37 °C overnight. Bacterial colonies were then counted. The age of the bacteria refers to the time the bacteria were stored on an LB agar plate in a 4°C room under ambient light before use.

10.5.3.2 Procedure alterations for work with S. aureus 8325-4

S. aureus was also treated with CO-RMs in the same way as *E. coli* W3110. However plates from viability studies with dilution were incubated overnight plus a further 24 h due to slower colony growth. All colonies that will actually grow on plain LB agar plates can be seen after the 40h-48h incubation. Lower dilutions are typically required in plating studies at the same OD compared to *E. coli* to get sensible colony numbers per plate.

Some initial studies were also carried out with CO-RM **9a** within set LB agar plates. The CO-RM was added to the medium at 40 °C before setting to reduce degradation. The plates were then stored in the dark at 4 °C prior to use. DMSO control plates were also made and stored in the same way.

10.5.3.3 Procedure alterations for work with *N. gonorrhoeae* MS11

N. gonorrhoeae was stored in 50% MH medium/glycerol stocks and was grown on Columbia agar plates with 5% defibrinated horse blood. The horse blood was added to warm melted Columbia agar (50 °C) to keep the cells intact before setting. Stocks of *N. gonorrhoeae* were plated out and grown at 37 °C under 5% CO_2 for 40 h to give sufficient numbers of bacteria to work with. Plates were used within four days of plating out stocks.

N. gonorrhoeae was either grown in RPMI medium or BHI medium with a yeast autolysate supplement. The supplement powder was dissolved in 15 ml sterile water and 1.5 ml liquid supplement was added to 50 ml of medium. RPMI medium already contains 20 mM Na_2CO_3 as a CO_2 source, where as 10 mM Na_2CO_3 is added to BHI medium *via* a 1M stock solution.

DMSO and CO-RM was added to the culture as done previously. After incubation the culture was diluted out and grown on plates for viability studies. Plates were grown for 40-48 h to ensure that all colonies could be seen by eye.

In most experiments only two sets of dilutions were chosen to reduce the time at non optimal growth conditions. These were chosen based on the starting OD to give sensible numbers of colonies to count.

10.5.4 LegHb expression, extraction and purification

A Leghaemoglobin DNA sequence from a soya bean plant was expressed in *E. coli* BL21 using a high copy number plasmid with an ampicillin resistance gene. From a −80 °C stock in 50/50 LB media/glycerol, *E. coli* was grown up overnight at 37 °C on an LB agar plate with 100 μg ml^{-1} ampicillin (added to liquid agar at 50 °C before setting). A single colony was transferred to 5 ml of LB media with 100 μg ml^{-1} ampicillin in a Sterilin™ tube. This was grown at 37°C on an orbital shaker with 225 rpm rotation for 6 hours.

The 5 ml culture was then transferred to 635 ml of auto induction medium in a 2 L baffled conical flask, which consists of the following:

1. ZY media (590 ml)
2. 20× NPS (31 ml)
3. 50×52 (12.5 ml)
4. 1M $MgSO_4$ (630 μl)
5. 100 mg ml^{-1} ampicillin (630 μl)
6. 1000× metals (630 μl)

Stocks of each of these reagents are made up of the following:

1. 5.99 g tryptone, 2.95 g yeast extract, 590 ml H_2O.
2. 33 g NH_4SO_4, 68g K_2HPO_4, 500 ml H_2O.
3. 25 g glycerol, 2.5 g glucose, 10 g α-lactose, 100 ml H_2O.
4. 12.04 g $MgSO_4$ in 100 ml.
5. 200 mg ampicillin sodium salt, 2ml H_2O.

6. 50 mM $FeCl_3$, 20 mM $CaCl_2$, 10 mM $MnCl_2$, 10 mM $ZnSO_4$, 2 mM $CoCl_2$, 2 mM $CuCl_2$, 2 mM $NiCl_2$, 2 mM Na_2MoO_4, 2 mM Na2SeO3, 2 mM H_3BO_3 in 60 mM HCl.

The culture in auto induction medium was grown at 37 °C overnight with shaking at 120 rpm. The culture which was now thick and dark in colour, was centrifuged at 5000 rpm for 15 mins at 4 °C. The medium was discarded from the red pellet of cells which was subsequently resuspended in 35 ml 50mM Tris Buffer pH 9. The suspension of cells was then sonicated in a 50 ml Falcon™ tube on ice using a standard probe with sonication for 10s/10s on/off cycles for a total sonication time of 3 minutes.

Cell debris was then removed by two centrifugation cycles at 11000 rpm for 15 minutes (4 °C). Liquid was transferred to a new Falcon™ after the first centrifugation to remove most of the debris.

The Protein was purified on a 1.5 cm diameter anionic exchange column using DEAE sepharose CL6B. The protein was loaded on to the column and was washed with 50mM Tris pH 9 until the red band indicative of the protein was running very close to the bottom of the column. The protein was then fully eluted using a gradient starting with 30 mM NaCl and 20 mM K_2HPO_4 moving to 500mM NaCl. 5 ml eluent fractions were taken and the protein typically eluted in fractions 5–12.

Purity of the protein was checked using an in-house 15% polyacrylamide SDS page gel using a set current of 400 mA.

Upon confirming sufficient purity, the protein solution was concentrated 10 fold using a Vivaspin 20 MWCO (PES) 5,000 Falcon ™ tube. The resultant protein solution was desalted by diluting 10 fold with 10 mM Tris pH 7.4 and concentrating the new solution with the Vivaspin tube 10 fold. This dilution with Tris buffer was performed once more to dilute any salt in the solution by a total 100 fold.

The protein was divided in to aliquots and was stored at −20 °C and was used within two months of preparation.

The concentration of the protein was determined by UV/visible spectroscopy using a literature molar extinction coefficient for Ferrous-Lb of 13000 mol^{-1} dm^3 cm^{-1} (555 nm).[127]

10.6 General X-ray Diffraction details and data

10.6.1 Details of general procedure from X-ray diffraction service

Diffraction data wascollected at 110 K on an Oxford Diffraction SuperNova diffractometer with Mo-K_a radiation (l = 0.71073 Å) using a EOS CCD camera. The crystal was cooled with an Oxford Instruments Cryojet. Diffractometer control, data collection, initial unit cell determination, frame integration and unit-cell refinement was carried out with "Crysalis". Face-indexed absorption corrections were applied using spherical harmonics, implemented in SCALE3 ABSPACK scaling algorithm. OLEX2 was used for overall structure solution, refinement and publication data. Within OLEX2, the algorithm used for structure solution was Superflip, refinement by full-matrix least-squares used theSHELXL-97. All non-hydrogen atoms were refined anisotropically. Hydrogen atoms were placed using a "riding model" and included in the refinement at calculated positions.

10.6.1.1 X-ray Crystal Structure Data and Images

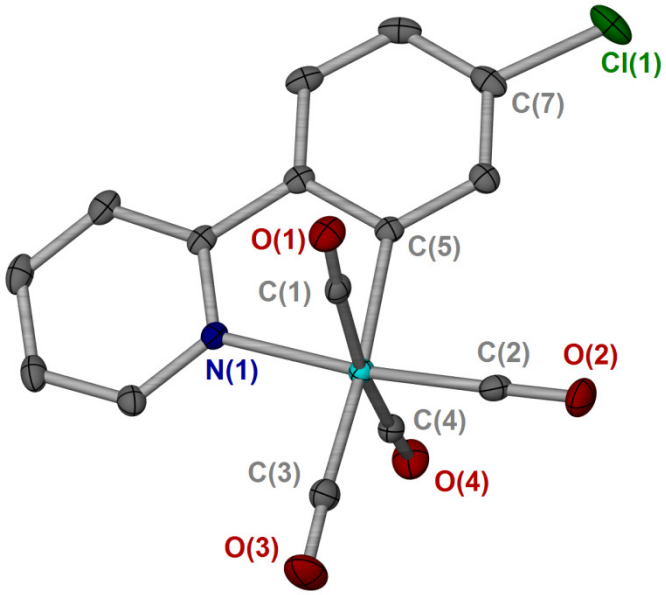

Figure 172. X-ray crystal structure of complex **39**. Atoms displayed as ellipsoids at 50% probability. Hydrogen atoms omitted for clarity. Crystallised from CH_2Cl_2/Hexane. Selected bond lengths (Å) and angles(°):Mn(1)-C(1) = 1.8530(16) , Mn(1)-N(1) = 2.0569(13), Mn(1)-C(2) = 1.7999(13), Mn(1)-C(3) = 1.8318(17), Mn(1)-C(4) = 1.8624(16), Mn(1)-C(5) = 2.0412(16); C(5)-Mn(1)-C(3) = 175.23(7), C(1)-Mn(1)-N(1) = 90.21(6), C(3)-Mn(1)-C(2) = 90.94(7), C(2)-Mn(1)-N(1) = 173.07(6), C(3)-Mn(1)-N(1) =95.98(6) , C(4)-Mn(1)-N(1) =88.22(6), N(1)-Mn(1)-C(5) = 79.54(6)

Table 33. Crystal data and structure refinement for complex **39**

Identification code	ijsf1224
Empirical formula	$C_{15}H_7NO_4ClMn$
Formula weight	355.61
Temperature/K	110.00(10)
Crystal system	monoclinic
Space group	$P2_1/c$
a/Å	10.1290(4)
b/Å	10.2171(2)
c/Å	13.7629(3)
α/°	90.00
β/°	101.871(3)
γ/°	90.00
Volume/Å^3	1393.86(6)
Z	4
ρ_{calc}mg/mm^3	1.695
m/mm^{-1}	1.155
F(000)	712.0
Crystal size/mm^3	0.2648 × 0.1908 × 0.03
2Θ range for data collection	5.72 to 64.18°
Index ranges	$-14 \leq h \leq 9$, $-14 \leq k \leq 14$, $-20 \leq l \leq 19$
Reflections collected	8831
Independent reflections	4427[R(int) = 0.0235]
Data/restraints/parameters	4427/0/199
Goodness-of-fit on F^2	1.052
Final R indexes [I>=2σ (I)]	R_1 = 0.0338, wR_2 = 0.0767
Final R indexes [all data]	R_1 = 0.0452, wR_2 = 0.0842
Largest diff. peak/hole / e Å^{-3}	0.48/-0.34

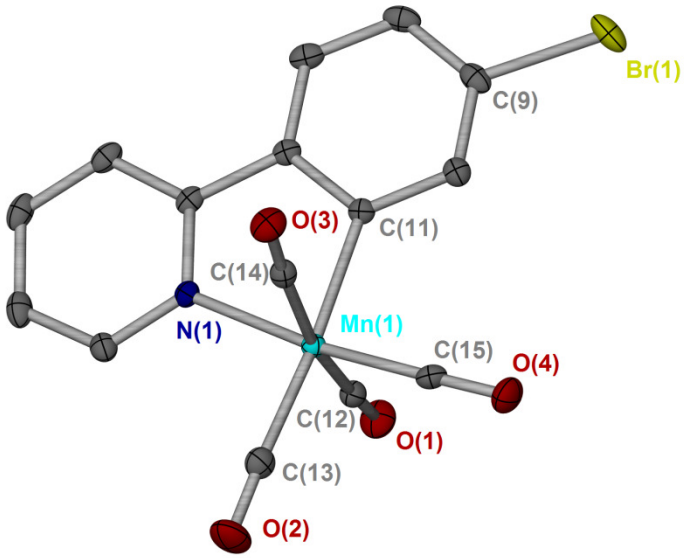

Figure 173. X-ray crystal structure of complex **40**. Atoms displayed as ellipsoids at 50% probability. Hydrogen atoms omitted for clarity. Crystallised from CH_2Cl_2/Hexane. Selected bond lengths (Å) and angles(°):Mn(1)-C(11) = 2.0477(17) , Mn(1)-N(1) = 2.0638(14), Mn(1)-C(15) = 1.8007(18), Mn(1)-C(12) = 1.8642(19), Mn(1)-C(13) = 1.8401(19), Mn(1)-C(14) = 1.8544(19); C(14)-Mn(1)-C(12) = 168.51(8), C(13)-Mn(1)-C(12) = 95.58(8), C(11)-Mn(1)-C(15) = 93.25(7), (13)-Mn(1)-N(1) =96.04(7), C(15)-Mn(1)-N(1) = 172.80(7), C(14)-Mn(1)-N(1) =90.03(7) , C(12)-Mn(1)-N(1) =88.03(7), N(1)-Mn(1)-C(11) = 79.55(6)

Table 34. Crystal data and structure refinement for complex **40**

Identification code	ijsf1123
Empirical formula	$C_{15}H_7NO_4MnBr$
Formula weight	400.07
Temperature/K	110.00(10)
Crystal system	monoclinic
Space group	$P2_1/c$
a/Å	10.2503(2)
b/Å	10.2194(2)
c/Å	13.8964(2)
α/°	90.00
β/°	100.7783(16)
γ/°	90.00
Volume/Å^3	1430.00(5)
Z	4
ρ_{calc}mg/mm^3	1.858
m/mm^{-1}	3.733
F(000)	784.0
Crystal size/mm^3	0.2326 × 0.2016 × 0.1628
2Θ range for data collection	5.68 to 64°
Index ranges	$-13 \leq h \leq 14$, $-7 \leq k \leq 14$, $-12 \leq l \leq 20$
Reflections collected	7682
Independent reflections	4528[R(int) = 0.0211]
Data/restraints/parameters	4528/0/199
Goodness-of-fit on F^2	1.056
Final R indexes [I>=2σ (I)]	R_1 = 0.0303, wR_2 = 0.0658
Final R indexes [all data]	R_1 = 0.0407, wR_2 = 0.0701
Largest diff. peak/hole / e Å^{-3}	0.53/-0.48

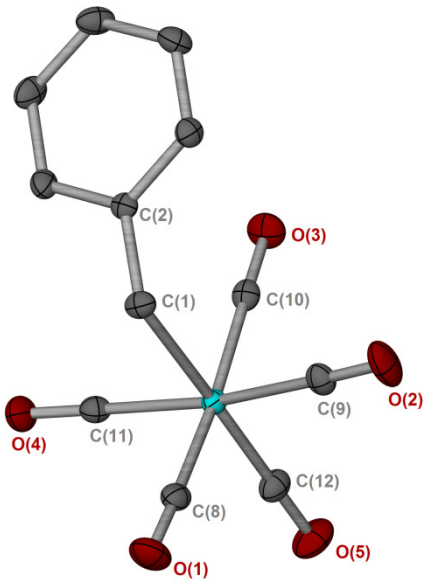

Figure 174. X-ray crystal structure of $BnMn(CO)_5$ (**42**)**.** Atoms displayed as ellipsoids at 50% probability. Hydrogen atoms omitted for clarity. Crystals obtained by sublimation. Selected bond lengths (Å) and angles(°):Mn(1)-C(1) = 2.2071(13) , Mn(1)-C(8) = 1.8483(14), Mn(1)-C(9) = 1.8501(14), Mn(1)-C(10) = 1.8720(14), Mn(1)-C(11) = 1.8514(14), Mn(1)-C(12) = 1.8292(15); C(1)-Mn(1)-C(12) = 177.78(6), C(1)-Mn(1)-C(11) = 84.58(6), C(1)-Mn(1)-C(10) = 88.93(5), C(1)-Mn(1)-C(9) =84.52(7), C(10)-Mn(1)-C(8) = 173.01(7), C(11)-Mn(1)-C(9) =169.06(6) , C(8)-Mn(1)-C(11) =89.15(6), Mn(1)-C(8)-O(1) = 178.16(13).

Table 35. Crystal data and structure refinement for complex **42**

Identification code	ijsf1229a
Empirical formula	$C_{12}H_7O_5Mn$
Formula weight	286.12
Temperature/K	109.95(10)
Crystal system	monoclinic
Space group	$P2_1/n$
a/Å	6.9018(3)
b/Å	6.5722(3)
c/Å	27.1897(13)
α/°	90.00
β/°	96.969(4)
γ/°	90.00
Volume/Å^3	1224.21(9)
Z	4
ρ_{calc}mg/mm^3	1.552
m/mm^{-1}	1.086
F(000)	576.0
Crystal size/mm^3	0.1428 × 0.1377 × 0.0636
2Θ range for data collection	5.96 to 60.04°
Index ranges	$-9 \leq h \leq 9$, $-9 \leq k \leq 9$, $-38 \leq l \leq 36$
Reflections collected	10916
Independent reflections	3583[R(int) = 0.0278]
Data/restraints/parameters	3583/0/163
Goodness-of-fit on F^2	1.076
Final R indexes [I>=2σ (I)]	R_1 = 0.0297, wR_2 = 0.0691
Final R indexes [all data]	R_1 = 0.0342, wR_2 = 0.0717
Largest diff. peak/hole / e Å^{-3}	0.37/-0.36

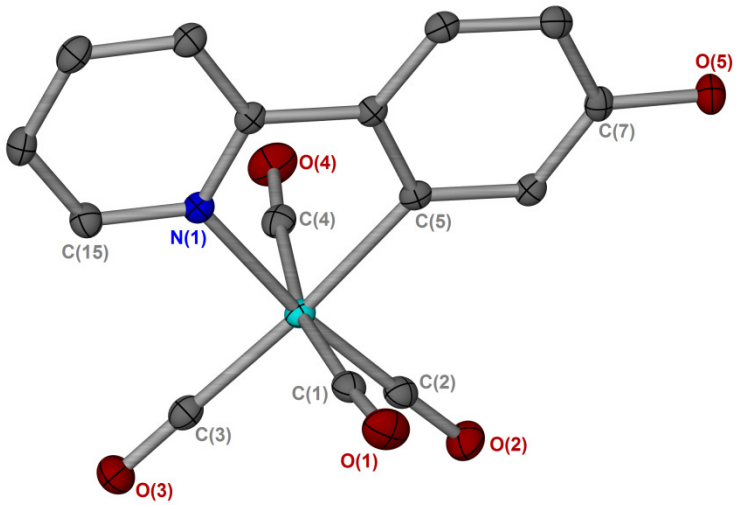

Figure 175. X-ray crystal structure of complex **64**. Atoms displayed as ellipsoids at 50% probability. Hydrogen atoms omitted for clarity. Crystallised from CH_2Cl_2/Hexane. Selected bond lengths (Å) and angles(°):Mn(1)-C(1) = 1.8459(17) , Mn(1)-N(1) = 2.0678(12), Mn(1)-C(2) = 1.8053(16), Mn(1)-C(3) = 1.8389(16), Mn(1)-C(4) = 1.8565(19), Mn(1)-C(5) = 2.0431(14); C(5)-Mn(1)-C(3) = 174.25(6), C(3)-Mn(1)-C(2) = 91.73(7), C(1)-Mn(1)-N(1) = 90.73(6), C(2)-Mn(1)-N(1) = 173.20(6), C(3)-Mn(1)-N(1) =96.89(7) , C(4)-Mn(1)-N(1) = 90.09(6), N(1)-Mn(1)-C(5) = 79.41(5).

Table 36. Crystal data and structure refinement for **64**

Identification code	ijsf1223
Empirical formula	$C_{15}H_8MnNO_5$
Formula weight	337.16
Temperature/K	110.00(10)
Crystal system	monoclinic
Space group	$P2_1/c$
a/Å	8.6436(3)
b/Å	6.9498(3)
c/Å	22.1788(8)
α/°	90.00
β/°	91.922(3)
γ/°	90.00
Volume/Å^3	1331.54(9)
Z	4
ρ_{calc}mg/mm^3	1.682
m/mm^{-1}	1.015
F(000)	680.0
Crystal size/mm^3	0.2531 × 0.2374 × 0.0543
2Θ range for data collection	5.88 to 60.06°
Index ranges	$-9 \leq h \leq 12$, $-9 \leq k \leq 9$, $-31 \leq l \leq 21$
Reflections collected	7330
Independent reflections	3892[R(int) = 0.0206]
Data/restraints/parameters	3892/0/203
Goodness-of-fit on F^2	1.053
Final R indexes [I>=2σ (I)]	$R_1 = 0.0321$, $wR_2 = 0.0748$
Final R indexes [all data]	$R_1 = 0.0372$, $wR_2 = 0.0776$
Largest diff. peak/hole / e Å^{-3}	0.43/-0.33

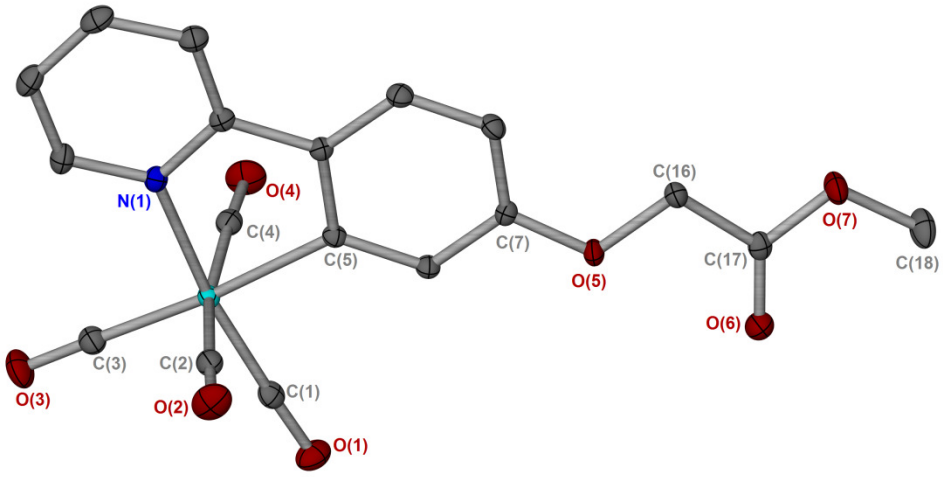

Figure 176. X-ray crystal structure of complex **45**. Atoms displayed as ellipsoids at 50% probability. Hydrogen atoms omitted for clarity. Crystallised from CH_2Cl_2/Hexane. Selected bond lengths (Å) and angles(°):Mn(1)-N(1) = 2.0672(11) , Mn(1)-C(1) = 1.8148(14), Mn(1)-C(2) = 1.8660(14), Mn(1)-C(3) = 1.8263(14), Mn(1)-C(4) = 1.8527(14), Mn(1)-C(5) = 2.0528(13); N(1)-Mn(1)-C(1) = 172.00(5), N(1)-Mn(1)-C(2) = 88.23(5), N(1)-Mn(1)-C(3) = 95.30(5), N(1)-Mn(1)-C(4) =90.38(5), N(1)-Mn(1)-C(5) = 80.08(5), C(2)-Mn(1)-C(4) =169.52(6) , C(1)-Mn(1)-C(3) =92.67(6).

Table 37. Crystal data and structure refinement for **45**

Identification code	ijsf1124
Empirical formula	$C_{18}H_{12}NO_7Mn$
Formula weight	409.23
Temperature/K	110.00(10)
Crystal system	triclinic
Space group	P-1
a/Å	7.0000(4)
b/Å	11.2458(6)
c/Å	12.1356(8)
α/°	67.181(6)
β/°	83.042(5)
γ/°	86.381(4)
Volume/Å^3	873.93(9)
Z	2
ρ_{calc}mg/mm^3	1.555
m/mm^{-1}	0.797
F(000)	416.0
Crystal size/mm^3	0.2161 × 0.1857 × 0.0987
2Θ range for data collection	5.86 to 64.52°
Index ranges	$-9 \leq h \leq 9$, $-15 \leq k \leq 16$, $-18 \leq l \leq 17$
Reflections collected	9348
Independent reflections	5500[R(int) = 0.0247]
Data/restraints/parameters	5500/0/245
Goodness-of-fit on F^2	1.062
Final R indexes [I>=2σ (I)]	R_1 = 0.0322, wR_2 = 0.0796
Final R indexes [all data]	R_1 = 0.0371, wR_2 = 0.0831
Largest diff. peak/hole / e Å^{-3}	0.48/-0.42

Appendix 1

^{1}H NMR spectra of prepared compounds

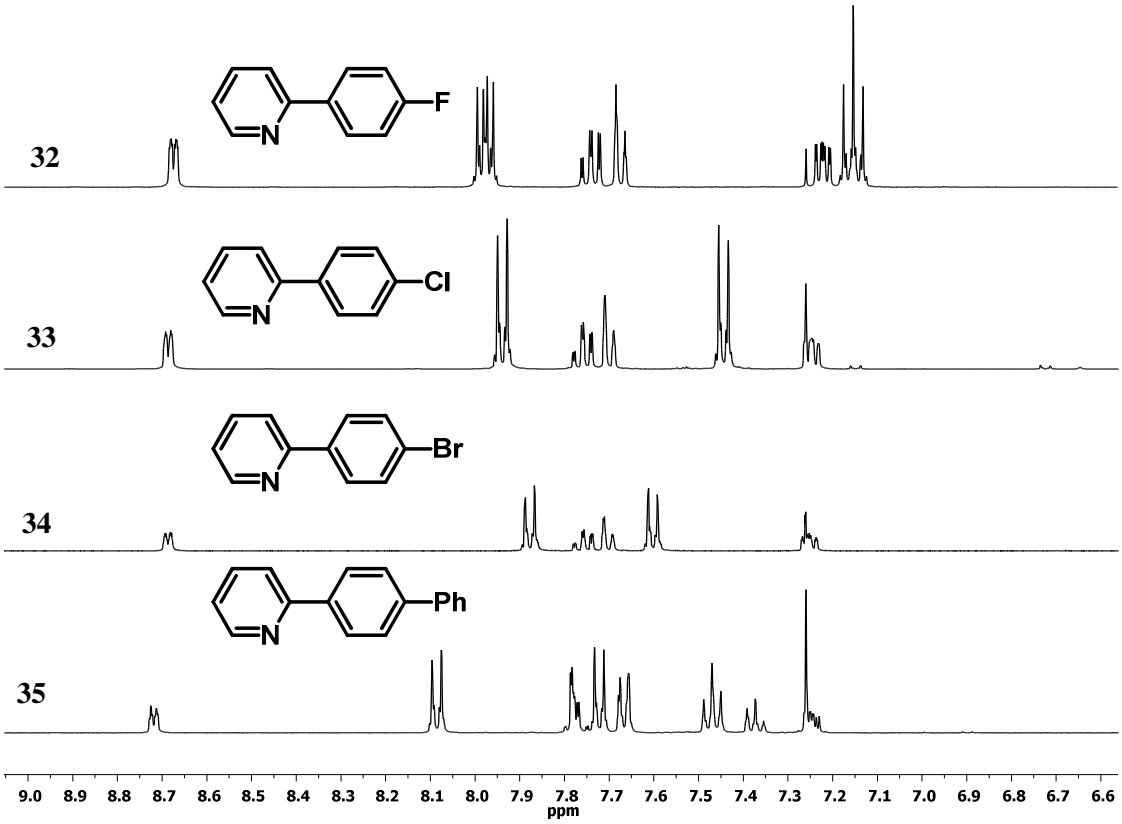

Figure A1. 400 MHz ^{1}H NMR spectra of phenylpyridine ligands **32-35** in $CDCl_3$ at 300 K.

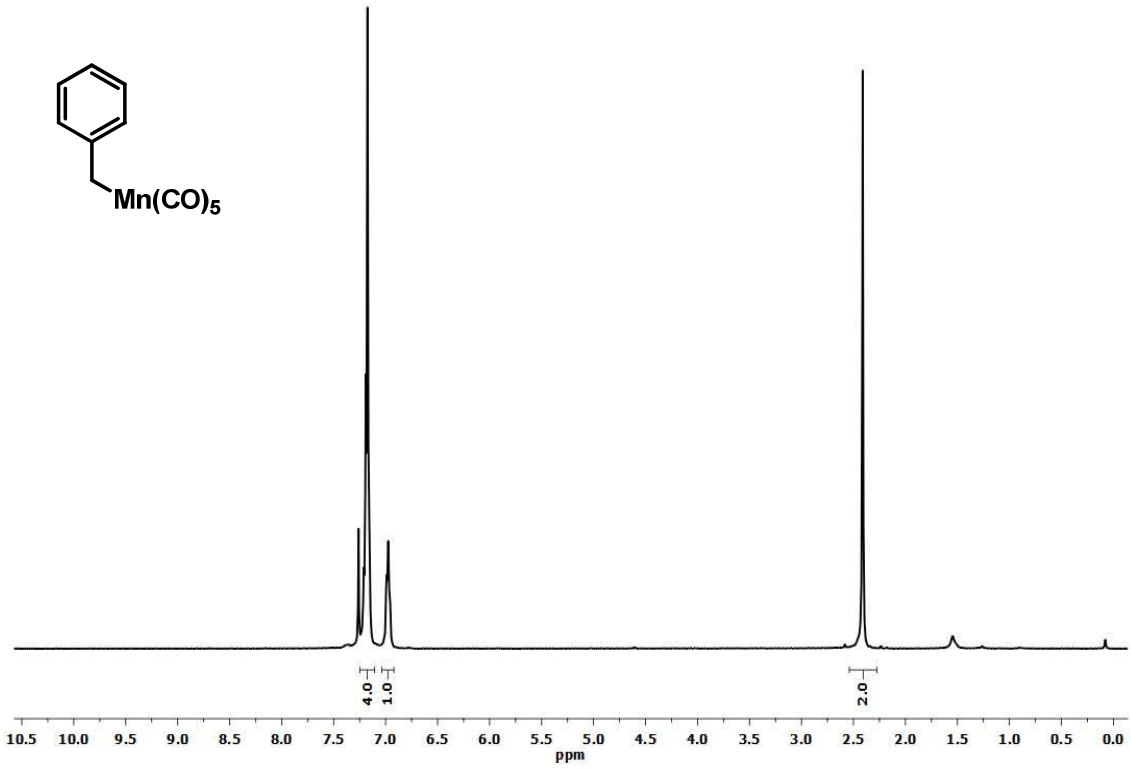

Figure A2. 400 MHz ^{1}H NMR spectra of $BnMn(CO)_5$ (**42**) in $CDCl_3$ at 300 K.

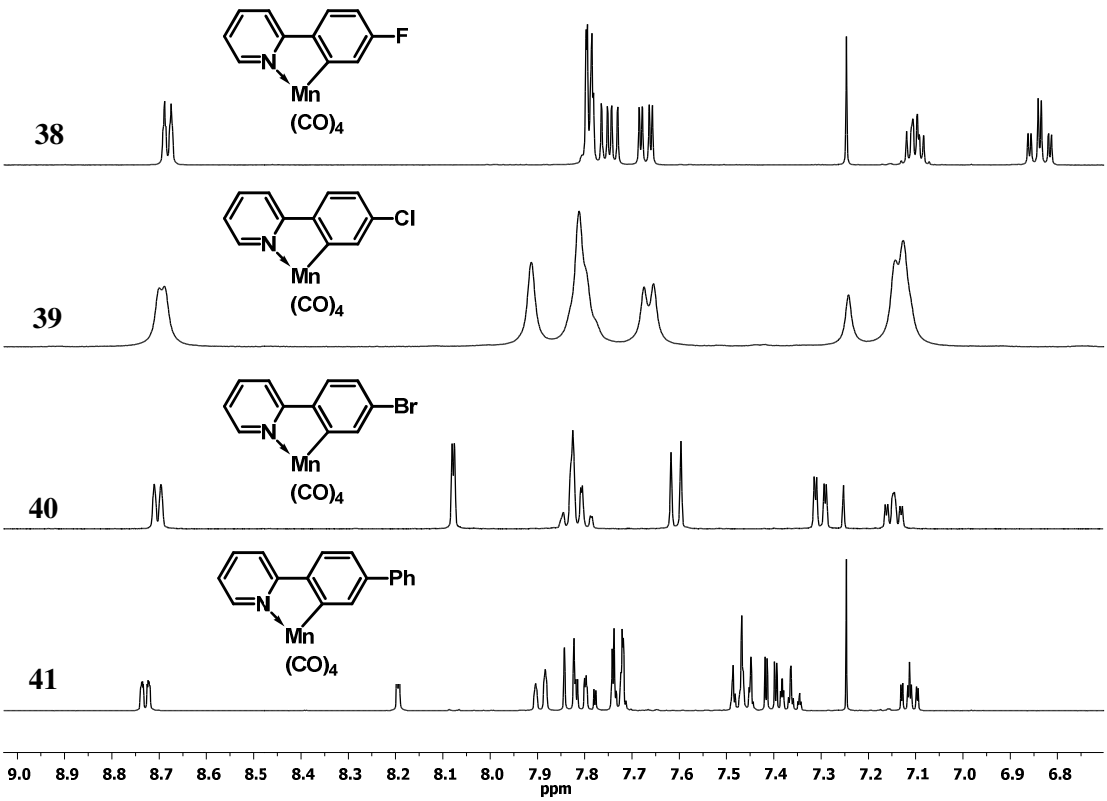

Figure A3. 400 MHz ^{1}H NMR spectra of manganese(**I**) complexes **38-41** in $CDCl_3$ at 300 K

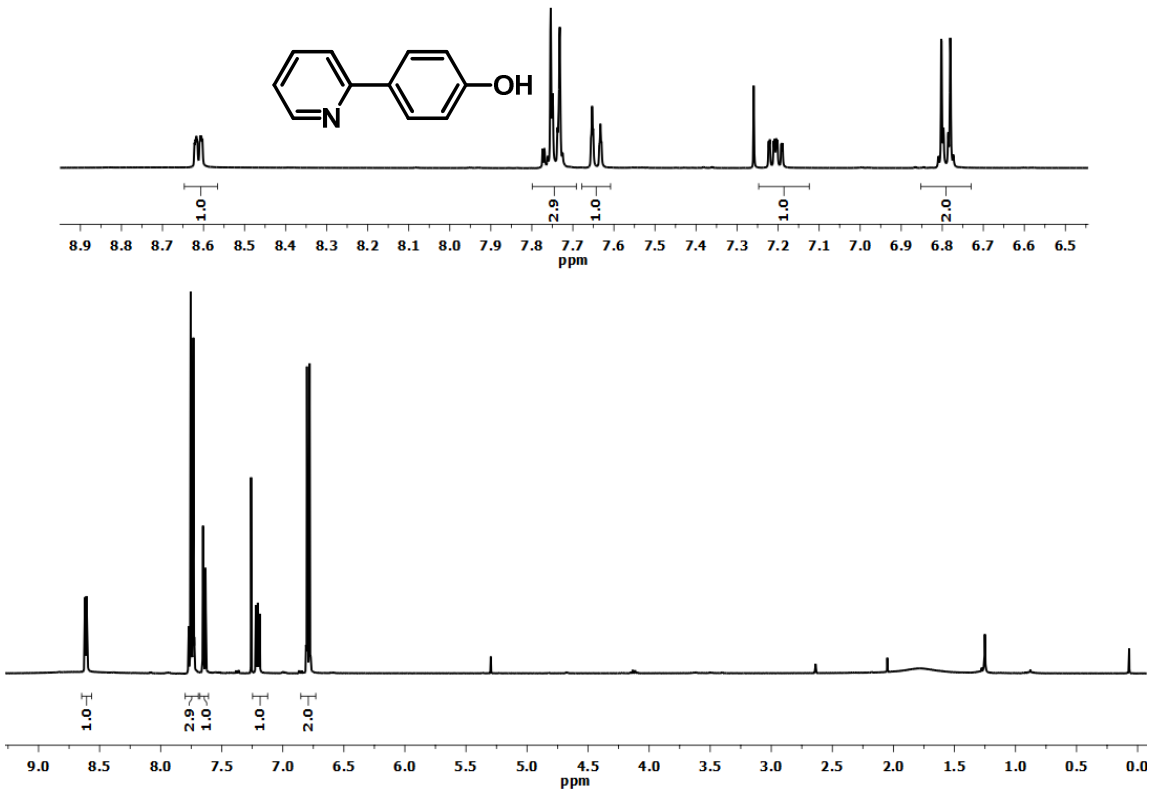

Figure A4. ^{1}H NMR spectrum of 2(4-hydroxyphenyl)pyridine(**43**) in $CDCl_3$ at 300 K

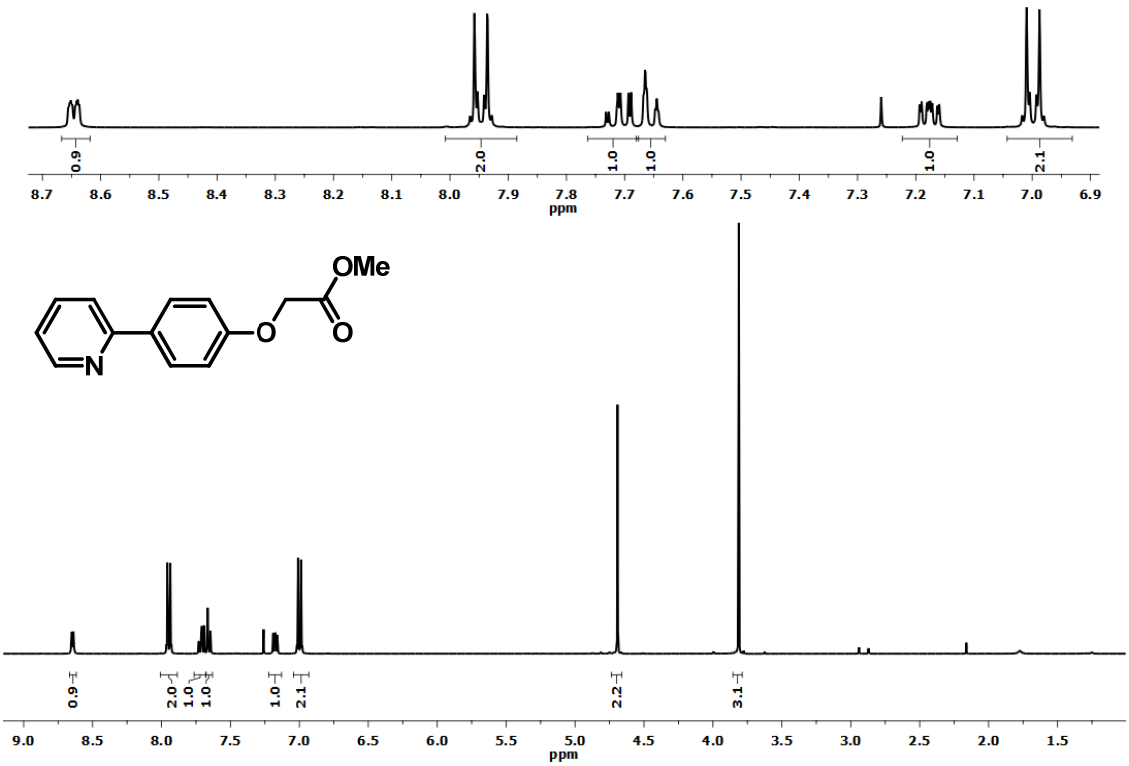

Figure A5. 400 MHz ^{1}H NMR spectrum of methyl [4-(pyridin-2-yl)phenoxy]acetate (**44**) in $CDCl_3$ at 300 K

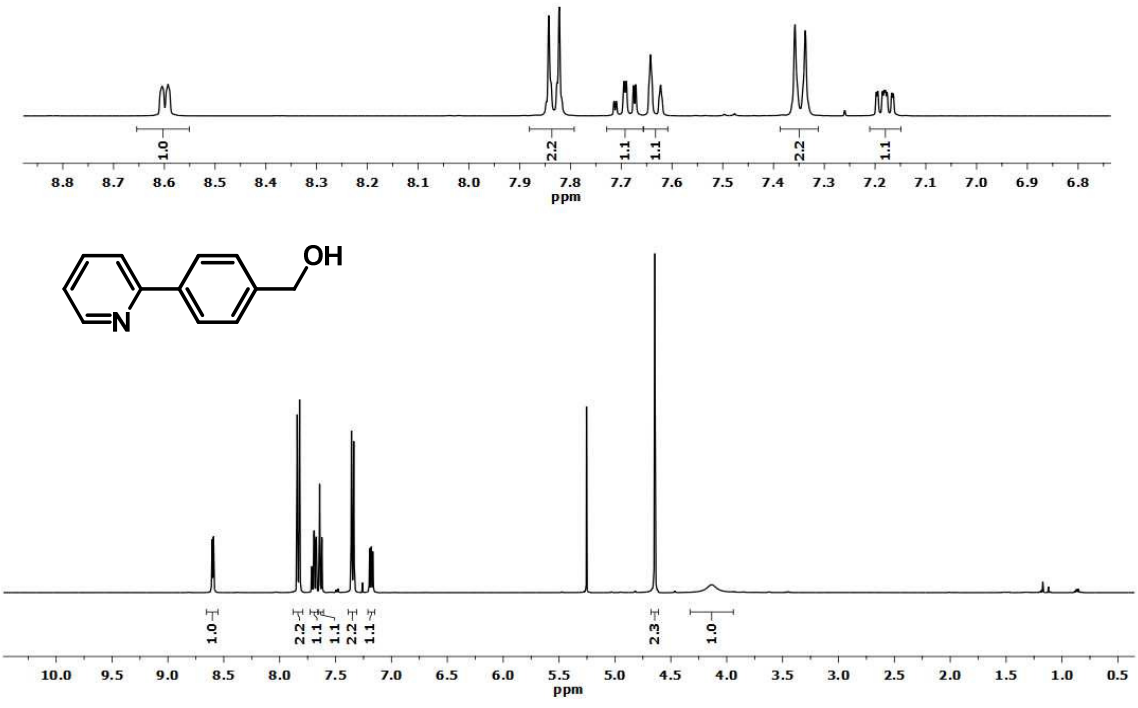

Figure A6.400 MHz ^{1}H NMR spectrum of 2-(4-hydroxymethyl-phenyl)pyridine (**50**) in $CDCl_3$ at 300 K

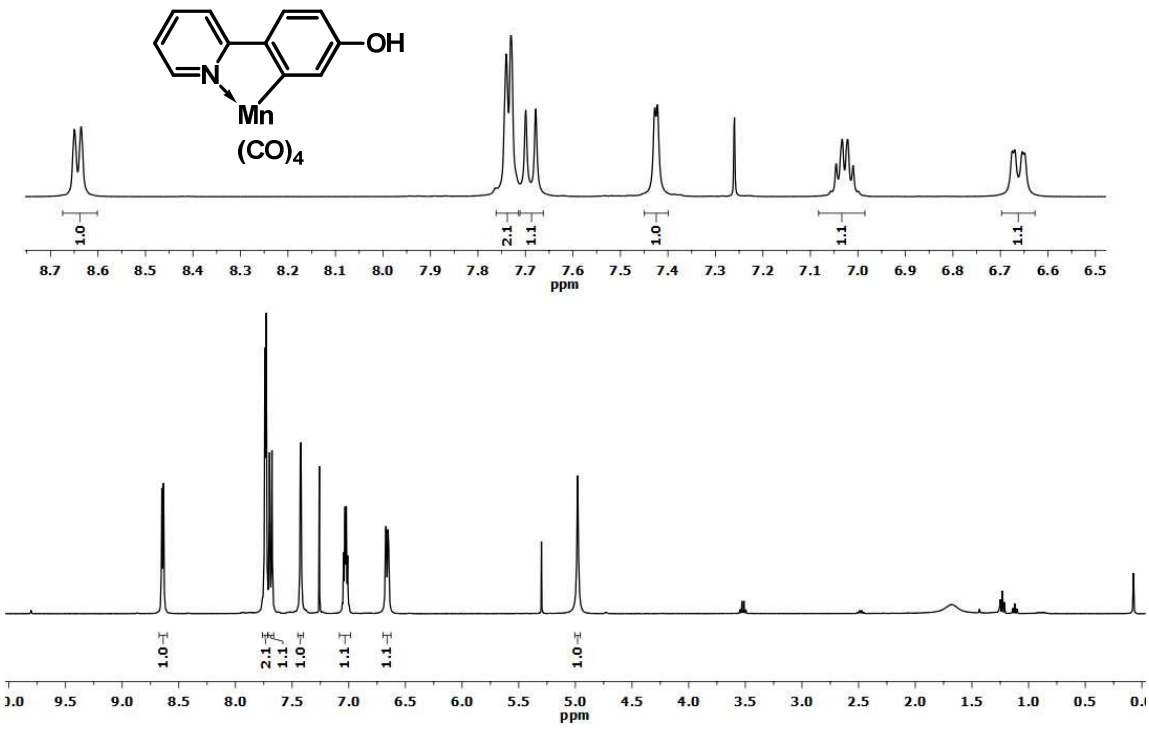

Figure A7. ^{1}H NMR spectrum of tetracarbonyl (2-(4-hydroxyphenyl)κ,C_2-pyridine-κ,N) manganese(I) (**64**) in $CDCl_3$ at 300 K.

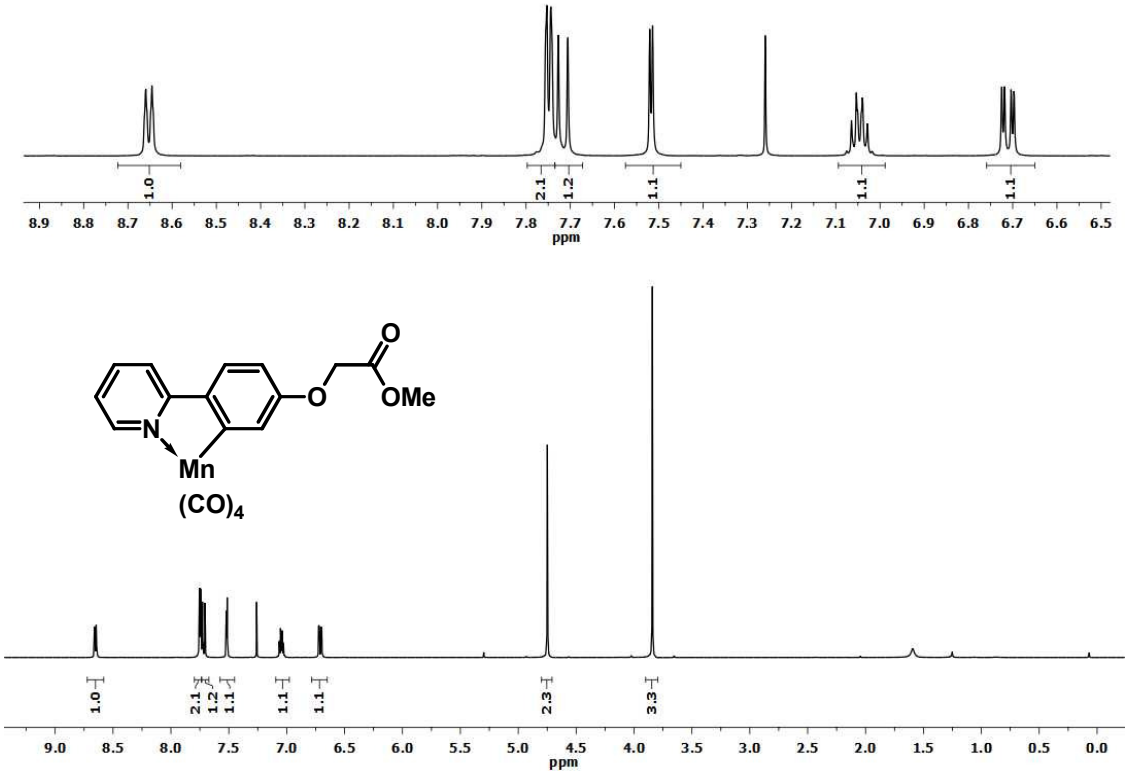

Figure A8. ^{1}H NMR spectrum of tetracarbonyl (methyl [4-(pyridin-2-yl-κ,N)phen-κ,C^{2}-oxy]acetate) manganese(I) (**45**) in $CDCl_3$ at 300 K.

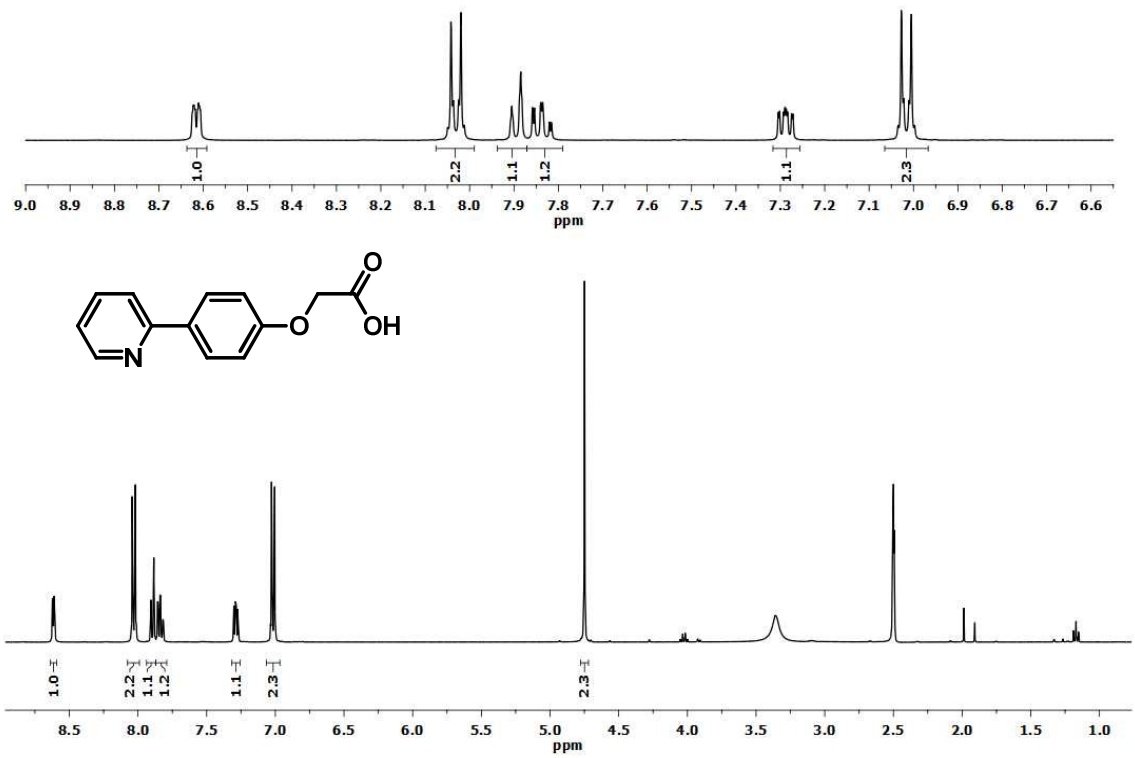

Figure A9. ^{1}H NMR spectrum of methyl [4-(pyridin-2-yl)phenoxy]acetic acid (**46**) in DMSO-d_6 at 300 K.

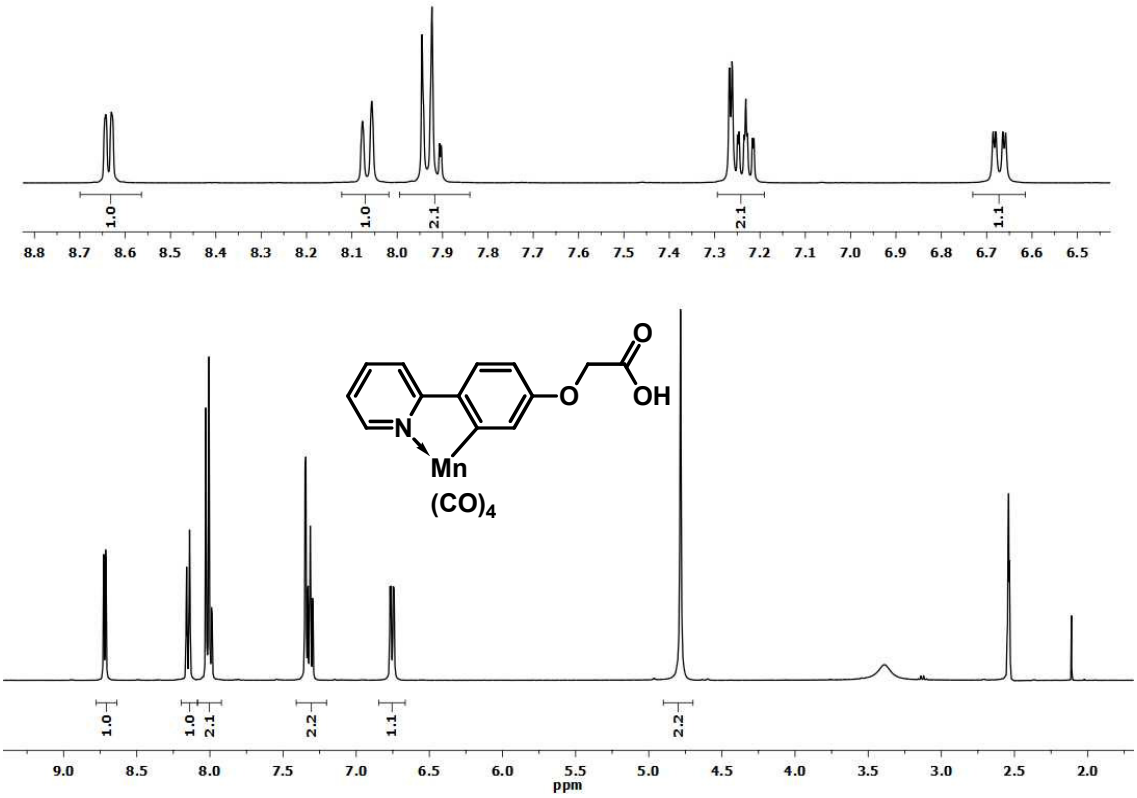

Figure A10. ^{1}H NMR spectrum of methyl tetracarbonyl (methyl [4-(pyridin-2-yl-κ,N)phen-κ,C^{2}-oxy]acetic acid) manganese(I) (**47**) in DMSO-d_6 at 300 K.

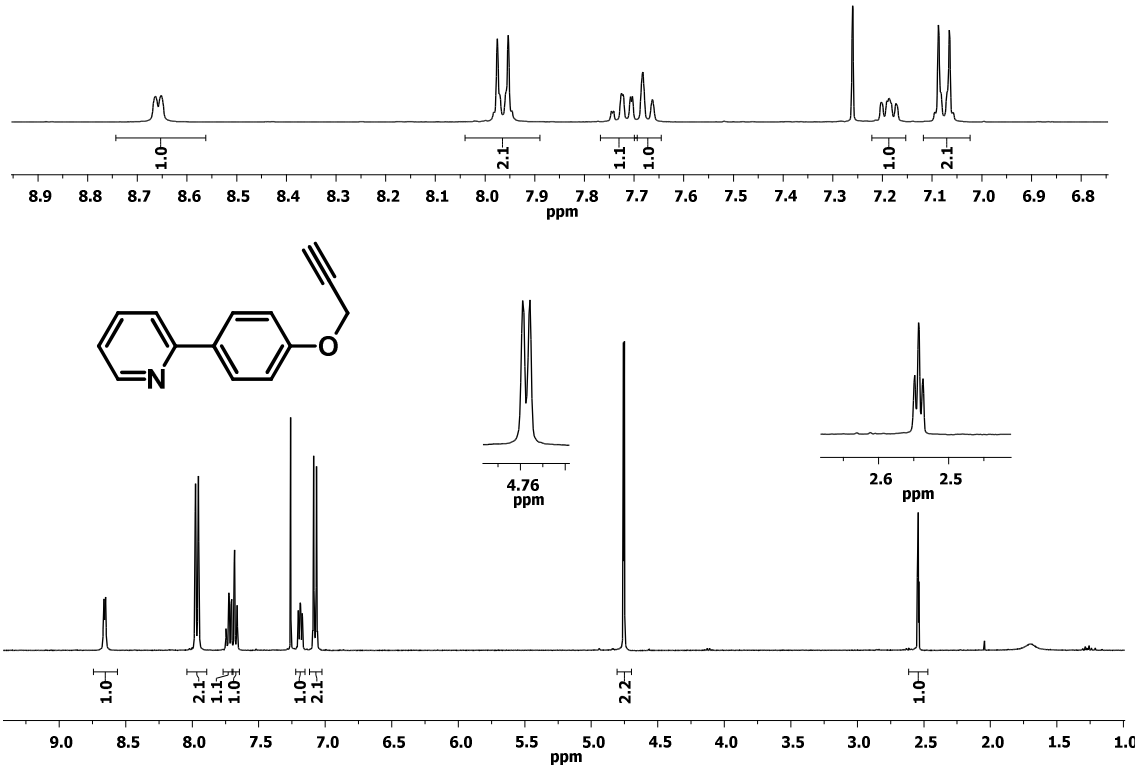

Figure A11. 400 MHz ^{1}H NMR spectrum of 2-[4-(prop-2-ynyloxy)phenyl]pyridine (**51**) in $CDCl_3$ at 300 K.

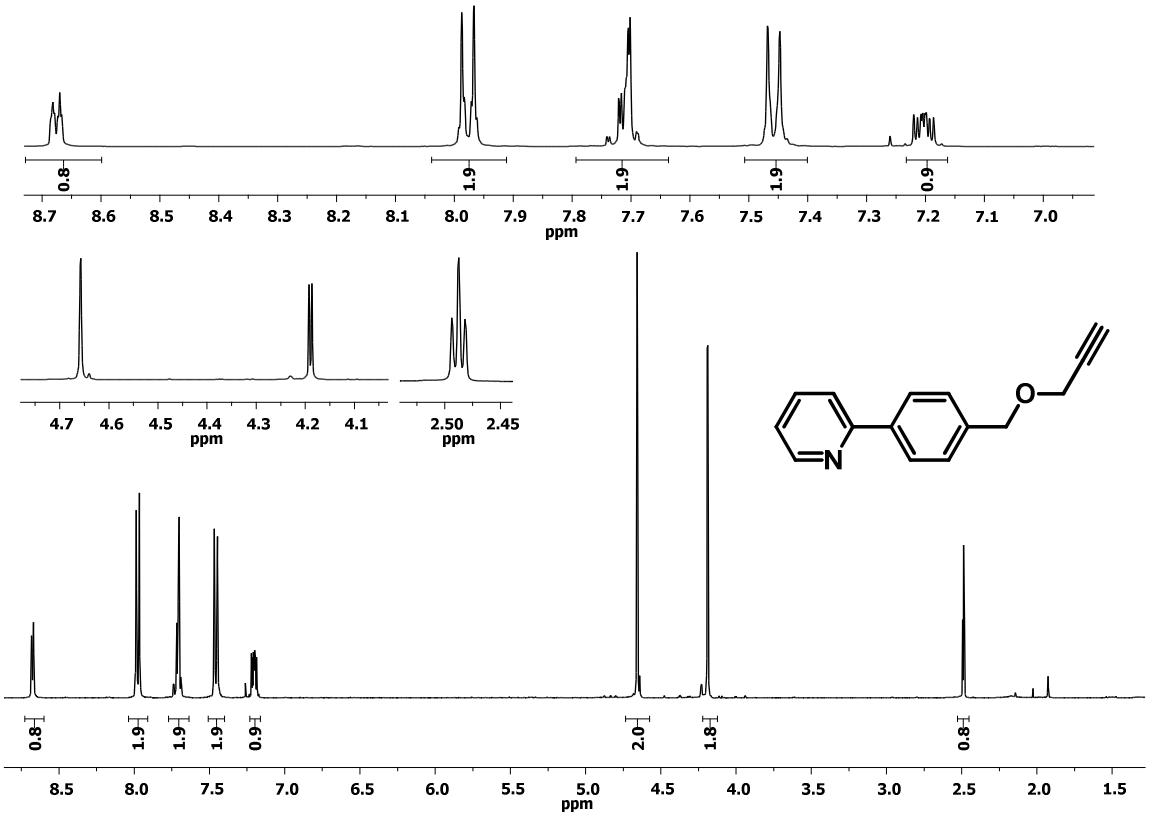

Figure A12. 400 MHz ^{1}H NMR spectrum of 2-(4-[(prop-2-ynyloxy)methyl]phenyl)pyridine (**52**) in $CDCl_3$ at 300 K.

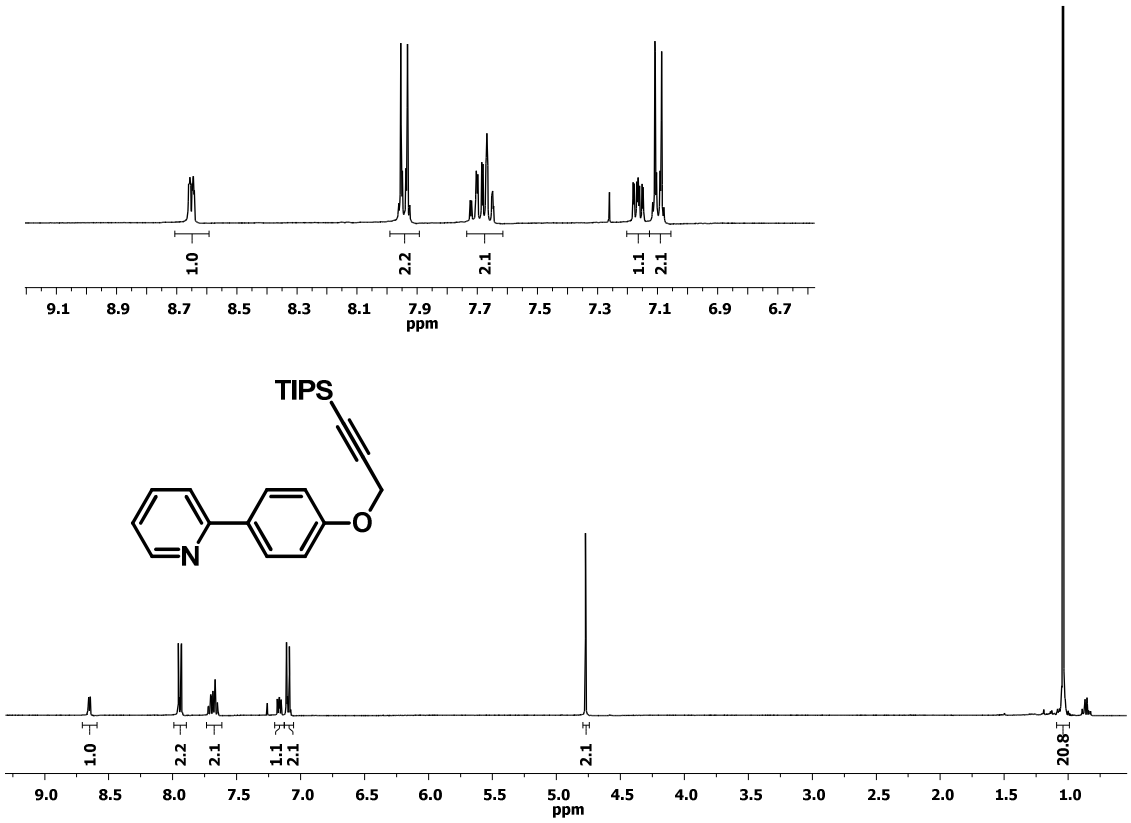

Figure A13. 400 MHz ^{1}H NMR spectrum of 2-[4-(3-triisopropylsilyl-prop-2-ynyloxy)phenyl]pyridine (**57**) in $CDCl_3$ at 300 K.

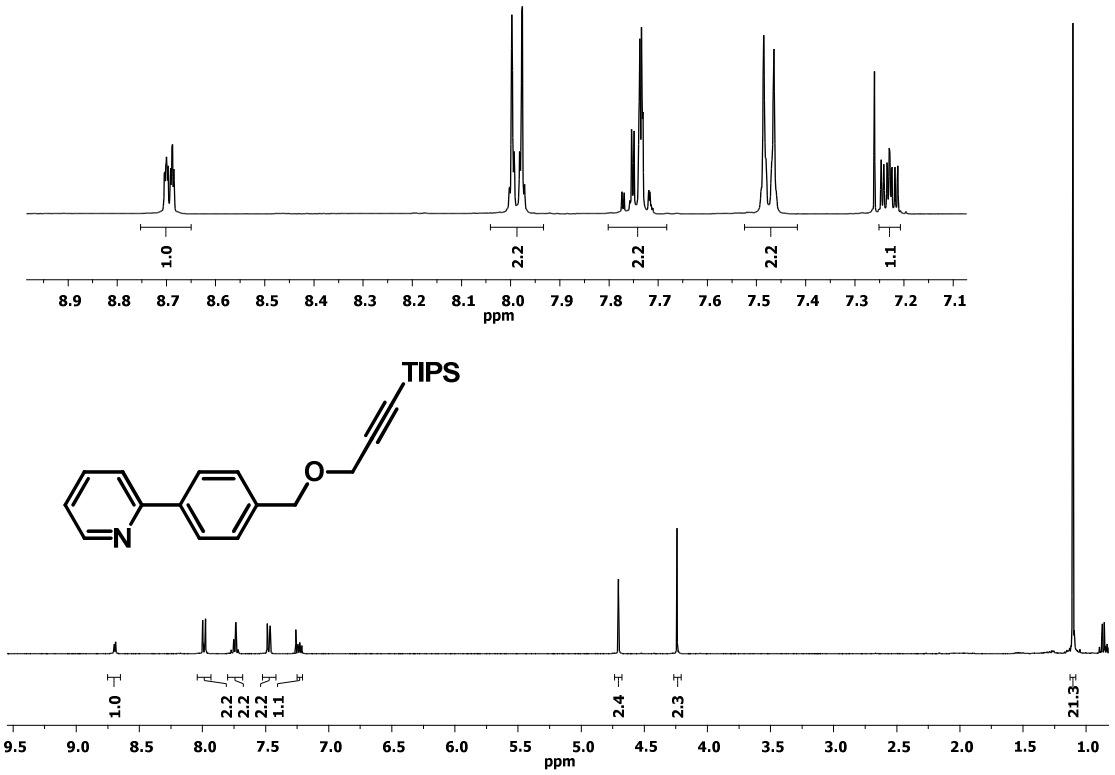

Figure A14. 400 MHz ^{1}H NMR spectrum of 2-(4-[(3-triisopropylsilyl-prop-2-ynyl-oxy)methyl]phenyl) pyridine (**58**) in $CDCl_3$ at 300 K.

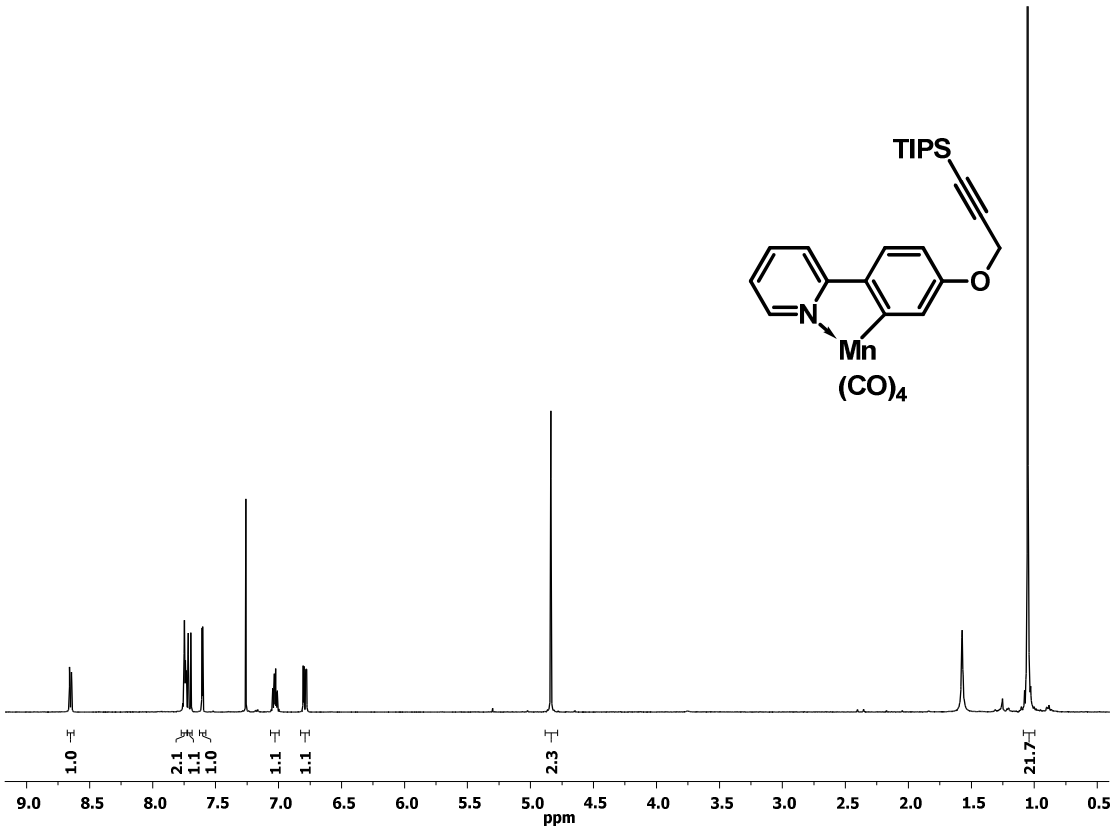

Figure A15. 400 MHz ^{1}H NMR spectrum of tetracarbonyl 2-[4-(3-triisopropylsilyl-prop-2-ynyloxy)phenyl]κ,C^{2}-pyridine-κ,N) manganese(I) (**59**) in $CDCl_3$ at 300 K.

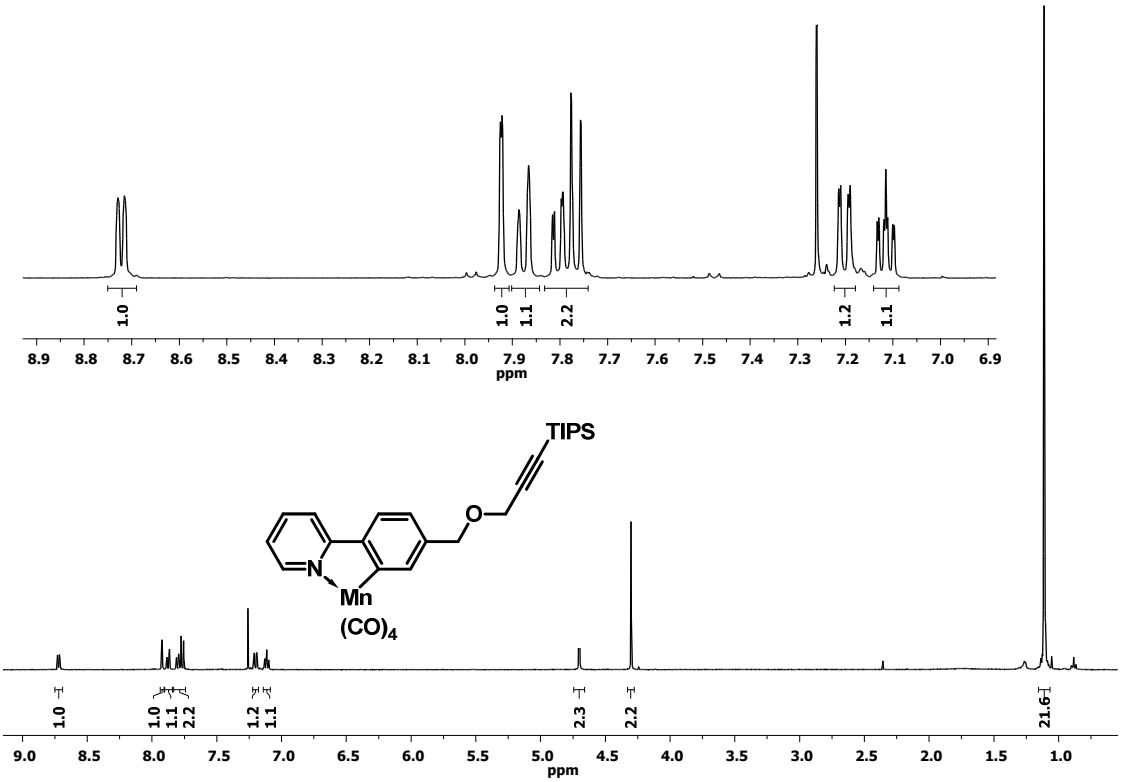

Figure A16. 400 MHz ^{1}H NMR spectrum of tetracarbonyl 2-(4-[(3-triisopropylsilyl-prop-2-ynyl-oxy)methyl]phenyl) κ,C^{2}-pyridine-κ,N) manganese(I) (**60**) in $CDCl_3$ at 300 K.

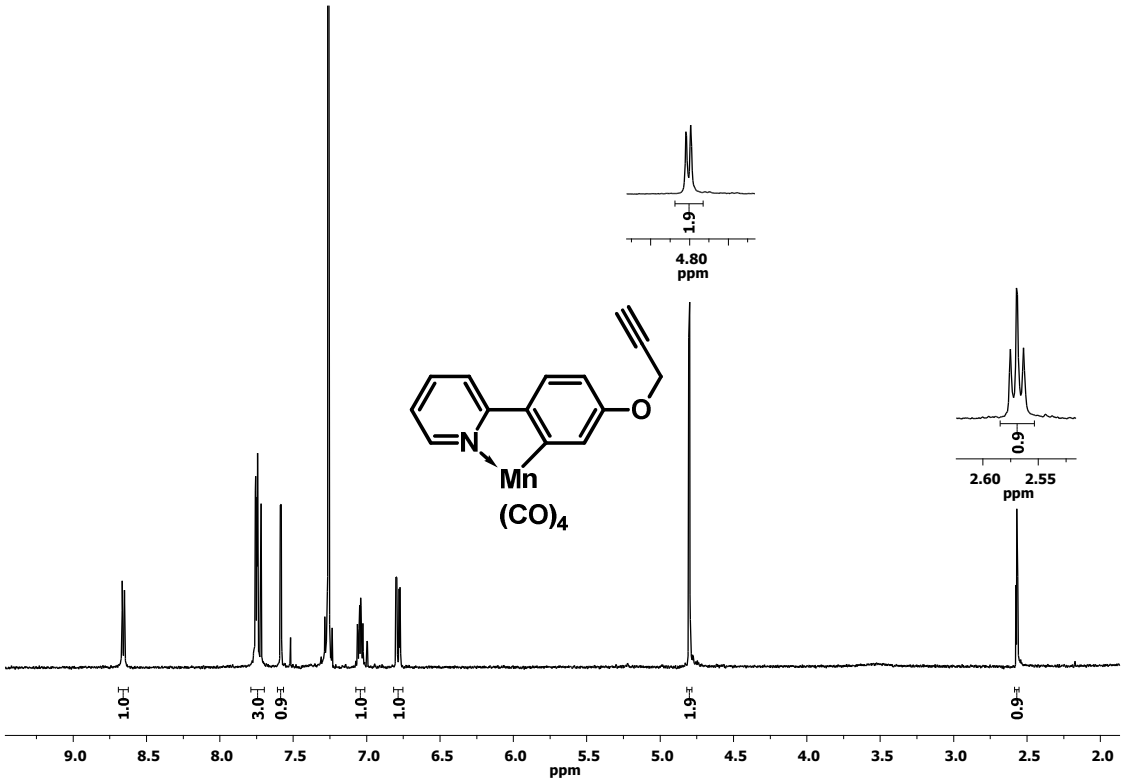

Figure A17. 400 MHz ^{1}H NMR spectrum of 2-[4-(prop-2-ynyloxy)phenyl] κ,C^{2}-pyridine-κ,N) manganese(I) (**62**) in $CDCl_3$ at 300 K.

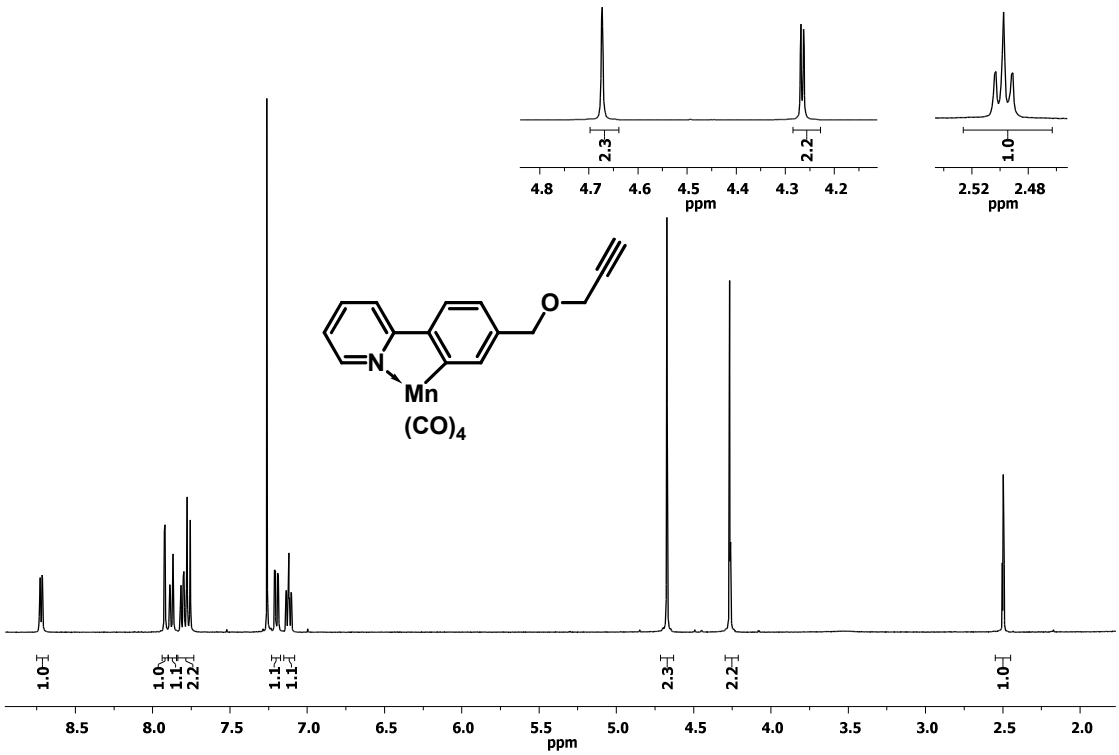

Figure A18. 400 MHz ^{1}H NMR spectrum of tetracarbonyl 2-(4-[(prop-2-ynyloxy)methyl]phenyl) κ,C^{2}-pyridine-κ,N) manganese(I) (**63**) in $CDCl_3$ at 300 K.

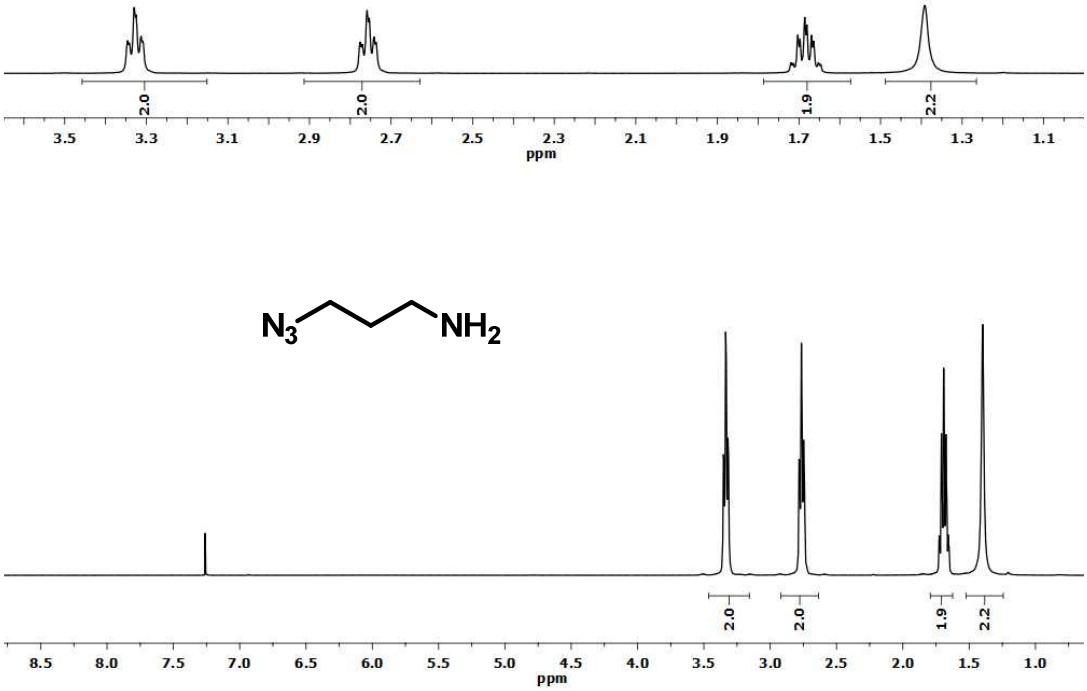

Figure A19. 400 MHz ^{1}H NMR spectrum of 3-azido-1-propylamine (**67**) in $CDCl_3$ at 300 K.

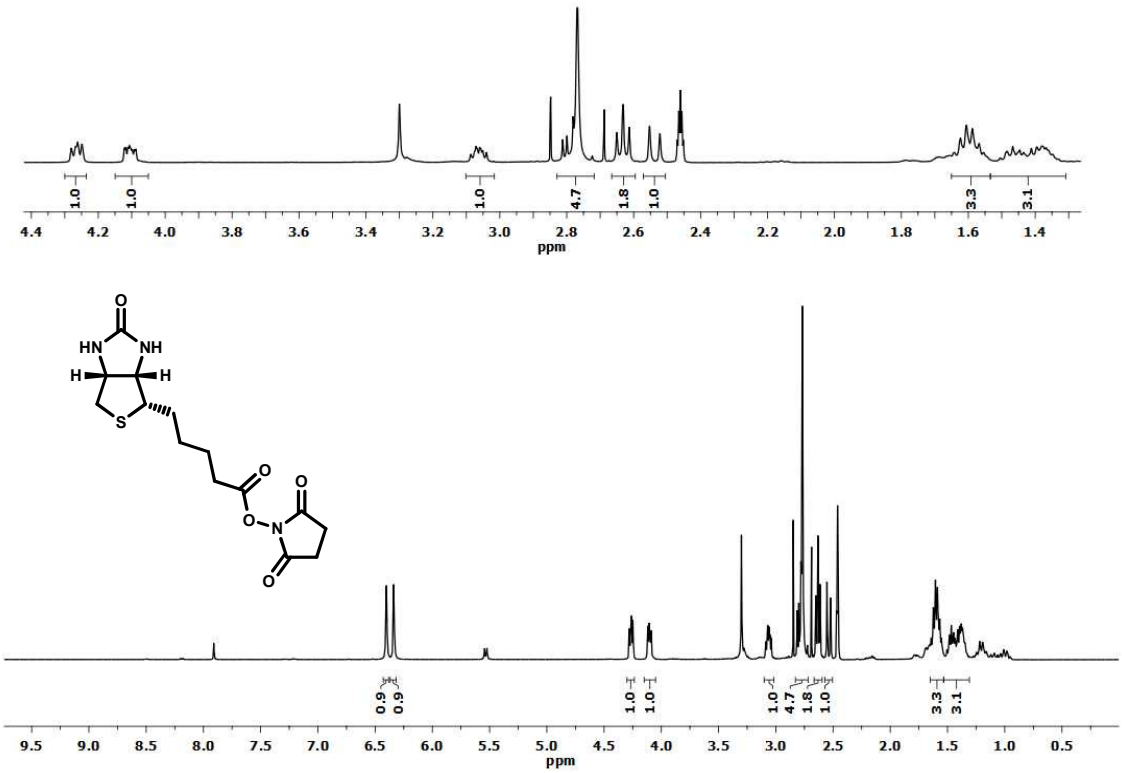

Figure A20. 400 MHz ^{1}H NMR spectrum of biotin-NHS(**69**) in DMSO-d_6 at 300 K.

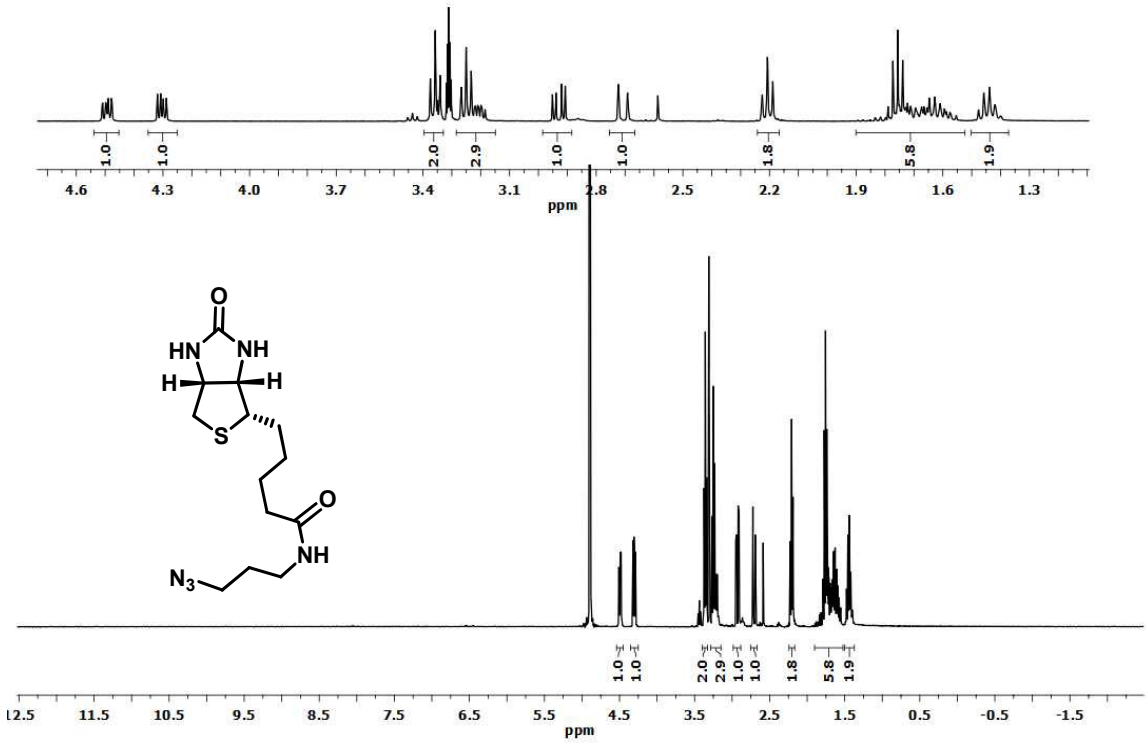

Figure A21. 400 MHz ^{1}H NMR spectrum of biotinyl-azide(**70**) in d_3-MeOD at 300 K.

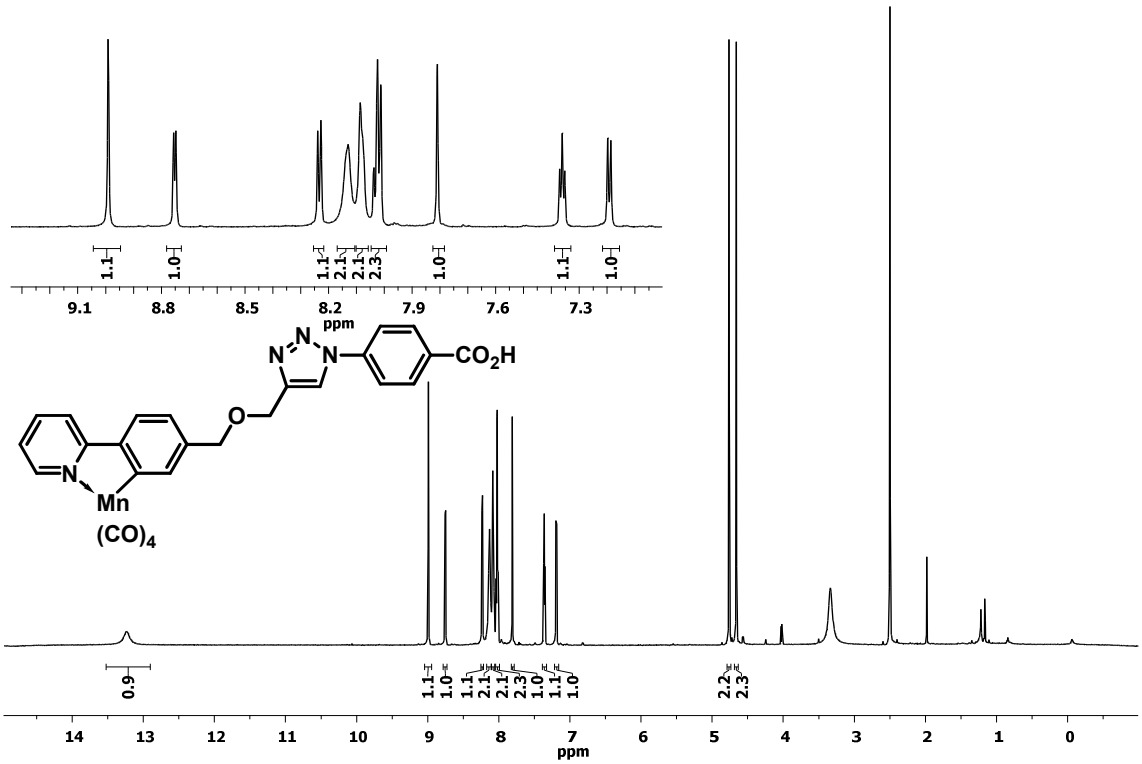

Figure A22. 700 MHz ^{1}H NMR spectrum of tetracarbonyl (2-[4-(([1-(4-carboxyphenyl)-1H-1,2,3-triazol-4-yl]methoxy)methyl)phenyl κ,C_2]pyridine κ,N) manganese(I) (**65**) in DMSO-d_6 at 300 K.

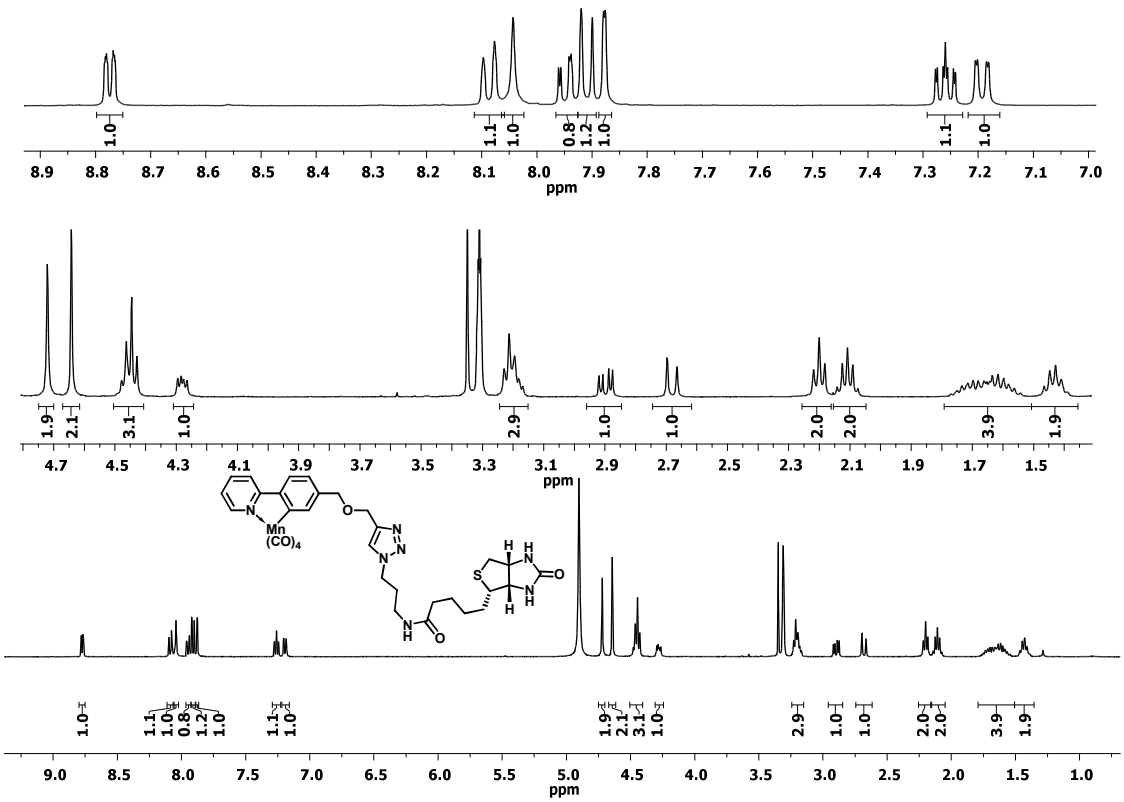

Figure A23. 400 MHz ^{1}H NMR spectrum of CO-RM (**71**) in MeOD-d_4 at 300 K

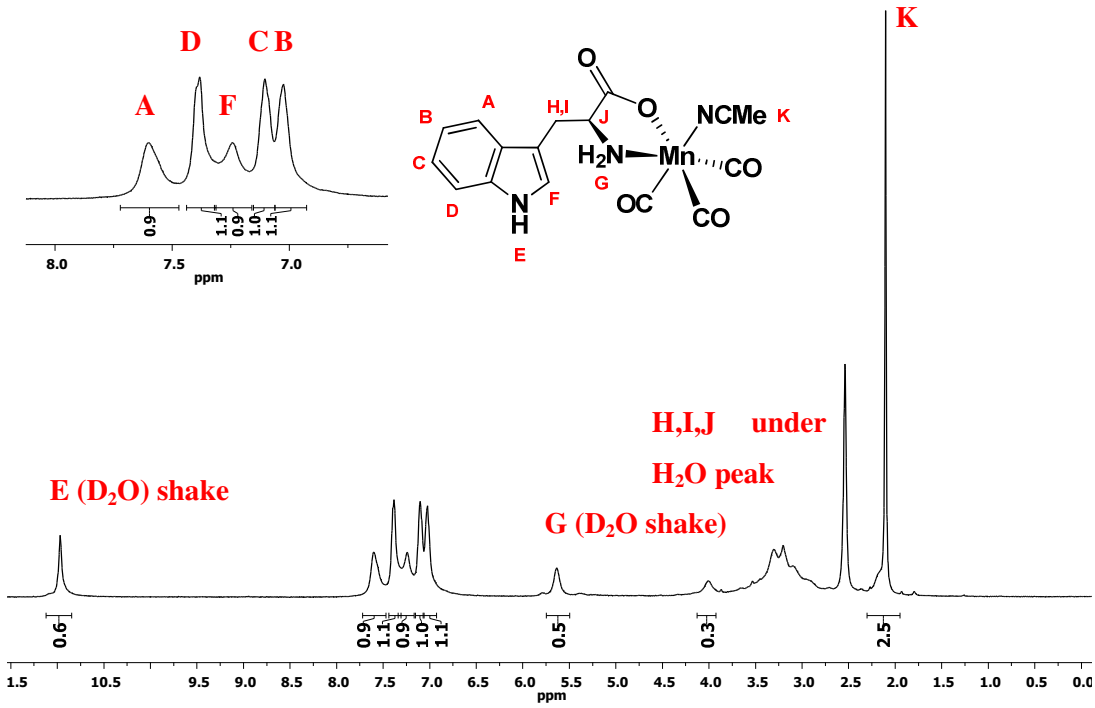

Figure A24. 400 MHz ^{1}H NMR spectrum of CO-RM L-**75** in DMSO-d_6 at 300 K

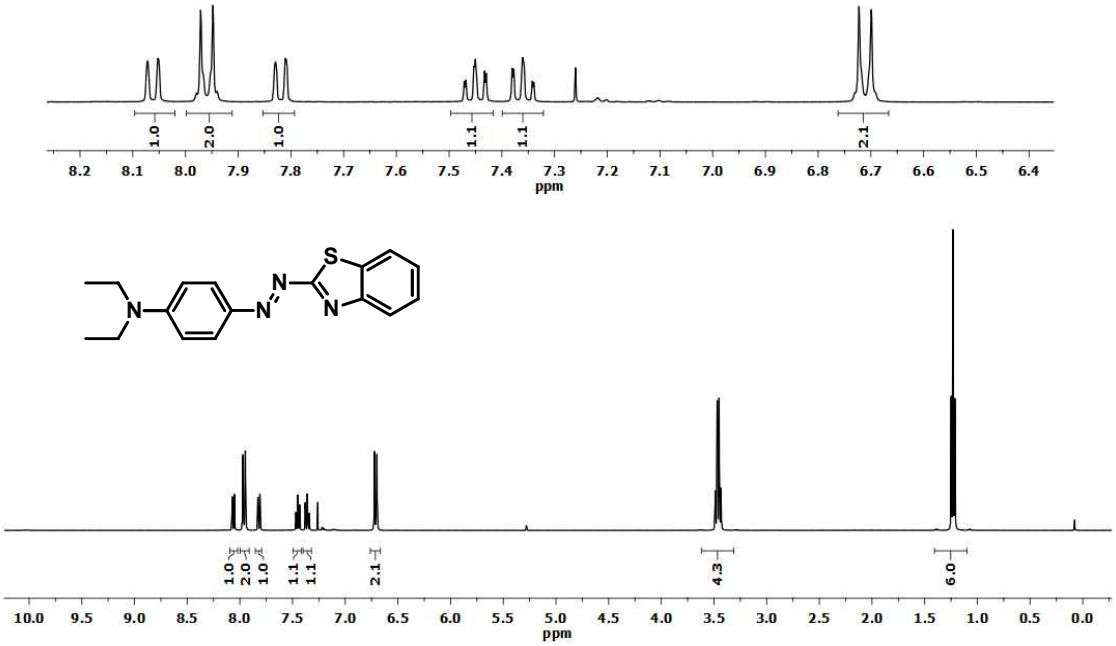

Figure A25. 400 MHz ^{1}H NMR spectrum of azodye **76** in $CDCl_3$ at 300 K

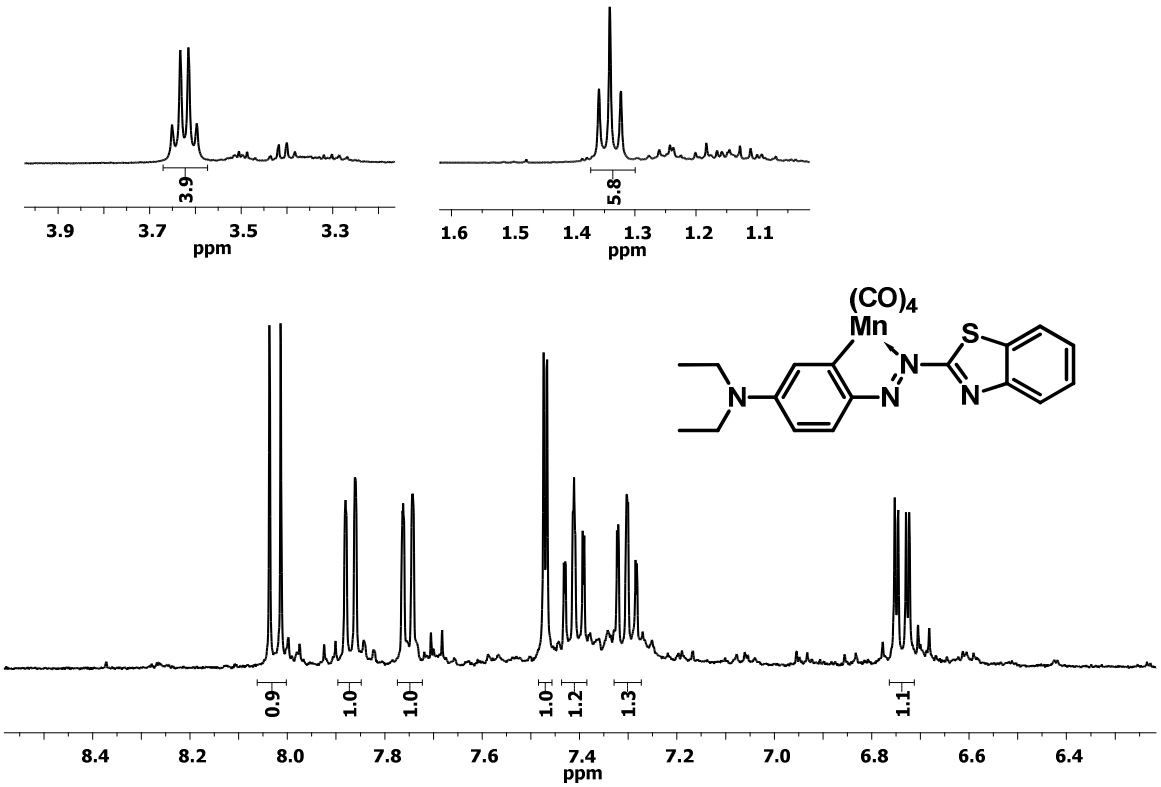

Figure A26. 400 MHz ^{1}H NMR spectrum of dye CO-RM **77** in CD_2Cl_2 at 300 K

^{13}C NMR spectra of prepared compounds

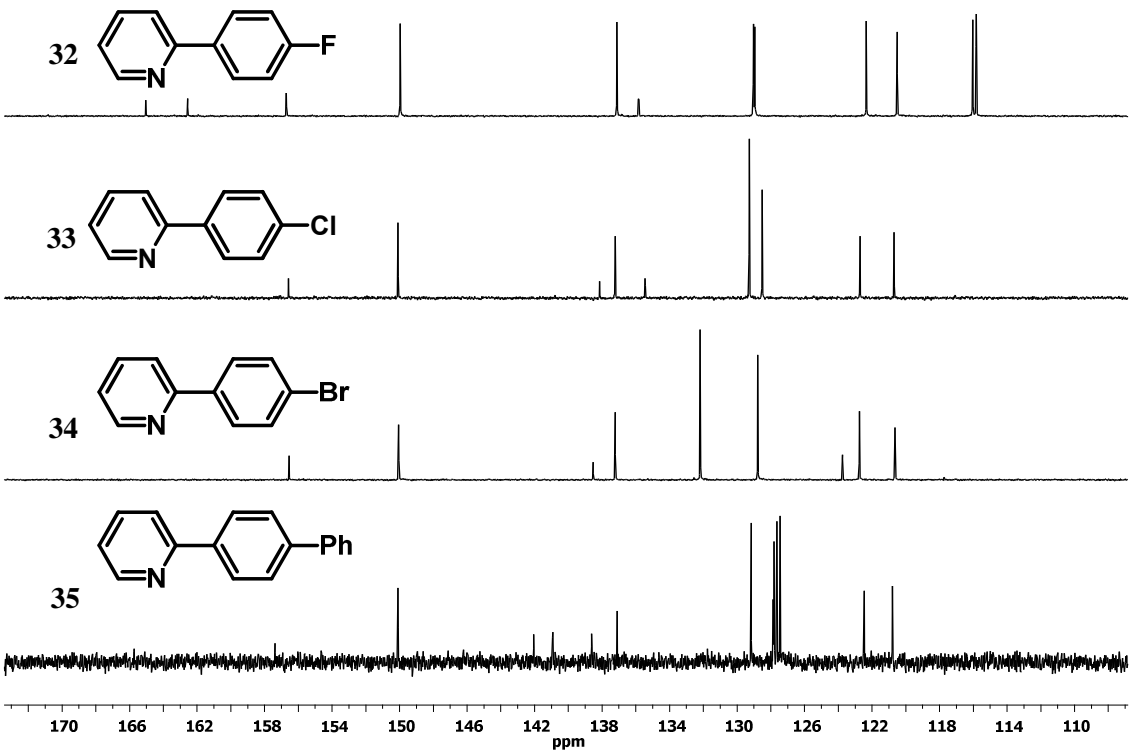

Figure A27. 100 MHz ^{13}C NMR spectra of manganese complexes **32**-**35** in $CDCl_3$ at 300 K

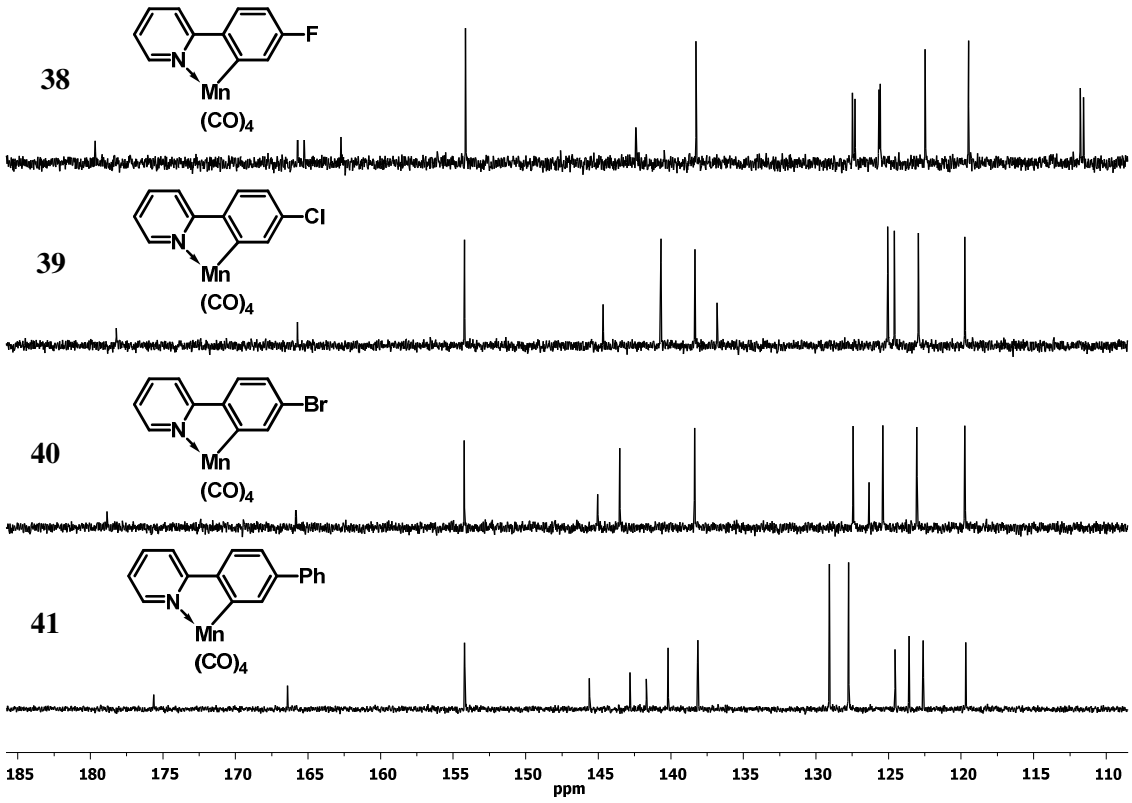

Figure A28. 100 MHz ^{13}C NMR spectra of manganese complexes **38**-**41** in $CDCl_3$ at 300 K

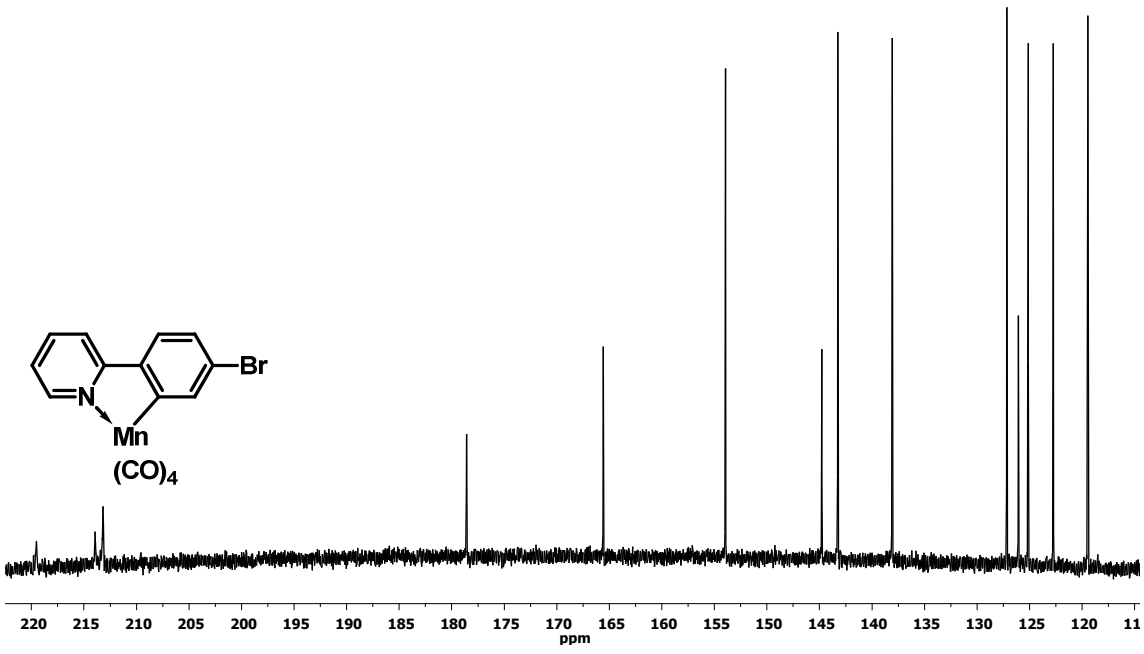

Figure A29. 121 MHz ^{13}C NMR spectra of manganese complex **40** in $CDCl_3$ at 298K with 10000 scans to show metal carbonyl signals.

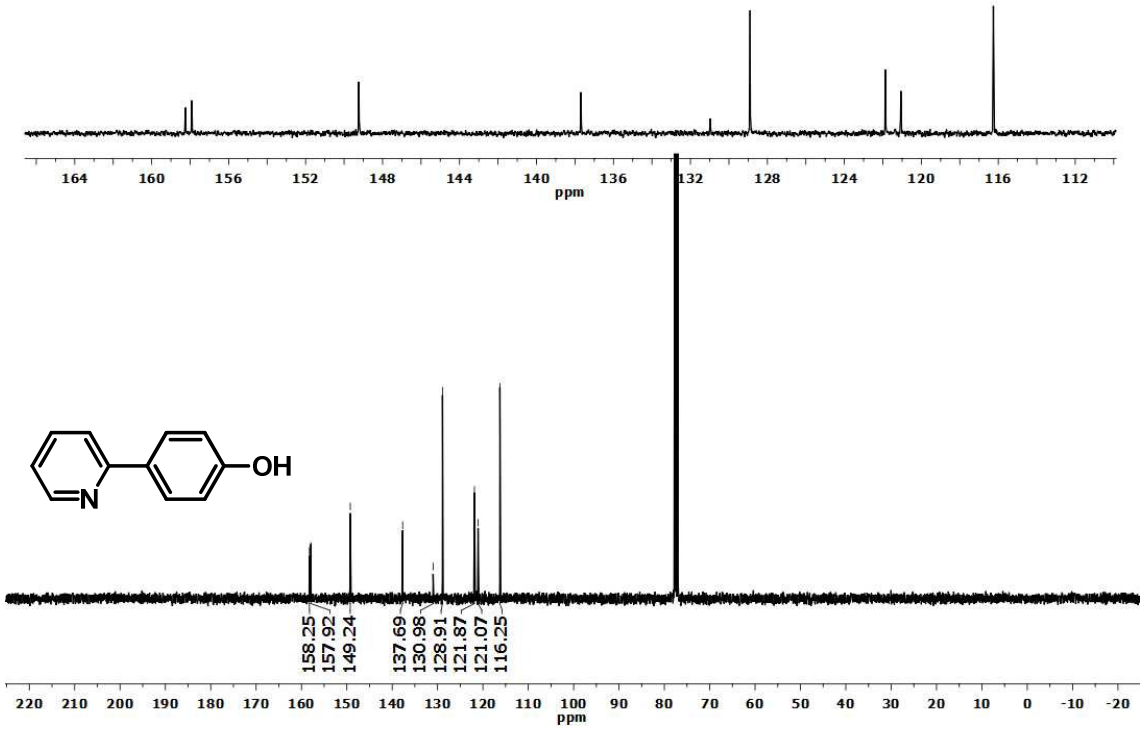

Figure A30. 100 MHz ^{13}C NMR spectrum of 2(4-hydroxy-phenyl)pyridine(**43**) in $CDCl_3$ at 300 K

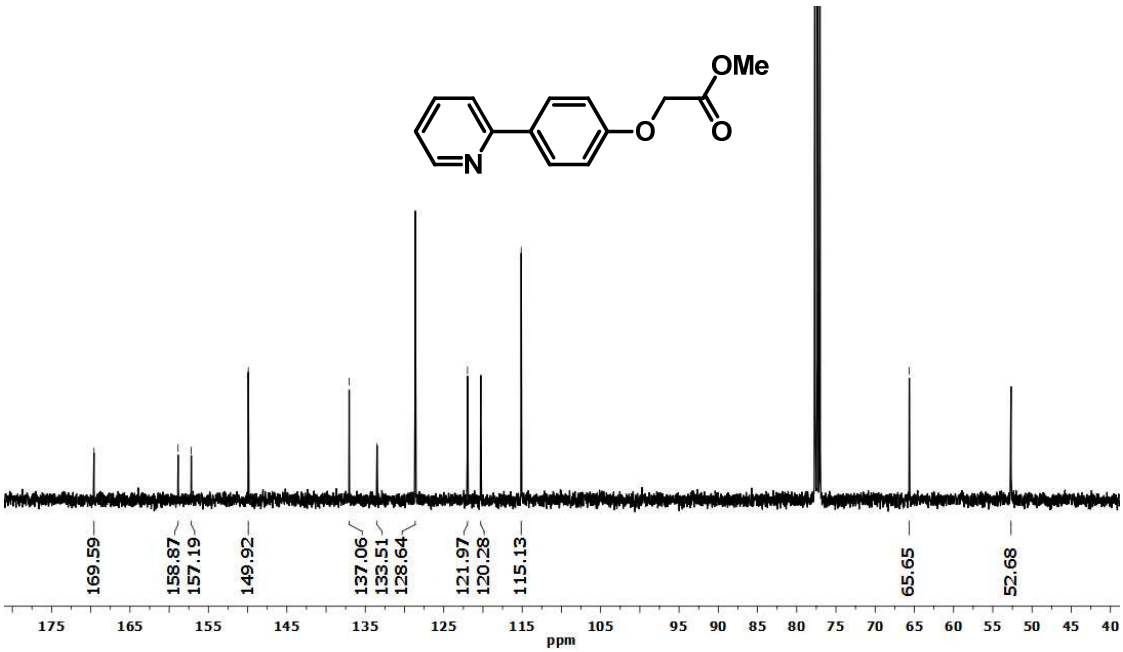

Figure A31.100 MHz ^{13}C NMR spectrum of methyl [4-(pyridin-2-yl)phenoxy]acetate (**44**) in $CDCl_3$ at 300 K.

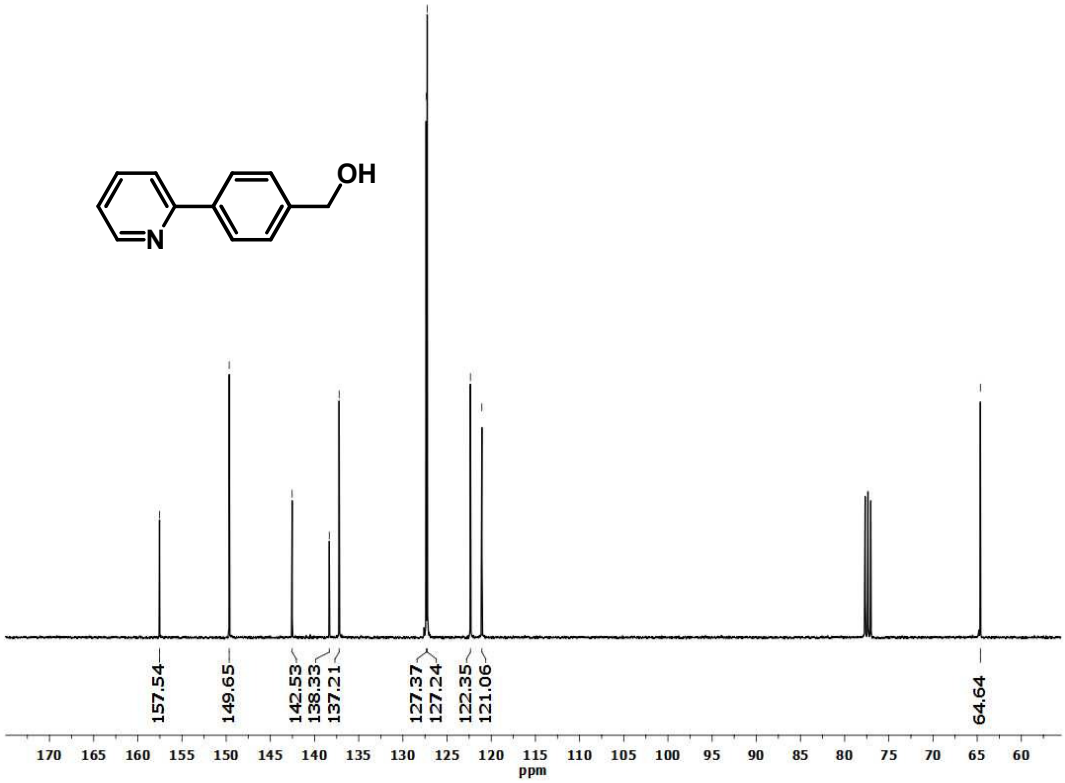

Figure A32. 100 MHz ^{13}C NMR spectrum of 2-(4-hydroxymethyl-phenyl)pyridine (**50**) in $CDCl_3$ at 300 K

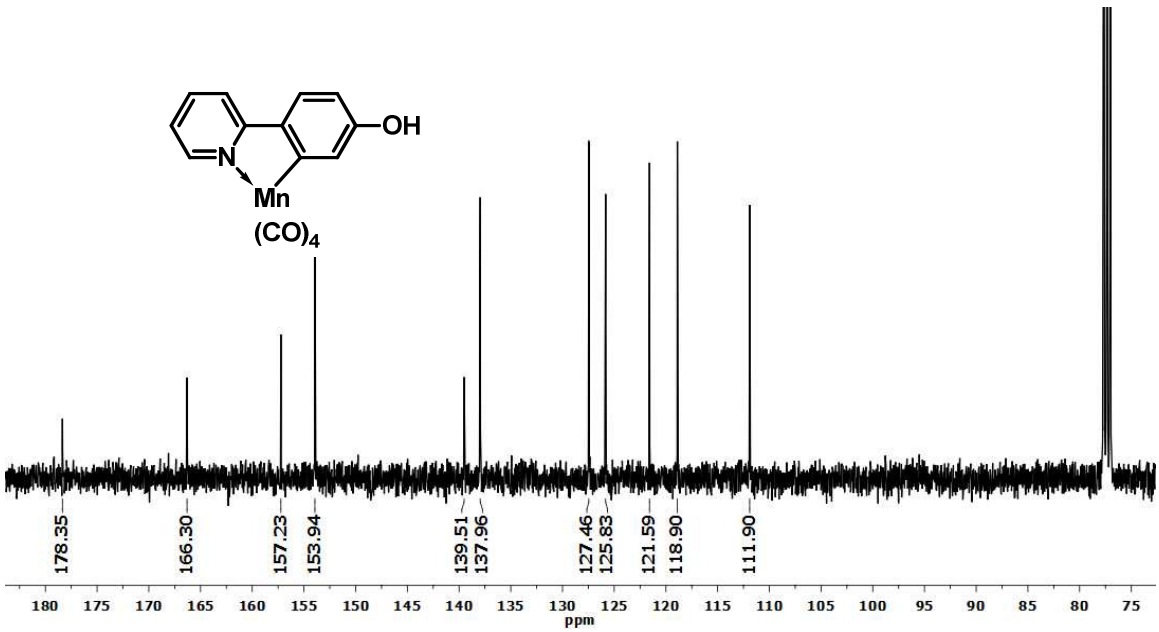

Figure A33. 100 MHz ^{13}C NMR spectrum of tetracarbonyl (2-(4-hydroxy-phenyl)κ,C^2-pyridine-κ,N) manganese(I) (**64**) in $CDCl_3$ at 300 K.

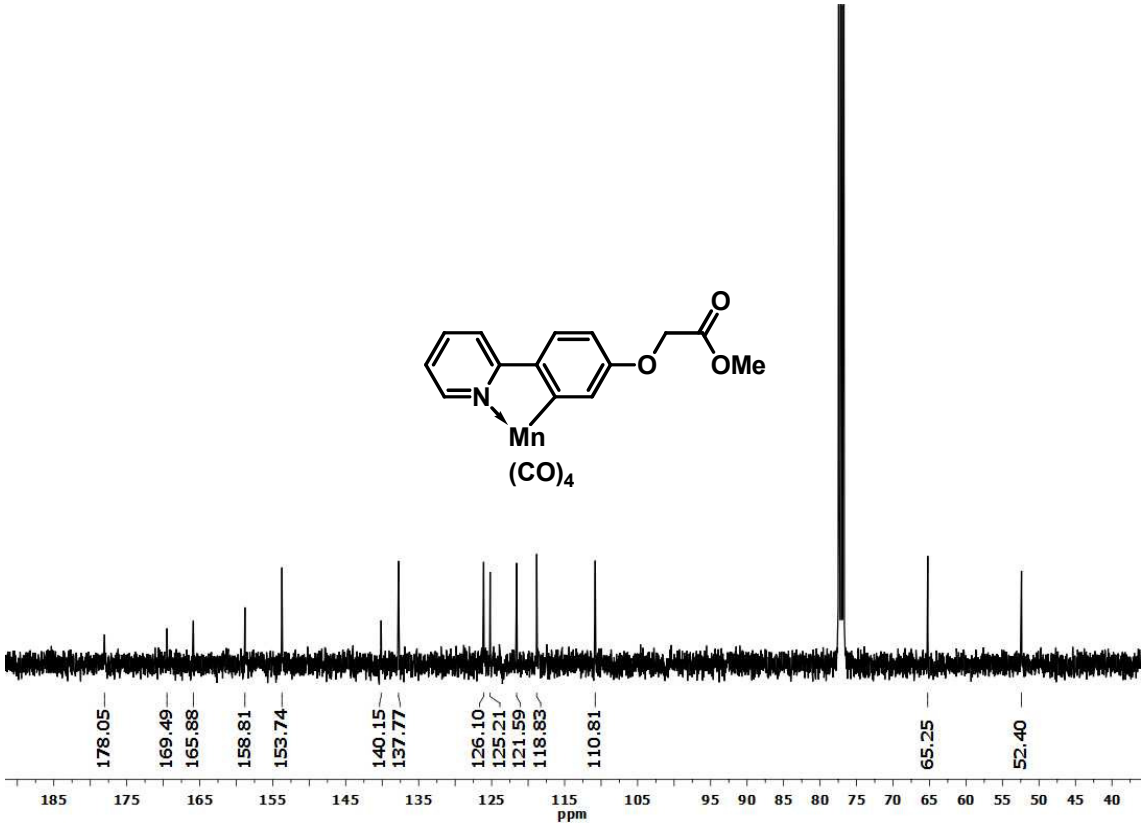

Figure A34. 100 MHz ^{13}C NMR spectrum of tetracarbonyl (methyl [4-(pyridin-2-yl-κ,N)phen-κ,C^2-oxy]acetate) manganese(I) (**45**) in $CDCl_3$ at 300 K.

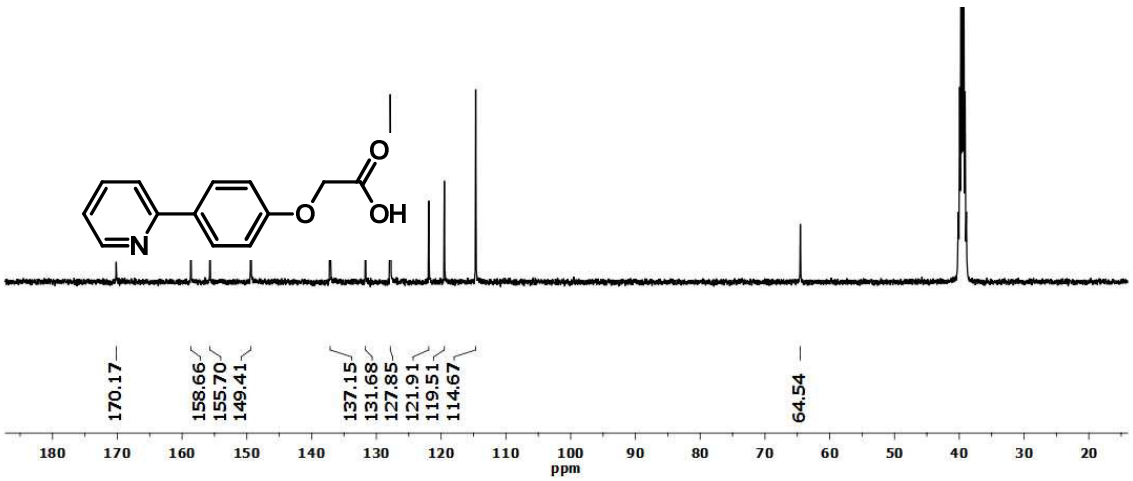

Figure A35. 100 MHz ^{13}C NMR spectrum of methyl [4-(pyridin-2-yl)phenoxy]acetic acid (**46**) in DMSO-d_6 at 300 K.

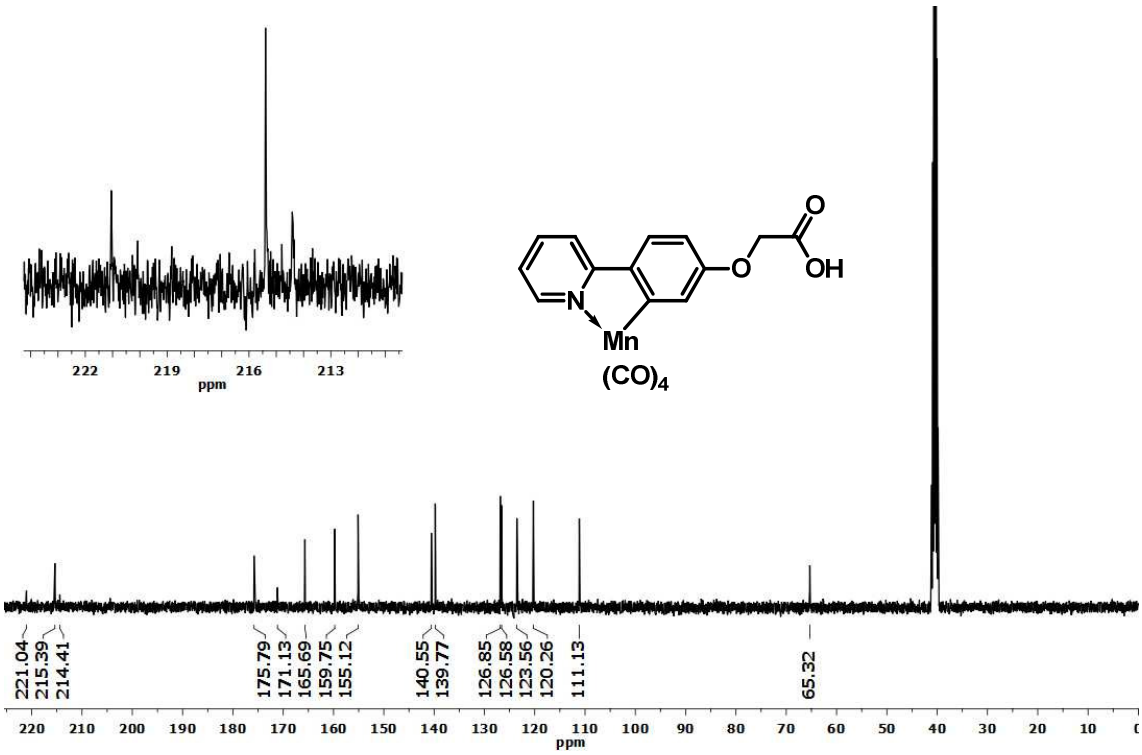

Figure A36. 100 MHz ^{13}C NMR spectrum of tetracarbonyl (methyl [4-(pyridin-2-yl-κ,N)phen-κ,C^{2}-oxy]acetic acid) manganese(I) (**47**) in DMSO-d$_6$ at 300 K.

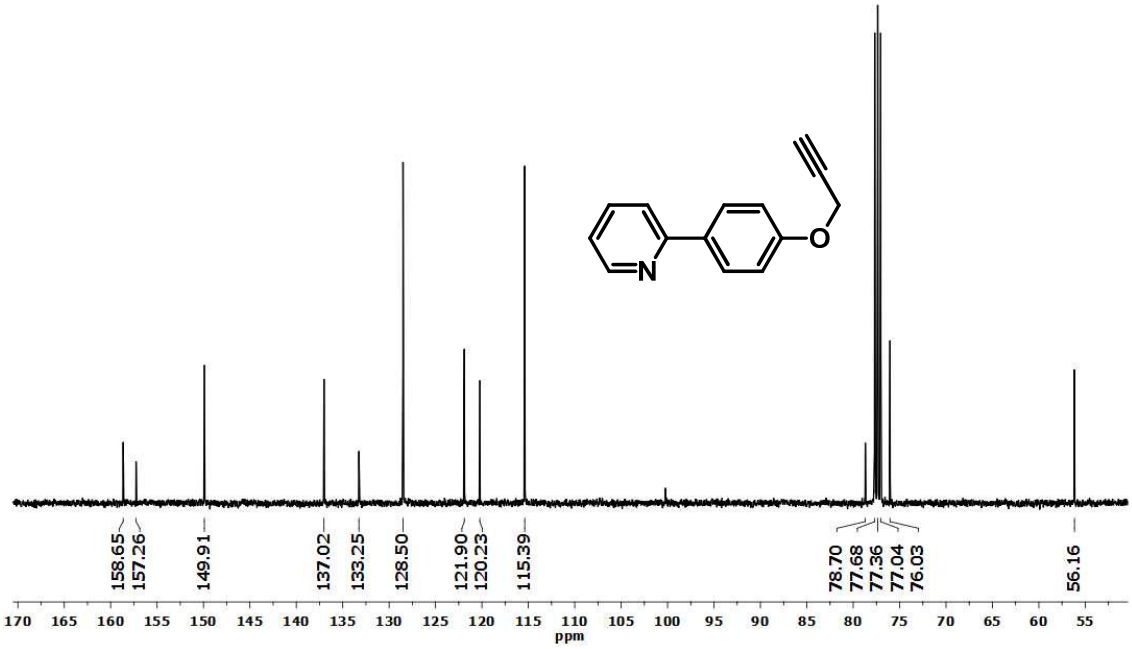

Figure A37. 100 MHz ^{1}H NMR spectrum of 2-[4-(prop-2-ynyloxy)phenyl]pyridine (**51**) in $CDCl_3$ at 300 K.

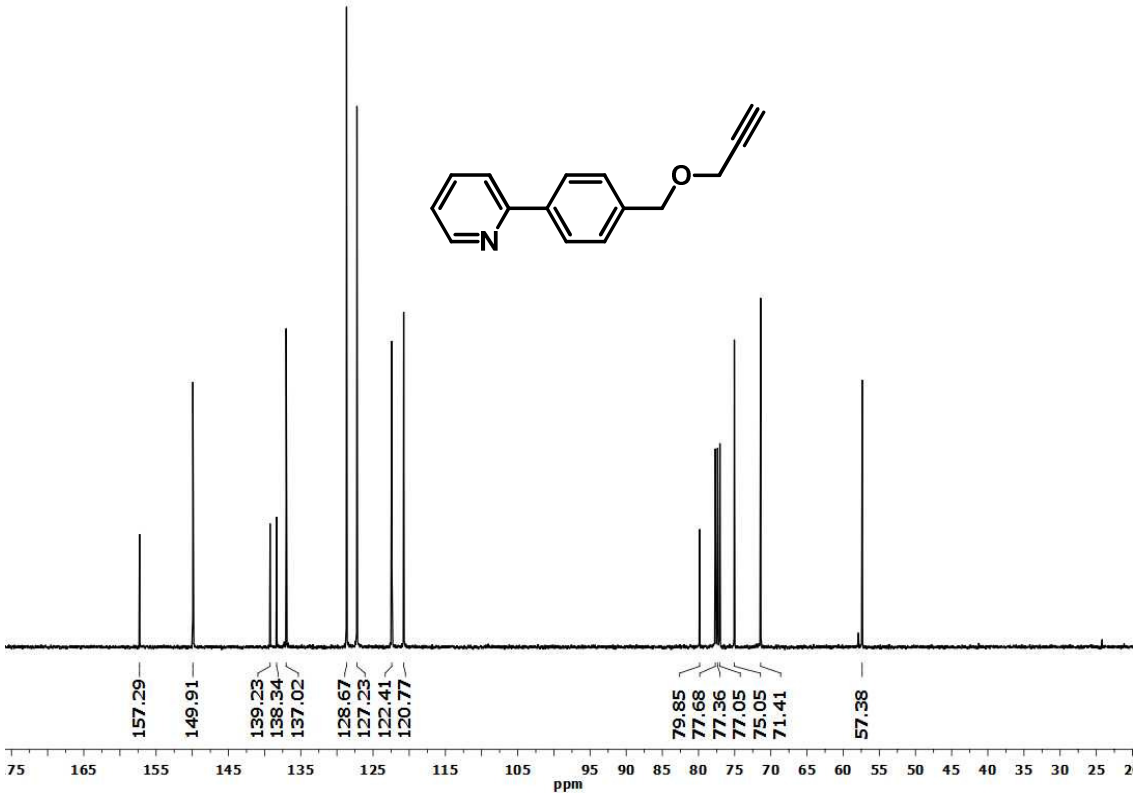

Figure A38. 100 MHz ^{13}C NMR spectrum of 2-(4-[(prop-2-ynyloxy)methyl]phenyl)pyridine (**52**) in $CDCl_3$ at 300 K.

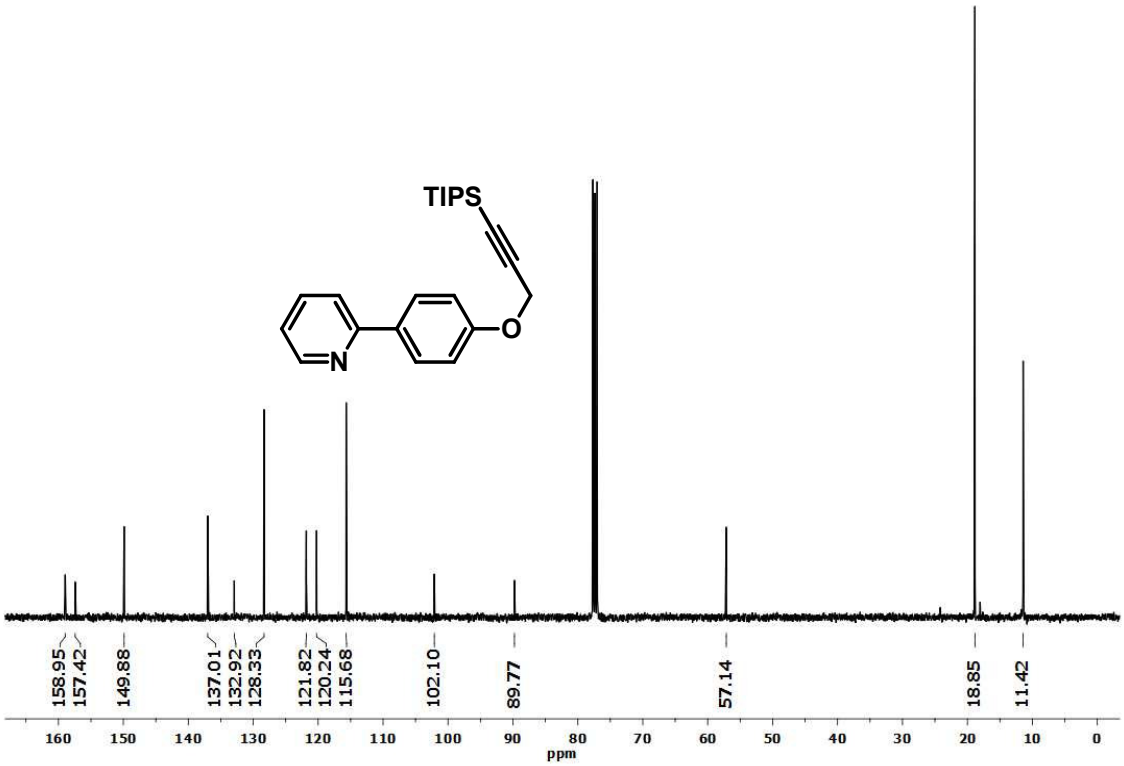

Figure A39. 400 MHz ^{1}H NMR spectrum of 2-[4-(3-triisopropylsilyl-prop-2-ynyloxy)phenyl]pyridine (**57**) in $CDCl_3$ at 300 K.

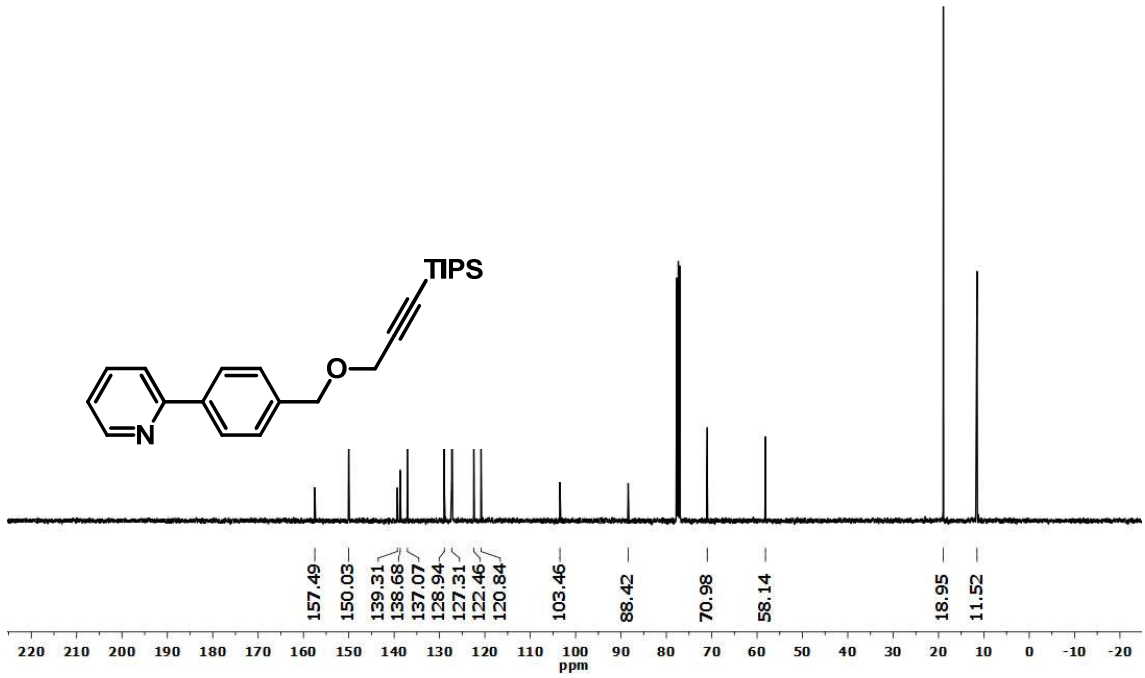

Figure A40: 100 MHz ^{13}C NMR spectrum of 2-(4-[(3-triisopropylsilyl-prop-2-ynyl-oxy)methyl]phenyl) pyridine (**58**) in $CDCl_3$ at 300 K.

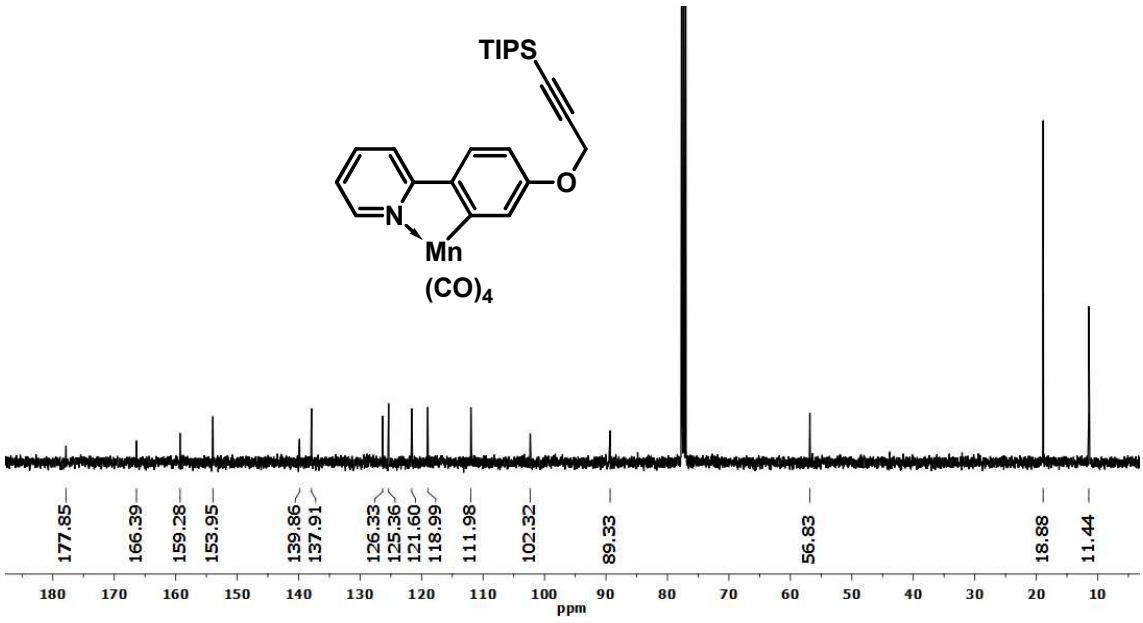

Figure A41. 100 MHz ^{13}C NMR spectrum of tetracarbonyl 2-[4-(3-triisopropylsilyl-prop-2-ynyloxy)phenyl]κ,C^2-pyridine-κ,N) manganese(I) (**59**) in $CDCl_3$ at 300 K.

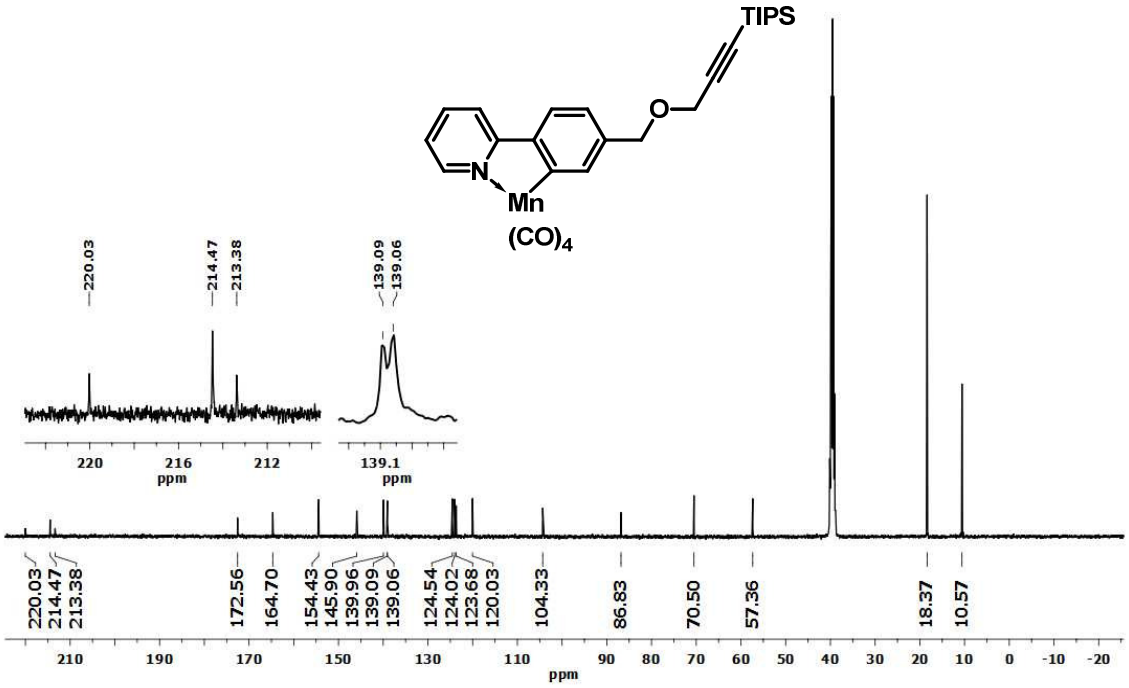

Figure A42. 100 MHz ^{13}C NMR spectrum of tetracarbonyl 2-(4-[(prop-2-ynyloxy)methyl]phenyl) κ,C^2-pyridine-κ,N) manganese(I) (**60**) in $CDCl_3$ at 300 K.

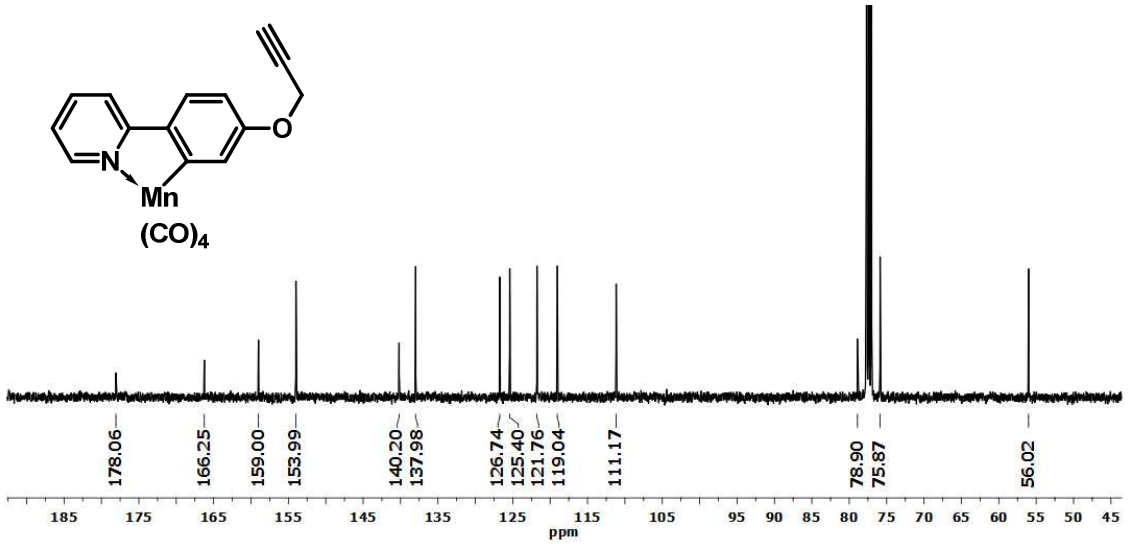

Figure A43. 100 MHz ^{13}C NMR spectrum of 2-[4-(prop-2-ynyloxy)phenyl] κ,C^2-pyridine-κ,N) manganese(I) (**62**) in $CDCl_3$ at 300 K.

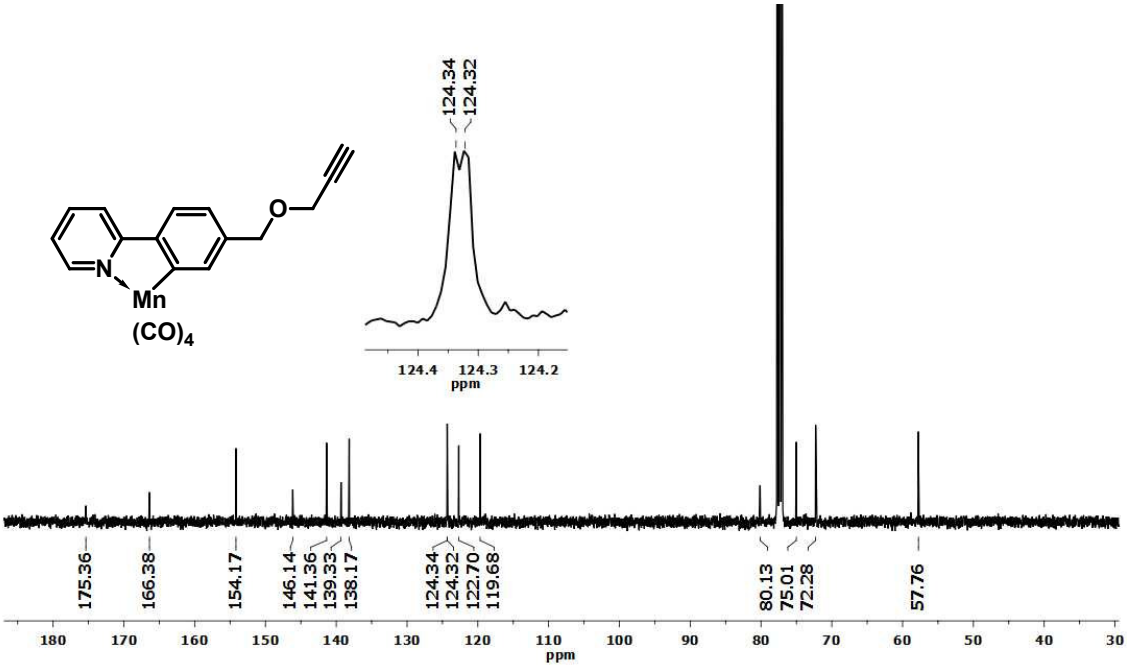

Figure A44. 100 MHz ^{13}C NMR spectrum of tetracarbonyl 2-(4-[(prop-2-ynyloxy)methyl]phenyl) κ,C^2-pyridine-κ,N) manganese(I) (**63**) in $CDCl_3$ at 300 K.

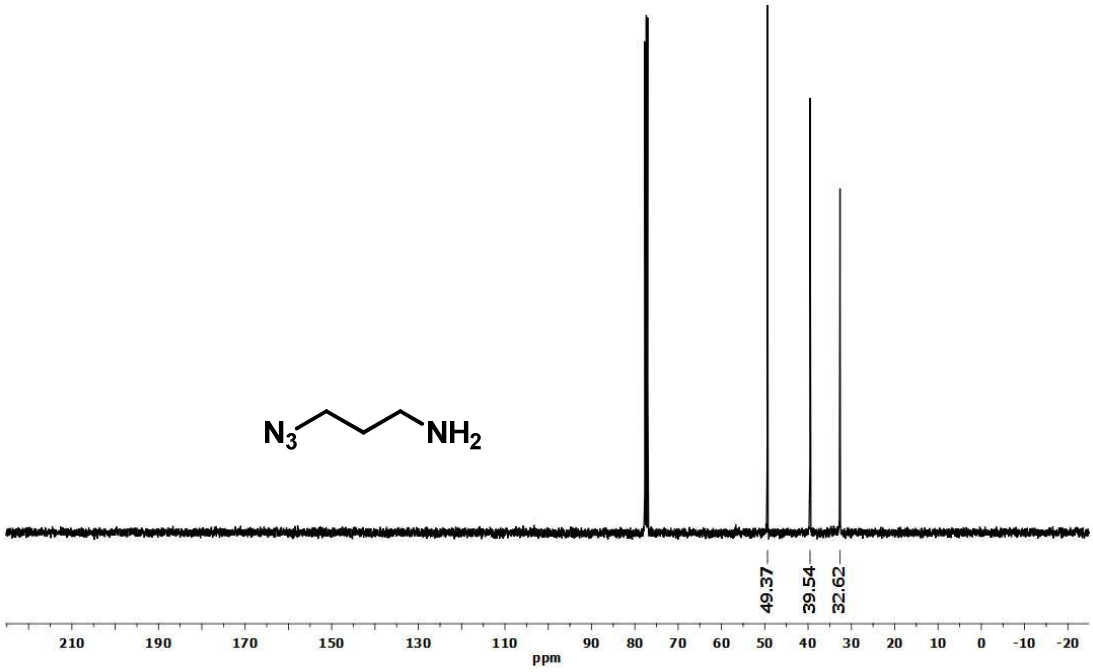

Figure A45. 100 MHz ^{13}C NMR spectrum of 3-aminopropylazide (**67**) in $CDCl_3$ at 300 K.

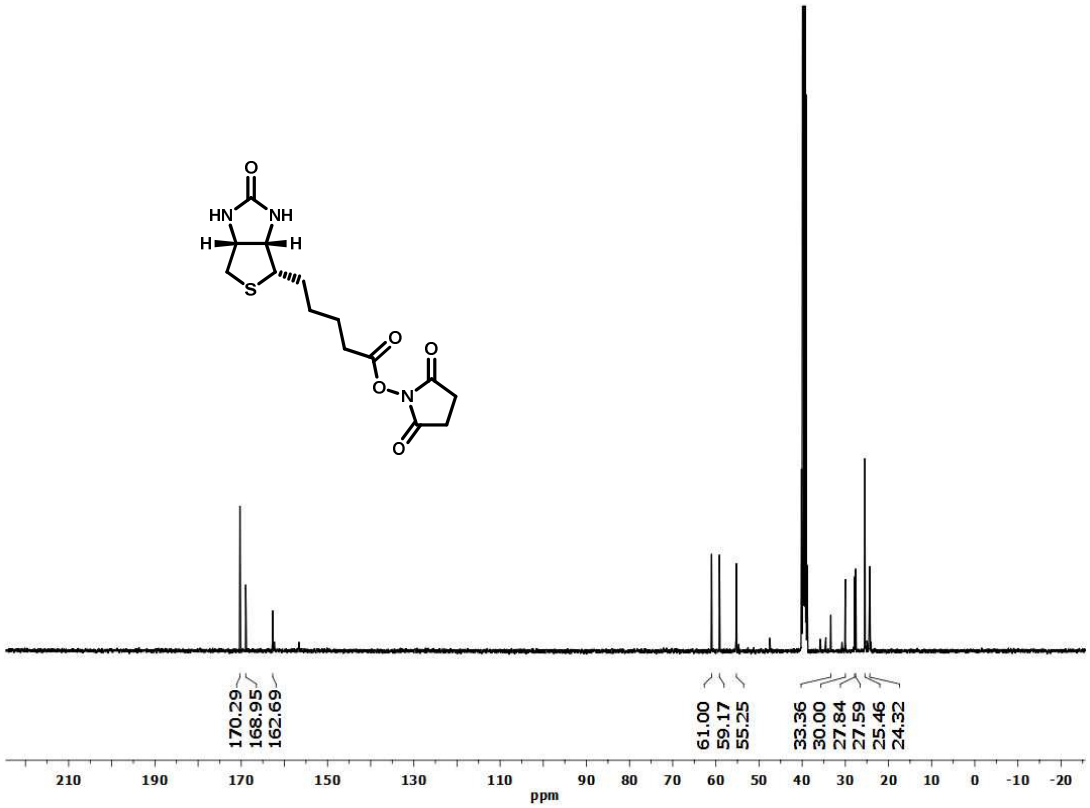

Figure A46. 100 MHz ^{13}C NMR spectrum of biotinyl-NHS(**69**) in DMSO-d_6 at 300 K.

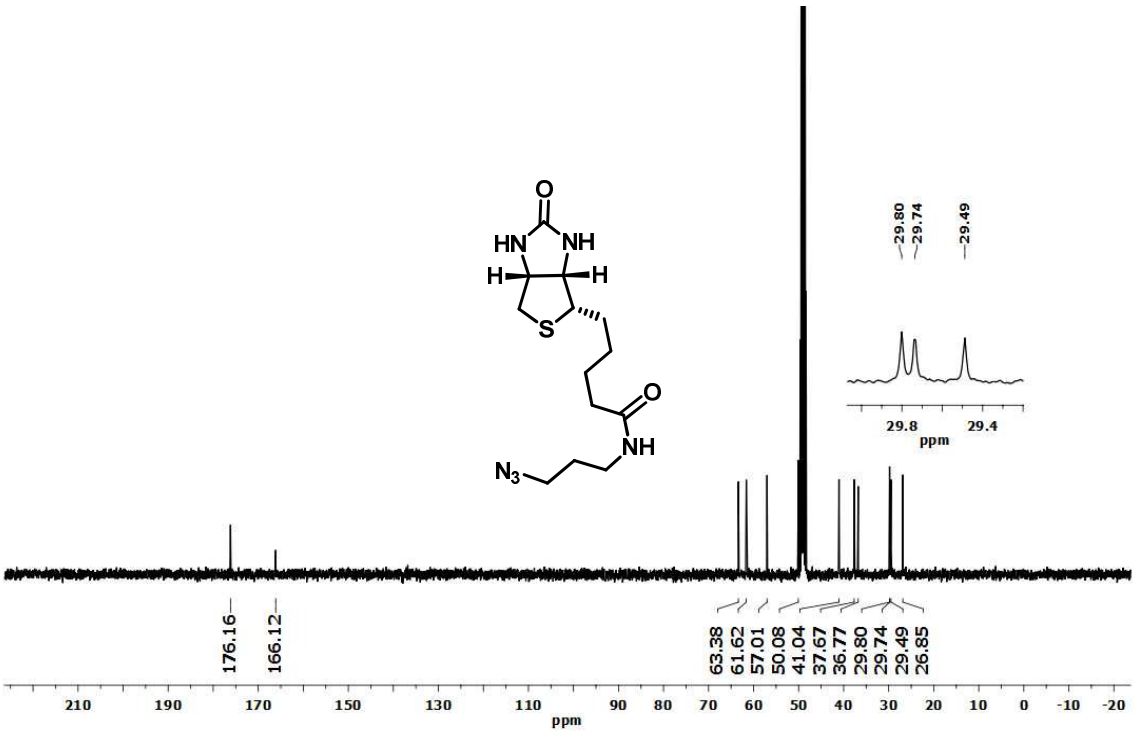

Figure A47. 100 MHz ^{13}C NMR spectrum of biotinyl-azide(**70**) in d_3-MeOD at 300 K.

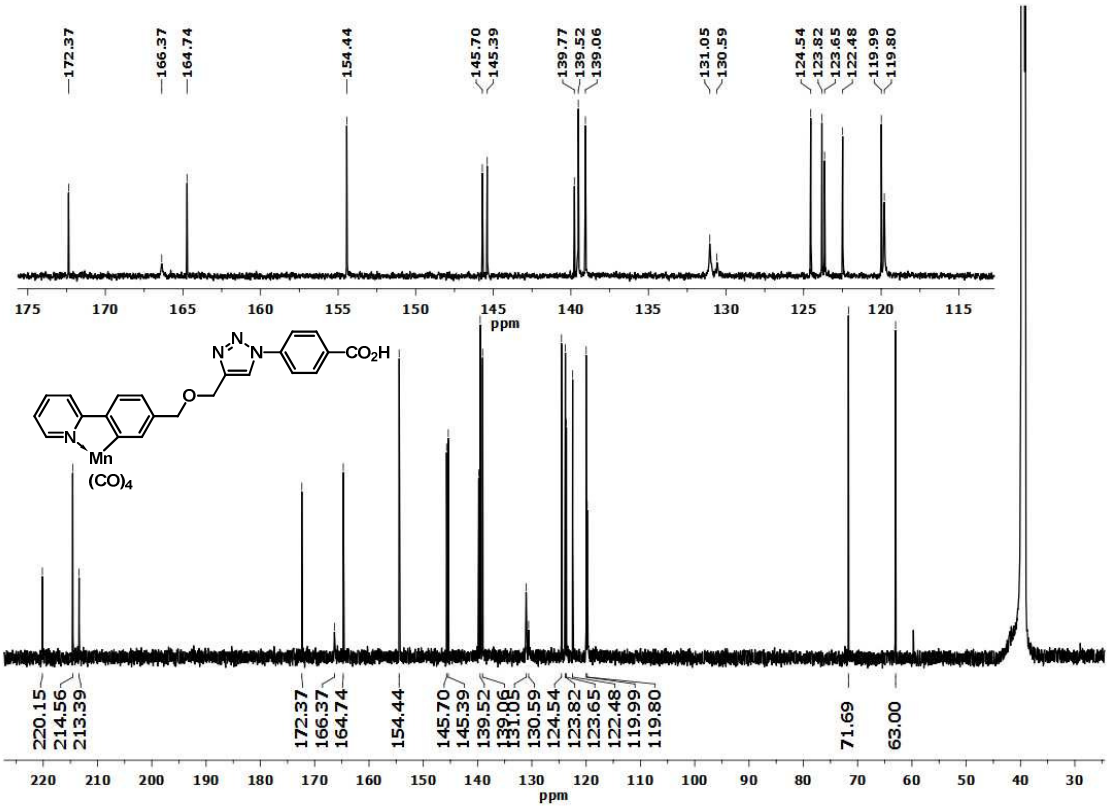

Figure A48. 176 MHz ^{13}C NMR spectrum of tetracarbonyl (2-[4-(([1-(4-carboxy-phenyl)-1H-1,2,3-triazol-4-yl]methoxy)methyl)phenyl κ,C2]pyridine κ,N) manganese(I) (**65**) in DMSO-d_6 at 299K.

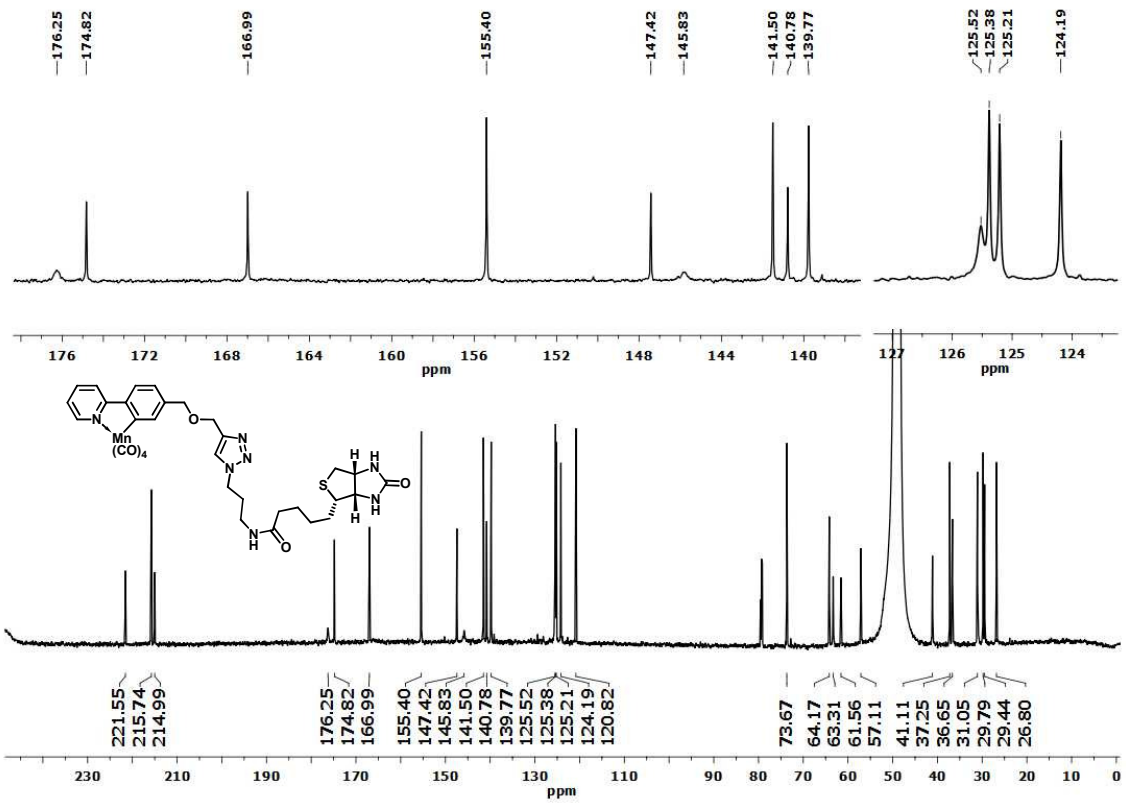

Figure A49. 176 MHz ^{1}H NMR spectrum of BB-CO-RM (**71**) in MeOD-d_4 at 263 K with 22000 scans.

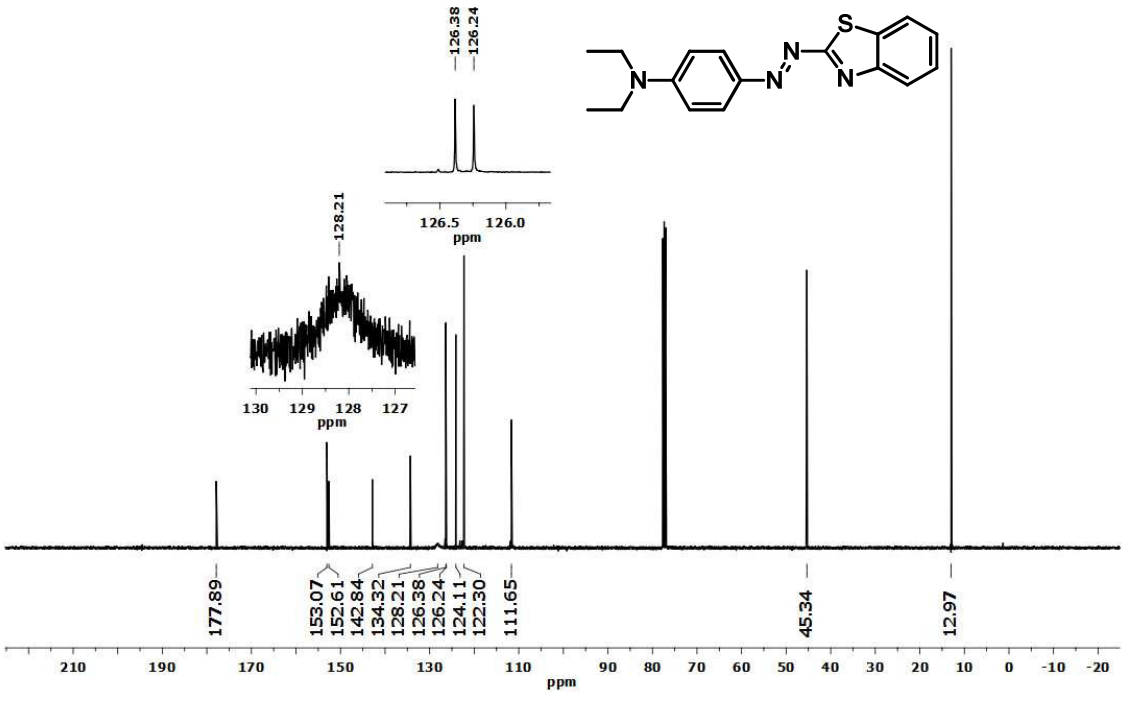

Figure A50. 100 MHz ^{13}C NMR spectrum of azodye **76** in $CDCl_3$ at 300 K

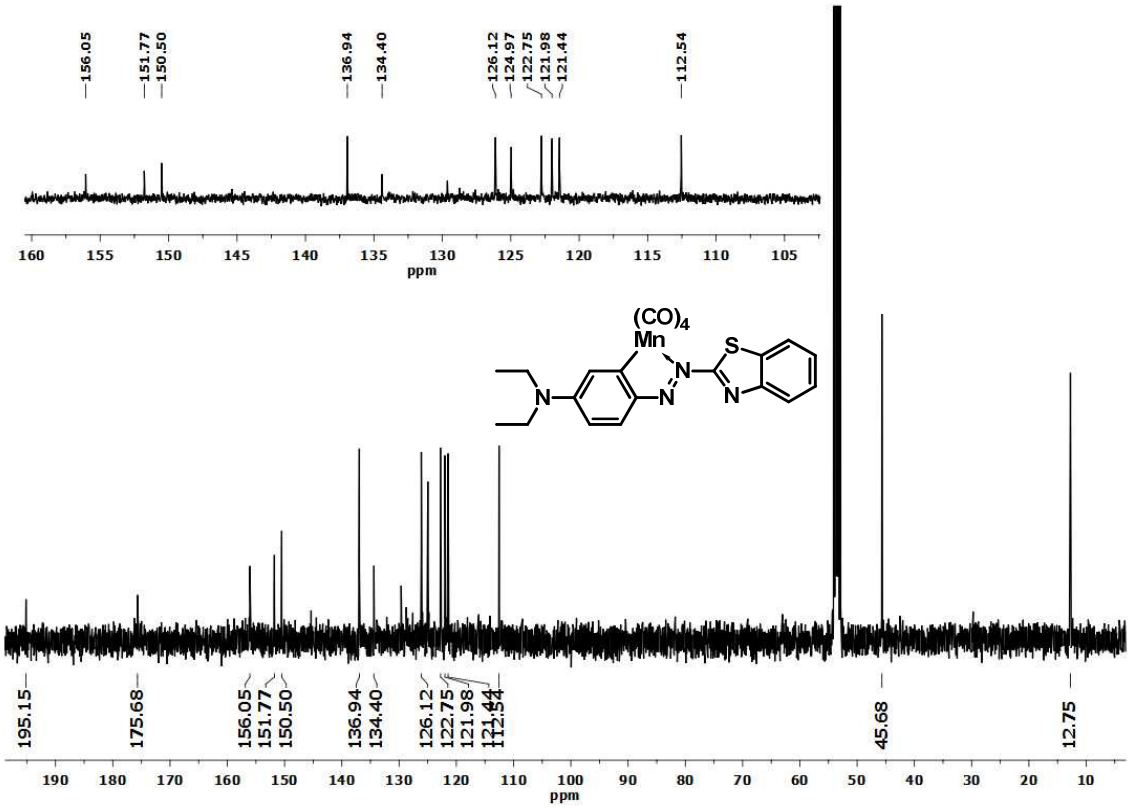

Figure A51. 100 MHz ^{13}C NMR spectrum of CO-RM **77** in CD_2Cl_2 at 300 K

11 Abbreviations

- CO-RM - Carbon monoxide-releasing molecule
- CO - Carbon monoxide
- NO - Nitric oxide
- DMSO - Dimethyl sulfoxide
- THF - Tetrahydrofuran
- +ve - Positive
- cGMP - Cyclic guanosine mono-phosphate
- GTP - Guanosine triphospphate
- HO - Haem oxygenase
- Hb - Haemoglobin
- Mb - Myoglobin
- Lb - Leghaemoglobin
- CO-Mb - Carboxy myoglobin
- CO-Hb - Carboxy haemoglobin
- NADPH - Nicotinamide adenine dinucleotide phosphate
- UDP - Uridine diphosphate
- VASP - Vasodilator-stimulated phosphoprotein
- TNF - Tumor necrosis factor
- NSAID - Non-steroidal anti-inflammatory drug
- sGC - soluble guanylyl cyclase
- EAE - Experimental allergic encephalomyelitis
- IR - Infrared
- NMR - Nuclear magnetic resonance
- PLE - Pig liver esterase
- 5-FU - 5-fluorouracil
- MDM2 protein - mouse double minute 2 protein
- DMF - *N*,*N*-dimethylformamide
- MCF-7 - Michigan Cancer Foundation cell strain 7
- LB medium - lysogency broth medium
- DMEM - Dulbecco's modified eagle medium
- FCS - foetal calf serium.
- PBS - Phosphate buffer saline
- LDH - Lactate dehydrogenase
- OD - optical density
- s - singlet
- d - doublet
- t - triplet
- q - quartet
- qn - quintet
- TMS - trimethylsilyl
- TIPS - triisopropylsilyl
- LDA - lithium diisopropylamide
- ITC - isothermal titration calorimetry
- ESI-MS - Electrospray ionisation mass spectrometry
- BHI - Brain heart infusion
- RPMI - Roswell Park Memorial Institute
- µM - micromolar
- nm - nanometres

- mM - millimolar
- mm - millimetres

12 References

[1] Clayden, J., *Organic chemistry*. Abridged ed.; Oxford University Press: Oxford ; New York, **2007**; p 103.

[2] Clayden, J., *Organic chemistry*. Abridged ed.; Oxford University Press: Oxford ; New York, **2007**; p 1315.

[3] Atkins, P. W., *Shriver & Atkins inorganic chemistry*. 4th ed.; Oxford University Press ;W.H. Freeman and Co.: Oxford ; New York, **2006**; p 532.

[4] Albright, T. A. *Tetrahedron* **1982**, *38*, 1339-1388.

[5] Hayton, T. W.; Legzdins, P.; Sharp, W. B. *Chem. Rev.* **2002**, *102*, 935-92.

[6] Pellicena, P.; Karow, D. S.; Boon, E. M.; Marletta, M. A.; Kuriyan, J. *Proc. Natl. Acad. Sci. U. S. A.* **2004**, *101*, 12854-9.

[7] Motterlini, R.; Otterbein, L. E. *Nat. Rev. Drug. Discov.* **2010**, *9*, 728-43.

[8] Van den Akker, F.; Ma, X. L.; Sayed, N.; Beuve, A. *Embo J.* **2007**, *26*, 578-588.

[9] Raub, J. A.; Benignus, V. A. *Neurosci. Biobehav, Rev,* **2002**, *26*, 925-940.

[10] Heinemann, S. H.; Hoshi, T.; Westerhausen, M.; Schiller, A. *Chem. Commun.* **2014**, *50*, 3644-60.

[11] Miro, O.; Alonso, J. R.; Cardellach, F.; Lopez, S.; Casademont, J. *Pharmacol Toxicol* **2003**, *93*, 142-146.

[12] Balsa, E.; Marco, R.; Perales-Clemente, E.; Szklarczyk, R.; Calvo, E.; Landazuri, M. O.; Enriquez, J. A. *Cell metabolism* **2012**, *16*, 378-86.

[13] Tsukihara, T.; Aoyama, H.; Yamashita, E.; Tomizaki, T.; Yamaguchi, H.; Shinzawa-Itoh, K.; Nakashima, R.; Yaono, R.; Yoshikawa, S. *Science* **1995**, *269*, 1069-74.

[14] Killick, E. M.; Marchant, J. V. *The Journal of physiology* **1959**, *147*, 274-98.

[15] Tenhunen, R.; Marver, H. S.; Schmid, R. *P. Natl. Acad. Sci. U. S. A.* **1968**, *61*, 748-55.

[16] Ryter, S. W.; Tyrrell, R. M. *Free Radic. Biol. Med.* **2000**, *28*, 289-309.

[17] Maines, M. D.; Gibbs, P. E. *Biochem. Bioph. Res. Co.* **2005**, *338*, 568-77.

[18] Slusher, T. M.; Olusanya, B. O.; Vreman, H. J.; Wong, R. J.; Brearley, A. M.; Vaucher, Y. E.; Stevenson, D. K. *Trials* **2013**, *14*, 446.

[19] Mazza, E.; Thakkar-Varia, S.; Tozzi, C. A.; Neubauer, J. A. *J. Appl. Physiol.* **2001**, *91*, 379-85.

[20] Ryter, S. W.; Otterbein, L. E.; Morse, D.; Choi, A. M. *Mol. Cell. Biochem.* **2002**, *234-235*, 249-63.

[21] Stocker, R.; Perrella, M. A. *Circulation* **2006**, *114*, 2178-89.

[22] George, J. F.; Chen, B.; Guo, L. L.; Fan, C. L.; Bolisetty, S.; Joseph, R.; Wright, M. M.; Agarwal, A. *Am. J. Pathol.* **2009**, *175*, 422-429.

[23] Gronert, K.; Seta, F.; Bellner, L.; Rezzani, R.; Regan, R. F.; Dunn, M. W.; Abraham, N. G.; Laniado-Schwartzman, M. *Am. J. Pathol.* **2006**, *169*, 1612-1623.

[24] Steegborn, C.; Rauch, A.; Leipelt, M.; Russwurm, M. *P. Natl. Acad. Sci. U. S. A.* **2008**, *105*, 15720-15725.

[25] Zhang, G. Y.; Xiang, B. G.; Skoda, R. C.; Smyth, S. S.; Du, X. P.; Li, Z. Y. *Blood* **2010**, *116*, 216-216.

[26] Schmidtko, A.; Gao, W.; Konig, P.; Heine, S.; Motterlini, R.; Ruth, P.; Schlossmann, J.; Koesling, D.; Niederberger, E.; Tegeder, I.; Friebe, A.; Geisslinger, G. *J. Neurosci.* **2008**, *28*, 8568-76.

[27] Massberg, S.; Gruner, S.; Konrad, I.; Garcia Arguinzonis, M. I.; Eigenthaler, M.; Hemler, K.; Kersting, J.; Schulz, C.; Muller, I.; Besta, F.; Nieswandt, B.; Heinzmann, U.; Walter, U.; Gawaz, M. *Blood* **2004**, *103*, 136-42.

[28] Ito, M.; Nakano, T.; Erdodi, F.; Hartshorne, D. J. *Mol. Cell. Biochem.* **2004**, *259*, 197-209.

[29] Miller, M. J. S.; Grisham, M. B. *Mediat. Inflamm.* **1995**, *4*, 387-396.

[30] White, K. A.; Marletta, M. A. *Biochemistry* **1992**, *31*, 6627-31.

[31] Stevenson, T. H.; Gutierrez, A. F.; Alderton, W. K.; Lian, L.; Scrutton, N. S. *Biochem. J.* **2001**, *358*, 201-8.
[32] Brayden, J. E.; Nelson, M. T. *Science* **1992**, *256*, 532-5.
[33] Meredith, A. L.; Thorneloe, K. S.; Werner, M. E.; Nelson, M. T.; Aldrich, R. W. *J. Biol. Chem.* **2004**, *279*, 36746-52.
[34] Yazejian, B.; Sun, X. P.; Grinnell, A. D. *Nat. Neurosci.* **2000**, *3*, 566-71.
[35] Jensen, B. S.; Odum, N.; Jorgensen, N. K.; Christophersen, P.; Olesen, S. P. *Proc. Natl. Acad. Sci. U. S. A.* **1999**, *96*, 10917-21.
[36] Berkefeld, H.; Fakler, B.; Schulte, U. *Physiol. Rev.* **2010**, *90*, 1437-59.
[37] Boczkowski, J.; Poderoso, J. J.; Motterlini, R. *Trends Biochem. Sci.* **2006**, *31*, 614-21.
[38] Dubuis, E.; Potier, M.; Wang, R.; Vandier, C. *Cardiovasc Res* **2005**, *65*, 751-61.
[39] Nakao, A.; Toyokawa, H.; Tsung, A.; Nalesnik, M. A.; Stolz, D. B.; Kohmoto, J.; Ikeda, A.; Tomiyama, K.; Harada, T.; Takahashi, T.; Yang, R.; Fink, M. P.; Morita, K.; Choi, A. M.; Murase, N. *Am. J. Transplant.* **2006**, *6*, 2243-55.
[40] BritishLiverTrust, Facts about liver disease. http://www.britishlivertrust.org.uk/media-centre/facts-about-liver-disease/, (accessed 8/5/2014).
[41] Zuckerbraun, B. S.; Billiar, T. R.; Otterbein, S. L.; Kim, P. K.; Liu, F.; Choi, A. M.; Bach, F. H.; Otterbein, L. E. *J. Exp. Med.* **2003**, *198*, 1707-16.
[42] Tsui, T. Y.; Obed, A.; Siu, Y. T.; Yet, S. F.; Prantl, L.; Schlitt, H. J.; Fan, S. T. *Shock* **2007**, *27*, 165-71.
[43] WorldHealthOrganisation, Antimicrobial Resistance Global Report. http://www.who.int/drugresistance/documents/surveillancereport/en/, (accessed 9/5/2014).
[44] Hendriks, J. H.; Prior, L.; Baker, A. R.; Thomson, A. J.; Saraste, M.; Watmough, N. J. *Biochemistry* **2001**, *40*, 13361-9.
[45] Pitcher, R. S.; Watmough, N. J. *Biochim. Biophys. Acta.* **2004**, *1655*, 388-99.
[46] Preisig, O.; Zufferey, R.; Thony-Meyer, L.; Appleby, C. A.; Hennecke, H. *J. Bacteriol.* **1996**, *178*, 1532-8.
[47] Jesse, H. E.; Nye, T. L.; McLean, S.; Green, J.; Mann, B. E.; Poole, R. K. *Bba-Proteins Proteom.* **2013**, *1834*, 1693-1703.
[48] Nobre, L. S.; Seixas, J. D.; Romao, C. C.; Saraiva, L. M. *Antimicrob. Agents Ch.* **2007**, *51*, 4303-4307.
[49] Mancuso, A. J.; Brownfain, D. S.; Swern, D. *Journal of Organic Chemistry* **1979**, *44*, 4148-4151.
[50] Pfeiffer, H.; Sowik, T.; Schatzschneider, U. *J. Organomet. Chem.* **2013**, *734*, 17-24.
[51] Atkin, A. J.; Fairlamb, I. J. S.; Ward, J. S.; Lynam, J. M. *Organometallics* **2012**, *31*, 5894-5902.
[52] Motterlini, R.; Sawle, P.; Hammad, J.; Bains, S.; Alberto, R.; Foresti, R.; Green, C. J. *FASEB J.* **2005**, *19*, 284-6.
[53] Clark, J. E.; Naughton, P.; Shurey, S.; Green, C. J.; Johnson, T. R.; Mann, B. E.; Foresti, R.; Motterlini, R. *Circ. Res.* **2003**, *93*, e2-8.
[54] Ryan, M. J.; Jernigan, N. L.; Drummond, H. A.; McLemore, G. R., Jr.; Rimoldi, J. M.; Poreddy, S. R.; Gadepalli, R. S.; Stec, D. E. *Pharmacol. Res.* **2006**, *54*, 24-9.
[55] Fagone, P.; Mangano, K.; Quattrocchi, C.; Motterlini, R.; Di Marco, R.; Magro, G.; Penacho, N.; Romao, C. C.; Nicoletti, F. *Clin. Exp. Immunol.* **2011**, *163*, 368-74.
[56] Pombeiro, A. J. L., *Advances in organometallic chemistry : the silver/gold jubilee International Conference on Organometallic Chemistry celebratory book*. **2014**; p 550.
[57] Rodrigues, S. S.; Seixas, J. D.; Guerreiro, B.; Pereira, N. M. P.; Romão, C. C.; Haas, W. E.; Gonçalves de Sousa, I. M., Prevention of gastric ulcery by carbon monoxide.Alfama, International Patent WO2009013612A1, **2012**.
[58] Crook, S. H.; Mann, B. E.; Meijer, A. J.; Adams, H.; Sawle, P.; Scapens, D.; Motterlini, R. *Dalton Trans.* **2011**, *40*, 4230-5.
[59] Ward, J. S.; Lynam, J. M.; Moir, J. W. B.; Sanin, D. E.; Mountford, A. P.; Fairlamb, I. J. S. *Dalton Trans.* **2012**, *41*, 10514-10517.

[60] Zobi, F.; Quaroni, L.; Santoro, G.; Zlateva, T.; Blacque, O.; Sarafimov, B.; Schaub, M. C.; Bogdanova, A. Y. *J. Med. Chem.* **2013**, *56*, 6719-31.
[61] Pfeiffer, H.; Rojas, A.; Niesel, J.; Schatzschneider, U. *Dalton Trans.* **2009**, 4292-8.
[62] Niesel, J.; Pinto, A.; Peindy N'Dongo, H. W.; Merz, K.; Ott, I.; Gust, R.; Schatzschneider, U. *Chem. Commun.* **2008**, 1798-800.
[63] Fairlamb, I. J. S.; Atkin, A. J.; Williams, S.; Sawle, P.; Motterlini, R.; Lynam, J. M. *Dalton Trans.* **2009**, 3653-3656.
[64] Bernardes, G. J. L.; Santos-Silva, T.; Mukhopadhyay, A.; Seixas, J. D.; Romao, C. C.; Romao, M. J. *J. Am. Chem. Soc.* **2011**, *133*, 1192-1195.
[65] Sun, B. W.; Sun, Z.; Jin, Q.; Chen, X. *Int. J. Biol. Sci.* **2008**, *4*, 176-183.
[66] Dong, D. L.; Chen, C.; Huang, W.; Chen, Y.; Zhang, X. L.; Li, Z.; Li, Y.; Yang, B. F. *Eur. J. Pharmacol.* **2008**, *590*, 99-104.
[67] Desmard, M.; Davidge, K. S.; Bouvet, O.; Morin, D.; Roux, D.; Foresti, R.; Ricard, J. D.; Denamur, E.; Poole, R. K.; Montravers, P.; Motterlini, R.; Boczkowski, J. *FASEB J.* **2009**, *23*, 1023-31.
[68] Stagni, E.; Privitera, M. G.; Bucolo, C.; Leggio, G. M.; Motterlini, R.; Drago, F. *Brit. J. Ophthalmol.* **2009**, *93*, 254-7.
[69] Chlopicki, S.; Olszanecki, R.; Marcinkiewicz, E.; Lomnicka, M.; Motterlini, R. *Cardiovasc Res* **2006**, *71*, 393-401.
[70] Coceani, F. *Circ. Res.* **2000**, *86*, 1184-1186.
[71] Fairlamb, I. J. S.; Lynam, J. M.; Moulton, B. E.; Taylor, I. E.; Duhme-Klair, A. K.; Sawle, P.; Motterlini, R. *Dalton Trans.* **2007**, 3603-5.
[72] Fairlamb, I. J. S.; Duhme-Klair, A. K.; Lynam, J. M.; Moulton, B. E.; O'Brien, C. T.; Sawle, P.; Hammad, J.; Motterlini, R. *Bioorg. Med. Chem. Lett.* **2006**, *16*, 995-8.
[73] Fairlamb, I. J. S.; Syvanne, S. M.; Whitwood, A. C. *Synlett* **2003**, 1693-1697.
[74] Sawle, P.; Hammad, J.; Fairlamb, I. J.; Moulton, B.; O'Brien, C. T.; Lynam, J. M.; Duhme-Klair, A. K.; Foresti, R.; Motterlini, R. *J. Pharmacol. Exp. Ther.* **2006**, *318*, 403-10.
[75] Fairlamb, I. J.; Marrison, L. R.; Dickinson, J. M.; Lu, F. J.; Schmidt, J. P. *Bioorg. Med. Chem.* **2004**, *12*, 4285-99.
[76] Romanski, S.; Kraus, B.; Schatzschneider, U.; Neudorfl, J. M.; Amslinger, S.; Schmalz, H. G. *Angew. Chem. Int. Ed.* **2011**, *50*, 2392-6.
[77] Boháč, A. L., M.; Hrnčiar,P.; Hutta, M. *J. Organomet. Chem.* **1996**, *507*, 23-29.
[78] Mohr, F.; Niesel, J.; Schatzschneider, U.; Lehmann, C. W. *Z. Anorg. Allg. Chem.* **2012**, *638*, 543-546.
[79] Schatzschneider, U. *Eur. J. Inorg. Chem.* **2010**, 1451-1467.
[80] Motterlini, R.; Clark, J. E.; Foresti, R.; Sarathchandra, P.; Mann, B. E.; Green, C. J. *Circ. Res.* **2002**, *90*, E17-24.
[81] Arregui, B.; Lopez, B.; Garcia Salom, M.; Valero, F.; Navarro, C.; Fenoy, F. J. *Kidney Int.* **2004**, *65*, 564-74.
[82] Zhang, W. Q.; Atkin, A. J.; Fairlamb, I. J. S.; Whitwood, A. C.; Lynam, J. M. *Organometallics* **2011**, *30*, 4643-4654.
[83] Kretschmer, R.; Gessner, G.; Gorls, H.; Heinemann, S. H.; Westerhausen, M. *J. Inorg. Biochem.* **2011**, *105*, 6-9.
[84] Trofimenko, S. *J. Am. Chem. Soc.* **1970**, *92*, 5118-5126.
[85] Kussie, P. H.; Gorina, S.; Marechal, V.; Elenbaas, B.; Moreau, J.; Levine, A. J.; Pavletich, N. P. *Science* **1996**, *274*, 948-53.
[86] Meister, K.; Niesel, J.; Schatzschneider, U.; Metzler-Nolte, N.; Schmidt, D. A.; Havenith, M. *Angew. Chem. Int. Ed.* **2010**.
[87] Peindy N'Dongo, H. W.; Neundorf, I.; Merz, K.; Schatzschneider, U. *J. Inorg. Biochem.* **2008**, *102*, 2114-9.
[88] Marques, A. R.; Kromer, L.; Gallo, D. J.; Penacho, N.; Rodrigues, S. S.; Seixas, J. D.; Bernardes, G. J. L.; Reis, P. M.; Otterbein, S. L.; Ruggieri, R. A.; Gonçalves, A. S. G.; Gonçalves, A. M. L.; Matos, M. N. D.; Bento, I.; Otterbein, L. E.; Blättler, W. A.; Romão, C. C. *Organometallics* **2012**, *31*, 5810-5822.

[89] Bruce, M. I.; Goodall, B. L.; Matsuda, I. *Aust. J. Chem.* **1975**, *28*, 1259-1264.
[90] Bennett, R. L.; Bruce, M. I.; Matsuda, I. *Aust. J. Chem.* **1975**, *28*, 1265-1272.
[91] Moulton, B. E. PhD. Dissertation, University of York, **2008**.
[92] Liu, C.; Han, N.; Song, X. X.; Qiu, J. S. *Eur. J. Org. Chem.* **2010**, 5548-5551.
[93] Beeby, A.; Bettington, S.; Fairlamb, I. J. S.; Goeta, A. E.; Kapdi, A. R.; Niemela, E. H.; Thompson, A. L. *New. J. Chem.* **2004**, *28*, 600-605.
[94] Atkin, A. J.; Lynam, J. M.; Moulton, B. E.; Sawle, P.; Motterlini, R.; Boyle, N. M.; Pryce, M. T.; Fairlamb, I. J. *Dalton Trans.* **2011**, *40*, 5755-61.
[95] Hamid, K. A.; Katsumi, H.; Sakane, T.; Yamamoto, A. *Int. J. Pharm.* **2009**, *379*, 100-8.
[96] Atkin, A. J.; Lynam, J. M.; Moulton, B. E.; Sawle, P.; Motterlini, R.; Boyle, N. M.; Pryce, M. T.; Fairlamb, I. J. *Dalton Trans.* **2011**, *40*, 5755-61.
[97] McLean, S.; Mann, B. E.; Poole, R. K. *Anal. Biochem.* **2012**, *427*, 36-40.
[98] Walker, S. D.; Barder, T. E.; Martinelli, J. R.; Buchwald, S. L. *Angew. Chem. Int. Ed.* **2004**, *43*, 1871-1876.
[99] Zhang, Y. M.; Wei, T. B.; Liu, H.; Li, M. L. *Synth. Comm.* **2005**, *35*, 1759-1764.
[100] Karlsson, S.; Mattsson, S.; Dahlstrom, M. *Tetrahedron Lett.* **2007**, *48*, 2497-2499.
[101] Motterlini, R.; Sawle, P.; Hammad, J.; Bains, S.; Alberto, R.; Foresti, R.; Green, C. J. *FASEB J.* **2005**, *19*, 284-6.
[102] Liu, D. *B. Environ. Contam. Tox.* **1981**, *26*, 145-149.
[103] Legrand, C.; Bour, J. M.; Jacob, C.; Capiaumont, J.; Martial, A.; Marc, A.; Wudtke, M.; Kretzmer, G.; Demangel, C.; Duval, D.; et al. *J. Biotechnol.* **1992**, *25*, 231-43.
[104] Giustarini, D.; Rossi, R.; Milzani, A.; Dalle-Donne, I. *Nitric Oxide, Part F* **2008**, *440*, 361-380.
[105] Schoenborn, J. R.; Wilson, C. B. *Adv. Immunol.* **2007**, *96*, 41-101.
[106] Bilous, P. T.; Weiner, J. H. *J. Bacteriol.* **1985**, *162*, 1151-5.
[107] Wilson, J. L.; Jesse, H. E.; Hughes, B.; Lund, V.; Naylor, K.; Davidge, K. S.; Cook, G. M.; Mann, B. E.; Poole, R. K. *Antioxid. Redox Signal* **2013**, *19*, 497-509.
[108] NHS, Information on *S. aureus* infections., http://www.nhs.uk/conditions/staphylococcal-infections/pages/introduction.aspx, (accessed 18/8/2014).
[109] Bumah, V. V.; Masson-Meyers, D. S.; Cashin, S. E.; Enwemeka, C. S. *Photomed. Laser Surg.* **2013**, *31*, 547-553.
[110] Maclean, M.; MacGregor, S. J.; Anderson, J. G.; Woolsey, G. *Appl. Environ. Microb.* **2009**, *75*, 1932-1937.
[111] Himo, F.; Lovell, T.; Hilgraf, R.; Rostovtsev, V. V.; Noodleman, L.; Sharpless, K. B.; Fokin, V. V. *J. Am. Chem. Soc.* **2005**, *127*, 210-216.
[112] Landi, F.; Johansson, C. M.; Campopiano, D. J.; Hulme, A. N. *Org Biomol Chem* **2010**, *8*, 56-59.
[113] Robinson, N. P.; Depree, G. J.; de Wit, R. W.; Main, L.; Nicholson, B. K. *J. Organomet. Chem.* **2005**, *690*, 3827-3837.
[114] Nicolai, S.; Erard, S.; Gonzalez, D. F.; Waser, J. *Org. Lett.* **2010**, *12*, 384-387.
[115] Zhou, B.; Chen, H.; Wang, C. *J. Am. Chem. Soc.* **2013**, *135*, 1264-7.
[116] Walker, J. R.; Altman, E. *Appl. Environ. Microb.* **2005**, *71*, 1850-1855.
[117] Green, N. M. *Biochem. J.* **1963**, *89*, 585-91.
[118] Campbell, A.; Del Campillo-Campbell, A.; Chang, R. *Proc. Natl. Acad. Sci. U. S. A.* **1972**, *69*, 676-80.
[119] Mayer, T.; Maier, M. E. *Eur. J. Org. Chem.* **2007**, 4711-4720.
[120] Suurkuusk, J.; Wadso, I. *Eur. J. Biochem.* **1972**, *28*, 438-41.
[121] ThermoScientific, HABA/avidin assay image. http://www.piercenet.com/product/pierce-biotin-quantitation-kit, (accessed 17/6/14).
[122] Kienle, A.; Lilge, L.; Vitkin, I. A.; Patterson, M. S.; Wilson, B. C.; Hibst, R.; Steiner, R. *Appl. Optics* **1996**, *35*, 1151.
[123] Belmont, J. A.; Wrighton, M. S. *Organometallics* **1986**, *5*, 1421-1428.
[124] Nagel, C.; McLean, S.; Poole, R. K.; Braunschweig, H.; Kramer, T.; Schatzschneider, U. *Dalton Trans.* **2014**, *43*, 9986-97.
[125] Silver, L. L. *Curr. Opin. Microbiol.* **2003**, *6*, 431-8.

[126] Ward, J. S.; Lynam, J.; Fairlamb, I. J. S.; Moir, J. W. *Chem. Eur. J.* **2014**, *Accepted: awaiting publication*.
[127] Appleby, C. A.; Wittenberg, B. A.; Wittenberg, J. B. *Proc. Natl. Acad. Sci. U. S. A.* **1973**, *70*, 564-8.
[128] Bertini, I.; Gray, H. B.; Lippard, S. J.; Valentine, J. S., *Bioinorganic chemistry*. University Science Books: Mill Valley, California, **1994**.
[129] Jones, D. K.; Badii, R.; Rosell, F. I.; Lloyd, E. *Biochem. J.* **1998**, *330 (Pt 2)*, 983-8.
[130] Bhattacharyya, P. *J. Bacteriol.* **1970**, *104*, 1307-11.
[131] Silver, S.; Johnseine, P.; King, K. *J. Bacteriol.* **1970**, *104*, 1299-306.
[132] Camara, J.; Serra, J.; Ayats, J.; Bastida, T.; Carnicer-Pont, D.; Andreu, A.; Ardanuy, C. *J. Antimicrob. chemother.* **2012**, *67*, 1858-60.
[133] Unemo, M.; Golparian, D.; Nicholas, R.; Ohnishi, M.; Gallay, A.; Sednaoui, P. *Antimicrob. Agents. Chemother.* **2012**, *56*, 1273-80.
[134] Ohnishi, M.; Saika, T.; Hoshina, S.; Iwasaku, K.; Nakayama, S.; Watanabe, H.; Kitawaki, J. *Emerg. Infect. Dis.* **2011**, *17*, 148-9.
[135] Wang, M. X.; Funabiki, K.; Matsui, M. *Dyes Pigments* **2003**, *57*, 77-86.
[136] Foresti, R.; Hammad, J.; Clark, J. E.; Johnson, T. R.; Mann, B. E.; Friebe, A.; Green, C. J.; Motterlini, R. *Brit. J. Pharmacol.* **2004**, *142*, 453-60.
[137] Kretschmer, R.; Gessner, G.; Gorls, H.; Heinemann, S. H.; Westerhausen, M. *J. Inorg. Biochem.* **2011**, *105*, 6-9.
[138] Sawle, P.; Foresti, R.; Mann, B. E.; Johnson, T. R.; Green, C. J.; Motterlini, R. *Brit. J. Pharmacol.* **2005**, *145*, 800-10.
[139] BBC, Antibiotic resistance: Cameron warns of medical 'dark ages'. http://www.bbc.co.uk/news/health-28098838, (accessed 19/8/14).
[140] Bradley, M.; Valeur, E. *Chem. Soc. Rev.* **2009**, *38*, 606-631.
[141] Williams, T. J.; Reay, A. J.; Whitwood, A. C.; Fairlamb, I. J. S. *Chem. Commun.* **2014**, *50*, 3052-4.
[142] Meister, K.; Niesel, J.; Schatzschneider, U.; Metzler-Nolte, N.; Schmidt, D. A.; Havenith, M. *Angew. Chem. Int. Ed.* **2010**, *49*, 3310-2.
[143] Atkin, A. J. PhD. Dissertation, University of York, **2010**.
[144] Coulson, D. R.; Satek, L. C.; Grim, S. O. *Inorg. Syn.* **1972**, *13*, 121-123.
[145] Bruce, M.; Liddel, M.; Pain, G. *Inorg. Syn.* **1989**, *26*, 171-172.
[146] Pfeffer, M.; Djukic, J. P.; Maisse, A. *J. Organomet. Chem.* **1998**, *567*, 65-74.
[147] Djukic, J. P.; Dotz, K. H.; Pfeffer, M.; DeCian, A.; Fischer, J. *Organometallics* **1997**, *16*, 5171-5182.
[148] Brase, S.; Gil, C.; Knepper, K.; Zimmermann, V. *Angew. Chem. Int. Ed.* **2005**, *44*, 5188-5240.